JOURNAL OF ATMOSPHERIC AND TERRESTRIAL PHYSICS

EDITORIAL ADVISORY BOARD

H. O. G. ALFVÉN-STOCKHOLM • J. BARTELS-GÖTTINGEN • P. M. S. BLACKETT-LONDON • E. G. BOWEN-SYDNEY • SIR DAVID BRUNT-LONDON • R. BUREAU-BAGNEUX • S. CHAPMAN-ALASKA • J. EGEDAL-COPENHAGEN • H. FICKER-VIENNA V. F. HESS-NEW YORK • E. O. HULBURT-WASHINGTON, D.C. • H. ISRAEL-TÜBINGEN D. H. MENZEL-CAMBRIDGE, MASS. • S. K. MITRA-CALCUTTA • M. NICOLET-UCCLE E. H. NORINDER-UPSALA • B. van der POL-GENEVA • J. A. RATCLIFFE-CAMBRIDGE O. E. H. RYDBECK-GOTHENBURG • SIR GEORGE SIMPSON-LONDON • H. SOLBERG-OSLO • C. STØRMER-OSLO • VELDKAMP-DE BILT • M. WALDMEIER-ZURICH R. v. d. R. WOOLLEY-CANBERRA • J. ZENNECK-ALTHEGNENBERG

EDITOR IN CHIEF

SIR EDWARD APPLETON, F.R.S.
EDINBURGH

VOLUME 7
JULY—DECEMBER
1955

PERGAMON PRESS • LONDON & NEW YORK

J. Atmosph. Terr. Phys.

VOL.
7
1955

CONTENTS

Nos. 1/2

F. Horner and C. Clarke: Some waveforms of atmospherics and their use in the location of thunderstorms 1

C. O. Hines: Hydromagnetic resonance in ionospheric waves 14

Gustav Ortner and Abdel Fattah El Nadi: Intermediate and large atmospheric ions at Cairo-Giza 31

J. Egedal and N. Ambolt: The effect on geomagnetism of the eclipse of 30 June, 1954 . . 40

Günther Lange-Hesse: Erdmagnetische Unruhe und Durchsmittsabweichungen der F_2–Schicht—Tagesgrenzfrequenzen in verschiedenen geomagnetischen Breiten 49

W. W. Mapleson and W. S. Whitlock: Apparatus for the accurate and continuous measurement of the earth's electric field 61

A. Omholt: The auroral E–layer ionization and the auroral luminosity 73

A. Sittkus: Untersuchung des Tagesganges der komischen Ultrastrahlung mit einer grossen Ionisationskammer 80

E. S. Cotton: Diurnal variations in natural atmospheric radioactivity 90

Research Notes:

A. P. Mitra: The lunar semi-diurnal oscillation in the ionospheric absorption of 150 kc/s radio waves . . 99

L. V. Wallace and R. W. Nicholls: The interpretation of intensity distributions in the N_2 second positive and N_2^+ first negative band systems 101

N. J. Skinner and R. W. Wright: Recombination and ion production from the total electron content . . 105

A. K. Saha and S. Ray: Some features of the E_2–layer observed at the ionosphere field station Haringhata Calcutta 107

Book Reviews:

"Meteor Astronomy" by A. C. B. Lovell (reviewed by D. W. R. McKinley) 109

"Variational Principles in Dynamics and Quantum Theory" by Wolfgang Yourgrau and Stanley Mandelstam (reviewed by L. Rosenfeld) 110

"Methoden und Problems der Wettervorhersage" by Heinz Reuter (reviewed by R. C. Sutcliffe) . . 111

Obituary: Professor Erich Regener (by J. Bartels) 112

No. 3

G. V. Groves: Geometric theory of sound propagation in the atmosphere 113

H. K. Paetzold: New experimental and theoretical investigations on the atmospheric ozone layer 128

D. M. Hunten: Some photometric observations of auroral spectra 141

Marcel Nicolet: The aeronomic problem of nitrogen oxides 152

Research Notes:

D. R. Barber: Changes in brightness, polarization and colour of the zenith day sky accompanying geomagnetic activity 170

C. M. Minnis: Electron production and recombination in the E-layer 172

Nos. 4/5

N. Davids and R. W. Parkinson: Wave solutions for critical and near-critical coupling conditions in the ionosphere 173

R. W. Parkinson: The night-time lower ionosphere as deduced from a theoretical and experimental investigation of coupling phenomena at 150 kc/sec 203

T. W. Bennington: Observations of the effects of ionospheric storms over a North Atlantic Circuit 235

W. R. Piggott: On the variation of ionospheric absorption at different stations 244

A. Omholt and L. Harang: Measurement of the mean lifetime of the metastable ^1S-state of the oxygen atom in the upper atmosphere during auroral displays 247

S. V. Chandrashekhar Aiya and K. R. Phadke: Atmospheric noise interference to broadcasting in the 3-Mc/s band at Poona 254

William C. Hoffman: A theoretical model for high-frequency backscatter from the sea surface via the ionosphere 278

H. P. Gush and A. Vallance Jones: Infra-red spectrum of the night sky from $1{\cdot}0\mu$ to $2{\cdot}0\mu$. 285

Research Note:

E. V. APPLETON, A. J. LYON, and A G. PRITCHARD: The detection of the S_q current system in ionospheric radio sounding 292

Book Review:

"Les Rayons Cosmiques dans leurs rapports avec l'Electricité atmospherique, la Métrologie, la Geomagnetisme et l'Astronomie," by A. DAUVILLIER (reviewed by H. ELLIOT) 296

No. 6

MARCEL NICOLET: Nitrogen oxides and the airglow 297

C. M. MINNIS: A new index of solar activity based on ionospheric measurements . . . 310

J. A. FEJER: The interaction of pulsed radio waves in the ionosphere 322

G. W. G. COURT: Ionospheric wind determination from spaced radio receiver fading records . 333

W. R. PIGGOTT: The measurement of normal E-layer critical frequencies at night . . . 341

Research Notes:

H. G. BOOKER: On the level at which fading is imposed on waves reflected vertically from the ionosphere . 343

L. W. ROSS: Accuracy of solar-flare observations. 345

A. OMHOLT: The recombination in the E-layer during aurorae 346

C. A. SHAIN: Changes in the absorption of cosmic noise observed during two ionospheric disturbances . . 347

HOPE I. LEIGHTON and DONALD E. BILLINGS: Solar H_α filaments and geomagnetic disturbances . . . 349

K-indices of geomagnetic activity from the observatories at Abinger, Eskdalemuir and Lerwick, from May to June, 1955 351

VOL. 7 1955

AUTHOR INDEX TO VOLUME 7

(B) denotes a book review

AIYA, S. V. C. p. 254
AMBOLT, N. p. 40
APPLETON, E. V. p. 292
BARBER, D. R. p. 170
BARTELS, J. p. 112.
BENNINGTON, T. W. p. 235
BILLINGS, D. E. p. 349
BOOKER, H. G. p. 343
CLARKE, C. p. 1
COTTON, E. S. p. 90
COURT, G. W. G. p. 333
DAVIDS, N. p. 173
EGEDAL, J. p. 40
ELLIOT, H. p. 296 (B)
EL NADI, ABDEL FATTAH, p. 31
FEJER, J. A. p. 322
GROVES, G. V. p. 113
GUSH, H. P. p. 285
HARANG, L. p. 247
HINES, C. O. p. 14
HOFFMAN, W. C. p. 278
HORNER, F. p. 1
HUNTEN, D. M. p. 141
JONES, A. VALLANCE p. 285
LANGE-HESSE, GÜNTHER p. 49
LEIGHTON, H. I. p. 349
LYON, A. J. p. 292
MAPLESON, W. W. p. 61
MCKINLEY, D. W. R. p. 109 (B)
MINNIS, C. M. pp. 172, 310
MITRA, A. P. p. 99
NICHOLLS, R. W. p. 101
NICOLET, M. pp. 152, 297
OMHOLT, A. pp. 73, 247, 346
ORTNER, G. p. 31
PAETZOLD, H. K. p. 128
PARKINSON, R. W. pp. 173, 203
PHADKE, K. R. p. 254
PIGGOTT, W. R. pp. 244, 341
PRITCHARD, A. G. p. 292
RAY, S. p. 107
ROSENFELD, L. p. 110 (B)
ROSS, L. W. p. 345
SAHA, A. K. p. 107
SHAIN, C. A. p. 347
SITTKUS, A. p. 80
SKINNER, N. J. p. 105
SUTCLIFFE, R. C. p. 111 (B)
WALLACE, L. V. p. 101
WHITLOCK, W. S. p. 61
WRIGHT, R. W. p. 105

Journal of Atmospheric and Terrestrial Physics, 1955, Vol. 7, pp. 1 to 13. Pergamon Press Ltd., London

Some waveforms of atmospherics and their use in the location of thunderstorms

F. Horner and C. Clarke
(Official communication from D.S.I.R. Radio Research Station, Slough)

(*Received* 7 *October* 1954)

ABSTRACT

Illustrations are given of the main types of waveforms which have been recorded in southern England, using the equipment described in an earlier paper. Particular emphasis is given to echo-type waveforms comprising a series of echoes arriving by different modes of reflection between the earth and the ionosphere. Practical difficulties arising in the use of this type for estimating the distance of the source are discussed.

The range is estimated from the measurement of the time-intervals between echoes, which under good conditions may be determined to an accuracy of two microseconds. Waveforms usually show discrepancies considerably greater than this figure when the time-intervals are compared with what would be expected from simple reflection theory and a graphical method of analysis is used which averages the errors on individual echoes. The effect of these discrepancies on the accuracy of distance estimation is discussed.

The frequency of occurrence of suitable types of waveform is derived from an analysis of routine recordings over a period of one year. Approximately three per cent of the waveforms recorded in daylight and five per cent at night were suitable for deriving an estimate of distance, but more detailed analysis of a proportion of the waveforms indicated that by changes in technique, the night-time figure might have been increased by a factor of about 2.

With experience it is not difficult to select by cursory inspection those waveforms which are likely, on analysis, to yield a useful distance estimate. Many of them, however, are rather complex, and considerable time is required to determine from these the most probable value of distance.

Most night-time storms within 2,000 km give rise to some waveforms from which a reliable distance estimate can be deduced; by day the corresponding range is about 500 km in summer and 1,000 km in winter. Within these ranges errors can be expected to be within ± 30 per cent.

It is concluded that waveform analysis would be of some value for thunderstorm location as an adjunct to a network of cathode-ray direction finders, but that the reliability and convenience of the technique are not yet sufficient for use as the sole method of estimating distance.

1. Introduction

The location of thunderstorms by radio means has become an accepted part of the worldwide system of meteorological observations, and various methods of location are in current use. In the British Isles, four direction finders operating at a frequency of 10 kc/s on baselines of about 500 km are used (Ockenden, 1947). This technique is in routine use and yields valuable results, but it involves difficulties and expense in manning four stations continuously and in maintaining telephone communication between them. In many other parts of the world a network of direction finders is impracticable because widely-spaced sites of adequate quality do not exist. Also in regions of high thunderstorm activity there might be difficulty in identifying a given flash at several stations. For these reasons much interest is attached to any possible method of making observations from a single station, by observing the direction of the storm and using an independent technique for assessing range. Analysis of the waveforms of atmospherics is one method of range measurement, and an investigation has been made of its possibilities and limitations as a routine technique. It is concluded that the technique has very limited application at present, and the reasons are discussed in this paper. The conclusions refer to observations in England, and do not necessarily apply to other regions of the world.

2. Technique for Recording Waveforms

Atmospheric waveforms have been recorded by a number of workers in many parts of the world (Schonland, 1941; Rivault, 1943 and 1945; Kessler and Goyder, 1950; Chapman, 1950; Kimpara, 1949; Caton and Pierce, 1952). It has been usual to record the time-variation of the vertical component of the electric field, but the first time-differential of the field is sometimes recorded. The main characteristics of the waveform are the same with both methods, except that the field-differential records do not contain large, slowly-varying components.

The waveform recorder used in the present work is essentially a vertical wire aerial connected to an amplifier with a passband from 50 c/s to 80 kc/s, and a cathode-ray tube display in which field-strength variations are displayed on a linear time-base. The instrument, a description of which has already been published (Clarke and Mortimer, 1951), was designed to record waveforms automatically on 35-mm film, and has proved satisfactory for routine investigation of the frequency of occurrence of various types of waveform. For the detailed study of echo-type waveforms it was found necessary to reduce optical distortion by the use of an additional display unit, with a flat-faced tube and a long-focus camera recording on 60-mm film. In addition, calibrating pulses were displayed on the record at 50-microsecond intervals (see Fig. 4). The time-base durations were usually between 1·5 and 7 milliseconds.

The previous paper (Clarke and Mortimer, 1951) also describes the method of determining the sources of the observed atmospherics, by co-ordinating the observations with those obtained with the Meteorological Office network of direction finders. This system was improved by sending an audible pulse, triggered by the atmospheric received on the waveform recorder, over the telephone network to the direction-finder observers.

VOL. 7 1955

3. The Estimation of Distance by Analysis of Echo-type Waveforms

Previous investigations have revealed the main types of form, and the mechanism which gives rise to these types is understood in a general way. The initial part of the waveform is frequently of the type shown in Fig. 1: it exhibits rapid variations in field due to the stepped-leader mechanism of discharge. It has been called the precursor, since it is usually, though not always, followed by further variations arising from a much larger discharge (the return stroke).

The type of waveform with which this investigation is mainly concerned is that showing a number of discrete impulses, originating in the return stroke of a lightning flash, and received by successive reflections at the earth and the ionosphere. It has been shown elsewhere (Schonland *et al.*, 1940) how the analysis of such waveforms can lead to an estimate of both the distance of the source and the effective height of reflection. It was desired to determine what practical difficulties would arise in the application of the technique to the routine location of thunderstorms.

The boundary between echo-type waveforms and other types is not clearly defined. A number of transition types are received which appear to exhibit echoes but which do not fit the simple reflection theory.

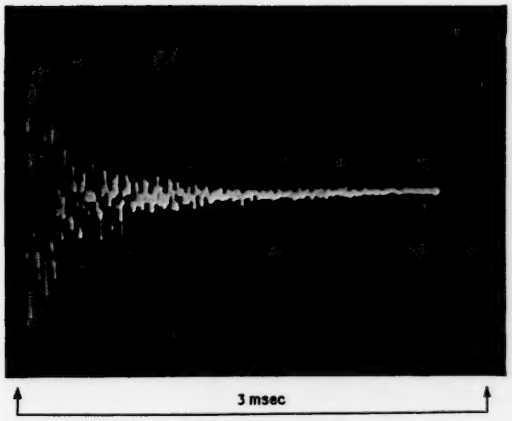

Fig. 1. Waveform arising from a stepped-leader discharge 21 July 1950, 0900 G.M.T., C.R.D.F. fix in North Sea, distance 850 km.

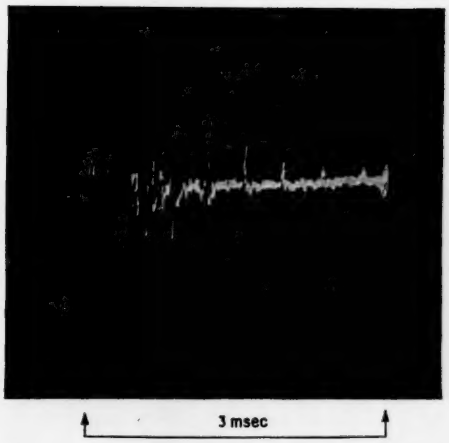

Fig. 2. Unusually well-defined echo type. 13 November 1950, 1900 G.M.T. Poor quality C.R.D.F. fix indicates location in widespread storm in north-west Europe; distance deduced from waveform—500 km.

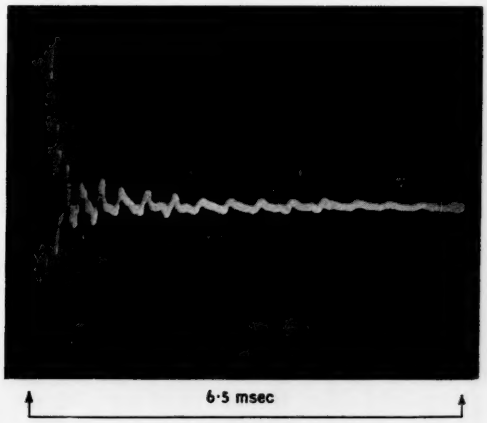

Fig. 3. Night-time echo-type form. 3 October 1949, 2100 G.M.T., one of a group of similar waveforms from a storm located by C.R.D.F. in the Pyrenees region—distance 1,050 km. Distance deduced from waveform 1,130 km.

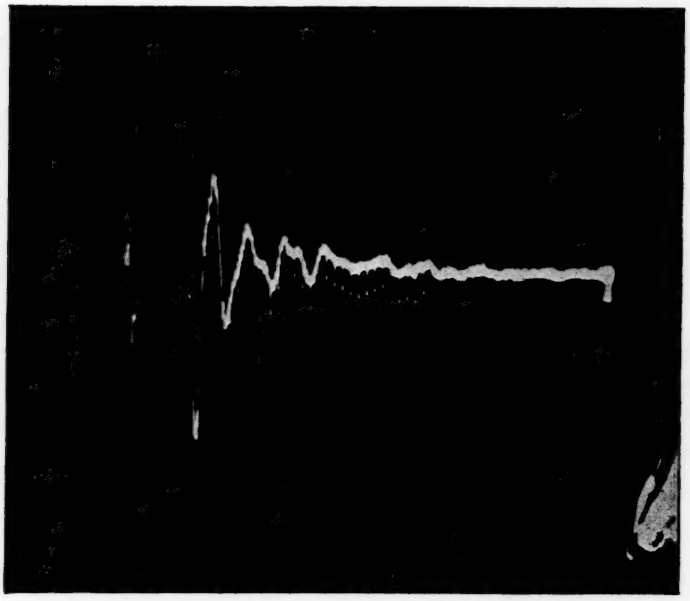

(a)

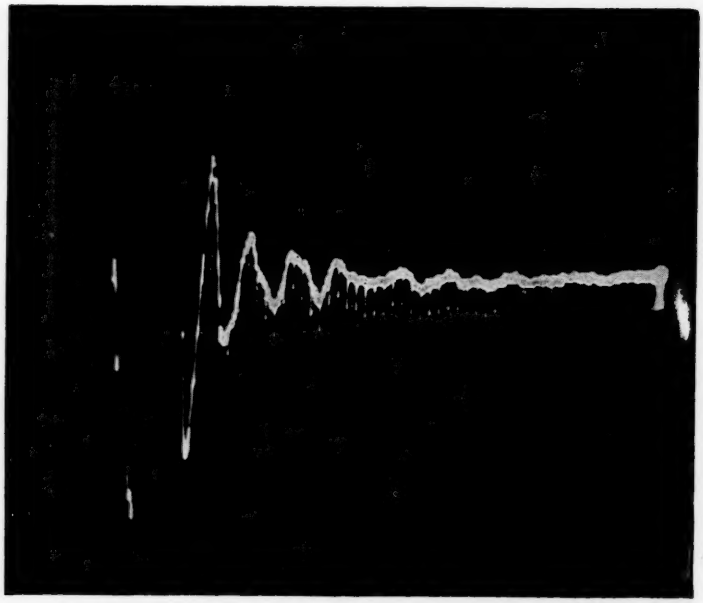

(b)

Fig. 4(a) and (b). Night-time echo-types, from a distant source in the Atlantic, showing similarity of fine structure. 5 December 1950. 2115 G.M.T., C.R.D.F. fix, 2,750 km, to south-west. Timing marks at 50-microsecond intervals.

VOL.
7
1955

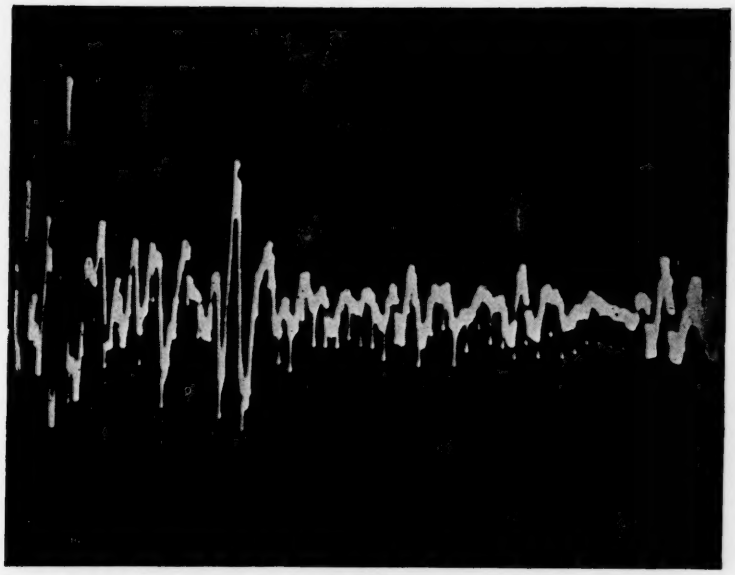

(a)

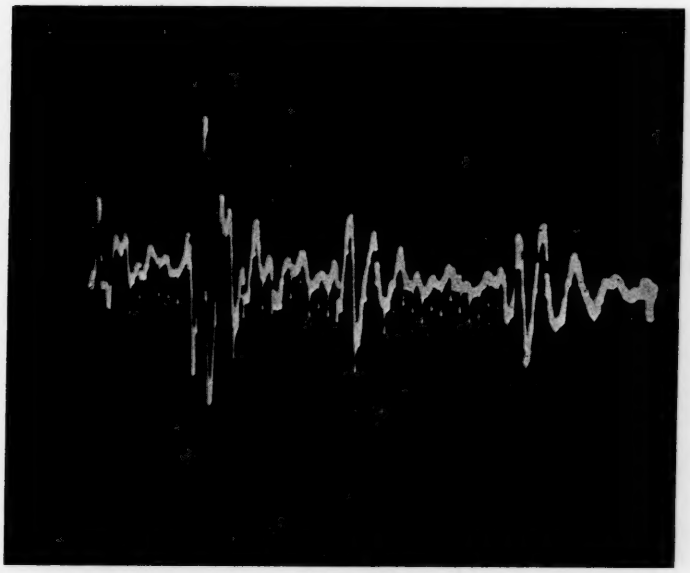

(b)

Fig. 5(a) and (b). Similar waveforms, probably originating in cloud discharges, 5 December 1950, 2115 G.M.T., C.R.D.F. fixes 3,000 km, to south-west. Timing marks at 50-microsecond intervals.

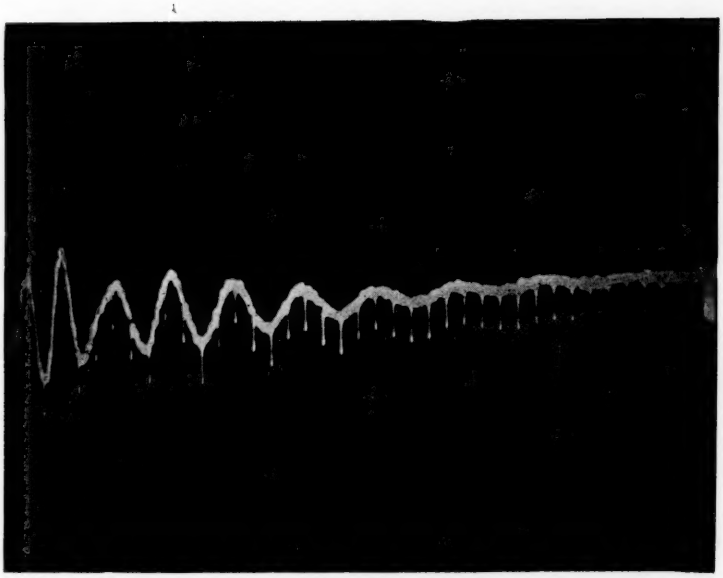

(a)

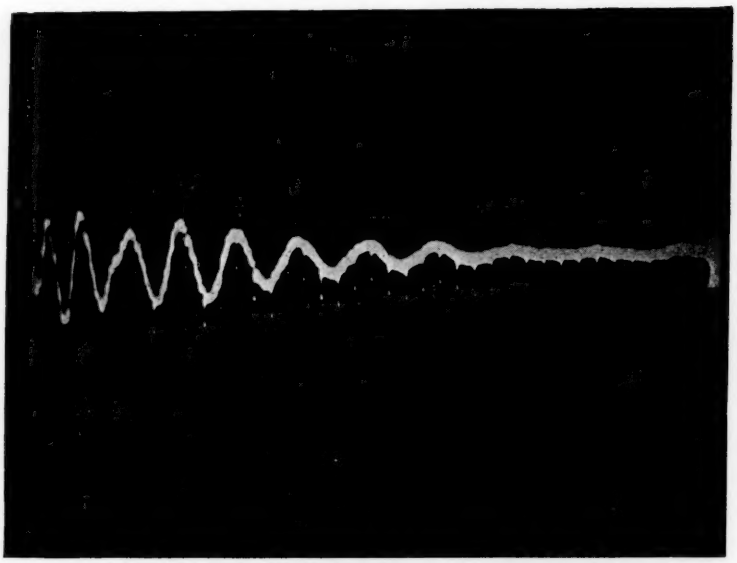

(b)

Fig. 6(a) and (b). Night-time quasi-sinusoidal types from a distant source showing similarity of fine structure. 12 and 14 December 1950, 2130 G.M.T., typical of a number for which the bearings did not give a positive fix but which indicate a distance of at least 3,000 km. Timing marks at 50-μ sec intervals.

VOL.
7
1955

In this paper the term "echo-type waveform" will be restricted to those which exhibit a series of at least four peaks which appear to arise from successive reflections of an initial impulse at the earth and at the ionosphere. To permit the accurate determination of the distance of the source, an echo-type waveform must exhibit sufficient number of echoes in relation to the distance, and the time-intervals between them must conform closely to the appropriate formula. The term will, however, be applied also to some waveforms which fall short of these requirements.

To clarify the definition, a few examples of waveforms will be shown, night-time and daytime types being considered separately, since they differ markedly.

3.1. *Night-time waveforms*

A few night-time waveforms can be classified as echo-type without any doubt; Fig. 2 shows an example in which the peaks are particularly well defined. The analysis of such a waveform is straightforward and leads to an accurate value for the distance of the source, but unfortunately such well-defined forms have rarely been recorded in the present series of experiments. The factors which produce these types are not definitely known. RIVAULT (1950) has suggested that the type is determined by the meteorological conditions at the source, and that the well-defined echo-types originate in storms in a standing mass of polar maritime air. This explanation, however, does not appear to account for all the observed facts. The example shown in Fig. 2 originated in a storm over Northern Europe at a distance of 500 km, and other records from the same storm and from other storms in similar positions failed to exhibit the same characteristics.

Fig. 3 shows a type of waveform which has been observed more frequently than the type shown in Fig. 2, though not in large numbers. The peaks are less clearly defined, but the analysis of this type is usually not difficult and leads to distance estimates of acceptable accuracy.

Most of the recorded echo-type waveforms have been more complex than these examples. Fig. 4 shows two typical forms. The peaks are more rounded than in the previous examples and they are not separated by long periods of zero field. Also there are often many more peaks than can be explained by assuming that energy originates in a single unidirectional current pulse and is reflected at a single ionospheric layer. Although the current discharge on some lightning flashes is known to be complex, it is difficult to deduce from the waveforms whether this is the main cause of the multiple peaks or whether reflection takes place at more than one height. These two possibilities can often be distinguished only if the low-order echoes can be seen, and they are frequently not recorded satisfactorily. Examination of a large number of these waveforms suggests that reflection from more than one height often occurs.

Analysis of the waveforms shown in Fig. 4, for example, indicates that they originated at a distance of 2,700 km (near the Azores) and that energy was reflected at heights of 77 and 85 km; the corresponding C.R.D.F. fix gave the distance as 2,750 km. Reflections from at least two heights, differing by a few kilometres, have been observed during very low-frequency vertical soundings of the ionosphere,

HELLIWELL, *et al.*, 1951; BROWN and WATTS, 1950), but the lowest frequency for which results have been published is 50 kc/s.

Whatever is the cause of these more complex waveforms, the result is to increase the difficulty of analysis. An estimate of distance is usually possible, but the accuracy is often low and the time taken to determine the most probable value is considerable.

It will be observed that the waveforms in Fig. 4 have almost identical fine structure; it is quite common for several waveforms from a given storm to show close similarity, a phenomenon which has been observed by other workers, (ZETROUER and KESSLER, 1951).

The different character of the various recorded echo-type waveforms is partly related to the length of the propagation path. Waveforms from near-atmospherics tend to show a simple series of well-defined peaks, while those from greater distances tend to be more complex and to have less well-defined peaks. Distance is not the only factor, however. Waveforms similar to Fig. 2 are rare even among the short-distance atmospherics, while those similar to Fig. 3 can be received from a wide range of distances. The more complex type of Fig. 4 tend to originate at the longer ranges, but there is a considerable range of distance over which waveforms of either of the types shown in Figs. 3 and 4 may be received. The proportions of the various types received does not therefore depend solely on the geographical distribution of the storms.

VOL. 7 1955

The examples shown illustrate waveforms which are classified as night-time echo-types. Other night-time forms consist largely of precursors (Fig. 1) which may or may not be followed by evidence of a main discharge, series of irregularly-spaced peaks (Fig. 5) which probably originate in cloud flashes, and from the greater distances, irregular waveforms of short duration. A further type, often called a quasi-sinusoidal form, is shown in Fig. 6. It originates at great distances and consists of a smooth oscillation which may be a limiting case of the echo-type form shown in Fig. 4.

3.2. *Daytime waveforms*

Useful echo-type waveforms occur in daylight mainly from close storms; at greater distances there are usually not a sufficient number of echoes for an analysis to be made. Even from close storms there are in general not more than four echoes, compared with at least ten at night, but as the first echo, and perhaps the ground pulse, are recorded, an analysis is frequently possible. Fig. 7 shows a typical form which is classed as an echo-type.

A more common form received in daylight is shown in Fig. 8. It consists of a smooth oscillation, and the time-intervals between the peaks do not generally conform to a simple reflection theory. Waveforms of this type received over a sea path are usually quite smooth, while those from an overland path are more irregular and of shorter duration. Daytime echo-types have been recorded mainly over distances of less than 1,000 km; at greater distances the waveform is more often of the smooth oscillatory type.

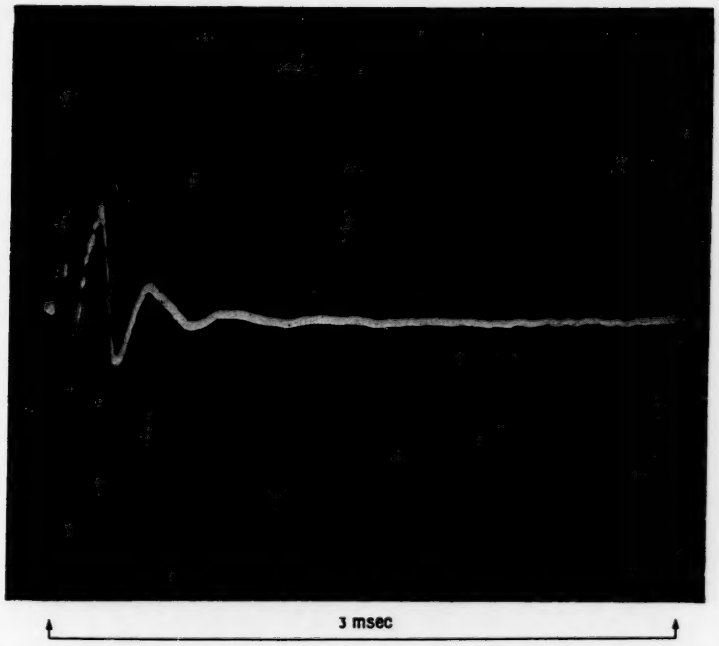

Fig. 7. Daytime echo-type form. 18 June 1951, 1600 G.M.T., C.R.D.F. distance 600 km to west

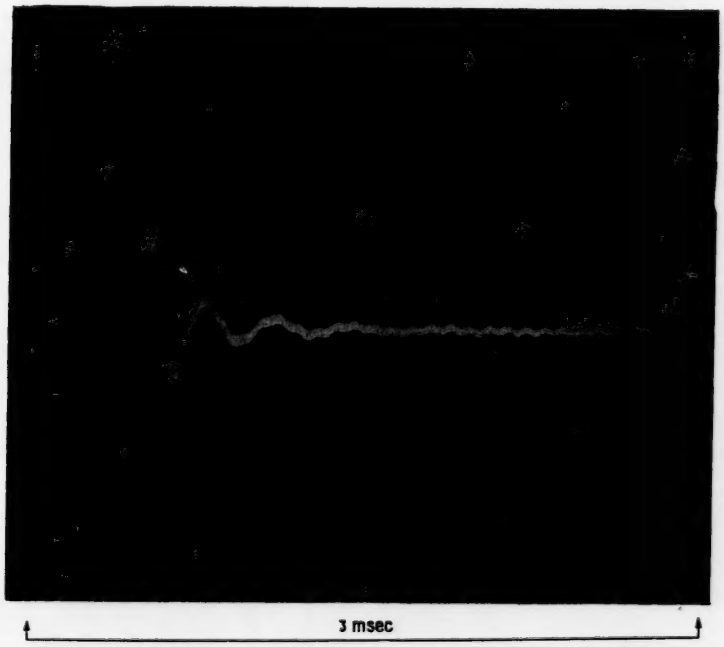

Fig. 8. Daytime waveform from a distant source, 15 February 1951, 1000 G.M.T., C.R.D.F. fix 2,500 km, to west.

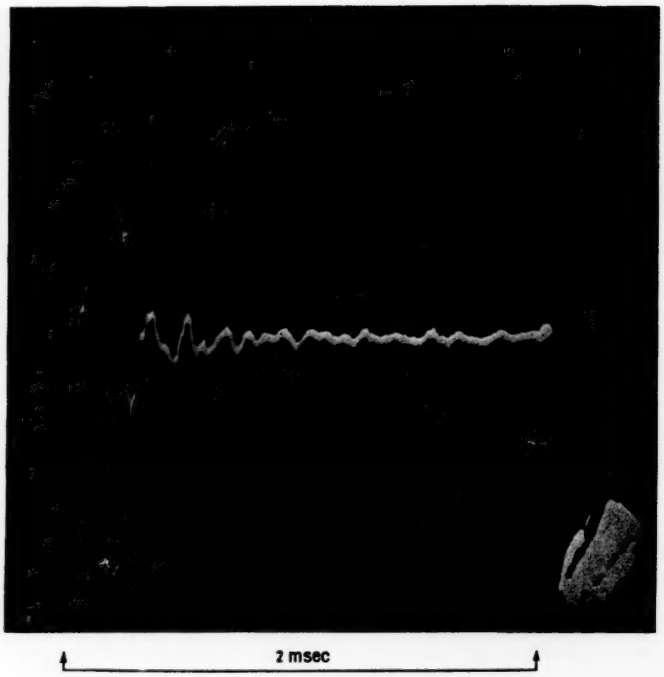

Fig. 12. Distant night-time echo-type form, 19 December 1950, 2115 G.M.T., C.R.D.F. location in the Balkans—distance 2,500 km.

VOL.
7
1955

3.3. *Methods of analysis*

Analysis of the waveforms involves the measurement of the time-intervals between successive echoes, either directly from the film, using a travelling microscope, or from a projected enlarged image. The method of analysis, leading to values of the distance of propagation (d) and the effective height of reflection in the ionosphere (h), have been discussed elsewhere (SCHONLAND *et al.*, 1940; RIVAULT, 1943). It is assumed that h is independent of the angle of incidence, and the records indicate that this is substantially true.

Measurements of the time relationships of four echoes are theoretically sufficient to determine both d and h, even if the order number n of the first visible echo is unknown. If the order number is known, three peaks are sufficient, and one such method of calculation has been described by RIVAULT (1943). Using this method, it is in fact found that with a waveform of the type shown in Fig. 2, the order numbers may be readily established, and an accurate value of distance calculated.

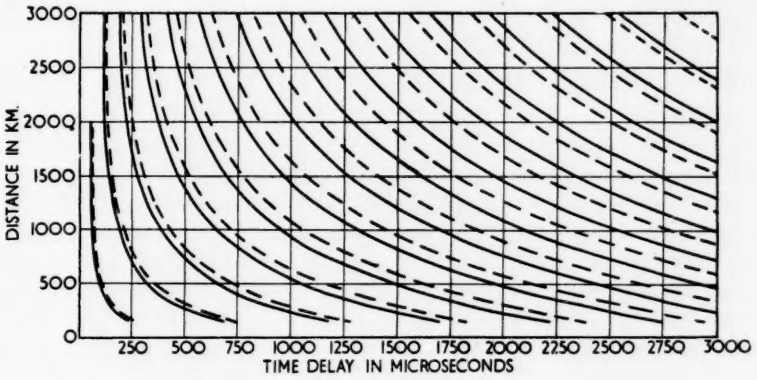

Fig. 9. Chart for deriving source distances from waveform sequences.
——— $h = 80$ km. – – – $h = 85$ km.

Examination of all the peaks leads to the values $d = 497 \pm 20$ km and $h = 87{\cdot}1 \pm 0{\cdot}3$ km. With the less well-defined echo-types the values of d and h derived from different sets of echoes may differ considerably. Calculations based on selected groups of echoes frequently lead to improbable values for the height of reflection or to distance estimates at variance with direction-finding observations. In such cases a graphical technique, by which the errors on the individual echoes can be averaged, is preferable to mathematical calculation.

The method used is similar to that described by other workers (CATON and PIERCE, 1952) and involves the use of charts of the form shown in Fig. 9. The two series of curves correspond to heights of reflection 80 and 85 km, and show the relationship between the time-delay of the echoes and the distance of the source; the interceptions of a line of constant d with the curves corresponding to various order numbers indicate the times of arrival of successive echoes with respect to that of the ground-pulse. The time-intervals measured on the recorded waveform are marked on transparent paper and fitted to the charts. The use of curves for two heights on one chart facilitates interpolation. Sets of curves at intervals of 5 km

in height have been found sufficient for most purposes, but for routine work there may be some advantage in using more charts with a smaller height separation.

3.4. *Errors in distance determination*

With waveforms of the type shown in Figs. 2 and 3, the technique described enables accurate values for d and h to be deduced, but with more commonly occurring types there is usually some difficulty in fitting the measured time-intervals to the charts. This difficulty is not due primarily to errors in reading the positions of the peaks on the record; it has been found that when several people read the position of even a broad peak, the results usually agree to about 2 microseconds. It can be shown that with the type of night-time waveform with a large number of echoes, timing errors of this magnitude introduce distance errors of only a few per cent up to 2,000 km. By day fewer echoes are recorded, but with errors of only 2 microseconds, distances up to 1,000 km could be estimated with reasonable accuracy with only five echoes, and four echoes would be sufficient up to 500 km. Within these ranges, therefore, inaccuracies in reading the positions of the peaks are not a serious limitation.

In practice, it is found that the measured time-intervals frequently cannot be fitted to the charts to an accuracy better than 20 microseconds. It appears that the peaks on the waveform become distorted, due possibly to interference between two echoes arriving almost simultaneously, or to dispersion effects or irregularities in the transmission medium. An additional difficulty in reading the positions of the peaks lies in the fact that the first echoes are usually much larger than the later ones. They may then produce a barely visible trace, due to the high writing speed, and the peak deflection may exceed the limits of the tube face (see Fig. 2).

VOL. 7 1955

The discrepancies which occur between the recorded and ideal sequences of echoes often make it difficult to assign order numbers to the echoes, and even if the orders are correctly assigned the derived values of d and h may be subject to large errors.

The practicability of estimating distance to a useful accuracy from such waveforms depends on the distance itself, on the number of recorded echoes, and on what knowledge exists of the height of reflection. Reported values of the height of reflection by night are between 75 and 90 km. From the present series of observations 85 km is the most common value, but some variations occur, and it cannot yet be assumed that the height is accurately known. By day the height appears to be about 15 km lower than by night.

The difficulties of assigning the correct order numbers to the echoes and deriving an estimate of distance can be illustrated by consideration of two hypothetical waveforms. Fig. 10 refers to a flash assumed to occur at a distance of 560 km and to produce an echo-type waveform by reflection of energy at a height of 80 km. Each reflected pulse is subject to a possible error up to 20 microseconds, and the lines show what corresponding values of d and h can be derived by fitting the waveform to the charts to this accuracy. Possible reflection heights in the range 75–90 km are considered.

The line marked "n" shows the range of values obtainable when the correct order numbers are assigned to the various echoes, the numbers of echoes used being

marked on the lines. If the first seven or eight echoes are visible, the maximum possible error in d is only about 20 per cent. If only the first four, five, or six echoes are visible, then a fit with the charts can be obtained for all assumed heights between 75 and 90 km, and a much larger error in d may result; this is indicated by the broken continuations of the line marked "n." If the first echo is missing, the error in d is not greatly affected, provided that the correct order numbers are chosen. It is possible however to obtain a tolerable fit if the wrong order numbers are chosen, and the line marked "$n + 1$" shows the values of d and h which can be

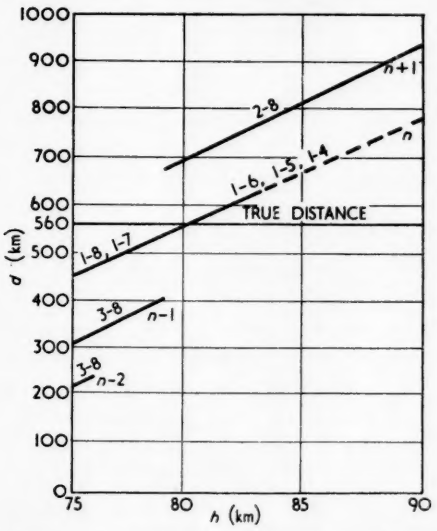

Fig. 10. Analysis of an echo-type waveform from a distance of 560 km for various sequences of recorded echoes. Possible solutions for d and h when echoes are subject to a displacement up to 20 μsec from their true positions.

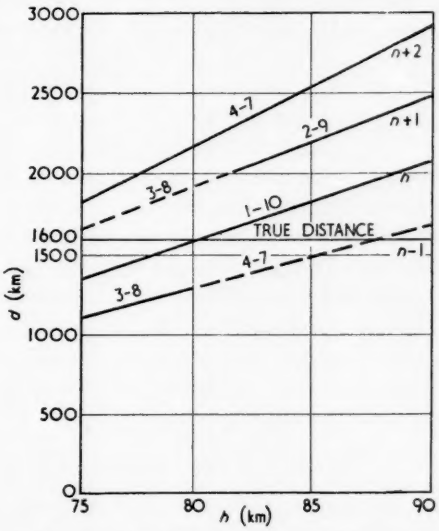

Fig. 11. Analysis of an echo-type waveform from a distance of 1,600 km for various sequences of recorded echoes; possible solutions for d and h when echoes are subject to a displacement up to 20 μsec from their true positions.

obtained if the second echo is wrongly assumed to be the third, and so on. Thus it is seen that if the first echo is missing, large errors in d may result. The other lines show that with the first two echoes missing other incorrect assessments of order number can be made, with correspondingly large errors in d. If the value of h were known from independent information, the maximum error in d would be greatly reduced.

Fig. 11 shows a corresponding set of curves for a distance of 1,600 km. If the first ten echoes are recorded, no incorrect order numbers are possible, but as the number of echoes is reduced, incorrect order numbers and large errors in distance may occur. For example, with echoes 2–9 the order number may be in error by one ($n + 1$ curve), a fit being obtained at heights above 81 km. With echoes 3–8 the fit may be obtained down to 75 km and a fit is also possible if the assumed order numbers are too low by one; with this number of echoes the total range of d giving tolerable fits is 1,100–2,500 km. It should be noted too that with only echoes

3–8, incorrect order numbers are possible even if the true height of reflection is known.

These examples show that large errors in distance may result from timing-errors of 20 microseconds, particularly when an incorrect assessment of order numbers is made. At close ranges the low-order echoes are visible and an unambiguous result may be obtained with a few echoes, such as occur in daytime waveforms (see Fig. 10). At longer ranges (Fig. 11) a larger number of echoes is necessary to establish the correct order numbers and distance estimation is practicable only at night.

This discussion shows the limitations of the technique due to the apparent displacements which have been found to occur in the positions of the peaks in practical waveforms. The conclusions regarding the magnitude of the errors in distance are pessimistic, since in a given waveform it may be that only one or two peaks are displaced by as much as 20 microseconds. The errors shown in Figs. 10 and 11 are therefore to be regarded as upper limits, and selection of the most probable value of distance from a number of possible fits will often give a result in reasonable agreement with a C.R.D.F. fix. In the absence of such supporting evidence, however, there may be little to choose between the various fits and the time required to explore all of them, and to decide on the most probable value of distance, is a serious drawback from the practical point of view.

Further research on the properties of the lower part of the ionosphere may enable the height of reflection h to be stated independently of the waveforms, and the derivation of the distance of the source of a waveform would then be much simplified and more precise.

VOL
7
195

4. Frequency of Occurrence of Echo-type Waveforms

Waveforms recorded on a routine basis for one year, October 1950 to September 1951 inclusive, at 0400, 1000, 1600, and 2000 hours local time, have been analyzed to determine the frequency of occurrence of echo-types, and the results are summarized in Table 1, which is based on examination of about 12,000 waveforms.

The first column for each observation time indicates the percentage of waveforms which show distinct echoes, and the second column indicates the percentage which, on cursory examination by an experienced worker, appeared to offer a reasonable prospect of yielding a useful estimate of the distance of the source. Those waveforms in the first category but not in the second either contained too few echoes for analysis or showed a number of echoes at irregular spacings. Detailed analysis of typical waveforms in the second category confirmed that nearly all these waveforms could in fact be analyzed and, although the analysis was often difficult, most of them yielded a distance estimate of accuracy comparable to that to be expected from the Meteorological Office, C.R.D.F. network.

It must be emphasized that the figures quoted in Table 1 were derived from a purely routine process of recording and analysis, and it is important to consider some of the factors which have a bearing on the percentages. One such factor is the recording technique. The use of a longer time-base would have increased the percentage of useful waveforms, because some of the recorded precursor types were probably followed by echo-types after an interval larger than the time-base. Also some records were unsatisfactory because the gain setting was not optimum. To

examine the importance of these limitations, the night-time records for September 1951 (0400 and 2200) were studied in detail. Of 2,250 waveforms, 149 (7 per cent) were capable of yielding a useful estimate of distance. There were a further 208 waveforms (9 per cent) which might possibly have been useful if the recording characteristics had been modified and if there had been no interference from

Table 1

Frequency of occurrence of echo-type waveforms in 1950–51

A—percentage classified as echo-types.
B—percentage capable of yielding a distance estimate of accuracy comparable with that obtained with C.R.D.F.
A blank denotes that no observations were made.

Local Time	0400		1000		1600		2200	
Month	A	B	A	B	A	B	A	B
October	—	—	—	—	2	2	39	27
November	—	—	10	9	8	4	41	29
December	—	—	10	5	5	3	16	5
January	—	—	10	5	8	2	16	4
February	—	—	12	9	6	3	10	3
March	—	—	1	0	4	2	5	2
April	—	—	3	3	14	9	—	—
May	—	—	—	—	—	—	13	8
June	6	1	7	2	8	2	11	3
July	5	1	15	6	24	7	11	1
August	8	3	4	0	7	1	8	1
September	20	10	11	4	11	1	18	6

station transmissions. There were also an unusually large number of precursor types during September (171 or 7½ per cent), some of which may have been followed by a useful echo-type. It is estimated that with no interference and with optimum recorder characteristics in respect of gain and time-base length, between 16 and 20 per cent of the night-time waveforms in September could have been used for estimating distance. If September was typical, therefore, the night-time figures in the columns B could probably be increased by a factor of about 2.

A similar examination of daylight records shows that the number of usable waveforms could be increased but probably by only a small factor. Many of the precursor types were received from distances such that even if a main waveform had been recorded, it would not have been possible to derive the source distance. The figures in Table 1 for daylight hours are therefore considered to be representative.

The results were also compared with information derived from the Meteorological Office C.R.D.F. network to determine the influence of storm position. It

was found that at night, in September 1951, echo-type waveforms were received on all occasions when storms within 2,000 km were reported, but their quality varied considerably. Storms at a particular distance would result in regular waveforms on some occasions and much more irregular ones on others. The occurrence of regular waveforms therefore depended not only on the locations of the storms, but also on either the characteristics of the storms or on the ionospheric conditions; the latter factor is believed to be the more important. The most regular waveforms probably occurred as a result of favourable combinations of storm positions and ionospheric conditions.

By day there was a marked difference between winter and summer. In winter useful echo-type waveforms were frequently, but not always, received from storms at distances up to 1,000 km; in summer the corresponding distance was only 500 km, and even from within this distance there were comparatively few useful waveforms. Close waveforms often have large very low-frequency components which increase the difficulty of measuring the time-intervals between the echoes; this effect could be minimized by reducing the low-frequency response of the amplifier.

The observed frequency of occurrence of echo-type waveforms by night is lower than has been indicated by other workers, (Schonland *et al.*, 1940; Caton and Pierce, 1953). The difference in the number classified as echo-types may be due in part to the difficulties of definition; there are many waveforms which show evidence of reflection of energy by the ionosphere but which have not been classified as echo-types in the present paper. The difference in the number which can be analyzed may be due partly to differences in recording technique and conditions, particularly interference from stations.

VOL.
7
195

5. Some General Comments on Waveforms

In the inspection of the waveforms, efforts have been made to recognize types of waveform which may be characteristic of sources in various localities even though they may not be suitable for detailed analysis. Caton and Pierce (1952) found, for example, that waveforms of the type shown in Figs. 6 and 8 arrive in England only from the west, possibly associated with the oversea paths; the present work confirms this finding.

It has been stated that similar waveforms are often received consistently from a given storm centre for a period of several days. Examples of nearly identical waveforms are shown in Figs. 4 and 6, and several waveforms similar to Fig. 4 were received from a storm centre near the Azores. During the same observation periods a second group of waveforms was received from the same area, and Fig. 5 shows two which are closely similar but quite different from those in Fig. 4. It is probable that those in Fig. 4 originated in a ground stroke, while those in Fig. 5 may have been from a cloud discharge. Fig. 12 shows a waveform, received from the Balkans two weeks later than those from the Azores and at the same time of day. There is some similarity between the forms shown in Figs. 4 and 12. Thus we have quite different waveforms received from approximately the same source and similar waveforms received from quite different sources.

In the present work the only general conclusions which have been drawn regarding waveform types are:—

(a) The smooth oscillatory type observed in the daytime (Fig. 8) is received mainly along oversea paths. The transition from the echo-type to the smooth oscillation occurs at about 1,500–2,000 km. Waveforms received by overland paths are often similar to the smooth oscillation, at a similar distance, but are usually more irregular and the oscillations are more rapidly damped;

(b) Quasi-sinusoidal forms received at night (Fig. 6) have been received only by long oversea paths. The transition from echo-types to quasi-sinusoids appears to occur at about 3,000 km. Atmospherics from similar distances overland usually have too small amplitude for their waveforms to be recorded satisfactorily;

(c) When a storm persists for several days there is a tendency for similar waveforms to be recorded at the same time of day. There may be more than one type of waveform from the same storm centre, however, and storms in the same area at other times may produce quite different waveforms.

The quoted distance for transition from echo-type to quasi-sinusoidal waveforms at night is much greater than that given by CATON and PIERCE (1952) (1,600 km). The figure of 3,000 km was obtained after critical examination of the bearings obtained by the C.R.D.F. network for each atmospheric. At this range the fixes are subject to large errors, but it is unlikely that the distances have been greatly overestimated. Furthermore, many echo-type waveforms have been recorded from distances greater than 2,500 km, as evidenced by their own structure.

OL.
7
955

6. CONCLUSIONS

The study of the waveforms of atmospherics has many applications. It is of interest to the meteorologist both in the study of the mechanism of the lightning discharge and in the location of thunderstorms. It is also of interest to the radio engineer in the study of the propagation of long radio waves, and because atmospherics constitute a source of interference to radio services. All these aspects are closely related, and information derived for one purpose has some application to the others.

In this paper, the main emphasis has been on the use of waveforms for locating thunderstorms in temperate regions. It is considered that by day suitable types would be received from most storms within about 500 km of the observing point, and sometimes, in winter, from distances up to 1,000 km. A range of about 500 km could be assessed to ± 20 per cent.

It is probable that at night waveforms suitable for analysis would be received on all occasions when there were storms within 2,000 km of the observing point, but the regularity of the waveforms, and therefore the difficulty of analysis, would vary considerably. The distances of storms within 2,000 km could in most cases be estimated with accuracies up to ± 30 per cent. It must be emphasized, however, that only a small percentage of recorded waveforms would be suitable for analysis (usually less than 20 per cent by night and 10 per cent by day) and it would also be necessary to measure the directions of arrival of these waveforms. The number of

atmospherics from which both the bearing and the distance could be deduced might be very small indeed, and the information derived from a short observation period would be much more sparse than is obtained by the present C.R.D.F. technique.

For routine work it would be desirable to limit the frequency response of the recorder. Lowering the upper limit would reduce interference from transmitting stations, and raising the lower limit would eliminate undesired low-frequency components of the atmospherics. It would also be desirable to record at least the first twenty milliseconds of the waveform without reducing the accuracy to which the time-intervals can be measured.

If thunderstorm location is required for weather-forecasting purposes, the time necessary for recording the waveforms, processing the film, and carrying out the necessary analysis may be too great for the results to be of value. The simplest echo-type forms can be analyzed in a few minutes, but the more complex types, which form a large proportion of those recorded, may need considerable study. The small percentage of waveforms which are suitable for analysis would also be an important limitation. The absence of suitable types may often be merely an indication that there are no storms within a few hundred kilometres of the observing point, but it is by no means certain that all close storms would be located in an observation period of only a few minutes. Further progress in the application of waveform analysis to meteorology is evidently dependent on improvements in knowledge of the structure of the ionosphere and its influence on the propagation of low-frequency radio waves. Considerable progress has been made in this field in recent years, (BRACEWELL *et al.*, 1952; BUDDEN, 1951 and 1952), but much remains to be done before the fine structure of many atmospheric waveforms can be satisfactorily explained.

It is therefore considered that the reliability of a location system based on waveform analysis cannot at present approach that obtained with a C.R.D.F. network. It might, however, be of some value in tracking the movement of particular storms during periods when the C.R.D.F. network was out of action—e.g., at night—for confirmation of distances derived from C.R.D.F. or for use in parts of the world where long base-line C.R.D.F. networks are impracticable.

Acknowledgments—The work described above was carried out as part of the programme of the Radio Research Board, and this paper is published by permission of the Director of Radio Research of the Department of Scientific and Industrial Research.

Much of the experimental and analytical work was done by Mr. D. E. MORTIMER and Miss C. M. BRIERLEY. The co-operation of the Meteorological Office in providing data from their thunderstorm location service is gratefully acknowledged.

REFERENCES

BRACEWELL, R. N., BUDDEN, K. G. RATCLIFFE, J. A., STRAKER, T. W., and WEEKES, K. 1952 The ionspheric propagation of low and very low frequency radio waves over distances less than 1,000 km. *Proc. Inst. Elect. Eng., Part III*, **98**, 221–236

BROWN, J. N., and WATTS, J. M. 1950 Ionosphere observations at 50 kc/s. *J. Geophys. Res.* **55**, 179–181

VOL. 7 1955

BUDDEN, K.	1951	The propagation of a radio atmospheric, Part I. *Phil. Mag.* **42,** 1–19
	1952	The propagation of a radio atmospheric, Part II. *Phil. Mag.* **43,** 1179–1200
CATON, P. G. F., and PIERCE, E. T.	1952	The waveforms of atmospherics. *Phil. Mag.* **43,** 393–409
CHAPMAN, F. W.	1950	On the waveform of atmospherics due to thundercloud discharges. *Proc. U.R.S.I.* **8,** 355–359
CLARKE, C., and MORTIMER, D. E.	1951	An automatic atmospherics waveform recorder. *Wireless Engineer* **28,** 359–370
HELLIWELL, R. A., MALLINCKRODT, A. J., and KRUSE, F. W.	1951	Fine structure of the lower ionosphere. *J. Geophys. Res.* **56,** 53–62
KESSLER, W. J., and GOYDER, C. W.	1950	Distance determination to thunderstorm areas through the analysis of associated atmospheric waveforms. *Proc. U.R.S.I.* **8,** 316–322
KIMPARA, A.	1949	On the waveform of atmospherics. *Mem. Fac. Eng. Univ. Nagoya* **1,** 1–8
OCKENDEN, C. V.	1947	Sferics. *Met. Mag.* **76,** 78–84
RIVAULT, R.	1943	Reflexions Multiples des atmospheriques entre le sol et l'ionosphere. Procede de deponillement des oscillogrammes d'atmospheriques. Notes Preliminaires du Laboratoire National de Radioelectricite No. 32
	1945	La Microstructure et la propagation des atmospheriques. *Comptes Rendus* **221,** 540
	1950	La Microstructure des atmospheriques. Applications ionospheriques et meteorologiques du type IV. *Comptes Rendus* **230,** 1846–47
SCHONLAND, B. F. J., ELDER, J. S., HODGES, D. B., PHILLIPS, W. E., and VAN WYK, J. W.	1940	The waveform of atmospherics at night. *Proc. Roy. Soc.* **A176,** 180–202
THOMAS, H. A., and BURGESS, R. E.	1947	Survey of existing information and data on radio noise over the frequency range 1–30 Mc/s. Radio Research Special Report No. 15, H.M. Stationery Office, London 1947, Code No. 47–29–15
ZETROUER, W. F., and KESSLER, W. J.	1951	A note on the similarity of certain waveforms. *J. Franklin Inst.* **252,** 137–141

Journal of Atmospheric and Terrestrial Physics, 1955, Vol. 7, pp. 14 to 30. Pergamon Press Ltd., London

Hydromagnetic resonance in ionospheric waves

C. O. Hines
Radio Physics Laboratory, Defence Research Board, Ottawa, Canada

(*Received* 29 *October* 1954)

ABSTRACT

The characteristics of one class of travelling ionospheric disturbance may be partially explained as the result of an observational selection, in which an atmospheric wave provides the basic disturbance and a hydromagnetic resonance the selection. This resonance occurs when natural modes of electromagnetic oscillation are generated through hydromagnetic coupling with the atmosphere, and it results in an enhanced motion of the ionospheric electrons which are alone observable. The quantitative comparison with observation provides estimates for the specific heat ratio ($\gamma \sim 1{\cdot}1$) and scale height ($C^2/\gamma g \sim 20$ km), which are lower than the values expected for the F_2-region concerned, but which are nevertheless possible and certainly valid in order of magnitude.

1. Introduction

Uniformly moving disturbances in the distribution of ionospheric charge have been detected and recorded by many observers in recent years. They reveal certain characteristics of scale and velocity which will have to be explained in any adequate theory of their occurrence. The movements themselves have been ascribed alternatively to winds and to waves—both mechanisms appear possible—but there have been few attempts to deduce the corresponding characteristics theoretically.

One relevant aspect of the wave interpretation is outlined in the present paper, namely, a phenomenon which may be termed "hydromagnetic resonance." This arises when an initial atmospheric disturbance generates natural modes of electromagnetic oscillation, and its significance derives from a related increase in the motion of ionospheric electrons. The resultant observational selection provides a plausible explanation for at least some of the characteristics actually found. Corresponding estimates of the atmospheric scale height and specific heat ratio are of the order expected, though perhaps somewhat low. A number of desirable extensions and modifications of the theory are indicated.

2. Ionospheric Oscillations

Oscillations in any conducting fluid must in principle be hydromagnetic by nature. Their mathematical investigation therefore involves both hydrodynamic and electromagnetic parameters, and, for the ionosphere, these enter in such profusion that a full development is extremely tedious and its immediate physical implications are extremely obscure. The work can be simplified and the picture clarified, however, by following an abridged physical development which is reasonably valid in the proposed application. Its quantitative justification will be found in the Appendix, together with a more complete outline of the full mathematical theory.

The central feature of hydromagnetics, as such, is the coupling which occurs between hydrodynamic and electromagnetic oscillations in a conducting fluid. This coupling, which results from collisions between charged and uncharged

VOL. 7 1955

components of the fluid, prevents the independent generation of either type of oscillation. Instead, both must occur together, if at all, with relative amplitudes which can be determined.

If the coupling action is strong, the characteristics of a disturbance may depend equally on the hydrodynamic and electromagnetic systems. With a weak coupling, however, either system may play a dominant part in determining those characteristics, almost to the exclusion of the other. The other would still be excited, but only into a forced oscillation whose modifying effects could largely be neglected. It is this case of weak coupling which would actually occur in the ionosphere, at least for disturbances having the space-time scales observed.

In the following development, it will be assumed that hydrodynamic oscillations of the atmosphere dominate the basic disturbance, though it will become apparent that secondary electromagnetic fields may nevertheless play an essential part in the observations. The medium considered is the simplest one which retains the essential features of the ionosphere, for it seems appropriate to neglect many practical complications in this initial investigation; the necessary extensions will be indicated at various points throughout the discussion.

The hydrodynamic oscillations will be taken as perturbations of an otherwise stationary isothermal atmosphere in the presence of a uniform gravitational field $\boldsymbol{g}$. They will be subject to the linearized equations of motion,

$$\rho_0 \, \partial \boldsymbol{U}/\partial t = \rho \boldsymbol{g} - \text{grad } p, \tag{1}$$

of adiabatic state,

$$\partial p/\partial t + \boldsymbol{U} \cdot \text{grad } p_0 = C^2(\partial \rho/\partial t + \boldsymbol{U} \cdot \text{grad } \rho_0), \tag{2}$$

and of continuous conservation of matter,

$$\partial \rho/\partial t + \boldsymbol{U} \cdot \text{grad } \rho_0 + \rho_0 \, \text{div } \boldsymbol{U} = 0, \tag{3}$$

wherein ρ and p are the actual density and pressure, ρ_0 and p_0 are their unperturbed values, $\boldsymbol{U}$ is the velocity perturbation of the atmosphere, and C is a constant —the "speed of sound"—given by

$$C^2 = \gamma p_0/\rho_0 \tag{4}$$

if γ is the usual ratio of specific heats. The condition for static equilibrium can be derived from (1), by setting the perturbations $\boldsymbol{U}$, $\rho - \rho_0$, and $p - p_0$ equal to zero, and it combines with (4) to show that ρ_0 and p_0 vary as $\exp \gamma \boldsymbol{g} \cdot \boldsymbol{r}/C^2$.

The velocity perturbation may be analyzed into complex Fourier components of the form

$$\boldsymbol{U}(\omega, \boldsymbol{k}) = \mathscr{U}(\omega, \boldsymbol{k}) \exp i(\omega t - \boldsymbol{k} \cdot \boldsymbol{r}), \tag{5}$$

with $\mathscr{U}$, ω, and $\boldsymbol{k}$ constant. These will satisfy the set (1)–(3) only if the scalar components of $\mathscr{U}$ have certain complex ratios, dependent on the mode of oscillation $\{\omega, \boldsymbol{k}\}$, and if ω and $\boldsymbol{k}$ themselves satisfy the dispersion relation

$$f_0 \equiv \omega^2 C^2 \boldsymbol{k} \cdot \boldsymbol{k} + i\omega^2 \gamma \boldsymbol{g} \cdot \boldsymbol{k} - \omega^4 - (\gamma - 1)(\boldsymbol{g} \times \boldsymbol{k}) \cdot (\boldsymbol{g} \times \boldsymbol{k}) = 0. \tag{6}$$

The corresponding fractional variations of ρ and p have the same space-time structure as (5), but their total variations contain the extra factor $\exp \gamma \boldsymbol{g} \cdot \boldsymbol{r}/C^2$.

Real ω's will be assumed for convenience of interpretation, without losing any generality in application.

The charged ionospheric particles which are set into motion by such a disturbance will exert a reactive force on the atmosphere. In the present context, the density of this force can be represented in order of magnitude by

$$\boldsymbol{J} \times \boldsymbol{B}_0 = \sigma_1[\boldsymbol{E} + \boldsymbol{U} \times \boldsymbol{B}_0] \times \boldsymbol{B}_0 - \sigma_2[(\boldsymbol{E} + \boldsymbol{U} \times \boldsymbol{B}_0) \times (\boldsymbol{B}_0/B_0)] \times \boldsymbol{B}_0. \quad (7)$$

(Cf. HINES, 1953, low-frequency approximations.) Here $\boldsymbol{E}$ and $\boldsymbol{J}$ are the electric field and current density generated hydromagnetically, while σ_1 and σ_2 are the "transverse conductivities" relative to the geomagnetic induction $\boldsymbol{B}_0$; σ_1, σ_2, and $\boldsymbol{B}_0$ will be assumed constant.

The $\boldsymbol{E}$ terms of (7) will normally be quite negligible in a disturbance controlled hydrodynamically, but the $\boldsymbol{U}$ terms should in principle be added to the right-hand side of (1). A formal inconsistency would arise if this were done, however, for these terms lack the factor $\exp \gamma \boldsymbol{g} \cdot \boldsymbol{r}/C^2$ implicit in all terms of (1); the assumed form of solution would no longer be valid. Fortunately this difficulty is of little importance in practice, for even the $\boldsymbol{U}$ terms of (7) are small compared to the forces in (1), except perhaps in those disturbances of the F_2-layer which have the very longest periods observed ($\sim$1 hour). The foregoing analysis will therefore be sufficiently valid for the purposes of this paper. In addition to the reactive forces, any more accurate development should take into account the effects of molecular (and perhaps eddy) viscosity and heat conduction, and Coriolis forces due to the earth's rotation; all introduce modifications of the same general order in the F_2-layer.

VOL. 7 1955

The atmospheric disturbance will normally generate secondary oscillations of the electromagnetic system, as already stated. This fact is illustrated by equation (7), for $\boldsymbol{E}$ and $\boldsymbol{J}$ cannot vanish there unless $\boldsymbol{U}$ itself vanishes—or at least, unless $\boldsymbol{U}$ is directed wholly along $\boldsymbol{B}_0$. The forced oscillations can be determined approximately from (7), in conjunction with MAXWELL'S relations

$$\text{curl } \boldsymbol{E} = -\partial \boldsymbol{B}/\partial t \quad (8)$$

and

$$\text{curl } \boldsymbol{B} = \mu_0 \boldsymbol{J}, \quad (9)$$

and with the approximate constitutive relation for the component of $\boldsymbol{J}$ in the direction of $\boldsymbol{B}_0$,

$$J_{B_0} = \sigma_0 E_{B_0}. \quad (10)$$

In these, σ_0 is the "longitudinal conductivity," which greatly exceeds σ_1 and σ_2 in the ionosphere; μ_0 is the permeability of free space and $\boldsymbol{B}$ the magnetic induction; the displacement current has been justifiably neglected, along with all diamagnetic effects.

The linear set (7)–(10) combines with (5) to determine the electromagnetic oscillations generated by each Fourier component of the original disturbance. Standard matrix methods supply solutions in the form

$$E_m(\omega, \boldsymbol{k}) = \sum_n \frac{\alpha_{mn}(\omega, \boldsymbol{k})}{\phi(\omega, \boldsymbol{k})} U_n(\omega, \boldsymbol{k}) \quad (11)$$

which explicitly indicates a scalar component of the secondary electric field in a certain mode of oscillation $\{\omega, \boldsymbol{k}\}$. The α_{mn} factor which appears in the numerator here changes with m and with n, and it changes further when the perturbations $\boldsymbol{J}$ and $\boldsymbol{B} - \boldsymbol{B}_0$ are considered in place of $\boldsymbol{E}$. On the other hand, ϕ is a characteristic function of the electromagnetic system, and it appears as a common denominator in all these cases. It is the determinant of the coefficients which multiply scalar components of $\boldsymbol{E}$, $\boldsymbol{J}$, and $\boldsymbol{B} - \boldsymbol{B}_0$ in (7)–(10), after these perturbations are given the form (5) and the differentiation is completed. The full expression for ϕ can be simplified in the present work without significant loss of accuracy, by neglecting all of its terms which contain σ_1 and σ_2; the remainder will then be found proportional to

$$\phi_0 \equiv k_{B_0}{}^2 \quad \boldsymbol{k} \cdot \boldsymbol{k}. \tag{12}$$

The factor of proportionality contains σ_0, and the appearance of $k_{B_0}{}^2$ indicates a geomagnetic control, but otherwise the specific features of the ionosphere play no explicit part in this approximation.

A detailed or an order-of-magnitude development of (11), combined with reasonable estimates for the relevant ionospheric parameters, will confirm that the $\boldsymbol{E}$ terms of (7) can normally be ignored relative to the $\boldsymbol{U}$ terms when determining the hydromagnetic reaction on the atmosphere. It will further indicate, in conjunction with the equations of electron motion, that the secondary electric field may usually be ignored in estimating the associated electron disturbances; the impressed electron motions normally result from collisional interactions exclusively, and they are comparable in magnitude to the atmospheric motion of the basic disturbance.

3. Hydromagnetic Resonance

It will be apparent from (11) that unusual effects might be obtained if ϕ were to become unusually small, for then the electromagnetic response to a given hydrodynamic stimulus might be greatly increased. Since $\phi = 0$ is the condition for free electromagnetic oscillations, such a phenomenon would be closely analogous to resonance in simpler systems, and indeed the term "hydromagnetic resonance" may be conveniently applied to it.

This resonance differs from that of the very simplest systems in one major respect: the oscillations here are characterized as much by their space structure ($\boldsymbol{k}^{-1}$) as by their time structure (ω^{-1}), whereas in the simplest mechanical and electrical systems the latter appears alone. Unless and until boundary conditions are imposed, restricting the permitted values of $\boldsymbol{k}$, there will then in general be resonant modes of oscillation and not specific resonant frequencies. A similar situation does arise, for example, with the oscillations of a stretched string. There the differential equation of motion introduces only a characteristic speed s, so that resonance is basically confined only to modes having

$$s^2 - \omega^2/k^2 = 0, \tag{13}$$

though in practice boundary conditions at the ends restrict the permitted k's and hence by (13) confine the resonant frequencies to a particular spectrum.

It is to be stressed that the occurrence of a modal resonance would be a prerequisite to any frequency resonance which might actually arise in practice; boundary effects can at most introduce subsidiary restrictions, as in the case of the string. Accordingly, the conditions which provide a modal resonance can be discussed with profit even though the further restrictions remain unknown. This is of particular importance in the present investigation, for the appropriate ionospheric boundary conditions may be difficult to determine.

These points have been emphasized because of the prominent part hydromagnetic resonance may play in interpreting the recorded data. In resonant modes, the secondary electric field may come to dominate the motion of the ionospheric electrons, and may enhance that motion considerably in the process. Since disturbances in the electron distribution are alone observable in this work, a marked observational selection would then be produced. Resonant waves would be particularly susceptible to detection, and they might in fact be the only ones actually observed. This possibility suggests an explanation for some of the characteristics found in practice: they may simply be the characteristics required for resonance. Such a suggestion underlies all further work in the present paper.

It should be remarked that the resonance could apparently become so strong that the neglect of $\boldsymbol{E}$ terms in the hydromagnetic reaction $\boldsymbol{J} \times \boldsymbol{B}_0$ would no longer be justified, and the approximate development no longer valid. The observational effects just described would, however, come into play before such a complication arose, so the preceding formalism remains applicable as it stands.

VOL.
7
1955

The following analogy, in terms of a simple frequency resonance, may prove helpful in understanding the observational selection and the interplay of forces involved here. If a vibrator were connected to a short horizontal piece of light coil-spring, and that in turn to one side of a freely suspended heavy pendulum, it would normally force both into slight oscillation at its own frequency. If that frequency approached the natural frequency ω_0 of the pendulum, however, corrected slightly by an effect of the spring, then the motion of the pendulum would become resonantly large. One end of the spring would follow suit, and unusually large compressions and rarefactions in its body would result. Finally, if a random series of arbitrary disturbances were produced by the vibrator, rather than a continuous oscillation, and if only the body of the spring were observable, then those disturbances having a relatively large Fourier component at ω_0 would be particularly susceptible to detection; indeed, for a sufficiently low over-all excitation, they might be the only ones detected. The vibrator corresponds to the atmosphere of course, the pendulum to the electromagnetic system, and the spring to the coupling plasma of ionospheric charge, particularly electrons.

The mathematical development which now ensues can be simplified by an assumption which seems fairly natural in the case of local atmospheric oscillations, that an exponential decay of amplitude can occur in horizontal planes only in the direction of horizontal phase propagation. This assumption corresponds to that of homogeneous plane waves common in preliminary investigations of homogeneous media, but here complete wave homogeneity is not assumed because of the basic vertical inhomogeneity of the atmosphere. Mathematically, the

requirement is that the ratio of any two horizontal components of $\boldsymbol{k}$ will be real. In this case a real reorientation of real co-ordinate axes is sufficient to reduce $\boldsymbol{k}$ to a two-component form, $\boldsymbol{k}_h$ in the direction of horizontal propagation, and $\boldsymbol{k}_g$ in the downwards direction given by $\boldsymbol{g}$. The hydrodynamic dispersion relation (6) governing the basic disturbance then becomes

$$\omega^2 C^2(k_g^2 + k_h^2) + i\omega^2\gamma g k_g - \omega^4 - (\gamma - 1)g^2 k_h^2 = 0. \tag{14}$$

The condition for hydromagnetic resonance, $\phi \to 0$, can be replaced by the approximation $\phi_0 = 0$ in the present work. This in turn provides two possible conditions, $k_{B_0}^2 = 0$ or $\boldsymbol{k} \cdot \boldsymbol{k} = 0$, of which only the latter will be adopted for general consideration. In component notation it now demands

$$k_g^2 + k_h^2 = 0, \tag{15}$$

a relation which combines with (14) to give the quadratic

$$(\gamma - 1)g^2 k_g^2 + i\omega^2\gamma g k_g - \omega^4 = 0, \tag{16}$$

and hence the solutions

$$k_h = ik_g = \omega^2/(\gamma - 1)g \qquad \text{or} \qquad k_h = ik_g = \omega^2/g. \tag{17}$$

The sign of k_h in (17) is conventional, while that of k_g is uniquely determined by (16).

4. Subsidiary Conditions

The resonance formulae will shortly be applied in an interpretation of observational data, but they may be supplemented in advance by certain subsidiary conditions which appear relevant. These are added in order to specify more closely the characteristics expected in practice, and so to provide a more stringent test of the wave and resonance hypotheses. They are admittedly only guesses at the actual controlling conditions, but they are perhaps the best that can be expected while lacking a fuller knowledge of the generating mechanisms and a detailed development of certain complicating features which are discussed in Section 6.

First, it might be expected that the basic atmospheric disturbances are generated with a roughly uniform distribution of energy throughout the region of excitation—that no great exponential increase or decrease of energy with height occurs—as in the case of atmospheric tides. This is purely an assumption, but perhaps the most natural one to add to that of a horizontal wave homogeneity when treating oscillations of the inhomogeneous atmosphere; it seems to provide the most reasonable physical extension of the assumption of homogeneous waves, frequently made in the treatment of homogeneous media. It would require $|U|$ to vary roughly as $\rho_0^{-1/2}$ in the vertical direction, since all the hydrodynamic forms of energy vary as $\rho_0|U|^2$ on the average, and hence

$$k_g = -i\gamma g/2C^2 \tag{18a}$$

if there is no vertical propagation. It will be seen that this condition is compatible with that of resonance, and in conjunction with it demands

$$k_h = \gamma g/2C^2 \tag{18b}$$

and

$$\omega = \sqrt{\gamma(\gamma-1)/2}\, g/C \qquad \text{or} \qquad \omega = \sqrt{\gamma/2}\, g/C. \tag{18c}$$

Again, the vertical component of atmospheric velocity must vanish at the earth's surface if boundary conditions there are at all relevant. This normally demands the superposition of two modes of oscillation, with common values for ω and $\boldsymbol{k}_h$, only one of which could be resonant at a time. But both modes can tend to resonance simultaneously as the conditions (18) are approached from different directions—indeed a continuous set can, since $\partial f_0/\partial k_g$ vanishes then—so the observable effects might be increased in this case without necessitating any increase of total energy. (In the exact limit these modes would cancel out at all levels, but before the limit is reached the argument is valid for sufficiently great heights.)

Further, the hydrodynamic group-speed in the horizontal direction,

$${}_HG_h \equiv (\partial\omega/\partial k_h)_{f_0=0} = \frac{k_h[(\gamma-1)g^2 - \omega^2C^2]}{\omega[C^2(k_g^2+k_h^2) + i\gamma g k_g - 2\omega^2]}, \tag{19}$$

has two degrees of freedom in general, being subject only to the condition $f_0 = 0$. This means that there may be a considerable dispersion of energy as the two free parameters—say ω and k_g—vary within a group. For physically acceptable γ's, between 1 and 5/3, the dispersion cannot be kept to an absolute minimum when resonance occurs; but it will be minimized under variations of k_g when $d_H G_h/dk_g$ vanishes, and in conjunction with the resonance condition this leads again to the set (18).

Finally, the conditions (18) provide equality between ${}_HG_h$ and the horizontal group-speed of the resonant components,

$${}_RG_h \equiv (d\omega/dk_h)_{f_0=\phi_0=0} = \omega/2k_h. \tag{20}$$

This means that the hydrodynamic disturbance as a whole then moves with the same horizontal speed as its resonant part, and so, physically, it could maintain the energy of that part in spite of appreciable ohmic losses introduced by the resonant electromagnetic system. The intermodal coupling necessary to effect this energy exchange could result from local inhomogeneities or from basic nonlinearities.

From (18b,c) it is apparent that the phase-speed ω/k_h occurring in these special modes is

$$P_h = \sqrt{2(\gamma-1)/\gamma}\, C \qquad \text{or} \qquad P_h = \sqrt{2/\gamma}\, C, \tag{18d}$$

while the group-speed is half as much,

$$G_h = \sqrt{(\gamma-1)/2\gamma}\, C \qquad \text{or} \qquad G_h = \sqrt{1/2\gamma}\, C \tag{18e}$$

as determined from (19) or (20).

VOL. 7 1955

Two of the preceding arguments can be developed on somewhat different lines with somewhat different conclusions. For example, a single mode of oscillation can satisfy the boundary condition previously employed, and so can provide an increase in amplitude without an increase in the total energy, if and only if its vertical component of U vanishes. The relations (1)–(4) can be used to show that this will occur if and only if

$$ik_g = (\gamma - 1)g/C^2. \tag{21a}$$

This result combines with the resonance formulae to give

$$k_h = (\gamma - 1)g/C^2 \tag{21b}$$

$$\omega = (\gamma - 1)g/C \quad \text{or} \quad \omega = \sqrt{\gamma - 1}\, g/C \tag{21c}$$

$${}_HG_h = C \quad \text{or} \quad {}_HG_h = 0 \tag{21d}$$

and

$${}_2{}_RG_h = P_h = C \quad \text{or} \quad {}_2{}_RG_h = P_h = C/\sqrt{\gamma - 1}. \tag{21e}$$

Again, if a minimum dispersion of hydrodynamic energy is demanded under variations of ω—if $d_H G_h/d\omega$ is made to vanish—and the conditions for resonance are applied, then the first alternatives in (21) provide one solution, and the set

$$\omega = g/C, \qquad k_h = ik_g = g/C^2,$$
$${}_2{}_RG_h = {}_HG_h = P_h = C \tag{22}$$

provides another. And finally, it may be noted that ω and k_g cannot be taken as independent when $\partial f_0/\partial k_h$ vanishes. However, $d_H G_h/dk_h = \partial_H G_h/\partial k_h = 0$ then, so there is a minimum dispersion of energy under variations of k_h (now regarded as an independent variable). The relevant conditions, when resonance occurs, are given by the second alternatives in (21) or by the set

$$\omega = \sqrt{\gamma - 1}\, g/C, \qquad k_h = ik_g = g/C^2,$$
$${}_HG_h = 0, \qquad {}_2{}_RG_h = P_h = \sqrt{\gamma - 1}\, C. \tag{23}$$

These several formulae render themselves suspect by their variety, though the general agreement on orders of magnitude is to be noted. The variety emphasizes the need of a more detailed development, perhaps along such lines as those indicated in Section 6, while the agreement provides some justification for an order of magnitude comparison with observation even at the present stage.

5. Comparison with Observation

Two classes of travelling ionospheric disturbance may be disposed of quickly, for their characteristics are difficult to reconcile with the resonance formulae. These are the small-scale (200 m, 3 sec) disturbances detected in the E-layer, and the medium-scale (5 km, 30 sec) disturbances in the upper ionospheric regions. In each case a quantitative comparison with the resonance formulae (17) provides an estimate for γ which lies well above the kinetic-theory maximum value of 5/3. Further comparison with the more restrictive formulae of the preceding section

leads to values for the atmospheric scale height, $C^2/\gamma g$, which are much too small on any reasonable estimate. Some possibility exists that the observed scale refers only to the fine structure of a diffraction pattern, and not at all directly to the ionospheric disturbance itself, in which case a better agreement with theory could be attained. This explanation may seem somewhat forced, however, especially for the higher-level disturbances which are probably free from diffractive distortion, and in any case it introduces still further defects. Accordingly, an interpretation of such disturbances is perhaps best sought on some other grounds than those proposed here.

Disturbances occur on a much larger scale in the main body of the F_2-layer (PIERCE and MIMNO, 1940; MUNRO, 1950; BRAMLEY, 1953), and these provide a more satisfactory comparison with the resonance theory. Their horizontal progression continues over large distances without appreciable attenuation, in qualitative agreement with the resonance formulae (17). In addition to the horizontal advance, a relatively small downwards component of progression has often been detected by MUNRO and by BRAMLEY. This component might be inherent in the basic disturbance, but MUNRO (following MARTYN, 1950) considers it more probable that the fundamental movement is horizontal and that the vertical progression is introduced by some secondary change of phase with height. Such an interpretation is certainly plausible, however debatable, and it accords with the theory of hydromagnetic resonance: the resonant waves described by (17) progress only in a horizontal direction. A further qualitative comparison might be made between predicted and observed amplitude variations with height, though the latter are seldom recorded, but it would be invalidated by a complicating effect of ionization gradients. This point will be discussed more fully in the next section.

Observational estimates of the time scale ($\sim$20 min) and horizontal structure size ($\sim$200 km) often depend in part on observational estimates of the horizontal speed ($\sim$10 km/min). It is not always clear whether this is a speed of phase surfaces, of the wave group, or indeed of either, so a certain amount of misinterpretation may occur. Even direct measurements of the apparent period and wavelength are subject to some error, as a consequence of distortion within the group profile. No exact values of ω and k_h can therefore be obtained, though the errors introduced by any direct interpretation of the data should certainly not exceed one order of magnitude; the rough estimates $2\pi/\omega \sim 20$ min and $2\pi/k_h \sim 200$ km will be adopted. These will be found incompatible with the second alternative in the resonance formulae (17), since $g \sim 9{\cdot}0$ m/sec^2 in the F_2-layer, but they correspond to the first alternative if $\gamma \sim 1{\cdot}1$. This value is lower than might be expected for the upper atmosphere, but at least it cannot be contradicted on general grounds. MARTYN (1950) has in fact been led to a similar low value of γ, in presenting his cellular-wave theory of the F_2-layer disturbances, and he has tentatively attributed it to dissociative processes in nitrogen molecules.

Comparison with the more restrictive formula (18b) provides an estimate for the scale height $C^2/\gamma g \sim 20$ km. This value is reduced by a factor of 5 if (21b) is employed, and increased by a factor of 2 if (23) is adopted. In contrast, previous estimates of the F_2 scale height have been rather higher—60 or 100 km, though

VOL. 7 1955

at least one recent investigation (KALLMANN, 1953) suggests a value nearer 40 km. In any case, the resonance estimate is certainly of the order expected.

6. NECESSARY MODIFICATIONS

This preliminary investigation was undertaken with the primary purpose of determining whether or not hydromagnetic resonance might play a significant part in the interpretation of the observed disturbances. The qualitative and quantitative comparisons have now indicated that this may well be the case, at least for the large-scale F_2-layer disturbances. Further detailed work therefore seems in order, and some of the following considerations seem likely to enter it.

Ionization gradients were neglected in the general development of Sections 2–4, and justifiably so, but they can introduce important modifications when the observational aspects are introduced. The impressed electron velocity $\boldsymbol{V}$ will have the exponential form (5), but a height variation of the unperturbed electron density N_0 will alter the form of the observable perturbation: in a linearized theory,

$$\partial(N - N_0)/\partial t + \operatorname{div}(N_0 \boldsymbol{V}) = 0,$$

$$\therefore \qquad N - N_0 = \omega^{-1}(N_0 \boldsymbol{k} + i \operatorname{grad} N_0) \,.\, \boldsymbol{V} \qquad (24)$$

where N is the actual electron density. The amplitude and the phase of $N - N_0$ will differ from those of the basic exponential in $\boldsymbol{V}$, as N_0 and grad N_0 take on different values at different heights. A detailed evaluation of the effect depends on a detailed determination of $\boldsymbol{V}$, but that lies outside the scope of the present paper. However, it does seem likely, though by no means necessary with hydromagnetic resonance, that $\boldsymbol{V}$ will be essentially in the direction of $\boldsymbol{B}_0$. In this case, (24) combines with the resonance formulae to indicate that a wave travelling towards the geomagnetic equator would contain an apparent upwards component of propagation, while a wave moving away from the equator would have an apparent downwards component. A similar reversal, though in the opposite sense, would occur in the theory of cellular waves on the elementary arguments presented by MARTYN (1950). Neither reversal is confirmed by observation: the vertical progression is nearly always downwards, regardless of the horizontal direction of travel.

A vertically increasing temperature might introduce just such a downwards component in the apparent progression. It would be accompanied by an increasing speed of sound C, and hence by an increasing speed in such observationally important modes as those listed in Section 4. The upper parts of an electron disturbance might therefore tend to precede the lower parts, and so introduce the observed downwards tilt in the apparent wave-front, in much the same way as water-waves tend to turn in towards a sloping beach.

The amplitude of the fractional perturbation, $|N - N_0|/N_0$, depends not only on the real exponential factor in $\boldsymbol{V}$ but also on the amplitude factor $|k_V + i \operatorname{grad}_V N_0/N_0|$. The latter may compensate, or over-compensate, for variations of the former in some regions. Even with resonance then, when the basic disturbance increases with height, $|N - N_0|/N_0$ may decrease. No general data are available for comparison, but in one disturbance illustrated in detail by MUNRO (1950) a slight increase at the lower levels was followed by a decrease higher up towards the F_2-layer peak (where grad $N_0 \to 0$). A rough quantitative agreement with the resonance formulae may be obtained in this case, again on the assumption that $\boldsymbol{V}$ lies nearly along $\boldsymbol{B}_0$. Any deficiency might result from a standing-wave effect, introduced by the superposition of different oscillation modes as suggested following equation (18c), or from a $\boldsymbol{V}$ which makes an appreciable angle with $\boldsymbol{B}_0$.

Inhomogeneities of atmospheric temperature, of electron density, and of other ionospheric parameters, have of course far graver consequences than those just described. They invalidate certain assumptions on which the form of the solution depended, and hence they invalidate the solution itself except perhaps as a good approximation. The value of this approximation can to some extent be judged from an estimate of the greatest inhomogeneity ignored, which is probably that imposed on C^2 by the increasing temperature, and which may amount to 10 per

cent per scale height (GLEDHILL and SZENDREI, 1950; KALLMANN, 1953). This value is probably not sufficient to invalidate the preceding formulae as order of magnitude relations, but it is certainly sufficient to call for further investigation.

An attempt has been made to anticipate probable boundary conditions, by assuming a horizontal wave homogeneity and subsequently by adopting a uniform vertical distribution of energy. Aside from these conditions, and from a suggested restriction on the atmospheric velocity at the earth's surface, no attention has yet been paid to hydrodynamic boundary conditions. Some such conditions must certainly be satisfied, but they can probably not be specified very closely until the original cause of the disturbances is known. It seems doubtful that boundary conditions on the secondary electromagnetic oscillations will affect the problem, except perhaps in demanding that the flow of energy be away from any localized hydrodynamic source.

Atmospheric tides must be taken into account in a complete development. Their basic motion can be represented fairly well in the present problem by a constant horizontal velocity vector, say $\boldsymbol{U}_0$. Equations (1)–(3) must be referred to co-ordinates moving with this velocity relative to the earth, if they are to remain valid in their present form. Associated geomagnetic forces and polarization fields must also be taken into account in principle, but they are of little consequence in the theory of hydromagnetic resonance: equations (7)–(10) can be referred directly to the moving system without appreciable change, though $\boldsymbol{E}$ and $\boldsymbol{J}$ may then include irrelevant constant components. Accordingly the principal modifications can be discovered simply by referring all previous formulae to the moving system, and hence by adding $\boldsymbol{U}_0 \cdot \boldsymbol{k}_h$ to the predicted ω, and $(U_0)_{k_h}$ to the predicted speed of the wave-front, before comparing them with observation. This could not be done in the preceding section, where mean values only were employed, for the corrections must be applied in each case individually. To illustrate the possible effect, however, it may be noted that the correction for a tidal wind which is equal in magnitude but opposite in direction to the observed horizontal movement would produce a fourfold increase in the estimate of $(\gamma - 1)$, to a resultant estimate $\gamma \sim 1{\cdot}4$ on the basis previously adopted. Estimates dependent on k_h alone are not affected by tidal winds.

VOL. 7 1955

It may be recalled that terms in σ_1 and σ_2 were neglected in deriving the function ϕ_0 used in the condition for hydromagnetic resonance. The omission of the force density (7) from the equation of motion (1) also amounts to a neglect of σ_1 and σ_2 terms, but now in the function f_0 of the basic hydrodynamic system. Accordingly, the treatment in the preceding sections is to be regarded only as a zero-order approximation, susceptible to modification by first- and higher-order terms in σ_1 and σ_2. The corrections can be readily calculated, and they naturally lead to alterations in the various resonance formulae which have been derived. They will not be quoted here, however, for in practice even further modifications of the same order must be introduced. These result from the effects of an electron partial pressure, and they can alter the relations (7) and (10) in detail though not in magnitude. Their full investigation must await a more thorough treatment of electron motions, and of the corresponding conductivities and reactions.

The concept of an "extended resonance" may well enter the final description of the observed disturbances. It arises when the forced system resonates to all, or at least to an infinitely increased number, of the oscillation modes which comprise the basic disturbance—when ϕ in the denominator of (11) vanishes not only for some particular set $\{\omega, \boldsymbol{k}\}$ which makes f_0 vanish, but also for all first-order differential variations from this set which continue to make f_0 vanish. In the zero-order approximation, the condition is that

$$\phi_0 = 0 = f_0 \tag{25}$$

and further that

$$\frac{\partial f_0/\partial \omega}{\partial \phi_0/\partial \omega} = \frac{\partial f_0/\partial k_g}{\partial \phi_0/\partial k_g} = \frac{\partial f_0/\partial k_h}{\partial \phi_0/\partial k_h}. \tag{26}$$

(More generally a third k-derivative could be included, but it adds nothing new to the present zero order development.)

The solutions (17) have already been formed for (25), and they can be shown compatible with (26) if and only if $k_{B_0} = 0$ or $\gamma = 2$. The first of these options has already been met as a

condition for simple resonance, but it was not developed in detail. In conjunction with (17) it could be satisfied only at the magnetic equator, and then only if $\boldsymbol{k}_h$ were directed towards the east or towards the west. These rather rigid conditions would be relaxed to some extent if first-order corrections were taken into account.

The $\gamma = 2$ alternative is, of course, excluded by the kinetic theory of gases, but that is not to say it is irrelevant. It is sufficiently "close" to a physically acceptable solution in a complex $\{\gamma, \omega, \boldsymbol{k}\}$ space to suggest that some influence of the extended resonance may be found in practice. Moreover, it will be modified by first-order corrections, and perhaps in such a way as to increase that influence. Indeed, the modification can in some cases be of "half order"—it can amount to one part in five, for example, when the basic first-order corrections are only one part in twenty-five, and that would be enough to bring the required value of γ into the acceptable range. The other conditions for resonance, incidentally, are altered by similar amounts in many cases; in particular, significant vertical components of phase propagation can be introduced.

The detailed development of these first-order corrections has been postponed, but in so far as a simple coupling relation of the type (7) is applicable their magnitudes may be quickly estimated. In the F_2-layer the most important modifications are probably those related to the reaction on the atmospheric motion, and they introduce fractional corrections of the order $\sigma_1 B_0^2/\omega\rho_0$. On occasion this can very likely achieve the value one-twentyfifth just mentioned.

The appearance of ω in the denominator here is perhaps of significance, for it implies that the corrections increase with the period of the wave. Normally the σ_1 corrections would lead to a damping and broadening of the resonance, but the damping effects may be more than offset by the closer fulfilment of extended resonance conditions. In this case the increased amplitudes associated with increased periods (Munro, 1950) could be explained, while the broadening effects would explain the corresponding decrease in the number of cycles observed. (With a very sharp resonance, the observable disturbance would extend well beyond a compact primary-wave group, for its Fourier spectrum would be more constricted.)

No restrictions on the direction of travel have emerged from the main analysis, except for the primary restriction to the horizontal plane, but a more detailed investigation will certainly introduce some. Extended resonance, for example, adds subsidiary first-order conditions on the direction of $\boldsymbol{k}_h$ in some cases. This direction will affect the response even in a simple resonance, for it will affect the α_{mn} factors in the numerator of (11), and similar factors in the expression for the electron response to the resonant field. Since these factors eventually affect the observable perturbations of electron density, any directional change in $\boldsymbol{k}_h$ can introduce some further observational selection. Here again the development must await a detailed study of electron motions.

The necessary investigation of electron motions has already been initiated. It has revealed a further possibility whose observational importance may greatly exceed that of the effects just considered: the possibility that the electrons themselves may be set into resonant oscillations. (To return to an earlier analogy, the spring itself may be set into resonant oscillation by the vibrator, while the pendulum remains relatively unmoved.) This phenomenon of "electron resonance" is at present under investigation, and its initial consequences have been outlined elsewhere (Hines, 1954). They need not be repeated here, but it may be remarked that the estimates they provide are perhaps more acceptable than those found in the preceding section, at least if the latter are taken at face value rather than as order of magnitude results. The details of the work are to be reported shortly.

7. Conclusion

The large-scale travelling disturbances now regularly detected in the F_2-layer appear to have many features in common with certain resonant hydromagnetic waves: their amplitudes vary with height in about the same manner, their primary progression is thought to be horizontal, and it is unattenuated, and their space-time scales have the same orders of magnitude. Indeed, it may be suggested that

these particular disturbances have been observationally selected from a far greater variety which may actually occur, simply because they do produce hydromagnetic resonance and hence large fluctuations of electron density. In this case quantitative estimates can be made for two independent atmospheric parameters:

$$\gamma \sim 1{\cdot}1 \qquad \text{and} \qquad C^2/\gamma g \sim 20 \text{ km}.$$

These values are lower than might be expected at the relevant height, but perhaps by no more than the errors involved. Certain secondary characteristics of the observed disturbances might be explained by an extension of the present approximate resonance conditions, and better quantitative estimates may result, but no definite conclusions on this aspect have yet been reached.

Observational records displaying variations of vertical and horizontal space scales with frequency, or at least variations of horizontal speed with frequency, would be helpful in testing and directing further developments of a wave hypothesis.

I should like to record here my debt to J. C. SCOTT and J. A. RATCLIFFE, through whose interest and advice I was led to the study of hydromagnetic waves and of their possible application to ionospheric disturbances; to H. BONDI, whose encouragement and advice as research supervisor are particularly appreciated, and a number of workers at the Cavendish Laboratories, for many stimulating and constructive discussions of the whole problem; and to the National Research Council of Canada and the Defence Research Board of Canada, which have in turn provided financial support.

VOL. 7 1955

REFERENCES

BRAMLEY, E. N.	1953	*Proc. Roy. Soc.* **A 220,** 39
GLEDHILL, J. A., and SZENDREI, M. E.	1950	*Proc. Phys. Soc.* **B 63,** 427
HINES, C. O.	1953	*Proc. Camb. Phil. Soc.* **49,** 299
	1954	*Nature* **173,** 1087
KALLMANN, H. K.	1953	*J. Geophys. Res.* **58,** 209
MARTYN, D. F.	1950	*Proc. Roy. Soc.* **A 201,** 216
MUNRO, G. H.	1950	*Proc. Roy. Soc.* **A 202,** 208
PIERCE, J. A., and MIMNO, H. R.	1940	*Phys. Rev.* **57,** 95

APPENDIX

In the development of Section 2, it was assumed that the reactive force (7) was omitted legitimately from the right-hand side of (1). This assumption was necessary to develop with clarity the relationship between the forced electromagnetic system and the forcing hydrodynamic oscillation. In a general hydromagnetic wave, however, such an analysis is normally invalid; the two systems are mixed inextricably in determining the possible modes of oscillation. To justify the procedure adopted, and to verify certain orders of magnitude involved, the following detailed formalism is presented.

When the force density $\boldsymbol{J} \times \boldsymbol{B}_0$ is added on the right of (1), a formal inconsistency arises because of the exp $\gamma \boldsymbol{g} \cdot \boldsymbol{r}/C^2$ variation in ρ_0 and p_0. This fact, which was noted before, will be ignored for the moment.

On adopting the exponential forms

$$\boldsymbol{U} = \mathscr{U} \exp i(\omega t - \boldsymbol{k} \cdot \boldsymbol{r}) \tag{A1}$$

$$\boldsymbol{E} = \mathscr{E} \exp i(\omega t - \boldsymbol{k} \cdot \boldsymbol{r}) \tag{A2}$$

$$(\rho - \rho_0)/\rho_0,\ (p - p_0)/p_0 \propto \exp i(\omega t - \boldsymbol{k} \cdot \boldsymbol{r}) \tag{A3}$$

and substituting from (2), (3), and (4) into the modified (1), three scalar equations can be obtained in which ρ, p, and p_0 do not appear. These may be written, after slight reduction, as

$$U_{mn} B_0 \mathscr{U}_n + e_{m\nu} \mathscr{E}_\nu = 0 \qquad \begin{cases} m, n = x, y, z \\ \nu = \xi, \eta, \zeta \end{cases} \tag{A4}$$

where: summation over each repeated index is implied; the right-handed x, y, z co-ordinates are such that the positive z axis points downwards in the direction of $\boldsymbol{g}$ and the y axis points towards magnetic north; in the similar ξ, η, ζ system the ζ axis points in the direction of $\boldsymbol{B}_0$, being separated from the y axis by the dip angle I (positive in the northern hemisphere), and the ξ axis parallels the x axis, pointing to magnetic west; and, if

$$R^2 = \omega^2/C^2, \qquad K = ig\boldsymbol{k}/C^2, \qquad \tilde{\gamma} = \gamma - 1$$

$$Q_{1,2} = i\omega\sigma_{1,2} B_0^2/\rho_0 C^2, \qquad c = \cos I, \qquad s = \sin I,$$

then

$$\begin{aligned} U_{xx} &= k_x^2 - R^2 + Q_1 & U_{xy} &= k_x k_y - Q_2 s & U_{xz} &= k_x k_z + K_x + Q_2 c \\ U_{yx} &= k_x k_y + Q_2 s & U_{yy} &= k_y^2 - R^2 + Q_1 s^2 & U_{yz} &= k_y k_z + K_y - Q_1 cs \\ U_{zx} &= k_x k_z + \tilde{\gamma} K_x - Q_2 c & U_{zy} &= k_y k_z + \tilde{\gamma} K_y - Q_1 cs & & \\ U_{zz} &= k_z^2 - R^2 + \gamma K_z + Q_1 c^2 & e_{m\zeta} &= 0 & & \\ Q_1 &= -e_{x\eta} = e_{y\xi}/s = -e_{z\xi}/c & Q_2 &= -e_{x\xi} = -e_{y\eta}/s = e_{z\eta}/c. & & \end{aligned} \tag{A5}$$

Further, $\boldsymbol{J}$ and $\boldsymbol{B}$ can be eliminated from the set (7)–(10) to give three scalar equations

$$u_{\mu n} B_0 \mathscr{U}_n + E_{\mu\nu} \mathscr{E}_\nu = 0 \qquad \begin{cases} \mu, \nu = \xi, \eta, \zeta \\ n = x, y, z \end{cases} \tag{A6}$$

where, if $q_{0,\,1,\,2} = i\omega\mu_0\sigma_{0,\,1,\,2}$, then

$$\begin{aligned} E_{\xi\xi} &= k_\eta^2 + k_\zeta^2 + q_1 & E_{\xi\eta} &= -k_\xi k_\eta - q_2 & E_{\xi\zeta} &= -k_\xi k_\zeta \\ E_{\eta\xi} &= -k_\xi k_\eta + q_2 & E_{\eta\eta} &= k_\xi^2 + k_\zeta^2 + q_1 & E_{\eta\zeta} &= -k_\eta k_\zeta \\ E_{\zeta\xi} &= -k_\xi k_\zeta & E_{\zeta\eta} &= -k_\eta k_\zeta & E_{\zeta\zeta} &= k_\xi^2 + k_\eta^2 + q_0 \\ q_1 &= u_{\xi y}/s = -u_{\xi z}/c = -u_{\eta x} & q_2 &= u_{\xi x} = u_{\eta y}/s = -u_{\eta z}/c & u_{\zeta n} &= 0. \end{aligned} \tag{A7}$$

The sets (A4) and (A6) provide six linear homogeneous equations in six unknowns, $B_0\mathscr{U}_n$, and $\mathscr{E}_\nu$. (The $B_0\mathscr{U}_n$ components are chosen, rather than just $\mathscr{U}_n$, to equalize dimensions in the unknowns and separately in their coefficients.) The condition for a nonvanishing solution is, then, that the determinant of the coefficients shall vanish: that

$$\Delta \equiv \begin{vmatrix} U_{mn} & e_{m\nu} \\ u_{\mu n} & E_{\mu\nu} \end{vmatrix} = 0. \tag{A8}$$

The elements of this determinant contain terms of the following form only (neglecting differences between γ, $\gamma - 1$, and 1), with estimated magnitudes of the following order, in metres^{-2}, in the F_2-layer:

$$|k_\mu k_\nu| \sim |k_m k_n| \sim 10^{-9} \qquad R^2 \sim 10^{-10\cdot5} \qquad |K_m| \sim 10^{-9}$$

$$|q_0| \sim 10^{-7} \qquad |q_1| \sim 10^{-12} \qquad |q_2| \sim 10^{-13}$$

$$|Q_1| \sim 10^{-11\cdot5} \qquad |Q_2| \sim 10^{-12\cdot5}$$

These estimates are based on the observed space-time scales, such that $k_h \sim 10^{-4.5}$/m and $\omega \sim 10^{-2.5}$/sec, on an assumed $C^2 \sim 10^{5.5}$ m^2/sec^2 (corresponding to a scale height $\sim$10 or 100 km, temperature $\sim$1,000°K), density $\sim 10^{-9}$ kg/m^3, electronic and ionic collisional frequencies $\sim 10^3$ and 10^1/sec, gyrofrequencies $\sim 10^7$ and 10^2 radians/sec, and numeric densities $\sim 10^{12}$/m^3, and on the standard values $g \sim 10^1$ m/sec^2, $\mu_0 \sim 10^{-6}$ henry/m, and $B_0 \sim 10^{-4.5}$ weber/m; standard formulae (cf. HINES, 1953) have been used in the calculation of σ_0, σ_1, and σ_2, taking account of the large measure of cancellation between electronic and ionic contributions to σ_2; $\sigma_0 \sim 10^{1.5}$, $\sigma_1 \sim 10^{-3.5}$, $\sigma_2 \sim 10^{-4.5}$ mho/m. It is obviously legitimate to neglect the effective displacement conductivity, $\omega\varepsilon_0 \sim 10^{-13.5}$ mho/m, relative to these. The estimates obtained are inaccurate, of course, particularly where they involve the density ρ_0. Nevertheless, they do tend to indicate one important conclusion, namely, that the terms containing σ_1 and σ_2 are small compared with all the others. This suggests that a truncated series expansion of Δ in (A8), using the Q_1, Q_2, q_1, q_2 terms as expansion parameters, should provide a legitimate approximation. The "zero-order" terms in the series would not contain any contribution from the $e_{m\nu}$ and $u_{\mu n}$ elements of Δ, for these all contain σ_1 or σ_2 as a factor. The zero-order approximation to (A8) would therefore be

$$|\, U_{mn} \,|_0 \cdot |\, E_{\mu\nu} \,|_0 = 0 \tag{A9}$$

in which the $\|_0$ notation indicates the zero-order part of the appropriate determinant. It is the approximate factorization of Δ, apparent from the form of (A9), which most readily indicates that the hydrodynamic and electromagnetic systems are but loosely coupled in ionospheric disturbances having the scales observed, for (A9) will be satisfied if either hydrodynamic relation

$$|\, U_{mn} \,|_0 = 0 \tag{A10}$$

or the electromagnetic relation

$$|\, E_{\mu\nu} \,|_0 = 0 \tag{A11}$$

is satisfied. Since the basic disturbance was assumed to be hydrodynamic in the earlier work, the option (A10) was adopted in the first instance; in reduced form, it appeared as the hydrodynamic dispersion relation (6). The subsequent condition for resonance, that $\phi_0 = 0$, was simply a reduced form of (A11).

The approximate development can be carried one stage farther. The $e_{m\nu}$ and $u_{\mu n}$ elements of (A8) must enter the expanded form of Δ in pairs, so they contribute only second- and higher-order terms to the full series. To the first order then, (A8) becomes

$$|\, U_{mn} \,|_0 \cdot |\, E_{\mu\nu} \,|_0 + |\, U_{mn} \,|_0 \cdot |\, E_{\mu\nu} \,|_1 + |\, U_{mn} \,|_1 \cdot |\, E_{\mu\nu} \,|_0 = 0 \tag{A12}$$

where the $\|_1$ notion is self-explanatory. No first-order error occurs if this is rewritten as

$$(|\, U_{mn} \,|_0 + |\, U_{mn} \,|_1) \cdot (|\, E_{\mu\nu} \,|_0 + |\, E_{\mu\nu} \,|_1) = 0, \tag{A13}$$

so to this order the two systems still appear to be only loosely coupled. Improvements on (A10) for the basic disturbance, and on (A11) for the resonance condition, are now indicated by (A13). These were not developed, for reasons discussed in Section 6.

In the loosely coupled case, the set (A6) takes on the aspect of a set of forcing equations imposed on $\mathscr{E}$, and it may be used to estimate the electric response to a given hydrodynamic stimulus. Under nonresonant conditions, it will be found that these equations give

$$\begin{aligned} \mathscr{E}_{\xi,\eta}/B_0\mathscr{U}_m &\sim 10^{-3} \\ \mathscr{E}_\zeta/B_0\mathscr{U}_m &\sim 10^{-5} \end{aligned} \tag{A14}$$

for the F_2-region disturbances, and that, when a "zero-order resonance" occurs by virtue of $\boldsymbol{k} \cdot \boldsymbol{k} = 0$, they give

$$\begin{aligned} \mathscr{E}_{\xi,\eta}/B_0\mathscr{U}_m &\sim 10^{0} \\ \mathscr{E}_\zeta/B_0\mathscr{U}_m &\sim 10^{-5}. \end{aligned} \tag{A15}$$

($\mathscr{E}_\zeta$ does not increase because, using the notation of equation (11), a cancellation occurs in the numerator factor, $\alpha_{\zeta n}$, which just compensates for the resonance cancellation in the denominator,

VOL. 7 1955

ϕ.) It will be found that the $\mathscr{E}_\nu$ terms of (A4) are not comparable with the principal $B_0\mathscr{U}_n$ terms, in either of these cases. Again, the $Q_{1,2}$ terms in the U_{mn} coefficients are small compared with the other terms. These facts provide the necessary justification of the omission of $\boldsymbol{J} \times \boldsymbol{B}_0$ from (1), in the development of Section 2.

The oversight of the formal inconsistency may be justified on the same basis: the various $Q_{1,2}$ terms, which introduce the unwanted ρ_0 variation in (A4), are small relative to the others present. (The actual first-order corrections introduced by the Q_1 terms in (A13) are of the relative order $\sigma_1 B_0^2/\omega\rho_0 \sim 10^{-1}$. One order of magnitude is really not a safe working margin, perhaps, but it must be remembered that the estimates are approximate. Indeed, if $\sigma_1 B_0^2/\omega\rho_0$ actually became as great as 10^{-1}, the wave motion might be quickly damped out. A corresponding conclusion applies to winds—they tend to decay in a time $\rho_0/\sigma_1 B_0^2$, so the observations, whatever their interpretation, indicate a value of $\sigma_1 B_0^2/\rho_0$ at least as small as that estimated here.)

The linearized equation of electron motion,

$$\partial \boldsymbol{V}/\partial t = (e/m)\,(\boldsymbol{E} + \boldsymbol{V} \times \boldsymbol{B}_0) + K_e(\boldsymbol{U} - \boldsymbol{V}), \tag{A16}$$

can be reduced to show that, when $|\,G_e\,| \gg K_e$, the electric field will control the electron motion if

$$\begin{aligned} \mathscr{E}_{\xi,\eta}/B_0\mathscr{U}_m &> 10^0 \\ \text{and/or} \qquad \mathscr{E}_\zeta/B_0\mathscr{U}_m &> |\,K_e/G_e\,| \sim 10^{-4}. \end{aligned} \qquad (m \neq x) \tag{A17}$$

Here e/m is the electronic charge/mass ratio, K_e is the electronic collisional frequency, and $-G_e \equiv -eB_0/m$ is the electronic gyrofrequency. Comparison with (A14) and (A15) will show that the electric field has little effect in nonresonance conditions, and even with a zero-order resonance its effect is only comparable to that of the hydrodynamic motion. An enhanced effect, of the type described in Section 3, actually arises only when conditions for a first-order resonance are approached—when the factors in (A13) are set equal to zero separately. The forcing equations (A6) then lead to the values

$$\begin{aligned} \mathscr{E}_{\xi,\eta}/B_0\mathscr{U}_m &\sim 10^3 \\ \mathscr{E}_\zeta/B_0\mathscr{U}_m &\sim 10^{-2}, \end{aligned} \tag{A18}$$

which certainly exceed the required amounts (A17). A difficulty arises here, however, for the $\mathscr{E}_\nu$ terms in (A4) now become comparable to the principal $B_0\mathscr{U}_n$ terms which would otherwise control the basic disturbance. Further, the ohmic energy losses become comparable to the energy available in the hydrodynamic oscillation. This marks a breakdown in the "loose coupling" approach, that is, in the use of (A6) simply as forcing equations; the complete set (A4, A6) must now be used in determining the various ratios $\mathscr{E}_\nu/B_0\mathscr{U}_m$, for example, as ratios of various pairs of five-by-five determinants culled from Δ. The proper procedure does confirm that electron motions can be enhanced under conditions of a first-order resonance, though perhaps not to the extent that (A18) might suggest. The first-order conditions approximate to the zero-order conditions, of course, and it is on this basis that Sections 3–5 are meaningful. Some auxiliary first-order conditions can also arise on occasion, and these might replace, or support and augment, the tentative conditions introduced in Section 4.

Coriolis force densities have been neglected in the foregoing analysis. They may be represented by $2\rho_0\boldsymbol{\Omega} \times \boldsymbol{U}$ in a linearized theory, where the earth's angular rotation $\boldsymbol{\Omega}$ is of the order 10^{-4}/sec. Relative to the inertial force density $i\omega\rho_0\boldsymbol{U}$, for example, this extra force is only of the order $\Omega/\omega \sim 10^{-1\cdot5}$. Molecular viscosity, with coefficient η', would introduce a force density $\eta'(\nabla\,.\,\nabla\,\boldsymbol{U} + \nabla\nabla\,.\,\boldsymbol{U}/3)$ of the order $k_m k_n \eta' U_n$. According to the kinetic theory of gases, η' is independent of pressure and varies only as the square root of the thermodynamic temperature, so that the s.t.p. value 10^{-5} kg m^3/sec should be approximately correct. (Smaller values have been suggested,* from a consideration of the effects of the diminishing density of the upper atmosphere.) Relative to the inertial force, this viscous effect is then of the order 10^{-2} or less. Molecular heat-conduction introduces effects of this same order, $k_m k_n \eta'/\omega\rho_0$.

The amount of eddy viscosity can only be guessed, but it would not be likely to affect the problem at great heights, where the rising atmospheric temperature provides a static stability.

Finally, the effects of electron partial pressures have been implicitly ignored, in adopting the standard form and formulae for electric currents and conductivities. These pressures introduce forces of the order $|C_e^2 k_\mu k_\nu / \omega K_e| \sim 1$ relative to collisional forces, so they must be taken into account in a detailed development. (Here C_e is the "speed of sound" in the electron plasma; the ratio C^2/C_e^2 is about equal to the ratio of electronic to molecular mass, assuming the electrons to be at the same temperature as the atmosphere.) The necessary corrections to the basic formulae for the current components would not exceed an order of magnitude, and, since the detailed form of those formulae has nowhere entered the zero-order development, the deduced conditions for resonance would remain valid. This aspect will be developed more fully elsewhere; in particular, in the detailed presentation of the electron resonance phenomenon.

While the foregoing estimates relate only to the F_2-layer and to the disturbances appearing therein, similar conclusions may be drawn for the E-layer. Extreme resonance effects could arise there, however, before any difficulty arose with the approximate "loose coupling" approach. Most correction terms are reduced at the lower level, but electron partial pressures are still important. These pressures may have even greater significance in the upper ionosphere, in application to the medium-scale disturbances detected above the F_2-layer peak (from observations of radio star scintillations), but the relevant atmospheric parameters cannot be estimated with any certainty at all.

---

* YERG, D. G., 1952, *J. Geophys. Res.* **57**, 217.

VOL.
7
1955

Journal of Atmospheric and Terrestrial Physics, 1955, Vol. 7, pp. 31 to 39. Pergamon Press Ltd., London

Intermediate and large atmospheric ions at Cairo-Giza

GUSTAV ORTNER and ABDEL FATTAH EL NADI
Physics Department, Faculty of Science, University of Cairo

(*Received* 22 *November* 1954)

ABSTRACT

The mobility spectrum of atmsopheric ions in the mobility range below 100 × 10^{-4} cm^2/volt-sec has been investigated, using types of the cylindrical condenser method.

Distinct ion groups with definite values of the mobilities have been found (discontinuous spectrum). The mobilities in the range between (10 and 100) × 10^{-4} cm^2/volt-sec change from day to day, but are fairly constant in the range below 10 × 10^{-4} cm^2/volt-sec.

Furthermore, a certain influence of visible light on the ion concentration was observed.

INTRODUCTION

The ions in the atmosphere can be classified according to ISRAEL (1933) as

(a) Ultra-large ions having mobilities below 2·5;
(b) Langevin ions with mobilities between 2·5 and 10;
(c) Large intermediate ions in the mobility range between 10 and 100;
(d) Small intermediate ions with mobilities between 100 and 1,000;
(e) Small ions having mobilities above 1,000.

The present paper gives the mobility spectrum (ion characteristic) of atmospheric ions found at Cairo-Giza with mobilities below 100.

APPARATUS

The air passes through a cylindrical electric condenser. The central electrode of 5·01 cm in external diameter was subdivided into five sections, electrically insulated from each other and kept together by polysterene cylinders inside the tube. The lengths of the sections were 100, 10, 10, 20, and 20 cm in the direction of the air-blast. Each section could be connected to the electrometer of the Compton type by wires leading through holes in the polysterene insulators inside the tube. The fifth section was earthed in all the experiments. The central electrode was enclosed coaxially by another cylinder of brass, 170 cm in length and 6·98 cm in internal diameter, connected to a variable voltage supplied by dry batteries. The blast passed between these two cylinders. A third cylinder of 10·5 cm in diameter enclosed the two forementioned cylinders in order to make the electrostatic shielding more efficient. The dry batteries were placed inside a shielded box. The air was drawn either from outside the laboratory directly through a short tube into the electric condenser or, as was done in many experiments, through a rectangular box of 70-litres volume inserted in the tube. The box had two glass windows on opposite sides. In some experiments the box was alternately exposed to light or covered by a black cloth.

Throughout this paper the values of mobilities are expressed in units 10^{-4} cm^2/volt-sec.

LOCAL CONDITIONS

The experiments have been carried out in the Physics Department of the Faculty of Science, situated on the west side of the Nile. The place is remote from the centre of the city of Cairo by about five kilometres. The district is very similar to a garden city. In general, the atmospheric conditions at Cairo are probably somewhat different from those in European cities. Coal fires are rare and the main fuels are petroleum and butangas. The weather is fairly constant, at least during the period from May to July, during which months most of the ion characteristics have been investigated. The temperature during the day ranges from round 30°C in May to between 35 and 40°C in July. The relative humidity in all the experiments did

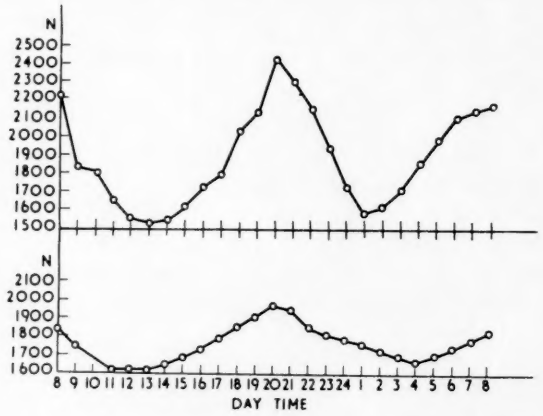

Fig. 1. Diurnal variation of the atmospheric ions.
Above: mean of January 1953
Below: mean of December 1952

not exceed 70 per cent, and was at the average about 60 per cent. Prevailing winds came from across the Mediterranean.

MEASUREMENTS WITH THE SUBDIVIDED CONDENSER

In the first experiments the subdivided condenser was used at a fixed voltage. The first section of the central electrode of 100 cm in length was earthed, and the three following sections totalling 40 cm in length were connected to the electrometer. The voltage was kept at a value at which only ions of mobilities below 23 could arrive at the electrometer. Readings were taken hourly over a whole day and night for ten days in December 1952 and eleven days in January 1953. The curves were fairly consistent and the means for each month are shown in Fig. 1. The curves may give an idea of the diurnal variation of large ions, though the ordinates do not represent the concentrations of all the ions with mobilities smaller than 23. The smaller the mobilities the smaller the fraction of ions arriving at the electrometer. Both curves exhibit a maximum number of ions at about 0800 hr, a gradual decrease to a minimum at about 1300 hr followed by an evening maximum at 2000 hr and a further decrease to a minimum at 0400 hr in the morning in December, which is shifted to 0100 hr in January. All data refer to local mean time of Cairo. These

VOL. 7 1955

results are in general agreement with observations of the diurnal variation of large ions by TORRESON and WAIT in Washington (1935), by HOGG at Kew Observatory in England (1939), and by LAUGHLIN in Paris (1927).

CHARACTERISTICS OF LARGE INTERMEDIATE IONS

The mobility range between 10 and 100 was investigated in the subdivided condenser, with the first three sections of together 120 cm in length earthed, and the

Table 1.

Date	*Daytime*	*Polarity*	*Mobility*	*Number/cc*
14 April 1953	0830–1030	negative	$k_1 = 550$ $k_2 = 20$ $k_3 = 11(?)$	470 560
14 April 1953	1200–1400	negative	$k_1 = 71$ $k_2 = 23$ $k_3 = 8(?)$	350 430
15 April 1953	0900–1100	positive	$k_1 = 48$ $k_2 = 23$	300 290
15 April 1953	1200–1400	positive	$k_1 = 83$ $k_2 = 29$	230 210
18 April 1953	1200–1400	negative	$k_1 = 29$	350
20 April 1953	1500–1700	negative	$k_1 = 57$ $k_2 = 20$	400 600
20 April 1953	1500–1700	positive	$k_1 = 57$ $k_2 = 20$	400 520
22 April 1953	1200–1400	negative	$k_1 = 45$ $k_2 = 11(?)$	520
22 April 1953	1200–1400	positive	$k_1 = 45$ $k_2 = 11(?)$	500
23 April 1953	1100–1400	negative	$k_1 = 45$ $k_2 = 11(?)$	680

following fourth section of 20 cm in length, connected to the electrometer. The ratio $(C_1 + C_2)/C_1 = 1{\cdot}17$. The air-blast was properly adjusted to the mobility range under investigation. Fig. 2 shows two characteristics obtained with different blasts: 10 litres/18·7 sec and 10 litres/26·5 sec respectively. Variation of the blast is a fairly reliable test of the reality of appearing steps or peaks in a characteristic. Table 1 gives the results of all the observations carried out in this range of mobilities.

The ion concentrations N have been calculated, using the expression derived by HOGG (1935):

$$N = E_m \cdot (C_2 + C_3) \cdot (1 + C_1/C_2)/Q \cdot t \cdot e,$$

C_1 being the capacity of the earthed sections, C_2 the capacity of the section connected to the electrometer, and C_3 the capacity of the electrometer and wires, E_m the electric potential attained by $C_2 + C_3$ during time t corresponding to a peak of the ion characteristic, Q the air transport in cc per second, and e the charge of the electron. It is assumed that all the ions are singly charged.

As regards the characteristics it may be said that it was not too difficult to obtain consistent readings over a couple of hours. In general, the procedure applied was similar to that of HOGG (*loc. cit.*). He used a standard condenser at a fixed voltage beside the variable-voltage condenser. Since a second condenser arrangement could not be made available, the current at a standard potential was measured in the same condenser between the measurements with variable voltage. In those

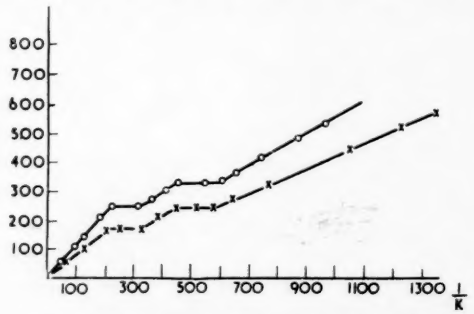

Fig. 2. Characteristics of large intermediate ions.
Upper curve: air draught 10 litres/18·7 sec.
Lower curve: air draught 10 litres/26·5 sec.

cases where the variations of the readings at standard potential were within reasonable limits, all the measurements were related to the average value at standard potential. Otherwise the experiment was rejected.

Summarizing, one can say that:

1. The mobilities of the ion groups change from one day to the other and even on the same day at different hours. Nevertheless, there is a certain coincidence on various days; a group with the mobility 20 appears with some preference.
2. The number of ions is comparatively small in this mobility range.

CHARACTERISTICS OF LARGE IONS WITH MOBILITIES BELOW 10

The condenser arrangement was the same as with the intermediate ions, but the blast was properly adjusted. Two characteristics obtained on subsequent days in July are shown in Fig. 3. Peaks appear at the mobilities $k_1 = 6{\cdot}7$, $k_2 = 2{\cdot}3$, $k_3 = 1{\cdot}0$, $k_4 = 0{\cdot}6$. The rise to each peak of the curves points towards the origin, as it should do. The fall after the peak corresponding to k_1 has somewhat less slope than would be expected if no ions between 6·7 and 2·3 were present: The

VOL. 7 1955

slope after the peak belonging to k_2 has nearly the theoretical value, whereas the slope after k_3 seems to indicate nonresolved groups of ions with mobilities between 1·0 and 0·6. All the ion characteristics investigated show with a surprising constancy the same groups, though the group at 0·6 could be verified in only 6 out of 40 characteristics because the voltage necessary for this group was not available when the other characteristics were investigated. In 38 characteristics the group

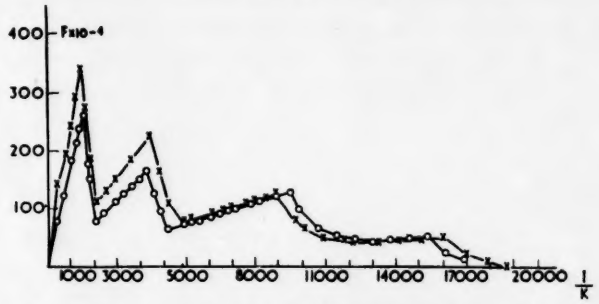

Fig. 3. Characteristics of large and ultra-large atmospheric ions.
⊙ 14 July, 1953
× 15 July, 1953

k_1 was found with mobility values between 6·5 and 7·0, in two characteristics k_1 7·7 and 8·0 respectively. The values of k_2 were between 2·3 and 2·4 and of k_3 between 0·94 and 1·04. Table 2 contains the ion concentrations for the groups shown in Fig. 3.

Table 2.

Date	*Mobility*	*Ion concentration*
14 July 1953	6·7	2,660
	2·3	1,660
	1·0	980
	0·61	430
15 July 1953	6·5	1,700
	2·3	950
	0·95	940
	0·59	510

After all, there seems to be no doubt about the existence of prominent ion groups in the atmosphere. Such groups have been found by previous authors, though the values of the mobilities observed by different authors are not in exact agreement. We refer to the most recent paper, published by P. J. Nolan and P. J. Kenny (1952).

In six cases characteristics have been investigated both for positive and negative ions. The average ratio $-/+$ was found to be 1·26.

CHARACTERISTICS OF IONS OBTAINED WITH THE SINGLE CONDENSER

In order to check the results obtained with the subdivided condenser the mobility spectrum was investigated with the first section of the central electrode of 100 cm in length connected to the electrometer. All the other sections were earthed. Altogether 18 characteristics were investigated with this arrangement. Fig. 4 shows an example. In this characteristic, steps appear at 12·5, 5·9, 2·3 and 1·0. The three smaller mobilities have been found in all the characteristics, though the step at 1·0 was hardly noticeable in some of the curves. The values range from 5·9 to 7·4 and from 2·2 to 2·4. Ion groups of higher mobilities, as, for example, in Fig. 4, appear sometimes, and indications of such groups appear also with the subdivided condenser.

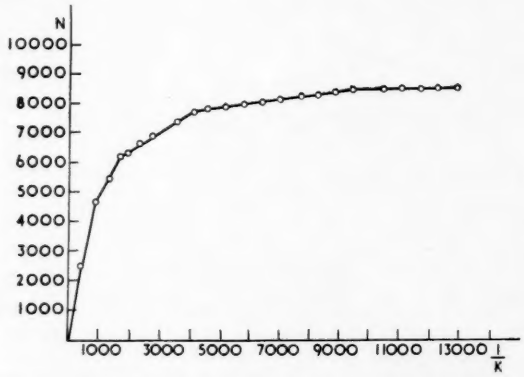

Fig. 4. Characteristic of atmospheric ions in the single condenser.

Summarizing, one can say that the mobilities below 10 are found to be in a satisfactory agreement with both of the condenser arrangements. The total ion concentration, including all mobilities, lies between 7,000 and 12,000 at various days.

INFLUENCE OF VISIBLE LIGHT ON THE MOBILITY SPECTRUM OF LARGE ATMOSPHERIC IONS

It was observed in experiments carried out at night that the ceiling lighting in the laboratory has some influence on the ion current. The walls of the laboratory have large windows covering the whole area round the air-inlet tube, so that the air outside was illuminated through the windows.

In order to investigate this curious phenomenon in the daytime, the rectangular box mentioned above was inserted in the inlet tube. Experiments were carried out with the box alternately covered by a black cloth ("dark box") and illuminated by either daylight or a tungsten filament lamp of 500 watts or a sodium lamp of 45 watts The tungsten lamp was used in a projector with glass lenses, 150 cm distant from the box. A mercury thermometer inside the box did not show a noticeable rise of temperature by illumination. The characteristics with dark box and illuminated box have always been taken one after the other. Most of the experiments have been carried out at noon and early afternoon, when the diurnal variation of the ions is comparatively small.

VOL. 7 1955

Characteristics Obtained with the Subdivided Condenser

(a) *Intermediate ions*

With intermediate ions an increase of ions was always observed in the illuminated box compared with the dark box, as is shown in Table 3, which contains the results of one experiment.

Table 3.

Mobility	*Ion concentration*	
	Dark box	*Illuminated box*
22	480	640
25	420	510

(b) *Ions with mobilities below* 10

The positions of the peaks have been found to be independent of the lighting conditions, as for the intermediate ions. One pair of the characteristics is shown in Fig. 5. The ion concentrations derived from it are given in Table 4.

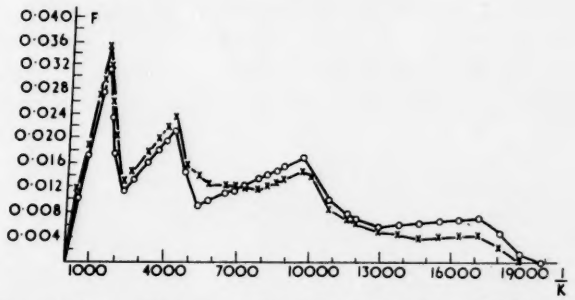

Fig. 5. Characteristics of large and ultra-large ions in the subdivided condenser.
○ dark box.
× box illuminated by tungsten filament lamp.

All the other pairs of characteristics show the same behaviour, independent of the polarity of the ions.

Summarizing, one can say that the ion groups of the mobilities 7 and 2·3 always show an increase of ions in light compared with the dark box, whereas the groups at 1·0 and 0·6 show a decrease. No distinct difference was observed between daylight and the light from the tungsten lamp, but a clear change was apparent with the sodium lamp. The crossing point of the characteristics obtained with the illuminated box and dark box is shifted from the mobility 1·35 in daylight and the light of the tungsten lamp, to 2·3 in presence of the sodium lamp. Furthermore, the slope of the characteristics between the peaks at 2·3 and 1·0 appears to be smaller in daylight and tungsten-lamp light compared with the slope of the characteristics obtained with the dark box.

These results lead to the conclusion that the equilibrium of the ions of various mobilities seems to depend on the lighting conditions.

CHARACTERISTICS OBTAINED WITH THE SINGLE CONDENSER

The subdivided condenser supersedes by far the single condenser with regard to the resolving power, particularly at the smallest mobilities, but it is not quite appropriate for investigating the total ion balance between dark and illuminated box.

Table 4.

Mobility	*Ion concentration*	
	Dark box	*Illuminated box*
6·7	2,480	2,770
2·3	1,420	1,760
1·0	1,310	1,260
0·58	700	430

VOL. 7 1955

Are new ions created in light not balanced by the loss of ions with other mobilities, or does only a new distribution in the mobility spectrum occur, without change of the total number? In order to make this point clear, characteristics have been investigated with the single condenser—first section of 100 cm in length connected

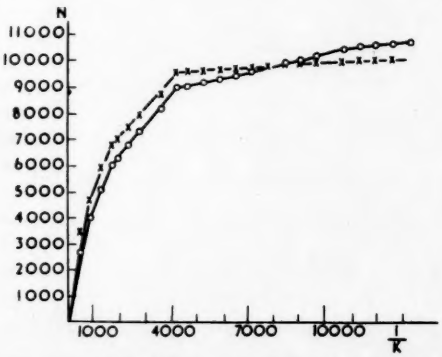

Fig. 6. Characteristics of atmospheric ions in the single condenser.
⊙ dark box.
× box illuminated by tungsten filament lamp.

to the electrometer—so that all the ions entering the condenser were measured, at least up to a certain lower limit of mobility depending on the available voltage. The pair of characteristics shown in Fig. 6 shows clearly a slight decrease of the total number of ions in light compared with the dark box. The same behaviour was observed in all the other characteristics. The reduction of the ions in light is

less than 500 ions and might be due to diffusion to the walls of the box and recombination, both effects being increased in light because of the greater average mobility of the ions. Furthermore, all the characteristics obtained with the single condenser show an increase in light of ions with mobilities greater than 6 and a decrease at mobilities smaller than 2 compared with dark box. This result is in qualitative agreement with that obtained with the subdivided condenser.

A few characteristics have been investigated, using the sodium lamp of 45 watts as light source. They also show a slight decrease in the total number of ions in the light as compared with the dark box.

Time Dependence of the Light Effect

The change of the characteristics does not occur suddenly after changing the lighting conditions, but gradually, within a few minutes. This holds both for alteration from light to dark and conversely, and was found from alternate illumination and darkening of the box as well as in experiments at night without box when the outside air round the inlet tube was alternately illuminated and darkened.

The investigation of this phenomenon will be continued with monochromatic light.

Summary

The mobilities of ions present in the atmosphere of Cairo-Giza have been investigated in the range below 100×10^{-4} cm²/volt-sec, using two different condenser arrangements. The mobility values between (10 and 100×10^{-4} change from one day to the other, but in the mobility range below 10×10^{-4} ion groups with fairly constant mobility values of $6{\cdot}8_4$, $2{\cdot}3_4$, $1{\cdot}0_1$, and 0·60, at the average, in units 10^{-4} cm²/volt-sec have been observed.

Furthermore, it was found that visible light has a certain influence on the characteristics. Both in daylight and in the light of a tungsten filament lamp the ions with mobilities greater than about 2×10^{-4} show an increase in concentration, and the ions with mobilities smaller than 2×10^{-4} a decrease compared with darkness.

References

Hogg, A. R.	1939	*Proc. Phys. Soc.* (London) **51**, 1014
Israel, H., and Schulz, L.	1933	*Terr. Magn. Atmosph. Electr.* **38**, 285
MacLaughlin, J.	1927	*C. R. Acad. Sci.* (Paris) **184**, 1183
Nolan, P. J., and Kenny, P. J.	1952	*J. Atmosph. Terr. Phys.* **2**, 266
Torreson, O. W., and Wait, G. R.	1935	*Terr. Magn. Atmosph. Electr.* **40**, 425

Journal of Atmospheric and Terrestrial Physics, 1955, Vol. 7, pp. 40 to 48. Pergamon Press Ltd., London

The effect on geomagnetism of the solar eclipse of 30 June 1954

J. EGEDAL* and N. AMBOLT†

(*Received* 27 *December* 1954)

ABSTRACT

After a short review of results of earlier investigations of the effect of solar eclipses on geomagnetism, observations of the magnetic declination, compiled from eleven observatories near the path of totality of the solar eclipse of 30 June 1954, have been examined. It is shown that the maximal magnetic effect takes place in close connection with the passage of the eclipse. On the assumption that the effect is a diminution of the departure of the daily variation, the said effect, derived according to a new method, has been examined, and it is shown that a diminution of the order found by CHAPMAN from an investigation based on theoretical considerations takes place in the present case.

1. INTRODUCTION

Since the beginning of the twentieth century efforts have been made to solve the question as to whether or not a solar eclipse has any influence on terrestrial magnetism. In particular, L. A. BAUER, Department of Terrestrial Magnetism, Washington, D.C., has taken an active part in these efforts. In connection with solar eclipses he established provisional observatories, arranged observations, and compiled and evaluated such data. The first observations arranged by BAUER (1900) showed a variation during the eclipse, but later observations gave doubtful results mainly on account of the occurrence of magnetic disturbances during the eclipses. VAN BEMMELEN (1905) examined observations from several eclipses and was convinced that an effect existed. CHARLES NORDMANN (1907) demonstrated the effect in a new way, forming differences between the magnetic values of the stations which the eclipse passed by. CHREE (1915) was sceptical as to the existence of the magnetic effect of a solar eclipse, and on the basis of data from the Kew observatory he pointed out that a variation at maximum obscuration was similar to a variation at the same time on the preceding day, and that the variation observed during the solar eclipse might therefore be due to influences other than those of the solar eclipse. During a long period from 1926 and onward no observations have been arranged, but CHAPMAN (1933), considering such an effect as existing, dealt with the question from a theoretical point of view, and later BARTELS and CHAPMAN (1940) stressed the importance of further examination of the question.

2. ARRANGEMENTS

In connection with the total solar eclipse of 30 June 1954, Avdelningen för jordmagnetism of the Royal Hydrographic Office of Sweden decided to establish a provisional magnetic observatory at Edh near Värnamo, below the central line of the track of totality in the *E*-layer.

The two authors agreed to compile magnetic data from their own countries (Denmark and Sweden) and from other countries near to the track of the eclipse (Iceland, United Kingdom, Belgium, Germany, Norway, Finland, Poland, and Russia), to evaluate the data, and to publish the result jointly. Applications

* Danish Meteorological Institute, Copenhagen, Denmark.
† Hydrographic Office, Stockholm, Sweden.

VOL. 7 1955

asking for observations to be used for the investigation were sent out to the countries mentioned. Observations were received from the following observatories: Reykjavik (Iceland); Lerwick, Eskdalemuir, and Abinger (United Kingdom); Manhay (Belgium); Wingst (Germany); Dombås (Norway); Rude Skov (Denmark); Abisko, Kiruna, Lovö, and Edh near Värnamo (Sweden); and Sodankylä and Nurmijärvi (Finland).

3. The Observations

From most observatories, copies of magnetograms for declination (D), horizontal force (H), and vertical force (Z) were received. As magnetic disturbances may hide a small effect caused by the solar eclipse, it was satisfying to note that 30 June was rather quiet until 2300 G.M.T. However, H and Z were least quiet, and therefore the examination has been confined to the declination. The observations from Abisko, Kiruna, and Sodankylä were slightly disturbed, so that these observations have been left out of consideration in some calculations mentioned later.

4. The Phenomenon

Bauer (1900) expected the effect of a solar eclipse on geomagnetism to be similar to the effect which would be produced if night hours were suddenly interposed among the day hours. In other words, the effect should be a diminution of departures from the mean value for the night hours, due to the daily variation. This view is just the view adopted at present and the basis of this investigation. When the sun disappears behind the moon the ionization of the E-layer is reduced, and consequently a diminution of the departures forming the daily variation takes place. According to ionospheric observations by Rydbeck (1946), the electron density of the E-layer during a solar eclipse varies with the solar radiation with a lag of about five minutes. It might be expected that the magnetic effect should vary in a similar way.

5. The Treatment

The examination of the observations during the solar eclipse has consisted firstly in a determination of the difference in time between the time of the passage of the totality, or of the maximal obscuration, and the time of maximal effect on the declination; and secondly, in a determination of the maximal diminution in percent of a derived departure of the daily variation for the time of maximal obscuration. The derived departure will be nearly equal to that for the night hours.

6. Occurrence of Maximal Effect and of the Minimum of Solar Radiation

The effect of the solar eclipse of 30 June on the declination was so pronounced that the time of the maximal effect could be determined. Table 1 gives the names of the stations, their latitude and longitude, time of maximal obscuration, and occurrence of maximal deviation from the normal variation.

The time of maximal obscuration has been determined with due regard to the azimuth of the sun and the direction of the path of totality. For Reykjavik no value for the occurrence of maximal deviation is given, because no deviation was traceable. Considering the values for the rest of the stations, it is found that the

maximal deviation on an average occurred two minutes before the maximal obscuration, but when Manhay is excluded the maximal deviation occurs on an average at the same time as the maximal obscuration. For Manhay two secondary maxima for the deviation are found at 1228 and 1244. It should be remembered that the determination of the time of the maximal deviation is rather uncertain.

Table 1. *Occurrence of maximal obscuration and of maximal deviation of the declination during the solar eclipse of* 30 *June* 1954

Station	φ	λ	*Maximal obscuration G.M.T.*	*Occurrence of maximal deviation G.M.T.*	*Remarks*
Reykjavik	64°08′	338°03′	1204	—	
Lerwick	60°08′	358°49′	1226	1219	Quick-run: 1231
Eskdalemuir	55°19′	356°12′	1226	1233	Reserve instr.: 1230
Abinger	51°11′	359°37′	1235	1231	
Dombås	62°04′	9°07′	1236	1236	
Manhay	50°18′	5°41′	1244	1216	
Wingst	53°45′	9°04′	1245	1243	
Rude Skov	55°51′	12°27′	1246	1243	
Edh (Värnamo)	57°10′	14°01′	1246	1246	
Lovö	59°21′	17°50′	1248	1247	Reserve instr.: 1244
Nurmijärvi	60°30′	24°39′	1252	1303	

VOL. 7 1955

In order to examine whether the maximal deviation at the different stations takes place in connection with the passage of the eclipse, a quantity, α, equal to the ratio for each station of the difference between the time of the observed deviation, T_0, and the mean time of all observed deviations, M_0, and of the difference between the time of maximal obscuration, T_m, and the mean time for all considered obscuration, M_m, has been determined:

$$\alpha = \frac{T_0 - M_0}{T_m - M_m}$$

If the maximal deviations take place in connection with the passage of the eclipse, the quality α should be equal to 1. The values for the ten stations have been examined and the following value for α has been found:

$$\alpha = 1{\cdot}0 \pm 0{\cdot}38$$

Leaving the value of Manhay out of consideration, the following result was found:

$$\alpha = 1{\cdot}2 \pm 0{\cdot}21$$

These values indicate with rather great certainty that the maximal deviation takes place in connection with the passage of the eclipse.

7. The Diminution in Percent of a Derived Departure

Earlier, the effect of a solar eclipse was often determined by a comparison with the variations of the preceding and the succeeding day. This method will produce no satisfactory result in the present case, since the daily variation of D for 30 June is abnormally large. The determination of the effect has therefore been carried out by means of mechanical adjustment of hourly departures according to a method proposed by Ryd (1917), using a special formula for adjustment of magnetic variations (see *Annuaire Magnétique*, 1923, Publ. Danish Meteorological Institute):

$$u_i = 0{\cdot}370o_i + 0{\cdot}283(o_{i+1} + o_{i-1}) + 0{\cdot}102(o_{i+2} + o_{i-2})$$
$$- 0{\cdot}026(o_{i+3} + o_{i-3}) - 0{\cdot}045(o_{i+4} + o_{i-4}) - 0{\cdot}012(o_{i+5} + o_{i-5})$$
$$+ 0{\cdot}008(o_{i+6} + o_{i-6}) + 0{\cdot}005(o_{i+7} + o_{i-7})$$

where u_i is the adjusted value for a certain hour i, and o_i the hourly value for the same hour, and the rest of the o-values are corresponding values for the hours indicated by their indices.

As one or two hourly values during the solar eclipse may be changed due to the eclipse, the formula has been used for amendment of such values through an iterating procedure. These calculations have been continued as long as the last interpolated values are numerically higher than the former ones. In order to illustrate the method, the result of an adjustment of the hourly departures of easterly declination from the Rude Skov magnetic observatory for 30 June 1954 has been given (Table 2). The hourly values for 1200 and 1300, originally, were $-6{\cdot}5'$ and $-6{\cdot}1'$ and are after the iteration $-7{\cdot}0'$ and $-7{\cdot}2'$, respectively. The value for 2300 is interpolated.

Table 2. Adjustment of hourly departures of D at Rude Skov for 30 June 1954

G.M.T.	Departures	Adjusted values	Differences	G.M.T.	Departures	Adjusted values	Differences
0000	$+0{\cdot}1'$	$+0{\cdot}08'$	$+0{\cdot}02'$	1200	$-7{\cdot}0'$	$-7{\cdot}02'$	$+0{\cdot}02'$
0100	$+0{\cdot}5'$	$+0{\cdot}43'$	$+0{\cdot}07'$	1300	$-7{\cdot}2'$	$-7{\cdot}23'$	$+0{\cdot}03'$
0200	$+0{\cdot}7'$	$+1{\cdot}08'$	$-0{\cdot}38'$	1400	$-6{\cdot}0'$	$-5{\cdot}94'$	$-0{\cdot}06'$
0300	$+2{\cdot}6'$	$+2{\cdot}13'$	$+0{\cdot}47'$	1500	$-3{\cdot}7'$	$-3{\cdot}86'$	$+0{\cdot}16'$
0400	$+3{\cdot}1'$	$+3{\cdot}43'$	$-0{\cdot}33'$	1600	$-1{\cdot}8'$	$-1{\cdot}79'$	$-0{\cdot}01'$
0500	$+5{\cdot}1'$	$+4{\cdot}84'$	$+0{\cdot}26'$	1700	$-0{\cdot}3'$	$-0{\cdot}37'$	$+0{\cdot}07'$
0600	$+5{\cdot}4'$	$+6{\cdot}06'$	$-0{\cdot}66'$	1800	$+0{\cdot}2'$	$+0{\cdot}19'$	$+0{\cdot}01'$
0700	$+6{\cdot}5'$	$+6{\cdot}47'$	$+0{\cdot}03'$	1900	$+0{\cdot}2'$	$0{\cdot}00'$	$+0{\cdot}20'$
0800	$+5{\cdot}8'$	$+5{\cdot}43'$	$+0{\cdot}37'$	2000	$-0{\cdot}8'$	$-0{\cdot}30'$	$-0{\cdot}50'$
0900	$+3{\cdot}4'$	$+2{\cdot}53'$	$+0{\cdot}87'$	2100	$-0{\cdot}4'$	$-0{\cdot}45'$	$+0{\cdot}05'$
1000	$-2{\cdot}4'$	$-1{\cdot}36'$	$-1{\cdot}04'$	2200	$-0{\cdot}2'$	$-0{\cdot}32'$	$+0{\cdot}12'$
1100	$-4{\cdot}8'$	$-4{\cdot}94'$	$+0{\cdot}14'$	2300	$(0{\cdot}0')$	$-0{\cdot}13'$	$+0{\cdot}13'$

In order to illustrate the result of the adjustment the adjusted values have been given in Fig. 1. A smooth curve has been drawn through the found values.

The standard deviation of the calculated departures from the observed values is $\pm 0{\cdot}37'$, so that the smooth curve of Fig. 1 may give a good basis for the determination of the departure at the time of totality or of maximal obscuration and of the deviation caused by the solar eclipse.

The determination of the diminution of the departure given in percent for totality is based on the assumption that the effect is proportional to that part of the

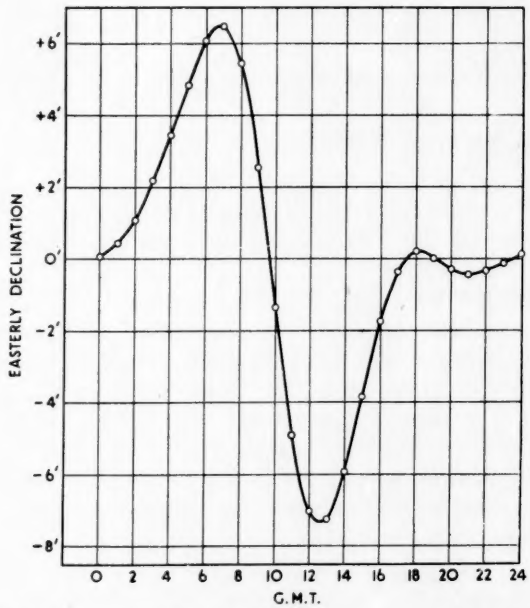

Fig. 1. Adjusted values representing the daily variation of D at Rude Skov, 30 June 1954.

sun's disc covered by the moon. From the present data it appears that the difference between the time of totality or of maximal obscuration and of the maximal effect is small, so that the assumption may be useful.

If the apparent radii of the sun and the moon are equal, the covered part of the sun's disc is given by the following formula:

$$\frac{2}{\pi}(\arcsin\sqrt{2x - x^2} - (1 - x) \,.\, \sqrt{2x - x^2})$$

where the apparent radius of the sun is put equal to 1, and x is half the width of the covered part of the sun given in the same unit. In Fig. 2 the covered part of the sun's disc is represented for the solar eclipse of 30 June 1954, interposing, in the middle of the curve given by the formula, a horizontal line representing the duration of the totality (2·5 minutes).

The effect at a given place depends on electric currents in a great area in the

VOL. 7 1955

E-layer. As the covered part of the sun will be different in each place in this area, this should be taken into consideration in the determination of the maximal effect.

Let us suppose that electric currents are flowing in a certain direction at an altitude of 100 km, and calculate the horizontal magnetic effect from overhead

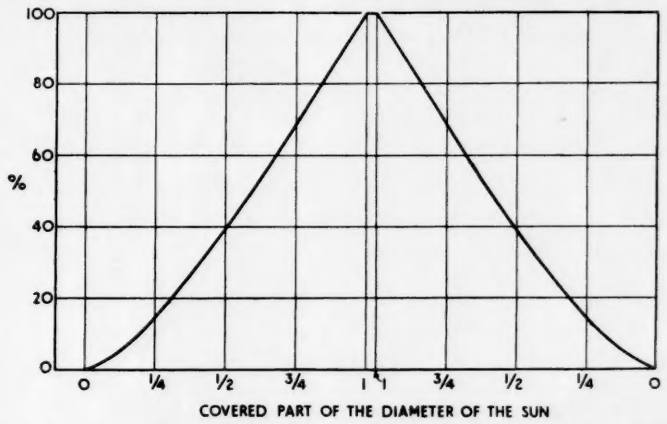

Fig. 2. The covered part of the disc of the sun during the solar eclipse of 30 June 1954.

currents in a direction at right angles to that of the current-system for a given place of observation.

The effect will be composed of effects from all the different parts of the current-system. For places on the earth lying in a direction at right angles to that of the

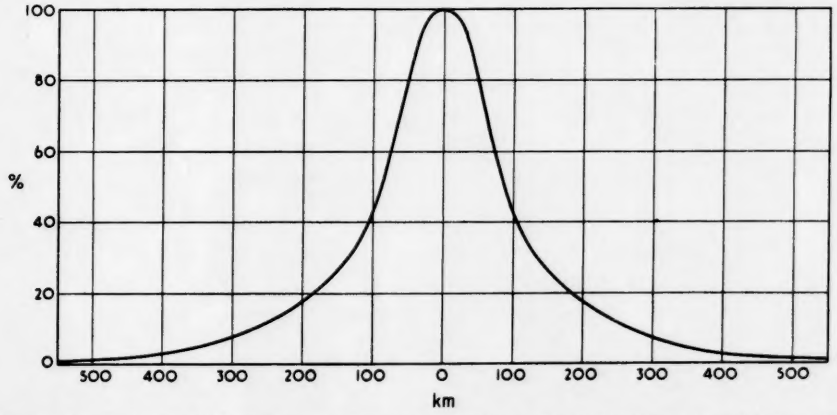

Fig. 3. Magnetic effects from electric currents flowing in a certain direction at an altitude of 100 km as observed in horizontal direction at right angles to the currents at a given place of observation, calculated for overhead currents at different distances at right angles to the direction of the currents and given in percent of the effect of overhead currents at the place of observation.

current-system the effect of the overhead currents as measured at the place of observation will vary as given in Fig. 3.

In Table 3 the magnetic effect is given in percent of the total effect for certain intervals.

By means of the values of Table 3 and data from Fig. 2 it has been possible to determine the amount percent of the effect at a given place compared with the maximal effect just below the central line of the totality in the *E*-layer (see Table 4, column 6).

Table 3. *Magnetic effect from electric currents flowing at an altitude of* 100 *km at different distances (laterally)*

Distances km	*Magnetic effect percent of the total effect*
0– 50	38·2
50–150	37·4
150–250	14·6
250–350	6·5
350–450	2·4
450–550	0·8

In Table 4 are given: Station, distance from central line of the totality (to the north +, and to the south −), $0{\cdot}9° \cot h_s \cos d$, where 0·9° is the height of the considered electric currents (100 km) expressed in latitude degrees, h_s the altitude of the sun at totality as observed from the point of the central line nearest to the place of observation in question (the magnetic observatory), and d the difference

Table 4. *Position of stations in relation to the track of totality, maximal effect expressed in percent of the derived departure*

Station	*Distance from central line*	$0{\cdot}9° \cdot \cot h_s \cdot \cos d$	*Distance from iono-spheric central line*	*Derived depart-ure*	*Deviations at maximal obscuration*	*Percent of maximal effect*	*The maximal effect in percent of the derived departure*
Reykjavik	+1·2°	+0·7°	+1·9°	−0·8′	untraceable	96	—
Lerwick	−1·1°	+0·7°	−0·4°	−7·4′	2·1′	99	29
Eskdalemuir	−6·3°	+0·6°	−5·7°	−5·0′	0·8′	84	19
Abinger	−9·6°	+0·5°	−9·1°	−4·9′	0·8′	71	23
Dombås	+2·4°	+0·7°	+3·1°	−7·8′	2·85′	93	39
Manhay	−9·0°	+0·5°	−8·5°	−6·3′	0·9′	74	19
Wingst	−5·0°	+0·5°	−4·5°	−6·8′	1·9′	88	32
Rude Skov	−2·3°	+0·6°	−1·7°	−7·4′	2·2′	97	31
Edh (Värnamo)	−0·7°	+0·6°	−0·1°	−7·5′	2·2′	100	29
Lovö	+2·2°	+0·7°	+2·9°	−7·8′	2·3′	93	30
Nurmijärvi	+5·1°	+0·7°	+5·8°	−7·5′	1·5′	85	24
						Mean: 27·5 ± 2·0	

VOL. 7 1955

between the azimuth of the line from the mentioned point to the place of observation and the azimuth of the sun at the above-mentioned moment of time, distance from the ionospheric central line (*E*-layer), derived departure, effect at maximal obscuration, percent of maximal effect, and the maximal effect in percent of the derived departure.

The distance of the stations from the central line of the totality has been calculated, and by means of the correction $0{\cdot}9° \cdot \cot h_s \cdot \cos d$ the distance from the ionospheric central line has been determined. The departure and the deviation at maximal obscuration have been determined by means of the adjusted daily variation for the station in question. Finally, the maximal effect has been derived and has been given in percent of the derived departure.

To illustrate the effect, the *D*-magnetogram for Edh (Värnamo), the station nearest to the place below the ionospheric central line, has been reproduced (see Fig. 4).

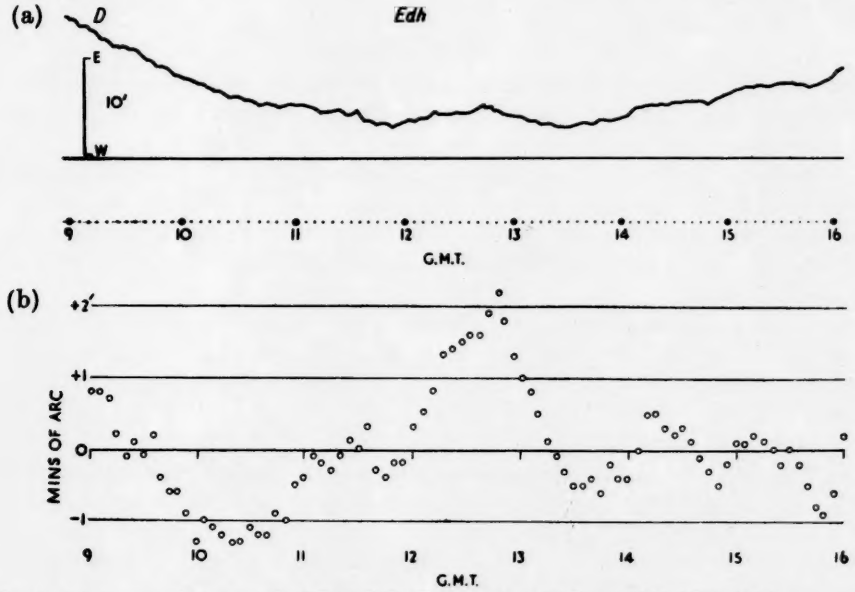

Fig. 4. (a) A copy of the record of *D* at Edh (Värnamo) on 30 June, 0900–1600, 1954.
(b) Representation of the difference between the observed and the adjusted values of *D* for every five minutes at the same place and time.

In Table 4 no value of the maximal effect has been given for Reykjavik, because it has not been possible to trace any deviation at the time of maximal obscuration, which might be expected, as the derived departure is small. The values of this station are uncertain. For the rest of the stations it has been possible to determine the maximal effect given in percent of the derived departure. The deviations from the mean of the values given in the last column of Table 4 are comparatively large, due to the uncertainty of the measurement of the small effects and due to masking by magnetic disturbances; however, the mean of all values has been found with a fair accuracy. CHAPMAN (1933) found that the

maximal diminution should be 28 per cent. The accordance between this theoretical value and the value $27{\cdot}5 \pm 2{\cdot}0$ found from the observations is satisfying.

8. The Present and Earlier Results

It is remarkable that the doubt as to the reality of an effect from solar eclipses has existed for so many years, but the explanation is certainly that the effect in many cases has been masked by magnetic disturbances, and that the effect has been studied in cases where the departure of the daily variation was small. As regards the effect during the solar eclipse of 30 June, it should be stated that this took place during relative quiet magnetic conditions, and that the range of the daily variation of 30 June as determined at Rude Skov was 30 per cent larger than the mean range of all days of June 1954. The conditions for an investigation were in this case extremely favourable, and, into the bargain, the track of totality passed near to several magnetic observatories.

9. Conclusions

The fact that the observed maximal deviation during the considered solar eclipse and the totality or maximal obscuration occur synchronically makes it evident that the deviations are due to the solar eclipse.

It is remarkable that the difference between the occurrence of maximal deviation and the occurrence of totality or of maximal obscuration seems to be small. This means that the sun shortly after the totality or maximal obscuration is able not only to compensate the recombination, but also to augment the ionization of the E-layer.

Even if the accordance between the observed and the theoretical values of the effect in the present case is great, the study of the phenomenon ought to be continued, comprising all magnetic elements, possibly through an international co-operation.

Acknowledgments—We acknowledge the receipt of copies of magnetograms and express our sincere thanks to: Geophysicist TH. SIGURGEIRSSON, Reykjavik; the Astronomer Royal, Sir HAROLD SPENCER JONES; the Director of the Meteorological Office, London; Professor B. TRUMPY, Bergen; Dr. L. KOENIGSFELD, Liege; Professor F. ERRULAT, Hamburg; and Dr. E. SUCKSDORFF, Helsinki.

References

BARTELS, J., and CHAPMAN, S.	1940	*Geomagnetism*, 354
BAUER, L. A.	1900	*Terr. Mag.* **5,** 143
BEMMELEN, W. VAN	1905	*Nat. Tijdschr. voor Ned. Indië*, **64,** afl. 3–4
CHAPMAN, S.	1933	*Terr. Mag.* **38,** 175
CHREE, C.	1915	*Terr. Mag.* **20,** 71
NORDMANN, CHARLES	1907	*Terr. Mag.* **12,** 15
RYD, V. H.	1917	*Publ. Danish Meteorological Institute Medd.* Nr. 3
RYDBECK, O. E. H.	1946	*Transactions of Chalmers University of Technology*, **53,** 14

VOL. 7 1955

Journal of Atmospheric and Terrestrial Physics, 1955, Vol. 7, pp. 49 to 60. Pergamon Press Ltd., London

Erdmagnetische Unruhe und Durchschnittsabweichungen der F_2-Schicht-Tagesgrenzfrequenzen in verschiedenen geomagnetischen Breiten

Geomagnetic activity and average deviations of daytime F_2-layer critical frequencies in different geomagnetic latitudes

GÜNTHER LANGE-HESSE
Institut für Ionosphärenforschung in der Max-Planck-Gesellschaft,
Lindau über Northeim/Han., Germany

(*Received* 20 *December* 1954)

ABSTRACT

The observational data of six ionospheric stations and one geomagnetic observatory is systematically analyzed in order to find out statistical relations between the degree of geomagnetic activity and the average deviations of the daytime F_2-layer critical frequencies from their median values. The observational data is arranged only according to the degree of geomagnetic activity; then the average deviations are determined for different degrees of geomagnetic activity.

There appears a distinct dependence on the geomagnetic latitude, the seasons, and the sunspot cycle. The practical significance of these results for the prediction of ionospheric disturbances is discussed. Figures are given representing the reliability of these predictions for different geomagnetic latitudes, different seasons, and phases of sunspot cycle.

A. EINLEITUNG

Über den zeitlichen Ablauf einzelner Ionosphärenstürme und den gleichzeitigen Verlauf der erdmagnetischen Unruhe ist wiederholt von verschiedenen Autoren berichtet worden. Darüber hinaus sind von APPLETON und PIGGOTT (1952, 1953) sowie von MARTYN (1953a, b) systematische Untersuchungen durchgeführt worden über den durchschnittlichen Ablauf von Ionosphärenstürmen und über die gleichzeitige Auswirkung von Ionosphärenstürmen an verschiedenen Punkten der Welt.

Über den näheren Zusammenhang zwischen den verschiedenen erdmagnetischen Unruhegraden und den Durchschnittsabweichungen der F_2-Schicht-Grenzfrequenzen vom Medianwert ist dagegen wenig bekannt, insbesondere darüber, von welchem Grade der erdmagnetischen Unruhe an im Durchschnitt eine F_2-Schicht-Grenzfrequenzerniedrigung merklich wird. Einen ersten Beitrag zu dieser Frage gaben die Untersuchungen von BERKNER und SEATON (1940) und zum Teil auch die von APPLETON und PIGGOTT (1952). Einen weiteren Beitrag gaben die Untersuchungen von LANGE-HESSE (1954) an der etwa $5\frac{1}{2}$ Jahre langen Meßreihe der Ionosphärenstation Lindau ($\varphi = 51{\cdot}65°$ N, $\lambda = 10{\cdot}13°$ E). In dieser Arbeit wurde unter anderem die günstigste Lage des Zeitintervalls für das erdmagnetische Unruhemaß ermittelt im Hinblick auf optimale Korrelation mit den F_2-Schicht-Grenzfrequenzabweichungen.

B. ARBEITSRICHTUNG

In den nachstehenden Untersuchungen wird an Hand des Beobachtungsmaterials von sechs europäischen Ionosphärenstationen und einem erdmagnetischen Observatorium ermittelt.

(1) Der Einfluß der geomagnetischen Breite und Länge auf den Zusammenhang zwischen dem Grade der erdmagnetischen Unruhe und den Durchschnittsabweichungen der F_2-Schicht-Grenzfrequenzen vom Medianwert.
(2) Die Änderung des in (1) genannten Einflusses mit der Jahreszeit und der Phase im Sonnenfleckenzyklus.
(3) Die Sicherheit, mit der aus dem Grade der erdmagnetischen Unruhe kurzfristig Ionosphärenstürme vorhergesagt werden können.
(4) Die Änderung der in (3) genannten Sicherheit mit der geomagnetischen Breite, mit der Jahreszeit und der Phase im Sonnenfleckenzyklus.

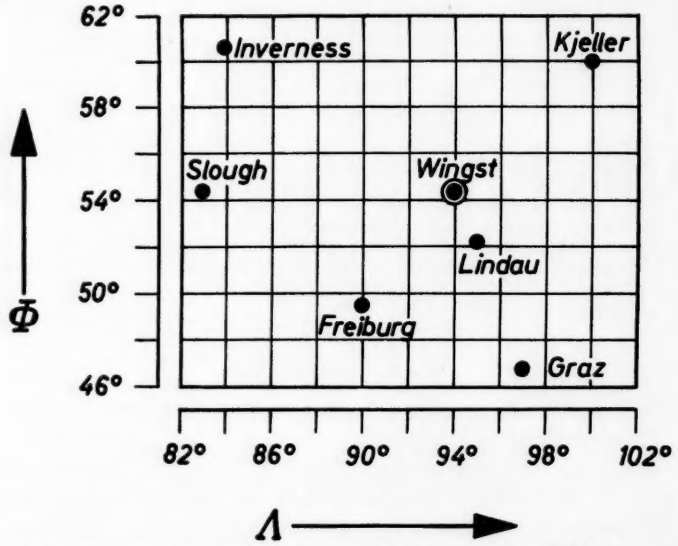

Abb. 1. Die Meßwerte dieser europäischen Stationen werden in den nachfolgenden Untersuchungen benutzt (Φ, Λ = geomagnetische Breite und Länge).
Fig. 1. The observational data of these European stations are used in the following investigations (Φ, Λ = geomagnetic latitude and longitude).

C. BEOBACHTUNGSMATERIAL

Es werden benutzt die Grenzfrequenzen der ordentlichen Komponente der F_2-Schicht (f^0F_2) aus der Zeit von November 1948 bis April 1954 von folgenden Stationen (Abb. 1):

(I)	Inverness:	$\varphi = 57{\cdot}45°\text{N};\ \lambda = 4{\cdot}25°\text{W}$	$(\Phi = 60{\cdot}7°;\ \Lambda = 084°)$
	Slough:	$\varphi = 51{\cdot}50°\text{N};\ \lambda = 0{\cdot}60°\text{W}$	$(\Phi = 54{\cdot}4°;\ \Lambda = 083°)$
	Freiburg:	$\varphi = 48{\cdot}10°\text{N};\ \lambda = 07{\cdot}80°\text{E}$	$(\Phi = 49{\cdot}5°;\ \Lambda = 90°)$
(II)	Oslo-Kjeller:	$\varphi = 60{\cdot}00°\text{N};\ \lambda = 11{\cdot}10°\text{E}$	$(\Phi = 60{\cdot}0°;\ \Lambda = 100°)$
	Lindau:	$\varphi = 51{\cdot}65°\text{N};\ \lambda = 10{\cdot}13°\text{E}$	$(\Phi = 52{\cdot}3°;\ \Lambda = 095°)$
	Graz:	$\varphi = 47{\cdot}10°\text{N};\ \lambda = 15{\cdot}50°\text{E}$	$(\Phi = 46{\cdot}9°;\ \Lambda = 097°)$*

Dieser Zeitraum erstreckt sich angenähert vom Sonnenfleckenmaximum zum Minimum. Zusätzlich herangezogen werden die erdmagnetischen Beobachtungen

* Von der Ionosphärenstation Graz sind regelmäßige Grenzfrequenzwerte erst ab. 1 Febr. 1951 vorhanden.

VOL. 7 1955

des Observatoriums Wingst $\varphi = 53{\cdot}7°$ N; $\lambda = 9{\cdot}7°$ E ($\Phi = 54{\cdot}5°$; $\Lambda = 94{\cdot}0°$) aus dem gleichen Zeitraum.

Die unter (I) und (II) genannten Ionosphärenstationen liegen etwa zwischen 61° und 47° geomagnetischer Breite und zwischen 83° und 100° geomagnetischer Länge (Abb. 1). Das erdmagnetische Observatorium Wingst liegt etwa in der Mitte dieses Raumes. Die unter (I) aufgeführten Ionosphärenstationen liegen im Westteil, die unter (II) im Ostteil dieses Raumes.

D. Das Beobachtungsmaterial wird folgendermaßen vorbereitet

(1) *Ionosphärenmaterial*

Für jede Station wird aus den f^0F_2-Werten von 10–14 h eines jeden Tages (insgesamt 5 Werte) der Mittelwert gebildet. Dieser Mittagsmittelwert (10–14 h) f^0F_2 genannt, wird als charakteristischer Kennwert angesehen für die Lage der f^0F_2-Tageswerte. Die Wahl dieses Wertes stellt zwar eine gewisse Schematisierung dar, jedoch würden die nachstehenden Untersuchungen bei der Wahl differenzierterer Angaben über die Tagesgrenzfrequenzen ins uferlose anwachsen. Aus den (10–14 h) f^0F_2-Werten werden in täglichen Abständen übergreifende 27 tägige Medianweret gebildet, anschließend die Differenz zwischen dem (10–14 h) f^0F_2-Wert und dem zugehörigen 27 tägigen Medianwert. Diese tägliche Differenz, $\Delta(1\text{–}27)$ f^0F_2 genannt, stellt die Abweichung des Mittagsmittelwertes (10–14 h) f^0F_2 vom zentrierten 27 tägigen Medianwert dar. Der 27 tägige Medianwert entspricht etwa dem Monatsmedianwert.

Ist der (10–14 h) f^0F_2-Wert an einer Station durch technische Störungen ausgefallen, so werden die (10–14 h) f^0F_2-Werte aller anderen Stationen dieses Tages aus den Meßreihen gestrichen. Durch diese Maßnahme erhält man für alle sechs Stationen zeitlich völlig gleiche Zeitreihen. Andererseits fallen jedoch durch diese strenge Auswahl etwa 20 Prozent der Beobachtungstage aus.

(2) *Erdmagnetisches Material*

Als Maß für die erdmagnetische Unruhe werden die täglichen C_k-Werte von Wingst benutzt. Während C_i (früher auch C_{int} abgekürzt) ein Maß ist für die planetarische 24stündige erdmagnetische Unruhe (siehe Landolt-Börnstein, 1952, S. 738), ist C_k ein Maß für die lokale 24stündige erdmagnetische Unruhe. C_k hat die gleiche Skala wie C_i von 0·0–2·0. Neben C_k, das ein logarithmisches Maß darstellt, und C_i gibt es für die 24stündige erdmagnetische Unruhe noch die linearen Maße A_k (lokal) und A_p (planetarisch). A_k wird aus den dreistündigen Kennziffern K und A_p aus den dreistündigen planetarischen Kennziffern K_p gebildet (siehe Landolt-Börnstein, 1952, S. 739; I.U.G.G. 1954, S. VIII). Umwandlung von A_k- in C_k-Werte geschieht ebenfalls nach der für A_p in C_i-Werte gültigen Tabelle (siehe I.U.G.G. 1954, S. IX).

Für die nachstehenden Untersuchungen wird ausschließlich der C_k-Wert für 06–06 h GMT benutzt, abgekürzt C_k (06–06 h). Nach [6] zeigt C_k (06–06 h) eine merklich bessere Korrelation mit den F_2-Schicht-Grenzfrequenzabweichungen als C_k (00–24 h). C_k (06–06 h) endet jeweils um 06 h des bezeichneten Tages, daher ist C_k (06–06 h) ein zeitlicher Vorläufer von dem (10–14 h) f^0F_2-Wert.

E. ZUSAMMENHANG ZWISCHEN DEN EINZELNEN ERDMAGNETISCHEN UNRUHEGRADEN UND DEN F_2-SCHICHT-GRENZFREQUENZABWEICHUNGEN VOM MEDIANWERT IN VERSCHIEDENEN GEOMAGNETISCHEN BREITEN

Die Tage der ganzen Beobachtungszeitreihe werden jetzt nach dem Grade der erdmagnetischen Unruhe in 21 Gruppen aufgeteilt (entsprechend $C_k = 0{\cdot}0$; $0{\cdot}1$; ...; $2{\cdot}0$), und zwar werden (für jede Station einzeln) unter den einzelnen C_k-Werten die Abweichungen $\Delta(1\text{–}27)\, f^0F_2$ der Tage eingetragen, die den entsprechenden C_k-Wert haben. Hierbei entstehen 21 Spalten. Von jeder Spalte wird der Durchschnitt der darinstehenden $\Delta(1\text{–}27)\, f^0F_2$-Werte gebildet. Die so gewonnenen Durchschnittsabweichungen $\Delta(1\text{–}27)\, f^0F_2$ von drei Stationen zeigt in Prozent

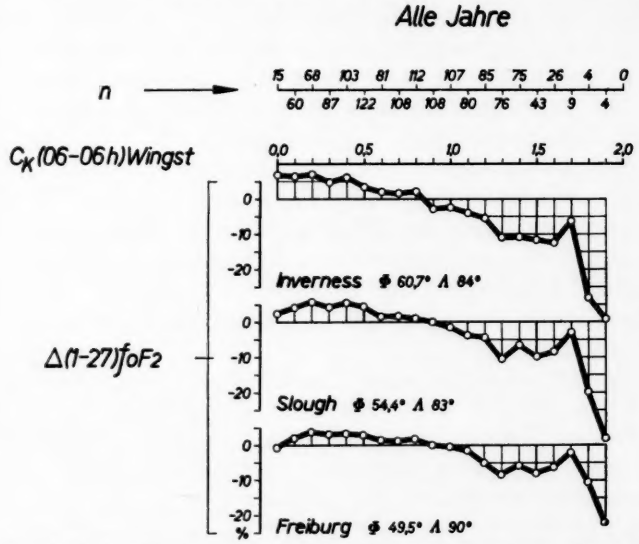

Abb. 2. Durchschnittsabweichungen $\Delta(1\text{–}27)\, f^0F_2$ in verschiedenen geomagnetischen Breiten in Abhängigkeit von dem Grade der erdmagnetischen Unruhe. [C_k(06–06 h) Wingst].

Fig. 2. Average deviations $\Delta(1\text{–}27)\, f^0F_2$ (= average noon value (10–14 h) f^0F_2 minus 27-day median) in different geomagnetic latitudes as a function of the degree of geomagnetic activity [C_k(06–06 h) Wingst]. n = Number of values used for each average deviation.

umgerechnet Abb. 2 in Abhängigkeit von C_k. Die für die einzelnen Durchschnittsabweichungen $\Delta(1\text{–}27)\, f^0F_2$ benutzte Anzahl Tage ist in der mit n bezeichneten Zeile angegeben. Diese Zeile gibt gleichzeitig eine Häufigkeitsverteilung der C_k-Werte.

Der Verlauf der drei Kurven in Abb. 2 zeigt, daß von $C_k = 0{\cdot}9\text{–}1{\cdot}0$ an die Abweichungen negativ werden. Mit zunehmender erdmagnetischer Unruhe nehmen auch die negativen Abweichungen zu. Nach einem kurzen Wiederanstieg aller drei Kurven bei $C_k = 1{\cdot}7$ wird die größte negative Abweichung bei $C_k = 1{\cdot}9$ erreicht. Alle drei Kurven erreichen bei $C_k = 1{\cdot}2$ etwa -5 Prozent Abweichung. Der Einfluß der erdmagnetischen Unruhe auf die f^0F_2-Werte ist demnach von $C_k = 1{\cdot}2$ an aufwärts besonders stark. Der Wiederanstieg aller drei Kurven bei $C_k = 1{\cdot}7$ scheint reell zu sein, da er unabhängig voneinander bei allen drei Stationen auftritt. Über die physikalische Ursache dieser sonderbaren Erscheinung kann vorerst

VOL. 7 1955

nichts ausgesagt werden. Aus der Abb. 2 geht weiterhin hervor, daß die positiven Abweichungen bei den niedrigeren C_k-Werten ($0{\cdot}0 \leqslant C_k \leqslant 0{\cdot}6$) und die negativen bei den höheren C_k-Werten dem Betrage nach mit abnehmender geomagnetischer Breite abnehmen.

Die bisherigen Resultate sagen noch nichts darüber aus, mit welcher Wahrscheinlichkeit beim Eintritt einer erdmagnetischen Unruhe bestimmter Größe eine vorgegebene Mindestabweichung in $\Delta(1\text{–}27)\, f^0F_2$ folgt. Hierüber geben jedoch die Kurven der Abb. 3 Auskunft. Dort ist für jede Durchschnittsabweichung $\Delta(1\text{–}27)$

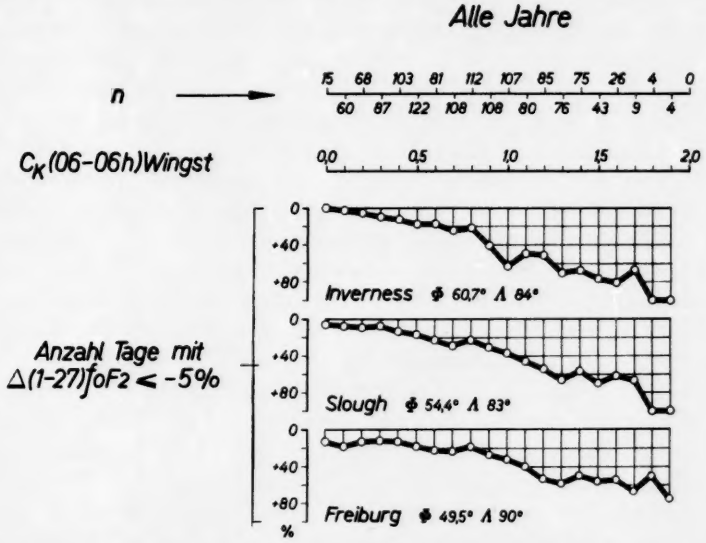

Abb. 3. Anzahl Tage (in Prozent) mit $\Delta(1\text{–}27)\, f^0F_2 < -5$ Prozent (hier gewählte Definition für einen Ionosphärensturm) in verschiedenen geomagnetischen Breiten in Abhängigkeit von dem Grade der erdmagnetischen Unruhe [C_k(06–06 h) Wingst].

Fig. 3. Number of days (in percent) with $\Delta(1\text{–}27)\, f^0F_2 < -5$ per cent (definition for an ionospheric storm taken here) in different geomagnetic latitudes as a function of the degree of geomagnetic activity [C_k(06–06 h) Wingst].

f^0F_2 der Abb. 2 die prozentuale Anzahl Tage angegeben mit Abweichungen $\Delta(1\text{–}27)$ $f^0F_2 \leqslant -5$ Prozent (das sind z.B. Abweichungen von -6 Prozent oder -10 Prozent, usw.). Mit anderen Worten ist das die prozentuale Anzahl der Tage, an denen eine merkliche F_2-Schicht-Grenzfrequenz-Depression (Ionosphärensturm)* stattfand.

Bei $C_k = 1{\cdot}2\text{–}2{\cdot}0$ beträgt für alle in Abb. 3 gezeigten Stationen die prozentuale Anzahl Tage mit Ionosphärenstürmen ($\Delta(1\text{–}27)\, f^0F_2 \leqslant -5$ Prozent) mehr als 50 Prozent. Diese Anzahl nimmt zwar mit abnehmender geomagnetischer Breite ab, liegt jedoch für Freiburg ($\varphi = 49{\cdot}5°$) noch über 50 Prozent. Bei $C_k < 1{\cdot}2$ beträgt diese Anzahl ($C_k = 1{\cdot}0$ von Inverness ausgenommen) weniger als 50 Prozent. Bei sehr niedrigen C_k-Werten ($0{\cdot}0 \leqslant C_k \leqslant 0{\cdot}2$) ist die Wahrscheinlichkeit des Eintritts

* Unter Ionosphärensturm wird in Rahmen dieser Untersuchungen verstanden eine Abweichung $\Delta(1\text{–}27)\, f^0F_2 < -5$ Prozent.

von Ionsophärenstürmen (= prozentuale Anzahl Tage mit $\Delta(1\text{–}27)\, f^0F_2 \leqslant -5$ Prozent) sehr gering, jedoch ist diese Wahrscheinlichkeit nach Abb. 3 in höheren geomagnetischen Breiten deutlich geringer als in niedrigeren. Das bedeutet, daß bei erdmagnetischer Ruhe ($0{\cdot}0 \leqslant C_k \leqslant 0{\cdot}2$) die F_2-Schicht-Grenzfrequenzen in höheren Breiten sehr selten um größere Beträge vom Medianwert abweichen, ganz im Gegensatz zu erdmagnetisch gestörten Zeiten ($1{\cdot}2 \leqslant C_k \leqslant 2{\cdot}0$), wo das Umgekehrte der Fall ist.

F. Einfluß des Sonnenfleckenzyklus

Um den Einfluß der geomagnetischen Breite und des Sonnenfleckenzyklus auf die Grenzfrequenzabweichungen und die Wahrscheinlichkeit des Eintritts von Ionosphärenstürmen bei hohen C_k-Werten ($1{\cdot}2 \leqslant C_k \leqslant 2{\cdot}0$) deutlich vor Augen zu führen, wird ein anderes Experiment durchgeführt. Für jeweils eine Station wird aus den Abweichungen $\Delta(1\text{–}27)\, f^0F_2$ von allen Tagen mit $1{\cdot}2 \leqslant C_k \leqslant 2{\cdot}0$ ein Durchschnittswert gebildet. Abb. 4 zeigt diese so gebildeten Durchschnittsabweichungen $\Delta(1\text{–}27)\, f^0F_2$ von drei Stationen verschiedener geomagnetischer Breite, sowohl für alle Jahre der benutzten Zeitreihe als auch nur für die maximumnahen und minimumnahen Jahre.* Die zweite Zeile der Abb. 4 gibt für die darüberstehenden Durchschnittsabweichungen $\Delta(1\text{–}27)\, f^0F_2$ die zugehörige prozentuale Anzahl Tage mit $\Delta(1\text{–}27)\, f^0F_2 \leqslant -5$ Prozent oder mit anderen Worten die Wahrscheinlichkeit des Eintritts eines Ionosphärensturmes bei $1{\cdot}2 \leqslant C_k \leqslant 2{\cdot}0$.

Nach Abb. 4 sind die Durchschnittsabweichungen $\Delta(1\text{–}27)\, f^0F_2$ der maximumnahen Jahre etwa um den Faktor zwei größer als die der minimumnahen Jahre. Entsprechend ist auch die Wahrscheinlichkeit des Eintritts eines Ionosphärensturmes in den maximumnahen Jahren (die hier etwa 70–75 Prozent beträgt) merklich größer als in den minimumnahen Jahren. Der Einfluß der geomagnetischen Breite auf die Durchschnittsabweichungen ist in beiden Phasen des Sonnenfleckenzyklus näherungsweise gleich, dagegen ist der Einfluß der Breite auf die Wahrscheinlichkeit des Eintritts eines Ionosphärensturmes in den maximumnahen Jahren geringer als in den minimumnahen.

G. Einfluß der Jahreszeiten

Um den Einfluß der Jahreszeiten erkennen zu können, wird ein gleiches Experiment durchgeführt wie in Abb. 4, jedoch dabei das Beobachtungsmaterial der minimum- und maximumnahen Jahre nach Jahreszeiten aufgeteilt. Das Ergebnis zeigt Abb. 5 und 6.

(a) *Maximumnahe Jahre*

Während der maximumnahen Jahre (Abb. 5) sind die Durchschnittsabweichungen $\Delta(1\text{–}27)\, f^0F_2$ in höheren Breiten ($\Phi \approx 60°$) im Winter am größten und im Sommer am geringsten. In niedrigeren Breiten ($\Phi \approx 50°$) dagegen zu den Äquinoktien am größten und im Winter am geringsten. Der Einfluß der Breite auf die Durchschnittsabweichungen ist im Winter am größten und im Sommer am geringsten. Die Wahrscheinlichkeit des Eintritts eines Ionosphärensturmes ($\Delta(1\text{–}27)\, f^0F_2$

* Die maximumnahen Jahre zählen bei diesen Untersuchungen von November 1948 bis September 1950, die minimumnahen Jahre von Februar 1951 bis April 1954.

VOL. 7 1955

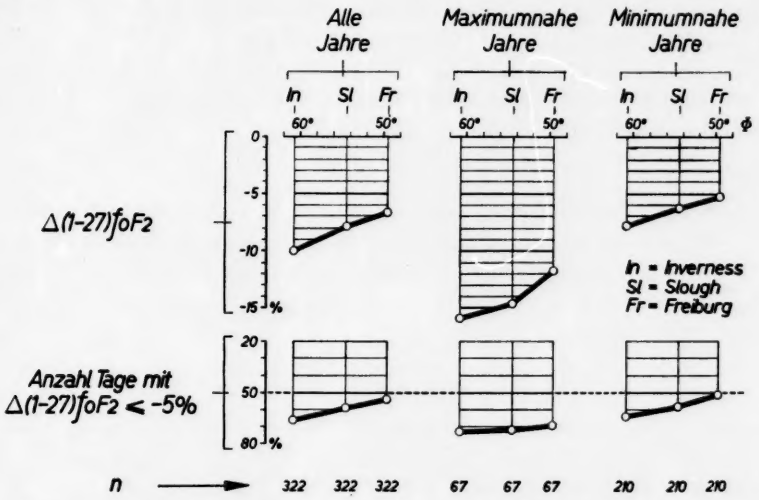

Abb. 4. Durchschnittsabweichungen $\Delta(1\text{–}27)\ f^0F_2$ für die erdmagnetischen Charakterzahlen $1{\cdot}2 \leqslant C_k \leqslant 2{\cdot}0$ in Abhängigkeit von der geomagnetischen Breite. In der 2. Zeile: Für jede Durchschnittsabweichung die Anzahl Tage (in Prozent) mit $\Delta(1\text{–}27)\ f^0F_2 \leqslant -5$ Prozent (Ionosphärensturm).

Fig. 4. Average deviation $\Delta(1\text{–}27)\ f^0F_2$ for the geomagnetic character figures $1{\cdot}2 \leqslant C_k \leqslant 2{\cdot}0$ as a function of geomagnetic latitude. Left column for all the years considered, middle column only the years near sunspot-maximum and right column only the years near sunspot-minimum. In the second line: for each average deviation the number of days (in percent) with $\Delta(1\text{–}27)\ f^0F_2 \leqslant -5$ per cent (ionospheric storm).

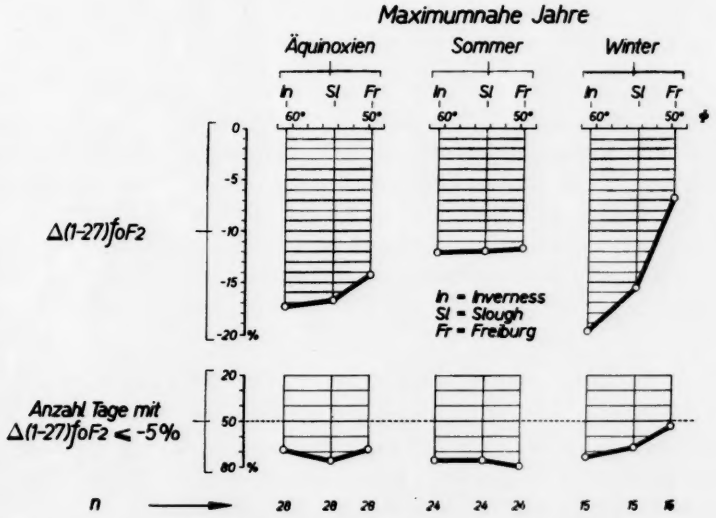

Abb. 5. Ergebnis eines gleichartigen Experiments wie in Abb. 4. Maximumnahe Jahre aufgeteilt nach Jahreszeiten.

Fig. 5. Result of a similar experiment as in Fig. 4. Years near sunspot-maximum divided in seasons. Equinox left, summer middle, and winter right.

$\leqslant -5$ Prozent) liegt im Sommer und zu den Äquinoktien etwa zwischen 70 Prozent und 80 Prozent. Ein merklicher Einfluß der Breite ist in diesen Jahreszeiten nicht zu erkennen, dagegen ist ein solcher im Winter deutlich erkennbar. Die Wahrscheinlichkeit des Eintritts eines Ionosphärensturmes liegt im Winter in $\Phi \approx 50°$ nur wenig über 50 Prozent.

(*b*) *Minimumnahe Jahre*

Während der minimumnahen Jahre (Abb. 6) ist der jahreszeitliche Einfluß auf die Durchschnittsabweichungen $\Delta(1\text{–}27)\, f^0F_2$ in höheren Breiten ($\Phi \approx 60°$) gering, in niedrigeren Breiten ($\Phi \approx 50°$) dagegen stark. Der Einfluß der Breite auf die

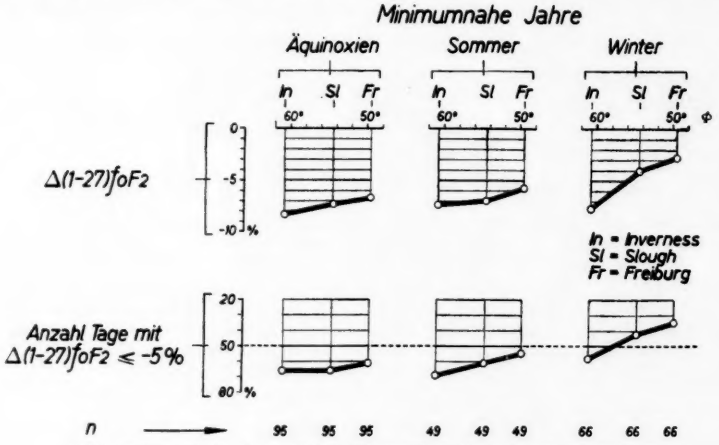

Abb. 6. Ergebnis eines gleichartigen Experiments wie in Abb. 4.
Minimumnahe Jahre aufgeteilt nach Jahreszeiten.

Fig. 6. Result of a similar experiment as in Fig. 4. Years near sunspot-minimum divided in seasons. Equinox left, summer middle, and winter right.

Durchschnittsabweichungen ist im Winter am größten, im Sommer und zu den Äquinoktien jedoch merklich geringer. Ein Einfluß der Breite auf die wahrscheinlichkeit des Eintritts eines Ionosphärensturmes ist zu allen Jahreszeiten zu erkennen. Im Winter ist dieser Einfluß am stärksten. Zu dieser Jahreszeit liegt diese Wahrscheinlichkeit für $\Phi \leqslant 55°$ unter 50 Prozent. Die C_k-Werte von 1·2 bis 2·0 können grundsätzlich nur dann als anzeigende Vorläufer von Ionosphärenstürmen benutzt werden, wenn die Wahrscheinlichkeit des Eintritts größer als 50 Prozent ist.

H. Einfluß der geomagnetischen Länge

Die bisher gezeigten Ergebnisse waren ausschließlich aus den Meßreihen der Stationen Inverness, Slough und Freiburg gewonnen. Diese Stationen liegen im Westteil des in Abb. 1 gezeigten Raumes. Um zu erkennen, welchen Einfluß die geomagnetische Länge auf die bisher gezeigten Ergebnisse hat, werden gleiche Untersuchungen wie vorhergehend durchgeführt mit den Meßreihen der drei im Ostteil dieses Raumes (Abb. 1) zwischen $\Lambda = 95°$ und 100° liegenden Stationen: Kjeller ($\Phi = 60°$), Lindau ($\Phi = 52{\cdot}3°$) und Graz ($\Phi = 46{\cdot}9°$). Da die Meßreihe von

VOL. 7 1955

Graz erst im Februar 1951 beginnt, mußten die nachstehenden Untersuchungen auf den Zeitraum der minimumnahen Jahre (Februar 1951–April 1954) beschränkt bleiben.

Abb. 7 zeigt das Ergebnis eines gleichen Experimentes wie Abb. 6, jedoch hier von den drei östlichen Stationen (Abb. 1). Die in Abb. 7 in den einzelnen Breiten aufgeführten Zahlenwerte sind näherungsweise den Werten entsprechender Breiten in Abb. 6 gleich.

Zum weiteren Studium des Längeneinflusses wird mit den Meßreihen der in Abb. 7 aufgeführten Stationen ein gleiches Experiment durchgeführt wie in Abb. 2. Die Ergebnisse zeigen die untersten Zeilen der Abb. 8, 9 und 10. In den Zeilen darüber sind zum Vergleich aufgetragen die entsprechenden Werte der im Westteil

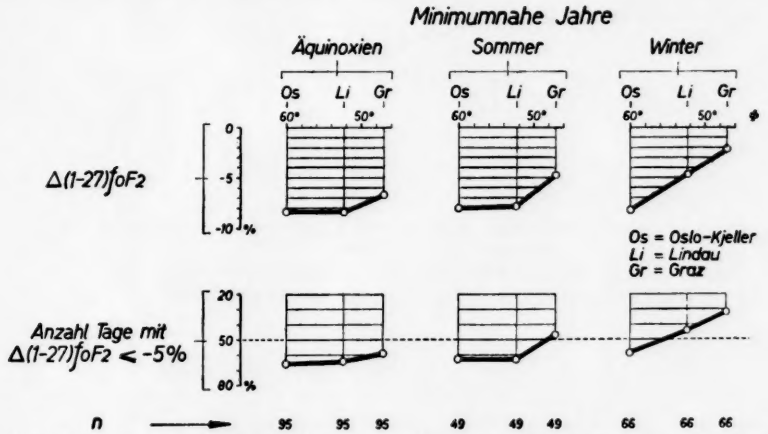

Abb. 7. Ergebnis eines gleichartigen Experimentes wie in Abb. 6 aber von den östlichen Ionosphärenstationen (siehe Abb. 1).

Fig. 7. Result of a similar experiment as in Fig. 6, but for the eastern ionospheric stations (see Fig. 1).

des Raumes in angenähert gleicher Breite liegenden Stationen. Eine nähere Überprüfung der Abb. 8, 9 und 10 zeigt, daß sich die Kurvenverläufe für Stationen näherungsweise gleicher Breite aber um etwa 10–15° verschiedener Länge weitgehendst ähneln. Längenänderungen von etwa 10–15° haben somit praktisch keinen Einfluß auf die Durchschnittsabweichungen der F_2-Grenzfrequenzen vom Medianwert.

I. Zusammenfassung der Ergebnisse

Die Durchschnittsabweichungen der F_2-Grenzfrequenzen vom Medianwert $\Delta(1–27)$ f^0F_2 als Funktion der erdmagnetischen Unruhe (C_k) zeigen sowohl bei niedrigeren als auch bei höheren C_k-Werten eine deutliche Abhängigkeit von der geomagnetischen Breite (Abb. 2). Die geomagnetische Länge hat dagegen bei Änderungen von etwa 10–15° keinen merklichen Einfluß (Abb. 8, 9 und 10).

Ein deutlicher Einfluß des Sonnenfleckenzyklus auf die Durchschnittsabweichungen $\Delta(1–27)\,f^0F_2$ für $1{\cdot}2 \leqslant C_k \leqslant 2{\cdot}0$ ist in allen vorstehend untersuchten geomagnetischen Breiten ($\Phi = 46–61°$) vorhanden (Abb. 4). Die Durchschnitts-

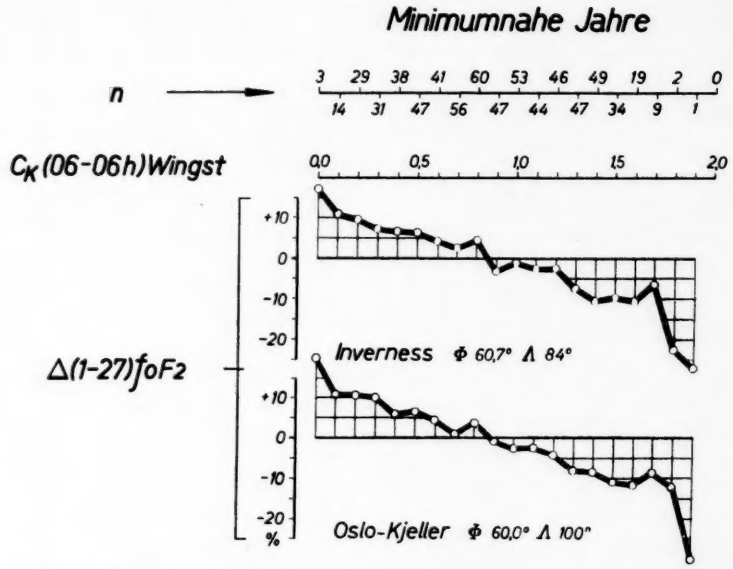

Abb. 8. Vergleich der Durchschnittsabweichungen von Inverness und Kjeller (gleiches Experiment wie in Abb. 2).

Fig. 8. Average deviations for Inverness in comparison to those for Kjeller (same experiment as in Fig. 2). Years near sunspot-minimum.

VOL. 7 1955

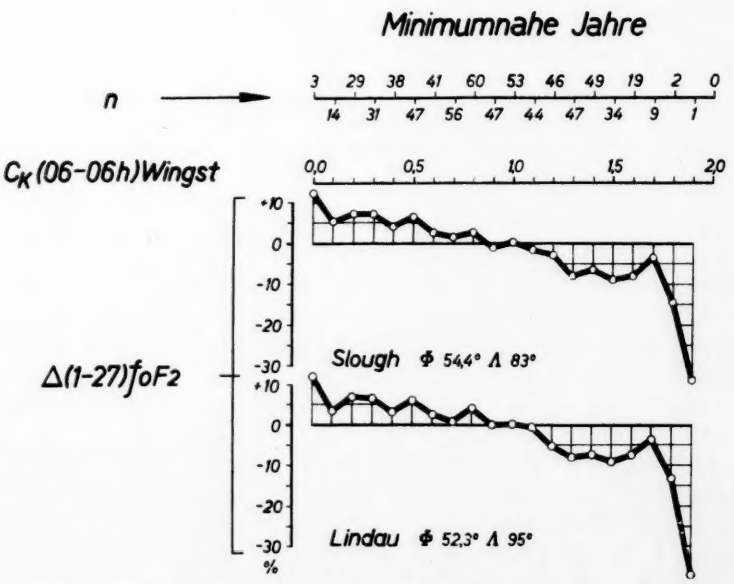

Abb. 9. Vergleich der Durchschnittsabweichungen von Slough und Lindau (gleiches Experiment wie in Abb. 2).

Fig. 9. Average deviations for Slough in comparison to those for Lindau (same experiment as in Fig. 2). Years near sunspot-minimum.

abweichungen der maximumnahen Jahre (hier Nov. 1948 bis Sept. 1950) betragen etwa das Zweifache von den der minimumnahen Jahre (hier Febr. 1951 bis April 1954).

Ein jahreszeitlicher Einfluß auf die Durchschnittsabweichungen für $1{\cdot}2 \leqslant C_k \leqslant 2{\cdot}0$ ist in niedrigeren Breiten ($\Phi \approx 50°$) sowohl während der maximumnahen als auch während der minimumnahen Jahre vorhanden. Die geringsten Durchschnittsabweichungen treten dort im Winter auf (Abb. 5, 6). In höheren Breiten ($\Phi \approx 60°$) ist ein merklicher jahreszeitlicher Einfluß nur während der maximum-

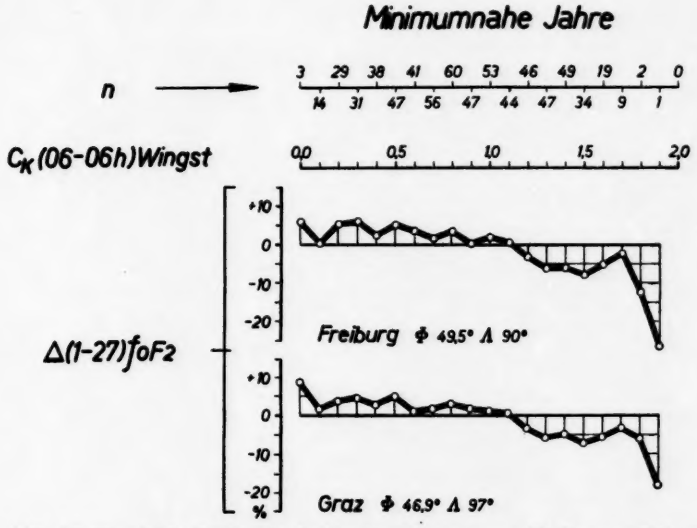

Abb. 10. Vergleich der Durchschnittsabweichungen von Freiburg und Graz (gleiches Experiment wie in Abb. 2).

Fig. 10. Average deviations for Freiburg in comparison to those for Graz (same experiment as in Fig. 2). Years near sunspot-minimum.

nahen Jahre erkennbar. Die geringsten Abweichungen treten dort im Sommer, die höchsten im Winter auf (Abb. 5).

C_k (06–06 h) von 1·2 bis 2·0 kann lediglich im Winter während der minimumnahen Jahre in $\Phi \leqslant 55°$ nicht als anzeigender Vorläufer von Ionosphärenstürmen benutzt werden (Abb. 6, 7).

Schrifttum

Appleton, E. V. und Piggott, W. R. (1952,) The morphology of storms in the F_2-layer of the ionosphere. *J. Atmosph. Terr. Phys.* **2**, 236–252.

Appleton, E. V. (1953), Storm phenomena in the ionsphere. Archiv der elektrischen Übertragung (A.E.Ü.) **7**, 271–273.

Berkner, L. V. und Seaton, S. L. (1940), Systematic ionospheric changes associated with geomagnetic activity. *Terr. Mag.* **45**, 419–424.

International Union of Geodesy and Geophysics. (1954), Association of Terrestrial Magnetism and Electricity (IATME), Bulletin No. 12h, Den Haag.

LANGE-HESSE, G. (1954,) Systematische Untersuchungen über den Einfluß der erdmagnetischen Unruhe auf die Tagesgrenzfrequenzen der F_2-Schicht. Archiv der elektrischen Übertragung (A.E.Ü.) **8**, 143–154.

LANDOLT-BÖRNSTEIN, (1952), Zahlenwerte und Funktionen aus Physik, Chemie, Astronomie, Geophysik und Technik, III. Band: Astronomie und Geophysik. Hersg. J. BARTELS und P. TEN BRUGGENCATE. Springer Verlag. 6. Aufl. Berlin.

MARTYN, D. F. (1953), Geo-morphology of F_2-region ionospheric storms. *Nature* **171**, 14–16.

MARTYN, D. F. (1953b), The morphology of the ionospheric variations associated with magnetic disturbance. *Proc. Roy. Soc.*, **A218**, 1–18.

VOL.
7
1955

Journal of Atmospheric and Terrestrial Physics, 1955, Vol. 7, pp. 61 to 72. Pergamon Press Ltd., London

Apparatus for the accurate and continuous measurement of the earth's electric field

W. W. MAPLESON,*
and
W. S. WHITLOCK,
Department of Physics, Durham Colleges in the University of Durham

(*Received* 29 *November* 1954)

ABSTRACT

Two new instruments of the "field mill" type, for the accurate measurement of the earth's electric field, are described. One mill, designed for operation in fair weather, gives a galvanometer deflection of ± 5 cm for a field of ± 250 V/m with an accuracy of $\pm 2\frac{1}{2}$ V/m with half-hourly calibration. The response time is about one second. The other mill, designed to work in all weathers, has a maximum sensitivity of ± 10 cm deflection for ± 75 V/m with an accuracy of ± 1 V/m with half-hourly calibrations. The response time is about one-tenth second. The theory of their operation is given, including an analysis of the disturbing effects of rain and air-earth currents, and of grid current in the first valve of the amplifier. The limitations to their accuracy are discussed and improvements in design are suggested. A review of earlier field mills and other "mechanical collectors" is included.

1. INTRODUCTION

In the course of some investigations in atmospheric electricity it was necessary to obtain accurate, continuous measurement of electric field by means of apparatus which was transportable and did not interfere with other atmospheric measurements in the vicinity. Some kind of mechanical collector was clearly the instrument of choice. Although a large number of instruments of this type have been developed in the past for the measurement of electric field both in the atmosphere and in the laboratory, only one claim has been found for accuracy in the measurement of the small fields of fair weather: LUEDER (1943), ± 2 per cent from 20 to 300 V/m; and little attention has been paid to the disturbing effects of rain-current. However, LUEDER'S instrument did not indicate the sign of the field. Consequently it is felt that a description of the two types of "field mill" which were constructed for the present research projects, with particular reference to the limitations to their accuracy, will be of interest, and that a brief review of previous instruments will not be out of place.

2. PRINCIPLE OF OPERATION OF THE MECHANICAL COLLECTOR

The mechanical collector has been developed in two main forms. In the first a conductor is first earthed and exposed to the field so that a charge, proportional to the field, is induced on it. The earth connection is broken and the conductor moved to some screened position, where it is connected to an electrometer with which it shares its charge. The conductor is then returned to its original position, and the procedure repeated continuously and rapidly so that the electrometer receives a sequence of unidirectional current pulses and eventually acquires a steady potential proportional to the electric field.

* Now at the Department of Anaesthetics, Welsh National School of Medicine, Cardiff.

This appears to have been the first form of mechanical collector built, since, when the Norwegian, Russeltvedt, reported it in 1926, it had then been in use for some years. This form has been further developed by Workman and Holzer (1939), Goto (1951), and Chalmers (1953). Chalmers usually keeps the repetition frequency constant and measures the current due to the sequence of pulses.

The first machine of the second form, described by the German, Matthias, in 1926, employed two semi-cylindrical conductors, electrically insulated from each other but mechanically joined to form a complete cylinder, which was rotated about its axis. The charges induced on the semi-cylinders gave a sine-wave current between them which provided a measure of the electric field. Later variations of this form have often had a fixed conductor or "stator" connected to earth through a high impedance and regularly exposed to and screened from the electric field by means of a suitable "rotor." An alternating voltage, proportional to the field, is developed across the impedance. This form has proved extremely popular, being used for measurements both in the atmosphere and in the laboratory. It has been used recently in an instrument which measures the three components of the electric field (Kasemir, 1951).

It will now be apparent that the principal difference between the two forms of mechanical collector is that the first is a d.c. and the second an a.c. instrument. Chalmers (1953) has shown that by using large conductors in the first form, measurement of the fair-weather field can be obtained without amplification. However, since the present instruments had to be transportable, only a comparatively small conductor could be tolerated and some amplification was therefore necessary. Collectors of the second form were therefore built in order to avoid the difficulties of d.c. amplification.

Collectors of this form have been given a variety of names. Here the term "field mill"—Rangs (c. 1942): "Feldmühle" is used on the ground that its undoubted brevity and uniqueness outweigh the descriptive merit of more cumbersome terms.

3. Review of Field Mills

In the arrangement used by Macky (1937), Trump, Safford, and van de Graaff (1940), Waddel (1948), Clark (1949), Cleveland (1950), von Kilinski (1950), and Cross (1953), the conductor consisted of a circle with alternate sectors removed. A similar set of earthed sectors rotated over them so that the output waveform was approximately triangular. Van Atta *et al.* (1936), Rangs (c. 1942), and Accardi (1952) used a similar arrangement with the sectors shaped to give a sinewave output. Lueder (1943), who was interested in obtaining a very rapid response, used a circular stator with a fixed perforated earthed plate over it and rotated a similar perforated plate, also earthed, between the two. The instrument of Harnwell and van Voorhis (1933) was similar, except that it used sector plates, and instead of the fixed plate being earthed it was connected to a known variable potential, thereby providing a null method of measurement. Malan and Schonland (1950), who were also interested in a very rapid response, used a set of eighteen studs arranged in a circle as their stator and rotated over them a plate with eighteen corresponding holes. By an ingenious elaboration of the sector type, Smith (1954) has devised an instrument which will respond to varying fields up to

VOL. 7 1955

22 kc/s. GOHLKE and NEUBERT varied the exposure of their "stator" by vibrating it up and down through a corresponding hole (1940), or to and fro below the hole (1942). SCHWENKHAGEN (1943) developed a number of models, using many of the methods already described. KIRKPATRICK and MIYAKE (1932), KIRKPATRICK (1932), HENDERSON, GOSS, and ROSE (1935), SCHUCHARD (1935), FELDENKRAIS (1937), THOMAS (1937), NEUBERT (1938), and KASEMIR (1944), used the original cylindrical arrangement of MATTHIAS. GUNN (1932, 1933, 1954) also used this arrangement amongst others.

In order to determine the direction of the field, the alternating current has been rectified by a commutator (KIRKPATRICK and MIYAKE, KIRKPATRICK, GUNN, HENDERSON, GOSS, and ROSE, SCHUCHARD, FELDENKRAIS, THOMAS, WADDEL, CLARK, VON KILINSKI, and CROSS), or by an electronic phase-sensitive detector (CROSS and GUNN, 1954); or the zero has been displaced by adding the output of an auxiliary synchronous generator to the output of the mill (RANGS, SCHWENKHAGEN, VON KILINSKI, and ACCARDI). A deliberate (MALAN and SCHONLAND) or accidental (LUEDER) asymmetry in the output waveform displayed on a C.R.O. has also been used for sign determination, while others have employed entirely independent methods (MATTHIAS, VAN ATTA *et al.*, MACKY, TRUMP *et al.*, GOHLKE and NEUBERT, and KASEMIR). HARNWELL and VAN VOORHIS could determine the sign of the field from the sign of the voltage to be applied to the fixed plate for zero output.

In almost all cases some degree of amplification was necessary prior to rectification or C.R.O. display.

4. Mode of Operation Adopted

There is some advantage in working at a frequency as high as a few hundred cycles per second: for ease of amplification, ease of discrimination against 50 c/s pick-up, and for a number of other reasons discussed in Section 5. In view of this, the cylindrical arrangement is unsuitable because of the inconveniently high rotor speed needed. The vibrating forms have the disadvantage of requiring moderate amounts of power at the operating frequency, particularly if that is high.

In one of the present mills, the "M-type," which was designed to operate only in fair weather, a high operating frequency was obtained by adopting the MALAN and SCHONLAND design with ten studs and a rotor speed of 3,000 r.p.m., while in other, the "S-type," which was designed to operate in all conditions, this was done by using a four-sector design with a rotor speed of 5,000 r.p.m.

To determine the direction of the field, phase-sensitive detection was used, because this is such a convenient way of limiting the bandwidth of the instrument and hence of discriminating against noise generated in the mill and amplifier. In view of the comparatively high frequency of operation, electronic phase-sensitive detection was considered to be more reliable than mechanical commutation.

5. Theory of the Fixed-conductor Field Mill

The theory of the d.c. form of mechanical collector has been treated by CHALMERS (1953) and that of the cylindrical mill by SCHUCHARD (1935). Some aspects of the theory of the fixed conductor, or stator, mill have been considered by DAHL (1951),

but here the matter will be developed further as a guide to the choice of parameter values in design. Two cases will be treated: Case M, where the exposed area of the stator varies sinusoidally (which is approximately true for the MALAN and SCHONLAND arrangement of the M-type mill) and case S, where the exposed area varies according to a triangular waveform (which is approximately the case for the sector arrangement of the S-type mill). The rationalized system of M.K.S. units will be used throughout.

In both cases let the stator have a capacity C and a resistance R to earth (composed of actual components and strays). Let the electric field be F and the exposed area at any time be a with a maximum area A. Let the angular velocity of the exposure-screening cycle be ω. If the exposure of the stator is unity, then the charge induced on it will be given by:

$$q = \varepsilon_0 Fa \qquad \text{and} \qquad q_{\max} = Q = \varepsilon_0 FA$$

In case M a varies sinusoidally. Therefore $a = (A/2)(1 + \sin \omega t)$ and hence $q = (Q/2)(1 + \sin \omega t)$, where t = time. Now this quantity of charge must flow through C and R. Therefore the instantaneous value of the current through C and R is given by

$$i = dq/dt = (\omega Q/2) \cos \omega t$$

and the peak value of i by

$$I = \omega Q/2 = \omega \varepsilon_0 FA/2.$$

The peak voltage across C and R is given by

$$V = IZ = \omega \varepsilon_0 FAZ/2$$

where Z, the impedance of C and R in parallel, is given by

$$Z = R/(\omega^2 C^2 R^2 + 1)^{1/2}$$

Therefore

$$V = \omega \varepsilon_0 FAR/2(\omega^2 C^2 R^2 + 1)^{1/2}$$

This relationship will be falsified if a does not vary sinusoidally and by the fact that C will vary somewhat in synchronism with a. If these effects are small and $\omega^2 C^2 R^2 \gg 1$, then the above equation simplifies to

$$V = \varepsilon_0 FA/2C \qquad (1M)$$

In case S, considering some half-cycle at the end of which the stator is fully exposed, then $a = At/t_p$, where t = time (measured from the start of the half-cycle) and $t_p = \pi/\omega$, the half-period of the exposure-screening cycle.

Therefore $q = q_0 + Q\omega t/\pi$, where q_0 is the charge on the stator at the start of the half cycle,

and

$$i = dq/dt = Q\omega/\pi = \varepsilon_0 FA\omega/\pi.$$

If v is the instantaneous voltage across C and R,

then

$$dv/dt = (1/C)(i - v/R)$$

Integrating with the condition $v = q_0/C$ at $t = 0$ and $v = V$ at $t = \pi/\omega$, and substituting for i, gives

$$V = (\varepsilon_0 FA\omega R/\pi)(1 - \exp(-\pi/\omega CR)) + (q_0/C) \exp(-\pi/\omega CR)$$

VOL. 7 1955

Since in a steady field no d.c. can persist across R, both the charge and the voltage waveform must be symmetrical about zero. Therefore in the steady state the voltage at the end of the half-cycle will be equal and opposite to the voltage at the beginning, i.e., $q_0/C = -V$

Therefore $$V = \frac{\varepsilon_0 FA\omega R(1 - \exp(-\pi/\omega CR))}{\pi(1 + \exp(-\pi/\omega CR))}$$

If $\exp(-\pi/\omega CR)$ is expanded as a series, this reduces to

$$V = \frac{FA}{2C}\left(1 - \frac{\pi^2}{12\omega^2C^2R^2} + \text{higher powers}\right)$$

As in case M, if $\omega^2C^2R^2 \gg 1$, this simplifies to

$$V = \varepsilon_0 FA/2C \tag{1S}$$

Thus in both cases the output voltage is proportional to the electric field and can be made virtually independent of frequency and the resistance of the stator to earth.

As a further guide to the choice of parameter values, consideration must now be given to the errors introduced by the grid current in the first valve of the amplifier, the charge carried by raindrops and the air-earth current.

If the stator is connected directly to the grid of a valve the grid current of which is I_g, then the stator will be at a potential $V_d = I_gR$ with respect to earth. First, this must be small or it will distort the field at the stator so that variations in it will vary the effective exposure. Second, variations in the capacity of the stator due to the movement of the rotor will produce, from this direct voltage, an alternating voltage which is indistinguishable from the signal voltage.

For both cases, if $2\Delta C$ is the range of the capacity variation and ΔV_d the peak value of the alternating voltage which it develops, then ΔV_d cannot exceed $V_d\Delta C/C$ or $I_gR\Delta C/C$. If this is to be small compared with the signal voltage and if the conditions for (IM, IS) are satisfied, then

$$I_gR\Delta C/C < \varepsilon_0 FA/2C \qquad \text{or} \qquad I_gR\Delta C/A < \varepsilon_0 F/2$$

Suppose ΔV_d is to be less than V for a field of 1 V/m, then

$$I_gR\Delta C/A < 4{\cdot}4 \times 10^{-12} \tag{2}$$

The flow of rain and air-earth currents to the stator will be interrupted by the movement of the rotor producing a current flow through C and R composed of an alternating component of the same frequency as that due to the field, superimposed on a direct component. Errors due to the alternating component will be considered first.

In case M for a current density J, the alternating voltage across C and R will be sinusoidal and have a peak value $JAZ/2$. If this is to be small compared with the signal voltage, $\varepsilon_0\omega FAZ/2$, then

$$J/\omega \ll \varepsilon_0 F$$

In case S, if $\omega^2C^2R^2 \gg 1$, then the amount of rain-current that leaks through R during the first half-cycle is negligible, and under these conditions the voltage

across the condenser will be $JAT_p/2C = JA\pi/2C\omega$. This gives the peak to peak value of the voltage developed during the first half-cycle. It can be shown that the peak voltage for any successive cycle is no greater than that developed during the first cycle. Therefore the effects of the rain-current will be small if

$$J/\omega \ll 2\varepsilon_0 F/\pi$$

Thus the effects of vertical currents are inversely proportional to ω, and for a current of 10^{-10} amps/m^2, which would be an upper limit for the air-earth current and which Chalmers (1949) gives as an upper limit for steady rain, the output due to this current can be made less than that due to a field of 1 V/m for both cases if

$$\omega > 6\pi \qquad (3)$$

Since larger rain-current will usually be accompanied by larger fields, any reasonable value of ω will keep the error negligible. However, the conditions assumed above are somewhat ideal, and in practice the error will be lower if the movement of the rotor is too rapid to allow all the drops to penetrate to the stator, or may be higher if intense charging occurs due to the shattering of the drops by the rotor.

Generally the direct component of the rain-current is negligible compared with the grid-current unless either an electrometer valve is used or the stator is unusually large: in both of the present mills a Mullard EF37A, operated with reduced heater and anode voltages, was used for the first stage, giving a grid-current of about 5×10^{-11} amp.

Finally, although the steady effect of rain may be small, individual drops may have a more marked effect. Hutchinson and Chalmers (1951) found that in the absence of point discharge (i.e., for fields less than, say, 500 V/m) the charge on a drop rarely exceeds 3×10^{-14} c. In both cases this would develop a potential of $3 \times 10^{-14}/C$ volts across C. If this is to be less than the peak alternating voltage due to a field of 1 V/m, then

$$3 \times 10^{-14}/C < \varepsilon_0 A/2C \qquad \text{or} \qquad A > 7 \times 10^{-3}\ \text{m}^2 \qquad (4)$$

If the drops are shattered by the rotor, a more stringent condition may have to be imposed. However, this voltage would decay in a period of about $5CR$, so that if the response of the final indicator was long compared to $5CR$, it would not respond to individual drops but only to the average output for rain-current.

6. Design of the Present Instruments

M-type mill

This was required by Chalmers and Mapleson (1955) to provide an accurate and absolute measurement of the earth's electric field in fine weather over the range -250 to $+250$ V/m with a response time of not more than five seconds.

One end plate of a motor alternator was replaced by a *Tufnol* disc into which were built the stator studs. These consisted of 10 0 BA cheese-head screws mounted at equal intervals on a circle of 5·9-cm radius. An earthed aluminium plate covered the surface of the *Tufnol* with a clearance of about 1 mm around each stud. The rotor, 15·2 cm in diameter, and about 1·5 mm thick, was fixed to the motor shaft to give a separation of about 1 mm from the surface of the studs. The studs

VOL. 7 1955

were connected to the grid of an EF37A which was mounted inside the casing and suspended by rubber bands to reduce microphony. It was connected as a cathode follower to isolate the mill from the large capacity of the connecting cable. The alternator output provided a reference voltage for the detector. The phase relation between this and the signal voltage could be varied by turning the rotor on the shaft and by an electrical phase-shift network. The motor was synchronous, so that variations of ω were slight. Two strips of phosphor bronze pinched the shaft to provide suitable earthing for the rotor.

The output of the mill was fed to a two-stage *RC*-coupled negative feedback amplifier with variable gain. Fig. 1 shows the phase sensitive detector, which is

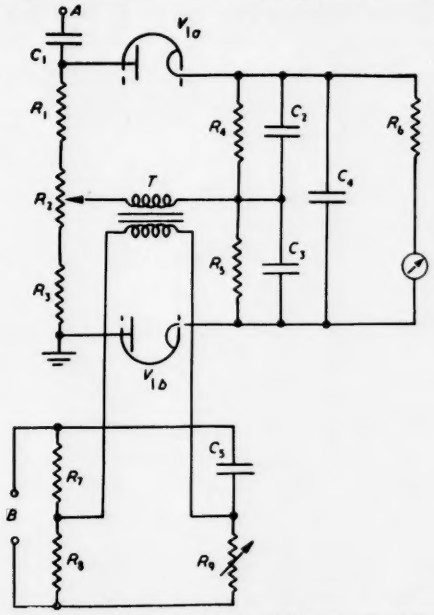

Fig. 1. Phase-sensitive detector and phase-shift network of the M-type mill.

R_1, R_2, R_3,	100 K	C_2, C_3, C_4	0·1 μF
R_4, R_5	1 M	C_5	3 μF
R_6	50 M	V_1	VR 54
R_7, R_8	50 Ω	T	1 : 3 step up
R_9	1 K (max)	A	Signal input from amplifier
C_1	2 μF	B	Reference input from alternator (3 V r.m.s.)

essentially similar to that of JAMES, NICHOLS, and PHILLIPS (1947), and the phase-shift network taken from TERMAN (1943). A field of 250 V/m was made to give an output of 1·5 V d.c. and a galvanometer deflection of 5 cm. The values of the instrument constants were as follows: $\omega = 1{,}000\,\pi$, $A = 7{\cdot}9 \times 10^{-4}$ m^2, $R = 5 \times 10^7$ ohms, $C = 7 \times 10^{-11}$ farad, $\Delta C = 4 \times 10^{-12}$ farad, $I_g = 5 \times 10^{-11}$ amp.

For this mill the conditions for (1M) and those of (3) were adequately met, whilst errors arising from grid current effects would be small. The condition (4) was not satisfied, but as the response time of the final recording instrument was long (one second) compared with $5CR$, individual drops had no appreciable effect.

In its working position the mill was mounted so that the rotor was 45 cm above the ground. This produced a field at the studs which was two to three times greater than that at the ground nearby. With half-hourly calibrations, measurements of field could almost always be relied upon to within $\pm 2{\cdot}5$ V/m over the range -250 to $+250$ V/m.

The S-type mill

Two identical instruments were constructed for investigations on the variations of the earth's electric field by CHALMERS and WHITLOCK (1955). They were required to have a high maximum sensitivity, a good short-period stability, a response time of less than one second, and were to be used in all weather conditions.

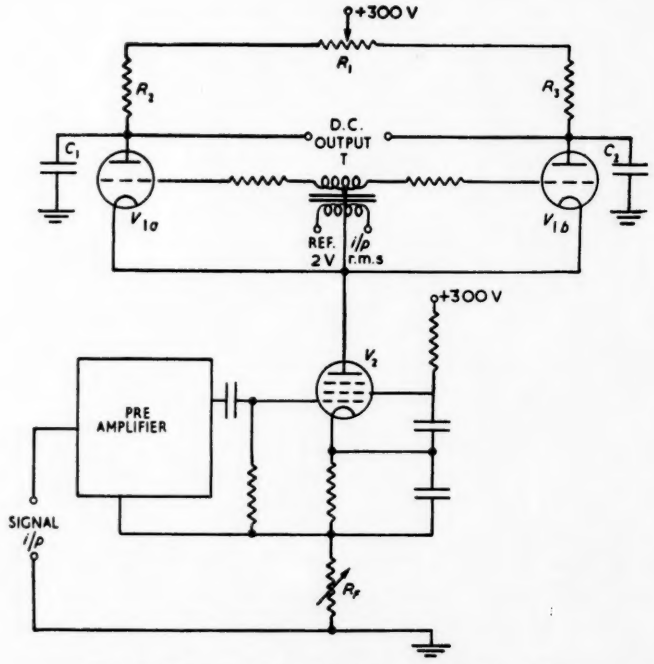

Fig. 2. Phase-sensitive detector of the S-type mill.

R_1	25 K	V_1	ECC 91
R_2, R_3	100 K	V_2	EF 50
C_1, C_2	0·5 μF	T	1 : 3 step up

The upper shaft of a d.c. motor carried the main rotor, which consisted of four 45° sectors of 6·75-cm external diameter and was separated by 3 mm from the lower identical stator. Fixed to the lower shaft was the rotor of a small electrostatic reference generator. Both the output from the stator and that from the reference generator were connected to their appropriate inputs in the electronic equipment by cathode follower stages. The motor and the adjoining valves were supported on anti-vibration mountings. Two small carbon brushes bearing against the upper

VOL. 7 1955

shaft provided suitable earthing for the rotor. In order to prevent any electrical interaction between the reference generator and the stator via the motor-shaft, the generator was electrically isolated from the shaft. All supplies to the mill were d.c., so avoiding any possibility of mains pick-up.

Seventy-five metres of cable connected the mill to a three-stage *RC*-coupled negative feedback amplifier, with step-gain control allowing the use of the mill over a wide range of field strengths. Fig. 2 shows the form of the phase-sensitive detector, which is a modification of that of SCHUSTER (1951). Many of the qualities of Schuster's detector are the result of introducing the high-anode impedance of a pentode in series with switching triodes so that variations in their impedance ($\simeq$7 KΩ) are small compared with the common impedance ($\simeq$1 MΩ). This idea has been extended by including part of the detector in the amplifier feedback loop thereby increasing the value of the common-series impedance and so improving the performance of the detector.

On the maximum sensitivity range the output was 25 V d.c. for a field of 75 V/m, and the corresponding galvanometer deflection was 10 cm. The values of the instrument constants were as follows: $\omega = 660\,\pi$, $A = 6{\cdot}3 \times 10^{-3}$ m^2, $R = 10^8$ ohms, $C = 1{\cdot}2 \times 10^{-10}$ farad, $\Delta C = 7 \times 10^{-12}$ farad, $I_g = 5 \times 10^{-11}$ amp. For this mill the conditions for (1S) and those of (3) were completely satisfied, whilst (2) and (4) were approximately satisfied. Owing to the short response-time of the final indicator (0·1 second) the effects of individual drops, although small, were often apparent. There has been no indication that any appreciable charge generation takes place when the drops are shattered by the rotor.

When an absolute calibration of the field was required, the mill was sunk into the ground with its rotor in the plane of the surface. Under these conditions half-hourly calibrations indicated that drift limited the accuracy of absolute measurement of the field to ± 1 V/m over the range -75 to $+75$ V/m. The fact that the final output noise-level over the range 10 to 0·1 cycles/sec was equivalent to 0·5 V/m indicates the degree of accuracy obtainable for very short-period measurements.

7. Discussion of Errors

(*a*) *Errors arising in the electronic equipment*

In both mills neither the cathode follower nor the main amplifier (nor the electric phase-shifter of the M-type mill) contributed significantly to the total error. The detectors, however, presented greater difficulties.

In the M-type mill, deviation from linearity at mid-scale did not exceed 0·5 per cent of the "full-scale" output. The additional error due to zero drift did not exceed 0·5 per cent of full-scale output with calibration at one-hourly intervals.

In the S-type mill nonlinearity and zero drift due to variations in the characteristics of the detector triodes were successfully made negligible by the method described in Section 6. Appreciable errors did, however, arise from the dependence of the operation of the circuit on the amplitude of the reference voltage. This was believed to be due to unsuitability of the transformer used, rather than to any fundamental defect in the design of the circuit. In the final arrangement, deviation from linearity at mid-scale did not exceed 1 per cent of full-scale output.

(*b*) *Errors arising in the field mills proper*

The field mill itself has an essentially linear field-voltage characteristic, and with the values of ω, C, and R employed, variations of ω did not contribute significant errors. The negligible effects of the air-earth current and rain-currents and the small effect of grid-current in the first stage have already been discussed in Section 5. Thus the only serious sources of error were the spurious outputs which occurred when the mills were fully screened. So long as these outputs were steady, they

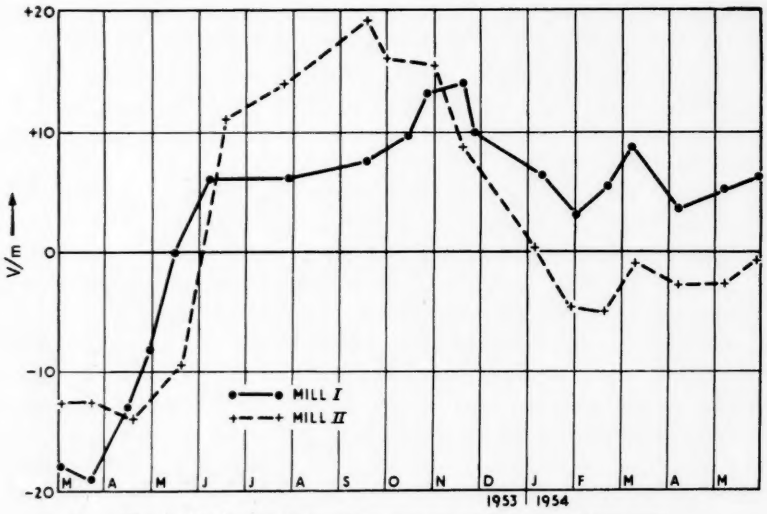

Fig. 3. Variation of spurious output with time—*S*-type mill.

could be balanced out, but variations in them contributed to zero drift in the final measurements. Such outputs have been noted by a number of workers and a number of sources suggested.

If there is a contact potential between the stator and the rotor, a charge will be induced on the stator which will vary at the operating frequency and so produce an output which will be indistinguishable from that due to an external field. This source has been mentioned by Rangs (c. 1942), Lueder (1943), and Kasemir (1944), and certainly existed and was very variable in both the present instruments when the stators and rotors were of brass or aluminium. By using nickel-plated surfaces in the M-type mill, this spurious output was reduced from about 300 V/m to about 50 V/m, and in the S-type mill with chromium-plated surfaces the output varied in the manner shown in Fig. 3.

Precisely similar effects will be obtained if a potential difference exists across the earthing contact of the rotor. This has been mentioned by Henderson, Goss, and Rose (1935), by Lueder (1943), and by Cross (1953), but evidently did not occur in either of the present mills, since the provision of additional temporary earthing contacts, composed of different pairs of metals, did not alter the outputs.

Stray charges on the surfaces of any insulators near the stator will induce a charge on it which will be modulated by the rotor and so produce a spurious output.

VOL. 7 1955

This source has been mentioned by LUEDER (1943), and probably occurred in the M-type mill, where it seems likely that it was the source most susceptible to variation. In the S-type mill all insulators were successfully screened from the test plate and rotor, and consequently caused no spurious output.

(c) *Errors arising in the calibration*

For routine calibration, metal boxes were constructed which fitted onto the faces of the mills in such a way that they fully excluded the earth's field and always had the same positions relative to the stators. The boxes could be earthed to provide zero field or raised to a known potential to provide a calibration field. The only likely source of error would therefore be contact potential between the stator and the box. Experimental checks showed that this effect was small for both mills, but might prove appreciable if the box were of a different metal and was close to the stator.

8. IMPROVEMENT OF THE PRESENT DESIGNS

From the foregoing discussion it will be apparent that the only significant errors arose from zero drift and nonlinearity in the phase-sensitive detector and from zero drift due to changes in the contact potential and stray charges on the insulators at the mill proper.

The errors in the detector could be made of negligible importance if, instead of applying negative feedback over only part of the circuit, it were applied over the whole instrument: making the output of the detector apply a field to the mill which tended to oppose the external field. This suggestion is now being carried out by ADAMSON at Durham.

This could well be combined with using a mill of the LUEDER or HARNWELL and VAN VOORHIS type, in which all insulating surfaces can readily be screened. The fixed plate could then be connected to the detector output instead of to earth. Finally, the stator, rotor, fixed plate, and calibrating box should all be well plated with nickel or chromium or possibly made of stainless steel (as was tried recently by CROSS).

Acknowledgments—The authors' thanks are due to Dr. J. A. CHALMERS for advice and encouragement and to the Durham Colleges Research Fund for grants for the equipment; also to the Durham Colleges Standing Committee for Research Awards for a research studentship for one of us (W. W. M.) and to the Ministry of Education for a Further Education and Training Grant for the other (W. S. W.).

REFERENCES

ACCARDI, L.	1952	*Geofis. pura. appl.* **22,** 84
CHALMERS, J. A.	1953	*J. Atmosph. Terr. Phys.* **4,** 124
CHALMERS, J. A., and MAPLESON, W. W.	1955	*J. Atmosph. Terr. Phys.* **6,** 151
CHALMERS, J. A., and WHITLOCK, W. S.	1955	To be published
CLARK, J. F., Jr.	1949	*Instruments* **22,** 1007
CLEVELAND, H. W.	1950	*J. Soc. Mot. Pict. Engrs.* **55,** 37
CROSS, A. S.	1953	*Brit. J. Appl. Phys.*, Supp. No.2, S47
DAHL, H.	1951	*On the Sensitivity of Generating Electrostatic d.c. Voltmeters.* Chr. Michelsens Institutt, Bergen, Norway.

FELDENKRAIS, M.	1937	*J. Phys. Radium* **8,** 383
GOHLKE, W., and NEUBERT, U.	1940	*Z. tech. Phys.* **21,** 217
	1942	*Z. tech. Phys.* **23,** 70
GOTO, M.	1951	*J. Geomagn. Geoelect.* **3,** 22
GUNN, R.	1932	*Phys. Rev.* **40,** 317
	1933	U.S. Patent 1,919,215
	1954	*Rev. Sci. Instr.* **25,** 432
HARNWELL, G. P., and VAN VOORHIS, S. N.	1933	*Rev. Sci. Instr.* **4,** 540
HENDERSON, J. E., GOSS, W. H., and ROSE, J. E.	1935	*Rev. Sci. Instr.* **6,** 63
HUTCHINSON, W. C. A., and CHALMERS, J. A.	1951	*Quart. J. R. Met. Soc.* **77,** 85
JAMES, H. M., NICHOLS, N. B., and PHILLIPS R. S.	1947	*Theory of Servomechanisms,* (McGraw-Hill, New York) p. 111
KASEMIR, H. W.	1944	*Die Zylinderfeldstärkenmühle mit Kleinen Segmenten,* (Flugfunkforschungsinstitut Oberpfaffenhofen E. V. Aussenstelle Gräfelfing.)
	1951	*Tellus* **3,** 240
KIRKPATRICK, P.	1932	*Rev. Sci. Instr.* **3,** 430
KIRKPATRICK, P., and MIYAKE, F.	1932	*Ibid.* **3,** 1
LEUDER, H.	1943	*Met. Z.* **60,** 340
MACKY, W. A.	1937	*Terr. Magn. Atmos. Elect.* **42,** 71
MALAN, D. J., and SCHONLAND, B. F. J.	1950	*Proc. Phys. Soc. Lond.,* B **63,** 402
MATTHIAS, A.	1926	*Electizitätswirtschaft* **25,** 297
NEUBERT, U.	1938	*Z. Phys.* **110,** 334
RANGS, –	c. 1942	"Gerat fur Messung der luftelektrischen Feldstarke". Z.W.B. Nr. 699. Ministry of Supply ref. IIB/6022
RUSSELTVEDT, N.	1926	"Beiheft zur Jb. norweg. met. Inst. für 1925" p. 11
SCHUCHARD, E. A.	1935	University of Washington Engineering Experiment Station, Bulletin No. 80, Seattle.
SCHUSTER, N. A.	1951	*Rev. Sci. Instr.* **22,** 254
SCHWENKHAGEN, H.	1943	*Elektrizitätswirtschaft* **42,** 120
SMITH, L. G.	1954	*Rev. Sci. Instr.* **25,** 510
TERMAN, F. E.	1943	*Radio Engineers' Handbook,* (McGraw-Hill, New York), p. 949
THOMAS, M. A.	1937	*Rev. Sci. Instr.* **8,** 448
TRUMP, J. G., SAFFORD, F. J., and VAN DE GRAAFF, R. J.	1940	*Rev. Sci. Instr.* **11,** 54
VAN ATTA, L. C., NORTHRUP, D. L., VAN ATTA, C. M., and VAN DE GRAAFF, R. J.	1936	*Phys. Rev.* **49,** 761
VON KILINSKI, E.	1950	*Z. Met.* **4,** 77
WADDEL, R. C.	1948	*Rev. Sci. Instr.* **19,** 31
WORKMAN, E. J., and HOLZER, R. E.	1939	*Rev. Sci. Instr.* **10,** 160

VOL. 7 1955

Journal of Atmospheric and Terrestrial Physics, 1955, Vol. 7, pp. 73 to 79. Pergamon Press Ltd., London

The auroral *E*-layer ionization and the auroral luminosity

A. OMHOLT
The Auroral Observatory, Tromsö, Norway

(*Received* 3 *February* 1955)

ABSTRACT

The photon emission within the negative nitrogen bands emitted from aurorae in zenith and the maximum electron density in the *E*-layer are measured simultaneously. A correlation is found between these two quantities. From the observations the recombination coefficient in the *E*-layer during aurorae is found to be greater than 10^{-7} cm^3 sec^{-1}. In medium to strong aurorae the mean electron density is found to be 2 to 10 . 10^5 electrons cm^{-3}. The radio echoes in the V.H.F.-band during aurorae are briefly discussed.

1. INTRODUCTION

The ionization process responsible for the increase in the *E*-layer ionization during magnetic storms and aurorae (designated as the E_a-layer) is probably identical with the primary excitation process causing the auroral luminosity. Attempts have been made (SEATON, 1954; OMHOLT, 1954) to deduce the electron density in the *E*-layer during aurorae from the absolute intensity of the negative nitrogen bands in the aurora (N_2^+, $B^2\Sigma_u^+ - X^2\Sigma_g^+$). The excitation of these bands is probably also an ionization process, namely

$$N_2(X^1\Sigma_g^+) + X \rightarrow N_2^+(B^2\Sigma_u^+) + e + X \tag{1}$$

where X is the incoming particle causing the aurorae.

This gives η(N.G.) N_2^+ molecules in the $B^2\Sigma_u^+$ state per sec per cm^3, and the same number of free electrons. The lifetime of this excited state is probably of the order of 10^{-8} sec, and collisional deactivation should not take place. η(N.G.) then give the photon emission per sec per cm^3 in the first negative band system of nitrogen from the aurora.

A number of other ionization processes may be assumed. The relative importance of these are not known. The low intensity of the OII and NII lines in the auroral spectrum (VEGARD and KVIFTE, 1951) indicates, however, that the ionization rate of these atoms is low.

We suppose the total electron production $\eta(e)$ to be at least proportional to η(N.G.):

$$\eta(e) = k\eta(\text{N.G.}) \tag{2}$$

where k is greater than 1, and we get for the electron density $n(e)$:

$$\frac{dn(e)}{dt} = k\eta(\text{N.G.}) - \alpha_{\text{rec}}\, n(e)^2 \tag{3}$$

α_{rec} being the recombination coefficient. Putting $\frac{d}{dt}\, n(e) = 0$ we have

$$n(e) = \left(\frac{k\eta(\text{N.G.})}{\alpha_{\text{rec}}}\right)^{1/2} \tag{4}$$

The photon emission per sec per cm^2 column of the aurora, π(N.G.), is given by

$$\pi(\text{N.G.}) = \int_r \eta(\text{N.G.})\, dr = l_0 \eta_{\max}(\text{N.G.}) \tag{5}$$

where r is the distance in radial direction from the observation point, $\eta_{\max}$(N.G.) is the photon emission in the maximum intensity point of the aurora, and l_0 a quantity defined by equation (5). If we, as an approximation, assume k and α_{rec} to be independent of r within the aurora, $\eta_{\max}$(N.G.) gives the photon emission in the point of maximum electron density due to the ionization process (1). The maximum electron density $n_{\max}(e)$ determines a critical penetration frequency f_0 given by

$$n_{\max}(e) = 1{\cdot}24 \,.\, 10^4 f_0{}^2 \qquad (f_0 \text{ in Mc/sec}) \tag{6}$$

and we get from equations (4) and (5)

$$\pi(\text{N.G.}) = 1{\cdot}54 \,.\, 10^8 \frac{l_0 \alpha_{\text{rec}}}{k} f_0{}^4 = 1{\cdot}54 \,.\, 10^8 \beta f_0{}^4 \tag{7}$$

where $\beta = \dfrac{l_0 \alpha_{\text{rec}}}{k}$

It is apparent from this that simultaneous measurements of π(N.G.) and of f_0 may give us informations about the recombination coefficient α_{rec}. Measurements have been made and the results are given in this paper. The observations were made at the Auroral Observatory, Tromsö, lying close to the auroral zone. The observations treated in the following sections are therefore of high-latitude aurorae.

VOL. 7 1955

2. The Experimental Equipment

The auroral form was by a lens focused on a small circular opening on the front of a RCA 931–A photomultiplier. The area of the sky covered by the opening was four degrees in diameter, and the instrument was always directed towards zenith. The time-constant of the photomultiplier circuit was about one sec. The current was amplified by a balanced valve voltmeter, the current from which was measured with a μA meter. Before the lens was placed an interference filter with maximum transmission for 4280 Å. The current was read with short intervals (1–3 minutes). Ionospheric soundings were made with 15-minute intervals during the time of observation, and the P'-f–curve were recorded at the observatory.

The sensitivity of the photometer was determined by a standard lamp constructed in the following way: An opal glass of size 18 cm in diameter was enlighted from behind by a small lamp through a small opening in a ground glass. The current through the lamp was controlled by a mA meter. The output from the opal glass was found to be constant over the whole surface. The emission of the lamp in erg sec^{-1} cm^{-2} Å^{-1} sterrad^{-1} was measured before and after the series of auroral observations, at the Physical Institute of Oslo University. By placing this lamp before the lens of the photometer we get this illuminated in the same way as by the aurora. Knowing the transmission profile of the filter and the sensitivity curve of the multiplier, we can easily calculate the intensity of any aurora in erg cm^{-2} sec^{-1}.

The total photon emission within the first negative nitrogen band system is given by

$$\pi(\text{N.G.}) = \pi(4278)\,\frac{\sum_{v',v''} I(v', v'')/h\nu(v', v'')}{\sum_{v',v''} T(v', v'')I(v', v'')/h\nu(v', v'')} \tag{8}$$

where $\pi(4278)$ is the photon emission from the aurora passing the filter. $I(v', v'')$ and $\nu(v', v'')$ are the relative intensities and the frequencies of the bands, and $T(v', v'')$ is the transmission of the interference filter for the (v', v'')-band. Other auroral emissions passing the filter are very weak, and the 4278(0–1), 4236(1–2), and 4200(2–3) bands are the only ones taken into account. Using the values published by BATES (1949, Tables 6 and 20), we find

$$\pi(\text{N.G.}) = 5\,.\,\pi(4278) \tag{9}$$

Measurements were made only during very clear nights, with no moon, thus avoiding errors from false light.

3. The Observations

The photon emission of the first negative nitrogen band system is measured within a small area in zenith. What we need to deduce from the ionospheric records is the electron density in the E_a-layer in this same point. The echo patterns during magnetic storms are, however, often very complex, and we cannot always decide whether the reflections come exactly from zenith or from some ionospheric irregularities close by. From the ionospheric records are deduced critical frequencies only in cases when unambiguous group retardation near the critical frequency appears. Records showing reflection from the E_a-layer, but no group retardation, were rejected. The records giving critical frequencies have been divided into two groups:

(a) Those showing multiple reflections from the E_a-layer or an F-layer on frequencies above the critical frequency for the E_a-layer. This is taken as an indication of a reflection point being in zenith.

(b) Those showing a single reflection from the E_a-layer only, thus giving no information about the position of the reflection point.

The results of the observations are given in Figs. 1 and 2. In Fig. 1 is given a typical set of records during a couple of hours when critical frequencies f_0 could be deduced from all the ionospheric records. In Fig. 2 are given the values of f_0 measured and the values of π(N.G.) in zenith measured simultaneously.

4. Discussion of the Observations

Although a considerable scatter appear in the points observed, Fig. 2 gives a strong indication of the validity of equation (7). This equation is satisfied by the straight line drawn in Fig. 2, when we put $\beta = l_0\alpha_{\text{rec}}/k = 0{\cdot}28$. There seem to be no principal differences between the observations belonging to the two different groups (a) and (b). In case (b), however, the aurora is usually somewhat stronger than in case (a). This will give a denser ionosphere and probably a stronger

absorption, thus no multiple reflections are observed. The considerable scatter in the points observed is to be expected from equation (7), as k, l_0, and α_{rec} may vary from time to time. In deducing equation (7) we also assumed $\frac{d}{dt} n(e) = 0$, which is not always valid. Dividing the observations in two sub-groups, with $\frac{d}{dt} n(e) < 0$ and > 0 we find, however, no significant difference between the two groups. This

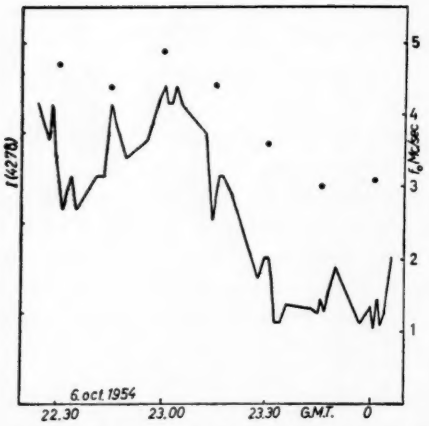

Fig. 1. The variation of the relative intensity $I(4278)$ of the negative nitrogen bands (drawn line) emitted from aurorae in zenith and the critical frequency f_0 of the E_a-layer (points) in Tromsö.

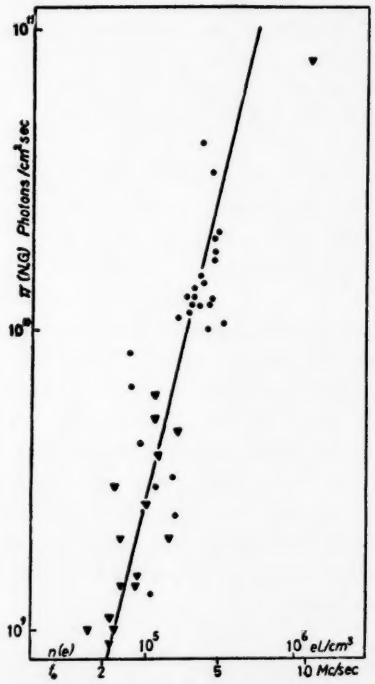

Fig. 2. The critical frequency f_0 of the E_a-layer against the photon emission π(N.G.) of the negative nitrogen bands from the aurora in zenith.
▼ group (a), ● group (b).

shows that the neglect of $\frac{d}{dt} n(e)$ is not important in explaining the scatter of the points observed. The value $\beta = 0{\cdot}28$ seems to represent the mean values of all the observations. From the auroral luminosity curves published by HARANG (1946) we find l_0 to be 25–30 km for a medium auroral arc in a height of 110 km (l_0 given by equation (5)). Adopting 28 km for l_0, we get $\alpha_{rec} = 10^{-7}\, k$ cm^3 sec^{-1}. Now we must suppose k to be greater than 1 (we have probably $1 < k < 2$) and we thus get $\alpha_{rec} > 10^{-7}$ cm^3 sec^{-1}.

This is a somewhat higher value than usually accepted for the normal E-layer, which is 1 to 3 . 10^{-8} cm^3 sec^{-1} (MITRA and JONES, 1954). This value is, however, valid only for daylight conditions, with photon ionization. The recombination

VOL. 7 1955

coefficient for the E-layer region (MITRA and JONES, 1954) is most probably given by

$$\alpha_{\text{rec}} = \frac{1}{N^+} \sum_r \alpha_{\text{Dr}} N(X_r Y_r^+) \tag{10}$$

where α_{Dr} is the coefficient of dissociative recombination of a molecule $X_r Y_r$, $N(X_r Y_r^+)$ is the concentration of its positive ion, and N^+ the total concentration of positive ions. As the relative concentration of the different positive ions may well be different in the two cases (photon and corpuscular ionization), we may easily explain the different values of α_{rec}.

The values of typical auroral intensities given in an earlier paper (OMHOLT, 1954) are confirmed by the new measurements, though they may probably be increased with about 50 per cent. The earlier calculated electron densities are, however, too great, as l_0 as well as α_{rec} were then underestimated.

The strongest auroral band measured during this series of measurements gave a photon emission of $4 \cdot 10^{11}$ photons $\text{cm}^{-2}\ \text{sec}^{-1}$. This is probably very near the upper limit of auroral luminosities. An extrapolation of the straight line in Fig. 2 to this value of π(N.G.) gives $f_0 = 11$ Mc/sec, or, allowing for the scatter of the observations, $f_0 = 15$ Mc/sec as an upper limit of the critical frequencies of the E_a-layer.

5. Auroral Electron Densities and Radio Reflections

The photon emission from medium to strong aurorae overhead is found to be 2 to $10 \cdot 10^{10}$ photons $\text{cm}^{-2}\ \text{sec}^{-1}$. From Fig. 2 we deduce critical frequencies of the corresponding E_a-layer ranging from 4 to 9 Mc/sec, allowing for the scatter of the observations, or an electron density ranging from 2 to $10 \cdot 10^5$ electrons cm^{-3}. This is in agreement with the observations in Tromsö on 41 Mc/sec (HARANG and STOFFREGEN, 1940) with 5-kW pulse effect, and on 35 and 74 Mc/sec (HARANG and LANDMARK, 1954) with 25-kW pulse effect. With antennas vertically directed against very intense aurorae, no indications of echoes within the range of the main auroral luminosity were found.

It should be pointed out, however, that the values of electron densities given here are mean values over a considerable volume of the aurora. Aurorae showing complex structure may include small volumes of considerably higher electron densities.

Radio echoes in the V.H.F.-band during aurorae are reported by several investigators. Echoes on 106 Mc/sec are reported by CURRIE, FORSYTH, and VAWTER (1953). To explain these echoes as critical reflections from small volumes of intense ionization will require electron densities in these of about $1{\cdot}4 \cdot 10^8$ el./cm^3. This is more than one hundred times the mean electron density in ordinary medium to strong aurorae. The photon emission required to explain this electron density is greater than 10^4 times the mean photon emission measured. Though hard to believe, this mechanism of echo reflection cannot be finally rejected, as the echoes are reported to appear only when the aurorae show a clear ray structure. Details of this structure need further investigation.

The observations of BULLOUGH and KAISER (1954) are by them explained as direct, critical reflection from an auroral arc. Using a frequency of 74 Mc/sec, this

seems hardly possible, as this will require an electron density of $7 \cdot 10^7$ el./cm^3 or a photon emission of 10^{15} photons/cm^3 sec in parts of an auroral arc. The auroral electron densities given in this paper are, however, not in conflict with the mechanisms of partial reflection (scatter) used for explaining radio echoes from aurorae.

An alternative explanation of the V.H.F.-echoes during aurorae is given by HARANG and LANDMARK (1954), according to which the V.H.F.-echoes are explained as indirect back-scatter from the ground, at low angles via an E_a-layer of patchy character. The electron density required for such a mechanism is about $2 \cdot 10^6$ el./cm^3 (on 74 Mc/sec). This value is in better agreement with the observations reported in this paper.

6. VARIATION OF β WITH THE VIRTUAL HEIGHT

The value of $\beta = l_0 \alpha_{rec}/k$ can be deduced from each observation by equation (7). We must expect that α_{rec}, l_0, and k, and thus β, will vary with the height of the E_a-layer. Although a considerable scatter appears in the results, there seems to be an increase in β with increasing virtual reflection height h'. The mean values of β, β_0, for three groups of h', and the mean value of $|\beta_n - \beta_0|$ are given in Table 1, columns 3 and 4. No variation in $n(e)$ with the virtual height h' could be found. The possible increase in β with increasing h' is probably due to the increasing value of l_0 with increasing height (HARANG, 1946).

VOL. 7 1955

Table 1

Mean values of β for different groups of virtual reflection heights h

Virtual height h'	*Number of observations*	*Mean values of* $\beta = \beta_0$	*Mean value of* $\lvert\beta_n - \beta_0\rvert$
98–107	12	0·19	0·07
108–117	15	0·25	0·12
118–127	11	0·38	0·24

To derive α_{rec} by the usual methods used for eclipses, sunset, and sunrise, i.e., by measuring the variation of $n(e)$ versus time and then to use equations (3) and (5), seems to be difficult for auroral ionization, as k, α_{rec}, and l_0 vary strongly with time.

Acknowledgments—The author is greatly indebted to Professor L. HARANG for discussions, and to chief scientist F. LIED and Mr. S. SKRIBELAND, head of the Wave Propagation Bureau at the Norwegian Defence Research Establishment, for valuable assistance in the interpretation of the ionospheric records. He is also indebted to the Norwegian Research Council for Science and the Humanities and to Kr. Birkelands Fund and Norsk Hydros Fund for financial support.

References

Bates, D. R.	1949	*Proc. Roy. Soc.* **A196,** 217
Bullough, K., and Kaiser, T. R.	1954	*J. Atmosph. Terr. Phys.* **5,** 189
Currie, B. W., Forsyth, P. A., and Vawter, F. E.	1953	*J. Geophys. Res.* **58,** 179
Harang, L.,	1946	*Geofys. Publ.* **16,** No. 6
Harang, L., and Landmark, B.	1954	*J. Atmosph. Terr. Phys.* **4,** 322
Harang, L., and Stoffregen, W.	1940	*Zz. f. Hochfrequenztech.* **55,** 105
Mitra, A. P., and Jones, R. E.	1954	*J. Geophys. Res.* **59,** 391
Omholt, A.	1954	*J. Atmosph. Terr. Phys.* **5,** 243
Seaton, M. J.	1954	*J. Atmosph. Terr. Phys.* **4,** 285
Vegard, L., and Kvifte, G.	1951	*Geofys. Publ.* **18,** No. 3

DL.
955

Journal of Atmospheric and Terrestrial Physics, 1955, Vol. 7, pp. 80 to 89. Pergamon Press Ltd., London

Untersuchung des Tagesganges der kosmischen Ultrastrahlung mit einer großen Ionisationskammer

(Studies on daily variations of cosmic radiation with a large ionization chamber)

A. SITTKUS
Phys. Institut der Universität Freiburg i. Br.

(*Received* 4 *November* 1954)

ABSTRACT

Studies of the daily variations of cosmic radiations in a shielded ionization chamber of 60-cm diameter and 180-cm length. The results of abnormal daily variations are discussed.

Die kosmische Ultrastrahlung (U.S.) zeigt einen sonnentäglichen Gang mit einer Amplitude von einigen Promille. Da durch die statistisch bedingte Meßunsicherheit der gebräuchlichen Apparaturen und zum Teil auch durch reelle unregelmäßige Änderungen der Strahlung Schwankungen der in einer Stunde gemessenen Intensität bis etwa 1% hervorgerufen werden, ist zur Feststellung des Tagesganges eine Summierung vieler Einzeltage nötig. Mit diesem Verfahren wurden zahlreiche Untersuchungen des sonnentäglichen Ganges gemacht. Es zeigte sich dabei, daß der Tagesgang eine sehr komplizierte Erscheinung ist, bei der viele Faktoren, wie eine mögliche Anisotropie der primären Weltraumstrahlung, die Einwirkung eines ev. vorhandenen Magnetfeldes der Sonne, erdmagnetische und atmosphärische Einflüsse eine Rolle spielen, ohne daß bisher eine einwandfreie Zergliederung der verschiedenen Anteile möglich war (Literatur bei WILSON, 1952). Nun fanden SEKIDO und YOSHIDA (1950), daß gelegentlich bei magnetischen Stürmen unmittelbar nach der Störung ein verstärkter Tagesgang mit Amplituden bis über 10 Promille auftritt, der in den Registrierungen direkt zu erkennen ist. Damit war zum ersten Mal die Möglichkeit gegeben, eine besondere Klasse von Tagesgängen zu isolieren und die Bedingungen des Auftretens zu untersuchen. Die japanischen Forscher nahmen auf Grund der wenigen direkt beobachteten Fälle an, daß bei jeder magnetischen Störung, gekennzeichnet durch den Verlauf der erdmagnetischen Komponenten oder einen charakteristischen Abfall der U.S.-Intensität, Tagesgänge mit anormaler Amplitude und anormalem Verlauf auftreten und führten mit dieser Annahme eine Analyse des Tagesganges bei magnetischen Störungen durch. Sie erhielten im statistischen Mittel eine Vergrößerung der Tagesgangamplituden und eine Verlagerung des zeitlichen Eintretens der Extremwerte. Unabhängig davon fanden EHMERT und SITTKUS (1951) mit Apparaturen großer Meßgenauigkeit (Ionisationskammer mit statistischer Streuung des Stundenmittels von etwa 1·5 Promille und Zählrohrkoinzidenzapparatur mit 6 Promille Schwankung) mehrere Fälle des Auftretens von *abnormalen Tagesgängen* (*A.T.G.*).* Eine vorläufige Analyse zeigte, daß es sich bei diesen Effekten um weltweite Erscheinungen handelt, deren Verlauf an die

* Inzwischen sind A.T.G. auch von ELLIOT und DOLBEAR (WILSON, 1952) beobachtet worden.

VOL. 7 1955

Ortszeit gebunden ist. Weiter ergab sich, daß das Auftreten von A.T.G. nicht immer mit deutlichen magnetischen Störungen verknüpft ist. Es schien daher nötig, unabhängig von irgendwelchen Annahmen über die Ursache, die Tage mit A.T.G. allein aus den Registrierungen der U.S. auszusuchen und dann eine Analyse dieses Effektes zu versuchen. Da für das einwandfreie Erkennen der A.T.G. eine möglichst große Meßgenauigkeit der Apparatur vorteilhalft ist, wurden für die folgende Untersuchung dieser Erscheinung nur die Dauerregistrierungen einer in Freiburg aufgestellten Ionisationskammer benutzt.

Die Registrierungen der Ultrastrahlung wurden in Freiburg i. Br. (geogr. Breite 48° N, geogr. Länge 8° E, geom. Breite 49° N, Höhe 240 m über N.N.) im Turm der Universität durchgeführt. Gemessen wird die Ionisation in einer 500 l. Kammer von 60 cm Durchmesser und 180 cm Länge, gefüllt mit 8 atü Stickstoff, hinter 105 g/cm² (75 g/cm² Eisen + 30 g/cm² Schwerspat) Panzer. Dabei wird der Hauptteil des Ionenstroms durch eine kleine Gegenkammer, die mit Ra-γ-Strahlung bestrahlt wird, kompensiert und die verbleibende Abweichung mit Hilfe eines Einfadenelektrometers kontinuierlich auf 10 cm breitem Film bei 8 cm Vorschub pro Stunde registriert. Bei dieser Art der Registrierung lassen sich größere Hoffmann'sche Stöße erkennen und ihre Extraionisation von der Gesamtionisation abziehen. Auf diese Weise können Stöße nicht als pseudostatistische Schwankungen in Erscheinung treten. Die Abweichungen des Ionenstromes vom Kompensationsstrom werden stündlich ausgewertet und als mittlere Abweichung von einem festen Bezugswert in Promille erhalten. Die statistische Streuung des Stundenmittels wurde zu etwa 1·5 Promille bestimmt. Aus einer längeren Meßserie wurde der Einfluß der meteorologischen Faktoren durch 4-fach-Korrelationsrechnung zu −0·91 Promille/mb luftdruckänderung, zu −0·38 Promille/10 m Höhenänderung der 96 mb-Fläche und zu +0·18 Promille/10 m Abstandsänderung der 96 mb-von der 225 mb Fläche berechnet. Mit diesen Werten wurde eine Reduktion der gemessenen Stundenwerte auf gleiche Werte des Luftdruckes, der 96 mb-Fläche und des Abstandes der 96 von der 225 mb-Fläche durchgeführt. Dabei wurde die Barometereffektkorrektur nach den stündlichen Registrierungen eines Aneroidbarographen vorgenommen, so daß ein Tagesgang des Luftdruckes nicht in den Tagesgang der U.S. eingehen kann. Für die 96 mb und die 225 mb-Fläche standen aus der Wetterkarten des deutschen Wetterdienstes für Freiburg nur je ein Wert täglich zur Verfügung. Die Korrektur der einzelnen Stundenwerte konnte deshalb nur mit linear interpolierten Werten gemacht werden. Dadurch kommt in die Einzelwerte eine Unsicherheit herein, die aber auch in Extremfällen 5 Promille nicht überschreiten wird. Außerdem wird bei dieser Art der Korrektur der Tagesgang der Druckflächen nicht auskorrigiert, so daß die ermittelten Tagesgänge der U.S. Effekte des Tagesganges der 96 mb-Fläche und der Schichtdicke zwischen der 96 mb und der 225 mb-Fläche voll enthalten (Wilson, 1952). Aus der laufenden Auftragung der vollständig korrigierten Stundenwerte wurden dann diejenigen Tage als A.T.G.-Tage ausgesucht, die einen deutlich erkennbaren regelmäßigen Tagesgang mit Maximum um Mittag aufwiesen, und in 3 Klassen eingeteilt. Klasse 1 enthält die zum Teil unsicheren Fälle mit einer maximalen Amplitude unter 7 Promille. Diese Tage wurden zu den Rechnungen im allgemeinen nicht benutzt. Klasse 2 enthält die Tage mit

Amplituden zwischen 7 und 10 Promille und Klasse 3 die wenigen Fälle mit Effekten über 10 Promille. Auch bei den Tagen der Klassen 2 und 3 ist die Sicherheit der Einordnung als A.T.G. durch Schwankungen der Strahlung teilweise beeinträchtigt, doch gaben unabhängige Auswertungen gleiche Ergebnisse, sodaß die Sicherheit der Bestimmung zu etwa 90% angesetzt werden darf.

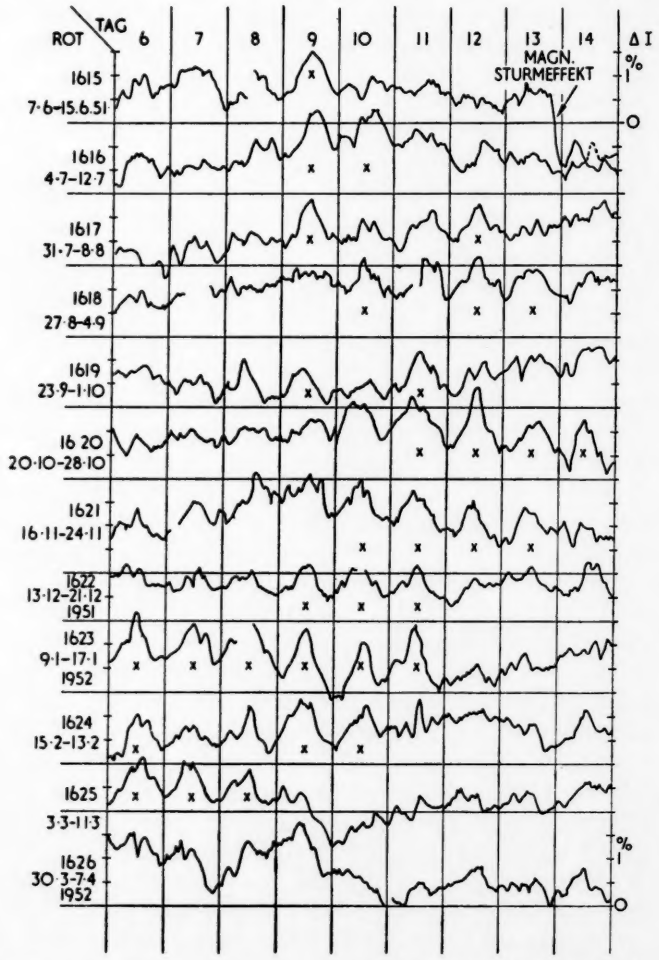

Fig. 1. Beispiele für das Auftreten ausgeprägter Tagesgänge in den Registrierungen einer gepanzerten Ionisationskammer.
(Records of a shielded ionization-chamber: Examples for the occurrence of pronounced daily variations.)

Die Untersuchung der 40 Registriermonate von Dezember 1949 bis März 1953 ergab 189 deutlich erkennbare A.T.G.-Tage. Beispiele für solche Tage sind in Fig. 1 dargestellt (s. auch A. EHMERT und A. SITTKUS, 1951).

Aus der Darstellung ist zu erkennen, daß der Effekt bevorzugt in Gruppen

VOL. 7 1955

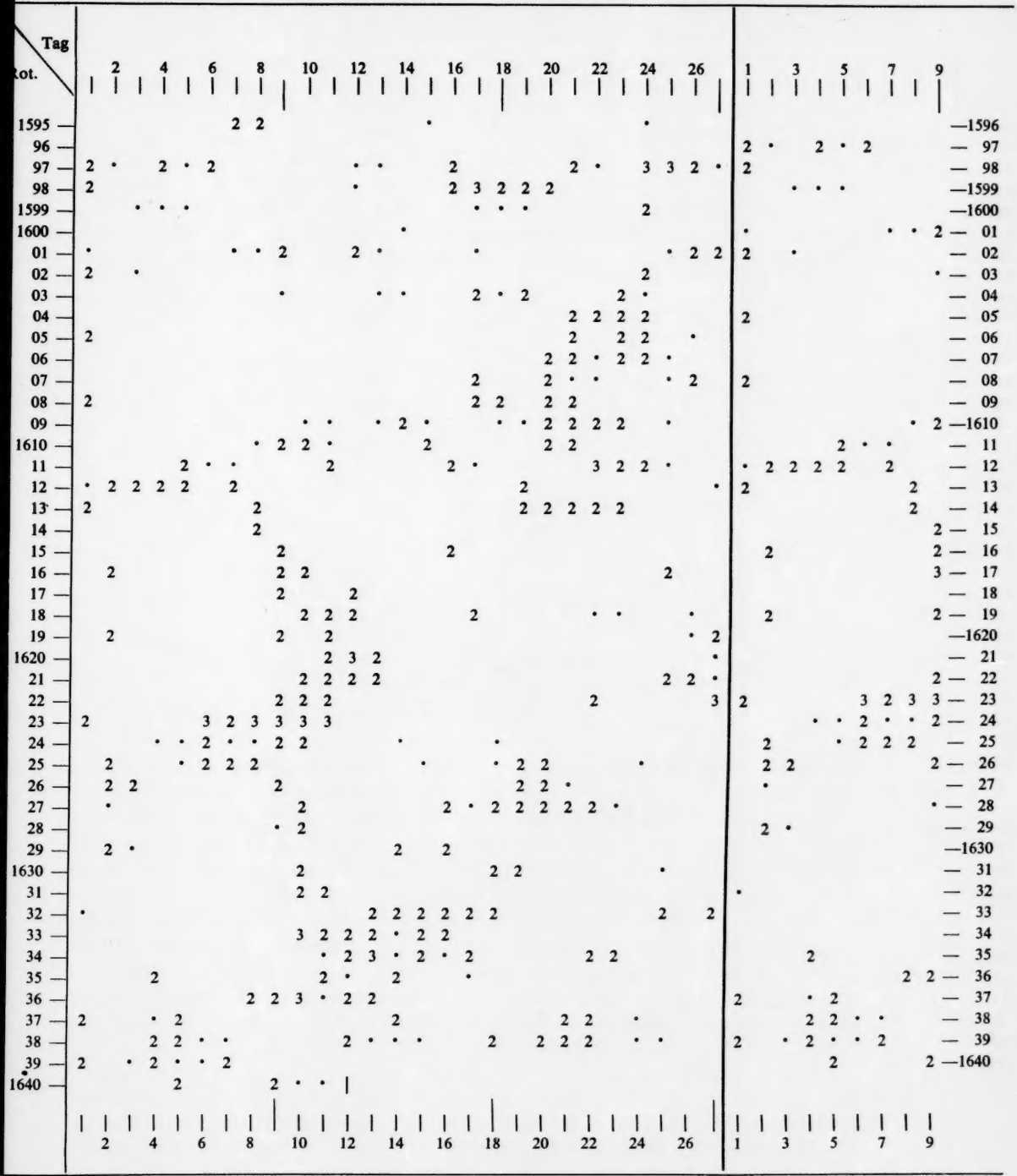

Fig. 2. Auftreten ausgeprägter Tagesgänge, nach Sonnenrotationen geordnet.
(•) Unsichere Fälle, (2) Tage mit Amplituden zwischen 7 und 10 Promille, (3) Tage mit Amplituden über 10 Promille.
Occurrences of pronounced daily variations, arranged according to solar rotations.
(•) Uncertain cases, (2) days with amplitudes between 7 and 10 per mille, (3) days with amplitudes greater than 10 per mille.

von mehreren Tagen Dauer auftritt und daß eine starke Wiederholungstendenz nach einer Sonnenrotation auftritt. Den gleichen Eindruck vermittelt Fig. 2, in der das gesamte Material in Form eines Teppichs nach Sonnenrotationen geordnet dargestellt ist. Die Darstellungen zeigen, daß es sich bei den A.T.G. um einen von der Sonne gesteuerten Vorgang handelt.

Zunächst wurde aus dem Material der 189 ausgewählten Tage der Verlauf der Intensität bei A.T.G. mit dem Tagesgang bei 189 normalen Tagen verglichen (N.T.G.), die dieselbe zeitliche Verteilung zeigen. Die Vergleichstage wurden allein aus dem U.S. Material ausgewählt mit der Bedingung, daß A.T.G. nicht erkennbar war und daß sie möglichst nahe bei den A.T.G.-Tagen lagen. Es wurde

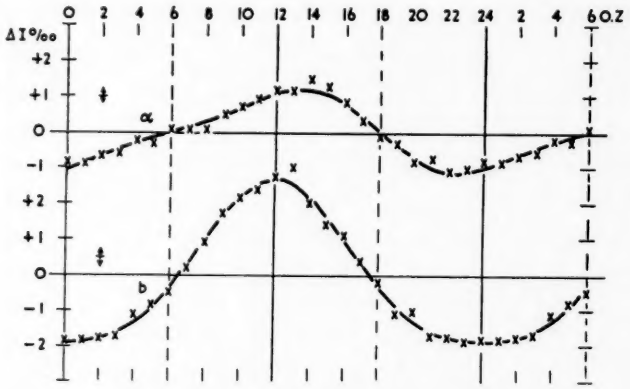

Fig. 3.
Kurve *a*, Verlauf des Tagesganges an normalen Tagen.
Kurve *b*, Verlauf des Zusatzeffektes an A.T.G. Tagen.
(Curve *a*, Daily variation on normal days.
Curve *b*, Additional daily variation on days with big daily variations.)

dabei keine Rücksicht darauf genommen, ob der magnetische Störungsgrad dieser Tage dem der A.T.G.-Tage entsprach. (Über die mögliche Auswirkung dieser Vernachlässigung siehe die weitere Diskussion). Das Ergebnis der Berechnung zeigt Fig. 3, dabei stellt die Kurve *a* den N.T.G. und Kurve *b* den Zusatzeffekt bei A.T.G. dar. Während der N.T.G. (Kurve *a*) den bekannten unsymmetrischen Verlauf mit langsamem Anstieg und steilerem Abfall (Max. um 14 ^{h} Ortszeit, Min. um 22 ^{h} O.Z.) zeigt, weist der Zusatzeffekt (Kurve *b*) innerhalb der statistischen Unsicherheit einen symmetrischen Verlauf zu Ortszeit-Mittag auf. Damit ist gezeigt, daß sich aus dem Tagesgang der Ultrastrahlung eine Komponente abspalten läßt, die symmetrisch zu Ortszeit-Mittag verläuft und deren Amplitude so stark schwankt, daß sie zeitweise nicht erkennbar ist, zeitweilig aber den Tagesverlauf vollkommen beherrscht.

Im Mittel tritt pro Woche ein Tag mit deutlichem A.T.G. auf. Durch diesen Tag wird bei Rechnungen, in denen A.T.G. Tage nicht ausgeschieden werden, die Gesamt-Amplitude des so bestimmten Tagesganges um 0·7 Promille von 2·5 Promille auf 3·2 Promille erhöht und der Zeitpunkt des Eintretens der Extremwerte verschoben. Wegen der starken Schwankungen im Auftreten deutlicher

VOL. 7 1955

A.T.G. Tage (Fig. 1 u. 2), tritt der Einfluß dieses Effektes bei Tagesgangauswertungen ohne Auswahl der Tage in verschiedenem Maße auf und muß bei Auswertungen über Änderungen des Tagesganges berücksichtigt werden.

Der in Fig. 3, Kurve *b*, dargestellte Verlauf des Zusatzeffektes bei A.T.G. ist das statistische Mittel einer großen Zahl von Einzelwerten. Die Art der Mittelbildung schließt nicht aus, daß der individuelle A.T.G. Tag einen vom Mittel abweichenden Verlauf zeigt z.B. kann eine jahreszeitliche Abhängigkeit des Verlaufs bestehen oder in einer Folge von A.T.G. Tagen können Amplitude und Phasenlage des Einzeltages, von der Nummer der A.T.G. Tages abhängen. Zur Prüfung der ersten Frage wurde aus 39 Sommer = A.T.G. = Tagen (Zeitraum

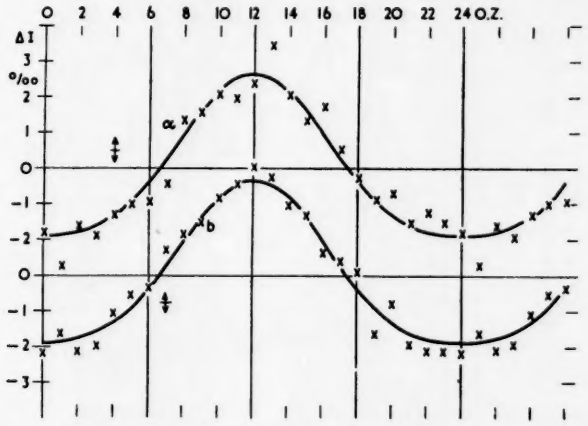

Fig. 4. Verlauf des an A.T.G. Tagen auftretenden Zusatzeffektes im Sommer (Kurve *a*) und Winter (Kurve *b*).
(Additional daily variations on days with big daily variations (Fig. 3*b*), shown separately for summer (curve *a*) and winter (curve *b*).)

16·4 bis 15·8) und 71 Winter=A.T.G.=Tagen (16·10 bis 15·2) der Verlauf des Zusatzeffektes für Sommer und Winter bestimmt und mit dem Ergebnis der Bestimmung aus allen Tagen verglichen (Fig. 4). Bei Berücksichtigung der statistischen Meßgenauigkeit ergibt sich im Sommer und Winter der gleiche Verlauf. Das vorliegende Material ist noch zu spärlich, um mit Sicherheit jahreszeitliche Änderungen des A.T.G. auszuschließen, doch zeigt der Vergleich, daß die ausgeprägten Tagesgänge wohl nicht durch die Aussendung von Ultrastrahlung durch die Sonne verursacht werden. Eine Erklärung des A.T.G. durch Zusatzstrahlung von der Sonne, verlangt wegen des Maximums um Ortszeitmittag die Annahme sehr energiereicher geladener Teilchen ($> 10^{11}$ eV), die durch das magnetische Erdfeld nicht mehr beeinflußt werden, oder die Existenz ungeladener Strahlung von einigen 10^9 eV. In beiden Fällen muß dann die Intensität vom Sonnenstande abhängig sein, also müßte im Winter die Amplitude im Mittel kleiner sein als im Sommer, auch müßte der Verlauf des A.T.G. wegen der ungleichen Tageslänge verschieden sein. Für beide Effekte ergeben sich keine Anhaltspunkte.

Zur Klärung des zweiten Punktes wurden aus den Registrierungen die Gruppen

ausgewählt, bei denen auf einen normalen Tag mindestens 3 A.T.G. Tage einander unmittelbar folgten. Dabei wurde zur Vermehrung des Materials eine Gruppe auch dann mitgezählt, wenn zwei Tage zu den A.T.G. Klassen 2 oder3 und ein Tag zur Klasse 1 gehörte. Auf diese Weise wurden 30 Gruppen erhalten und aus diesen der Tagesverlauf für den letzten Tag vor der Störung (Vortag) und die 3 folgenden A.T.G. Tage berechnet. Das Ergebnis ist in Fig. 5 dargestellt. Die Darstellung zeigt, daß beim Auftreten ausgeprägter Tagesgänge innerhalb der Gruppe keine systematischen Änderung der Amplitude und der Phasenlage von Tag zu Tag erfolgt. In den 30 Gruppen sinkt die mittlere Intensität um 3 Promille ab. Ob diese Abnahme reell ist oder ob sie nur durch statistische Effekte hervorgerufen ist, läßt sich nur durch Häufung der Beobachtungen entscheiden. Die

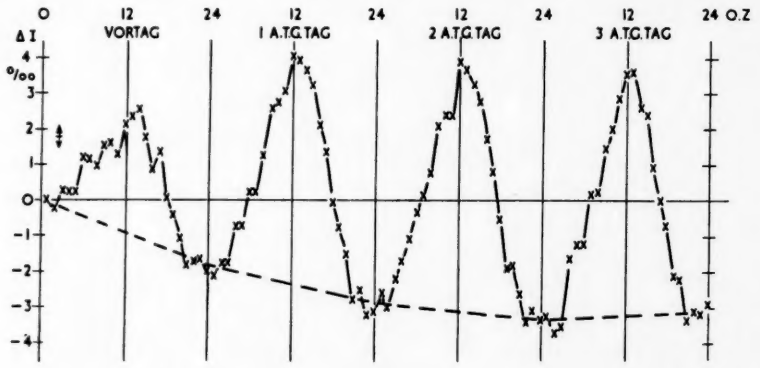

Fig. 5. Verlauf des Tagesganges in einer Folge von mindestens 3 A.T.G. Tagen.
(Daily variations for a sequence of days with big daily variations, and for the day before. Average for thirty such sequences.)

geringe Abnahme (0·4 Promille) des mittleren Stundenwertes bei der Auswertung aller A.T.G. Tage spricht gegen die Realität der in Fig. 5 erhaltenen Verminderung.

Bei der Ordnung der A.T.G.-Tage nach Sonnenrotationen (Fig. 2) zeigte sich eine ausgeprägte 27-tägige-Wiederholungstendenz, die darauf hinweist, daß der Effekt durch die Sonnenaktivität bedingt ist. Es wurde nun versucht, die Bedingungen für das Auftreten von A.T.G. durch Vergleich mit direkt beobachtbaren Vorgängen auf der Sonne oder mit solchen Ereignissen auf der Erde (erdmagnetische Schwankungen, Ionosphärenmessungen), die von der Aktivität der Sonne abhängig sind, festzulegen. Dabei können die erzielten Ergebnisse nur sehr vorläufigen Charakter haben, da die Zahl der A.T.G. Tage für genaue Untersuchungen noch nicht ausreicht und das Beobachtungsmaterial nur einen kleinen Teil eines 11-jährigen Sonnenzyklus überdeckt.

Zunächst wurde untersucht, ob das Auftreten von A.T.G. bevorzugt an einen bestimmten magnetischen Störungsgrad des Erdfeldes gebunden ist. Als Störungsmaß für die Einwirkung solarer Materieströme wurden die Charakterzahlen $C = 0{\cdot}1$ oder 2 des Erdmagnetischen Observatoriums Wingst benutzt (Errulat). Für die Sonnenrotationen 1595 bis 1623 wurde ausgezählt, wie oft ein A.T.G. Tag der Klasse 2 oder 3 auf einen Tag mit $C = 0{\cdot}1$ oder 2 fällt. Das Ergebnis zeigt

VOL. 7 1955

Tab. 1. Es ergibt sich keine Bevorzugung eines Störungsgrades. Das einfache Auszählungsverfahren wurde in der Weise erweitert, daß nach der Methode der überlagerten Stichtage die Verteilung der Charakterzahl C in der Nähe von A.T.G. Tagen bestimmt wurde. Dabei wurde jeder A.T.G. Tag der Klasse 2 und 3 als Stichtag Null gewählt und die Verteilung der C vom $-3.$ bis $+3.$ Tag berechnet. Das Ergebnis ist ebenfalls negativ, d.h. innerhalb des ausgewählten Zeitraums geht dem A.T.G. kein Tag mit einem ausgezeichneten magnetischen Störungszustand voraus oder umgekehrt. Eine Beschränkung des Stichtagverfahrens auf isolierte A.T.G. und 1. Tag von Gruppen, sowie eine Verfeinerung der Beschreibung des magnetischen Störungsgrades durch Benutzung der 3-h-Kennziffern Kp

Tabelle 1

Störungsmaß C	0	1	2
Zahl der Tage in den Rot 1595–1623	362	313	108 783 Tage = 29 Rotationen
Zahl der A.T.G. Tage	54	42	16 112 A.T.G. Tage
rel. Anteil der A.T.G. Tage	14·9%	13·4%	14·8% Mittel 14·3%

(Bartels) ergab wiederum keine Zusammenhänge. Der negative Ausfall der Versuche läßt den Schluß zu, daß im Beobachtungszeitraum das Auftreten von A.T.G. nicht mit erkennbaren korpuskelbedingten Störungen des magnetischen Erdfeldes verknüpft ist.

Nach der Methode der überlagerten Stichtage und durch Vergleich der A.T.G. Tagverteilung mit den Jahresübersichten aus dem Sonnenzirkular (Kiepenheuer) wurden Zusammenhänge mit der Sonnenfleckenrelativzahl der ganzen Scheibe, die ein Maß für erdmagnetisch wirksame Wellenstrahlung ist (Bartels, 1946), mit der Relativzahl der Zentralzone, mit der Intensität der grünen Koronalinie und mit der Flächenbedeckung der Filamente gesucht. Auch hier ließen sich keine Kopplungen entdecken. Alle verwendeten Sonnenelemente zeigen im Verlauf der Meßzeit eine starke Abnahme der Intensität im Lauf des 11-jährigen-Zyklus; so sinkt z.B. die ausgeglichene Sonnenfleckenrelativzahl nach dem Maximum von 1947 im Beobachtungszeitraum von dem Wert 83·9 im Jahre 1950 über 69·3, für 1951 auf 31·5 im Jahre 1952. Dagegen bleibt die Zahl der sicheren A.T.G. Tage mit 44 Tagen im Jahre 1950, 59 Tagen für 1951 und 64 Tagen für 1952 in erster Näherung konstant.

Zusammenfassend lässt sich das Ergebnis der Analyse so formulieren. In den Registrierungen einer großen gepanzerten Ionisationskammer läßt sich an zahlreichen Tagen (15%) des Beobachtungszeitraumes von Dezember 1949 biz März 1953 ein anormal großer Tagesgang (A.T.G.) direkt erkennen. Der Effekt ist eine weltweite Erscheinung, deren Ablauf an die Ortszeit gebunden ist. Die Vergrößerung der Gesamtamplitude beträgt im statistischen Mittel 0·5%. Der Zusatzeffekt hat im Gegensatz zum normalen Tagesgang sein Maximum um Ortszeitmittag und der Verlauf ist symmetrisch. A.T.G.-Tage treten bevorzugt

in Gruppen von mehreren Tagen Dauer auf. In den Gruppen zeigen die Einzeltage gleiche Amplitude und gleichen Verlauf des Tagesganges. A.T.G.-Tage zeigen starke Wiederholungsneigung nach einer Sonnenrotation, was auf einen Zusammenhang mit der Sonnentätigkeit hinweist, ohne daß es bisher möglich war, die genauen Bedingungen für das Auftreten von A.T.G. zu bestimmen. Insbesonderes zeigen sich keine Zusammenhänge mit dem Störungsgrad des erdmagnetischen Feldes.

Die Resultate der Untersuchung der A.T.G. Tage, die ohne Annahme über Zusammenhänge mit anderen Erscheinungen allein aus den Messungen der Ultrastrahlung ausgesucht wurden, zeigen, daß die beobachteten Veränderungen

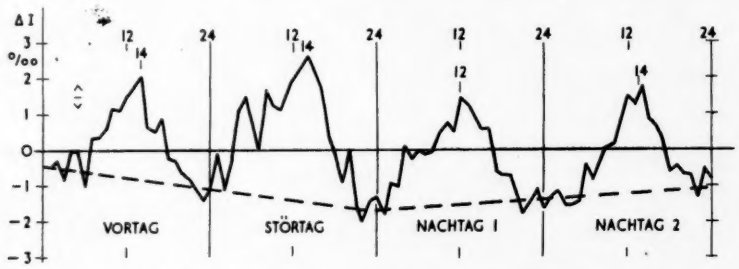

Fig. 6. Änderung des Tagesganges bei magnetischen Störungen.
(Charge of the daily variation on four successive days, with geomagnetic disturbance on the second day. Average of twenty cases.)

des Tagesganges nicht identisch sind mit den Änderungen, die Sekido und Mitarbeiter (SEKIDO und YOSHIDA, 1950) als Folge magnetischer Störungen (hohe Kennziffer) fanden. Die japanischen Forscher finden eine Zunahme der Tagesgangamplitude und eine Vorverlegung der Zeit des Maximums bei magnetischen Störungen dann, wenn die mittlere Intensität der Ultrastrahlung gleichzeitig abnimmt. Dabei ergibt sich zwischen der Intensitätsabnahme der Strahlung und der Amplitudenzunahme bez. der Zeitverlagerung des Maximums des Tagesganges eine hohe Korrelation. Eine Magnetsturmabnahme der U.S. Intensität um 5% bewirkt eine Erhöhung der Tagesgangamplitude von 4 Promille auf etwa 14 Promille und eine Vorverlegung der Zeit des Maximums um 5 Stunden von 14 h O.Z. auf 09 h O.Z. Nimmt man diese Werte auch für die Freiburger Registrierungen als gültig an, so läßt sich auf Grund der beobachteten Intensitätsschwankungen der Einfluß magnetischer Störung auf den Tagesgang abschätzen. Im ganzen Zeitraum der Beobachtung und besonders in der Nachbarschaft der A.T.G. Tage wurden kaum Magnetsturmeffekte beobachtet, die Intensitätsabnahmen über 1% bewirken. Das bedeutet, daß magnetische Einflüsse die Tagesgangamplitude höchstens von 2·5 Promille auf 4·5 Promille und die Zeit des Maximums von 14 h auf 13 h ändern könnten. Deutet man den Abfall der mittleren Intensität in Fig. 5 als Magnetfeldeinwirkung, so sollte der Tagesgang an den A.T.G. Tagen um nur 0·6 Promille in der Amplitude wachsen und das Maximum auf 13·30 O.Z. verschoben werden. Die beobachteten Änderungen sind wesentlich größer und daher wohl nicht auf solche Einflüsse zurückzuführen.

Zur Prüfung, ob die von Sekido und Mitarbeitern gefundenen Werte für die

VOL. 7 1955

Beeinflussung des Tagesganges durch magnetische Störungen auch für die vorliegenden Messungen gültig sind, wurde eine vorläufige Aufrechung des Tagesganges bei magnetischer Erdfeldstörung durchgeführt. Aus dem Material der 40 Monate wurden zunächst alle A.T.G. Tage der Klassen 2 und 3 ausgesondert. Aus dem Rest wurden 20 Serien von je 4 Tagen ausgesucht, bei denen die magnetische Kennziffer C Wingst am 1, 3, und 4 Tag O oder 1 war, während am 2, Tag $C = 2$ verlangt wurde. Der Verlauf des Tagesganges für diese Gruppen mit "singulärer" Störung ist in Fig. 6 dargestellt. Er ist eine Bestätigung der japanischen Messungen. Im Verlauf der Störung tritt eine Abnahme der mittleren Intensität ein, gleichzeitig damit wächst die Amplitude des Tagesganges am Störtag, während die Vorverlegung der Eintrittszeit des Maximums verzögert erfolgt. Die mindestens qualitative Übereinstimmung der Ergebnisse, läßt die Verwendung der bei der Diskussion des A.T.G. benutzten Größen gerechtfertigt erscheinen.

Der Deutschen Forschungsgemeinschaft habe ich für die Bereitstellung der Mittel für die Untersuchungen zu danken, ebenso dem Institutsdirektor Prof. Dr. W. Gentner für zahlreiche fördernde Diskussionen.

References

Bartels, J.	1946	*Naturwissenschaften* **33**, 140
		Regelmässige Mitteilungen des Geophys. Inst. Göttingen, *J. Geophys. Res.*
Ehmert, A., und Sittkus, A.	1951	*Physikal. Verhandlungen H.*2, 29
	1951	*Z. Naturforsch.* 6a, 618
Errulat, Fr.		*Monatliche Mitteilungen des Deutschen Hydrographischen Inst.*
Kiepenheuer, K. O.		Sonnen-Zirkular, Verofftl. des Fraunhofer-Instituts Freiburg i. Br.
Sekido, Y., und Yoshida, S.	1950	*Rept. on Ionospheric Research in Japan* **4**, 37 und 479
Täglicher Wetterbericht des deutschen Wetterdienstes, Bad Kissingen.		
Wilson, J. G.	1952	*Progress in Cosmic Ray Physics*, S. 455

Journal of Atmospheric and Terrestrial Physics, 1955, Vol. 7, pp. 90 to 98. Pergamon Press Ltd., London

Diurnal variations in natural atmospheric radioactivity

E. S. COTTON
Geophysics Research Directorate, Air Force Cambridge Research Center,
Air Research and Development Command, Cambridge, Massachusetts

(*Received* 9 *October* 1954)

ABSTRACT

The diffusion of radium emanation in the atmosphere is considered, using several simplifying assumptions in order to gain an understanding of diurnal changes in the concentration within the surface layer. The order of magnitude of the night-to-day ratio for various daytime concentrations is calculated and compared with continuous ionization records made during the 1952 and 1953 autumn seasons. The importance of meteorological factors is pointed out and typical records shown.

I. INTRODUCTION

The trapping of radioactive emanation in the surface layer of the atmosphere has long been recognized as the principal mechanism governing diurnal variations in ion production at surface stations. The effects of meteorological factors have been noted, although in most studies of diurnal changes the average variation in a certain season has been considered to be the most important result. The experiments to be described indicate that these daily changes are explicable on the basis of individual events and that meteorological effects are directly associated with them.

VOL. 7 1955

II. DIFFUSION OF EMANATION

The density of the effective radioactive materials (chiefly Em^{222} and its short-lived alpha-emitting daughter products, Po^{218} and Po^{214}) is determined by the rate of exhalation from the ground, the decay of the substances while present, and the rate of loss from the top of the surface layer. The surface layer of the atmosphere is that region near the ground where the motion of the atmosphere is completely controlled by frictional effects, and, as used here, will denote a layer of varying thickness according to the prevailing conditions. If we let s represent the density of emanation in curies per cubic centimetre and F the flux in curies per square centimetre per second, then the continuity equation becomes

$$\frac{\partial s}{\partial t} = -\frac{dF}{dz}, \tag{1}$$

since the flux of emanation is assumed to vary only with the height in the surface layer, denoting height by z. We assume also that the flux is composed of two terms, one which is proportional to the vertical gradient of emanation, and a second term which expresses the rate of emanation entering the atmosphere, or exhalation from the earth. Thus

$$F = -\frac{A}{\rho}\frac{ds}{dz} - E \tag{2}$$

where A is the so-called exchange coefficient in grams per centimetre per second, ρ is the density of the air in grams per cubic centimetre, and E is the exhalation in

curies per square centimetre per second. The change of s with time is given by the familiar exponential law,

$$\frac{\partial s}{\partial t} = -\lambda s \tag{3}$$

where λ is the disintegration constant of the emanation. Using (2) and (3) in equation (1), we obtain

$$-\frac{dE}{dz} = \lambda s - \frac{1}{\rho}\frac{dA}{dz}\frac{ds}{dz} - \frac{A}{\rho}\frac{d^2s}{dz^2} \tag{4}$$

Equation (4) is the atmospheric diffusion equation for emanation written in such a form that it includes exhalation as a separate part of the flux.

LETTAU (1941, 1949) has solved (4) using $\frac{dE}{dz} = 0$ and assuming that $A = A_0 + A_1 z$ where $0 \leq z \leq h$. He shows that this assumption leads to an ordinary Bessel equation, and that for various exchange conditions with radium emanation the concentration s in the surface layer is nearly constant. Using this result, we may neglect the term in $\frac{d^2s}{dz^2}$ in (4) and write the integral over the surface layer as

$$-\int_0^h \frac{dE}{dz}\,dz = \int_0^h \lambda s\,dz - \int_0^h \frac{1}{\rho}\frac{dA}{dz}\frac{ds}{dz}\,dz \tag{5}$$

$\frac{dE}{dz}$ is not a proper function, but it can be treated by using the delta-function concept. Since we know that $\frac{dE}{dz} = 0$ except at $z = 0$, and that

$$E(z) = 0, \qquad z > 0$$
$$E(z) = E_0, \qquad z < 0,$$

we may represent the delta function by

$$\delta(z) = -\frac{dE}{dz}/E_0$$

where

$$\int_{-\infty}^{\infty} \delta(z)\,dz = 1$$

The integral need not have the limits shown; instead we shall use the vertical extent of the surface layer, starting just below the ground level. Thus

$$-\frac{1}{E_0}\int_x^h \frac{dE}{dz}\,dz = 1, \qquad x < 0$$

where x is very small compared to h. We can shift the height variable so that $x = 0$ with no error being introduced in the other integrals of (5). Then, finally

$$-\int_0^h \frac{dE}{dz}\,dz = E_0$$

The determination of $\frac{ds}{dz}$ at the top of the layer is quite difficult, since the emanation content changes rapidly above the surface layer, but is almost constant within it. We shall try the very simple assumption that the variation of s within the surface layer obeys the relation

$$S = S_0 - S_1 Z, \tag{6}$$

where $0 \leq z \leq h$, and $S_0 \gg S_1 z$. Thus, putting this in (5),

$$E_0 = \lambda S_0 h - \frac{\lambda s_1 h^2}{2} + \frac{1}{\rho} A_1 S_1 h \tag{7}$$

Since the middle term on the right-hand side can be shown to be small compared to the other terms, this reduces to

$$S_0 = \frac{E_0 - A_1(h/\rho)S_1}{\lambda h} \tag{8}$$

a relation expressing S_0 in terms of the exhalation, the gradients of content and exchange, the disintegration constant, and the height of the surface layer.

Equation (8), derived under rather severe simplifying assumptions, can only be used as a means of verifying the order of magnitude variations of S_0 as a result of large changes in atmospheric exchange conditions. Such large changes are most noticeable in the nocturnal inversions developed in valley location during fine weather. Lettau (1941) estimates that the following values are representative of such conditions:

Strong Convection $A_1 = 0{\cdot}02$ g/cm² sec, $h = 200$ m.

Nocturnal Inversion $A_1 = 0{\cdot}004$ g/cm² sec, $h = 50$ m.

If we use the average values given by Israel (1951) as $E_0 = 40 \times 10^{-18}$ curies/cm² sec and daytime $S_0 = 1 \times 10^{-16}$ curies/cm³, we obtain for the midday gradient of emanation content

$$S_1 = \frac{E_0 - \lambda S_0 h}{A_1 h} \rho$$

or,

$$S_1 = 1{\cdot}1 \times 10^{-22} \text{ curies/cm}^4.$$

During the nocturnal inversion, when equilibrium has been reached, the gradient must be larger than this, at least due to the decrease in layer-height. Thus, taking S_1 to be about $4{\cdot}4 \times 10^{-22}$ curies/cm⁴, we can solve (8) for S_0 under these conditions. Thus we obtain

$$S_0 = 3300 \times 10^{-18} \text{ curies/cm}^3$$

The ratio of night to day content is thus

$$\frac{3300}{100} = 33$$

VOL. 7 1955

Using other values of daytime emanation content S_0, we obtain Table 1.

Table 1. *Night-to-day ratios for various values of daytime emanation content, using the specified exchange conditions.*

Daytime S_0 c/cm^3	*Daytime gradient* c/cm^4	*Night-time gradient* c/cm^4	*Night-time* S_0 c/cm^3	*Night-to-day ratio*
10×10^{-18}	$1{\cdot}2 \times 10^{-22}$	$4{\cdot}8 \times 10^{-22}$	$3{,}200 \times 10^{-18}$	320
100×10^{-18}	$1{\cdot}1 \times 10^{-22}$	$4{\cdot}4 \times 10^{-22}$	$3{,}300 \times 10^{-18}$	33
400×10^{-18}	$0{\cdot}7 \times 10^{-22}$	$3{\cdot}2 \times 10^{-22}$	$3{,}500 \times 10^{-18}$	9
$1{,}000 \times 10^{-18}$	0	0	$4{,}000 \times 10^{-18}$	4

The data in Table 1 show that the ratio of night to day content should be variable, even for constant exhalation, and that the value of the daytime content determines the ratio even under the same exchange conditions. Actually, the values of content, exchange coefficient, and exhalation are all quite variable and, of course, are not independent of one another as this model has assumed.

It is of interest to see whether the calculated ratios of night to day readings correspond to measurable data; this comparison will be considered in the next section. It should be noted first that the ratios shown in Table 1 are calculated using the given exchange conditions for nocturnal inversions. If the exchange mechanism were constant during the day-night cycle, the ratio of night to day content would be unity, regardless of the value of daytime content.

III. Experimental Data

The experimental equipment consisted of two ionization chambers of cylindrical shape; the first was constructed of 0·5 cm wire mesh, 0·12 cm wire diameter, supported at the ends by wooden discs, and covered by cellophane of 1·6 mg/cm² thickness. The collecting electrode was a brass rod 3·2 mm in diameter; the mesh cylinder was 21·8 cm in diameter and 36·5 cm in length. (This chamber was built and used for several experiments by the late Dr. G. Wait of the Carnegie Institution of Washington.) The second chamber consisted of an interior wire-mesh cylinder 20 cm in diameter and 60 cm in length, supported on lucite discs at the ends. This cylinder was the high-voltage electrode and in its centre, supported by a teflon insulator, was a 0·95 cm diameter collecting electrode. The entire chamber was surrounded by a second cylinder of wire mesh, 2·86 cm from the inside cylinder, and mounted on aluminium discs on either end. The lower disc was the base plate and guard ring; this entire outer assembly was maintained at the potential of the electrometer case.

The field which existed between the outer grounded screen and the inner high-voltage screen was presumed to collect and remove most atmospheric ions which

would have disturbed the chamber. It was found by introducing artificial sources of ions that this filter was quite effective for small ions, but that it did not remove all large ions. Thus, if the atmosphere were polluted by large nuclei, the reading of the screen-wall chamber could be different from that due only to radioactive materials. The exposed metal parts of the screen-wall chamber were silver-plated in order to reduce contamination background.

Each chamber was mounted on the pre-amplifier unit of a Model 30, Applied Physics Corporation vibrating reed electrometer, and resistors were attached so that the electrometer measured the voltage developed across the resistor. This voltage was recorded continuously. The calculated ratio of the alpha-particle contribution to the current in the thin-wall chamber to that in the screen-wall chamber was about 0·15; the observed ratio of diurnal current changes (presumed to be due only to alpha particles) averaged over all the cases studied was 0·12, which agrees well with the calculated value.

The chambers were operated in a truck located at three sites in the vicinity of Bedford, Massachusetts. During the autumn of 1952 the cellophane-wall chamber was operated alone at a valley location, 140 ft above sea-level. In the summer of 1953 both chambers were operated on a small hill, 306 ft above sea-level. No useful diurnal changes were observed there, and in the autumn of 1953 the chambers were again operated in the valley at 125 ft above sea-level. Air was continuously exchanged between the truck and the outside by means of an air-conditioner fan.

VOL. 7 1955

Those days on which significant diurnal effects were observed were selected from the two autumn periods of measurement and displayed on the same time axis with simultaneous records of surface temperature and wind velocity obtained from the Hanscom Air Force Base weather station. The meteorological records used were not continous measurements, but gave at least hourly observations. In all cases except one, where pronounced nocturnal increases in ionization were observed, there existed also a period of calm, or windspeed less than one knot. Figs. 1, 2, and 3 show five of these diurnal changes in detail. Twenty-four cases of large diurnal effects were selected in all, for consideration of their relative characteristics.

Fig. 1 shows a period when only the cellophane-wall chamber was in use. Full scale on the ionization record corresponds to $10{\cdot}3 \times 10^{-14}$ amperes, or forty-seven ion pairs per cubic centimetre per second. The period shown is forty-eight hours. Cross-hatched areas in the wind plot indicate changes in direction as shown by arrows at the top of the chart; a wind directed from the north is shown as a downward arrow, and so forth. The general characteristics of all the diurnal curves are to be seen in this figure; a single large maximum is observed in the morning at about 7 o'clock, as is well known. The rapidity of the decrease from this maximum and the onset of wind after the nocturnal calm are characteristic of surface temperature inversions and their subsequent dissolution. No secondary maxima are seen in this period. Fine weather associated with a high-pressure area dominated the period; ground fog was visible from midnight until 0630 during the morning of 9 September.

Fig. 2 shows a 48-hour period in October 1953, when both chambers were in operation. Full scale for the screen-wall chamber corresponds to $21{\cdot}8 \times 10^{-14}$ amperes, or seventy-two ion pairs per cubic centimetre per second, and for the

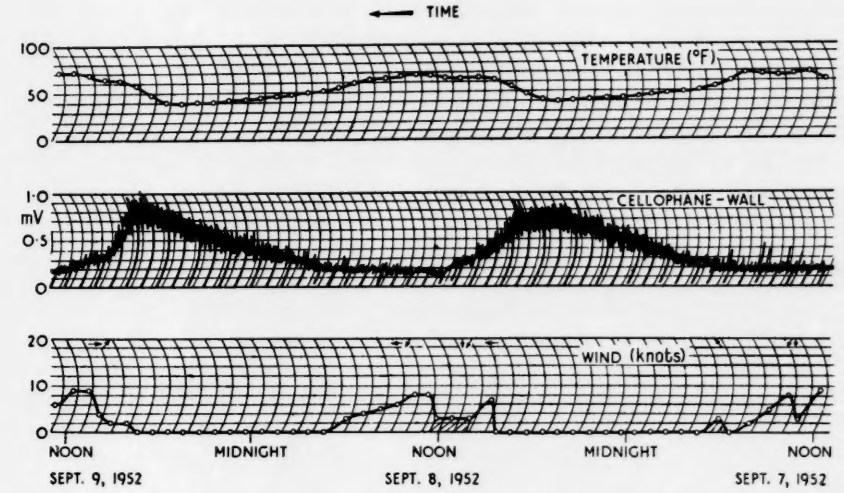

Fig. 1. 7–9 September 1952. (Full-scale ionization = 47 *I*).

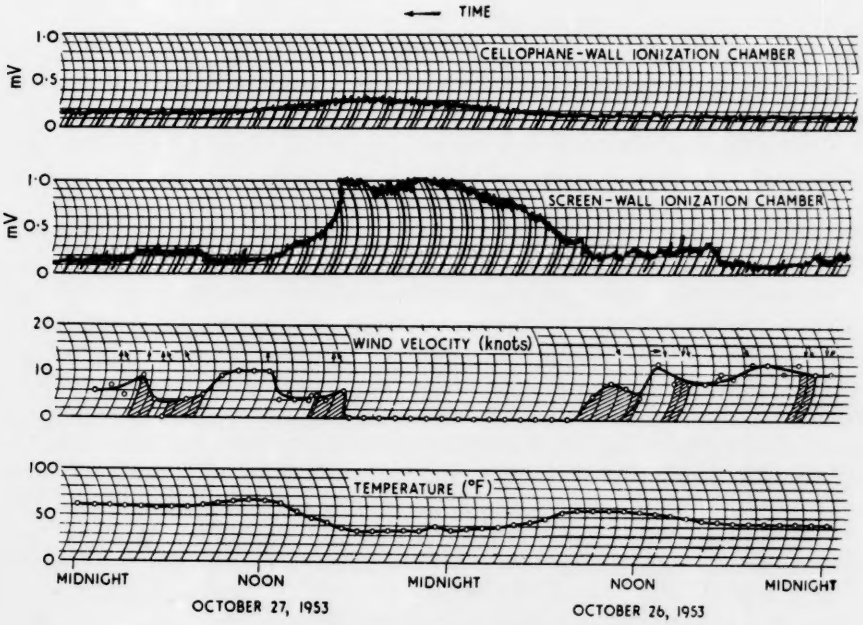

Fig. 2. 19–21 October 1953. (Full-scale screen-wall ionization = 72 *I*.
Full-scale cellophane-wall ionization = 46 *I*).

cellophane-wall chamber to $10{\cdot}1 \times 10^{-14}$ amperes, or forty-six ion pairs per cubic centimetre per second. An increase in emanation content of short duration at about 0800 on 20 October can be seen on both chamber records, and a correspondent wind-shift with a very short calm period can be seen on the wind record. The readings before and after this small maximum seem to show a difference between north and south winds. North winds passed over wooded land, while south winds passed over the runways, roads, and buildings of the air base. The influence of large ions, which reach a maximum density as convection increases, cannot be ignored here, although the cellophane-wall chamber also shows a slight increase in the ionization after the maximum. A large maximum developed during the next night, but did not continue until the usual time (0700–0800) because of the wind rise at about 0130, when a new air mass began to dominate the area.

In Fig. 3 a single large maximum is shown, with a secondary maximum at about 0200 on 27 October. The development of the secondary seems to be correlated with a small increase in temperature at the same time, indicating that perhaps local convection currents temporarily disturbed the inversion. No wind was indicated. Similar occurrences were seen on many of the records, usually between 2200 and 0200.

Two frequency distributions are shown in Fig. 4, one showing the time difference in hours between the minimum nocturnal temperature and the ionization maximum and the other showing the time difference between the beginning of wind on such days and the ionization maximum. Number of events is plotted as the ordinate and time differences as the abscissa, where positive numbers indicate that the temperature minimum (or onset of wind) occurred *prior* to the ionization maximum. It is seen that the ionization maximum occurs most often one to two hours after the surface heating begins, and that the decrease from the maximum is quite closely associated with the onset of wind for days when a nocturnal calm prevails.

VOL. 7 1955

IV. CONCLUSION

The formation of quite dense layers of radioactive emanation can be understood from the simple flux considerations given here. Verification of the order of magnitude of night to day ratios was made in this series of measurements. Accepting the values obtained by HESS and VANCOUR (1951) for the contribution to the total ionization of all other radiations except alpha particles, and correcting for background in the chambers, we arrive at an average daytime *minimum* emanation contribution of 4 I for the screen-wall chamber and 1 I for the cellophane-wall chamber. The night-to-day ratios on the charts shown here vary from 10 to 18 for the 1953 location, and from 33 to 35 for the 1952 location. As seen in Table 1, such values are to be expected for average amounts of emanation density from 100 to 400×10^{-18} curies/cm^3. The emanation content at night changes very little as the daytime content is varied over two orders of magnitude; we would expect from this that completely developed maxima with the same meteorological conditions should reach about the same amplitude, and this seems to be the case in the limited number of samples considered here. Smaller maxima are observed of course, for different exchange coefficients; we have considered only the average exchange conditions postulated by LETTAU.

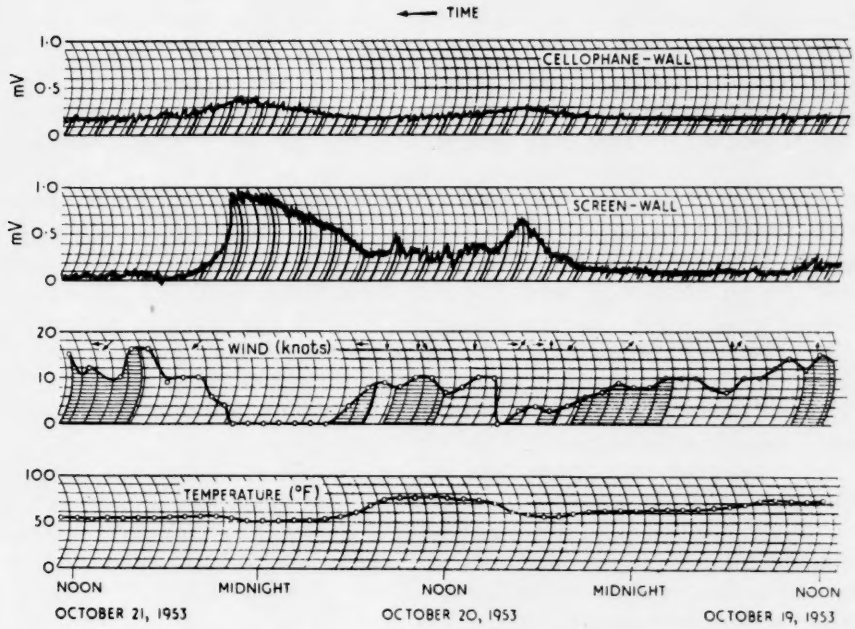

Fig. 3. 26–27 October 1953. (Full scale screen-wall ionization = 72 *I*.
Full-scale cellophane-wall ionization = 46 *I*.)

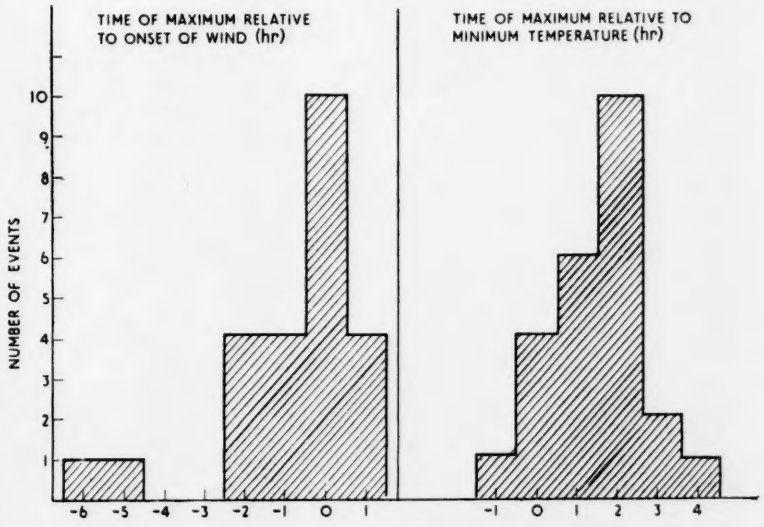

Fig. 4. Frequency distribution of diurnal maxima with respect to temperature and wind.
(Positive times indicate delay of ionization maximum.)

The significance of these results is determined mainly by the ability to explain individual diurnal variations on the basis of meteorological conditions. This seems feasible, not only for time correlation, but also for order of magnitude comparisons. Many investigators have studied this type of variation, as pointed out in the discussion by ISRAEL (1951); in general, the meteorological correlation has been indicated only by deduction from prevailing conditions. BURKE and NOLAN (1950) found a diurnal variation in RaA (Po^{218}) content which depended upon the wind-speed in the same manner as the data discussed here. Their data also showed a correlation between nuclei content and RaA density; however, the diurnal variations in these quantities are quite different, thus indicating that nuclei variations could not greatly affect the *diurnal* changes measured in the screen-wall chamber. (The simultaneous records of the cellophane-wall chamber also indicate this.) The results of WILKENING (1952) and of BLIFFORD, LOCKHART, and ROSENSTOCK (1952) also show diurnal variations which depend upon meteorological variables in the same manner as those described in this paper.

A more quantitative study of these phenomena would include measurements of ionization and of meteorological quantities on a continuous basis at several heights within the surface layer. In this way the gradients could be measured and used to explain the diffusion of the emanation in much greater detail. Such a procedure might shed additional light on the nature of exchange processes within the surface layer and at its upper boundary.

VOL. 7 1955

REFERENCES

BLIFFORD, I. H., LOCKHART, L. B., and ROSENSTOCK, H. B.	1952	U.S. Naval Research Laboratory Report No. 4036
BURKE, T., and NOLAN, J. J.	1950	*Proc. Roy. Irish Acad.* **A53,** 145
HESS, V. F., and VANCOUR, R. P.	1951	*J. Atmosph. Terr. Phys.* **1,** 13
ISRAEL, H.	1951	*Compendium of Meteorology,* pp. 157–159, American Met. Society, Boston
LETTAU, H.	1941	*Beitr. Geophys.* **57,** 365
	1949	Research Paper No. 1, Geophysics Research Directorate, U.S. Air Force Cambridge Research Center
WILKENING, M. H.	1952	*Nucleonics* **10,** 36

RESEARCH NOTES

The lunar semi-diurnal oscillation in the ionospheric absorption of 150 kc/s radio waves*

(*Received* 17 *January* 1955)

Vertical incidence absorption measurements using pulse transmission at 150 kc/s were started in the Ionosphere Research Laboratory of the Pennsylvania State University by BENNER (1952) in 1949, and were continued till 1953. Some preliminary analysis for lunar semi-diurnal periodicity was attempted by Mrs. LETHBRIDGE of the Laboratory with some of the earlier data, but no conclusive result was obtained. The present note describes the results of more detailed analysis, using a longer period of data.

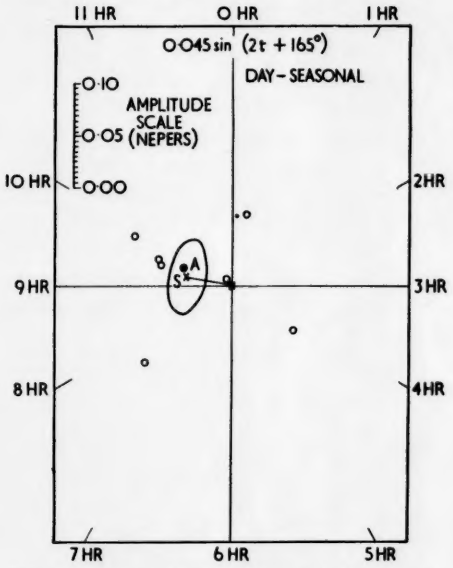

Fig. 1. Harmonic dial for lunar semi-diurnal oscillation in daytime absorption of radio waves at 150 kc/s.

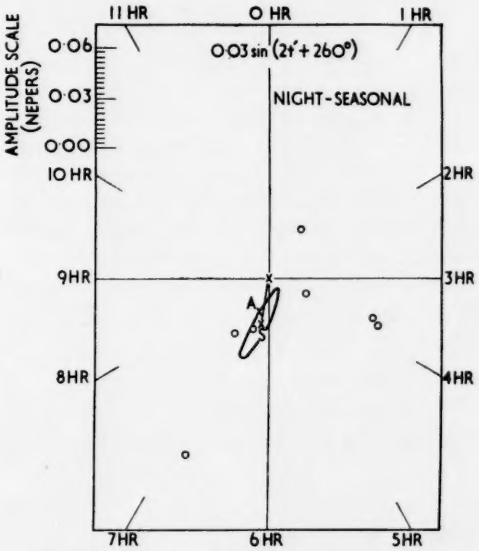

Fig. 2 Harmonic dial for lunar semi-diurnal oscillation in night-time absorption of radio waves at 150 kc/s.

In analyzing the data it was considered advisable to deal with the daytime and the night-time observations separately, since it is believed that at this frequency the daytime absorption is principally due to region *D* (Nertney, 1953), while the night-time absorption is due, of course, to region *E* alone. This was confirmed by the results of some preliminary analysis in which day and night data were treated separately. The results showed appreciable differences in amplitude and phase for the daytime and the night-time conditions.

The values around sunrise and sunset were always rejected for two reasons; firstly, at

* The research reported in this note has been sponsored by the Geophysics Research Directorate of the Air Force Cambridge Research Center, Air Research and Development Command, under Contract AF19(122)–44.

these times there is a transition from predominant *D*-absorption to predominant *E*-absorption, and vice versa; and secondly, errors due to polarization are most severe at these times.

The data were analyzed by the Chapman-Bartels method, as described in *Geomagnetism* (Vol. 1) (CHAPMAN and BARTELS, 1940). "Poor" data were discarded. In deciding as to the quality of the data, considerations were given to equipment conditions as well as to the existence, or otherwise, of the various disturbing phenomena.

The data after treatment were subjected to harmonic analysis, both in units of months and in units of seasons (summer (J), winter (D), and equinox (E)). The results for the seasonal groups are displayed in the harmonic dials in Figs. 1 and 2, in which the probable error ellipses are also drawn. For the entire period the lunar semi-diurnal oscillations for the daytime and the night-time conditions are given by $0{\cdot}05 \sin (2t' + 160°)$ neper and by $0{\cdot}025 \sin (2t' + 260°)$ neper, respectively.

As already been mentioned, the daytime result is believed to refer to the *D*-region. Earlier analysis of the noon absorption data at Slough by APPLETON and BEYNON (1949) gave a lunar semi-diurnal variation of amplitude 0·03 neper with maximum absorption occurring 10·9 lunar hours after transit. If the Appleton-Beynon tide refers to *D*-region, it is in reasonable agreement with the present daytime results for this region. If, however, it refers to region *E*, it is almost out of phase with the night-time *E*-region results recorded in this note.

The geophysical significance of these results is not easy to understand. For *D*-region heights, it is perhaps permissible to assume a bodily movement of the ionization without any distortion in *N*. In such a case, an oscillation in absorption given by $0{\cdot}05 \sin (2t' + 160°)$ neper will be caused by a height oscillation of the layer of amplitude only about 0·1 km, with maximum occurring approximately four hours after lunar transit.

For our night-time observations, the assumption of a simple bodily movement of the layer is not permissible. However, if such an assumption is made, the corresponding height oscillation comes out to be $0{\cdot}20 \sin (2t' + 80°)$ km.

A. P. MITRA

Ionosphere Research Laboratory,
The Pennsylvania State University,
State College, Pennsylvania.
(Now at *National Physical Laboratory of India, New Delhi* 12.)

VOL. 7 1955

REFERENCES

BENNER, A. H. 1952 *Proc. Inst. Radio Eng.*, **39**, 186

CHAPMAN, S., and BARTELS, J. 1940 *Geomagnetism*, Vol. 1, Ch. 8, Oxford University Press.

APPLETON, E. V., and BEYNON, W. J. G. 1949 *Nature*, **164**, 308.

The interpretation of intensity distributions in the N_2 second positive and N_2^+ first negative band systems

(*Received* 17 *February* 1955)

ABSTRACT

Photoelectric band intensities of the N_2 second-positive and N_2^+ first-negative systems, are interpreted, with the aid of Franck-Condon factors $q(v'v'')$ and r-centroids $\bar{r}_{v'v''}$ to show the dependence of the electronic transition moment $R_e(r)$ of these systems upon internuclear separations. Smoothed arrays of vibrational transition probabilities have been derived for these band systems.

Introduction

As part of a general laboratory study of molecular band systems of astrophysical interest, the intensity distributions of the first (Turner and Nicholls, 1954) and second positive systems of N_2 and the first negative system of N_2^+ have been measured photoelectrically. In view of the importance of these band-systems to the study of the aurora, it has been thought worthwhile briefly to report here upon the apparent variation of electronic transition moment $R_e(r)$ with internuclear separation which has been observed, and its effect upon the array of vibrational transition probabilities for the last two band systems.

The integrated intensity $I_{v'v''}$ of a molecular band depends upon the energy quantum $E_{v'v''}$, vibrational transition probability $p_{v'v''}$, and population $N_{v'}$ in the upper level according to equation (1), where D is a constant which depends upon geometry of the optical system and the units of measurement employed.

$$I_{v'v''} = DN_{v'}E^4_{v'v''}p_{v'v''} \tag{1}$$

The conditions under which it is possible to write

$$p_{v'v''} = R_e^2(\bar{r}_{v'v''})q_{v'v''} \tag{2}$$

where $\bar{r}_{v'v''} = \dfrac{\int \psi^{v'}(r) r \psi^{v''}(r)\, dr}{\int \psi^{v'}(r)\psi^{v''}(r)\, dr}$ and is the r-centroid of the $v' \rightarrow v''$ transition, have been discussed by Fraser (1954). $\psi^{v'}(r)$, $\psi^{v''}(r)$ are the vibrational wavefunctions. $q_{v'v''} = \left| \int \psi^{v'}(r)\psi^{v''}(r)\, dr \right|^2$ and is the Franck-Condon factor of the band. Accordingly, equation (1) may be written

$$I_{v'v''} = DN_{v'}E^4_{v'v''}q_{v'v''}R_e^2(\bar{r}_{v'v''}) \tag{3}$$

Methods have been developed (Fraser and Jarmain, 1953, 1954) to compute arrays of $q_{v'v''}$ without undue tedium, and data on them is available for a number of systems (Fraser, Jarmain, Nicholls, 1953, 1954). Methods (Jarmain, Nicholls) have also been developed to compute $\bar{r}_{v'v''}$. Fraser (1954) has suggested that equation (3) may be employed to find $R_e(r)$ from arrays of measured intensities $I_{v'v''}$ and of computed values of $q_{v'v''}$ and $\bar{r}_{v'v''}$. This has already been applied to the first positive system (Turner and Nicholls, 1954) and a number of other band-systems which will be reported upon elsewhere.

Equation (3) may be recast as

$$DN_{v'}R_e^2(\bar{r}_{v'v''}) = I_{v'v''}/E^4_{v'v''}q_{v'v''} \tag{4}$$

Thus a plot of the square root of the right-hand side as a function of $\bar{r}_{v'v''}$ for v'' progressions ($N_{v'}$ = const) will show, after suitable scaling of segments for each v', how $R_e(r)$ varies with r.

Experimental

The second positive system was excited in purified nitrogen, using a Hunter-Pearse (1936) water-cooled capillary discharge tube and a 15-kilovolt transformer. The first negative system was excited in two ways: (a) in a condensed a.c. discharge in the Hunter-Pearse

tube in commercial helium (using the nitrogen impurity), and (b) in the hollow cathode of an H-shaped capillary discharge tube. Purified nitrogen was excited by a 2,000-volt power d.c. supply in this case.

A photoelectric scanning attachment employing a 1P28 photomultiplier was built for the Bellingham and Stanley medium quartz spectrograph employed in this work. The band-intensity profiles were recorded in ink on a paper trace by a Leeds and Northrup recording microammeter. During each experiment a Hilger constant deviation spectrometer fitted with a photomultiplier was used to monitor the intensity of one band, using another recording microammeter. The trace from this instrument served to verify that source conditions remained essentially constant during a run. The optical and recording systems were calibrated against a Philips standard lamp. The areas under the band profiles could then be interpreted as relative integrated intensities $I_{v'v''}$.

Results

The conventional method of determining, band by band, the relative vibrational transition probabilities from an array of integrated intensities is, from equation (1), to divide $I_{v'v''}$ by $E^4_{v'v''}$. In general, the smaller the $I_{v'v''}$, the greater will be the experimental error in such a determination. $I_{v'v''}/E^4_{v'v''}$ (measured photoelectrically by the authors), $q_{v'v''}$ (Fraser,

Table 1. *Comparison between* $I_{v'v''}/E^4_{v'v''}$, $p_{v'v''}$ (Omholt, 1954), $q_{v'v''}$ (Jarmain, Fraser, Nicholls, 1953, 1954) *for the second positive system of* N_2

v' \ v''	0	1	2	3	4	5	6	7	8	9
	0·45	0·34	0·16	0·05	—	—				
0	0·44	0·36	0·15	0·04	—	—				
	0·448	0·328	0·146	0·05	0·016	0·005				
	0·39	0·02	0·27	0·25	0·15	0·06	0·03	—		
1	0·38	0·02	0·24	0·21	0·11	—	—	—		
	0·392	0·019	0·203	0·195	0·115	0·047	0·020	0·006		
	0·12	0·32	0·03	0·06	0·20	0·16	0·12	0·05	0·02	
2	0·12	0·43	0·02	0·07	0·16	0·15	—	—	—	
	0·135	0·323	0·032	0·062	0·157	0·142	0·082	0·039	0·015	
	—	—	0·16	0·10	—	0·09	0·15	0·11	0·06	0·03
3	—	—	—	—	—	—	—	—	—	—
	0·022	0·256	0·163	0·116	0·002	0·092	0·141	0·187	0·057	0·024
	0·001	—	—	—	0·156	—	0·054	0·16	0·16	—
4	—	—	—	—	—	—	—	—	—	—
	0·001	0·07	0·303	0·048	0·156	0·0181	0·032	0·098	0·118	0·077

Legend:

v' \ v''
$I_{v'v''}/E^4_{v'v''}$
$p_{v'v''}$
$q_{v'v''}$

VOL. 7 1955

Table 2. Comparison between $I_{v'v''}/E^4_{v'v''}$ and $q_{v'v''}$ for the first negative system of N_2^+

v' \ v''	0	1	2	3	4
0	0·68	0·31	0·09	0·02	—
	0·68	0·30	—	—	—
	0·677	0·246	0·062	0·013	0·002
1	—	—	0·36	0·22	0·07
	0·28	—	0·36	0·23	—
	0·283	0·283	0·289	0·120	0·035
2	—	—	—	—	—
	0·04	0·40	—	0·27	0·21
	0·038	0·397	0·076	0·251	0·165

Legend:

v' \ v''

I/E^4 N_2 negative glow

I/E^4 N_2 + *He*

$q_{v'v''}$

Table 3. r-Centroids for the second positive and first negative band-systems

v' \ v''	0	1	2	3	4	5	6	7	8	9
0	1·182	1·148	1·116	1·086	1·058	1·032				
	1·097	1·053	1·013	0·974	—	—				
1	1·228	1·189	1·154	1·122	1·002	1·056	1·039	1·014		
	1·159	1·102	1·057	1·017	0·98	—	—	—		
2	1·280	1·234	1·195	1·160	1·129	1·099	1·072	1·046	1·021	
	1·265	1·162	1·106	1·061	1·022					
3	1·344	1·287	1·241	1·202	1·166	1·135	1·106	1·079	1·064	1·029
	—	—	—	—	—	—	—	—	—	—
4	1·426	1·351	1·294	1·247	1·298	1·173	1·141	1·113	1·086	1·061
	—	—	—	—	—	—	—	—	—	—

Legend:

v' \ v''

$\bar{r}_{v'v''}$ Second Positive

$\bar{r}_{v'v''}$ First Negative

JARMAIN, and NICHOLLS 1953, 1954), and $p_{v'v''}$ (determined from photographic intensity measurements by OMHOLT (1954), are presented in Table 1, for bands of the second positive system of N_2. Table 2 presents similarly $I_{v'v''}/E^4_{v'v''}$ and $q_{v'v''}$ for bands of the first negative system of N_2^+. In these tables, the increasing discrepancy between $I_{v'v''}/E^4_{v'v''}$ and $q_{v'v''}$ along a v'' progression is due to the variation of $R_e(r)$ with r. This variation was determined for the two band systems by the previously described method. $I_{v'v''}/q_{v'v''}\ E^4_{v'v''}$ was plotted, after suitable scaling for each progression, as a function of $\bar{r}_{v'v''}$ for each of the band systems. Table 3 presents an array of $\bar{r}_{v'v''}$ values for these systems computed by Mr. W. R. JARMAIN.

By a least-squares treatment, it was found that the data for the second positive system was best represented by

$$R_e(r) = \text{const}\,[-4{\cdot}74r^2 + 10{\cdot}0r - 4{\cdot}30] \qquad (5)$$

$$1{\cdot}02 < r < 1{\cdot}35\ \text{A}$$

while the data for the first negative system of N_2^+ was best represented by

$$R_e(r) = \text{const}\,[10{\cdot}1r^2 - 23{\cdot}5r - 14{\cdot}5] \qquad (6)$$

$$0{\cdot}974 < r < 1{\cdot}265\ \text{A}$$

From equation (2) it is evident that a "smoothed" array of vibrational transition probabilities $p_{v'v''}$ may be computed by multiplying the Franck-Condon factor $q_{v'v''}$ by $R_e^2(\bar{r}_{v'v''})$. Arrays of the smoothed vibrational transition probabilities are presented for the second positive system in Table 4 and for the first negative system in Table 5. Such "smoothed" data is superior to that in Tables 1 and 2, because experimental scatter has been substantially reduced and all of the intensity measurements play a part in determining $R_e(r)$ and thus $p_{v'v''}$.

Table 4. "Smoothed" relative vibrational transition probabilities $p_{v'v''} = R_e^2(\bar{r}_{v'v''})q_{v'v''}$ of the second positive band-system of N_2

v' \ v''	0	1	2	3	4	5	6	7	8	9
0	0·41	0·32	0·15	0·06	0·02	0·005				
1	0·31	0·02	0·20	0·13	0·05	0·02	0·01			
2	0·09	0·25	0·03	0·06	0·16	0·15	0·09	0·04	0·02	
3	0·01	0·16	0·13	0·10	—	0·09	0·15	0·11	0·06	0·03
4	—	0·03	0·18	0·04	0·13	0·02	0·03	0·10	0·12	0·08

Table 5. Smoothed relative vibrational transition probabilities $p_{v'v''} = R_e^2(\bar{r}_{v'v''})q_{v'v''}$ of the first negative band-system of N_2^+

v' \ v''	0	1	2	3	4
0	0·54	0·23	0·07	0·02	
1	0·21	0·21	0·27	0·26	0·05
2	0·04	0·29	0·06	0·23	0·17

VOL. 7 1955

Finally it may be noticed that, when required, relative vibrational populations $N_{v'}$ may be obtained by using equation (1) from a plot of $I_{v'v''}/E^4_{v'v''}R_e^2(\bar{r}_{v'v''})q_{v'v''}$ against v'.

Acknowledgments—The authors would like to acknowledge the invaluable assistance which they received during this work from Drs. P. A. Fraser and R. G. Turner and Messrs. W. R. Jarmain and B. G. Young.

One of us (L. V. W.) wishes to thank the Research Council of Ontario for the award of a scholarship during the tenure of which this work was carried out.

This work was supported by the Air Force Cambridge Research Center under contract AF19(122)–470.

Department of Physics,
University of Western Ontario.

L. V. Wallace*
R. W. Nicholls

References

Fraser P. A., and Jarmain W. R.	1953	*Proc. Phys. Soc.* **A66** 1145
Fraser P. A.	1954	*Can. J. Phys.* **32** 515
Fraser P. A.	1954	*Proc. Phys. Soc.* **A67** 939
Fraser P. A., Jarmain W. R., and Nicholls R. W.	1954	*Ap. J.* **119** 286
Hunter A., and Pearse R. W. B.	1936	*J. Sci. Instr.* **13** 403
Jarmain W. R., and Fraser P. A.	1953	*Proc. Phys. Soc.* **A66** 1153
Jarmain W. R., Fraser P. A., and Nicholls R. W.	1953	*Ap. J.* **118** 228
Jarmain W. R., and Nicholls R. W.	1954	*Can. J. Phys.* **32** 201
Jarmain W. R., and Nicholls R. W.	1955	Scientific Report No. 20, Dept. of Physics, University of Western Ontario, Contract AF19(122)–470
Nicholls R. W., Jarmain W. R., and Fraser P. A.	1953	*Can. J. Phys.* **31** 1019
Omholt A.	1954	*J. Atmosph. Terr. Phys.* **5** 63
Turner R. G., and Nicholls R. W.	1954	*Can. J. Phys.* **32** 468, 475

Recombination and ion production from the total electron content

(*Received* 4 *April* 1955)

In a recent paper (1954) we have suggested a method by which values of the coefficient of recombination α and the rate of ion production q may be deduced from the diurnal variation of the total electron content of a column of unit cross-section below the maximum of the layer. The mean coefficient of recombination $\bar{\alpha}$ and the mean rate of ion production $\bar{q}$ throughout the F-layer are defined by the equations

$$\bar{\alpha}\left(\frac{n}{y_m}\right)^2 y_m = \int_{h_0}^{h_m} \alpha N^2 \, dh \qquad \text{and} \qquad \bar{q}y_m = \int_{h_0}^{h_m} q \, dh$$

where the symbols have their usual interpretation. We suggested that if a parabolic layer is considered, then $\bar{\alpha} = 3\alpha/4$ and $\bar{q} = q/3$. Dr. W. Becker has been kind enough to point out that these figures result from an over-approximation, and that the assumption of a parabolic distribution of ionization density actually leads to $\bar{\alpha} = 6\alpha/5$ and $\bar{q} = 8q/15$.

* Now in the Department of Astronomy, University of Michigan, Ann Arbor.

This difference necessitates a slight revision of the values of q and α deduced from $\bar{q}$ and $\bar{\alpha}$ given in Table 1 of the previous paper. If a Chapman layer is assumed, then it may be shown that for small values of χ

$$\bar{q} = \frac{q_0}{2} \frac{\exp(1 - \sec\chi)}{\sec\chi} \qquad \text{and} \qquad \bar{\alpha} = \frac{9\alpha}{8} \exp(1 - \sec\chi)$$

It is perhaps an over-elaboration to include the terms in χ, since the deduction assumes that $y_m = 2H$, where H is the scale-height. At noon, when $\chi = 0$, it will be seen that there is very little difference between the correct deductions from the parabolic assumption and those from the Chapman layer.

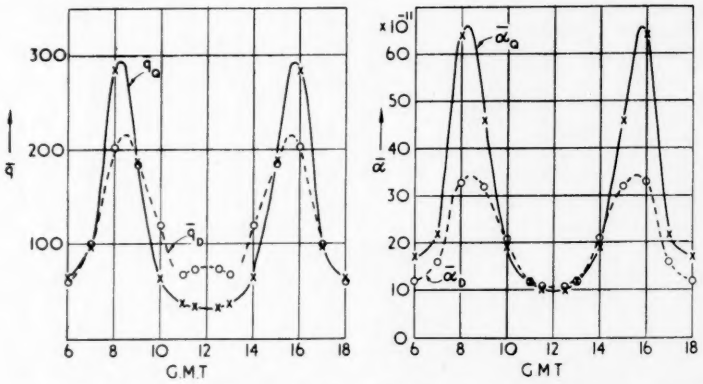

Fig. 1. Annual mean diurnal variation of $\bar{q}$ and $\bar{\alpha}$, $\bar{q}_D$ and $\bar{\alpha}_D$ on magnetically disturbed days, $\bar{q}_Q$ and $\bar{\alpha}_Q$ on magnetically quiet days.

Before using the method further, it is important to consider its advantages and limitations. It is an important improvement on the method of deducing α and q for the F-layer from the diurnal variation of N_m, since it takes into account variations in the thickness of the layer due to vertical ion drift. However, it must be remembered that both the method and the regular diurnal variation of n will be affected by any changes which may occur in the fraction of the total ionization which lies below the maximum of the layer. Such changes will occur in general when vertical ion drift is present, and will affect the values of $\bar{\alpha}$ and $\bar{q}$ obtained by the method. It is also assumed that $\bar{\alpha}$ and $\bar{q}$ vary symmetrically about noon.

Despite these limitations we have utilized the method further to deduce values of $\bar{\alpha}$ and $\bar{q}$ from the diurnal variations of n observed at Ibadan on magnetically quiet days, and also on magnetically disturbed days. The diurnal variations of n on quiet days (when the total of the geomagnetic planetary three-hour-range indices K_p is less than 16) and on disturbed days (when the total K_p is greater than 30) during the year 1952 have been given elsewhere (1955). The values of $\bar{\alpha}$ and $\bar{q}$ obtained from this data are shown in Fig. 1.

We feel that these results are of particular significance with respect to the vertical ion drift theories proposed by MARTYN (1947) to account for the behaviour of the F_2-layer. One would normally expect both $\bar{\alpha}$ and $\bar{q}$ to vary regularly with the time of day. The strong maxima observed for both 0800 hr and 1600 hr on quiet days indicates that some process is occurring that is not included in the theory. This, we would suggest, is a change, brought about by vertical ion drift, of the fraction of the ionization which lies below the maximum. On disturbed days it is seen that these anomalous maxima in the variation of $\bar{\alpha}$ and $\bar{q}$ are

VOL. 7 1955

considerably reduced. This is to be expected, since we have previously (1955) pointed out that the vertical ion drift is greatly reduced on disturbed days at Ibadan when the S_D motions oppose those of S_Q.

We conclude that although the mean diurnal variation of n shows no midday minimum, these results indicate that the effects of vertical ion drift, so conclusively shown by the midday minimum in the diurnal variation of N_m, are still to be seen in the distribution of n. A decrease of n below the normally expected values around midday on quiet days indicates either (1) a loss of ions due to increased α, or (2) loss of 'visible' ionization, i.e., ions contained in n, due to vertical ionic drift.

N. J. Skinner
R. W. Wright

University College,
Ibadan, Nigeria.

References

Becker, W.	1955	Private communication
Martyn, D. F.	1947	*Proc. Roy. Soc.* **A189,** 241
Skinner, N. J., and Wright, R. W.	1954	*J. Atmosph. Terr. Phys.* **5,** 290
Skinner, N. J., and Wright, R. W.	1955	*J. Atmosph. Terr. Phys.* **6,** 177

Some features of the E_2-layer observed at the ionosphere field station, Haringhata, Calcutta

(*Received* 19 *April* 1955)

An automatic ionospheric recorder has recently been installed at Haringhata, twenty-eight miles north of the city of Calcutta. During the short period that it has been in operation, some interesting features of the E_2-layer have been observed. These are briefly described below:

Appearance of the E_2-layer on the records is a normal daytime feature of this station. The hour at which it is formed is not, however, the same on all days. Sometimes it can be distinguished in the forenoon traces, but it is more usually observed in the afternoon records at or after 1300 hours local time. The E_2-layer first appears as a sort of "ridge" in the F_1-layer trace (Skinner, Brown, and Wright, 1954). Records (a), (b) and (c) of Fig. 1 show the beginning of the process. It then moves downwards and merges with the E_1-layer (Fig. 2). The process will be clear from the plot of the time variations of $h'F_1$, $h'E_2$, and $h'E_1$ shown in Fig. 3. The merging of the E_2-layer with E_1 is frequently associated with scatter at frequencies near f^0E_1 (Fig. 2c), followed by formation of sporadic E ionization (Fig. 2e).

It is to be noted that this downward movement of the E_2-layer is essentially different from the descent of ion-clouds from F-region to E-region as reported from auroral latitude stations (Hagg and Hanson, 1954). In this case the ionization is patchy and its occurrence is of sporadic nature. The E_2-layer movement recorded above is of regular occurrence and the layer concerned is not patchy, but is thick and extended as shown by the P'-f traces.

The ionospheric recorder in operation is of the type developed by the Commonwealth Scientific and Industrial Research Organization, Australia, and has been presented to the

University of Calcutta on permanent loan. The operational characteristics of the recorder are as follows:

Frequency sweep:	1·0 to 13·0 Mc/s in 1 min 55 sec, at intervals of ten minutes.
Peak power:	About 1 kW.
Aerial system:	Vertical deltas.

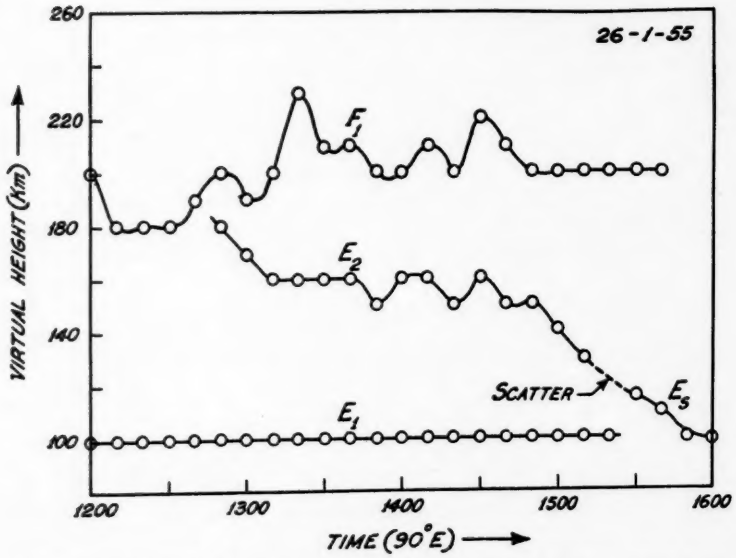

Fig. 3. Time variation of the virtual heights of E_1-, E_2-, and F_1-layers. The E_2-layer originates at the F_1-layer level (180 km). It then moves downwards and finally forms a sporadic E-layer at the E_1-layer height.

The observations described form part of the programme of the Radio Research Committee, Council of Scientific and Industrial Research, Government of India.

The authors are grateful to Professor S. K. Mitra for encouragement and advice.

Institute of Radio Physics and Electronics,
University of Calcutta,
Calcutta, India.

A. K. Saha
S. Ray

References

Hagg, E. L., and Hanson, G. H. 1954 *Canad. J. Phys.* **32**, 790
Skinner, N. J., Brown, R. A., and Wright, R. W. 1954 *J. Atmosph. Terr. Phys.* **5**, 92

VOL. 7 1955

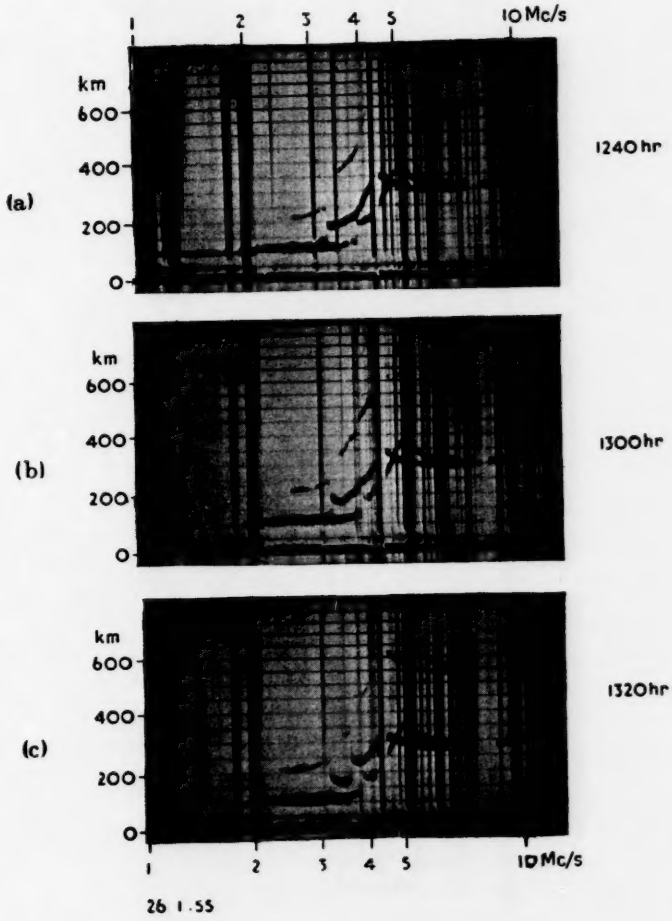

Fig. 1. Illustrating the formation of the E_2-layer originating from a "ridge" in the F_1-layer trace.

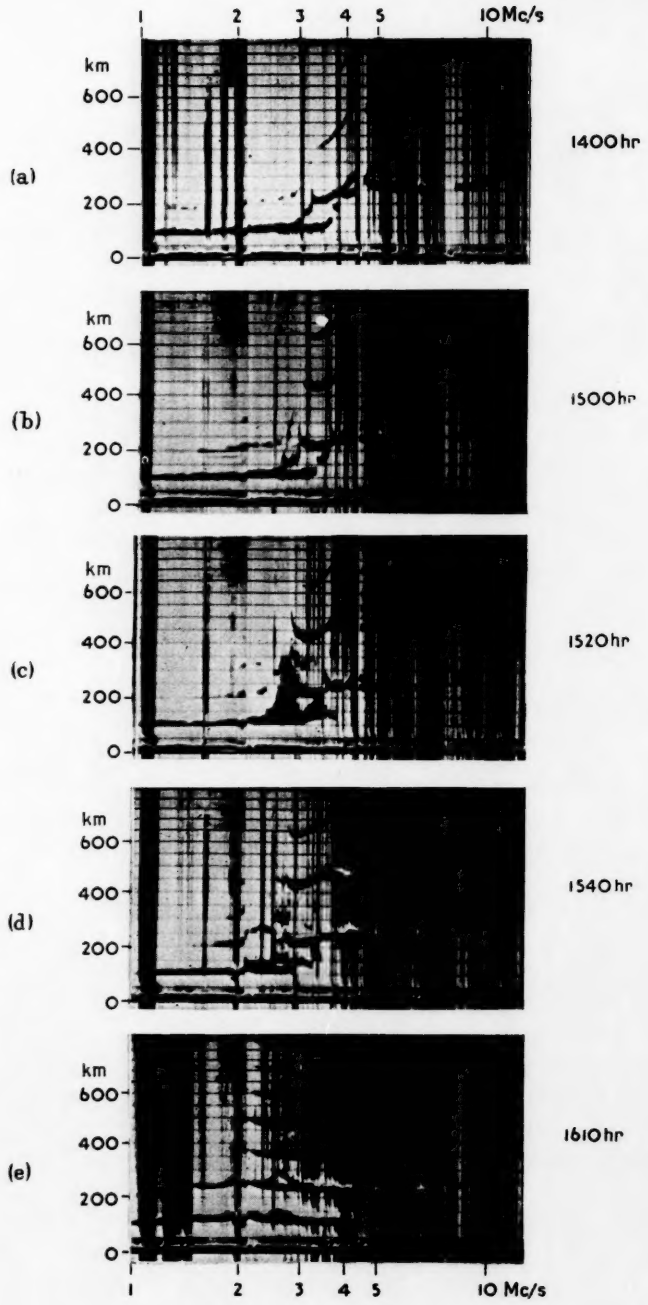

Fig. 2. Illustrating the downward movement of the E_2-layer and the subsequent formation of sporadic E ionization at the E_1-layer height.

VOL.
7
1955

Book reviews

LOVELL, A. C. B.: **Meteor Astronomy.** xiv + 463 pp., 3 plates, 187 figs., 175 tables. Clarendon Press, Oxford, 1954. 60s. net.

OLIVIER's treatise on meteors has stood for thirty years as the classical text on the subject, and it will continue to be of value for its exhaustive treatment of the earlier visual observations. However, the new and powerful radio techniques, together with recent improvements in the photographic methods, have so greatly increased our knowledge of meteoric phenomena that the need of a modern and comprehensive summary has become acutely apparent. This book by LOVELL may be fairly said to meet the requirement admirably, both as a reference volume for the experienced worker, and as an advanced text for scientists in allied fields who are finding more and more that their own disciplines are affected by these studies. This is not to say that the book has no appeal for the educated layman—quite the contrary—the freely flowing style throughout, combined with a trenchant ability to paraphrase in concise and easily understood terms some of the more recondite literature on the subject, will definitely attract the reader who is mainly interested in extending his scientific horizon.

It should be emphasized that the major theme is meteor astronomy, which, by definition, describes the history of the small particles up to the moment they are vaporized in the earth's upper atmosphere. Most of the work on meteor physics has been reserved for a complementary text promised at some future date, with the exception of some brief discussions of physical effects in the upper air which are necessary to an understanding of the astronomical observations. Little or no reference is made to spectroscopic studies or ionization measurements, and the subject of meteorites is not touched. As the reader peruses the book he may feel somewhat regretful on occasion that these matters are not presented in more detail, but nevertheless he should congratulate the author on having made a firm decision to stick to a natural division of the broad field and on covering that selected portion so thoroughly. Any attempt to embrace the entire range of meteoric phenomena in one volume would have seriously limited its usefulness as an authoritative reference work.

The opening chapter on visual and photographic techniques seems to treat the naked-eye observations rather sketchily, particularly as for some time to come the visual observer will continue to play an important part. ÖPIK's rocking-mirror method of measuring velocities is described, as well as the Harvard photographic methods, including a reference to the new Super-Schmidt cameras. The next two chapters outline the various radio-echo techniques, using both pulsed and continuous-wave transmissions, in somewhat greater detail, as these may not be as familiar to the classical astronomer. Conversely, the next chapter deals with the equations of meteoric motion for the benefit of the radiophysicists who may lack an astronomical background.

The two chapters on diurnal and seasonal variation and number and mass distribution of sporadic meteors tend to redress the balance for the neglected visual observer, as much of the information is visual or telescopic. It is indeed interesting to review the attempts of many brilliant men, such as SCHIAPARELLI and HOFFMEISTER, to resolve a large mass of confusing and complicated data, much of which were later shown to be erroneous, in order to draw a coherent picture. While the general problem is still far from being clarified and presents a continuing challenge to future workers, certain aspects of it have been put on a more solid footing by the application of new techniques, which hold out hope for rapid advancement of our knowledge. In particular, the measurement of the velocities of the sporadic meteors has received special attention in recent years because of its bearing on the long-standing question of whether meteors come from interstellar space or are members of the solar system.

LOVELL devotes four chapters to this velocity problem, roughly one-quarter of his book. This has been necessary because the rocking-mirror experiments of ÖPIK yield results in contradiction with WHIPPLE's photographic velocities and the radio-echo observations. The lengthy analysis of ÖPIK's work has failed to show decisively whereby his reasoning might be reconciled with the later observations, but it does serve the purpose of summarizing his data and conclusions in a form more palatable to the average reader—particularly to this reviewer, who has found

some of ÖPIK's original papers to be very brilliant but difficult reading. PORTER's analysis of the British meteor data is discussed, and the very precise photographic measurements of velocities and radiants, made by WHIPPLE and JACCHIA, are covered in considerable detail in the book. To date the photographic results are the most accurate available but they are few in number and apply only to meteors brighter than zero magnitude. The Super-Schmidts are expected to extend the observations to the third magnitude. The apex and anti-apex velocity experiments carried out at Jodrell Bank, and the similar Canadian observations, are thoroughly discussed. These radio methods have extended the range of observations to the eighth magnitude and also have included the daylight hours. The conclusions to be drawn from all the contemporary investigations, with the exception of OPIK's work, is that very few sporadic meteors can be reaching us from interstellar space. In fact, at the time of writing this book there was no clear-cut and positive evidence of the existence of any meteors with highly hyperbolic velocities, but the search will be continued and extended to fainter magnitudes. In the light of present information, it would be just as implausible to assert that we are receiving no visitors at all from outside the solar system as it would be to say that the majority are from interstellar space.

The major meteor showers are each discussed fully, using data from all available sources. In the case of the daytime showers, of course, practically all of the information comes from the Jodrell Bank workers, who are unchallenged in this particular field. LOVELL discusses the number and mass distribution of the shower meteors, and enlarges on the cosmological relationships of meteors, indicating the probability that some streams have cometary associations and others have not. Both WHIPPLE and LOVELL have pointed out that many of the sporadic meteors have short-period direct orbits near the plane of the ecliptic and hence are more likely to be asteroidal in nature. There is further speculation on the origin and history of some of the showers, in view of current theories on the dispersive effects acting on the particles.

The volume contains a large number of very useful tables and is copiously illustrated with line drawings, although the paucity of half-tone plates is to be regretted—this is presumably dictated by the publisher. It contains the essential background information needed not only by every scientific worker in the field but also by radar and communications engineers, who are beginning to realize that meteoric effects may be assets in some of their projects and liabilities in others; in either case the meteors cannot be ignored.

D. W. R. MCKINLEY

WOLFGANG YOURGRAU and STANLEY MANDELSTAM; **Variational Principles in Dynamics and Quantum Theory**, Sir Isaac Pitman & Sons, Ltd., London, 1955. ix + 155 pages. 25s.

The aim of this book is to review the historical development of variational principles in physics and to assess their epistemological significance. The authors do not delve very far below the surface, but they are clearly aware of the limited scope of their enquiry and they have the great merit of going directly back to the sources. The result is a clear, straightforward, reliable account of the subject, from the treatment of the reflection of light attributed to HERO of Alexandria to the ideas of DE BROGLIE and SCHRÖDINGER, with due emphasis on the work of HAMILTON and JACOBI. The authors develop all calculations in great detail, writing out every step; a feature which will no doubt be welcomed by the student and may in fact be a valuable help to him, provided that he has sufficient self-discipline to try to do the job by himself first. The epistemological chapter must be commended for its sound common sense and its polite, but quite effective, exposure of the incredible childishness with which some very great men have approached the philosophical aspect of the problem. Altogether a neat, unpretentious piece of work, which will be read with interest by experienced physicists, but which above all will be profitably used by students as a first introduction into an important subject of great educative value.

L. ROSENFELD

VOL. 7 1955

HEINZ REUTER; **Methoden und Probleme der Wettervorhersage.** 161 pp. 46 figs. Springer-Verlag, Vienna, 1954. 37s. 6d.

Although containing short paragraphs on the forecasting of temperature, cloud, and precipitation, this attractive work is concerned almost exclusively with the problem of predicting the future pressure and contour patterns over time-intervals of some twenty-four hours.

The methods of attacking this problem, which may be called the basic forecasting problem, are at the present time in a rather confusing stage which will in later years come to be regarded as a stage of transition. Until the period of the last World War the methods had remained largely a matter of experience and simple extrapolation backed up by a growing body of physical and dynamical understanding, but with this rather in the nature of background thinking than of systematic method.

In recent years the dynamical behaviour of the atmosphere on the synoptic scale has been greatly clarified, and three-dimensional analysis, coupled with dynamical principles, now competes with experience and extrapolation for pride of place in the derivation of the forecast chart.

Almost certainly we are moving rapidly towards the next phase, when systematic calculation will establish the dynamical forecast as the primary step, with experience and extrapolation then relegated to the more subordinate position. One may expect that electronic computing methods will, in this special problem, take over from the "expert", although, so far as can yet be seen, the prediction of details of winds, temperatures, cloud, visibility, and precipitation must remain a matter of expert judgment for much longer.

With the subject in such a state of change, a textbook is at the same time both exceptionally difficult to write and exceptionally valuable to the forecasting profession if it is well written. And Dr. REUTER has succeeded quite remarkably well. He has struck upon a level of mathematics which needs neither be despised by the theoretician nor avoided by the practical forecaster whose theoretical tools may have become rusty. The style is direct and economical, avoiding on the one hand the stringent presentation beloved of the mathematician and on the other hand the tedious prolixity which so often mars the writing of the synoptic meteorologist, too aware of his subject's complexities.

We find, of necessity, the classical gradient wind and the thermal wind equations together with MARGULES'S equations for the slope of a surface of discontinuity, but almost at once we meet modern ideas with zonal indices and ROSSBY'S wave equation. Kinetic formulae, after PETTERSSEN, occupy one chapter, to be followed by two chapters of a kind peculiar to present-day synoptic forecasting, a sort of descriptive mixture of three-dimensional dynamics, kinematics, and extrapolation.

There is nothing more difficult than to describe how these ideas are combined to produce a forecast chart (a prebaratic), but Chapter V is a successful digest supported by a definite illustrative example.

The more mathematical and dynamical treatment of Chapter VI discusses models, introduces pressure as a vertical co-ordinate, deals with the tendency equation and divergence, derives the equations for the barotropic atmosphere, which then lead to an excellent introduction to numerical forecasting by integration. "Development theory" as evolved in England is very fairly treated.

The book will be particularly acceptable in this country, as the basic techniques are familiar through English texts and through our national forecasting procedures. No forecaster who can manage the German, written in particularly lucid and uninvolved style, should miss this work, while the university teacher wishing to complete an introductory course on dynamical meteorology with a discussion on current methods of practical forecasting might well use the book as an additional text. There is no work available in English at the present time covering this particular field.

It should, however, be noted that the comprehensive title is a little misleading. There is no attempt to cover the broad field of weather prediction problems; thermodynamical processes, as distinct from the dynamical and kinematical, receive scant attention, but as a monograph of limited scope the work is useful and timely.

R. C. SUTCLIFFE

Obituary

Professor ERICH REGENER

On 27th February 1955 ERICH REGENER died, after a short illness, aged 73. He had still been at work a week before, pursuing his geophysical collaboration with colleagues abroad, and conducting the last of his typical experiments: he produced molecular beams emitted from a cooled ice-surface and directed them to a mirror cooled with liquid air; the ice was deposited on the mirror in a thin, slowly growing layer with beautiful interference colours, which could be measured and interpreted to indicate the very low densities of the molecular beam.

REGENER was born on the 12th November 1881 near Bromberg. Fortunately for geophysics, his doctor's dissertation (with WARBURG, Berlin) dealt with the ozone spectrum, and this may explain why REGENER found the way from the laboratory to the outside study of the physical phenomena provided by Nature. He is perhaps best known for his famous ascents, made with three or four huge balloons, to measure ozone and cosmic rays high in the stratosphere. Other characteristic and pioneer experiments were the measurement of the intensity of cosmic radiation in the greatest depth (250 m) of Lake Constance, and the development of apparatus for measuring pressure and temperature as well as for photographing the solar spectrum, intended for the first scientific ascent of a V2-rocket.

REGENER was professor of physics—from 1911 at the Landwirtschaftliche Hochschule Berlin; from 1920 at the Technische Hochschule Stuttgart. When, in the midst of a most successful career in research and teaching, he was, in 1937, forced to give up his chair at Stuttgart, the Max Planck-Gesellschaft (then Kaiser Wilhelm-Gesellschaft) provided him with a research institute for the physics of the stratosphere, first at Friedrichshafen, then at Weissenau near Ravensburg, Württemberg.

His many friends and collaborators all over the world will always remember his outstanding personality, combining rare experimental ability with the gift of inspiring others to excellent work.

For more detailed accounts of REGENER's life and work, see W. BOTHE and O. HAHN, *Zs. Naturforschung* **6a**, 565 and 568 (1951); W. BRAUNBEK, *Physikal. Blätter* **7**, 516 (1951); A. EHMERT, *Physikal. Blätter* **11** (1955).

J. BARTELS

VOL. 7 1955

Journal of Atmospheric and Terrestrial Physics, 1955, Vol. 7, pp. 113 to 127. Pergamon Press Ltd., London

Geometrical theory of sound propagation in the atmosphere

G. V. Groves
Department of Physics, University College, London

(*Received* 29 *March* 1955)

ABSTRACT

This paper deals with the geometry of sound waves and rays propagated in a moving inhomogeneous medium with particular reference to the atmosphere. The theory developed is, essentially, a generalization of that in geometrical optics for the propagation of light in an inhomogeneous isotropic medium to the case where the medium is in motion. Differential equations defining the wavefront and rays of a sound propagation in an inhomogeneous moving medium are derived, and then transformed by expressing the unit normal of the wavefront in terms of certain trace velocities. With the equations in this form, an integral is immediately obtainable for sound propagated in the atmosphere by assuming that the velocity of sound and wind-velocity vector are functions of height only. From this solution the law of refraction, the condition for total reflection of a sound ray, and the equations for the wavefront at any time are found.

By way of example, the theory is applied to a simple velocity of sound v. height relation, and expressions are obtained for the range and time at which the abnormal sound propagation from a ground-level source returns to earth. Numerical results calculated from these formulae are found to be in accord with observations that have been made on this phenomenon.

1. Introduction

It is a well-known result of optics that the wave theory of propagation of light can be replaced by a geometrical theory in the limiting case when the wavelength becomes zero. The concept of a ray of light can then be introduced, and the propagation can be described in terms of bundles of such rays. For a medium whose properties vary continuously in both space and time, the geometrical theory remains a valid approximation to the wave theory, as long as the changes in refractive index are small over distances of a wavelength, and for the duration of a period of the wave motion: atmospheric refraction of light is dealt with on this assumption. In acoustics the situation is analogous; and the propagation of sound in a continuous medium can be treated by a geometrical theory even when the medium is in motion, provided the variations in the properties of the medium are sufficiently small. This result has been established by Blokhintzev (1946), starting from the wave equations for the propagation of sound in an inhomogeneous moving medium.

As changes in the state of the atmosphere are generally small over distances of say 100 m and during time intervals of the order of a second, the geometrical approximation will be valid for wavelengths well into the infrasonic region, and will therefore cover most cases of practical interest. A number of problems on sound propagation in the atmosphere have been treated on this assumption, and some of the more interesting results are surveyed briefly in the next section. These developments, however, fail to provide an adequate theoretical structure for the satisfactory solution of some of the more complicated problems that can arise, such as the determination of upper atmosphere properties by sound propagation methods. The present paper has been written to meet this need; and its object is to obtain a general solution for the propagation in the atmosphere

of sound rays and wavefronts in terms of the velocity of sound and wind fields. The inverse problem of deducing atmospheric properties from observations on sound propagation will be dealt with in a later paper.

2. PREVIOUS THEORETICAL DEVELOPMENTS ON SOUND IN THE ATMOSPHERE

The presence of a wind gradient in the atmosphere as a cause of refraction of a sound wave was suggested by STOKES (1857) to account for the increased intensity of a sound down-wind from its source. This explanation was also given by REYNOLDS (1874), who pointed out that changes in air temperature would also cause refraction on account of the dependence of the velocity of sound on temperature. One of the first theoretical accounts of these two effects was given by RAYLEIGH (1896), who introduced the concept of sound rays and derived equations for their paths. He obtained the law of refraction at the interface between two different horizontal wind streams by considering the velocity of trace of the wavefront along the surface of separation. This argument still applies when the velocity of sound also changes across the boundary; and RAYLEIGH's formula

$$c \sec \theta + u = \text{const.}, \tag{1}$$

where θ is the inclination of the wavefront normal to the horizontal, holds when both the velocity of sound c and horizontal wind velocity u are functions of height.

RAYLEIGH did not reckon, however, with the fact that in the presence of wind the direction of a sound ray in space is not necessarily along the wavefront normal. This was pointed out by BARTON (1901), who showed that when wind speed increases with height, total reflection of a sound ray can occur. BARTON considered the case of a linear increase of wind speed with height, and derived the equation of sound rays from a source at the origin: in the case where the wavefront is horizontal initially, the paths are parabolas, and the wavefront remains horizontal during propagation. The corresponding problem for a linear temperature variation with height has been considered by LAMB (1925), who showed that the sound rays are cycloids generated by circles rolling on the horizontal line of zero absolute temperature.

During the first world war and at times since, sound propagation in the atmosphere has received attention in connection with the detection and location of aircraft. One of the problems considered has been the determination of corrections for temperature and wind variations to be applied to the observed direction of arrival of the sound wavefront, in order to find the true direction of the aircraft. In his account of this work, MILNE (1921) gave the first generalized treatment of sound propagation in three dimensions. He obtained the differential equations for the path of a ray in space, and also the partial differential equation satisfied by the wavefronts, but the correspondence between rays and wavefronts was not made apparent. For a stratified medium MILNE obtained an integral in the form of the refraction formula (1) and also showed that the azimuth angle of the wavefront normal along a particular ray remains constant. These two results have since provided the principal means for discussing sound propagation in the atmosphere.

VOL. 7 1955

3. Choice of Notation for Wavefronts and Rays

A wavefront is defined as the surface of sound disturbances which were emitted from the source at the same time. This definition applies not only to a pulse of short duration, but also to a continuous emission, and in the case of a vibration of single frequency means that a wavefront is a surface containing all points of the medium that are in the same phase of vibration.

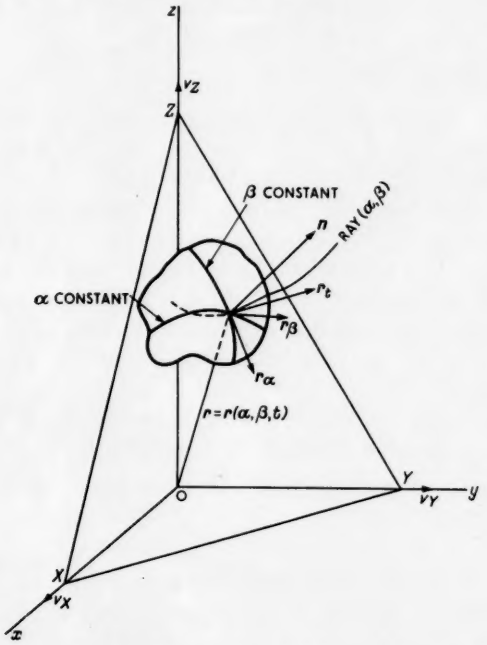

Fig. 1. Diagram showing notation used for wavefront and rays.

Consider a certain wavefront, and let its equation at time t be

$$\boldsymbol{r} = \boldsymbol{r}(\alpha, \beta, t) \tag{2}$$

with reference to a fixed origin O. The values (α, β) are taken as parametric co-ordinates to the points of the surface. See Fig. 1. Write

$$\boldsymbol{n} = \boldsymbol{n}(\alpha, \beta, t) \tag{3}$$

for the unit normal at the point (α, β), then

$$\boldsymbol{n}^2 = 1 \tag{4}$$

and

$$\boldsymbol{n} \cdot \boldsymbol{n}_\alpha = \boldsymbol{n} \cdot \boldsymbol{n}_\beta = \boldsymbol{n} \cdot \boldsymbol{n}_t = 0, \tag{5}$$

where the suffixes α, β, and t denote partial differentiation with respect to these quantities. The vectors $\boldsymbol{r}_\alpha$ and $\boldsymbol{r}_\beta$ can readily be shown to lie in the tangent plane at (α, β), and so

$$\boldsymbol{n} \cdot \boldsymbol{r}_\alpha = \boldsymbol{n} \cdot \boldsymbol{r}_\beta = 0. \tag{6}$$

Furthermore, $\boldsymbol{r}_\alpha \wedge \boldsymbol{r}_\beta$ is a vector perpendicular to the tangent plane at (α, β), and therefore

$$\boldsymbol{n} = (\boldsymbol{r}_\alpha \wedge \boldsymbol{r}_\beta)/|\boldsymbol{r}_\alpha \wedge \boldsymbol{r}_\beta|. \tag{7}$$

Let P be a point on the wavefront with the co-ordinates

$$\alpha = \alpha(t) \qquad \beta = \beta(t)$$

at time t. Then

$$\boldsymbol{r} = \boldsymbol{r}(\alpha(t), \beta(t), t)$$

is the locus of P in space; and

$$d\boldsymbol{r}/dt = \boldsymbol{r}_t + \alpha'(t)\boldsymbol{r}_\alpha + \beta'(t)\boldsymbol{r}_\beta \tag{8}$$

is the velocity vector of P. So far the parametric co-ordinate system (α, β) on the wavefront at time t has been arbitrarily assigned. It will now be supposed that the co-ordinates (α, β) are chosen on each successive wavefront surface, so that when the locus of P is a sound ray, $\alpha(t)$, $\beta(t)$ are independent of t for all points P. Then by (8), $\boldsymbol{r}_t$ is the velocity vector of the sound ray in space at time t. As all points on the same ray now have the same co-ordinates (α, β), these can be taken as co-ordinates defining the ray; and the equation of the ray (α, β) is (2).

4. Geometrical Equations of Sound Propagation in an Inhomogeneous Moving Medium

Let the phase of the sound propagation under consideration be

$$\psi = \omega[t - \theta(\boldsymbol{r})/c_0]$$

at point $\boldsymbol{r}$ and time t, where c_0 is a reference velocity and ω the frequency. The equation of the wavefront defined by the phase $\psi = \psi_0$ is then

$$\theta(\boldsymbol{r}) = c_0(t - \psi_0/\omega). \tag{9}$$

The condition defining the propagation of a wavefront in geometrical acoustics has been derived by Blokhintzev (1946) in the form of the eiconal equation

$$|\nabla\theta| = c_0/(c + \boldsymbol{w} \cdot \boldsymbol{n}), \tag{10}$$

where c is the velocity of sound and $\boldsymbol{w}$ the velocity of the medium. Putting $\boldsymbol{r} = \boldsymbol{r}(\alpha, \beta, t)$ in (9), and differentiating partially with respect to α, β, and t, it is seen that

$$\boldsymbol{r}_\alpha \cdot \nabla\theta = \boldsymbol{r}_\beta \cdot \nabla\theta = 0 \tag{11}$$

$$\boldsymbol{r}_t \cdot \nabla\theta = c_0. \tag{12}$$

Hence by (6) and (11), $\nabla\theta$ is parallel to $\boldsymbol{n}$ and so can be written

$$\nabla\theta = |\nabla\theta|\,\boldsymbol{n}.$$

Substituting this equation into (12) and using (10), the equation defining the wavefront becomes

$$\boldsymbol{r}_t \cdot \boldsymbol{n} = c + \boldsymbol{w} \cdot \boldsymbol{n}. \tag{13}$$

VOL. 7 1955

If P is the point of the wavefront whose co-ordinates are

$$\alpha = \alpha(t) \qquad \beta = \beta(t),$$

it follows from (6), (8), and (13) that

$$(d\boldsymbol{r}/dt) \cdot \boldsymbol{n} = c + \boldsymbol{w} \cdot \boldsymbol{n}, \tag{14}$$

i.e. the component of the velocity of P along the normal is independent of $\alpha(t)$, $\beta(t)$. If the locus of P is orthogonal to the wavefront at all times, then

$$d\boldsymbol{r}/dt = q\boldsymbol{n}, \tag{15}$$

where, by (14),

$$q = c + \boldsymbol{w} \cdot \boldsymbol{n}. \tag{16}$$

$q\boldsymbol{n}$ is the velocity of propagation of the wavefront in space. A partial differential equation for this surface is obtained by substituting from (7) and (8) into (15).

Although (15) and (16) define the wavefront and the system of orthogonal curves, the ray paths themselves cannot be determined without introducing some more general assumption such as FERMAT's principle of least time. It appears simpler though to start from a principle defining the kinematics of an element of the wavefront (MILNE, 1921), and this will be adopted here. It is assumed that the velocity of the element of the wavefront at the point (α, β) at time t is the sum of

(i) the velocity of sound $c(\boldsymbol{r}, t)$ in the direction of the wavefront normal;

(ii) the velocity of the medium $\boldsymbol{w}(\boldsymbol{r}, t)$.

This assumption is expressed by

$$\boldsymbol{r}_t = \boldsymbol{w}(\boldsymbol{r}, t) + c(\boldsymbol{r}, t)\boldsymbol{n}. \tag{17}$$

It is seen that this relation satisfies (13), showing that the wavefront is still propagated according to the eiconal equation. A partial differential equation for $\boldsymbol{r}(\alpha, \beta, t)$ is obtained by substituting for $\boldsymbol{n}$ from (7). An alternative treatment is to derive $\boldsymbol{n}_t$ in terms of $\boldsymbol{r}$ and $\boldsymbol{n}$ and solve this relation simultaneously with (17). In this way one partial differential equation can be replaced by two ordinary differential equations. The procedure is as follows. Equation (6) is differentiated with respect to t to give

$$\boldsymbol{r}_\alpha \cdot \boldsymbol{n}_t + \boldsymbol{r}_{\alpha t} \cdot \boldsymbol{n} = 0;$$

and (17) is differentiated with respect to α to give

$$\boldsymbol{r}_{\alpha t} = (\boldsymbol{r}_\alpha \cdot \nabla)\boldsymbol{w} + (\boldsymbol{r}_\alpha \cdot \nabla c)\boldsymbol{n} + c\boldsymbol{n}_\alpha,$$

where ∇ operates on scalar functions of $\boldsymbol{r}$ to give the gradient vector while α, β and t are kept fixed. Eliminating $\boldsymbol{r}_{\alpha t}$ from these equations, it is seen on using (4) and (5) that

$$\begin{aligned} \boldsymbol{r}_\alpha \cdot \boldsymbol{n}_t &= -[\boldsymbol{r}_\alpha \cdot \nabla(\boldsymbol{w} \cdot \boldsymbol{n}) + \boldsymbol{r}_\alpha \cdot \nabla c] \\ &= -\boldsymbol{r}_\alpha \cdot \nabla q \end{aligned} \tag{18}$$

by (16). By a similar argument (18) can be shown to hold when α is replaced by β.

This means that the vector $\boldsymbol{n}_t + \nabla q$ is perpendicular to both $\boldsymbol{r}_\alpha$ and $\boldsymbol{r}_\beta$ and hence lies in the direction of $\boldsymbol{n}$, i.e.

$$\boldsymbol{n}_t + \nabla q = \kappa \boldsymbol{n}.$$

Using (4) and (5) it is seen that

$$\kappa = \boldsymbol{n} \cdot \nabla q,$$

and therefore

$$\boldsymbol{n}_t = (\boldsymbol{n} \cdot \nabla q)\boldsymbol{n} - \nabla q. \tag{19}$$

(17) and (19) are two first-order equations which could be solved simultaneously for $\boldsymbol{r}(\alpha, \beta, t)$ and $\boldsymbol{n}(\alpha, \beta, t)$ in terms of the initial form of the wavefront.

5. Equations of Propagation in Terms of Trace Velocities v_X, v_Y, and v_Z

It is now proposed to derive an alternative form to equation (19) with $\boldsymbol{n}(\alpha, \beta, t)$ replaced by a new vector $\boldsymbol{h}(\alpha, \beta, t)$ defined below.

Let $Oxyz$ be three mutually perpendicular axes of reference and write

$$\boldsymbol{r} = (x, y, z)$$
$$\boldsymbol{n} = (\lambda, \mu, \nu)$$
$$\boldsymbol{w} = (u, v, w).$$

Define $v_X(\alpha, \beta, t)$, $v_Y(\alpha, \beta, t)$, $v_Z(\alpha, \beta, t)$ by

$$\lambda(\alpha, \beta, t)v_X(\alpha, \beta, t) = \mu(\alpha, \beta. t)v_Y(\alpha, \beta, t) = \nu(\alpha, \beta, t)v_Z(\alpha, \beta, t) = q(\boldsymbol{r}(\alpha, \beta, t), \boldsymbol{n}(\alpha, \beta, t), t). \tag{20}$$

These velocities can be given a simple interpretation. If the tangent plane at the point (α, β) of the wavefront at time t moves instantaneously in the direction of the normal, the points X, Y, Z where this plane cuts Ox, Oy, Oz have velocities q/λ, q/μ, q/ν, i.e. v_X, v_Y, v_Z, along Ox, Oy, Oz respectively (see Fig. 1). The relationship between λ, μ, ν and v_X, v_Y, v_Z is found from (16) and (20) to be

$$\left.\begin{aligned} \lambda &= 1\Big/v_X\left(\frac{1}{v_X^2}+\frac{1}{v_Y^2}+\frac{1}{v_Z^2}\right)^{\frac{1}{2}} \\ \mu &= 1\Big/v_Y\left(\frac{1}{v_X^2}+\frac{1}{v_Y^2}+\frac{1}{v_Z^2}\right)^{\frac{1}{2}}, \\ \nu &= 1\Big/v_Z\left(\frac{1}{v_X^2}+\frac{1}{v_Y^2}+\frac{1}{v_Z^2}\right)^{\frac{1}{2}} \end{aligned}\right\} \tag{21}$$

where v_X, v_Y, and v_Z are related by

$$c + \left(\frac{u}{v_X}+\frac{v}{v_Y}+\frac{w}{v_Z}\right)\Big/\left(\frac{1}{v_X^2}+\frac{1}{v_Y^2}+\frac{1}{v_Z^2}\right)^{\frac{1}{2}} = 1\Big/\left(\frac{1}{v_X^2}+\frac{1}{v_Y^2}+\frac{1}{v_Z^2}\right)^{\frac{1}{2}} = q. \tag{22}$$

Equation (19) will be transformed to the new variables v_X, v_Y, v_Z by writing it out in components as

$$\frac{1}{\lambda}\left(\frac{\partial \lambda}{\partial t}+\frac{\partial q}{\partial x}\right) = \frac{1}{\mu}\left(\frac{\partial \mu}{\partial t}+\frac{\partial q}{\partial y}\right) = \frac{1}{\nu}\left(\frac{\partial \nu}{\partial t}+\frac{\partial q}{\partial z}\right) = \boldsymbol{n} \cdot \nabla q. \tag{23}$$

VOL. 7 1955

A relation for $\boldsymbol{n} \cdot \nabla q$ is then found by taking the scalar product of (17) and (19) and using (4), (5), and (16):

$$\boldsymbol{w} \cdot \boldsymbol{n}_t + \boldsymbol{r}_t \cdot \nabla q = q(\boldsymbol{n} \cdot \nabla q).$$

This can be written, using (16), as

$$\partial q/\partial t - (\boldsymbol{w}' \cdot \boldsymbol{n} + c') = q(\boldsymbol{n} \cdot \nabla q), \tag{24}$$

where

$$\boldsymbol{w}' = [\partial \boldsymbol{w}(\boldsymbol{r}, t)/\partial t]_{\boldsymbol{r}\ \text{constant}}$$

$$c' = \partial c(\boldsymbol{r}, t)/\partial t]_{\boldsymbol{r}\ \text{constant}}.$$

Hence on eliminating $\boldsymbol{n} \cdot \nabla q$ from (23) and (24), it is found that

$$\begin{aligned}\partial q/\partial t - (c' + \lambda u' + \mu v' + \nu w') &= (q/\lambda)(\partial\lambda/\partial t + c_x + \lambda u_x + \mu v_x + \nu w_x)\\ &= (q/\mu)(\partial\mu/\partial t + c_y + \lambda u_y + \mu v_y + \nu w_y)\\ &= (q/\nu)(\partial\nu/\partial t + c_z + \lambda u_z + \mu v_z + \nu w_z),\end{aligned}$$

where suffixes x, y, and z denote partial differentiation with respect to these quantities. Using (21) and (22), the terms in these equations can be rearranged to give

$$\frac{\partial}{\partial t}\left(\frac{1}{v_X}\right) + \left(c_x + \frac{c'}{v_X}\right)\left(\frac{1}{v_X{}^2} + \frac{1}{v_Y{}^2} + \frac{1}{v_Z{}^2}\right)^{\frac{1}{2}} + \left(u_x + \frac{u'}{v_X}\right)\frac{1}{v_X} + \left(v_x + \frac{v'}{v_X}\right)\frac{1}{v_Y} + \left(w_x + \frac{w'}{v_X}\right)\frac{1}{v_Z} = 0 \tag{25}$$

$$\frac{\partial}{\partial t}\left(\frac{1}{v_Y}\right) + \left(c_y + \frac{c'}{v_Y}\right)\left(\frac{1}{v_X{}^2} + \frac{1}{v_Y{}^2} + \frac{1}{v_Z{}^2}\right)^{\frac{1}{2}} + \left(u_y + \frac{u'}{v_Y}\right)\frac{1}{v_X} + \left(v_y + \frac{v'}{v_Y}\right)\frac{1}{v_Y} + \left(w_y + \frac{w'}{v_Y}\right)\frac{1}{v_Z} = 0 \tag{26}$$

$$\frac{\partial}{\partial t}\left(\frac{1}{v_Z}\right) + \left(c_z + \frac{c'}{v_Z}\right)\left(\frac{1}{v_X{}^2} + \frac{1}{v_Y{}^2} + \frac{1}{v_Z{}^2}\right)^{\frac{1}{2}} + \left(u_z + \frac{u'}{v_Z}\right)\frac{1}{v_X} + \left(v_z + \frac{v'}{v_Z}\right)\frac{1}{v_Y} + \left(w_z + \frac{w'}{v_Z}\right)\frac{1}{v_Z} = 0. \tag{27}$$

In terms of the vector $\boldsymbol{h}(\alpha, \beta, t)$ defined by

$$\boldsymbol{h}(\alpha, \beta, t) = (1/v_X(\alpha, \beta, t),\ 1/v_Y(\alpha, \beta, t),\ 1/v_Z(\alpha, \beta, t)),$$

(25) to (27) can be written

$$\boldsymbol{h}_t + (|\,\boldsymbol{h}\,|\,c' + \boldsymbol{h} \cdot \boldsymbol{w}')\boldsymbol{h} + \nabla(|\,\boldsymbol{h}\,|\,c + \boldsymbol{h} \cdot \boldsymbol{w}) = 0. \tag{28}$$

Unlike $\boldsymbol{n}$, $\boldsymbol{h}$ is of course dependent on the choice of reference axes. (28) now replaces (19), and could be solved simultaneously with (17) for $\boldsymbol{r}(\alpha, \beta, t)$ and $\boldsymbol{h}(\alpha, \beta, t)$.

6. SOUND PROPAGATION IN THE ATMOSPHERE

A solution of equation (28) applicable to the case of a sound wave in the atmosphere will be derived under the following simplifying assumptions.

A.1—The velocity of sound $c(\boldsymbol{r}, t)$ and the wind velocity vector $\boldsymbol{u}(\boldsymbol{r}, t)$ are independent of t in the time interval for which the propagation is being considered.

A.2—Propagation takes place over a sufficiently small region of the earth's surface for the curvature of the earth to be neglected, and over this region $\boldsymbol{w}(\boldsymbol{r}, t)$ and $c(\boldsymbol{r}, t)$ are independent of horizontal displacements.

Taking the Oz axis in the vertical direction, these assumptions mean that $\boldsymbol{w}$ and c are functions of z alone, so that

$$c' = u' = v' = w' = c_x = u_x = v_x = w_x = c_y = u_y = v_y = w_y = 0.$$

In view of these relations, (25) and (26) become

$$\frac{\partial}{\partial t}\left(\frac{1}{v_X}\right) = \frac{\partial}{\partial t}\left(\frac{1}{v_Y}\right) = 0.$$

$v_X(\alpha, \beta, t)$ and $v_Y(\alpha, \beta, t)$ are therefore independent of t and can be written as

$$\begin{aligned} v_X &= a(\alpha, \beta) \\ v_Y &= b(\alpha, \beta) \end{aligned} \tag{29}$$

This means that along any ray (α, β), v_X and v_Y remain constant; and it is convenient to introduce a new parametric system of co-ordinates (a, b) defined by the transformation

$$\begin{aligned} a &= a(\alpha, \beta) \\ b &= b(\alpha, \beta). \end{aligned}$$

In the new co-ordinates the ray (α, β) becomes the ray (a, b) and a clear physical interpretation can be given to these co-ordinates as they are in fact the trace velocities v_X and v_Y. In practice, the co-ordinates of the ray received at a point O' on the ground can be determined directly by positioning microphones along axes parallel to Ox, Oy, and timing the arrival of the sound wave at each microphone. From the distance v. time curves for the passage of the wave along each axis the velocities at O' in each direction are found, and these are of course a and b. Should the microphone array at O' be situated on axes $O'x'$, $O'y'$ rotated at an angle ω from Ox, Oy, a and b can be obtained from the measured velocities a', b' by the transformation

$$\begin{aligned} 1/a &= \cos\omega/a' - \sin\omega/b' \\ 1/b &= \sin\omega/a' + \cos\omega/b' \end{aligned}$$

The solution for v_Z as a function of a, b, and z now comes from (22) and (29). These give

$$1/v_Z^2 = 1/q^2(a, b, z) - 1/k^2(a, b) \tag{30}$$

and

$$w(z)/v_Z = p(a, b, z)/k(a, b) - c(z)/q(a, b, z), \tag{31}$$

VOL. 7 1955

where

$$k(a, b) = + (1/a^2 + 1/b^2)^{-\frac{1}{2}} \tag{32}$$

$$p(a, b, z) = k(a, b)[1 - u(z)/a - v(z)/b]. \tag{33}$$

$k(a,b)$ is called the characteristic velocity* of the ray (a, b) and is independent of the choice of axes Ox and Oy.

Eliminating $q(a, b, z)$ from (30) and (31), it is found that

$$(c^2 - p^2)v_Z^2 + 2wpkv_Z + (c^2 - w^2)k^2 = 0.$$

Hence

$$v_Z/k = [wp \pm c(p^2 + w^2 - c^2)^{\frac{1}{2}}]/(p^2 - c^2), \tag{34}$$

and therefore

$$k/v_Z = [-wp \pm c(p^2 + w^2 - c^2)^{\frac{1}{2}}]/(c^2 - w^2). \tag{35}$$

Substituting (35) into (31) gives

$$k/q = [cp \mp w(p^2 + w^2 - c^2)^{\frac{1}{2}}]/(c^2 - w^2), \tag{36}$$

and therefore

$$q/k = [cp \pm w(p^2 + w^2 - c^2)^{\frac{1}{2}}]/(p^2 + w^2). \tag{37}$$

In (34) to (37), upper and lower signs correspond. This completes the solution for v_X, v_Y, v_Z.

7. Law of Refraction

The direction cosines of the wavefront normal are readily found from (20) and (29) to be

$$\lambda = q/a = (k/a)[cp \pm w(p^2 + w^2 - c^2)^{\frac{1}{2}}]/(p^2 + w^2) \tag{38}$$

$$\mu = q/b = (k/b)[cp \pm w(p^2 + w^2 - c^2)^{\frac{1}{2}}]/(p^2 + w^2) \tag{39}$$

$$\nu = (q/k)(k/v_Z) = [-cw \pm p(p^2 + w^2 - c^2)^{\frac{1}{2}}]/(p^2 + w^2), \tag{40}$$

using (35) and (29). Only two of these equations are independent in view of the relation $\lambda^2 + \mu^2 + \nu^2 = 1$. Substituting for q from equation (16), (38) and (39) give the law of refraction in the form

$$[c(z) + \lambda u(z) + \mu v(z) + \nu w(z)]/\lambda = a \tag{41}$$

$$[c(z) + \lambda u(z) + \mu v(z) + \nu w(z)]/\mu = b. \tag{42}$$

For fixed values of a and b these relations give the direction cosines of the wavefront normal along the ray (a, b). The solution of (41) and (42) for λ, μ, and ν as functions of a, b, and z is of course (38) to (40).

In the special case when the wavefront is parallel to the Oy axis, i.e., when $\mu = 0$, and when the wind velocity vector is everywhere horizontal, i.e., when $w(z) \equiv 0$, (41) becomes

$$c(z)/\lambda + u(z) = a.$$

* The term "apparent velocity" is sometimes used, because to an observer on the ground receiving the ray (a, b) the sound appears to be travelling along the ground with velocity k.

(42) gives $b = \infty$ and hence that $\mu \equiv 0$. This is the case for which (1) had been deduced previously. When $u(z) \equiv 0$, SNELL's law of geometrical optics is obtained.

From (41) and (42) it is seen that

$$\lambda/\mu = b/a. \tag{43}$$

This relation was derived by MILNE (1921), and means that along any ray the normal to the wavefront remains parallel to the same vertical plane.

8. Total Reflection of a Sound Ray

Total reflection of a ray occurs at heights for which $\partial z/\partial t = 0$, i.e., by the Oz-component of (17) for which

$$w(z) + c(z)\nu(a, b, z) = 0.$$

From (40), this condition holds when

$$p^2(z) + w^2(z) - c^2(z) = 0;$$

i.e., when

$$[c^2(z) - w^2(z)]^{\frac{1}{2}}/[1 - u(z)/a - v(z)/b] = k(a, b). \tag{44}$$

For λ, μ, ν to be real, (38) to (40) require $p^2 + w^2 - c^2 \geqslant 0$; and hence the ray must lie between two consecutive height levels satisfying (44). The path of the ray is a periodic curve.

The significance of the positive and negative signs in (38) to (40) is easily established. On an upwards path $\partial z/\partial t > 0$ and hence $\nu > -w/c$. Applying this condition to (40) it can be shown that the positive sign holds, provided p and $c^2 - w^2$ are positive quantities. Now, by (33), (41), and (42)

$$p = (c + \nu w)/(1 - \nu^2)^{\frac{1}{2}};$$

from which it follows that p has the minimum value $(c^2 - w^2)^{\frac{1}{2}}$ at $\nu = -w/c$. Hence p and $c^2 - w^2$ are always positive, since $c > w$ in reality. In the same way it can be shown that on the downwards path the negative sign holds in (40).

When no wind is present (44) reduces to $c(z) = k$, i.e., rays are reflected at heights where the velocity of sound equals their characteristic velocities. If the function $c(z)$ decreases and then increases with height, as for instance the function in Fig. 2, the rays from an aerial source having $k < c_0$, where c_0 is the ground-level velocity of sound, will remain trapped between two levels and not reach the ground.

9. Solution for Wavefront and Rays

Under assumptions A.1 and A.2, equation (17) can be written out in components as

$$\begin{aligned} \partial x/\partial t &= u(z) + c(z)\lambda(a, b, z) \\ \partial y/\partial t &= v(z) + c(z)\mu(a, b, z) \\ \partial z/\partial t &= w(z) + c(z)\nu(a, b, z), \end{aligned}$$

where $\lambda(a, b, z)$, $\mu(a, b, z)$, and $\nu(a, b, z)$ are the expressions (38) to (40). If these

VOL. 7 1955

equations are integrated along the ray (a, b), the equation of the wavefront at time t is obtained in the form

$$x \equiv x(a, b, z) = x_0(a, b) + \int_{z_0(a,b)}^{z} \frac{u(z) + c(z)\lambda(a, b, z)}{w(z) + c(z)\nu(a, b, z)}\, dz \tag{45}$$

$$y \equiv y(a, b, z) = y_0(a, b) + \int_{z_0(a,b)}^{z} \frac{v(z) + c(z)\mu(a, b, z)}{w(z) + c(z)\nu(a, b, z)}\, dz \tag{46}$$

$$t \equiv t(a, b, z) = t_0 + \int_{z_0(a,b)}^{z} \frac{dz}{w(z) + c(z)\nu(a, b, z)} \tag{47}$$

f denotes integration along the ray (a, b) and

$$x = x_0(a, b) \quad y = y_0(a, b) \quad z = z_0(a, b)$$

is the equation of the wavefront at time t_0. Only for certain special forms of $c(z)$ and $w(z)$ is it possible to evaluate (45) to (47); in other cases numerical methods would have to be utilized.

Tables for the calculation of sound-ray paths have been constructed by ROTHWELL (1947) in connection with experiments on the location of aircraft by sound carried out in 1930 and 1931. In order to find the path of a ray and its time of travel, the atmosphere is divided into horizontal layers sufficiently thin for $c(z)$ and $u(z)$ to be regarded as linear functions of z. The increments in x and t arising from each layer are then found and added together. Diagrams of sound rays are presented by ROTHWELL for atmospheres in which the function $c(z) + u(z)$ consists of one, two, three, and four contiguous straight lines. An elementary method for computing rays, also based on the procedure of matching a series of straight-line segments to the function $c(z)$, is given by SABY and NYBORG (1946). An example on the propagation of sound to great distances is considered in the next section.

10. Abnormal Propagation of Sound

The problem is now considered where sound from a ground-level source is reflected back to earth by a temperature inversion in the upper atmosphere. For simplicity it is assumed that there is no wind and that the variation of absolute temperature, and hence of $c^2(z)$, with altitude is the function shown in Fig. 2. Taking the source of sound at the origin, the co-ordinates of the point at which the ray (a, b) returns to earth are, by (45) and (46),

$$x = \int_{z=0}^{z=0} \frac{\lambda}{\nu}\, dz = [\pm]\frac{k}{a} \int_{z=0}^{z=0} \frac{c(z)\, dz}{[k^2 - c^2(z)]^{\frac{1}{2}}} \tag{48}$$

by (33), (38), and (40), and

$$y = \int_{z=0}^{z=0} \frac{\mu}{\nu}\, dz = \frac{a}{b}\, x \tag{49}$$

by (43) and (48).

In (48) the positive sign holds on the upwards path and the negative sign on the

downwards path. By (44) the vertex is reached when $c(z) = k$. (48) can therefore be expressed as

$$x = \frac{2k}{a}\left[\frac{1}{\gamma_1}\int_{c_0}^{c_m}\frac{c^2\,dc}{(k^2-c^2)^{\frac{1}{2}}} + \frac{c_m(h_2-h_1)}{(k^2-c_m^2)^{\frac{1}{2}}} + \frac{1}{\gamma_2}\int_{c_m}^{k}\frac{c^2\,dc}{(k^2-c^2)^{\frac{1}{2}}}\right], \tag{50}$$

where

$$2\gamma_1 = dc^2/dz = (c_m^2 - c_0^2)/h_1 \qquad (o < z < h_1)$$
$$2\gamma_2 = dc^2/dz \qquad (h_2 < z).$$

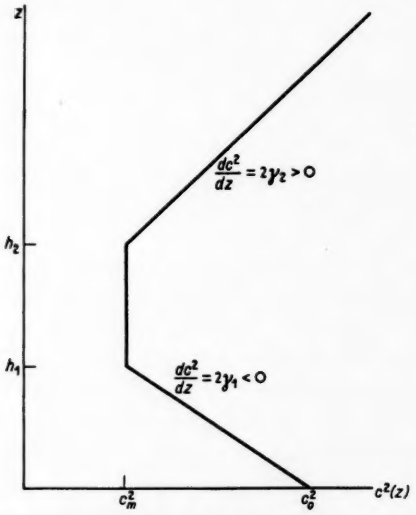

Fig. 2. Adopted form for $c^2(z)$, where $c(z)$ is the velocity of sound at height z.

The distance from the source at which the ray (a, b) returns to earth is

$$R(a, b) = (x^2 + y^2)^{\frac{1}{2}}$$
$$= |\, ax \,|/k \qquad \text{by (32) and (49);}$$

and on evaluating (50), this becomes

$$R(a, b) = |\, \{[k^2 \cos^{-1} c_0/k + c_0(k^2 - c_0^2)^{\frac{1}{2}}] - [k^2 \cos^{-1} c_m/k + c_m(k^2 - c_m^2)^{\frac{1}{2}}]\}/\gamma_1$$
$$+ 2c_m(h_2 - h_1)/(k^2 - c_m^2)^{\frac{1}{2}} + [k^2 \cos^{-1} c_m/k + c_m(k^2 - c_m^2)^{\frac{1}{2}}]/\gamma_2 \,|. \tag{51}$$

In the same way the time of travel of the ray is found from (47) to be

$$= \int_{z=0}^{z=0}\frac{dz}{cv} = [\pm]k\int_{z=0}^{z=0}\frac{dz}{c(z)[k^2 - c^2(z)]^{\frac{1}{2}}} \qquad \text{by (40)}$$
$$= (2k/\gamma_1)(\cos^{-1} c_0/k - \cos^{-1} c_m/k) + 2k(h_2 - h_1)/c_m(k^2 - c_m^2)^{\frac{1}{2}}$$
$$+ (2k/\gamma_2)\cos^{-1} c_m/k. \tag{52}$$

Knowing c_0, c_m, and h_1 from observations at the lower altitudes, (51) and (52) can be used to determine h_2 and γ_2 from measurements of the time of travel t and the characteristic velocity k of a sound ray from a source at known distance R.

VOL. 7 1955

This is essentially the method that has been used in the past for analyzing the results of sound propagation experiments (WHIPPLE, 1933).

Equation (51) shows that R depends only on the characteristic velocity k, and not on a and b separately. This means that the points where the rays (a, b) for which $1/a^2 + 1/b^2$ is constant return to earth lie on a circle centred on the source. The variation of R with k is plotted in Fig. 3 for typical values of the remaining quantities: the ground-level velocity of sound c_0 is taken to be 340 m/sec, and the value in the isothermal layer c_m to be 290 m/sec; the isothermal layer is taken to extend from $h_1 = 10$ km to $h_2 = 30$ km; γ_2 is taken equal to 1·0, 1·5, and 2·0 times $-\gamma_1$. The corresponding times of travel are shown in Fig. 4. k can vary from c_0 to ∞, but the graphs are plotted only as far as $k = 420$ m/sec, as reflected rays with values as large as this have only occasionally been received and most values have been found to be about 350 m/sec (WHIPPLE, 1935).

Fig. 3 shows that sound reaches points between 184 km and 211 km from the source when $\gamma_2 = -\gamma_1$; between 150 km and 187 km when $\gamma_2 = -\frac{3}{2}\gamma_1$; and between 132 km and 175 km when $\gamma_2 = -2\gamma_1$. These values are in agreement with the general conclusion that the inner boundary of an abnormal zone is roughly part of a circle of radius 100 km to 200 km (WHIPPLE, 1935). Fig. 3 also shows that the inner boundary does not arise from rays which leave the source along the ground ($k = 340$ m/sec), as might be expected. On account of the concentration of rays in the vicinity of the boundary, it should be possible to define it quite accurately from aural observations. Figs. 3 and 4 taken together show that at certain ground locations two rays are received in close succession. Several cases of double reception were recorded in the series of observations on gunfire carried out in 1929–1930 in England; the interval between pulses being most often three or four seconds (WHIPPLE, 1931). Triple reception also frequently occurred, and this phenomenon could no doubt be explained in terms of a more sophisticated temperature structure than that of Fig. 2.

It should be remarked that the above explanation of abnormal sound propagation needs some modification in order to represent the true state of affairs. A feature common to almost all observations that have been made on abnormal sound propagation is that the sound is usually received only on the west side of the source in summer and on the east side in winter. This was first noticed in connection with the firing on the western front in the first world war, and later in the gunfire experiments reported by WHIPPLE (1931), which could be successfully conducted in summer months only, as all observation points were situated in the north-west quadrant relative to the firing point. The reason for this seasonal change of conditions is undoubtedly the presence of stratospheric winds from the east in summer and the west in winter. The effect of wind on the abnormal propagation of sound is approximately to replace $c(z)$ by the algebraic sum of the velocity of sound in still air and the wind velocity component in the direction of the ray; and this interpretation needs to be given to $c(z)$ in Fig. 2. The existence of high winds in the stratosphere means that air temperatures can only be determined reliably by sound propagation experiments that are capable of separating out the wind contributions. This has been attempted with some success in more recent work (CRARY, 1952; RICHARDSON and KENNEDY, 1952).

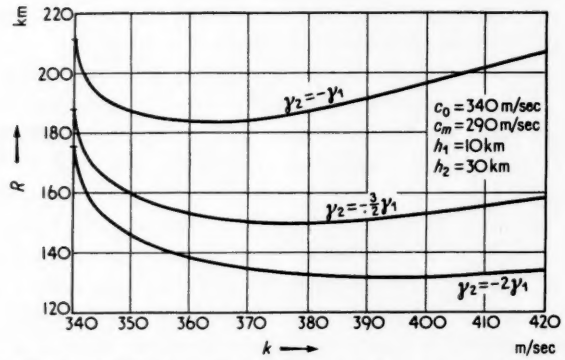

Fig. 3. Horizontal distance R at which a ray from a ground-level source returns to earth as a function of its characteristic velocity k.

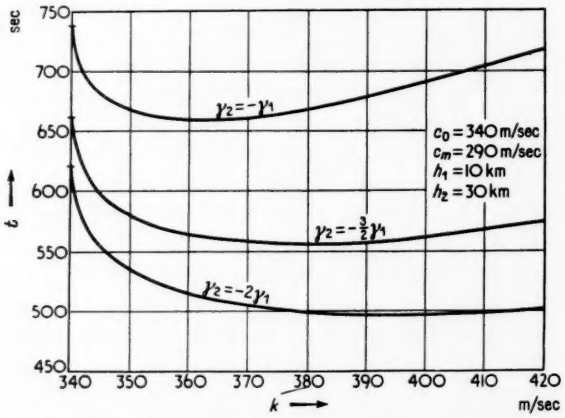

Fig. 4. Time to return to earth of a ray from a ground-level source as a function of its characteristic velocity k.

11. CONCLUSIONS

A solution has been obtained for the wavefront and rays of a sound propagation in the atmosphere on the assumption that the atmospheric properties are functions of height. Assumptions that have been made in previous treatments of this problem—e.g., that the vertical wind velocity component is zero, that the ray paths lie in vertical planes, that the wavefront is plane—have been found to be unnecessary. Of particular interest is the generalized form of SNELL's law given by (41) and (42).

A special feature of the theory is the assignment of co-ordinates to the sound rays. It has been shown that these co-ordinates can be chosen to be the trace velocities of the incident sound wave along two perpendicular lines on the ground at their point of intersection. They therefore have a distinct practical significance, as these two velocities can readily be measured; and it is indeed customary to do so in certain sound propagation experiments.

The problem of abnormal propagation of sound has been considered, and it

VOL. 7 1955

is shown that the theory explains the principal characteristics of this phenomenon in terms of a simple velocity of sound v. height relation.

References

Barton, E. H.	1901	*Phil. Mag.* **1,** 159
Blokhintzev, D.	1946	*J. Acoust. Soc. Amer.* **18,** 322
Crary, A. P.	1952	*J. Met.* **9,** 93
Lamb, H.	1925	*Dynamical theory of sound,* 2nd ed., 221
Milne, E. A.	1921	*Phil. Mag.* **42,** 96
Rayleigh, Lord	1896	*Theory of sound,* **2,** 2nd ed., 129
Reynolds, O.	1874	*Proc. Roy. Soc.* **22,** 531
Richardson, J. M., and Kennedy, W. B.	1952	*J. Acoust. Soc. Amer.* **24,** 731
Rqthwell, P.	1947	*J. Acoust. Soc. Amer.* **19,** 205
Saby, J. S., and Nyborg, W. L.	1946	*J. Acoust. Soc. Amer.* **18,** 316
Stokes, G. G.	1857	Brit. Assoc. Rep., 22
Whipple, F. J. W.	1931	*Quart. J. R. Met. Soc.* **57,** 331
Whipple, F. J. W.	1933	*Terr. Mag. At. El.* **38,** 13
Whipple, F. J. W.	1935	*Quart. J. R. Met. Soc.* **61,** 285

OL.
955

Journal of Atmospheric and Terrestrial Physics, 1955, Vol. 7, pp. 128 to 140. Pergamon Press Ltd., London

New experimental and theoretical investigations on the atmospheric ozone layer*

H. K. PAETZOLD
Max-Planck-Institut für Physik der Stratosphäre, Weissenau bei Ravensburg

(*Received* 20 *November* 1954)

ABSTRACT
A summary is given of theoretical and experimental investigations on the atmospheric ozone layer carried out by the author, discussing the photochemical constitution of ozone, determination of the vertical zone distribution, dependence of ozone on the latitude, ozone household, annual ozone course, and ozone as indicator for the transport of air (circulation and mass exchange).

ALTHOUGH a large number of investigations on the atmospheric ozone are already available, no qualitative satisfactory solution of the ozone problem has been attained as yet. The main reason for this is our poor knowledge of the vertical distribution of the ozone. This distribution is caused in a complicated way by several factors, such as photochemical constitution and destruction of ozone, horizontal and vertical air motions and oxidation processes. For this reason measurements of the total ozone amount on the ground are not sufficient for a satisfactory analysis of the household, of the dependence on latitude, of the annual course, etc., of ozone and its connection with the meteorological elements (circulation and mass exchange).

VOL. 7 1955

In order to supplement the available material, we have tried at the Weissenau Institute, during the last few years, to obtain more extensive material on the vertical ozone distribution. For this purpose we developed three methods:

1. Ascents with recording ultraviolet balloon-spectrographs.
2. Eclipses of the moon.
3. A cheap and easily fitted radiosonde.

The radiosonde is still being tested, so there are no measuring results as yet. The first two methods, however, produced a series of valuable observations which allow, with previous results of other authors, a more detailed analysis of the factors which influence ozone and its vertical distribution. The following gives a short summary of this subject.

METHODS FOR DETERMINATION OF THE VERTICAL OZONE DISTRIBUTION

1. *Method of balloon ascents*

We developed a spectrograph for ascents which was to be as stable as possible, but at the same time of little weight (PAETZOLD, 1954a; 1955a; 1954b). The optics, barograph, and thermograph were fitted in a closed metal case. It was important for the reproductive clearness of the spectrograph to be maintained, because the photographic-photometrically measured course of intensity in the sun's spectrum depends—due to the Fraunhofer-lines—on a well-focused clearness.

* Reported at the UGGI-assembly at Rome, 1954.

The apparatus proved to be so stable that even after rough landings it needed no readjustment, so that the observation material is homogeneous.

The dependence on wavelength of the quartz three-stage filter in front of the slit was determined by a method developed by us, which is based on diffraction at the slit (PAETZOLD, 1947, 1950a). An MgO-plate irradiated by the sun served as source of light, in the same way as with the first ascents with UV-spectrographs (REGENER, 1938). A ring-diaphragm was used for reducing the scattered light of the sky to 40 per cent. The influence of the remaining scattered light was determined separately on the ground. Its value did not amount to more than 3 per cent of the measured ozone value. The precision of the evaluation procedure was so intensified that the error in the determination of the vertical ozone distribution at 10-, 25-, and 30-km altitude was only $1 \cdot 10^{-3}$, $0{\cdot}5 \cdot 10^{-3}$, and $0{\cdot}3 \cdot 10^{-3}$ cm O_3/km.

The height of the balloon equipment was determined by barometer, and additionally at clear sight by telescope and ocular-micrometer. Even at altitudes above 30 km there were no greater differences between the two methods than 1 km, so that the error in the determination of altitude never exceeded 0·5 km.

Up to the present time we have carried out seventeen successful ascents during the different seasons. The highest altitude we reached was 38 km, the average altitude 31 km.

2. *Method of eclipses of the moon*

For the determination of ozone distributions up to the altitude of 45 km and in various latitudes, the method of eclipses of the moon, which has lately been developed by us, proved to be very suitable and should therefore be considered in future (PAETZOLD, 1950b, 1951a). By this method we measure, in the spectral region of the Chappuis bands, the distribution of light on the surface of the moon vertical to the limit of the earth's shadow and in the vicinity of it. If the moon is suitably passing through the earth's shadow, one can also determine with this method the ozone distribution at latitudes where observations are normally difficult to carry out. By measurements carried out by the author and from material obtained at previous eclipses of the moon, a total of eight ozone distributions (four at the equator and four at 65° geographical latitude) could be derived (PAETZOLD, 1952a, 1952b). It is interesting that the ozone absorption in the Chappuis bands causes a narrow greenish-coloured zone in the vicinity of the limit of the earth-shadow (PAETZOLD, 1951b, 1954c).

RESULTS AND DISCUSSION

1. *Photochemical theory of ozone, dependence on latitude, and ozone household*

First of all we are interested in the comparison between the observed ozone distribution and the distribution resulting from the photochemical theory. As the ozone distributions determined by balloon ascents and by lunar eclipses show strong variations—as pointed out below—one has to start from the averaged distributions.

The vertical ozone distribution resulting from the photochemical equilibrium was recalculated with the latest data (distribution of intensity of the sun's

spectrum, formation of the terrestrial atmosphere, spectral absorption of oxygen, etc.), whereby the still existing uncertainties were limited by various assumptions of the parameters (PAETZOLD, 1953a). The result was that above 24 km, up to 60-km altitude, the average measured ozone distribution at various latitudes is in satisfactory agreement with the distribution resulting photochemically, considering the uncertainties of the calculating basis (PAETZOLD, 1953b, 1953c). On the other hand, too little ozone is measured as against the theory, between 10- and 24-km altitude, with the discrepancy strongly increasing towards the equator. Moreover, there should be no ozone at all below 10-km altitude according to the photochemical theory, whereas in this region one observes an average ozone concentration of 2–4 . 10^{-3} cm O_3/km*).

Investigations have been carried out to ascertain if this tropospheric ozone is caused by cosmic radiation or electrical discharges in the atmosphere (PAETZOLD, 1954b). According to the strength of the cosmic radiation the tropospheric ozone could only be accumulated in 2 . 10^3 years. Accordingly, a time of 5 . 10^3 years will result with electrical discharges (mean discharge power in the atmosphere $\approx$ 1 . 10^{-16} coul/cm^2 sec, and ozone constitution by discharge of 1 . 10^{22} O_3 molecules/coul). Such enormous accumulation times make no sense, as near the ground, at places where in the evening and at night an inversion of temperature takes place, the ozone content can after sunset be reduced to zero (AUER, 1939; EHMERT, 1949; BOWEN and REGENER, 1951). With the assumption that, due to the inversion of temperature, an air layer of 10-m thickness is secluded from the vertical mass exchange, there will be—according to measurements—an ozone destruction on the ground of 4 . 10^{10} O_3 molecules/cm^2 sec.†

The origin of the tropospheric ozone is therefore to be sought in the stratosphere (REGENER, 1943). And, indeed, ozone must be continually reconstituted photochemically in the region between 15- and 22-km altitude, where the measured ozone content is smaller than the photochemically calculated content. Furthermore, there must be a continual ozone transport downward caused by the mass exchange, because below 24-km altitude the relation ozone/air permanently decreases with the height. The resulting quantity of this ozone current is given by:

$$\vec{O}_3 = -\frac{N_A}{\rho_0}\left(A(h)\,\frac{d\left(\frac{[O_3]}{[L]}\right)}{dh}\right)$$

It means: N_a, the Avogadro constant; ρ_0, air density (NTP); $A(h)$, Austausch-coefficient; $[O_3]/[L]$, the ratio ozone/air.

The table gives the photochemically calculated ozone reconstitution and the ozone current O_3 at 10-km altitude (PAETZOLD, 1954b). Both factors are thus in good agreement, if one considers the fact that the respective values are determined quite independently of each other. There is also good agreement

* Our measurements with spectrographs are in satisfactory agreement with those obtained with the chemical method in this region, as reported by G. M. B. DOBSON at the Ozone Symposium at Rome, 1954.

† This value is in very good agreement with new measurements of the surface ozone made by V. H. REGENER in New Mexico, which were reported at the UGGI-Assembly at Rome, 1954.

VOL. 7 1955

with the above-mentioned value of ozone destruction on the ground of $4 \cdot 10^{10}$ O_3 molecules/cm²/sec.

Table 1. *Ozone current and photochemical ozone reconstitution*

	$\overrightarrow{O_3}$ $\frac{O_3 \text{ molecules}}{cm^2 \text{ sec}}$.	*Ozone reconstitution* $\frac{O_3 \text{ molecules}}{cm^2 \text{ col sec}}$.
0° latitude	$8 \cdot 10^{10}$	$1{\cdot}4 \cdot 10^{11}$
45° latitude	$5 \cdot 10^{10}$	$2{\cdot}5 \cdot 10^{10}$

According to the above, the mean ozone distribution at various latitudes can be interpreted as a dynamic balance between photochemical constitution, turbulent ozone current, and ozone destruction in the troposphere and on the ground. Nothing certain can be said yet about the effect of the influence of circulation on this problem, because our knowledge of the variations of the vertical ozone distribution with latitude and season is too poor. The two above-mentioned factors seem to be so balanced, that the high ozone in all latitudes shows nearly the same amount, whereas, by the photochemical theory alone, the greatest amount should be at the equator. So the photochemical ozone value, averaged over the whole earth, will be 0·30 cm O_3, whereas in fact it amounts to 0·2 cm O_3.

The total quantity of ozone which is annually destroyed on the earth is quite imposing, amounting to $1 \cdot 10^{12}$ kg O_3/year, earth. As the total amount of atmospheric oxygen is $1 \cdot 10^{18}$ kg, the latter passes the ozonized stage in 10^6 years, a period which is rather short on the geological scale. This fact leads to very interesting questions about the origin and the household of atmospheric oxygen, and to a comparison of the conditions in the atmosphere of the earth and Mars (Paetzold, 1953d). Without photochemical reconstitution the ozone would in three years be reduced to a tenth of its present amount, which is an instructive confirmation of the fact that the ozone layer is characterized by a dynamic and not by a stationary equilibrium.

2. *Variations of the single ozone distributions*

The ozone distributions determined by balloon ascents as well as by eclipses of the moon are so manifold that we could not find two entirely equal distributions. This is shown in Fig. 1, which gives the integral curves of distributions measured at Weissenau at the various seasons. They give the total ozone amount $x(h)$ in the height h above the apparatus. It is striking that in spring and summer there is a particular variation in the curves below 20 km. Furthermore, there are also strong fluctuations of the ozone above 30 km, which are far beyond measuring precision. This is in agreement with measurements made at lunar eclipses.

One can roughly categorize three types of ozone distributions:

Type I: One maximum (at 23-km altitude).
Type II: Two maxima (at 23- and 15- or 5-km altitude).
Type III: Three maxima (at 23-, 15-, and 5-km altitude).

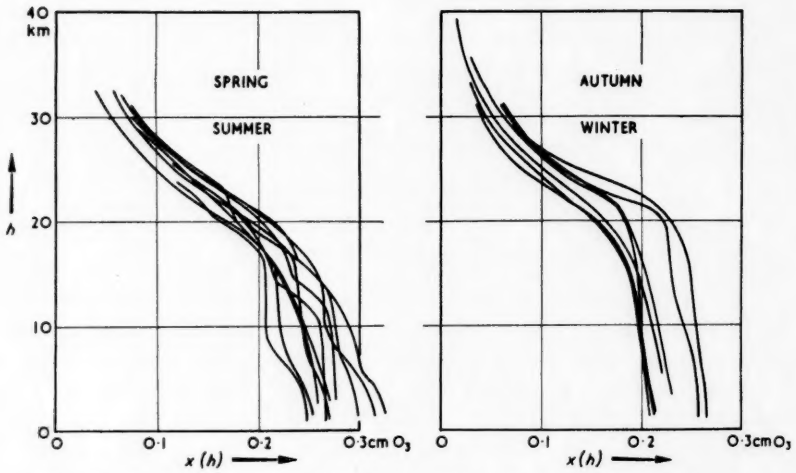

Fig. 1. The integral curves $x(h)$ of ozone of the balloon ascents at Weissenau.

VOL. 7 1955

With particular regard to the highest maximum, one must further distinguish a smooth and a peaked shape. Furthermore, the two maxima at 23- and 15-km altitude do not always appear separately, but take their course together into a broad hump. As the photochemical factors are not sufficiently variable, and the period of establishment of the photochemical equilibrium below 30-km altitude is far too slow (at 25-km altitude 1–3 years), the observed fluctuations of the vertical ozone distribution must be attributed to horizontal and vertical air motions (PAETZOLD, 1953b).

(a) *Horizontal air motions*

The influence of advection is shown most clearly at the secondary ozone maximum at 15-km altitude. By the single ascents we analyzed the air trajectories at 11- and 16-km altitude. Whenever the air in these altitudes originates from latitudes north of 65°N, we observe in spring the secondary ozone maximum, more or less separated from the first maximum which is demonstrated in Fig. 2 (PAETZOLD, 1954b, 1954d). It diminishes during the course of summer and does not exist in autumn and winter. This is in agreement with measurements of the ozone distribution by the Umkehreffekt at Tromsö (TONSBERG and OHLSEN, 1944). According to this, there is a high ozone concentration ($1 \cdot 10^{-2}$ cm O_3/km) in spring below 20 km down to 10 km, whereas in autumn it also rapidly decreases in this region, as in lower latitudes. The simplest explanation for this lower polar ozone is an increased ozone transport from altitudes above 30 km, where the ozone can be quickly enough reconstituted photochemically, down to lower

air layers where it can accumulate photochemically protected. With the assumption that the photochemically reconstituted ozone is brought down from the region between 30- and 50-km altitude, an increase of the total ozone amount of 0·002 cm O_3/day results, which is in sufficient agreement with observation. For this downward ozone transport in spring, the turbulent exchange coefficient at 30-km altitude must be of the magnitude of 1 to 5 g/cm/sec. This temporary increase of the exchange coefficient can be examined by the strong horizontal meridional descent of temperature in this altitude, as it must exist at the limit of the polar night in spring (MOSER, 1949). There is another possibility to explain the source of the lower polar ozone: a horizontal transport of ozone

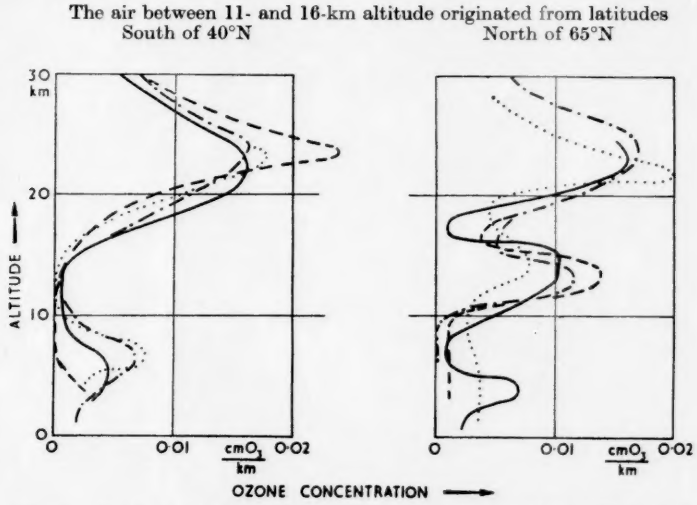

Fig. 2. Vertical ozone distribution and advection in spring at Weissenau.

at greater altitude from equatorial regions.* One cannot decide between the two explanations until the annual variations of the vertical ozone distributions in the polar region are better known. It may be that both effects, the horizontal transport and the photochemical restitution in conjunction, are of influence. The lower polar ozone is gradually exhausted in the course of summer, so that the secondary ozone maximum is not observed in autumn.

Fig. 3 demonstrates instructively that the secondary maximum is caused by advection. At the altitude of the secondary ozone maximum there is an abrupt change in the wind direction. On the other side the wind direction in this region remains unchanged if the secondary maximum in spring is not observed.

As concerns the tertiary ozone maximum, a closer co-ordination with the advection has not been found yet. This is not surprising, as the observation material for the circumstances in the troposphere is still too small. It seems, however, that the tertiary ozone maximum is also principally caused by different air supplies at the various heights.

* Dütsch, UGGI-Assembly at Rome, 1954.

(b) *Vertical air motions*

With regard to the vertical air motions, one must distinguish two kinds:

(1) vertical air currents, and

(2) the turbulent mass exchange.

The air currents leave the relation ozone/air of an air body unchanged, but in general the total ozone amount is varied by compression or expansion of the ozone. Contrary to this, the mass exchange tries to establish the same relation ozone/air over the whole height. The total ozone amount, however, remains unchanged, disregarding the influence of the regions where the ozone is destroyed, or photochemically reconstituted. However, this influence can only take effect slowly, in the course of several days or weeks (see the increase of polar ozone at the end of the polar night).

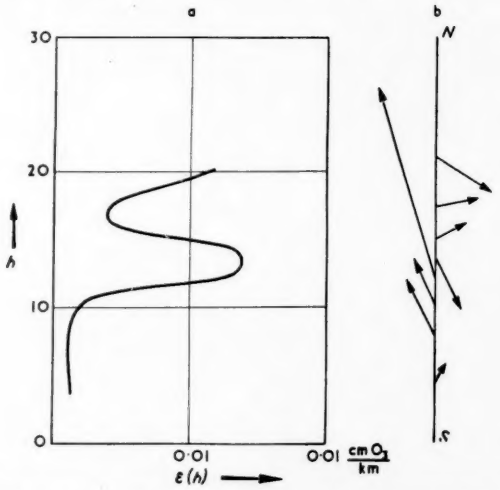

Fig. 3. Vertical ozone distribution (a) and wind distribution with height (b). Ascent of 26.3.1953, Weissenau.

We have investigated the influence of vertical motions especially with ascents in autumn, as at this time of the year the meridional gradient of the total ozone amount and the influence of advection are at a minimum (PAETZOLD, 1954b, 1954d). Fig. 4 shows four ascents in autumn 1953 at Weissenau, which partly reach 38-km altitude. The shape of the curves 2 and 3 of the relation ozone/air is obviously the same, with the only difference that above 20-km altitude they lie at somewhat different heights. The same applies for the curves 1 and 4 in Fig. 4. The upper maximum of the curves ozone/air of the distributions measured by rocket ascents (JOHNSON *et al.*, 1952) lies also at different heights between 30 and 45 km. The four equatorial ozone distributions determined by eclipses of the moon show the same signs as are demonstrated by Fig. 5. This displacement in altitude of the curves ozone/air must be attributed to vertical upward and downward air currents. For the magnitude of these vertical currents there follows from the data in Fig. 5 and the period of establishment of the photochemical equilibrium, a lower limit of 1–10 cm/sec in the region between

VOL. 7 1955

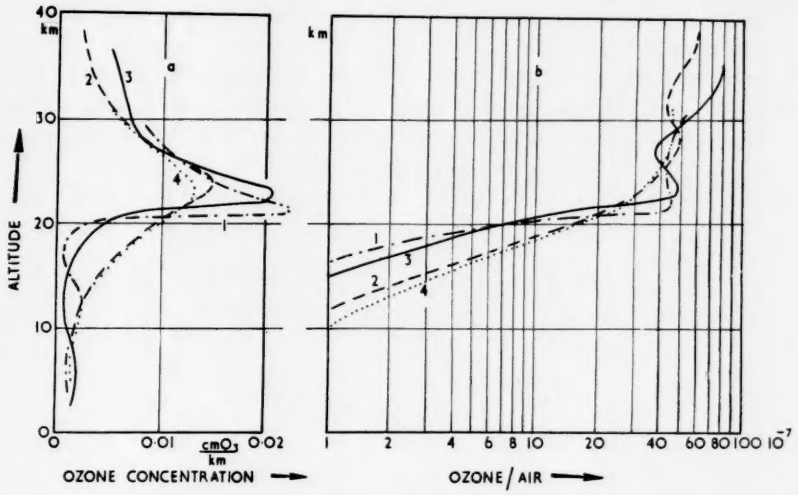

Fig. 4. Vertical ozone distribution in autumn at Weissenau.
1, 8.9.1953; 2, 28.9.1953; 3, 23.10.1953; 4, 28.10.1953.

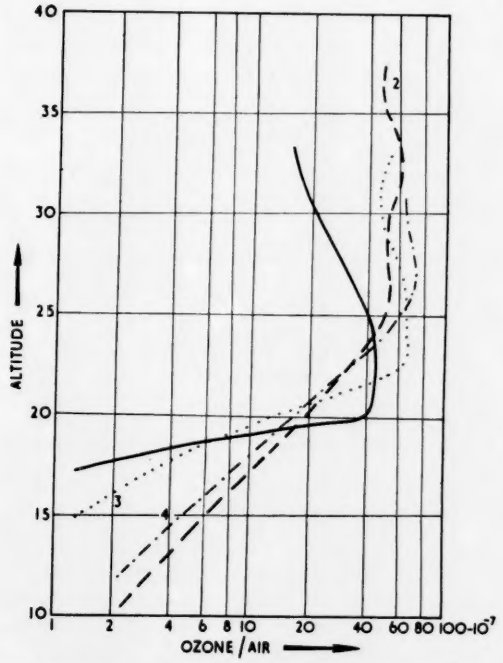

Fig. 5. The curves ozone/air of four equatorial ozone distributions after eclipses of the moon.
1, 2.3.1942; 2, 29.9.1941; 3, 14.9.1932; 4, 15.8.1943.

30- and 50-km altitude. For more exact values we need ascents at shorter intervals with an ozone radiosonde.

According to Figs. 4 and 5, it is striking that the curves ozone/air cross each other at 20-km altitude, i.e., that the vertical motions change their signs in this altitude. Accordingly there would be a kind of wave in the stratosphere, similar to the so-called "Föhnwaves" above the mountains. The change between peaked and smooth first ozone maxima can now easily be explained by this vertical form of

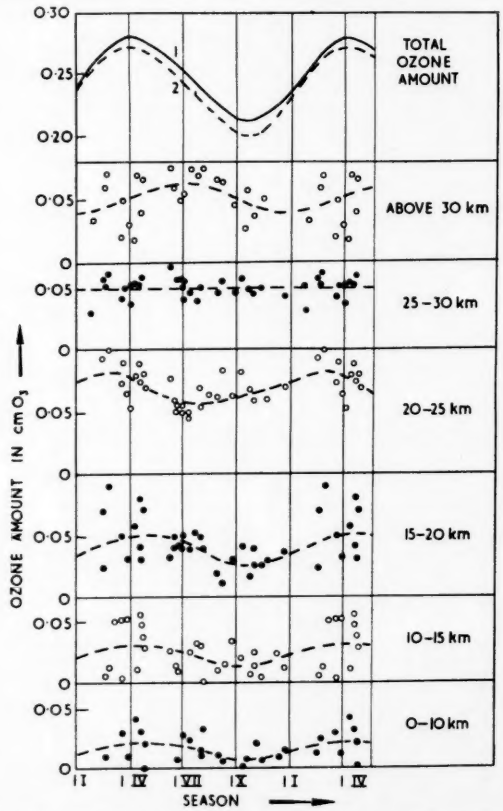

Fig. 6. The annual ozone course in different heights. The drawn-out curve 1 demonstrates the annual variation of the total ozone amount after the balloon ascents, whilst curve 2 represents the result of measurements with the Dobson apparatus at Arosa during many years.

air motion, whilst a plausible explanation from the vertical mass exchange is not possible.

It must be pointed out that the low dependence on height of the relation ozone/air above 24 km, cannot be taken for an intense mixing up of the air, because also according to the photochemical theory there will be an exponential decrease with height of the ozone concentration in this region, similar to the density of air (PAETZOLD, 1953a). Nothing definite can be said yet from the hitherto existing observations about the changing influence of the mass exchange on the ozone

VOL. 7 1955

distribution. If at 30-km altitude a notable alteration is to be effected by the exchange, the Austausch-coefficient must temporarily show—in accordance with a period of establishment of the photochemical equilibrium of approximately ten days—values of 0·1–1 g/cm/sec, and this seems to be the case sometimes (PAETZOLD, 1952c). It seems, however, that the vertical air currents influence the ozone distribution decisively.

3. *The annual variation of the total ozone amount in mean latitudes*

The work of previous investigations indicated the probability that the annual course of the ozone in mean latitudes is also caused by different factors, and that an analysis of these factors does not seem possible from the observations of the total ozone amount alone. Therefore we have tried to derive the annual variation of the ozone in the various altitudes from the Weissenau ascents and previous ascents of other authors (PAETZOLD, 1954b; 1954d; 1955b). In spite of the strong dispersion of the single points in Fig. 6, one can ascertain a different reaction of the ozone at different heights, which is probably to be attributed to various causes:

(1) Between 10 and 20 km in spring a maximum of the ozone amount caused by the advective polar ozone (secondary ozone maximum at 15-km altitude). The amplitude is 0·04 cm O_3.

(2) Between 20- and 25-km altitude in summer a minimum of the ozone amount, which must probably be attributed to the increased downward ozone transport due to the increased turbulence.

(3) In early summer a maximum of the ozone amount above 30-km altitude, which is caused photochemically. At this altitude the photochemical ozone distribution can follow the annual course of the sun's zenith distance. The observed amplitude of the annual photochemical ozone variation of 0·02 cm O_3 corresponds to the theoretical expectations.

It is remarkable that, between 25- and 30-km altitude, no annual variation of ozone content is observed (Fig. 6). It is obvious that at this height the influence of the photochemistry and the turbulence no longer reaches up and down, or else both are balanced against each other.

If the three above-mentioned factors are linked up, the resulting amplitude of the annual ozone course is too small according to Fig. 8 (dotted curve). Furthermore, these factors alone cannot explain plausibly the new increase of the ozone value from early November onward. Due to the curves ozone/air for the different seasons in Fig. 7, one must assume a fourth factor: between 10- and 20-km altitude, an air current of an average strength of 0·1 mm/sec going down in autumn and up in spring, and causing a respective compression and expansion of the ozone. At this height, this vertical current must be connected with a respective equalizing horizontal current from the summer to the winter hemisphere, of an average strength of about 1 m/sec.

With regard to this fourth factor, there is a further connection with the interdiurnal ozone fluctuations. If, with the annual course of the height of the tropopause in mean latitudes (winter 10 km, summer 11·5 km), one considers the formerly found correlation that the total ozone amount decreases by 0·01 cm

with an increase of the height of the tropopause of 1 km (MEETHAM,1937; DOBSON and HARRISON, 1926), there is, according to Fig. 8 (drawn-out curve), good agreement with the observed annual variation of ozone amount (circles). The above-mentioned average dropping of the stratosphere from 1.XII till 1.I by 1 km can therefore be explained by the increased low-pressure activity (tropopause vortex) in autumn and winter.

An interpretation of the annual ozone course by the four factors mentioned seems to be satisfactory, as it does not stress only one cause as was done hitherto, and adapts itself without disagreement to the general picture.

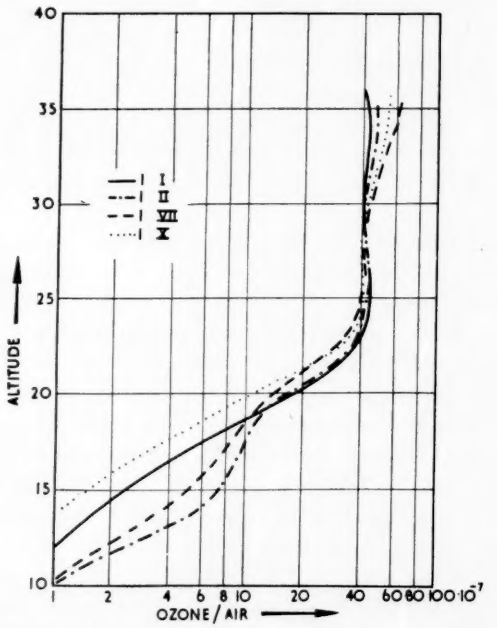

Fig. 7. The ratio ozone/air for the different seasons.

The local differences in the various climates (monsoon, maritime, and continental climate), as for instance the second maximum of the annual ozone course which has been observed at some places (KALEK, 1953), can only be determined by further measurements of ozone distributions. They will then give variable information about the circulation of air and large-scale mixing processes.

(4) *Ozone and weather*

The last point to be mentioned refers to the interdiurnal ozone fluctuations. In this field the observation material of the vertical ozone distributions is still too small to give any details. However, we can suppose that in spring the interdiurnal fluctuations of the total ozone amount are caused on the one hand advectively (secondary ozone maximum) and on the other by vertical currents. In autumn, however, the latter are the decisive factors. The same result follows from a newer, careful discussion about the interdurnal fluctuations of the total ozone

VOL. 7 1955

amount (NORMAND, 1953). From the observed interdiurnal fluctuations of the total ozone amount one can suppose that in autumn the vertical displacements of air up to 20-km altitude must amount to at least 1 km (PAETZOLD, 1954b).

An impressive demonstration of the effectiveness of the vertical air motions was given by our observation of an "ozone hole" above the Alps in November 1953 (PAETZOLD and ZSCHÖRNER, unpublished). According to this, the total ozone content in a narrow horizontal region of approximately 20-km width amounted to only about half of the value measured in its vicinity. This "ozone hole" can satisfactorily be explained by the existence of "Föhnwaves," which were caused by a strong NW wind above the Alps.

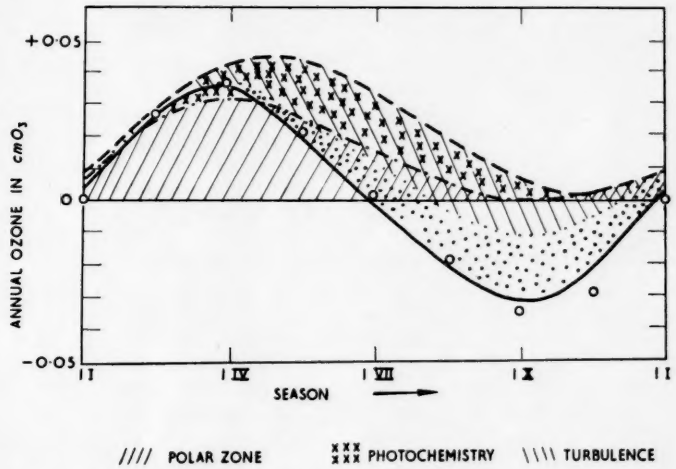

Fig. 8. The various contributions to the annual ozone course. Circles: the annual ozone course at Arosa measured with the Dobson spectral-photometer.

In order to obtain more detailed associations between ozone and weather, it will be necessary in future to carry out simultaneous ascents with ozone radiosondes at different places in marked weather conditions. Then it is to be expected that in connection with measurements of the total ozone amount with the Dobson spectral-photometer, valuable information for weather forecasts will be obtained. Furthermore, measurements of the surface ozone will be useful. These measurements should be carried out on peaks of mountains in order to exclude local secondary influences.

CONCLUSION

The reported results show the importance of worldwide measurements of the vertical ozone distribution, which are to be combined with the measurements of the total amount with the Dobson spectrometer. In order to give the indirect measurements of the ozone distribution by the Umkehr-effect a firm basis, it is necessary to make comparisons with simultaneous direct measurements by balloon ascents. Apart from this, it is necessary to work with a cheap but sufficiently precise ozone radiosonde in order to determine sufficiently the dependence of the ozone distribution on the season, the geographical latitude, and the

weather conditions. The polar regions and the jet-stream regions seem to be of special importance. Then one can expect valuable results regarding circulation, large-scale mixing processes, mass exchange, and perhaps weather forecasts. It must be pointed out that such low vertical air motions, as they result from Figs. 4, 5a, and 7, and as they can be directly measured by the ozone, can otherwise only be determined indirectly and statistically, and accordingly with uncertainty.

REFERENCES

AUER, R.	1939	*Gerl. Beitr. Geophys.* **54,** 137
BOWEN, I. G., and REGENER, V. H.	1951	*J. Geophys. Res.* **56**
DOBSON, G. M. B., and HARRISON, D. N.	1926	*Proc. Roy. Soc.* **A110,** 660
EHMERT, A.	1949	*Ber. Dtsch. Wetterd. US-Zone*, Nr. 11, 47
JOHNSON, F. S., PURCELL, J. D., TOUSEY, R., and WATANABE, K.	1952	*Geophys. Res.* **57,** 157
KALEK, A. K.	1953	Thêse Paris
MEETHAM, A. R.	1937	*Quart. J. Roy. Meteorol. Soc.* **63,** 289
MOSER, H.	1949	*Ber. Dtsch. Wetterd. US-Zone*, Nr. 11, 28
NORMAND, CH.	1953	*Quart. J. Roy. Meteorol. Soc.* **79,** 39
PAETZOLD, H. K.	1947	*Z. Naturforsch.* **2a,** 219
	1950a	*Optik.* **6,** 327
	1950b	*Z. Naturforsch.* **5a,** 661
	1951a	*Z. Naturforsch.* **6a,** 639
	1951b	*Naturwissenschaften.* **38,** 544
	1952a	*Z. Naturforsch.* **7a,** 325
	1952b	*J. Atmosph. Terr. Phys.* **2,** 183
	1952c	*Ber. Dtsch. Wetterd. US-Zone*, Nr. 38, 292
	1953a	*Geophys. p.e.appl.* **24,** 1
	1953b	*Geophys. p.e.appl.* **24,** 15
	1953c	*J. Atmosph. Terr. Phys.* **3,** 131
	1953d	*Mitt. Astron. Ges.*, p. 19
	1954a	*Geophys. Res.* **59,** 365
	1954b	Über die Photochemie der Erdatmosphäre unter besonderer Berücksichtigung der Ozonschicht, Habilitationsschrift München
	1954c	*Die Sterne* **30,** 13
	1954d	*Naturwissenschaften* **41,** 318
	1955a	*Z. Naturforsch.* **10a,** 33
	1955b	*Meteor. Abhlg. d. Inst. Meteor. Geophys. F. U. Berlin,* **II,** 92
PAETZOLD, H. K., and ZSCHÖRNER, H.	1955	*Z. Meteorol.* To be published
REGENER, E. u. V. H.	1938	*Phys. Z.* **35,** 788
REGENER, E.	1943	*Meteor. Z.* **60,** 253
TÖNSBERG, E., and OHLSEN, K. L.	1944	*Geophys. Pol.* **13,** No. 12

VOL. 7 1955

Journal of Atmospheric and Terrestrial Physics, 1955, Vol. 7, pp. 141 to 151. Pergamon Press Ltd., London

Some photometric observations of auroral spectra*

D. M. HUNTEN
University of Saskatchewan, Saskatoon

(*Received* 7 *March* 1955)

ABSTRACT

A variety of measurements of auroral spectra has been made with a photoelectric spectrometer. These include relative and absolute intensity measurements of the more prominent features, and a verification of SEATON's absolute intensity scale. Observations of Hβ seem to indicate more erratic behaviour than has been assumed. The intensity of the N II lines 5001–5 Å shows little or no excitation by helium ions. A very intense feature observed in Type B red aurora appears to be due to sodium. The vibrational development of the N_2^+ first negative system indicates electron excitation from the ground state of N_2 at a temperature of 0–700°K. The results show the spectrometer to be useful for intensity measurement and the observation of short-lived effects. It is, however, limited to the brighter forms of aurora.

1. INTRODUCTION

A photoelectric spectrometer capable of producing a tracing of an auroral spectrum in ten seconds with 10-Å resolution has been described in another paper (HUNTEN, 1953). When this instrument was first put into operation (the spring of 1952), a large number of spectra were taken with the main object of testing its performance. Since that time, the aurora has been considerably fainter; consequently all the spectra taken have covered a very restricted range of wavelength, so that the sensitivity could be increased. The original spectra covered a range of about 2500 Å, and since they were the only ones of this type available, they were examined and found to contain a good deal of interesting information. This information is the subject of the present paper. Many of the features could well be studied in more detail when bright aurora is again available in sufficient quantity.

The resolution used was sometimes 10 Å, sometimes 20. On some of the nights, spectra were also taken of a secondary standard low-brightness source which gives a continuous spectrum. This source has recently been provided with an absolute calibration against a black body at a known temperature by G. G. SHEPHERD (1954). Absolute intensities could therefore be found from some of the auroral spectra. Another group gave relative but not absolute intensities.

We have found it convenient to express the emission rates in quanta per second per unit solid angle from a square centimetre in the line of sight. The emission rate at wavelength λ will be written $Q(\lambda)$ and the units understood to be 10^7 quanta/cm^2 sec steradian.

Besides measuring intensities, we have been able to identify a few new minor features, to study the spectrum of Type B red aurora, to make some observations on forbidden transitions, and to estimate the vibrational temperature given by the N_2^+ first negative system.

* The research reported in this paper has been sponsored by the Geophysics Research Directorate of the Air Force Cambridge Research Center, Air Research and Development Command, under Contract AF 19 (122)–152.

2. LINES AND BANDS IDENTIFIED

In general, the features observed were the strong ones; however, some could not be resolved from neighbouring ones of greater intensity. A few bands could be identified with some certainty by their correlation with known ones of the same system. These are:

N_2	second positive	2-7	4490 Å	
		3-8	4417	
N_2^+	first negative	0-4	5865	(probable)
		1-5	5755	(probable)
N_2^+	Meinel	4-0	6130	(probable)
		5-1	6270	(possible, but badly blended)

The last four are further discussed in Section 3.

A fairly prominent feature appears at about 5000 Å. The two multiplets of N II to which it might belong are shown in Table 1, which is taken mostly from Miss MOORE's multiplet table (1945). PETRIE and SMALL (1952) identify the feature with the first three lines of multiplet 19, but say that the intensity distribution in the multiplet is anomalous, presumably because the lines at 5016 Å and 5026 Å are weaker than expected from the intensities given by Miss MOORE. These may, however, have been merely eye estimates; we have therefore calculated the expected intensities from the tables of RUSSELL (1936), and found them to be much lower for these two lines. CHAMBERLAIN and OLIVER (1953) prefer to

Table 1.

The two multiplets (both N II) that have lines near 5001 Å, as listed in Miss MOORE's table (1945). The last two columns give the intensities from this table and those calculated from the tables of RUSSELL (1936).

Multiplet and No.	J	λ	I_M	I_R
$3s^3P^0$–$3p^3S$	2–1	5045·1	8	5
	1–1	5010·6	6	3
4	0–1	5002·7	2	1
$3p^3D$–$3d^3F^0$	3–4	5005·1	10	100
	2–3	5001·5	8	69
19	1–2	5001·1	7	47
	2–2	5016·4	5	8·7
	3–3	5025·7	6	8·7
	3–2	5040·8	0	0·25

assign the 5000-Å feature to multiplet 4, but Table 1 immediately shows that this is incorrect, since the line at 5003 Å is the weakest of the multiplet. The objections to the identification of multiplet 19 seem to have been removed, and the feature may be called N II 5001-5 Å. The same conclusion appears to have been reached by CHAMBERLAIN and MEINEL (1954).

VOL. 7 1955

3. Red Aurora of Type B

This is the name given to aurora with a red lower border. It is usually bright, but lasts only a short time; conventional spectrographs are thus not well suited to its study. It has already been reported (Dahlstrom and Hunten, 1951) that bands of the O_2^+ first negative system are responsible for the red colour. Further observations have shown that these are usually, if not always, accompanied by N_2 first positive bands. Both systems make an important contribution to the red sensation.

A typical spectrum is shown in Fig. 1. A sequence of N_2 first positive bands shows from 6500 to 7000 Å; the bump at 6400 Å and the large peak at 6000 Å are produced by O_{2+} bands. While there are more first positive bands between

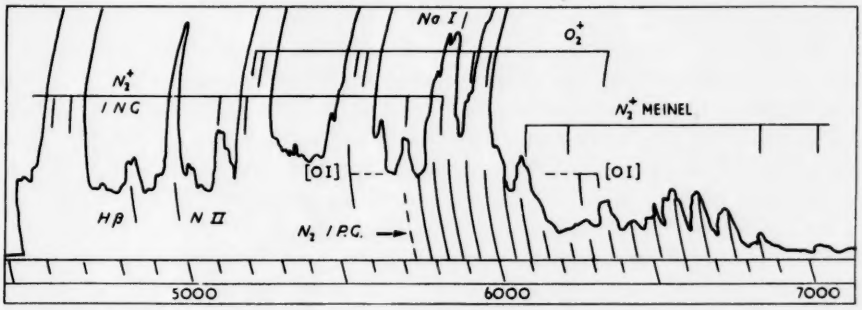

Fig. 1. A spectrum of Type B aurora taken on March 31, 1952, with 20 Å resolution. Wavelengths of band maxima for several systems are shown; the lengths of the lines for the N_2 first positive bands indicate either observed or expected intensities. It should be noted that the sensitivity decreases by a factor of 10 for each 650 Å beyond 5500 Å. (The same spectrum has been reproduced by Chamberlain and Meinel, 1954, Fig. 10a.)

5700 and 6200 Å, it does not appear that they could account for the features at 5750, 5870, and 6130 Å. The contribution of first positive bands was estimated by the following procedure:

(1) The intensities of the bands from 4-1 to 8-5 were measured.

(2) The intensities of the corresponding bands from 5-1 to 8-4 were then found from these by means of the intensity ratios measured by Turner and Nicholls (1954); for the 4-0 band the intensity ratio was found from the relative transition probabilities calculated by Jarmain and Nicholls (1954).

(3) The bands from 9-5 to 11-7, and 9-6 to 11-8, were estimated relative to 8-4 and 8-5 by means of the auroral intensities given by Petrie and Small (1953).

The resulting intensities, corrected for the response of the spectrometer, are shown in Fig. 1 by means of vertical lines at the wavelengths of the band maxima (Pearse and Gaydon, 1950). It seems probable that first positive bands cannot entirely account for the features observed.

It is natural first of all to see whether the N_2^+ first negative bands 0-4 (5865 Å) and 1-5 (5754 Å) are capable of accounting for the features at 5870 and 5750 Å. The expected intensity of the 0-4 band can be found from the observed intensity

of the 0-3 band, if the relative intensities are known. Unfortunately, HERZBERG (1928) was unable to measure the 0-4 band, because it was obscured by N_2 first positive bands; but his results suggest that an intensity ratio of about 0·2 is reasonable. The relative transition probabilities calculated by JARMAIN, FRASER, and NICHOLLS (1953) are very uncertain for these two bands, but give an intensity ratio of 0·25. Using the last figure, the expected intensity of the 0-4 band is about one-third of the intensity of the 5870-Å feature. It appears that the 0-4 band may give the inflection on the short-wavelength side, but cannot account for the whole feature. The identification of the 5750-Å feature with the 1-5 band appears satisfactory.

It is difficult to avoid the conclusion that the sodium *D* lines are responsible for most of the intensity at 5870 Å. The wavelength match with the red side of the feature is excellent, and the *D* lines are by far the strongest to be seen in this region of the spectra of PETRIE and SMALL (1952), on tracings reproduced by CHAMBERLAIN and MEINEL (1954). It is known from twilight observations (HUNTEN and SHEPHERD, 1954) that the density of sodium atoms follows approximately that of the atmosphere as a whole from 85 to at least 110 km. Since the Type B aurora observed was presumably at a lower-than-average altitude, a very strong radiation from sodium is perhaps not so strange as might appear at first sight.

It is interesting to estimate the maximum observed emission rate and to compare it with that observed in the twilight. The brightest spectrum recorded on March 3, 1952, gave $Q(5893) = 130$, after allowing for the first positive bands. The twilight scattering gives $Q(5893) = 30$ on the average at this season, and may give as much as 45 (HUNTEN and SHEPHERD, unpublished). All the observations of Type B aurora were made with 20-Å resolution. Higher resolution studies will be necessary before the identification of such a strong feature with the sodium lines is established with certainty.

A search was made for the second principal doublet of sodium at 3303 Å on some of the brightest spectra. If present, it was masked by ultraviolet radiations of second order or red ones of first order.

The feature at 6130 Å may most naturally be assigned to the 4-0 band of the MEINEL system of N_2^+. On some spectra there is an inflection corresponding to the 5-1 band at 6270 Å, but the identification is very uncertain.

It is noteworthy that the red lines of oxygen, normally much stronger than anything else in their region, are not visible at all in Fig. 1 and many other spectra of Type B aurora.

Emission rates for some of the principal features were measured from the same spectrum used for the sodium, and are given in Table 2. Since the 3914-Å band and the green line went off scale, their emission rates had to be estimated. The ratio $Q(3914)/Q(5228)$ is 110, according to the calculations of JARMAIN, FRASER, and NICHOLLS (1953). $Q(3914)$ is then 19,000. This may be checked by means of the ratio $Q(3805)/Q(3914) \doteqdot 0{\cdot}06$ given in Section 4; the result is $Q(3914) = 4000$. A rough average of these two was adopted for Table 2. Since the green line is normally only a little stronger than the 3914-Å band (Section 4), the value $Q(5577) \doteqdot 10{,}000$ was assumed. This, of course, is rather uncertain, since there is no assurance that the green line is not relatively weaker in Type B

VOL. 7 1955

aurora. The relative weakness of the red lines could be taken as evidence of this, and the cause could be assumed to be the scarcity of atomic oxygen at lower levels. However, since the red lines are weakened by collisional de-excitation at lower levels, it is impossible to be sure.

Table 2. Emission rates in units of 10^7 *quanta cm*^{2} *sec sterad. for the strongest spectrum of March 3, 1952.*

3914 and 5577 went off scale and were estimated by the method given in the text.

λ	*Identification*	$Q(\lambda)$	λ	*Identification*	$Q(\lambda)$
5893	Na I?	130	6875	1PG 3–0	2000
6000	O_2^+ 0–0, 1–1	270	6789	4–1	2300
6130	MEINEL 4–0	210	6705	5–2	1850
5228	N_2^+ 0–3	170	6624	6–3	1500
3805	2PG 0–2	250	6545	7–4	900
3914	N_2^+ 0–0	(10,000)	6469	8–5	850
5577	(OI)	(10,000)			

4. Emission Rates in Normal Aurora

The emission rates of the green line in aurorae estimated to be of brightness coefficient II and III on the international scale, were found to be about $Q(5577) = 80$ and 800. If these are multiplied by 4π they agree perfectly with the omnidirectional emission rates 10^{10} and 10^{11} quanta/sec cm^2 estimated by SEATON (1954). The Type B aurora reported in Table 2 must have been of brightness IV; the emission rate for it is a little over 10^{12} quanta/sec cm^2, rather lower than SEATON's figure. For photometric work it would be convenient to standardize the values 10^9, 10^{10}, 10^{11}, 10^{12} quanta/sec cm^2 ($Q(5577) = 8$, 80, 800, 8000) for brightness coefficients I, II, III, and IV.*

Relative emission rates for various pairs of the strongest or most interesting radiations were measured; the results are given in Table 3. The usual custom is to measure all radiations relative to the green line, but this has the disadvantages (1) that it is not always possible in practice, because the ratio may be very small, and (2) that some other pair of radiations may be associated with each other but not with the green line. (Possible examples are the various emissions of nitrogen.) The pairs chosen were usually close together in wavelength, so that uncertainties in the correction for atmospheric extinction would give small errors. All the spectra measured were taken at a zenith distance near 45°, so that the corrections were small. The extinction coefficients given by VAN DE HULST (1952) were used.

* Note added in proof: J. W. CHAMBERLAIN, in a recent discussion with the writer, has pointed out that SEATON's estimates are probably of surface brightness rather than omnidirectional emission rate. The conversion factor 4π should then be replaced by one approaching 2π (depending on the angular dependence of intensity). The agreement, while no longer perfect, is still good. A great advantage of the "Q" scale used here is that it is free of any such ambiguity, being directly related to an observed quantity. The proposed photometric scale should be established in "Q" units for this reason.

Many of the intensity variations shown in Table 3 are probably real, especially since some of the values given are the average from several successive spectra.

Table 3. *Ratios of the emission rates for several prominent auroral features.*

Values in italics are averages from several successive spectra; values bracketed together are from individual successive spectra. Intensity ratios by VEGARD and KVIFTE (1945) have been converted to emission-rate ratios, and are given when available.

Ratio	*Values found*	*Averages*	VEGARD-KVIFTE	*Remarks*
$Q(3914)/Q(5577)$	*0·42, 0·56, 0·81, 1·28,*	*0·77*	0·33	
$Q(4278)/Q(3914)$	(0·20, 0·17, 0·18), (0·42, 0·37, 0·38)	*0·29*	0·57	Lab. value 0·29
$Q(3805)/Q(3914)$	0·027 to 0·144	0·046 to 0·066	0·10	
$Q(5001\text{–}5)/Q(5577)$	0·0041 to 0·0086	*0·074*		
$Q(5001\text{–}5)/Q(4709)$	0·16 to 0·30	*0·22*		
$Q(5001\text{–}5)/Q(5228)$	1·0 to 1·8	*1·3*		Assumes $Q(4709)/Q(5228)=6·1$
$Q(H\beta)/Q(4709)$	0·01 to 0·15	0·02 to 0·10		normal aurora
	0·01 to 0·09	0·02 to 0·04		Type B
	(110, 130, 260)			flickering
	(24, 67)			very active rays

The ratio $Q(4278)/Q(3914)$ is of course a constant of the N_2^+ ion, so that the variations shown for it are certainly false. The average for the six spectra, however, agrees very well with the laboratory value. (That this is not so for the measurements of VEGARD and KVIFTE has already been pointed out by SEATON, 1954.) The agreement gives a useful check on the other measurements.

The ratio of N_2 second positive to N_2^+ first negative is usually constant to ± 20 per cent, but sometimes varies a good deal more.

The N II lines 5001-5 Å have been studied in the laboratory by FAN and MEINEL (1953). They found that the ratio of intensity of these lines to that of the N_2^+ band 5228 Å depended on the type of ion exciting the spectrum. For hydrogen ions the ratio was 1·3, and for helium ions it was 10. We were able to measure $Q(5001\text{-}5)/Q(4709)$ on a few spectra, and converted this to the desired ratio by means of the known value of $Q(4709)/Q(5228)$. The result, $Q(5001\text{-}5)/Q(5228) = 1·3$, shown in Table 3, indicates excitation by protons. (Because of the small difference in wavelength the Q ratio and the intensity ratio do not differ appreciably.)

The only hydrogen line which is far enough from other features to be observable is Hβ. The spectra studied showed large and often sudden variations in the intensity of Hβ, and it was never possible to predict when it would be present. No spectra were obtained in the earliest stages of a display, when hydrogen lines are usually strongest (MEINEL, 1952; PETRIE and SMALL, 1952). Hβ was observed with remarkably high relative intensity (though the absolute intensity

VOL. 7 1955

was normal) on two occasions in the faint, very active aurora which is usually seen just after a big display. These spectra were examined carefully to make sure that the feature was indeed Hβ, and not the 2-15 band of the Vegard-Kaplan system. Though one might doubt that a scanning spectrometer could get reliable spectra from this type of aurora, experience has shown that it can, since successive spectra are found to be very similar.

An estimate of the absolute emission rate of Hβ is of interest, since CHAMBERLAIN (1954) has shown how a value of the proton flux can be found from it. Only a rough absolute calibration of the spectrometer was available for the observations of Hβ reported in Table 4, but it is felt that the results should be correct within a factor of 2.

According to CHAMBERLAIN, one proton gives about eleven quanta of Hβ; thus a flux of 10^7 protons/cm^2 sec gives $Q(\mathrm{H}\beta) = 1$.* The flux estimated by

Table 4. Absolute emission rates of Hβ *for the same spectra as in Table 3.* Corresponding proton fluxes were deduced from the work of CHAMBERLAIN (1954).

Aurora	$Q(\mathrm{H}\beta)$	*Proton flux (protons/cm^2 sec)*
Normal	<1 to 10	$<10^7$ to 10^8
Type B	<2 to 16	$<2 \times 10^7$ to $1{\cdot}6 \times 10^8$
Flickering	(7, 12, 6)	7×10^7, $1{\cdot}2 \times 10^8$, 6×10^7
Very active rays	(3, 6)	3×10^7, 6×10^7

CHAMBERLAIN for an arc, 6×10^7 protons/cm^2 sec, is seen to be of the same order as the values in Table 4.

Another observation was made on the "afterglow" type of aurora when studying the $\Delta v = 2$ sequence of the N_2 second positive system. Fig. 2 shows one of three almost identical successive spectra taken on September 25, 1952, with 10-Å resolution; a normal spectrum is superposed in dotted lines. It is

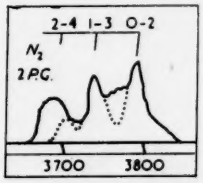

Fig. 2. An auroral spectrum covering the wavelengths from 3650 to 3850 Å with 10-Å resolution. In addition to the usual N_2 second positive bands shown with dotted lines, there are two strong Vegard-Kaplan bands. The aurora was of the very active "afterglow" type, in which radiation continues for some time after a bright outburst.

immediately evident that the relative intensity of the Vegard-Kaplan bands 1-11 (3684 Å) and 2-12 (3768 Å) is much greater than normal; they are almost as strong as the 1-3 band of the second positive system. This suggests that a large concentration of excited molecules was built up during the bright display,

* Note added in proof: This is strictly true only if the observation is made along the path of the protons, as pointed out by CHAMBERLAIN in a discussion. The observations quoted were made at zenith angles of 45° or less; the error introduced should be small.

and that, when the source of excitation disappeared, these molecules continued to radiate for some time. If this is so, the radiative mean life for the $A^3\Sigma$ excited state which leads to the Vegard-Kaplan bands must be at least twenty or thirty seconds.

Indirect evidence has been found that the forbidden line [N I] at 5199 Å behaves similarly. On photographic spectra this line is nearly as strong as the 0-4 band of the N_2^+ negative system at 5228 Å (PETRIE and SMALL, 1952). The photoelectric spectra, on the other hand, have never shown any sign of it; it would probably be visible if it were one-tenth as strong as the band. If the intensity of the [N I] line is smaller, it must be present for a much larger fraction of the time than the other radiations.

5. VIBRATIONAL TEMPERATURE FROM N_2^+ BANDS

The relative intensities in several band systems were discussed some years ago in a well-known paper by BATES (1949). He showed for the N_2^+ negative system how observations could give information about the method of excitation and the vibrational temperature existing before the excitation. The mechanisms considered were: electron excitation from (1) the ground state of N_2; (2) the ground state of N_2^+; and (3) electron and photon excitation as in (2) but with the vibrational distribution determined, not by thermal equilibrium, but by

Table 5. Relative intensity of the 1-2 N_2^+ *band expressed as a percentage of the intensity of the* 0-1 *band, and relative population rates for the* $v' = 0$ *and* 1 *levels.*

Set No.	*Relative int.*	*Population rates*
1	15·5	100 : 13·3
2	13·7	100 : 11·8
3	10·3	100 : 8·9
4	11·3	100 : 9·7
5	13·1	100 : 11·3
6	12·0	100 : 10·3
Average		100 : 10·9

equilibrium between excitation and emission. For high-latitude aurora he concluded that the measurements available favoured mechanism (1), but required that this state have a vibrational temperature around 2000°K. It was suggested that excitation by heavy particles might be important. There were, however, serious uncertainties in the measurements. More recently, PETRIE and SMALL (1953) made some further observations at Saskatoon, and found a vibrational temperature near 1000°K; the same excitation mechanism was indicated. (Comparison of their figures for relative population rates with Table 5 suggests a temperature a little higher than 1000°K.)

VOL. 7 1955

Several of the negative group bands showed up well on the spectrometer tracings. Relative intensity measurements were made only on one sequence at a time in order to eliminate the need for extinction corrections. The $\Delta v = -1$ sequence was not resolved from strong second positive bands. The intensities in the $\Delta v = 0$ sequence fall off much too rapidly for it to be useful. Measurements were therefore confined to the $\Delta v = 1$ and 2 sequences. It was found that the 1-3 band (4652 Å) always gave high results; this was attributed to the presence of a strong O II line at 4639 Å (PETRIE and SMALL, 1953). Finally, the 2-3 band (4199 Å) could not be measured because of the 2-6 band (4200 Å) of the second positive system. This left only the 0-1 (4278 Å) and 1-2 (4236 Å); however, a large number of independent measurements were possible. These were averaged in suitable groups; the results are given in Table 4. To compare them with theory, it is convenient to find the relative population rates for the levels with $v' = 0$ and 1. This is done by means of BATES's equation (10):

$$g(v') = \frac{Q(v', v'')}{p(v', v'')\nu^3(v', v'')} \sum_{v''} p(v', v'')\nu^3(v', v'').$$

Here $g(v')$ is the population rate for the level v', ν is the frequency of the radiation, and p is the relative transition probability for the band. The calculated values of the p's by JARMAIN, FRASER, and NICHOLLS (1953) were used, giving

$$\frac{g(1)}{g(0)} = 0{\cdot}86 \frac{Q(1\text{-}2)}{Q(0\text{-}1)}$$

The relative population rates resulting are given in the last column of Table 4. The corresponding vibrational temperature may be found by comparison with Table 5, adapted from BATES's paper with an added entry for 0°K. The average

Table 6. Relative population rates for the vibrational levels of the N_2^+ ion resulting from electron impact with the N_2 molecule in the ground state. Calculations by BATES (1949).

Vibrational temperature (°K)	0	500	1000	2000
$v' = 0$	100	100	100	100
1	11	11	13	26
2	0	0	1	7

result $g(1) = 10{\cdot}9$ is seen to indicate a temperature in the range 0 to perhaps 700°K. This is consistent with the expected temperature of about 300°K. The only excitation mechanism giving any agreement with observation is electron impact with the N_2 molecule in the ground state, as was found by other workers already mentioned.

6. CONCLUSIONS

The variety of results obtained in this paper shows that the photoelectric spectrometer is useful for certain types of auroral studies. These are the quick,

easy, and fairly accurate measurement of absolute and relative intensities, and the observation of short-lived effects. Measurements are usually limited to the brighter auroral forms, and seldom extend much to the red of 6200 Å. Results from aurora whose intensity is changing rapidly must be interpreted with caution, but can still be useful.

The main conclusions of this paper are the following:

(1) A few new bands of well-known nitrogen systems have been observed.

(2) The identification of the atomic feature near 5000 Å has been discussed. There seems little doubt that it is the three strongest lines of the multiplet $3p^3D - 3d^3F^0$ of N II, with wavelengths 5001-5 Å.

(3) The red colour of Type B aurora has been found due to O_2^+ first negative and N_2 first positive bands in about equal proportions.

(4) A strong feature observed in Type B aurora seems to be the sodium *D* lines. An intensity has been observed three times as great as that found in the twilight.

(5) Absolute intensities have been estimated for the strongest features in a bright spectrum of Type B aurora.

(6) The absolute intensity of the green line has been measured for aurorae of international brightness coefficient II, III, and IV, and found to agree well with the estimates of SEATON. A photometric scale has been suggested in which each unit increase in the brightness coefficient corresponds to a factor of 10 in intensity.

(7) Relative emission rates have been measured for several pairs of radiations; as would be expected, there is evidence of variations. One of the ratios agrees with that found by FAN and MEINEL for proton excitation, and indicates little or no contribution from helium ions.

(8) The relative emission rate of Hβ has been found to show large and sudden variations. The absolute emission rate leads to proton fluxes up to about 10^8 protons/cm^2 sec.

(9) Evidence has been found for a very slow decay in intensity of the Vegard-Kaplan bands and the [N I] line at 5199 Å.

(10) Measurements of the vibrational excitation of the N_2^+ first negative system show that it is produced by electron impact on N_2 molecules in the ground state at a vibrational temperature between zero and 700°K. A closer specification of the temperature appears experimentally almost impossible.

Many of the results should be regarded as preliminary and the measurements should be repeated when bright aurora becomes more plentiful.

Acknowledgements—The writer would like to acknowledge the value of many discussions with Dr. A. VALLANCE JONES.

REFERENCES

BATES, D. R.	1949	*Proc. Roy. Soc.* **A196**, 217
CHAMBERLAIN, J. W.	1954	*Astrophys. J.* **120**, 360
CHAMBERLAIN, J. W., and MEINEL, A. B.	1954	The earth as a planet (Ed. G. P. Kuiper) University of Chicago Press
CHAMBERLAIN, J. W., and OLIVER, N. J.	1953	*J. geophys. Res.* **58**, 457

VOL. 7 1955

DAHLSTROM, C. E., and HUNTEN, D. M.	1951	*Phys. Rev.* **84**, 378
FAN, C. Y., and MEINEL, A. B.	1953	*Astrophys. J.* **118**, 205
HERZBERG, G.	1928	*Ann. Phys.* **86**, 189
HUNTEN, D. M.	1953	*Canad. J. Phys.* **31**, 681
HUNTEN, D. M., and SHEPHERD, G. G.	1954	*J. Atmosph. Terr. Phys.* **5**, 57
JARMAIN, W. R., and NICHOLLS, R. W.	1954	*Canad. J. Phys.* **32**, 201
JARMAIN, W. R., FRASER, P. A., and NICHOLLS, R. W.	1953	*Astrophys. J.* **118**, 1228
MEINEL, A. B.	1952	*Mém. Soc. Roy. Sci. Liege* **12**, 203
MOORE, C. E.	1945	A multiplet table of astrophysical interest, Princeton University Observatory
PEARSE, R. W. B., and GAYDON, A. G.	1950	The identification of molecular spectra, 2nd ed., Chapman and Hall
PETRIE, W., and SMALL, R. G.	1952	*Astrophys. J.* **116**, 433
	1953	*Canad. J. Phys.* **31**, 911
RUSSELL, H. N.	1936	*Astrophys. J.* **83**, 129
SEATON, M. J.	1954	*J. Atmosph. Terr. Phys.* **4**, 285
SHEPHERD, G. G.	1954	Scientific Report No. AR-16, Contract AF19(122)–152, University of Saskatchewan
TURNER, R. G., and NICHOLLS, R. W.	1954	*Canad. J. Phys.* **32**, 468
VAN DE HULST, H. C.	1952	The atmospheres of the earth and planets (Ed. G. P. Kuiper), 2nd ed., University of Chicago Press
VEGARD, L., and KVIFTE, G.	1945	*Geofys. Publ.* **16**, No. 7

L.
55

Journal of Atmospheric and Terrestrial Physics, 1955, Vol. 7, pp. 152 to 169. Pergamon Press Ltd., London

The aeronomic problem of nitrogen oxides

MARCEL NICOLET*
Ionosphere Research Laboratory, The Pennsylvania State University, University Park, Pennsylvania

(*Received* 28 *March* 1955)

ABSTRACT

From consideration of the observational data on atmospheric nitric oxide, it is found that its concentration at any height must be less than 10^{11} cm^{-3}. Theoretical deductions from an aeronomic study show that its concentration could be of the order of 10^8 cm^{-3} (or 5×10^8) at about 80 km, and 10^9 cm^{-3} (or 5×10^9) at about 65 km. At any height below 70 km the nitric oxide concentration must be less than the ozone concentration.

The dissociation of nitrogen molecules involved in nitric oxide formation depends strongly on photo-ionization by ultraviolet or X-ray radiation and subsequent dissociative recombination. The vertical distribution of nitrogen atoms cannot be determined by a dissociation equilibrium, since it is subject to dynamical effects such as diffusion and atmospheric mixing.

Whatever the processes involved in the formation of nitric oxide, its vertical distribution will tend to follow the atmospheric distribution until it becomes dissociated. A departure from photo-equilibrium conditions cannot occur for nitrogen peroxide molecules, for their lifetime in a sunlit atmosphere is very short.

Nitrous oxide seems to play no role in the mesosphere.

In anticipation of the importance attached to the aeronomic problem of nitrogen oxides in the mesosphere and lower thermosphere, various provisional numerical data are presented.

I. INTRODUCTION

THE aeronomic problem of nitrogen oxides can only be studied on a theoretical basis, for no observational evidence concerning nitrogen oxides in the high atmosphere has been obtained to date.

Nitric oxide was first considered as an important constituent of the high atmosphere by NICOLET (1945). He found there is a possibility that this gas is quite abundant below the transition region in which molecular oxygen is transformed into atomic oxygen. He judged that the nitric oxide molecule could suitably explain the ionization below 100 km, that is, that "The essential phenomenon in region *D* results from NO photo-ionization." He pointed out that this molecule, with an ionization potential of the order of 9·5 eV, is able to absorb solar radiation of λ1300 Å and, in particular, the Lyman-α radiation at λ1215·7 Å, which is very sensitive to solar flares.

Since this mechanism was proposed, BATES and SEATON (1950) have set forth reasons indicating why it is difficult to consider any other acceptable alternatives such as O_2 and Na photo-ionization. WATANABE, MARMO, and INN (1953), after having measured the absorption coefficients of NO, O_2, and other molecules, concluded that the formation of the *D*-layer by NO as indicated by NICOLET (1945) can be a satisfactory explanation, since Lα lies in an atmospheric window. Use of the absorption coefficients of molecular oxygen in the region of its first continuum (WEISSLER and LEE, 1952; CLARK, 1952) shows that O_2 photo-ionization cannot account for the ionization in region *D*, but can occur at altitudes corresponding to the bottom of the *E*-layer. At the threshold, $\lambda = 1029$ Å (INN, 1953), the ionization cross-section may be very small (consider the ionization efficiency of O_2

* Present address: Royal Meteorological Institute of Belgium, Department of Radiation, Uccle, Belgium.

VOL. 7 1955

obtained by WAINFAN, WALKER, and WEISSLER, 1953). The cross-section at the threshold* may be as low as 10^{-19} cm^2 (INN, private communication), but the absorption coefficient is probably of the order of 4×10^{-18} cm^2 between 1000 Å and 910 Å. Therefore, an ionization peak of O_2 may occur at 90 km, the height at which the electron concentration could be of the order of 2×10^4 cm^{-3}. Furthermore, the observation of L-α radiation by rockets down to 74 km (BYRAM, CHUBB, FRIEDMAN, and GAILAR, 1953; BYRAM, CHUBB, and FRIEDMAN, 1954) and in the solar spectrum (PIETENPOL, RENSE, WALZ, STACEY, and JACKSON, 1953; TOUSEY, 1954) shows that the monochromatic radiation of chromospheric hydrogen can be a very effective agent for an ionization process below the mesopause level.

BATES (1952) in studying the atmospheric photo-equilibrium of nitrogen oxides, has shown that the formation of nitric oxide, resulting possibly from three body collisions of nitrogen and oxygen atoms, is counterbalanced by a loss due to a photo-dissociation process, and a chemical reaction between NO and N.

Some time ago it was believed that the absorption band centred at 2264 Å in the solar spectrum observed by DURAND, OBERLY, and TOUSEY (1949) could be identified as a band of *atmospheric* nitric oxide. With this interpretation, the band must correspond to a column of about 10^{18} molecules cm^{-2} at about 55 km (BATES and SEATON, 1950). Since MIGEOTTE and NEVEN (1952) have not detected atmospheric nitric oxide in their observations of the solar infrared spectrum, they deduce, by comparison with laboratory measurements, that the total number of nitric oxide molecules is less than 5×10^{17} molecules cm^{-2}. More recently, it has been shown (JOHNSON, PURCELL, TOUSEY, and WILSON, 1954) that the absorption observed in rocket spectra, which depresses the solar spectrum, cannot be due to nitric oxide and, therefore, the infrared investigation leads to a possible upper limit for the atmospheric nitric oxide abundance. It can be concluded that the observed absorption is due to solar absorption as yet unidentified.

Possible atmospheric spectroscopic evidence was suggested by NICOLET (1948) when he drew attention to coincidences between β-bands of NO and auroral radiations. The coincidences were found again by VEGARD in subsequent publications, but according to PETRIE and SMALL (1952) NO should not be present in auroral spectra.

Nitrous oxide, however, is observed by infrared spectroscopy. Following discovery of the fundamental band of N_2O at 7·8 μ by ADEL (1939), other bands have been found by various workers (MIGEOTTE, 1949); SHAW, SUTHERLAND, and WORMELL, 1948, . . .). From measurements of the absorption of infrared lines, MCMATH and GOLDBERG (1949) and MIGEOTTE, BENESCH, and NEVEN (1953) have found a spectroscopically determined abundance of the order of 10^{19} molecules cm^{-2}. N_2O follows the atmospheric vertical distribution (GOLDBERG and MULLER, 1953), or at least may be taken to be a tropospheric constituent. The photochemistry of tropospheric nitrous oxide has been investigated by BATES and WITHERSPOON (1952), who indicate that this molecule is not a member of the main photochemical series of nitrogen oxides. More recently, HARTECK and DONDER (1954) have also considered this problem without any reference to preceding work.

* This was written before we had received from Dr. G. L. WEISSLER a manuscript by Dr. P. LEE on the photo-ionization cross-section of O_2. At 1030 Å the cross-section is 5×10^{-19} cm^2, indicating that the absorption coefficient of O_2 is very small.

Nitrogen peroxide cannot be considered an important constituent in the mesosphere during daylight, because the dissociation rate coefficient is high. However, the laboratory results show many interesting processes, and NO_2 formation during the night remains to be investigated. From spectroscopic studies (NORRISH, 1929; BAXTER, 1930) it has been found that *visible* phenomena occur particularly in two bands lying in the red-orange and yellow-green parts of the spectrum; namely, between 6200–6300 Å and 5600–6050 Å. Furthermore, the formation of NO_2 by a radiative process involving nitric oxide and atomic oxygen is also a process leading to a continuous emission spectrum (GAYDON, 1944). Other laboratory investigations (RAYLEIGH, 1910; STODDARD, 1934; NEWMAN, 1935; SPEALMAN and RODEBUSH, 1935; KONDRATJEW, 1936; TANAKA and SHIMAZU, 1948) point to the fact that there is an afterglow which is related to nitrogen peroxide. Just as for every constituent which can affect the air-glow, it is necessary to study the possible equilibrium with ozone and atomic oxygen, and the departure from photo-equilibrium due to an atmospheric mixing.

In principle, the behaviour of nitrogen oxides must depend on the dissociation of molecular nitrogen. The conditions in the mesosphere and thermosphere indicate that the vertical distribution of nitrogen atoms is determined by atmospheric mixing or diffusion, rather than by local equilibrium. The change in the relative populations of nitrogen oxides must be studied by considering to what extent departure from equilibrium can exist.

After delineating the rate of absorption of solar radiation, the subsequent discussion shows the possible effects produced by atmospheric motions. This analysis will also indicate the rate with which chemical equilibrium is approached and, finally, the effects produced by processes involving nitrogen oxides and leading to possible day and night air-glow.

VOL. 7 1955

II. DISSOCIATION OF NITROGEN MOLECULES

The dissociation of nitrogen molecules has been studied by BATES (1952), who considered the predissociation found by HERZBERG and HERZBERG (1948) in the bands of the Lyman-Birge-Hopfield system. His determination of the dissociation-rate coefficient yields a value $J_{N_2} = 10^{-12}$ sec^{-1} at zero optical depth. Taking this value, MITRA (1954) has calculated the effect of the optical depth, using a cross-section of 10^{-19} cm^2 and, therefore, found a rate coefficient decreasing rapidly downward with height in the mesosphere.

Another process is operative in the ionosphere (BATES, 1954). Molecular nitrogen is ionized by ultraviolet radiation of $\lambda < 796$ Å, and at shorter wavelengths $\lambda < 661$ Å, for which the absorption coefficient is of the order of 2×10^{-17} cm^2 (WEISSLER, LEE, and MOHR, 1952). As the number of photons available at the top of the earth's atmosphere is not less than 2×10^9 photons cm^{-2} sec^{-1} (NICOLET, 1952), the ionization-rate coefficient at zero optical depth (in region F at 160–170 km for an overhead sun) cannot be less than $4{\cdot}4 \times 10^{-8}$ sec^{-1}.

Furthermore, X-ray action is a possible mechanism (NICOLET, 1952a), for the absorption of solar radiation from 175 Å to the shortest wavelengths can be effective for ionization. According to rocket results (BURNIGHT, 1952; TOUSEY, 1952; BYRAM, CHUBB, and FRIEDMAN, 1953), X-rays near 7 Å were detected above 90 km.

More recently, BYRAM, CHUBB, and FRIEDMAN (1954, private communication) have obtained new values. According to their latest two results, the number of photons $cm^{-2}\,sec^{-1}$ is equal to 2×10^7 or 10^9 for the spectral range 20 Å to 8 Å, and 3×10^8 or 3×10^9 for wavelengths shorter than 60 Å.

From these two sets of values, which are, however, widely divergent, it can be stated that, if the scale height is of the order of 10 km, the rate of direct ionization at the peak for $\lambda < 60$ Å must be between 1000 and 100 electrons $cm^{-3}\,sec^{-1}$. Since about 70 per cent of the electron production with $\lambda < 60$ Å arises from N_2, only 30 per cent must be associated with the *E*-layer formation.* It must be pointed out that the solar X-ray emission is not limited to wavelengths shorter than 60 Å. So far as the ionization of nitrogen molecules is concerned, we can state that at least 100 N_2 molecules are ionized per sec and cm^3 in region *E*. Therefore, about 1000 nitrogen atoms can be produced per sec and cm^3 at such low heights as 110 km. In fact, ionization of molecular nitrogen is followed by dissociative recombination (BATES and MASSEY, 1947) after a very short time. The lifetime $\tau_{N_2^+}$ of a nitrogen ion is

$$\tau_{N_2^+} = 1/\alpha n_e,$$

and depends on the electron concentration n_e in the ionosphere. The dissociative recombination coefficient of N_2^+ is not less than $10^{-7}\,cm^3\,sec^{-1}$ (BIONDI, 1951; FAIRE, FUNDINGSLAND, and ADEN, 1954), and as low an electron concentration as $10^4\,cm^{-3}$ results in a lifetime of N_2^+ of less than one hour. Thus, in the whole ionosphere, the photo-ionization by ultraviolet radiation and X-rays leads to a yield of nitrogen atoms which is larger than the production by the primary dissociation process.

The results, however, concern only a static atmosphere in which no transport process is involved. It was shown by NICOLET and MANGE (1954), and NICOLET (1954), that dynamic processes such as diffusion and mixing are acting on the vertical distribution of molecular oxygen. A similar problem exists for atomic nitrogen after its production. It can be shown that the downward diffusion velocity at 160 km (unit optical depth for an overhead sun) is about 1 m sec^{-1}. The yield of nitrogen atoms versus height, therefore, cannot be computed without consideration of atmospheric transport. Downward transport of nitrogen atoms following an ionization process is strongly effective, and modifies the vertical distribution of the nitrogen atom concentration, computed on the basis of a photo-equilibrium in a static atmosphere.

This analysis of N_2 dissociation is different from those of DEB (1952) and SATO (1953), for these authors do not consider the possibility of ionization by X-rays, and have adopted a radiative recombination of normal nitrogen atoms with a coefficient not less than $10^{-21}\,cm^3\,sec^{-1}$. With such a value the lifetime τ_N of a nitrogen atom is

$$\tau_N = 1/10^{-21} n(N);$$

* It must be pointed out that only a fraction of the total electron production by X-ray action (1/5 at wavelengths for which the absorption coefficients for oxygen and nitrogen are of the same order) is associated with the ionospheric layers as observed by radio methods. The excess observed in the X-ray spectrum by BYRAM, CHUBB, and FRIEDMAN (1954) does not necessarily mean a high ratio of negative ions to electrons in the *E*-layer, but can be interpreted by means of rapid dissociative recombination of N_2^+ compared with that of O_2^+.

that is to say, a very long time. In fact, the loss of nitrogen atoms primarily depends on the association of nitrogen and oxygen atoms in a three-body collision, and the shortest lifetime is

$$\tau_N = 1/10^{-32} n(\mathrm{M})\, n(\mathrm{O})$$

in which $n(\mathrm{M})$ denotes the third-body concentration. In order to have a lifetime shorter than one year, it is necessary that the concentrations $n(\mathrm{M})$ and $n(\mathrm{O})$ be larger than 10^{12} cm^{-3}. Therefore, ionization of molecular nitrogen followed by dissociative recombination and vertical transport due to diffusion and mixing is a powerful process for the production of atomic nitrogen in the lower thermosphere. Furthermore, the vertical distribution of nitrogen atoms does not depend on a dissociation equilibrium state, but on atmospheric motions affecting a static equilibrium.

III. The Vertical Distribution of Nitrogen Oxides in the Mesosphere

The formation of nitric oxide is due *a priori* to a three-body collision process

$$\mathrm{N} + \mathrm{O} + \mathrm{M} \rightarrow \mathrm{NO} + \mathrm{M} \qquad (1)$$

or to nitrous oxide formation and subsequent photo-dissociation

$$\mathrm{N_2} + \mathrm{O} + \mathrm{M} \rightarrow \mathrm{N_2O} + \mathrm{M} \qquad (2)$$

$$\mathrm{N_2O} + h\nu \rightarrow \mathrm{NO} + \mathrm{N} \qquad (2')$$

Reaction (1) is certainly the primary process of NO formation; it requires the dissociation of nitrogen as indicated in Section II. Process (2) should lead to NO formation in a region in which the atomic oxygen concentration is maximum; namely, above the mesopause level. However, in their study of the absorption coefficients of nitrous oxide, ZELIKOFF, WATANABE, and INN (1953) and ZELIKOFF and ASCHENBRAND (1954) have interpreted absorption continua in terms of possible dissociation processes without dissociation into nitric oxide and atomic nitrogen. According to this interpretation, process (2) should not be considered as a fundamental mechanism for the production of nitric oxide, and it is, therefore, difficult to believe that the photo-dissociation of $\mathrm{N_2O}$ provides a contribution to the production of nitrogen atoms at levels of the order of 80 km, as MITRA (1954) has found. Consequently, reference must be made to the results of BATES and WITHERSPOON in which $\mathrm{N_2O}$ is a tropospheric constituent.

Since the loss of nitric oxide molecules is due to photo-dissociation, for which the rate coefficient (BATES, 1952) is of the order of 10^{-7} sec^{-1}, and to the reaction (BATES, 1952)

$$\mathrm{N} + \mathrm{NO} \rightarrow \mathrm{N_2} + \mathrm{O} \qquad (3)$$

the time of dissociation, $\tau_{\mathrm{diss}}(\mathrm{NO})$, of nitric oxide may be very long. Consequently, it is unrealistic to deduce its concentration from photo-equilibrium conditions. Furthermore, a reaction such as

$$\mathrm{NO_2} + \mathrm{N} \rightarrow \mathrm{NO} + \mathrm{NO} \qquad (4)$$

is to be considered, and may be important at night.

VOL. 7 1955

A study of nitrogen peroxide formation and photo-dissociation

$$NO + O \rightarrow NO_2 \tag{5}$$

$$NO_2 + h\nu \rightarrow NO + O \tag{6}$$

shows that the ratio $n(NO_2)/n(NO) \ll 1$, and there is no practical effect on the daytime nitric oxide concentration.

It is clear, therefore, that atmospheric mixing, acting during the day, can play a leading role in fixing the vertical distribution of NO. Nitric oxide can follow the variation of the atmospheric distribution in the mesosphere more closely than a vertical distribution determined by photo-equilibrium conditions.

We make one further comment about the influence of NO_2. As will be shown later, the ratio $n(NO_2)/n(NO)$ varies very rapidly, and is different during day and night. However, so far as the region D problem is concerned, the photo-dissociation-rate coefficient of nitrogen peroxide must be considered. Because its value is about 5×10^{-3} sec^{-1} (BATES, 1952), the lifetime of an NO_2 molecule is very short, 200 seconds, and a daytime photo-equilibrium exists for this molecule. But, since the ratio $n(NO_2)/n(NO)$ remains less than unity, the other vertical distributions are not affected.

IV. The Total Number of Nitric Oxide Molecules

Since it is obvious that there is no possibility of avoiding a departure from photochemical equilibrium for nitric oxide in the mesosphere, the formation of a D-layer is to be found, to a first approximation, with NO molecules following the atmospheric vertical distribution.

No direct experimental data are available concerning this, and one must conjecture concerning possible numerical values. Dissociative recombination of NO^+ is certainly an important process, but it is not possible to determine which value of the recombination coefficient is the most probable in the range 10^{-6} cm^3 sec^{-1} to 10^{-8} cm^3 sec^{-1}. On the other hand, it is not easy to obtain a correct value from ionospheric data, as may be seen from the values collected by MITRA and JONES (1954). These authors obtain a smooth curve leading to a recombination coefficient varying continuously with height. However, the actual heights cannot be well determined. If, for example, 10^{-7} cm^3 sec^{-1} is adopted as the value of the recombination coefficient, it may be in error by one order of magnitude, and it may be concluded that any deductions from an ionization equilibrium equation will be subject to considerable uncertainty. Nevertheless, it is possible to find permissible limits for the nitric oxide concentration.

MIGEOTTE and NEVEN (1952) have determined an upper limit for $n(NO)H$ of $<5 \times 10^{17}$ cm^{-2}; hence, H being the scale height, any concentration $n(NO) > 10^{12}$ cm^{-3}, found by theory, cannot be acceptable. If a layer of 10 km thickness exists with more than 5×10^{11} NO molecules cm^{-3}, nitric oxide would have been detected by infrared methods. Thus, it is safe to conclude that a NO concentration larger than 10^{11} cm^{-3} does not exist in the mesosphere, and the large concentrations found by MITRA (1954) are not acceptable. This conclusion is confirmed from the interpretation of rocket data.

Because NO has an absorption coefficient of the order of 2×10^{-18} cm^2 (SUN

and WEISSLER, 1952; WATANABE, MARMO, and INN, 1953) a unit optical depth is found for 5×10^{17} molecules cm^{-2}, or less than 10^{12} molecules cm^{-3}. Since solar Lyman-α is observed down to 74 ± 2 km for a solar elevation of 18–20° (BYRAM, CHUBB, FRIEDMAN, and LICHTMAN, 1952), NO does not absorb Lα more than O_2. At about 80 km, the unit optical depth at Lα for an overhead sun can occur only if O_2 molecules are the effective absorbing constituent. The transmission factor would be about 10 per cent near 72·5 km and 1 per cent near 67·5 km, when O_2 absorbs alone and the sun is overhead. With an 18–20° solar elevation, a 1 per cent transmission factor would correspond to about 75 km. Hence, it is not possible to include NO as an atmospheric constituent strongly affecting the optical depth for Lα, because the solar radiation could not arrive at so low a height as 75 km. The ratio $n(\mathrm{NO})/n(\mathrm{M})$, namely the ratio of nitric oxide to all the atmospheric constituent concentrations, is less than 1/1000. A more recent analysis by BYRAM, CHUBB, FRIEDMAN, and GAILAR (1953) shows that no influence of nitric oxide can be detected. Since the absorption cross-section for NO is $2{\cdot}4 \times 10^{-18}$ cm^2, with an ionization cross-section equal to $2{\cdot}1 \times 10^{-18}$ cm^2 (WATANABE, 1954), and since the absorption cross-section of O_2 is of the order of 10^{-20} cm^2 (PRESTON, 1940; WATANABE, INN, and ZELIKOFF, 1953; DITCHBURN, 1954), a ratio $n(\mathrm{NO})/n(\mathrm{M}) = 1/1000$ should give an almost identical absorption for NO and O_2. Therefore, the concentration of nitric oxide cannot be more than 10^{11} cm^{-3} at 80 km. Consequently, rocket data and infrared spectroscopy yield consistent results indicating that there are, at any height, less than 10^{11} NO molecules cm^{-3}.

VOL. 7 1955

V. THE PHOTO-IONIZATION OF NITRIC OXIDE AND ITS CONCENTRATION

The rate of electron production by photo-ionization of NO may be written as follows.

$$n(\mathrm{NO})K(\mathrm{NO})Q_\infty(\mathrm{L}\alpha)e^{-n(\mathrm{O}_2)K(\mathrm{O}_2)H\sec\chi}, \tag{7}$$

in which $K(\mathrm{NO})$ denotes the ionization cross-section of NO, and $K(O_2)$ the absorption coefficient of molecular oxygen. The absorption cross-section of NO must not be considered in the optical depth.

The vertical distribution of the number of photons available for the photo-ionization of NO depends on the molecular oxygen concentration at efficient optical depths; the peak of the electron production by NO lies practically at the O_2 absorption peak for Lα radiation. If the nitric oxide concentration does not behave very differently from the concentrations of the principal atmospheric constituents, the peak of photo-ionization is fixed by the condition, (7),

$$n(\mathrm{O}_2)K(\mathrm{O}_2)H\sec\chi = 1 + \beta, \tag{8}$$

where $\beta = dH/dz$ is the gradient of the atmospheric scale height, H.

If the nitric oxide distribution is different from the atmospheric distribution, but related to it through the parameter X according to

$$[n(\mathrm{NO})/n_0(\mathrm{NO})]^X = n(\mathrm{O}_2)/n_0(\mathrm{O}_2),$$

the peak of photo-ionization is determined by

$$n(\mathrm{O}_2)K(\mathrm{O}_2)H\sec\chi = X(1 + \beta). \tag{8'}$$

Thus, the actual problem of NO ionization is not so complex as when a photo-equilibrium of nitrogen oxides is to be considered. The number of photons available for the ionization is known, the atmospheric absorption of Lα can be determined, and the vertical distribution of NO is not unknown. Consequently, it should be possible to determine the concentration of NO. Condition (8) shows a peak, for an overhead sun, of between 75 and 77 km, where the total number of atmospheric molecules is of the order of 7×10^{20} cm^{-2} or 5×10^{20} cm^{-2}.

The number of photons available at zero optical depth for a quiet sun has been obtained by BYRAM, CHUBB, FRIEDMAN, and GAILAR (1953). It is of the order of 6×10^{9} photons sec^{-1} cm^{-2}. At the absorption peak the number available must be of the order of $2{\cdot}2 \times 10^{9}$ photons sec^{-1} cm^{-2}. Since the ionization cross-section of NO is $(2{\cdot}1 \pm 0{\cdot}2) \times 10^{-18}$ cm^{2} (WATANABE, 1954), the ionization rate coefficient equals $4{\cdot}5 \times 10^{-9}$ sec^{-1} at the absorption peak, and $1{\cdot}3 \times 10^{-8}$ sec^{-1} at zero optical depth for a quiet sun. These values may be compared with those considered by MITRA (1954). Introduction of his reduction factor, namely $2{\cdot}6 \times 10^{-3}$ or $1{\cdot}6 \times 10^{-1}$, cannot be accepted, and shows that the concentrations deduced from his equations are not correct.

Using the conventional equation for an ionization equilibrium, that is,

$$\frac{n^{+}(\mathrm{NO})n_e}{n(\mathrm{NO})} = \frac{4{\cdot}5 \times 10^{-9}}{\alpha}\, e^{-n(\mathrm{O_2})K(\mathrm{O_2})H \sec \chi}, \tag{9}$$

in which n^{+}(NO) denotes the number of positive ions, n_e the electron concentration, and α the ionospheric recombination coefficient, it is clear that the concentration of NO could be deduced if the ionospheric parameters such as electron concentration and recombination were well known. It is difficult to say what value of n_e between 10^{3} and 10^{4} cm^{-3} is acceptable for the largest concentration in region D, and what value of α can be chosen.

Arbitrarily taking 10^{8}/NO molecules cm^{-3} at 80 km, that is to say a concentration of 2×10^{-7} times the atmospheric concentration, the rates of ionization for an overhead sun would be:

km	85	80	75	70	65
n_e cm^{-3} sec^{-1}	0·58	0·77	0·78	0·30	0·025

A recombination coefficient equal to 10^{-6} cm^{3} sec^{-1} would give an electron concentration of 1000 cm^{-3} at 77 km.* However, the effect of negative ions should be taken into account at the lowest heights. Therefore, the peak value of the electronic concentration depends on the assumed values of the parameters.†

Since neutral sodium has a concentration peak above 80 km (HUNTEN, 1954) of the order of 10^{4} cm^{-3}, the number of electrons produced by ionization of this atmospheric constituent at 85 km is not more than $10^{4} \times 10^{-5} = 10^{-1}$ cm^{-3} sec^{-1};

* For example, $\alpha = 10^{-7}$ cm^{3} sec^{-1}, and $n(\mathrm{NO}) = 5 \times 10^{8}$ cm^{-3} at 80 km, lead to about 6×10^{3} electrons cm^{-3} at the peak.

† A photo-detachment rate coefficient of 0·5 sec^{-1}, and an attachment coefficient of the order of 10^{-15} cm^{3} sec^{-1}, lead to a value of $\lambda = n^{-}/n_e$ of the order of unity at 68 km. But, at 80 km, λ would be only 0·2, and therefore, the electron concentration peak cannot be more than one scale height above the electron production peak. In other words, if the dissociative recombination coefficient were 10^{-6} cm^{3} sec^{-1}, the ionospheric coefficient would be 4×10^{-6} at 60 km, $2{\cdot}5 \times 10^{-6}$ at 65 km, about 2×10^{-6} at 70 km, and $1{\cdot}2 \times 10^{-6}$ at 80 km.

a maximum value. This demonstrates how important it is to obtain exact ionospheric data on recombination coefficients and of electronic concentration versus exact height. In conclusion, if a nitric oxide concentration of 10^8 cm^{-3} is considered correct to within one order of magnitude, it leads to a possible explanation of the behaviour of region D under normal conditions as well as under solar flare conditions. Sodium atoms cannot be responsible for the ionization at the bottom of the region, for their concentration appears to decrease too rapidly below their peak at 85 km. Insofar as the upper part of region D is concerned, at altitudes of 90 km, it will be necessary to take into account the variation of the ionospheric recombination coefficient with height, or the penetration of solar radiation ionizing O_2 near its threshold at about 1030 Å, for here the absorption coefficient is less than 10^{-18} cm^2 and permits the penetration of solar radiation below 100 km.

VI. PROCESSES IN THE CHEMOSPHERE

In the chemosphere, the aeronomic problem depends on the recombination processes leading to a loss of oxygen atoms. In a pure oxygen atmosphere, the loss of oxygen atoms is due to ozone formation, and association of atoms into oxygen molecules. It was shown by BATES and NICOLET (1950) that by its catalytic action hydrogen may have an effect on the ozone concentration in the mesosphere. Furthermore, dynamic motions which tend to increase the atomic oxygen concentration downward (NICOLET and MANGE, 1954; NICOLET, 1954) modify the photoequilibrium picture when the times involved in the reactions are too long. These motions are particularly effective near the mesopause level.

VOL. 7 1955

At night, atomic oxygen can enter into various reactions leading, finally, to a molecular recombination as follows:

$O + O + M \rightarrow O_2 + M,$	coefficient k_1
$O + O_2 + M \rightarrow O_3 + M,$	coefficient k_2
$O + OH \rightarrow H + O_2,$	coefficient a_2
$O + NO \rightarrow NO_2 + h\nu,$	coefficient b_2

Subsequently, the following reactions are also possible leading to O_2:

$O + O_3 \rightarrow O_2 + O_2,$	coefficient k_3
$O + NO_2 \rightarrow NO + O_2,$	coefficient b_3
$H + O_3 \rightarrow OH + O_2,$	coefficient a_3
$NO + O_3 \rightarrow NO_2 + O_2,$	coefficient b_4

An approximate equilibrium equation may be obtained at a height of the order of 70 km, the processes being considered as sufficiently rapid, namely,

$$n(H)/n(OH) \simeq n(O)/n(O_3).$$

At greater heights, departure from the equilibrium can exist, because the time of recombination of oxygen atoms increases with height (NICOLET and MANGE, 1954). Thus, the processes involving nitrogen oxides are subject to the variation of the atomic oxygen concentration.

In the mesosphere above 50 km, the atomic oxygen concentration is larger than the ozone concentration under *daytime* photo-equilibrium conditions. Therefore, the aeronomic problem is different above or below 50 km. If the mesosphere were a pure oxygen atmosphere, the ozone vertical distribution (BATES and NICOLET, 1950) would be

$$n(O_3)_{\text{limit}} = \frac{k_2}{k_3} n(O_2)n(M).$$

Above 80 km $n(O_3)_{\text{limit}} < n(O)_{\text{day}}$, and the atomic oxygen concentration always remains larger than the ozone concentration. Below 75 km, the ozone concentration cannot be larger than the daytime atomic oxygen concentration.

The fundamental process involving ozone and atomic oxygen depends on a reaction with an energy of activation of the order of 6 kcal leading to a rate coefficient, k_3, of about 10^{-15} cm^3 sec^{-1} at 250°K. But the processes affecting atomic oxygen and ozone through the catalytic action of hydrogen require a lower activation energy, perhaps of the order of 3 kcal, leading to a rate coefficient, $a_2 \approx a_3$, of more than 10^{-13} cm^3 sec^{-1} at 250°K. Thus, as was shown by BATES and NICOLET (1950), the atomic oxygen-ozone equilibrium in the mesosphere is subject to the catalytic action of hydrogen. Nevertheless, these estimates may be in error by a considerable factor, due to lack of precise values for the chemical reactions; it is difficult to study the exact variation of OH, H, O, and O_3 during dark hours.

The chemical reactions concerning the nitrogen oxides will be processes of the same kind. However, a considerable amount of attention must be given to the possible concentrations before studying the aeronomic problem. In the following, it is possible to suggest a scheme which is not a combination of all possibilities, but based on reactions of high efficiency due to low energies of activation.

VII. NITROGEN PEROXIDE

As may be readily verified from Bates's equations (1952) and the rate coefficient values, the photo-ionization of nitrogen peroxide is so rapid during the day that its action on the nitric oxide concentration can be neglected in the upper mesosphere.

The essential night-time mechanisms affecting NO_2 are:

(i) $$O + NO \rightarrow NO_2 + h\nu \qquad (10)$$

for which the rate coefficient b_2 is about 10^{-17} cm^3 sec^{-1} (BATES, 1954).

(ii) $$O + NO_2 \rightarrow NO + O_2 \qquad (11)$$

for which the rate coefficient b_3 depends on the activation energy chosen. Data may be deduced from SCHUMACHER (1930), SPEALMAN and RODEBUSH (1935), and HENRIQUES, DUNCAN, and NOYES (1938). The probability of this reaction is of the order of 10^{-5} per collision at a temperature of 313°K. Without any steric factor the activation would be 7 kcal, and with a steric factor of 0·01, as indicated by HENRIQUES, DUNCAN, and NOYES (1938), the activation energy may be 4·3 kcal. However, a steric factor of the order of 10^{-3} cannot be excluded after one considers other reactions of the same type. With such a value, the activation energy would

be only 2·9 kcal. Adopting as extreme values 7 kcal and 2·9 kcal, the following values are obtained:

T(°K)	$E = 7$ kcal	$E = 4{\cdot}2$ kcal	$E = 2{\cdot}9$ kcal
150	$1{\cdot}2 \times 10^{-20}$	$7{\cdot}0 \times 10^{-18}$	$1{\cdot}1 \times 10^{-17}$
200	$4{\cdot}8 \times 10^{-18}$	$5{\cdot}2 \times 10^{-17}$	$1{\cdot}4 \times 10^{-16}$
250	$1{\cdot}8 \times 10^{-16}$	$4{\cdot}9 \times 10^{-16}$	$6{\cdot}9 \times 10^{-16}$
300	$2{\cdot}1 \times 10^{-15}$	$2{\cdot}3 \times 10^{-15}$	$2{\cdot}0 \times 10^{-15}$
350	$1{\cdot}2 \times 10^{-14}$	$6{\cdot}8 \times 10^{-15}$	$4{\cdot}3 \times 10^{-15}$

If a value of 2×10^{-15} cm^3 sec^{-1} is accepted at 300°K, a minimum value of 5×10^{-18} cm^3 sec^{-1} and a maximum value of 1×10^{-16} cm^3 sec^{-1} must be adopted at 200°K. Because the experimental value given by SPEALMAN and RODEBUSH (1935) is an estimate correct only to an order of magnitude (10^{-5} per collision at 40°C), it is difficult to determine an exact value at temperatures of the upper mesosphere.

(iii) $$O_3 + NO \rightarrow NO_2 + O_2 \qquad (12)$$

The rate coefficient for (iii), b_4, has been determined (JOHNSTON and CROSBY, 1951, 1954).

Taking a steric factor of 5×10^{-3} and an activation energy of 2·4 kcal, the following values are obtained for b_4:

$150°K$, 3×10^{-16}; $200°K$, $2{\cdot}5 \times 10^{-15}$

$250°K$, $9{\cdot}5 \times 10^{-15}$; $300°K$, $2{\cdot}3 \times 10^{-14}$

Of the reactions

$$O_3 + NO_2 \rightarrow NO_3 + O_2 \qquad (13a)$$

followed by

$$NO_3 + NO \rightarrow NO_2 + NO_2 \qquad (13b)$$

(13a) has been studied in the laboratory by JOHNSTON and YOST (1949) and can be neglected to a first approximation, since its activation energy of about 7 kcal with a steric factor of the order of 4×10^{-2} leads to a rate coefficient of less than 10^{-17} at 250°K. For this reason, (13b), which has no activation energy (JOHNSTON, 1951), may be neglected.

(iv) The reaction $$N + NO_2 \rightarrow NO + NO \qquad (14)$$

is a fairly rapid reaction studied by SPEALMAN and RODEBUSH (1935). According to their conclusion, the reaction (14) and

$$N + NO \rightarrow N_2 + O \qquad (3)$$

are of the same order of rapidity at 40°C as that (11) between nitrogen peroxide and oxygen atoms. It should be of extreme importance to know the steric factors and activation energies associated with b_5 and b_6, the rate coefficients of (14) and (3), respectively.

VETTER (1949) has obtained values for the steric factors and activation energies of (3), (11), and (14). However, the whole study of VETTER depends on a reaction

VOL. 7 1955

$O + NO \rightarrow O_2 + N$, which is endothermic to the extent of 32 kcal. Therefore, the activation energy deduced by VETTER is 29 kcal; that is to say, a smaller value than that needed by the endothermic reaction. Data presented by WISE and FRECH (1952) lead to an activation energy of about 23 kcal. These various results cannot be accepted, since the equilibrium constant $K(N_2)$ of the reaction $N_2 = 2N$ is based on heats of dissociation of the order of 170 kcal instead of 225 kcal.

Consequently, the lack of exact data necessitates very crude estimates. Because an almost linear collision is involved in such reactions, we consider that a steric factor of 10^{-2} should be a maximum value, and that a value of 10^{-3}, which will be a minimum, cannot be far from the real steric hindrance. Such a value leads to the adoption of an activation energy of about 2·9 kcal. A steric factor of 5×10^{-3}, like that for (12), would lead to an activation energy of about 4 kcal.

(v) $$NO_2 + h\nu \rightarrow NO + O \qquad (15)$$

is a reaction for which the dissociation rate coefficient J_{NO_2} is 5×10^{-3} sec^{-1} (BATES, 1954), when NO_2 is subject to solar radiation.

Neglecting possible reactions with hydrogen, the differential equation involving processes affecting NO_2 may be the following:

$$\frac{dn(NO_2)}{dt} = [b_2 n(O) + b_4 n(NO) n(O_3)] n(NO) - [b_3 n(O) + b_5 n(N) + J_{NO_2}] n(NO_2). \qquad (16)$$

During the day, the time of dissociation, $\tau_{diss}(NO_2)$, of nitrogen peroxide will be given by

$$\tau_{diss}(NO_2) = 1/J_{NO_2} = 200 \text{ sec} \qquad (17)$$

which is a very short time. A photo-equilibrium must, therefore, exist and the equation is

$$\frac{n(NO_2)}{n(NO)} = \frac{b_2 n(O) + b_4 n(O_3)}{J_{NO_2} + b_3 n(O) + b_5 n(N)}. \qquad (18)$$

Inserting numerical values in (18), we see that $n(NO_2)$ is only a fraction of $n(NO)$, for $T = 250°K$,

$$\frac{n(NO_2)}{n(NO)} = 2 \times 10^{-15} n(O) \qquad (19)$$

or

$$\frac{n(NO_2)}{n(NO)} = 2 \times 10^{-12} n(O_3). \qquad (20)$$

After twilight, the ratio $n(NO_2)/n(NO)$ increases according to the solution to the differential equation (16) in which $J_{NO_2} = 0$, and $b_3 n(O) > b_5 n(N)$,

$$n(NO_2) = n_0(NO_2) e^{-b_3 n(O) t} + \frac{b_2 n(O) + b_4 n(O_3)}{b_3 n(O)} n(NO) [1 - e^{-b_3 n(O) t}] \qquad (21)$$

provided $n(NO)$ and $n(O)$ do not vary appreciably.

At sunset, the concentration of nitrogen peroxide increases according to the rate equation

$$\frac{dn(NO_2)}{dt} = [b_2 n(O) + b_4 n(O_3)]\, n(NO). \tag{22}$$

Above the mesopause $b_2 n(O) > b_4 n(O_3)$ and (22) becomes

$$\frac{dn(NO_2)}{dt} = 10^{-17}\, n(O) \tag{23}$$

which gives, after only 10^3 seconds,

$$n(NO_2) \geq n(NO)/100 \tag{24}$$

if

$$n(O) \geq 10^{12}\ \text{cm}^{-3}.$$

In the mesosphere at $T = 250°\text{K}$ where $n(O_3) > n(O)/1000$, (22) becomes

$$\frac{dn(NO_2)}{dt} = 10^{-14} n(O_3) n(NO) \tag{25}$$

which yields, after 10^3 seconds, if $n(O_3)$ is of the order of $10^{10}\ \text{cm}^{-3}$,

$$n(NO_2) = n(NO)/10. \tag{26}$$

In fact, the time τ_{neq} to reach the nocturnal equilibrium value,

$$\frac{n(NO_2)}{n(NO)} = \frac{b_2 n(O) + b_4 n(O_3)}{b_3 n(O)}, \tag{27}$$

which is expressed by

$$\tau_{neq} = 1/b_3 n(O), \tag{28}$$

depends on the atomic oxygen concentration and varies with height. Adopting the daytime value of $n(O)$, the time of NO_2 formation defined by (28) should be of the order of 10^4 to 5×10^4 sec between 50 km and 90 km. In other words, one night may be necessary to reach equilibrium instead of the 200 sec for a sunlit atmosphere. If we consider daytime values, the ratio $n(NO_2)/n(NO)$ is less than unity above 50 km, while it is larger than unity below 50 km where the temperature is still sufficiently high.

During dark hours, the equilibrium ratio $n(NO_2)/n(NO) > 1$ in the whole region where ozone is efficient. At 90 km, for example, where the reaction involves oxygen atoms, the equilibrium value cannot reach unity.

Day and night conditions may become identical in the thermosphere. For example, with the values adopted, $n(NO_2)/n(NO)$ should be of the order of 3×10^{-3} during night and day at 120 km.

Although it is necessary to avoid conclusions based only on night-time equilibrium conditions, it may still be remarked that, during the dark hours, the transformation of NO into NO_2 is important throughout the entire mesosphere. At lower heights, ozone molecules play the leading role, while above mesopause levels the reaction is due, essentially, to oxygen atoms.

VOL. 7 1955

It is important to point out that ozone would be destroyed during dark hours in the mesosphere if the nitric oxide concentration were larger than the ozone concentration. If not, the loss of ozone molecules is given by

$$\frac{dn(O_3)}{dt} = -b_4 n(O_3) n(NO). \tag{29}$$

Therefore,

$$n(O_3) = n_0(O_3) e^{-b_4 n(NO) t} \tag{30}$$

would lead to about one-third of the initial concentration, $n_0(O_3)$, in less than 2000 sec at 50 km, where the temperature is 280°K and $n_0(O_3) = 3 \times 10^{10}$ cm^{-3}; consequently, $n(NO)$ should be less than $n_0(O_3)$. It seems that the nitric oxide concentration should be less than the ozone concentration below 70 km ($n(NO) \leq 10^9$ cm^{-3}) to avoid an ozone loss during the night. Furthermore, the nocturnal concentration of nitrogen peroxide is limited to that of the daytime nitric oxide in the entire mesosphere.

Using the complete set of reactions written above, the equation governing the rate of change of $n(NO)$ is

$$\frac{dn(NO)}{dt} = b_1 n(M) n(O) n(N) + [J_{NO_2} + b_3 n(O) + 2b_5 n(N)] n(NO_2) - [J_{NO} + b_2 n(O) + b_4 n(O_3) + b_6 n(N)] n(NO). \tag{31}$$

Using (18), (31) can be written

$$\frac{dn(NO)}{dt} = b_1 n(M) n(O) n(N) - [J_{NO} + b_6 n(N)] n(NO),$$

for

$$b_3 n(O) > b_5 n(N). \tag{32}$$

One can say from (32), written for photo-equilibrium conditions, that the ratio $n(NO)/n(N)$ would decrease from about 50 at 50 km to about unity at 90 km. Maximum equilibrium values corresponding to night-time conditions would lead to NO concentrations of about 5×10^9 cm^{-3}.

These results are only estimates which suffer from lack of precision of experimental data. Furthermore, since an equilibrium cannot be reached, departures from photo-equilibrium conditions occur throughout the whole mesosphere and in the thermosphere. The mixing effect will be prevalent in the mesosphere and lower thermosphere, while diffusion will play the leading role above the production peak of nitrogen atoms.

In any case, it is important to distinguish between day and night conditions which affect the equilibrium between NO and NO_2 in the mesosphere, particularly in the region where the night-time equilibrium ratio $n(NO_2)/n(NO)$ is larger than unity.

Before studying the exact variation of the NO_2 nocturnal concentration, it is necessary to study the complete problem involving ozone, OH, H, and other processes, in a nitrogen-oxygen atmosphere in which departures from equilibrium conditions do exist.

VIII. CONCLUSIONS

Following BATES's analysis of the photochemistry of nitrogen oxides, it is possible to develop the study of the aeronomic problem of nitric oxide and nitrogen peroxide.

First, it is necessary to consider the dissociation of molecular nitrogen due to the photo-ionization of N_2 by ultraviolet radiation in region F with a departure from photochemical equilibrium conditions. Second, the photo-ionization of N_2 by X-rays in region E leads to a peak production of about 1000 nitrogen atoms per cm^3 and sec. Since the mean lifetime of a nitrogen atom before molecular formation is $1/b_1 n(M)n(O)$, it is shorter in the E-layer than in region F, and departures from photochemical equilibrium are less severe than at higher levels. Nevertheless mixing effects do play a role, and lead to fluctuations in the nitric oxide production below 100 km. These may give increases in the electron density in region D even when the sun is quiet. In other words, variations in the ionization of the D-layer may occur as a result of atmospheric motions affecting the downward transport of NO.

It was shown by NICOLET (1954) that concentrations of atomic oxygen which are larger than those given by photochemical equilibrium do exist in the O_2-O transition region because of atmospheric motions. The same kind of problem exists for nitric oxide. Therefore a special study should be made near 100 km.

In considering the problem of the origin of region D, the nitric oxide concentration may be taken to be about 5 to 1×10^8 cm^{-3} near 80 km, and would be of the order of 5 to 1×10^9 cm^{-3} at 65 km, generally corresponding to a vertical distribution following the atmospheric distribution, or even decreasing more slowly than the atmospheric constituents.

Such concentrations are able to provide an interpretation of the D-layer, subject to the effect of Lα emitted by a quiet sun, and also to the effect of solar flares Furthermore, fluctuations occurring in nitric oxide concentrations and subject to atmospheric motions may modify the ionization rate without any variation in Lα. Unfortunately, exact values of the ionospheric parameters cannot be used, for the altitudes deduced from ionospheric measurements are not precise enough, nor are the electron concentrations well known.

Between 90 km and 100 km ionospheric behaviour is difficult to determine without any knowledge of the X-ray radiation between 40 Å and 30 Å. Now, considering the ionization produced by ultraviolet radiation, it is easy to show (NICOLET, 1952) that the solar radiation at 1030 Å depends on free-free coronal transitions. Adopting coronal temperatures between 740,000°K and 1,440,000°K, numerical results can be obtained, using NICOLET's formulae (1952). The number of photons sec^{-1} cm^{-2} at the top of the earth's atmosphere between 1040 and 920 Å, i.e., in the spectral range not subject to a continuous absorption by atomic oxygen and molecular nitrogen, would be 10^7 to 5×10^7. Therefore, the solar emission cannot be represented by radiation temperatures less than 4500°K at about 1040 Å.

The aeronomic process of O_2 ionization depends on the continuous absorption of O_2 at its first ionization potential. At the threshold, the ionization cross-section is small (as low as 5×10^{-19} cm^2). However, the absorption coefficient is not less than 4×10^{-18} cm^2 between 1000 Å and 910 Å. Near Lyman-β at 1025 Å the cross-section is of the order of 2×10^{-18} cm^2. Using 5×10^{-19} cm^2, we find a unit

VOL. 7 1955

optical depth between 90 km and 95 km for an overhead sun. Therefore, the rate of ionization is of the order of

$$N_e(\text{U.V.}) = 0{\cdot}37 \times 2{\cdot}5 \times 10^7/7 \times 10^5 = 23 \text{ electrons cm}^{-3} \text{ sec}^{-1}$$

and is not negligible. With a recombination coefficient of the order of 3×10^{-8}, the electron concentration should be of the order of $2{\cdot}5 \times 10^4$ cm^{-3} and, of course, should be different from the X-ray ionization in the E-layer.

Finally, the maximum production of nitric oxide molecules occurs near the peak of the atomic oxygen concentration in the E-layer. Therefore, a charge transfer between atomic oxygen ions and nitric oxide molecules similar to the charge transfer between atomic oxygen ions and oxygen molecules must also be considered; it may lead to another peak of nitric oxide ions.

Acknowledgements—The author is indebted to Professor D. R. Bates for his comments on the draft manuscript written at The Pennsylvania State University.

The research reported in this paper has been sponsored by the Geophysics Research Directorate of the Air Force Cambridge Research Center, Air Research and Development Command, under Contract AF19(122)-44.

References

Adel, A.	1939	*Astrophys. J.* **90,** 627
Bates, D. R.	1952	*Ann. Géophys.* **8,** 194
Bates, D. R.	1954	The Physics of the Upper Atmosphere, Chapter 12 of *The Solar System*, Vol. 2, Ed. G. P. Kuiper, University of Chicago Press
Bates, D. R., and Massey, H. S. W.	1947	*Proc. Roy. Soc.* **A192,** 1
Bates, D. R., and Nicolet, M.	1950	*J. Geophys. Res.* **55,** 301
Bates, D. R., and Seaton, M. J.	1950	*Proc. Phys. Soc.* **B63,** 129
Bates, D. R., and Witherspoon, A. E.	1952	M. N. **112,** 101
Baxter, W. P.	1930	*J. Amer. Chem. Soc.* **52,** 3920
Biondi, M. A.	1951	*Phys. Rev.* **83,** 1078
Burnight, T. R.	1952	"Physics and Medicine of the Upper Atmosphere," Chap. XIII, (Albuquerque: Univ. New Mexico Press)
Byram, E. T., Chubb, F., and Friedman, H.	1954	"Rocket Exploration of the Upper Atmosphere," Pergamon Press, London, p. 274
Byram, E. T., Chubb, F., Friedman, H., and Gailar, N.	1953	*Phys. Rev.* **91,** 1278
Byram, E. T., Chubb, F., Friedman, H., and Lichtman, S.W.	1952	*J. Opt. Soc. Amer.* **42,** 876
Clark, K. C.	1952	*Phys. Rev.* **87,** 271
Deb, S.	1952	*J. Atmosph. Terr. Phys.* **2,** 309
Ditchburn, R. W.	1954	"Rocket Exploration of the Upper Atmosphere," Pergamon Press, London, p. 313
Durand, E., Oberly, J. J., and Tousey, R.	1949	*Astrophys. J.* **109,** 1
Faire, A. C., Fundingsland, C. T., and Aden, A. L.	1954	*Phys. Rev.* **93,** 650
Friedman, H., Lichtman, S. W., and Byram, E. T.	1951	*Phys. Rev.* **83,** 1025

GAYDON, A. G.	1944	*Proc. Roy. Soc.* **A183,** 111
GOLDBERG, L., and MÜLLER, E. A.	1953	*J. Opt. Soc. Amer.* **43,** 1033
HARTECK, P., and DONDER, S.	1954	*Phys. Rev.* **95,** 320
HENRIQUES, F. C., DUNCAN, A. B. F., and NOYES, W. A.	1938	*J. Chem. Phys.* **6,** 518
HERZBERG, G., and HERZBERG, L.	1948	*Nature* **161,** 283
HUNTEN, D. M.	1954	*J. Atmosph. Terr. Phys.* **5,** 57
INN, E. C. Y.	1953	*Phys. Rev.* **91,** 1194
JOHNSON, F. S., PURCELL, J. D., TOUSEY, R., and WILSON, N.	1954	"Rocket Exploration of the Upper Atmosphere," Pergamon Press, p. 279
JOHNSTON, H. S.	1951	*J. Amer. Chem. Soc.* **73,** 4542
JOHNSTON, H. S., and CROSBY, H.	1951	*J. Chem. Phys.* **19,** 799
JOHNSTON, H. S., and CROSBY, H.	1954	*J. Chem. Phys.* **22,** 689
JOHNSTON, H. S., and YOST, D. M.	1949	*J. Chem. Phys.* **17,** 386
KONDRATJEW, V.	1937	*Phys. Z. Sowjetunion* **11,** 320
MARMO, F., ZELIKOFF, M., and TANAKA, U.	1952	*J. Opt. Soc. Amer.* **42,** 870
MCMATH, R. R., and GOLDBERG, L.	1949	*Proc. Amer. Phil. Soc.* **93,** 362
MIGEOTTE, M.	1948	*Astrophys. J.* **107,** 400
MIGEOTTE, M., and NEVEN, L.	1952	*Soc. Roy. Sc. Liège Mémoires* **12,** 165
MITRA, A. P.	1954	*J. Atmosph. Terr. Phys.* **5,** 28
MITRA, A. P., and JONES, R. E.	1954	*J. Atmosph. Terr. Phys.* **5,** 104
NEWMAN, F. H.	1935	*Phil. Mag.* **20,** 777
NICOLET, M.	1945	*Inst. Roy. Météor,* Belgium, Mémoirs **19,** 124
NICOLET, M.	1948	"The Emission Spectra of the Night Sky and Aurora," *Phys. Soc.* London, p. 105
NICOLET, M.	1952	*Ann. Géophys.* **8,** 441
NICOLET, M.	1952b	"Physics and Medicine of the Upper Atmosphere," Chap. XII (Albuquerque; Univ. of New Mexico Press)
NICOLET, M.	1954	*J. Atmosph. Terr. Phys.* **5,** 132
NICOLET, M., and MANGE, P.	1954	*J. Geophys. Res.* **59,** 15
NORRISH, R. W.	1929	*J. Chem. Soc.* p. 1611
PETRIE, W., and SMALL	1953	*Canad. J. Phys.* **31,** 911
PIETENPOL, W. B., RENSE, W. A., WALZ, F. C., STACEY, D. S., and JACKSON, J. M.	1953	*Phys. Rev.* **90,** 156
PRESTON, W. M.	1940	*Phys. Rev.* **57,** 887.
RAYLEIGH, LORD (R. J. STRUTT)	1910	*Proc. Phys. Soc.* **23,** 66
SATO, T.	1953	*Geomag. and Geoelect.* **5,** 71
SHAW, J. H., SUTHERLAND, G. B. M., and WORMELL, T. W.	1948	*Phys. Rev.* **74,** 978
SPEALMAN, M. L., and RODEBUSH, W. H.	1935	*J. Amer. Chem. Soc.* **57,** 1474
STODDART, E. M.	1934	*Proc. Roy. Soc.* **A147,** 454
SUN, K., and WEISSLER, G. L.	1952	*J. Opt. Soc. Amer.* **42**
TANAKA, Y., and SHIMAZU, M.	1948	*J. Soc. Res. Inst.* **43,** 241
TOUSEY, R.	1952	*J. Opt. Soc. Amer.* **42,** 871
VETTER, K.	1949	*Z. Elektrochemie* **53,** 369
WATANABE, L., MARMO, F., and INN, E. C. Y.	1953	*Phys. Rev.* **90,** 155
WATANABE, K.	1954	*J. Chem. Phys.* **22,** 1564
WATANABE, K., INN, E. C. Y., and ZELIKOFF, M. J.	1953	*J. Chem. Phys.* **21,** 1026

VOL. 7 1955

WAIFAN, N., WALKER, W. C., and WEISSLER, G. L.	1953	*J. Appl. Phys.* **24,** 1318
WEISSLER, G. L., and LEE, Po	1952	*J. Opt. Soc. Amer.* **42,** 200
WEISSLER, G. L., LEE, Po, and MOHR, E. I.	1952	*J. Opt. Soc. Amer.* **42,** 84
WISE, H., and FRECH, M. F.	1952	*J. Chem. Phys.* **20,** 22
ZELIKOFF, M., WATANABE, K., and INN, E. C. Y.	1953	*J. Chem. Phys.* **21,** 1643
ZELIKOFF, M., and ASCHENBRAND, L. M.	1954	*J. Chem. Phys.* **22,** 1680 and 1685

RESEARCH NOTES

Changes in brightness, polarization, and colour of the zenith day sky accompanying geomagnetic activity

(*Received* 16 *June* 1955)

FROM the Smithsonian records of pyranometric observations of sky-brightness in the immediate vicinity of the sun, at air-mass 2·5, made on days preceding and following thirty magnetic storms, C. G. ABBOT (1948) has found evidence for an enhanced brightness amounting to ~10 per cent immediately following the onset of the storm. He interprets this result as demonstrating the entrance of ions from the solar corpuscular stream into the high atmosphere, where they can "act as centres of condensation of water-molecules and dust," thereby increasing both haziness and brightness of the sky.

Some results obtained here on fifty cloudless days with a photo-electric polarization photometer suggest that measures of zenith skylight may afford a more sensitive index of geomagnetic activity than do observations made in the immediate neighbourhood of the sun-path.

Sky-brightness and polarization were measured in each of two rather broad spectral bands, one through a Chance OB2 filter λ max. 4800 Å (band-width at half-intensity, 1200 Å), and the second through a OR2 filter at λ max. 6200 Å (band-width, 650 Å). The filtered light was analyzed by a rotating type-H Polaroid filter placed in front of a selenium photovoltaic cell. Observations were made at various solar zenith distances between 29° and 83°. The zenith sky subtended at the photometer a field of 17° radius.

Before a comparison with the relevant Abinger 3-hour-range-index, K, kindly supplied by the Astronomer-Royal, was attempted, the observed values of zenith brightness, B_z, and polarization, P_z, for the two colours were plotted against log. solar air-mass, and reduced to a standard solar air-mass, 2. The reduced measures were next arranged to form five separate groups representing progressive increases of geomagnetic activity, viz., (i) $K = 0$ to 0·5; (ii) $K = 1$ to 1·5; (iii) $K = 2$ to 3; (iv) $K = 3{\cdot}5$ to 4·5; (v) $K = 5$ to 6, inclusive. The observations comprised in each group numbered 2, 7, 22, 12, and 6, respectively; and although these were restricted in three of the five groups, they were sufficiently well distributed to minimize any gross effects of seasonal changes in sky transparency.

Finally the grouped values were plotted, and from the smoothed curves connecting B_z with K, and P_z with K for each colour, mean values of sky-brightness and polarization were found for representative K groups: 0, quiet; 2–3, moderately active; 5–6, strongly active; and 8–9, intensely active geomagnetic conditions.

The results are summarized in the table following. In each instance, the tabulated percentage of B_z or P_z is relative to the corresponding value for quiet geomagnetic conditions. In lines 3 and 6 of the table there are entered polarization values for the excess scattered light. These have been computed on the tacit assumption that the average value of the total contribution of Rayleigh and low-level (dust) scatter observed under quiet conditions, i.e., $K = 0$ group, will remain constant for the remaining groups; any additional light observed in the latter may then be attributed solely to high-level scattering. Since no observations for $K > 6$ were available, the tabulated data in column 5 (marked with an asterisk) have been computed by extrapolation from the smoothed curves, and should be regarded as provisional values only. Probable errors to be assigned to the tabulated group values are entered in column 6 of the table.

VOL. 7 1955

A useful criterion of the possible effect of geomagnetic conditions on the colour of the clear sky may readily be found by computing the ratio of sky-brightness at 4800 Å to that at 6200 Å (B_{4800}/B_{6200}), for quiet conditions, and for each of the three K groups included in the table. This has been done for total skylight, and for the added light separately. The results appear in the lower two lines of the table.

The results presented here suggest a systematic increase of zenith brightness in both

Per cent changes of brightness, polarization, and colour of zenith sky with geomagnetic activity

K groups		*Moderate* 2–3	*Strong* 5–6	*Intense* 8–9	*Probable error* %
4800 Å	ΔB_z	+17	+33	+40*	±18
	ΔP_z	+3	+2	±0*	±6
	p_z	46	35	27*	±9
6200 Å	ΔB_z	+32	+50	+53*	±23
	ΔP_z	−2	−1	+1*	±8
	p_z	19	22	26*	±12
B_{4800}/B_{6200}	Sky†	3·1	3·1	3·2*	
	Added light	1·9	2·3	2·6*	

At $K = 0$, $(B_{4800}/B_{6200}) = 3{\cdot}5$. * Extrapolated values. † Total light.

blue and red light with a progressive increase of geomagnetic disturbance. The effect is more pronounced at 6200 Å, where the increase is ~50 per cent of the mean sky-brightness observed when $K = 0$, or more than twice the estimated probable error. Also, the relative increase of brightness at the two wavelengths is greatest for the group, K 2–3, where the ratio of percentage increase of brightness in red and blue light is 2 : 1. In all probability these features are connected with the actual size-distribution characteristics of the high-level particles which are responsible for the additional scattered light. The enhanced brightness is accompanied also by a marked decrease in the blue/red intensity ratio, doubtless due to a dilution effect similar to that observed with a clear sky whenever thin alto-cirrus clouds appear (MINNAERT, 1940). This fact, taken by itself, suggests that a majority of the scattering particles have sizes which are large compared with the wavelengths considered. Thus, the Rayleigh component will not be appreciably augmented: this is to be expected if the scatter is mainly from centres formed by condensation of water-vapour on the solar particles, following ABBOT's suggestion. The significantly lower (B_{4800}/B_{6200}) values found for the added light appear to confirm this argument.

The changes in the polarization of total skylight with increasing geomagnetic activity all lie within the probable error of observation, and exhibit no striking trends, though they appear to be reversed in the two colours taken separately. When the polarization values for the added light alone are compared, the effect is much more pronounced. For blue light, the trend is towards a lower polarization under intensely disturbed conditions, the change amounting to −19 per cent; whereas for red light a reverse trend is found, with a smaller variation of +7 per cent. It seems likely that these changes are again associated with variations in the size-distribution of the scattering particles.

Taking the results together, it appears that measurements of the kind described above can yield a rather sensitive index of existing geomagnetic conditions. For example, the

increase of zenith brightness for red light, with strong activity, is ~50 per cent of that observed when $K = 0$, or about five times that found by ABBOT within a few radii of the sun's limb. Moreover, there is some less trustworthy evidence from the extrapolated data that, under true magnetic storm conditions, the sky-brightness will be enhanced still further. The observed changes of polarization of the added light in both colours also tend to support this conclusion.

It is intended to continue the day-sky observations through the present sunspot-cycle; and to include additional wavebands in the near ultraviolet and infrared.

A theoretical study of the probable mechanism and particle size-distribution involved in the high-level scattering process is also being undertaken in collaboration with Mr. G. F. LOTHIAN, Department of Physics, University College of the South-West, Exeter.

Acknowledgements—I am indebted to the Director, Mr. D. L. EDWARDS, for his interest in this investigation; and to Mr. A. J. DENNER for assistance in operating the photometer.

D. R. BARBER

Norman Lockyer Observatory of the University College of the South-West, Sidmouth, Devon.

REFERENCES

ABBOT, C. G. 1948 Smithsonian Misc. Collections **110**, No. 6, p. 8.
MINNAERT, M. G. J. 1940 *Light and Colour in the Open Air* (Bell, London), pp. 238, 247.

VOL. 7 1955

Electron production and recombination in the *E*-layer

In a recent account of results obtained during the 1952 eclipse (MINNIS, 1955) upper and lower limiting values were given for the electron production ($q_0 D$) in the E-layer due to the fraction (D) of the radiation emitted uniformly over the whole of the Sun's disc (Table 3, p. 103). Owing to an error made in attaching a sign to dq_1'/dx, the values quoted as lower limits are, in fact, upper limits. We have then:

$$q_0 D < 330 \text{ cm}^{-3} \text{ s}^{-1}$$

and from other evidence:

$$q_0/\alpha' = 258 \times 10^8 \text{ cm}^{-6}$$

and hence:

$$\alpha' < (1{\cdot}3/D)\ 10^{-8} \text{ cm}^3 \text{ s}^{-1}$$

This reinforces the conclusion already reached, that α' is unlikely to be as high as 10^{-7} cm^3 s^{-1}.

C. M. MINNIS

Radio Research Station, Slough.

REFERENCE

MINNIS, C. M. 1955 *J. Atmosph. Terr. Phys.* **6**, 91-112

Journal of Atmospheric and Terrestrial Physics, 1955, Vol. 7, pp. 173 to 202. Pergamon Press Ltd., London

Wave solutions for critical and near-critical coupling conditions in the ionosphere*

N. DAVIDS and R. W. PARKINSON
Ionosphere Research Laboratory, The Pennsylvania State University,
State College, Pennsylvania

(*Received* 27 *January* 1955)

ABSTRACT

Principal dielectric axis co-ordinates are used to put the coupled wave equations for ionospheric propagation into a form which is suitable for an analysis of critical coupling. This approach removes the singularity formerly associated with critical coupling. The analysis is carried out through the second order and compared with some recent data on polarization. The results compare favourably for several ionospheric models considered. A satisfactory analysis of split echoes at 150 kc/s is developed.

1. INTRODUCTION

EXPERIMENTAL observations at low frequencies (LINDQUIST, 1953; HELLIWELL *et al.*, 1951) have shown that the night-time first-hop echo is frequently split into two main components. Measurements at 150 kc/sec (KELSO *et al.*, 1951) indicate that, while the polarization of the echo apparently reflected from the higher level exhibits definite diurnal and seasonal variations, that of the lower echo is substantially different. Similar results have been obtained by HELLIWELL *et al.* (1951) at 100 and 325 kc/sec. The pronounced differences in polarization, and the fact that the lower echo is observed only at night, indicate that different reflection mechanisms are responsible for the two echoes. Several years ago, GIBBONS and NERTNEY (1952) obtained solutions of the Rydbeck coupled wave equations (RYDBECK, 1944) which seemed to indicate that, when the coupling term in these equations becomes large, there may be appreciable back-scatter from a region below the main reflection level. This back-scatter would thus provide a mechanism for the appearance of split echoes. However, since the coupling terms in the Rydbeck equations become infinite under certain coupling conditions, hereinafter called critical, the Gibbons-Nertney solutions were limited to conditions rather far removed from the critical case. It is the purpose of this paper to bridge the gap over the critical values by putting the propagation equations in a different form which avoids such singularities and which is, therefore, better adapted to theoretical analysis.

2. FUNDAMENTAL THEORY

The basic equations of the magneto-ionic theory have been presented in detail by many authors (see, for instance, FOSTERLING, 1942). For our purpose, it is sufficient at this point to note that the anisotropic properties of the medium are given by the vector relation

$$\vec{E} = \underline{\underline{\lambda}}\vec{P} \tag{2.1}$$

* The research reported in this paper has been sponsored by the Geophysics Research Directorate of the Air Force Cambridge Research Center, Air Research and Development Command, under Contract AF19(122)-44.

where $\underline{\underline{\lambda}}$ is the polarization tensor. If we choose a right-handed system of coordinate axes with positive x in the direction of magnetic east, y magnetic north, and z vertically upward, and then assume that the time variation of all quantities is of the form $\exp(j\omega t)$, the connection between $\vec{E}$ and $\vec{P}$ is given explicitly by

$$\begin{bmatrix} E_x \\ E_y \\ E_z \end{bmatrix} = -4\pi \begin{bmatrix} \frac{\omega^2}{\omega_0^2}\left(1 - \frac{j\nu}{\omega}\right) & -j\gamma_L & j\gamma_T \\ j\gamma_L & \frac{\omega^2}{\omega_0^2}\left(1 - \frac{j\nu}{\omega}\right) & 0 \\ -j\gamma_T & 0 & \frac{\omega^2}{\omega_0^2}\left(1 - \frac{j\nu}{\omega}\right) \end{bmatrix} \begin{bmatrix} P_x \\ P_y \\ P_z \end{bmatrix} \tag{2.2}$$

We further assume the ionosphere to be horizontally stratified and that the incident wave front is also horizontal, so that all spatial quantities vary with vertical height z only. Then MAXWELL's equations for the wave field, neglecting the presence of any constant electric field, lead to

$$E_x'' + k^2(E_x + 4\pi P_x) = 0 \tag{2.3}$$

$$E_y'' + k^2(E_y + 4\pi P_y) = 0 \tag{2.4}$$

$$D_z = E_z + 4\pi P_z = 0 \tag{2.5}$$

where primes denote differentiation with respect to z. The last equation, with $\operatorname{div} \vec{H} = 0$, implies that $\vec{D}$ and $\vec{H}$ are transverse to the direction of propagation, or horizontal.

In this form of the propagation problem, we have a system of six equations, (2.2) and (2.3) to (2.5), for the six unknown components E_x, E_y, E_z, P_x, P_y, P_z after the variation of N and ν with height (the ionospheric model) has been specified.

The usual approach is to use equations (2.2) and (2.5) to reduce the number of unknowns. This, however, is at the expense of simplicity in form of the differential equations and may be done in several different ways. A rather interesting general treatment of this aspect of the problem has recently been carried out by CLEMMOW and HEADING (1954). FOSTERLING (1942) and later RYDBECK (1944) chose to use the transversality condition (2.5) to eliminate the vertical components, thereby reducing the field problem to a system of four equations for the four quantities E_x, E_y, P_x, and P_y. The resulting two-dimensional equations are then diagonalized by what is essentially a principal axis transformation which leads to the so-called "π" modes, where

$$\pi_1 = (1 - u_1^2)^{1/2} E_x^{(1)} \tag{2.6}$$

$$\pi_2 = (1 - u_1^2)^{1/2} E_y^{(2)} \tag{2.7}$$

with

$$u_1 = \frac{E_y^{(1)}}{E_x^{(1)}},$$

VOL. 7 1955

and where the superscripts refer to the well-known principal modes, or magneto-ionic components. We are then left with the pair of differential equations

$$\left.\begin{aligned} \pi_1'' + (k^2\varepsilon_0 + M^2)\pi_1 &= -\pi_2 M' - 2\pi_2' M \\ \pi_2'' + (k^2\varepsilon_x + M^2)\pi_2 &= -\pi_1 M' - 2\pi_1' M \end{aligned}\right\} \tag{2.8}$$

where the subscripts 0 and x refer to the usual ordinary and extraordinary dielectric coefficients.

The coupled wave equations (2.8) have two properties which are of particular interest in any investigation of coupling phenomena. First, calculations have shown (Davids, 1952) that the coupling terms are negligible everywhere except over a narrow height interval (about 2 km for a frequency of 150 kc/sec) below the usual night-time E-region heights. This enables us to define an isolated coupling region and investigate coupling effects separately from those associated with the normal reflection region. Secondly, Davids (1953) has shown that for certain critical conditions the coupling term M becomes infinite. These conditions, which must be satisfied simultaneously, are, for conditions at State College and an operating frequency of 150 kc/sec,

$$\left.\begin{aligned} N = N_c &= \frac{m\omega^2}{4\pi e^2} = 278{\cdot}454 \text{ cm}^{-3} \\ \nu = \nu_c &= \frac{\omega_H \sin^2\theta}{2\cos\theta} = 5{\cdot}348 \times 10^5 \text{ sec}^{-1} \end{aligned}\right\} \tag{2.9}$$

From this latter property we see that the Rydbeck coupled wave equations are unsuited to analysis for critical and near-critical coupling conditions. This has led to a search for new components which are well-behaved in such cases, the results of which will be discussed in detail in the following sections.

3. The Principal Axis Reference System

As has been pointed out by Davids (1953), there are advantages in retaining the three-dimensional form of the polarization tensor appearing in (2.1). The propagation equations which result after diagonalization of this tensor turn out to be simpler and more useful for the critical coupling problem. When this work is carried out (see this last reference for details), equation (2.1) reduces to

$$E_i = -4\pi\lambda_i P_i, \qquad i = 1, 2, 3$$

where

$$\left.\begin{aligned} \lambda_1 &= \frac{\omega^2}{\omega_0^2}\left(1 - j\frac{\nu}{\omega}\right) \\ \lambda_2 &= \frac{\omega^2}{\omega_0^2}\left(1 - j\frac{\nu}{\omega} + \frac{\omega_H}{\omega}\right) \\ \lambda_3 &= \frac{\omega^2}{\omega_0^2}\left(1 - j\frac{\nu}{\omega} - \frac{\omega_H}{\omega}\right) \end{aligned}\right\} \tag{3.1}$$

The components E_i of the electric field in the principal axis reference system are related to those in the original x, y, z co-ordinate system by the equation

$$\begin{bmatrix} E_1 \\ E_2 \\ E_3 \end{bmatrix} = \begin{bmatrix} 0 & \sin\theta & \cos\theta \\ j/\sqrt{2} & \cos\theta/\sqrt{2} & -\sin\theta/\sqrt{2} \\ j/\sqrt{2} & -\cos\theta/\sqrt{2} & \sin\theta/\sqrt{2} \end{bmatrix} \begin{bmatrix} E_x \\ E_y \\ E_z \end{bmatrix} \tag{3.2}$$

The coefficients in this equation give the direction cosines of the principal axes of the polarization tensor $\underline{\underline{\lambda}}$. It should be noted that the first principal axis is along the direction of the earth's magnetic field, with the other two directions orthogonal to the first.* All three directions are constant to within the limits of variation of the earth's field, and may thus be considered constant over the lower ionosphere at any given geographical location.

The equations of propagation then become

$$(E_2'' + E_3'') + k^2(\varepsilon_2 E_2 + \varepsilon_3 E_3) = 0 \tag{3.3}$$

$$(E_1'' + k^2\varepsilon_1 E_1)\sin\theta + [E_2'' - E_3'' + k^2(\varepsilon_2 E_2 - \varepsilon_3 E_3)]\frac{\cos\theta}{\sqrt{2}} = 0 \tag{3.4}$$

$$\varepsilon_1 E_1 \cos\theta - (\varepsilon_2 E_2 - \varepsilon_3 E_3)\frac{\sin\theta}{\sqrt{2}} = 0 \tag{3.5}$$

These equations involve the principal dielectric coefficients of the medium, ε_1, ε_2, and ε_3, given by

$$\varepsilon_i = 1 - \frac{1}{\lambda_i}, \qquad i = 1, 2, 3 \tag{3.6}$$

This follows from $\vec{D} = \vec{E} + 4\pi\vec{P}$, so that we then have

$$D_i = \varepsilon_i E_i, \qquad i = 1, 2, 3 \tag{3.7}$$

4. The General Equations of Propagation

Let us consider equations (3.3) to (3.6). If we let

$$\left.\begin{aligned} \varepsilon_2 E_2 + \varepsilon_3 E_3 &= p \\ \varepsilon_2 E_2 - \varepsilon_3 E_3 &= q \\ E_1 &= r \end{aligned}\right\} \tag{4.1}$$

then

$$\left.\begin{aligned} E_2 + E_3 &= \frac{1}{2}\left[\left(\frac{1}{\varepsilon_2} + \frac{1}{\varepsilon_3}\right)p + \left(\frac{1}{\varepsilon_2} - \frac{1}{\varepsilon_3}\right)q\right] = \frac{1}{2}(\beta p + \gamma q) \\ E_2 - E_3 &= \frac{1}{2}\left[\left(\frac{1}{\varepsilon_2} - \frac{1}{\varepsilon_3}\right)p + \left(\frac{1}{\varepsilon_2} + \frac{1}{\varepsilon_3}\right)q\right] = \frac{1}{2}(\gamma p + \beta q) \end{aligned}\right\} \tag{4.2}$$

where

$$\left.\begin{aligned} \beta &= \frac{1}{\varepsilon_2} + \frac{1}{\varepsilon_3} \\ \gamma &= \frac{1}{\varepsilon_2} - \frac{1}{\varepsilon_3} \end{aligned}\right\} \tag{4.3}$$

* Orthogonality of two complex vectors $\vec{A}$ and $\vec{B}$ is defined by the condition $\vec{A}\cdot\vec{B}^* = 0$, where $\vec{B}^*$ is the complex conjugate of $\vec{B}$.

VOL. 7 1955

Differentiating (4.2) and substituting into (3.3) to (3.6), we obtain

$$\tfrac{1}{2}[\beta p'' + 2\beta' p' + \beta'' p + (\gamma q)''] + k^2 p = 0 \tag{4.4}$$

$$(r'' + k^2\varepsilon_1 r)\sin\theta + \{\tfrac{1}{2}[\beta q'' + 2\beta' q' + \beta'' q + (\gamma p)''] + k^2 q\}\frac{\cos\theta}{\sqrt{2}} = 0 \tag{4.5}$$

$$\varepsilon_1 r\cos\theta - q\frac{\sin\theta}{\sqrt{2}} = 0 \tag{4.6}$$

From the last of these equations we have

$$r = \frac{q}{\varepsilon_1\sqrt{2}}\frac{\sin\theta}{\cos\theta},$$

so that the first term of (4.5) becomes

$$\left[\left(\frac{q}{\varepsilon_1}\right)'' + k^2 q\right]\frac{\sin^2\theta}{\sqrt{2}\cos\theta}$$

If the indicated differentiations are then carried out and the terms collected, (4.5) becomes

$$\left(\frac{2}{\varepsilon_1}\sin^2\theta + \beta\cos^2\theta\right)q'' + 2\left[\left(\frac{2}{\varepsilon_1}\right)'\sin^2\theta + \beta'\cos^2\theta\right]q'$$
$$+\left[\left(\frac{2}{\varepsilon_1}\right)''\sin^2\theta + \beta''\cos^2\theta + 2k^2\right]q = -(\gamma p)''\cos^2\theta \tag{4.7}$$

We now make the transformation

$$\left.\begin{aligned} U &= \beta p \\ V &= \left(\frac{2}{\varepsilon_1}\sin^2\theta + \beta\cos^2\theta\right)q = \delta q \end{aligned}\right\} \tag{4.8}$$

Then the pair of equations (4.4) and (4.7) reduce to

$$\left.\begin{aligned} U'' + \frac{2k^2}{\beta}U &= -\left(\frac{\gamma}{\delta}V\right)'' \\ V'' + \frac{2k^2}{\delta}V &= -\left(\frac{\gamma}{\beta}U\right)''\cos^2\theta \end{aligned}\right\} \tag{4.9}$$

Finally, we write these in the form

$$\left.\begin{aligned} U'' + k^2 n_1^2 U &= -(M_1 V)'' \\ V'' + k^2 n_2^2 V &= -(M_2 U)''\cos^2\theta \end{aligned}\right\} \tag{4.10}$$

where

$$\left.\begin{aligned} n_1^2 &= \frac{2}{\beta} = \frac{2}{\dfrac{1}{\varepsilon_2} + \dfrac{1}{\varepsilon_3}} \\ n_2^2 &= \frac{2}{\delta} = \frac{2}{\dfrac{2}{\varepsilon_1}\sin^2\theta + \left(\dfrac{1}{\varepsilon_2} + \dfrac{1}{\varepsilon_3}\right)\cos^2\theta} \\ M_1 &= \frac{\gamma}{\delta} = \frac{\dfrac{1}{\varepsilon_2} - \dfrac{1}{\varepsilon_3}}{\dfrac{2}{\varepsilon_1}\sin^2\theta + \left(\dfrac{1}{\varepsilon_2} + \dfrac{1}{\varepsilon_3}\right)\cos^2\theta} \\ M_2 &= \frac{\gamma}{\beta} = \frac{\dfrac{1}{\varepsilon_2} - \dfrac{1}{\varepsilon_3}}{\dfrac{1}{\varepsilon_2} + \dfrac{1}{\varepsilon_3}} \end{aligned}\right\} \tag{4.11}$$

In order to distinguish equations (4.10) from the Rydbeck coupled wave equations, they will be referred to in all discussions to follow as the "general equations of propagation."

5. First-Order Theory—Coupling Along H

The possibility of integrating the general equations of propagation (4.10) is enhanced, and a reasonably approximate solution is obtained for the forward-scattered wave, if we take advantage of certain properties of the medium for the propagation frequency used. For 150 kc/sec propagation at State College we have

$$\left.\begin{aligned} \omega &= 0{\cdot}94248 \times 10^6 \text{ sec}^{-1} \\ \omega_H &= 9{\cdot}406 \times 10^6 \text{ sec}^{-1} \\ \frac{\omega_H}{\omega} &= 9{\cdot}99 \\ \theta &= 160^\circ\ 52' \end{aligned}\right\} \tag{5.1}$$

Since $\nu \cong 5 \times 10^5 \text{ sec}^{-1}$ in the coupling region and $N \cong 300 \text{ cm}^{-3}$ near critical coupling, we have $\dfrac{\nu}{\omega} \cong \dfrac{1}{2}$ and $\omega_0^2 \cong \omega^2$ for the cases of interest here. Consequently, referring to equations (3.1), we have

$$\lambda_2 \cong \frac{\omega^2}{\omega_0^2}(10 + \delta_2) \cong (10 + \delta_2)$$

$$\lambda_3 \cong \frac{\omega^2}{\omega_0^2}(10 + \delta_3) \cong (10 + \delta_3)$$

VOL. 7 1955

where the δ's represent complex quantities of the order of unity. From (3.6), then,

$$\left.\begin{aligned} \varepsilon_2 &\cong 1 - \frac{1}{10 + \delta_2} \cong 1 \\ \varepsilon_3 &\cong 1 - \frac{1}{10 + \delta_3} \cong 1 \end{aligned}\right\} \tag{5.2}$$

This is essentially equivalent to neglecting the ratio $\frac{\omega}{\omega_H}$ with respect to 1. Fig. 2 from DAVIDS (1953) shows the actual values of these coefficients plotted for a particular model. It confirms the conclusion that most of the variation in the coupling region takes place in the coefficient ε_1, which is associated with the principal component along the earth's magnetic field. Indeed, at the critical coupling point, for the model in question, we have the values

$$\varepsilon_2 = 0{\cdot}92 - j0{\cdot}005$$

$$\varepsilon_3 = 1{\cdot}09 - j0{\cdot}007$$

We shall now show that equations (4.10) can be integrated if the assumption (5.2) is made. Accordingly, we suppose that

$$\varepsilon_2 = \varepsilon_3 = 1 \tag{5.3}$$

which are their free-space values. Then (4.11) reduces to

$$\left.\begin{aligned} n_1^2 = 1; \qquad n_2^2 &= \frac{1}{\frac{1}{\varepsilon_1}\sin^2\theta + \cos^2\theta} \\ M_1 &= M_2 = 0 \end{aligned}\right\} \tag{5.4}$$

so that the propagation equations, now uncoupled, become

$$U'' + k^2 U = 0 \tag{5.5}$$

$$V'' + k^2 n_2^2 V = 0 \tag{5.6}$$

The first of these gives the free space solution, using (3.2),

$$U = \beta p = 2(E_2 + E_3) = 2\sqrt{2}\, jE_x = A_1 e^{jkz} + B_1 e^{-jkz} \tag{5.7}$$

Thus we have the results: to the order of $\frac{\omega}{\omega_H}$, the x-component of the electric field is unaffected by coupling.

The remaining equation (5.6) is that for a wave function $V(z)$ propagating through a (fictitious) medium of index n_2 given by (5.4). Putting $\varepsilon_1 = 1 - \frac{1}{\lambda_1}$, we may simplify the expression for n_2 into the form

$$n_2^2 = \frac{\lambda_1 - 1}{\lambda_1 - \cos^2\theta} \tag{5.8}$$

where λ_1 is given by (3.1).

For the specific models considered below in Section 7, it is found that W.K.B. functions are good approximate solutions to (5.6), since the W.K.B. criterion

$$\left| -\frac{1}{2}\frac{n''}{n} + \frac{3}{4}\left(\frac{n'}{n}\right)^2 \right| \ll \left| k^2 n^2 \right|, \tag{5.9}$$

is satisfied to within a few percent. This approximation is certainly applicable to within the order of accuracy being employed for this first-order analysis, so that we may write

$$V = \frac{A}{\sqrt{n}} e^{jk\int_0^z n d\zeta} + \frac{B}{\sqrt{n}} e^{-jk\int_0^z n d\zeta} \tag{5.10}$$

in which, for convenience, we have written simply n for n_2.

From (4.1), (4.8), (4.11), and (5.2),

$$U = \beta p = \beta(E_2 + E_3) = 2(E_2 + E_3)$$

$$V = \delta q = \frac{2}{n^2} q = \frac{2}{n^2}(E_2 - E_3)$$

and from (4.6), $E_1 = r = \dfrac{q}{\varepsilon_1\sqrt{2}} \tan\theta$. These relations then give

$$E_1 = \left(\frac{1}{\varepsilon_1\sqrt{2}} \tan\theta\right) \frac{n^2}{2} V$$

$$E_2 = \tfrac{1}{4} n^2 V + \frac{U}{4}$$

$$E_3 = -\tfrac{1}{4} n^2 V + \frac{U}{4}$$

Multiplying the constants in (5.10) by $\dfrac{1}{2\sqrt{2}} \tan\theta$, we may rewrite these expressions in the form

$$\left.\begin{aligned} E_1 &= \frac{\lambda}{\lambda - \cos^2\theta} V = \frac{n^2}{\varepsilon_1} V \\ E_2 &= \frac{\sqrt{2}}{2} n^2 V \cot\theta + Ce^{jkz} + De^{-jkz} \\ E_3 &= -\frac{\sqrt{2}}{2} n^2 V \cot\theta + Ce^{jkz} + De^{-jkz} \end{aligned}\right\} \tag{5.11}$$

The principal axis components may be transformed into the original x, y, z components by the relation

$$\begin{bmatrix} E_x \\ E_y \\ E_z \end{bmatrix} = \begin{bmatrix} 0 & -j/\sqrt{2} & -j/\sqrt{2} \\ \sin\theta & \cos\theta/\sqrt{2} & -\cos\theta/\sqrt{2} \\ \cos\theta & -\sin\theta/\sqrt{2} & \sin\theta/\sqrt{2} \end{bmatrix} \begin{bmatrix} E_1 \\ E_2 \\ E_3 \end{bmatrix}$$

VOL. 7 1955

Using this transformation and equations (5.4), we obtain

$$\left.\begin{aligned} E_x &= -j(Ce^{jkz} + De^{-jkz}) \\ E_y &= n^2V\left(\frac{\sin\theta}{\varepsilon_1} + \cos\theta\cot\theta\right) = \frac{1}{\sin\theta}\frac{1}{\sqrt{n}}(Ae^{jk\int ndz} + Be^{-jk\int ndz}) \\ E_z &= n^2V\cos\theta\left(\frac{1}{\varepsilon_1} - 1\right) = \frac{\cos\theta}{\lambda - \cos^2\theta}\frac{1}{\sqrt{n}}(Ae^{jk\int ndz} + Be^{-jk\int ndz}) \end{aligned}\right\} \tag{5.12}$$

The third propagation equation (2.5), which expresses the transversality of the $\vec{D}$ vector, i.e., $D_z = 0$, is then satisfied to the order of the approximation originally made.

6. Boundary Value Problem—First-Order Theory

If we consider an incident upgoing wave in free space, we have, with $A = C = 0$ and $n = 1$,

$$E_x = De^{-jkz}$$

$$E_y = \frac{1}{\sin\theta}\frac{1}{\sqrt{n}}Be^{-jk\int ndz} = \frac{B}{\sin\theta}e^{-jkz}$$

with the polarization given by

$$u = \frac{E_y}{E_x} = \frac{B}{D}\frac{1}{\sin\theta}, \qquad \text{or} \qquad B = uD\sin\theta$$

I—Free Space (Below)	II—Coupling Region	III—Free Space (Above)
$E_x = e^{-jkz} + C_1e^{jkz}$	$E_x = C_2e^{jkz} + D_2e^{-jkz}$	$E_x = D_3e^{-jkz}$
$E_y = ue^{-jkz} + \frac{A_1}{\sin\theta}e^{jkz}$	$E_y = \frac{B_2}{\sin\theta}\frac{1}{\sqrt{n}}e^{-jk\int_0^z ndz} + \frac{A_2}{\sin\theta}\frac{1}{\sqrt{n}}e^{jk\int_0^z ndz}$	$E_y = \frac{B_3}{\sin\theta}e^{-jkz}$
$E_z = \frac{\cos\theta\sin\theta}{\lambda - \cos^2\theta}ue^{-jkz} + \frac{A_1\cos\theta}{\lambda - \cos^2\theta}e^{jkz}$	$E_z = \frac{B_2\cos\theta}{\lambda - \cos^2\theta}\frac{1}{\sqrt{n}}e^{-jk\int_0^z ndz} + \frac{A_2\cos\theta}{\lambda - \cos^2\theta}\frac{1}{\sqrt{n}}e^{jk\int_0^z ndz}$	$E_z = \frac{B_3\cos\theta}{\lambda - \cos^2\theta}e^{-jkz}$
$z = a$		$z = b$

Fig. 1. Boundary value problem—first-order theory.

Let us now consider an isolated coupling region with free space above and below, and an incident upgoing wave of unit amplitude and polarization u. The wave solutions in each region may then be represented by the diagram of Fig. 1, in which the coefficients A_1 and C_1 represent the back-scattered amplitudes into Region I

and B_3 and D_3 represent those of the forward-scattered wave in Region III. The values $z = a$ and $z = b$ $(a < b)$ represent the boundaries (arbitrarily chosen) of the coupling region.

The conditions that the $\vec{E}$ vector and its spatial derivative be continuous at these points leads to the relations:

(A) from matching the x components:

$$C_1 = C_2 = 0$$

$$D_2 = D_3 = 1$$

which implies at once that the scattered wave has no x component, as remarked above.

(B) from matching the y components:

$$A_1 = A_2$$

$$B_2 = u \sin \theta$$

and, putting $A_1 = A_2 = R$ (for reflection coefficient),

$$B_3 = B_2 e^{jk\left(b - \int_0^b n d\zeta\right)} = u \sin \theta e^{jk\left(b - \int_0^b n d\zeta\right)}$$

$$R = 0$$

The transmitted y component is, therefore,

$$E_y = u e^{jk\left(b - \int_0^b n d\zeta\right)} e^{-jkz},$$

and if we denote the forward-scatter coefficient by T we have

$$|T| = |u| \left| e^{-jk \int_0^b n d\zeta} \right| \tag{6.1}$$

The results give zero back-scatter, as would be expected from the fact that the original assumption resulted in uncoupled equations, and imply that second-order analysis is necessary to obtain the back-scattered amplitudes.

7. Numerical Results of First-Order Theory

The behaviour of the index $n = n_2$, which governs the first-order theory, was studied for several models of ionospheric distributions for conditions at State College. The electron density models, shown in Fig. 2a, were based on the Chapman formula neglecting variation of the height of the maximum electron density with zenith angle χ and assuming a constant scale height of 10 km. The collision frequency model, shown in Fig. 2b, was obtained from NICOLET (1953); according to this model, the ν_c level occurs at $z = 90{\cdot}2$ km. Five N models are shown, which were chosen so that the $N = N_c$ level is located an integral number of quarter wavelengths (one-quarter wavelength $= \frac{1}{2}$ km at 150 kc/sec) both above and below the $\nu = \nu_c$ level. It should be noted that Model 3 exhibits critical coupling conditions,

VOL. 7 1955

a case which was discussed to some extent by DAVIDS (1953), so that with this choice of models we flank the critical model on both sides.

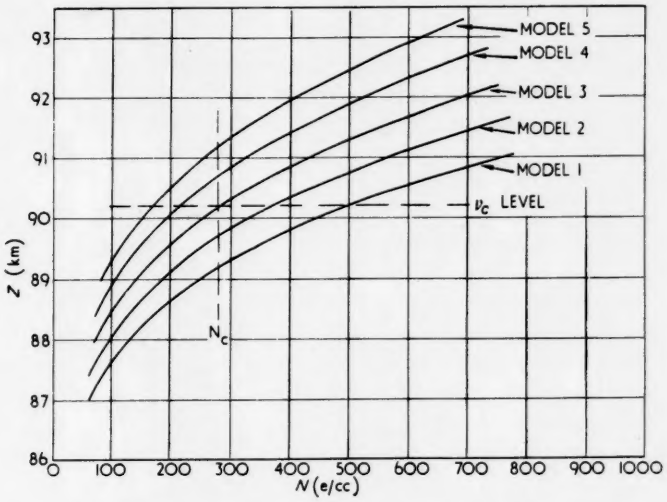

Fig. 2a. Electron density models used in first-order theory.

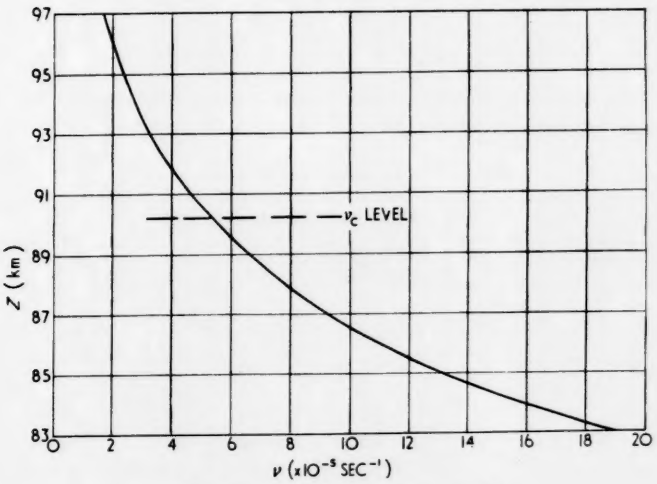

Fig. 2b. Collision frequency model.

The real and imaginary parts of n^2 are shown as a function of height in Fig. 3, and may be compared with the curves for the exact indices shown below in Section 8B. We note for the lower heights, where $N \to 0$, that $n \to 1$, its free space value. A plot of the index in the complex plane shows that the curves all start out from this free space value and sweep around an approximately circular arc back towards this point. Of course, actually the presence of the E-layer will modify the above behaviour at higher levels.

The amplitude, polarization and other information for the total transmitted wave is presented in Table 1. The results are based on an incident upgoing wave

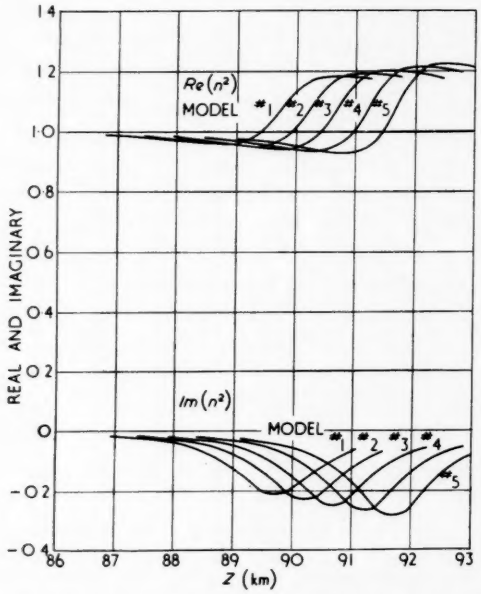

Fig. 3. Variation of n^2 with height in the region near critical coupling

unit amplitude and circular polarization; those for an incident downgoing wave are not sufficiently different to warrant separate tabulation.

Table 1. *Transmitted wave data.*

Model	*Transmitted wave magnitude,* $\lvert T \rvert$ *(y-component)*	*Phase shift (radians)*	φ, for *polarization* $e^{i\varphi}$		*Critical frequency* (Mc/s)
			(1)	(2)	
1	0·52	−0·572	1·00	−2·14	1·7
2	0·51	−0·540	1·03	−2·11	1·4
3	0·47	−0·641	0·93	−2·21	1·2
4	0·45	−0·600	0·97	−2·17	1·1
5	0·43	−0·585	0·98	−2·15	0·96

(1) For an incident total wave of circular polarization $u = j = e^{j(\pi/2)}$.
(2) For an incident total wave of circular polarization $u = -j = e^{-j(\pi/2)}$.

8. Preliminary Investigation of Second-Order Theory

As mentioned above, a second-order analysis is necessary in order to obtain back-scatter coefficients. The natural extension of the preceding work would be to take into account the previously neglected ratio $\frac{\omega}{\omega_H}$, but neglect its square.

VOL. 7 1955

However, an examination of the properties of the U, V components of the general equations of propagation, and of their relationship to the Rydbeck π components, has shown that it is possible to obtain second-order solutions of the exact equations directly. The present section will, therefore, be devoted to a discussion of these relationships and properties, while explicit second-order solutions of the general equations of propagation will be obtained in Section 9.

A. *Relationship between U, V Components and Rydbeck π Components*

The electric field components are related to those in the original x, y, z co-ordinate system by equation (3.2). The relationship between the latter and the Rydbeck π components is easily obtained. Using the transversality condition (2.5) on the dielectric displacement vector, we obtain from (2.2) the equation

$$E_z = \rho E_x + \sigma E_y \tag{8.1}$$

where

$$\left.\begin{aligned} \rho &= \frac{j\eta\gamma_T}{(1-\eta)(\gamma_L{}^2 - \eta^2) - \eta\gamma_T{}^2} \\ \sigma &= \frac{-\gamma_L\gamma_T}{(1-\eta)(\gamma_L{}^2 - \eta^2) - \eta\gamma_T{}^2} \\ \eta &= \frac{\omega^2}{\omega_0{}^2}\left(1 - j\frac{\nu}{\omega}\right) \end{aligned}\right\} \tag{8.2}$$

From Rydbeck (1944), we have the relations

$$\frac{E_y^{(1)}}{E_x^{(1)}} = u_1; \qquad \frac{E_y^{(2)}}{E_x^{(2)}} = u_2; \qquad u_1 u_2 = 1 \tag{8.3}$$

so that, using u_1 only and dropping its subscript, we have

$$\left.\begin{aligned} E_x &= E_x^{(1)} + E_x^{(2)} = E_x^{(1)} + uE_y^{(2)} \\ E_y &= E_y^{(1)} + E_y^{(2)} = uE_x^{(1)} + E_y^{(2)} \end{aligned}\right\} \tag{8.4}$$

For the definition of the π components—equations (2.6) and (2.7)—and equations (8.4) and (8.1), we obtain the transformation

$$\begin{bmatrix} E_x \\ E_y \\ E^z \end{bmatrix} = \begin{bmatrix} (1-u^2)^{-1/2} & u(1-u^2)^{-1/2} \\ u(1-u^2)^{-1/2} & (1-u^2)^{-1/2} \\ (1-u^2)^{-1/2}(\rho + \sigma u) & (1-u^2)^{-1/2}(\rho u + \sigma) \end{bmatrix} \begin{bmatrix} \pi_1 \\ \pi_2 \end{bmatrix} \tag{8.5}$$

Now, from equations (4.8) and (4.1) we have the relation

$$\begin{bmatrix} U \\ V \end{bmatrix} = \begin{bmatrix} \beta\varepsilon_2 & \beta\varepsilon_3 \\ \delta\varepsilon_2 & -\delta\varepsilon_3 \end{bmatrix} \begin{bmatrix} E_2 \\ E_3 \end{bmatrix} \tag{8.6}$$

Therefore, from (8.6), (3.2), and (8.5) we obtain finally the transformation

$$\begin{bmatrix} U \\ V \end{bmatrix} = \begin{bmatrix} F_1 & G_1 \\ F_2 & G_2 \end{bmatrix} \begin{bmatrix} \pi_1 \\ \pi_2 \end{bmatrix} \tag{8.7}$$

$$\left.\begin{aligned} F_1 &= [j(\varepsilon_2+\varepsilon_3) + u\cos\theta(\varepsilon_2-\varepsilon_3) - (\rho+\sigma u)(\varepsilon_2-\varepsilon_3)\sin\theta]\frac{\beta}{\sqrt{2(1-u^2)}} \\ G_1 &= [ju(\varepsilon_2+\varepsilon_3) + \cos\theta(\varepsilon_2-\varepsilon_3) - (\rho u+\sigma)(\varepsilon_2-\varepsilon_3)\sin\theta]\frac{\beta}{\sqrt{2(1-u^2)}} \\ F_2 &= [j(\varepsilon_2-\varepsilon_3) + u\cos\theta(\varepsilon_2+\varepsilon_3) - (\rho+\sigma u)(\varepsilon_2+\varepsilon_3)\sin\theta]\frac{\delta}{\sqrt{2(1-u^2)}} \\ G_2 &= [ju(\varepsilon_2-\varepsilon_3) + \cos\theta(\varepsilon_2+\varepsilon_3) - (\rho u+\sigma)(\varepsilon_2+\varepsilon_3)\sin\theta]\frac{\delta}{\sqrt{2(1-u^2)}} \end{aligned}\right\} \tag{8.8}$$

It is of interest to determine the form which (8.7) assumes in free space. In this case the electron density N is zero and we have

$$\varepsilon_1 = \varepsilon_2 = \varepsilon_3 = 1,$$

$$\beta = \delta = 2.$$

Also, it may be easily shown (see Appendix I) that in free space

$$\rho = \sigma = 0$$

Upon substitution of these relations into (8.8), the latter reduces to

$$\left.\begin{aligned} F_1 &= 2\sqrt{2}j(1-u^2)^{-1/2} \\ G_1 &= 2\sqrt{2}ju(1-u^2)^{-1/2} \\ F_2 &= 2\sqrt{2}\cos\theta u(1-u^2)^{-1/2} \\ G_2 &= 2\sqrt{2}\cos\theta(1-u^2)^{-1/2} \end{aligned}\right\} \tag{8.9}$$

Equation (8.7) therefore becomes

$$\begin{bmatrix} U \\ V \end{bmatrix} = \begin{bmatrix} 2\sqrt{2}j(1-u^2)^{-1/2} & 2\sqrt{2}ju(1-u^2)^{-1/2} \\ 2\sqrt{2}\cos\theta u(1-u^2)^{-1/2} & 2\sqrt{2}\cos\theta(1-u^2)^{-1/2} \end{bmatrix} \begin{bmatrix} \pi_1 \\ \pi_2 \end{bmatrix} \tag{8.10}$$

which, on comparison with (8.5), yields the relations

$$\left.\begin{aligned} U &= 2\sqrt{2}jE_x \\ V &= 2\sqrt{2}\cos\theta E_y \end{aligned}\right\} \tag{8.11}$$

We see, therefore, that in free space the U, V components are simply proportional to the x and y components of the electric field.

VOL. 7 1955

B. *Properties of the General Equations of Propagation*

At first glance, it would seem that the general propagation equations (4.10) are worse than the Rydbeck coupled wave equations (2.8), since coupling occurs through second derivatives instead of through first derivatives as with the latter. However, it may be shown analytically (see Appendix II) that, as long as N and ν and their spatial derivatives are well-behaved (i.e., have no singular points), the indices and coupling factors of the general equations of propagation are also well-behaved. This is an extremely important and useful property, since, as mentioned above, the work of GIBBONS and NERTNEY on coupling theory was limited to conditions rather far from critical coupling by the infinity which occurs in the coupling factor of the Rydbeck π equations under critical conditions.

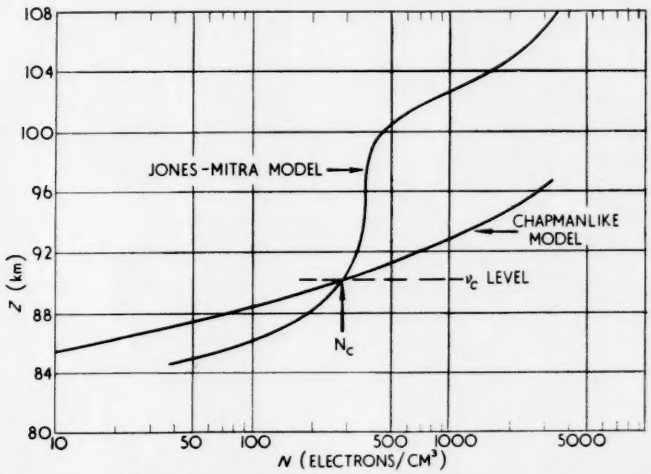

Fig. 4. Electron density models, for critical coupling conditions, used in second-order theory.

Before proceeding to a further investigation of the properties of the general equations of propagation, it was found necessary to choose several night-time electron density models in order to calculate values for the indices and coupling factors and determine their spatial variations. These models were felt to represent the best picture of the lower ionosphere available at the time, and were thus felt to provide better representations of actual conditions than the rather idealized Chapmanlike models used in Section 7. To obtain such distributions, an E-region model for $\chi = 90°$, as obtained from phase height measurements by JONES (1955), was combined with a D-region model, also for $\chi = 90°$, from MITRA (1954a). One of two recombination coefficient models, described in more detail below, was then applied in the usual manner to obtain composite N models for different times after sunset. In order to ascertain the effect of a rather drastic change in model shape upon the final results, calculations were also carried out for the Chapmanlike N distribution, chosen to provide critical coupling conditions, which was used in Section 7. The Nicolet ν model mentioned in Section 7 was also used for the second-order theory, and has been shown previously in Fig. 2b.

Initial calculations were made on the Jones-Mitra critical coupling model shown in Fig. 4. This was obtained from the sunset model described above by application of the Mitra-Jones (1954) recombination coefficient model, shown as Model 1 in Fig. 5, and corresponds to a time $t = 1{\cdot}67$ hours after sunset. Four other models, shown in Fig. 6, were obtained from the sunset model by application of the recombination coefficient model shown as Model 2 in Fig. 5. The latter was obtained by MITRA (1954b) from experimental results shortly after the critical case had been

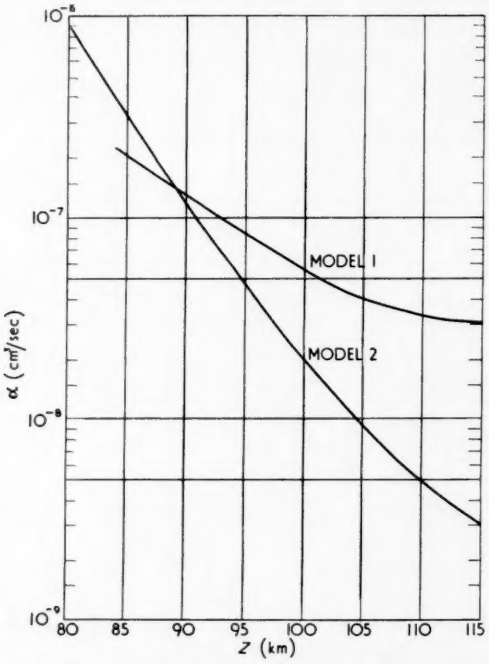

Fig. 5. Night-time recombination coefficient models.

calculated, and was felt to be a better representation of the recombination coefficient, for the hours just after sunset, than was Model 1. These four N models were chosen such that the $N = N_e$ level fell at approximately equal intervals both above and below the $\nu = \nu_e$ level, and correspond to times $t = 1{\cdot}0$, $1{\cdot}5$, $2{\cdot}5$, and $3{\cdot}0$ hours after sunset, respectively. The Chapmanlike distribution for critical coupling conditions, chosen for comparison as mentioned previously, is shown in Fig. 4.

The indices and coupling factors of the general equations of propagation, as calculated for the two critical coupling models of Fig. 4, are shown in Figs. 7 and 8; values for the models bracketing the critical point are not sufficiently different from those shown in Fig. 7 to warrant individual figures. It is evident that the U, V components are well-suited to an investigation of coupling phenomena, for the reasons discussed above. The derivatives of the coupling factors, which also appear in (4.10), are not shown, but both first and second derivatives were found to be well-behaved. In fact, it was found, in obtaining the second-order coupling solutions,

VOL. 7 1955

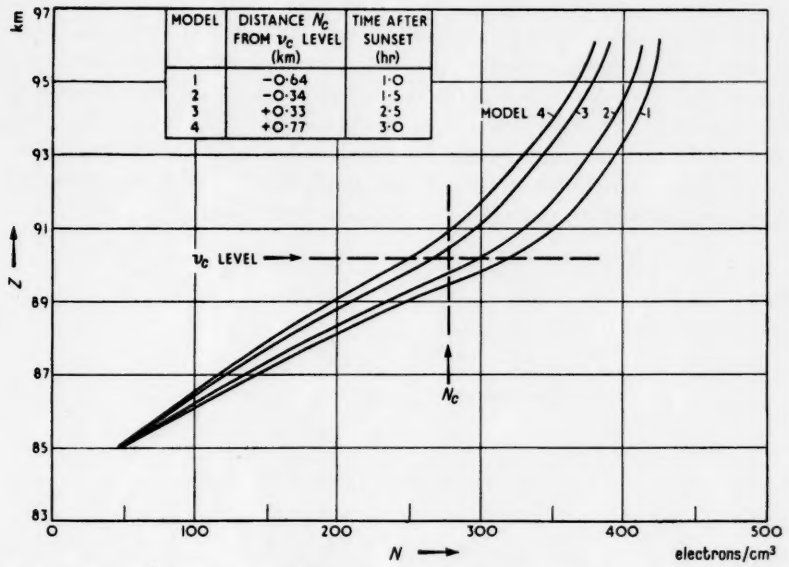

Fig. 6. Electron density models, bracketing critical coupling conditions, used in second-order theory.

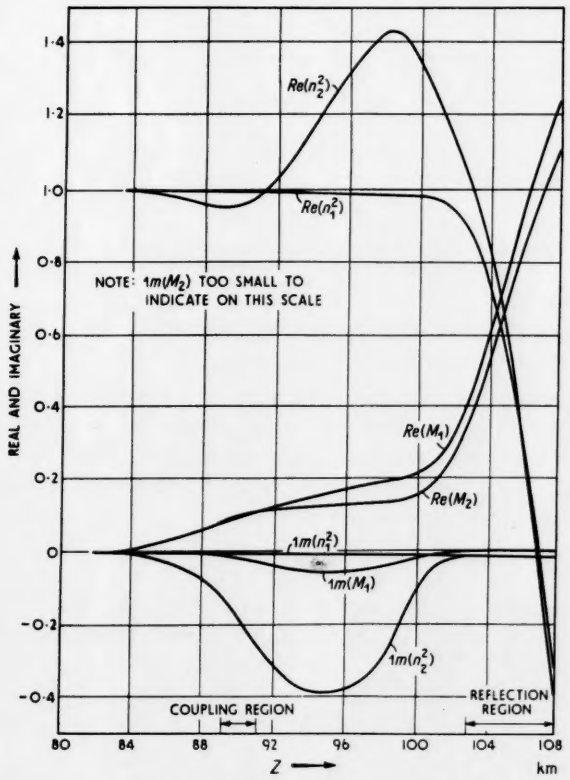

Fig. 7. Variation of indices and coupling factors with height—Jones-Mitra critical coupling model.

that the second derivatives could be completely neglected with respect to other terms involved; this will be discussed further in the next section. It was also found that the indices were such that W.K.B. functions are very good approximate solutions to the uncoupled general propagation equations, satisfying the W.K.B. criterion (5.9) to better than 0·1 per cent in all cases except for the Chapman-like model, where the criterion was still satisfied to better than one per cent. The fact that very good zero-order solutions are available is quite important for the second-order step, as will be brought out in more detail in the next section.

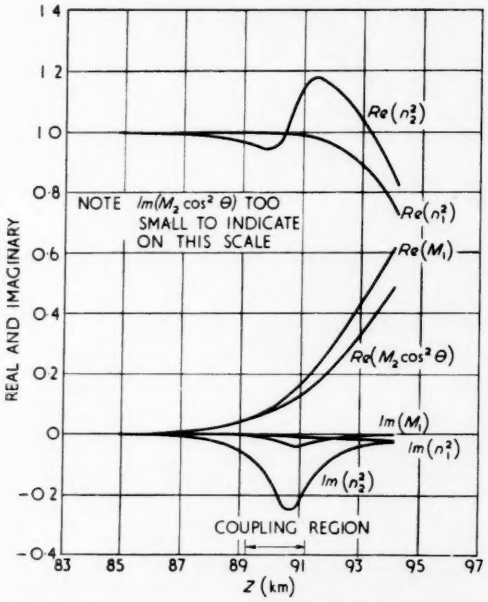

Fig. 8. Variation of indices and coupling factors with height—Chapmanlike critical coupling model.

9. Second-Order Solutions of the General Equations of Propagation

Since the indices and coupling factors of the general equations of propagation are well behaved throughout the coupling region, it is possible to obtain solutions by the method of variation of parameters in a manner similar to that used by Gibbons and Nertney (1952). This method may be very briefly summarized as follows:

Consider the second order differential equation

$$y'' + P(z)y' + Q(z)y = R(z) \tag{9.1}$$

If two independent solutions of this equation are known for $R(z) = 0$, the general solution for an arbitrary $R(z)$ may be obtained by variation of parameters in the form

$$y = Ay_{01} + By_{02} - y_{01}\int^{z} \frac{Ry_{02}}{y_{01}y_{02}' - y_{01}'y_{02}}\,dz + y_{02}\int^{z} \frac{Ry_{01}}{y_{01}y_{02}' - y_{01}'y_{02}}\,dz \tag{9.2}$$

VOL. 7 1955

where $y_0 = Ay_{01} + By_{02}$ is the general solution for $R(z) = 0$. In order to simplify the problem of obtaining numerical results in physical applications, the lower limits of integration are chosen arbitrarily, and the constants A and B are then determined by the solution of a boundary value problem.

Now let us consider our general propagation equations (4.10). Here we have two equations formally similar to (9.1) with the exception that the right-hand side of each contains the dependent variable from the other equation. However, we know from the discussion of the last section that W.K.B. functions are very good approximate solutions to the uncoupled equations. Therefore, we may use these as driving forces in the right-hand side of (4.10) and obtain second-order solutions by variation of parameters as outlined above. When this is carried out, the solutions in the coupling region take the form

$$\begin{aligned} U &= AU_u + BU_d + \frac{U_u}{2jk}\int_a^z (M_1V_0)''U_d\,dz - \frac{U_d}{2jk}\int_b^z (M_1V_0)''U_u\,dz \\ V &= CV_u + DV_d + \frac{V_u}{2jk}\int_a^z (M_2U_0\cos^2\theta)''V_d\,dz - \frac{V_d}{2jk}\int_b^z (M_2U_0\cos^2\theta)''V_u\,dz \end{aligned} \tag{9.3}$$

where A, B, C, and D are factors to be evaluated, a and b are arbitrary limits of integration, and U_0 and V_0 are the solutions of the uncoupled equations,

$$\left.\begin{aligned} U_0 &= AU_u + BU_d \\ V_0 &= CV_u + DV_d \end{aligned}\right\} \tag{9.4}$$

in which the subscripts refer to the upgoing and downgoing W.K.B. "waves,"

$$\left.\begin{aligned} U_{u,d} &= \frac{1}{\sqrt{n_1}}\exp\left[\mp jk\int_0^z n_1\,d\xi\right] \\ V_{u,d} &= \frac{1}{\sqrt{n_2}}\exp\left[\mp jk\int_0^z n_2\,d\xi\right] \end{aligned}\right\} \tag{9.5}$$

It is evident from Figs. 7 and 8 that we do not have an isolated coupling region, since the coupling factors tend to increase quite rapidly above this level. However, we know that there is an interval between the coupling and reflection regions in which the Rydbeck π components are of W.K.B. form, at least to a very good approximation. The difficulty of a non-isolated coupling region may be overcome, therefore, by matching the solutions (9.3), obtained above, to the π components in the interval above the coupling region where the latter are known. This enables us to set up the general boundary value problem illustrated in Fig. 9. Here, F_i, G_i are the functions, given by equation (8.8), relating the π components to the U, V components; $E, \ldots, H$ and $J, \ldots, P$ are factors to be determined; and the subscripts on the π's in Region III refer to the "upgoing" and "downgoing" W.K.B. solutions to the Rydbeck π equations in this region.

At State College, the transmitted wave is linearly polarized in a north-south direction. Referring to the expressions (8.9) for the U, V components in free space,

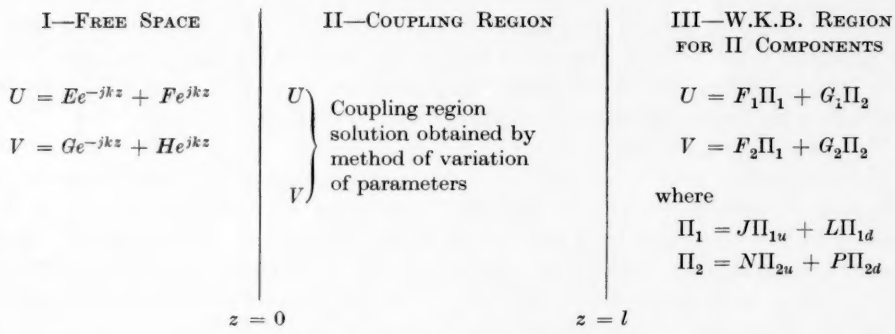

Fig. 9. General boundary value problem.

this corresponds to an incident V wave only. Also, under normal conditions for operation at 150 kc/sec, only the ordinary (π_1) component is reflected from the ionosphere. We may now proceed to obtain solutions for these two cases of interest.

A. *Upgoing Incident V Wave*

For this case we assume unit amplitude for the upgoing incident V wave, no upgoing incident U wave, and no downcoming waves in Region III. This gives us the conditions $G = 1, E = L = P = 0$. Also, since the lower limits of the integrals in equations (9.3) are arbitrary, we choose $a = b = 0$.

We now match the functions and their derivatives at the level $z = 0$. Since at this point

$$\begin{aligned} n_1 &= n_2 = 1 \\ n_1' &= n_2' = 0 \\ U_{u,d} &= V_{u,d} = 1 \\ U'_{u,d} &= V'_{u,d} = \mp jk \end{aligned}$$

we obtain the conditions

$$\left.\begin{aligned} A &= 0 \\ B &= F \\ C &= 1 \\ D &= H \end{aligned}\right\} \tag{9.6}$$

The solutions to the uncoupled equations, (9.4), thus reduce to

$$\begin{aligned} U_0 &= BU_d \\ V_0 &= V_u + DV_d \end{aligned}$$

so that the coupling region solutions become

$$\left.\begin{aligned} U &= BU_d + \frac{U_u}{2jk}\int_0^z [M_1(V_u + DV_d)]'' U_d\, dz - \frac{U_d}{2jk}\int_0^z [M_1(V_u + DV_d)]'' U_u\, dz \\ V &= V_u + DV_d + \frac{BV_u}{2jk}\int_0^z (M_2 U_d \cos^2\theta)'' V_d\, dz - \frac{BV_d}{2jk}\int_0^z (M_2 U_d \cos^2\theta)'' V_u\, dz \end{aligned}\right\} \tag{9.7}$$

VOL. 7 1955

Matching the functions and their derivatives at the level $z = l$, we obtain the equations

$$\left.\begin{aligned} BU_d + D(U_uI_1 - U_dI_2) - JF_1\pi_{1u} - NG_1\pi_{2u} &= U_dI_8 - U_uI_7 \\ B(V_uI_4 - V_dI_6) + DV_d - JF_2\pi_{1u} - NG_2\pi_{2u} &= -V_u \\ BU_d' + D(U_u'I_1 - U_d'I_2) - J(F_1\pi_{1u})' - N(G_1\pi_{2u})' &= U_d'I_8 - U_u'I_7 \\ B(V_u'I_4 - V_d'I_6) + DV_d' - J(F_2\pi_{1u})' - N(G_2\pi_{2u})' &= -V_u' \end{aligned}\right\} \tag{9.8}$$

where all functions are understood to be evaluated at the level $z = l$ and the following abbreviations have been used:

$$I_1 = \frac{1}{2jk}\int_0^l (M_1V_d)''U_d\,dz \tag{9.91}$$

$$I_2 = \frac{1}{2jk}\int_0^l (M_1V_d)''U_u\,dz \tag{9.92}$$

$$I_3 = \frac{1}{2jk}\int_0^l (M_2U_u\cos^2\theta)''V_d\,dz \tag{9.93}$$

$$I_4 = \frac{1}{2jk}\int_0^l (M_2U_d\cos^2\theta)''V_d\,dz \tag{9.94}$$

$$I_5 = \frac{1}{2jk}\int_0^l (M_2U_u\cos^2\theta)''V_u\,dz \tag{9.95}$$

$$I_6 = \frac{1}{2jk}\int_0^l (M_2U_d\cos^2\theta)''V_u\,dz \tag{9.96}$$

$$I_7 = \frac{1}{2jk}\int_0^l (M_1V_u)''U_d\,dz \tag{9.97}$$

$$I_8 = \frac{1}{2jk}\int_0^l (M_1V_u)''U_u\,dz \tag{9.98}$$

Let us consider one of these expressions, say (9.91), in more detail. From (9.5), we have

$$U_{u,d} = \frac{1}{\sqrt{n_1}}\exp\left[\mp jk\int_0^z n_1 d\xi\right]$$

$$U_{u,d}' = -\frac{1}{2}\frac{n_1'}{n_1}U_{u,d} \mp jkn_1U_{u,d}$$

$$U_{u,d}'' = -\frac{1}{2}\frac{n_1''}{n_1}U_{u,d} + \frac{3}{4}\left(\frac{n_1'}{n_1}\right)^2U_{u,d} - k^2n_1^2U_{u,d}$$

But since $U_{u,d}$ are W.K.B. functions, they must satisfy the condition

$$\left|\frac{1}{2}\frac{n_1'}{n_1}\right| \ll |jkn_1|$$

and the criterion of equation (5.9). We may write, therefore, to a very good approximation,

$$\left.\begin{aligned} U'_{u,d} &= \mp jkn_1 U_{u,d} \\ U''_{u,d} &= -k^2 n_1^2 U_{u,d} \end{aligned}\right\} \tag{9.10}$$

with similar expressions for $V'_{u,d}$ and $V''_{u,d}$. Writing out (9.91), we have

$$I_1 = \frac{1}{2jk}\int_0^l (M_1'' V_d + 2M_1' V_d' + M_1 V_d'') U_d \, dz$$

Substituting for U_d, and V_d and its derivatives, this becomes

$$I_1 = \frac{1}{2jk}\int_0^l \frac{(M_1'' + 2jkn_2 M_1' - k^2 n_2^2 M_1)}{\sqrt{n_1 n_2}} \exp\left[jk\int_0^z (n_2 + n_1)\, d\xi\right] dz \tag{9.11}$$

Similar expressions are obtained for $I_2, I_3, \ldots, I_8$. It was found, for all electron density models investigated, that the second derivatives of the coupling factors were negligible with respect to the other terms appearing in equation (9.11); this was also true in the expressions for the other seven integrals. The term involving the first derivative was included in all calculations, although it is probable that it, too, could have been neglected without too much error in the final results.

Returning to equations (9.8), we obtain the final determinantal expressions for the total back-scattered components in the form

$$B(=F) = \frac{\begin{vmatrix} U_d I_8 - U_u I_7 & U_u I_1 - U_d I_2 & -F_1\pi_{1u} & -G_1\pi_{2u} \\ -V_u & V_d & -F_2\pi_{1u} & -G_2\pi_{2u} \\ U_d' I_8 - U_u' I_7 & U_u' I_1 - U_d' I_2 & -(F_1\pi_{1u})' & -(G_1\pi_{2u})' \\ -V_u' & V_d' & -(F_2\pi_{1u})' & -(G_2\pi_{2u})' \end{vmatrix}}{\begin{vmatrix} U_d & U_u I_1 - U_d I_2 & -F_1\pi_{1u} & -G_1\pi_{2u} \\ V_u I_4 - V_d I_6 & V_d & -F_2\pi_{1u} & -G_2\pi_{2u} \\ U_d' & U_u' I_1 - U_d' I_2 & -(F_1\pi_{1u})' & -(G_1\pi_{2u})' \\ V_u' I_4 - V_d' I_6 & V_d' & -(F_2\pi_{1u})' & -(G_2\pi_{2u})' \end{vmatrix}} = \frac{\text{Numerator } (B)}{\Delta} \tag{9.12}$$

$$D(=H) = \frac{\begin{vmatrix} U_d & U_d I_8 - U_u I_7 & -F_1\pi_{1u} & -G_1\pi_{2u} \\ V_u I_4 - V_d I_6 & -V_u & -F_2\pi_{1u} & -G_2\pi_{2u} \\ U_d' & U_d' I_8 - U_u' I_7 & -(F_1\pi_{1u})' & -(G_1\pi_{2u})' \\ V_u' I_4 - V_d' I_6 & -V_u' & -(F_2\pi_{1u})' & -(G_2\pi_{2u})' \end{vmatrix}}{\Delta} \tag{9.13}$$

VOL. 7 1955

B. *Downcoming Incident Ordinary (π_1) Wave*

For this case we assume unit amplitude for the downcoming incident π_1 wave, no downcoming incident π_2 wave, and no upgoing waves in Region I. This gives us the conditions $L = 1$, $P = E = G = 0$. Matching at the level $z = 0$, we obtain the relations

$$A = 0$$

$$B = F$$

$$C = 0$$

$$D = H$$

A similar analysis to the above at the level $z = l$ yields the determinantal expressions for the total main echo components:

$$B(=F) = \frac{\begin{vmatrix} F_1\pi_{1d} & U_uI_1 - U_dI_2 & -F_1\pi_{1u} & -G_1\pi_{2u} \\ F_2\pi_{1d} & V_d & -F_2\pi_{1u} & -G_2\pi_{2u} \\ (F_1\pi_{1d})' & U_u'I_1 - U_d'I_2 & -(F_1\pi_{1u})' & -(G_1\pi_{2u})' \\ (F_2\pi_{1d})' & V_d' & -(F_2\pi_{1u})' & -(G_2\pi_{2u})' \end{vmatrix}}{\Delta} \tag{9.14}$$

$$D(=H) = \frac{\begin{vmatrix} U_d & F_1\pi_{1d} & -F_1\pi_{1u} & -G_1\pi_{2u} \\ V_uI_4 - V_dI_6 & F_2\pi_{1d} & -F_2\pi_{1u} & -G_2\pi_{2u} \\ U_d' & (F_1\pi_{1d})' & -(F_1\pi_{1u})' & -(G_1\pi_{2u})' \\ V_u'I_4 - V_d'I_6 & (F_2\pi_{1d})' & -(F_2\pi_{1u})' & -(G_2\pi_{2u})' \end{vmatrix}}{\Delta} \tag{9.15}$$

It will be noted that the integrals I_3 and I_5 do not appear in equations (9.12) to (9.15). However, it is found that they do appear in the final expressions when an upgoing incident wave is assumed which is linearly polarized in an east-west direction. Since it may be desirable, for some applications, to obtain solutions to the coupling problem for an incident wave of arbitrary polarization, which may be resolved into quadrature components with appropriate phase differences, the explicit expressions for these integrals have been included in the analysis.

10. Numerical Results of Second-Order Theory

Solutions were obtained for the six models shown in Figs. 4 and 6 for both cases of interest considered in the last section. Calculations for the Jones-Mitra critical coupling model, which was the first model for which numerical results were obtained, were carried out in their entirety by hand. It immediately became obvious,

however, that hand calculation only would entail a prohibitive amount of labour if solutions were desired for several additional models. Accordingly, the most laborious part of the calculations, the computation of integrals I_1 to I_8, was carried out on the University's IBM card programmed calculator; while these were being computed, the rest of the factors necessary for the solution of the boundary value problem were obtained by hand.

The final values of back-scatter and forward-scatter coefficients were also computed by hand, rather than on the IBM calculator, in order to be able to keep a close check on the results for consistency. In all cases, the level $z = 0$ (Fig. 9) was taken to be at 85 km, and in all cases except that of the Chapmanlike critical model the level $z = l$ was chosen to be 95 km. For the latter model, the level $z = l$ was chosen as 94 km, since the W.K.B. criterion (5.9) begins to break down at higher levels. Results of the boundary value problem are summarized in Table 2:

Table 2. Results of boundary value problem

Model	1	2	*Jones-Mitra critical*	3	4	*Chapmanlike critical*
Distance, N_c from ν_c level (km)	−0·64	−0·34	0	0·33	0·77	0
Coupling echo						
Tilt angle	149°	151°	148°	150°	152°	139°
θ	∼1°	∼2°	∼1°	∼1°	8°	14°
Rotation	L.H.	L.H.	R.H.	R.H.	R.H.	L.H.
Amplitude	0·107	0·113	0·103	0·120	0·124	∼0·6
Main echo						
Tilt angle	154°	152°	147°	152°	151°	177°
θ	7°	∼3°	∼3°	∼3°	∼2°	24°
Rotation	L.H.	L.H.	L.H.	L.H.	L.H.	L.H.
Amplitude	0·484	0·507	0·492	0·576	0·615	∼0·2

In this table, all tilt angles are measured counterclockwise from magnetic east. θ is the ellipticity angle, defined by the relation

$$\tan \theta = \frac{b}{a},$$

where b is the semi-minor axis of the polarization ellipse and a the semi-major axis. The sense of rotation is defined to be that observed when looking along the direction of propagation.

11. General Discussion and Conclusions

It will be noted that the results for the Jones-Mitra critical coupling model seem slightly inconsistent when compared with those for Models 1 to 4. This is primarily due to the fact, mentioned in Section 8B, that this model was obtained by the use of a different recombination coefficient model than was used to obtain the other

VOL. 7 1955

four. The shape of this model, therefore, is somewhat different than it would have been if calculated in the same manner as the others, having a slightly smaller electron density gradient at the ν_c level than otherwise. Since the Chapmanlike critical coupling model has a high gradient at this level, inspection will show that the results are, in general, consistent if this parameter is considered. Even so, the results for coupling echo tilt angle and main echo amplitude do not show consistent trends at critical coupling which can be explained by differences in electron density gradient between the models. It is evident, therefore, that the actual shape of the model must have an effect on the theoretical values for at least these two parameters. It would of course be desirable to be able to separate effects due to electron density gradients from those due to overall model shapes. However, a complete study for this purpose would require a very extensive programme of calculation, and, since many of the factors to be considered in any comparison of theory with experiment are themselves uncertain, it does not seem practicable to attempt a more detailed investigation of the "fine structure" of coupling phenomena, as it may be termed, at the present time.

For the five Jones-Mitra type models, coupling echo results show the tilt angle to be approximately constant with no particularly significant trend. The sense of rotation is seen to reverse as the N_c level goes above the ν_c level. Amplitudes are approximately constant, approaching a maximum for N_c levels slightly above that of Model 4. Results for the main echo, if the difference in electron density gradient of the critical case is considered, show that as high coupling conditions are approached the tilt angle swings from the normal night-time value of about 20 to 50 degrees (KELSO *et al.*, 1951; NERTNEY, 1953) through zero and "backs," so to speak, into the second quadrant. A minimum tilt angle is then reached for N_c levels slightly above that of Model 4, after which it increases again and "backs" once more into the first quadrant. As the minimum in tilt angle is approached, the polarization ellipse approaches linearity, although the sense of rotation continues to be left-handed.

The effect of a large increase in electron density gradient at the critical level is seen from the results for the Chapmanlike critical coupling model. The tilt angle for the coupling echo decreases, the polarization ellipse becomes broader, and a high back-scatter coefficient is obtained. On the main echo, the tilt angle is almost exactly east–west, the ellipse is quite broad, and the forward-scatter coefficient decreases to a rather low value. For high electron density gradients at the critical level, therefore, we see that the amplitude of the coupling echo may rise sharply while at the same time that of the main echo decreases, a phenomenon which has actually been observed but which has a fairly rare frequency of occurrence.

It is extremely interesting and important to note that the results show nothing extraordinary happening as the N_c level passes through the ν_c level. This shows, first, the inadequacy of ray theory, which predicts a discontinuous change in tilt angle at this point, and second, that the concepts of coupling phenomena which have been held up to this time are in error in assuming that the back-scatter should have a sharp maximum for critical coupling. The latter idea is thus shown to be a fiction caused by the use of the Rydbeck π components, whose coupling factors go to infinity at the critical point; if the general propagation equations (4.10) had

been in general use prior to the Rydbeck equations nothing unusual would have been expected, as the coupling factors of these equations exhibit no unusual behaviour for critical conditions. In fact, the term "critical coupling" actually does not apply when the general equations of propagation are used, since these have no singular points.

In attempting to compare the theoretical results with experiment, it must be remembered that the calculated amplitudes for main echo do *not* represent the amplitudes which would be observed at the ground for a unit transmitted wave. Rather, they are the amplitudes transmitted through the coupling region for a unit ordinary wave incident upon this region from above. Although second-order results have not been obtained for the transmitted wave due to the upgoing incident wave—and in general they will not be the same as for the downgoing case actually calculated—the results of the first-order theory above indicate that the values should be approximately equal. If we make this assumption, and also assume that there is little dissipative absorption in the reflection region, we obtain estimated absorption values (the logarithm of the ratio of ground pulse to first hop amplitudes) for the Jones-Mitra models of about 1·3 to 1·4 nepers, which are of the order of those actually observed (NERTNEY, 1953).

The amplitudes calculated for the coupling echo, on the other hand, do represent the amplitudes which should be observed at the ground for a unit transmitted wave. If we compare them with the estimated amplitudes of main echo as observed at the ground, we obtain values for the ratio of main echo to coupling echo amplitudes which range, again for Jones-Mitra models, from about 2·5 to 1 to 3·0 to 1. Amplitude ratios of this magnitude are more than sufficient to explain the ratios observed in the experimental records.

A third important conclusion may be obtained from the numerical results and the above discussion, namely, that it is not necessary to have a sharply stratified ionosphere in order to obtain split echoes of appreciable magnitude. HELLIWELL *et al.* (1951) have reported that multiple echoes are observed at 100 and 325 kc/sec which fall into groups, with heights of $2h_1$, $h_1 + h_2$, and $2h_2$; $3h_1$, $2h_1 + h_2$, $h_1 + 2h_2$, and $3h_2$, etc., where h_1 and h_2 are the group heights of the first hop split echoes. They conclude that these results indicate stratification, since any back-scatter from the coupling region would be too small for the $h_1 + h_2$, $2h_1$, etc. echoes to be observed. We may conclude from our theoretical coupling results, however, that such multiples are not only possible, but should be observable and are thus to be expected, and, therefore, that sharp stratification is not necessary to satisfactorily explain the experimental data.

Acknowledgements—The authors wish to express their appreciation to Dr. A. H. WAYNICK for the original suggestion of the problem and for his advice and assistance in the course of the work. They also wish to acknowledge the helpful advice and criticism which has been obtained from other members of this Laboratory.

Portions of this work are to be submitted by R. W. PARKINSON in partial fulfilment of the requirements for the Ph.D. degree in the Department of Physics, the Pennsylvania State University.

VOL. 7 1955

APPENDIX I

Values assumed by ρ and σ in free space

The expressions for ρ and σ, as given by equation (8.2), are

$$\rho = \frac{j\eta\gamma_T}{(1-\eta)(\gamma_L{}^2 - \eta^2) - \eta\gamma_T{}^2} \tag{1}$$

$$\sigma = \frac{-\gamma_L\gamma_T}{(1-\eta)(\gamma_L{}^2 - \eta^2) - \eta\gamma_T{}^2} \tag{2}$$

where

$$\left.\begin{aligned} \eta &= \frac{\omega^2}{\omega_0{}^2}\left(1 - \frac{j\nu}{\omega}\right) = \frac{278{\cdot}454}{N}\left(1 - \frac{j\nu}{\omega}\right) \\ \gamma_L &= \frac{\omega_H}{\omega}\,\frac{\omega^2}{\omega_0{}^2}\cos\theta = \frac{278{\cdot}454\omega_H}{\omega N}\cos\theta \\ \gamma_T &= \frac{\omega_H}{\omega}\,\frac{\omega^2}{\omega_0{}^2}\sin\theta = \frac{278{\cdot}454\omega_H}{\omega N}\sin\theta \end{aligned}\right\} \tag{3}$$

It will be noted that, since the quantities η, γ_L, and γ_T as given by (3) are dimensionless, ρ and σ are also dimensionless. Now, for our location and operating frequency, ω_H, ω, $\cos\theta$, and $\sin\theta$ are constants; therefore, we may write (3) as

$$\left.\begin{aligned} \eta &= \frac{k_1}{N}\left(1 - j\,\frac{\nu}{\omega}\right) \\ \gamma_L &= \frac{k_2}{N} \\ \gamma_T &= \frac{k_3}{N} \end{aligned}\right\} \tag{4}$$

where

$$\left.\begin{aligned} k_1 &= 278{\cdot}454 \\ k_2 &= \frac{278{\cdot}454\omega_H}{\omega}\cos\theta = k_1\frac{\omega_H}{\omega}\cos\theta \\ k_3 &= \frac{278{\cdot}454\omega_H}{\omega}\sin\theta = k_1\frac{\omega_H}{\omega}\sin\theta \end{aligned}\right\} \tag{5}$$

Substituting from (4) into (1), the expression for ρ may be reduced to

$$\rho = \frac{jk_1k_3}{\dfrac{k_2{}^2}{1 - j\,\dfrac{\nu}{\omega}} - k_1{}^2\left(1 - j\,\dfrac{\nu}{\omega}\right) - \dfrac{k_1}{N}(k_2{}^2 + k_3{}^2) + \dfrac{k_1{}^3}{N}\left(1 - j\,\dfrac{\nu}{\omega}\right)^2} \tag{6}$$

The dominant factor in this expression is obviously the electron density, N, except for the case where $\nu = \infty$; in this case the denominator goes to infinity and ρ goes

to zero for N either finite or zero. If $\nu \neq \infty$, $\frac{\nu}{\omega}$ is finite or zero, the denominator goes to infinity for $N = 0$, and ρ again goes to zero. Therefore, in free space ($N = 0$), we conclude that

$$\rho = 0 \tag{7}$$

Again, substituting from (4) into (2), the expression for σ may be reduced to

$$\sigma = \frac{-k_2 k_3}{k_2^2 - k_1^2\left(1 - j\frac{\nu}{\omega}\right)^2 - \frac{k_1}{N}(k_2^2 + k_3^2)\left(1 - j\frac{\nu}{\omega}\right) + \frac{k_1^3}{N}\left(1 - j\frac{\nu}{\omega}\right)^3} \tag{8}$$

By a similar argument to that used above, we conclude that, in free space ($N = 0$),

$$\sigma = 0. \tag{9}$$

APPENDIX II

Investigation of coupling factors of the general equations of propagation for singularities

Consider the expressions for M_1 and M_2 as given by equation (4.11). Utilizing equations (3.6) and (3.1), these reduce to

$$M_1 = \frac{-\frac{\omega_H}{\omega}\left[x_0^2\left(1 - \frac{j\nu}{\omega}\right) - 1\right]}{x_0^4\left(1 - \frac{j\nu}{\omega}\right)\left(1 - \frac{\omega_H^2 + \nu^2}{\omega^2} - \frac{2j\nu}{\omega}\right) - 2x_0^2\left(1 - \frac{j\nu}{\omega}\right)^2 + x_0^2\frac{\omega_H^2}{\omega^2}\cos^2\theta + \left(1 - \frac{j\nu}{\omega}\right)} \tag{10}$$

$$M_2 = \frac{-\frac{\omega_H}{\omega}}{x_0^2\left(1 - \frac{\omega_H^2 + \nu^2}{\omega^2} - \frac{2j\nu}{\omega}\right) - \left(1 - \frac{j\nu}{\omega}\right)} \tag{11}$$

Let us investigate these expressions and their first and second derivatives for singular points under conditions at State College as given by (5.1). Obviously, the only possibility for (11) to be infinite is for the denominator to be zero. For this case, we obtain two sets of conditions, namely,

$$\left\{\frac{\nu}{\omega} = 0, \quad x_0^2 = \frac{1}{1 - \frac{\omega_H^2}{\omega^2}}\right\} \quad \text{and} \quad \left\{\frac{\omega_H^2 + \nu^2}{\omega^2} = -1, \quad x_0^2 = \tfrac{1}{2}\right\}.$$

However, both of these are impossible for any real ionosphere, so we may conclude at once that there is no infinity in M_2.

The proof that (10) can have no infinity is somewhat more complicated, as we must consider both numerator and denominator. Since $x_0^2 = \frac{278}{N}$, the numerator has an infinity at $N = 0$; however, at this point the denominator also has an

VOL. 7 1955

infinity, and after multiplying numerator and denominator by N^2 we find that the limiting value, for $N = 0$, is actually zero. The possibility still remains that the denominator may be zero, and we find, separating real and imaginary parts, that we must satisfy the relations

$$\left.\begin{aligned} x_0^4\left(1 - \frac{\omega_H^2}{\omega^2} - \frac{3\nu^2}{\omega^2}\right) - 2x_0^2\left(1 - \frac{\nu^2}{\omega^2}\right) + x_0^2\frac{\omega_H^2}{\omega^2}\cos^2\theta + 1 = 0 \\ x_0^4\left(\frac{\omega_H^2 + \nu^2}{\omega^2} - 3\right) + 4x_0^2 - 1 = 0 \end{aligned}\right\}$$

Solution of these equations by graphical methods shows immediately that they are inconsistent for all positive values of $\frac{\nu^2}{\omega^2}$, and we thus conclude that there is no infinity in M_1.

We now proceed to investigate the derivatives of M_1 and M_2. Writing

$$M_{1,2} = \frac{A(z)}{B(z)}$$

we have

$$M'_{1,2} = \frac{A'B - B'A}{B^2} \tag{12}$$

$$M''_{1,2} = \frac{A''B^2 - ABB'' - 2A'B'B - 2A(B')^2}{B^3} \tag{13}$$

The denominators in these expressions are just higher powers of the denominators of (10) and (11), and we have shown above that the latter cannot be zero. The numerators, however, will contain the factors $(x_0^2)'$, $(x_0^2)''$, ν', and ν'' as well as x_0^2 and ν. Since

$$(x_0^2)' = \frac{-278N'}{N^2}$$

and

$$(x_0^2)'' = \frac{557(N')^2 - 278NN''}{N^3},$$

we see that, for $N \neq 0$, the numerators in (12) and (13) will have no infinity as long as the derivatives of N and ν are finite. For $N = 0$, on the other hand, both numerators and denominators simultaneously go to infinity. As before, it may be shown that the limiting values of the ratios are finite, but in the case of (13) we must impose the additional condition that $N' = 0$ at this point. Since the above conditions merely mean that both N and ν and their first derivatives must be continuous and finite, a condition which is practically certain to obtain physically, this causes us no difficulty.

We conclude, therefore, that the coupling factors in the general differential equations (4.10), together with their first and second derivatives, have no infinity under conditions which will be satisfied by any physically real ionosphere.

References

Clemmow, P. C., and Heading, J.	1954	*Proc. Cambridge Phil. Soc.* **50,** 319
Davids, N.	1952	*J. Atmosph. Terr. Phys.* **2,** 324
Davids, N.	1953	*J. Geophys. Res.* **58,** No. 3, 311
Fosterling, K.	1942	*Hoch. Teck. und Eleck. Aus.* **59,** 10
Gibbons, J. J., and Nertney, R. J.	1952	*J. Geophys. Res.* **57,** No. 3, 323
Helliwell, Mallinckrodt, and Kruse	1951	*J. Geophys. Res.* **56,** No. 1, 53
Jones, R. E.	1955	Accepted for publication in *J. Atmosph. Terr. Phys.*
Kelso, Nearhoof, Nertney, and Waynick	1951	*Ann. Geophys.* **7,** 215
Lindquist, R.	1953	*J. Atmosph. Terr. Phys.* **4,** 10
Mitra, A. P.	1954a	*J. Atmosph. Terr. Phys.* **5,** 28
Mitra, A. P.	1954b	Private communication
Mitra, A. P., and Jones, R. E.	1954	*J. Geophys. Res.* **59,** No. 3, 391
Nertney, R. J.	1953	*J. Atmosph. Terr. Phys.* **3,** 92
Nicolet, M.	1953	*J. Atmosph. Terr. Phys.* **3,** 200
Rydbeck, O. E. H.	1944	*Trans. Chalmers Univ. Gothenburg,* No. 34

VOL.
7
1955

Journal of Atmospheric and Terrestrial Physics, 1955, Vol. 7, pp. 203 to 234. Pergamon Press Ltd., London

The night-time lower ionosphere as deduced from a theoretical and experimental investigation of coupling phenomena at 150 kc/sec*

R. W. Parkinson
Ionosphere Research Laboratory, The Pennsylvania State University State College, Pennsylvania

(*Received* 27 *January* 1955)

ABSTRACT

Final results of an experimental programme for the investigation of coupling phenomena at 150 kc/sec, which covered a period of some ten months in all, are presented. Conclusions are obtained, from a comparison of the theoretical results presented in the preceding paper and the experimental data, regarding the shape of the night-time *D*-layer in the coupling region and its seasonal and diurnal variations.

Sunset *D-E* region models for July and November 1953 are proposed. A theoretical recombination coefficient model suggested by Mitra (1954a) is then applied in the usual manner to determine the variation of these models with time of night. Finally, comparison is made both with the conclusions obtained from the data on coupling phenomena and with all other available low-frequency data; very good agreement is obtained in all cases. It is concluded that the theoretical analysis satisfactorily explains the experimental observations.

1. Introduction

The theoretical aspects of coupling phenomena have been investigated for critical and near-critical coupling conditions in the preceding paper (Davids and Parkinson, 1955). It was shown that, by a suitable transformation, it is possible to obtain coupled wave equations with coupling factors which are well behaved under critical conditions. This enabled solutions to be obtained for such cases, and numerical results were presented for six ionospheric models of interest.

An experimental programme specifically designed for the investigation of coupling phenomena has been under way since March 1953; the instrumentation for this programme has been described elsewhere (Parkinson, 1955). The purpose of the present paper is threefold: first, the final results of the experimental investigation will be presented; second, certain conclusions regarding the shape of the night-time ionosphere in the coupling region, together with seasonal and diurnal variations of the *D*-layer, will be obtained from a comparison of the experimental and theoretical results on coupling phenomena; and third, sunset *D-E* region models will be proposed for summer and winter months whose variations with time of night, as obtained by the application of a theoretical night-time recombination coefficient model suggested by Mitra (1954a), agree very well both with the data on coupling phenomena and also with all other available low-frequency experimental data.

2. Data and Data Analysis

A. *Sample Data*

The experimental programme to investigate coupling phenomena extended from 19 March 1953 to 26 January 1954. A continuous recording programme,

* The research reported in this paper has been sponsored by the Geophysics Research Directorate of the Air Force Cambridge Research Center, Air Research and Development Command, under Contract AF19(122)-44.

however, was not initiated until 2 June 1953; during the first two months of the above period only night-time data were obtained, since the equipment was being tested for resolution of split echoes. This fact, combined with the usual transmitter and instrument breakdowns, high summer-time absorption and atmospherics, local interference, and so on, made the overall continuity of data rather spotty up to the beginning of July, although usable data were obtained in June. Also, many of the data for January 1954 were lost because of periodic equipment breakdown caused by a need for a general overhaul of the apparatus. Since the Laboratory's experimental programme on 150 kc/sec was terminated on 26 January, the general overhaul was postponed until after this time, when the equipment was also modified for operation on a lower frequency.

In view of the above, the data analysis to follow will be restricted to the period July 1953–December 1953, with data being included for June 1953 and January 1954, when available. Since primary emphasis is centred upon diurnal and seasonal variations of the parameters of interest, the experimental records were scaled at intervals of approximately 10 min. In order to reduce the possibility of obtaining false polarization data, which may result if main and coupling echoes overlap sufficiently, care was taken to choose points which showed the split echoes to be well resolved in height. That this effort was successful is evidenced by the fact that the results obtained when both main and coupling echoes were present simultaneously were essentially the same as those obtained when either was present by itself. It should be mentioned that no h'-t records were available for correlation from early in September up to the end of the recording programme. Since the equipment used for the investigation of coupling phenomena (PARKINSON, 1955) does not distinguish between coupling and main echoes *when only one is present*, the lack of h'-t records greatly increased the difficulty of identification of echoes under such circumstances. In cases where a reasonable doubt existed, therefore, the records were not scaled at all; although this caused the loss of quite a bit of data, particularly in the case of the coupling echo, it was felt to be necessary in order that final results might be regarded as significant.

VOL. 7 1955

Before proceeding further, let us consider the expressions for the polarization of the Rydbeck π-components (RYDBECK, 1944). From his paper, after adjusting the equations for an $e^{+j\omega t}$ time variation, we find the polarizations given by the relation

$$u_{1,2} = \frac{E_y^{(1,2)}}{E_x^{(1,2)}} = \frac{\dfrac{{\gamma_T}^2}{1 - {x_0}^2\left(1 - \dfrac{j\nu}{\omega}\right)} \pm \sqrt{\left[\dfrac{{\gamma_T}^2}{1 - {x_0}^2\left(1 - \dfrac{j\nu}{\omega}\right)}\right]^2 + 4{\gamma_L}^2}}{2j\gamma_L} \tag{2.1}$$

Substituting for ${x_0}^2$, γ_T, and γ_L, this may be reduced to

$$u_{1,2} = \frac{\dfrac{-k_1}{k_2 N - \left(1 - \dfrac{j\nu}{\omega}\right)} \pm \sqrt{\dfrac{{k_1}^2}{{k_2}^2 N^2 - 2k_2 N\left(1 - j\dfrac{\nu}{\omega}\right) + \left(1 - j\dfrac{\nu}{\omega}\right)^2} + {k_3}^2}}{jk_3}$$

where k_1, k_2, k_3 are constants for any given operating conditions. For $N = 0$ (free space) and ν finite, we have

$$u_{1,2} = \frac{\dfrac{k_1}{1 - j\dfrac{\nu}{\omega}} \pm \sqrt{\dfrac{{k_1}^2}{\left(1 - j\dfrac{\nu}{\omega}\right)^2} + {k_3}^2}}{jk_3}$$

At the ground, ν is of the order of 10^{11} or greater (NICOLET, 1953). For State College conditions and an operating frequency of 150 kc/sec, $k_1 \cong 10$, $k_2 \cong 0{\cdot}004$, $k_3 \cong 400$, and $\frac{\nu}{\omega} \cong 10^5$ at this level. Thus, in orders of magnitude, we may write

$$u_{1,2} \cong \frac{10^{-4} \pm \sqrt{10^{-8} + 10^4}}{j10^2}$$

$$\cong \frac{\pm 10^2}{j10^2}$$

$$\cong \mp j$$

At ground level, then, the polarization of the Rydbeck π-components is circular, with opposite sense of rotation, at least to within about 0·01 per cent. Since this is just what the coupling equipment records, channels 1 and 2, which correspond to the two circularly polarized components of the polarization ellipse, will henceforth be termed the ordinary and extraordinary modes. It should be noted that there may be some doubt as to the validity of the above argument for $N = 0$, since it is questionable whether the expression (2.1) holds in such a case. Physically, however, there is no difficulty, since from a wave-theory viewpoint the important consideration is not the actual number of electrons per cm^3, but rather the number of electrons per wavelength for a given cross-sectional area. For the wavelength of 2 km corresponding to our operating frequency, an electron density as low as 1 e/cc would correspond to 2×10^5 e/wavelength/cm^2, certainly a sufficiently high value to avoid the above difficulty. Inspection will show that polarizations of the ordinary and extraordinary components at the ground, as already derived, are not affected by electron densities as large as 300 e/cc, and since some cosmic-ray ionization is always present, the conclusions obtained are felt to be physically reasonable.

Sample diurnal plots of tilt angle, ellipticity angle, and ratio of extraordinary to ordinary modes are shown in Figs. 1 to 3. The examples given were chosen to illustrate typical diurnal characteristics with good data continuity. Times of ground sunrise and sunset for the particular dates chosen, together with values of international character figure, C, geomagnetic planetary index, K_p, and ionospheric character figure (Washington), I, (as obtained from CRPL-F bulletin data), are indicated on each figure; all times indicated are local mean solar time. The data of Fig. 1 were obtained on one of the ten magnetically selected quiet days of October, and show the typical bell-shaped diurnal variation of tilt angle obtained by previous workers (KELSO, NEARHOOF, NERTNEY, and WAYNICK, 1951). The data of Fig. 2, obtained on a day only slightly more magnetically disturbed, show a large number of high tilt angle values during the night-time hours in addition to the normal diurnal behaviour. These high night-time tilt angles were observed with increasing frequency as winter approached, and are attributed to high coupling conditions; this will be discussed at length in a later section.

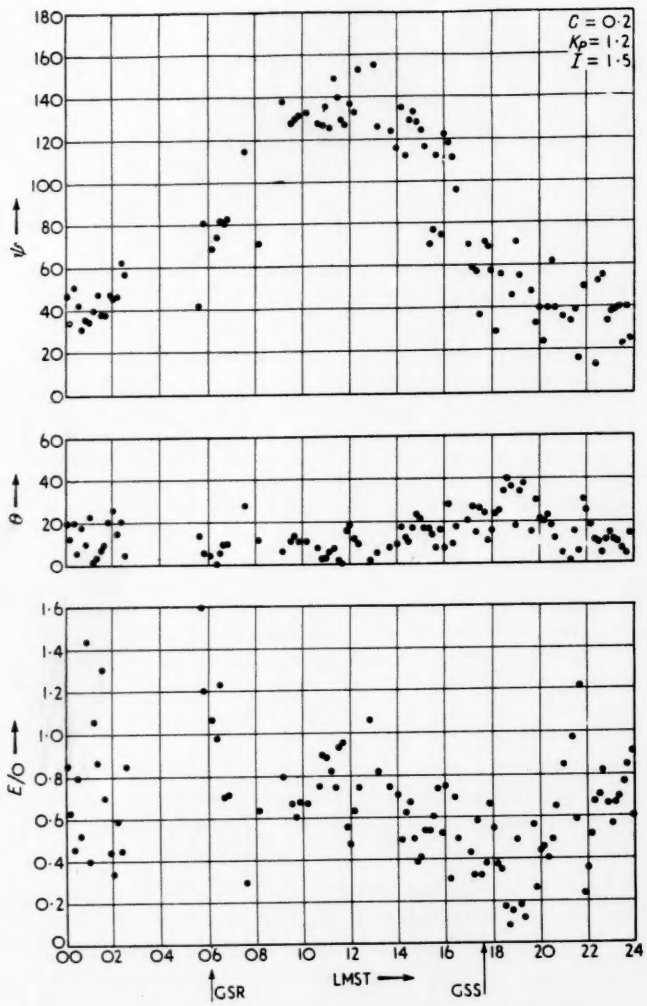

Fig. 1. Sample data, main echo, 4 October 1953.

VOL. 7 1955

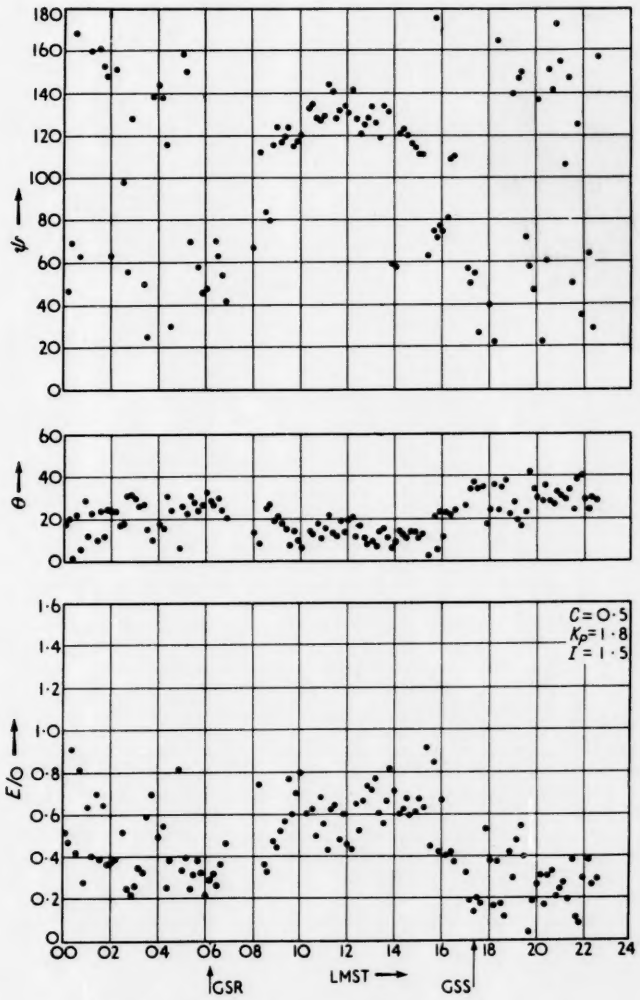

Fig. 2. Sample data, main echo, 11 October 1953.

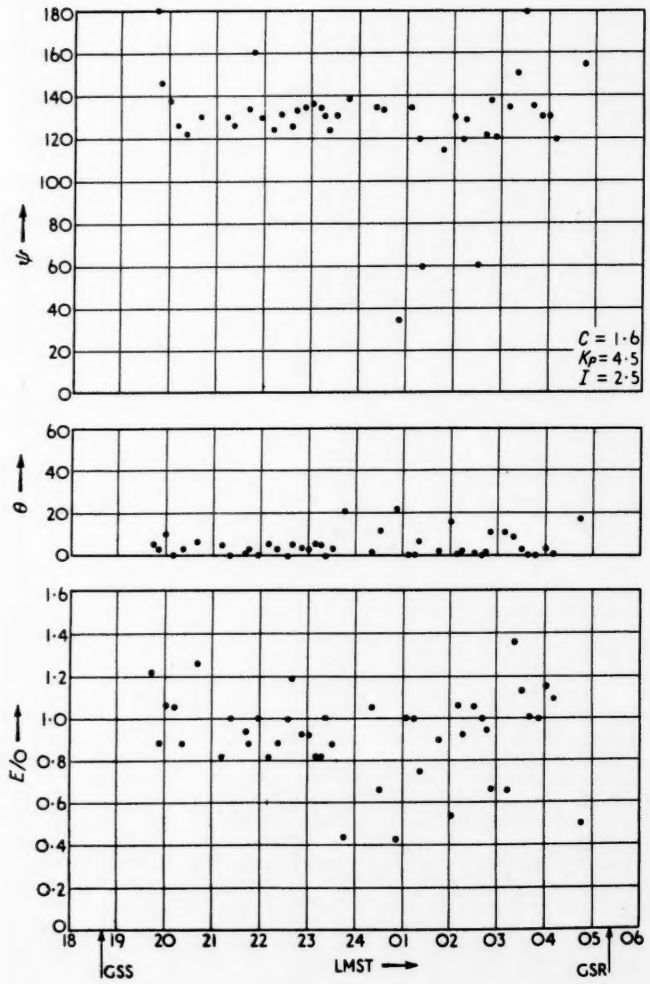

Fig. 3. Sample data, coupling echo, 23–24 August 1953.

VOL. 7 1955

Examples of the rapid variations which occur over short periods of time may be seen in Fig. 4. The wide fluctuations which occur over these short periods obviously account for most of the scatter which is observed in the diurnal plots.

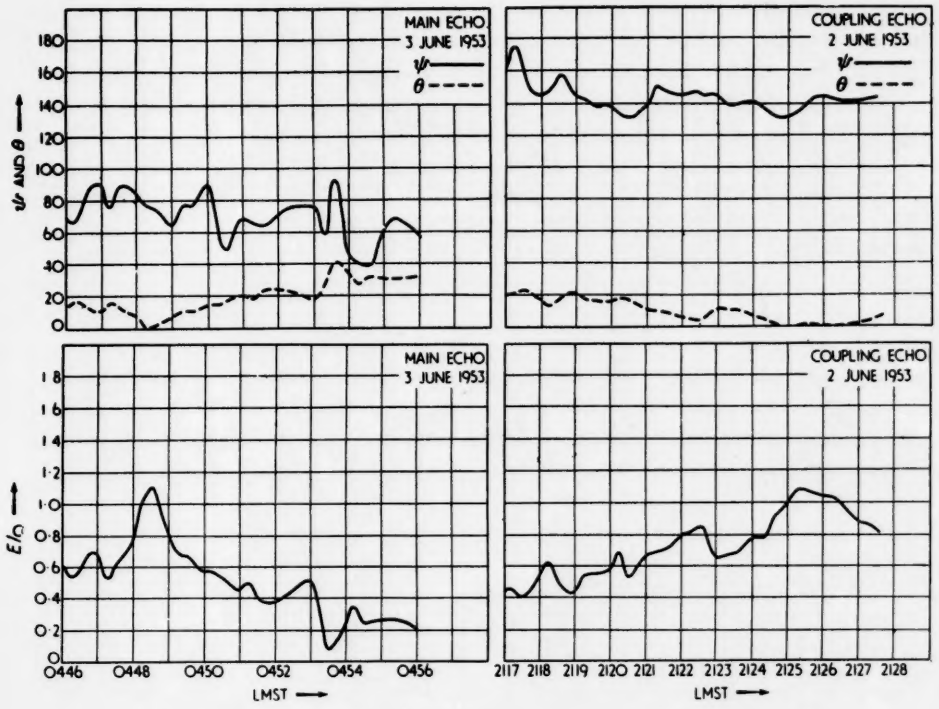

Fig. 4. Examples of continuous variation of tilt angle, ellipticity angle, and mode ratio.

B. *Monthly Averages*

Monthly average values, by hours, for main echo tilt angle, ellipticity angle, and mode ratio are shown in the curves of Figs. 5 to 7, tilt angle being measured counter-clockwise from magnetic east and the ellipticity angle being defined by the relation

$$\tan\ \theta = \frac{b}{a}$$

where a and b are the semi-major and semi-minor axes of the polarization ellipse, respectively. In obtaining these results, the high night-time tilt angles mentioned previously were averaged separately from values which seemed to correspond to the normal diurnal variation; the two averages thus obtained are shown separately on each curve. Values of ellipticity angle and mode ratios which corresponded to the high tilt angle values were also averaged separately from the rest, and are indicated as such on the curves. For all cases, averages obtained

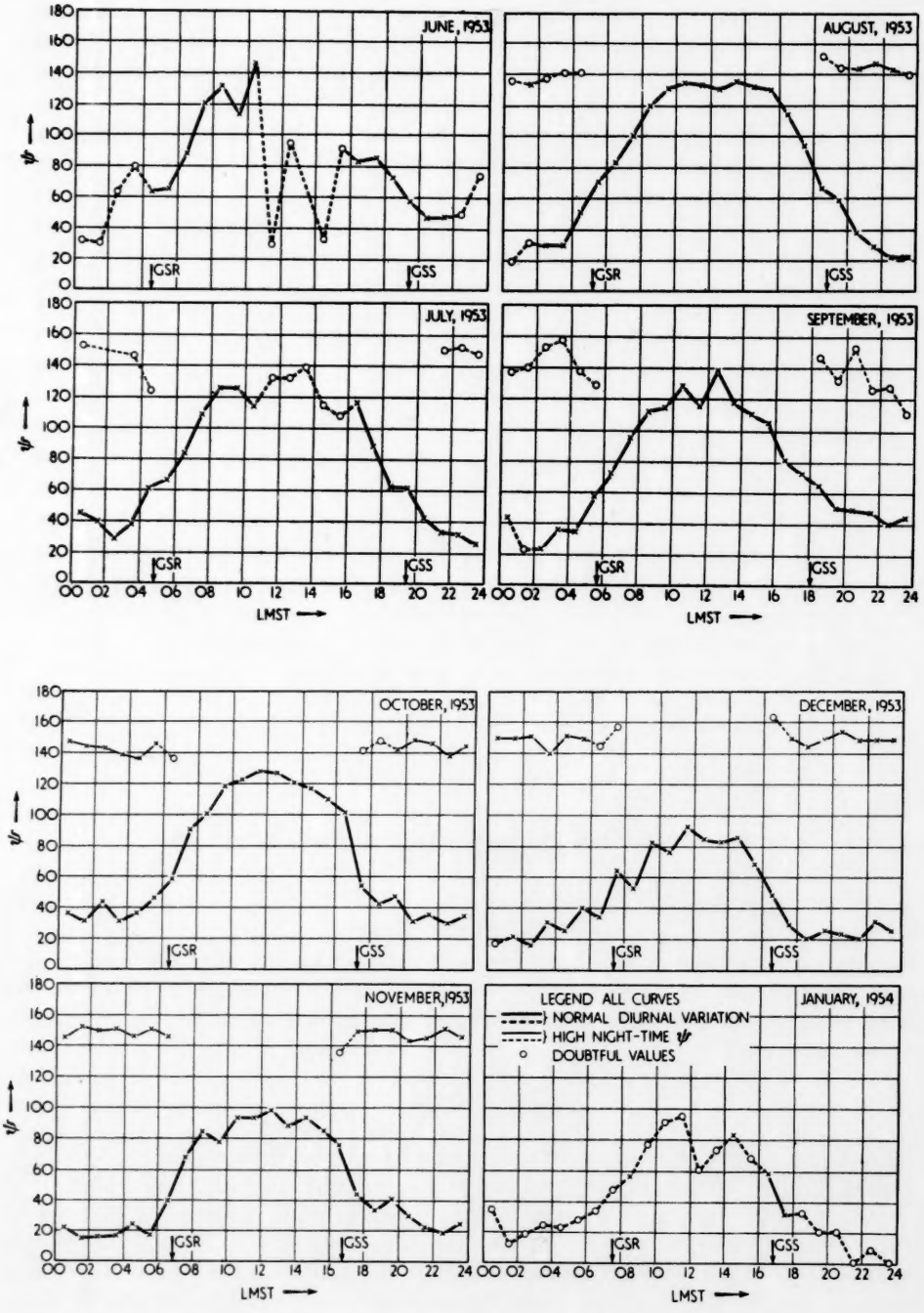

Fig. 5. Monthly average curves of main echo tilt angle.

VOL. 7 1955

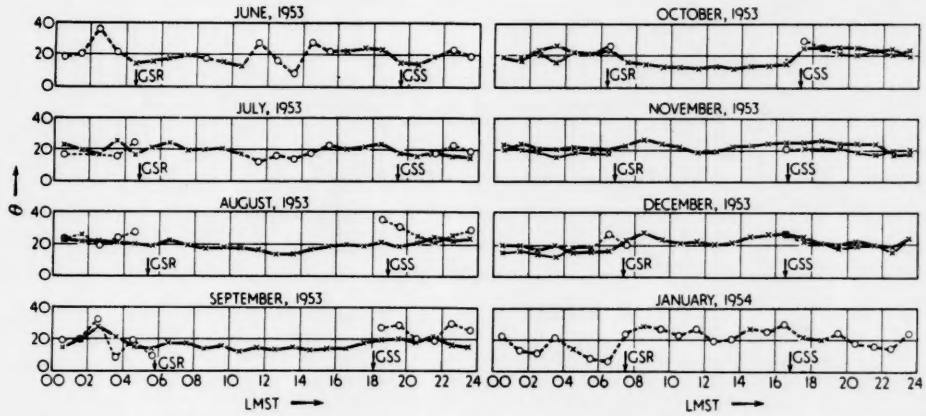

Fig. 6. Monthly average curves of main echo ellipticity angle.

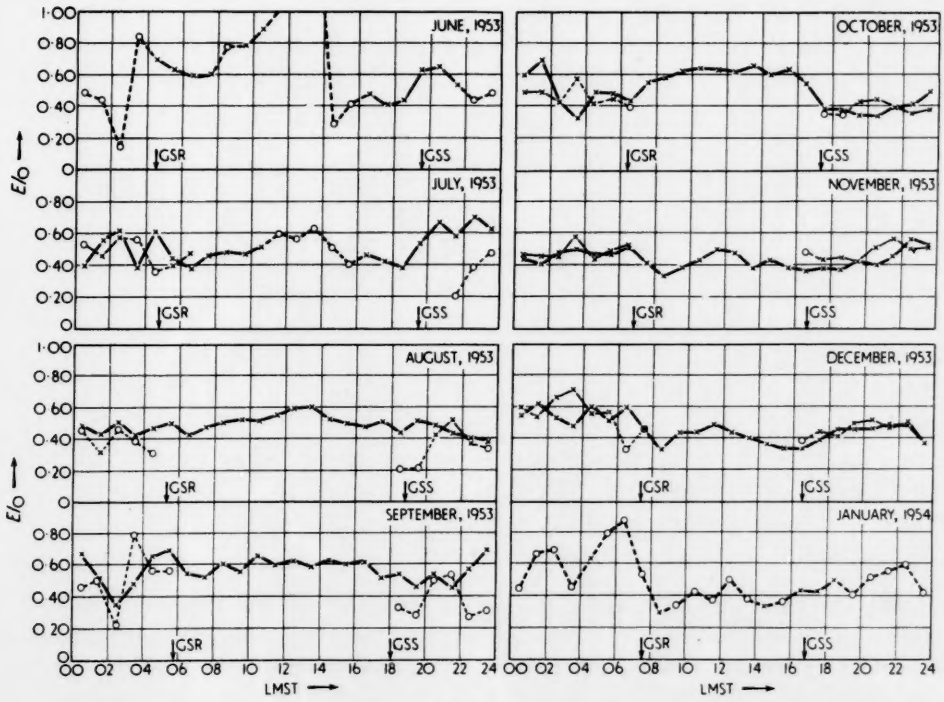

Fig. 7. Monthly average curves of main echo mode ratio.

from less than ten readings were considered doubtful; although the choice of a point at which to separate "doubtful" and "significant" averages was arbitrary, in view of the results it seems quite satisfactory.

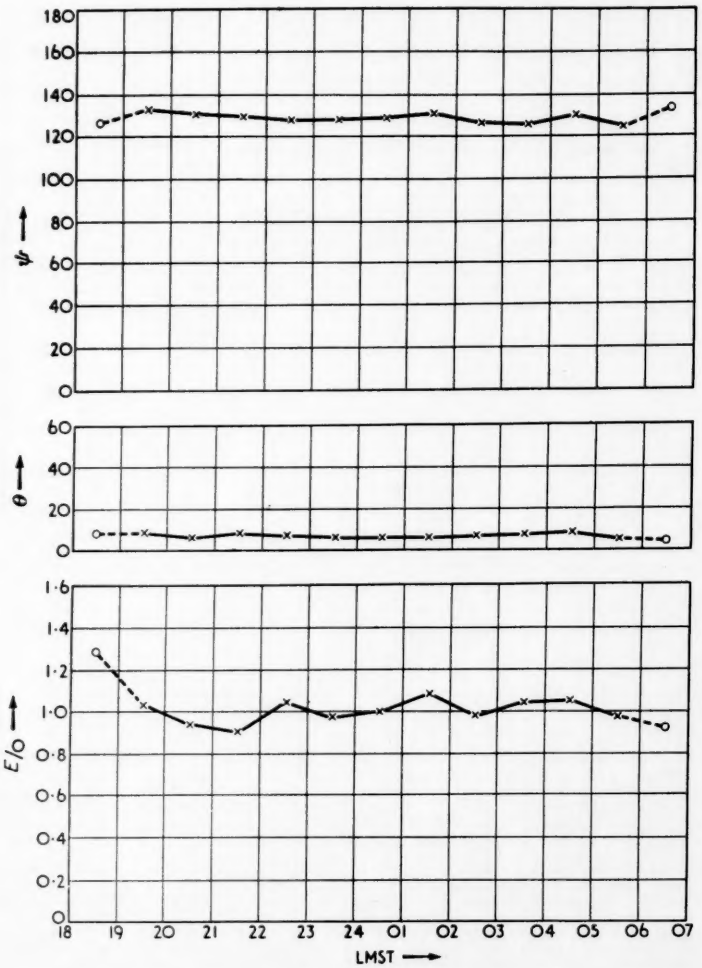

Fig. 8. Average curves of coupling echo tilt angle, ellipticity angle, and mode ratio, all data.

Monthly average values, by hours, for coupling echo tilt angle, ellipticity angle, and mode ratio were also obtained, but the results showed no significant diurnal or seasonal trends. Therefore, all coupling echo data obtained during the period August 1953 to January 1954 inclusive were combined and hourly averages again taken. The resulting curves are shown in Fig. 8; doubtful points are designated as such under the same criterion used to separate the values for main echo.

VOL. 7 1955

C. *Discussion of Experimental Results*

Ignoring, for the moment, the high night-time values, it is observed that the diurnal variation of main echo tilt angle compares very favourably with the theoretical results obtained by NERTNEY (1953). In addition, a seasonal variation in the noon-time maximum and in the width of the bell-shaped portion of the curves is evident, which also compares well with theory. The diurnal variation of ellipticity angle, while in fairly good agreement with theoretical values (KELSO *et al.*, 1951) during the night-time hours, shows a minimum during the day in most of the curves instead of the maximum which would be expected. This may also be observed in the curves for mode ratio, most of which show a rise during the day rather than the expected decrease.

Since the problem at hand is concerned primarily with night-time phenomena, the above discrepancy will not be investigated in detail at the present time. However, it is felt that a few remarks should be made as a guide for future work. NERTNEY'S work utilized the procedure of obtaining theoretical polarizations, absorptions, and so on, for a Chapmanlike *E*-region and comparing the results, for various frequencies, with experimental data. Since agreement was not obtained, an empirical *D*-layer model was postulated, its effect on the theoretical results calculated, and a comparison with experimental data again made. If agreement was still not obtained, the *D*-layer model was altered and the procedure repeated until theoretical results compared favourably with experiment. The entire process, therefore, depended largely upon the *E*-layer model originally assumed. Since that time, however, JONES (1955) has obtained an *E*-region model from phase height measurements which is substantially different from a Chapmanlike model. Also, MITRA'S theoretical *D*-region (1954b), which was used for the theoretical investigation of coupling phenomena, lies at a height about 10 km higher than NERTNEY'S empirical model, and has an overall shape quite different from the latter. It is evident, therefore, that this type of investigation should be repeated, taking account of the change in the *E*-layer suggested by JONES and at least starting the work on the *D*-layer with a model obtained from theoretical considerations such as that suggested by MITRA.

Returning to a consideration of the experimental data presented in Figs. 5 to 8, we note that the high night-time tilt angles for main echo tend to average about 140° to 150°. Referring to the theoretical results presented in the preceding paper, we see that such high night-time tilt angles for main echo would be expected to be associated with high coupling conditions. If this is true, there should be an experimental correlation between the appearance of the coupling echo and the occurrence of these high tilt angles. In order to determine whether such a correlation exists, all night-time experimental records were re-examined and high and low tilt angles tabulated with respect to presence or non-presence of the coupling echo. The results of this investigation are shown in Table 1. Although it is obvious from an inspection of the figures that an excellent correlation exists, a Chi-square test was made on the data to determine the statistical probability that the distribution shown in Table 1 might be due to chance. This analysis gave a Chi-square value of 1500; since a value of about 6 would indicate a probability of only 0·01 that the results are due to chance, it may be concluded that the correlation between the high night-time tilt angles for main echo and the appearance of the coupling echo is definitely established, and that both phenomena may, therefore, be attributed to the coupling effects investigated.

With this conclusion in mind, we may examine the experimental data with

the object of determining the characteristics of the night-time ionosphere at and near the coupling level. Comparing the experimental results with the theoretical results of the preceding paper, we may infer the following:

Table 1. *Correlation between high night-time tilt angles for main echo and appearance of coupling echo*

	Coupling echo present	*No coupling echo present*
"High" night-time ψ, main	1068	330
"Low" night-time ψ, main	347	2127

(All figures are total number of occurrences).

1. From high night-time tilt angles, main echo: the average values of 140° to 150° indicate either a smaller electron density gradient near the critical coupling level, or a different type of model shape (such as a Chapmanlike model, which has a more rapid variation of tilt angle near critical coupling). There also seems to be a tendency for the monthly average values to approach a minimum about October, and then increase again; this would imply a seasonal variation, with the average N_c level at its highest point somewhere around October.

2. From ellipticity angle values corresponding to the high tilt angles of main echo: these data tend to average about 20°, which would indicate a higher electron density gradient than the Jones-Mitra models. There is also a tendency for higher values to be observed before midnight, indicating that the N_c level rises during the night, as would be expected. No significant seasonal trend is evident.

3. From mode ratio values corresponding to high tilt angles of main echo: these data tend to average from 0·40 to 0·50, implying a fairly high election density gradient at the coupling level. The values before midnight tend to be generally lower than those after midnight, indicating a rise in the N_c level during the night. Finally, the monthly averages show a tendency to increase from summer to winter, indicating a seasonal variation with the N_c level at its highest point during the winter months.

4. From tilt angle data for the coupling echo: as stated before, the monthly data plots showed no significant diurnal or seasonal tendencies; this is what would be expected from the theoretical results. The average of all data shows tilt angles of about 130°which remain approximately constant throughout the night, implying a high electron density gradient at the coupling level.

5. From ellipticity angle data for the coupling echo: again, the monthly data show no significant diurnal or seasonal tendencies, as would be expected from the theoretical results. The average of all data gives an approximately constant value of about 8° throughout the night, implying a fairly high electron density gradient around the critical level.

VOL. 7 1955

6. From mode ratio data for the coupling echo: the average of all data for this parameter shows an approximately constant value throughout the night of about 1·0. This would mean that the coupling echo was, on the average, linear—a result which is in some disagreement with the average ellipticity angle results above. However, the latter data do not take account of sense of rotation, whereas right-handed rotation appears here as a mode ratio greater than 1·0. Since a substantial percentage of the coupling echo data showed right-handed rotation, which was not true of main echo, we have a difference between ellipticity angle and mode ratio results which was not evident in the main echo data. The mode ratio for left-handed rotation may vary from 0·0 to 1·0, while that

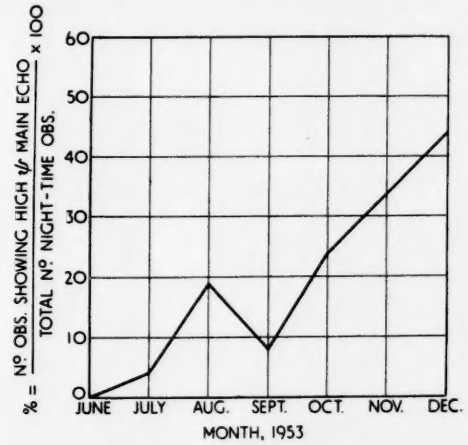

Fig. 9. Monthly percentage of night-time main echo observations with high tilt angles.

for right-handed rotation may vary from 1·0 to ∞. In interpreting the data for mode ratios, therefore, we must take account of the fact that a value showing right-handed rotation may carry much more weight in the averaging process than one showing left-handed rotation, since the range of values which it may assume is so very much greater.

It has been mentioned previously that the high night-time tilt angles for main echo were observed with increasing frequency as winter approached. This, combined with the seasonal tendency in their average values pointed out in Part 1, above, implies a seasonal variation in the height of the N_c level which we may further investigate by determining the percentage of all night-time observations, by months, for which these high tilt angles occurred. The results of this analysis are shown in Fig. 9, and the seasonal variation is quite apparent. We must, however, inquire as to the mechanism which may cause such a phenomenon, that is, why both high and low tilt angles are observed at irregular intervals on any given night, as in Fig. 2, rather than the smooth transition which might be expected. Now, focusing effects on multiple hop echoes have been observed on 3·5 mc/sec (*F*-region) by Pierce and Mimno (1940) and on 150 kc/sec (lower *E*-region) by Schrag (1955). These effects have been attributed to large-scale

irregularities, travelling over the transmitting site, which must be concave downward for focusing to occur. Since these travelling disturbances have been observed both at heights of 100 km and 250 km, there seems to be no good reason why they should not also exist at lower heights, as at the coupling levels in which we are interested here. Pierce and Mimno place an outside limit on the amplitude of these disturbances of 1–2 km, while Schrag, assuming a drift velocity of 5 km/min, obtains vertical depths for irregularities at 100 km of 0·2 to 3·0 km, with values above 1·0 km occurring quite rarely.

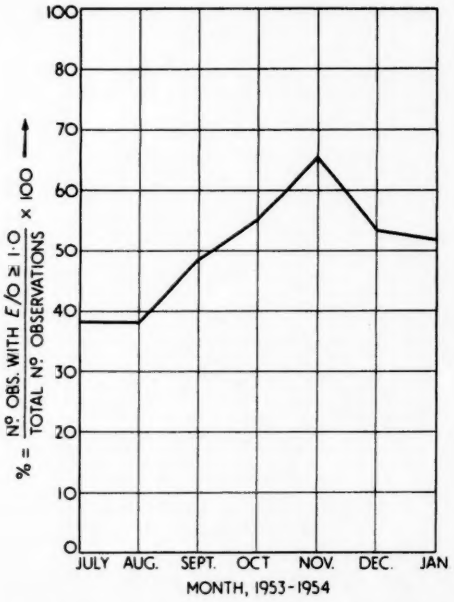

Fig. 10. Monthly percentage of coupling echo observations with mode ratios equal to or greater than 1·0.

The effect of such a travelling irregularity at the coupling level would be to decrease the electron density in that region for a short period of time. If the N_c level is a kilometre or two below the ν_c level, it would thus be raised toward the critical coupling region, causing the main echo tilt angle to swing through zero into the second quadrant if the N_c level is raised high enough. As the disturbance passes, the N_c level will drop back to its normal height and the main echo tilt angle will return to the first quadrant. This is precisely the type of behaviour that is observed in Fig. 2, so that this interpretation, combined with the results shown in Figs. 5 and 9, should enable us to form a picture of the average seasonal variation in the height of the N_c level. Before proceeding further, however, we shall investigate a third type of data from which we may obtain information regarding this seasonal behaviour. According to the theoretical results, the sense of rotation of the coupling echo, if the layer shape in the coupling region is somewhat similar to the Jones-Mitra models used for calculation, should reverse for the N_c level

VOL. 7 1955

at or above the ν_e level. Therefore, the percentage of all coupling-echo observations, by months, having mode ratios equal to or greater than 1·0 was determined, with results which are shown in Fig. 10.

Attributing the rather irregular appearance of the high night-time tilt angles for main echo to travelling disturbances at the coupling level, then, the data of Figs. 5, 9, and 10 enable us to draw several conclusions regarding the seasonal variation in height of the N_e level. First, the N_e level rises from summer to winter, with a minimum occurring during the summer months. In evaluating these data

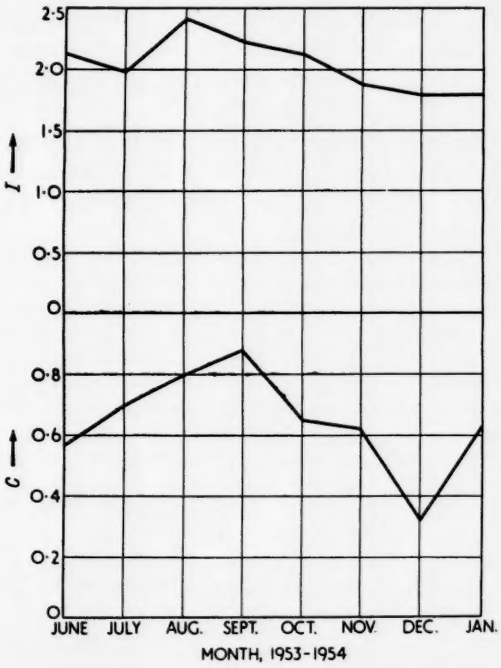

Fig. 11. Monthly average ionospheric storminess index, Washington, D.C. (I) and international character figure (C).

in order to specify the time of year at which this minimum occurs, it should be stated that the percentage of main echo readings showing high tilt angles for June should be considered doubtful, since relatively few night-time data were available for this particular month. Also, the rather large percentage for August is attributed to the fact that August was the most ionospherically disturbed month during the entire period for which data are presented. Monthly average values of ionospheric storminess index (Washington, D.C.) and international character figure from CRPL-F bulletin data are shown in Fig. 11. Since the effects of interest are due to travelling irregularities, the former index is felt to be a better indication of possible turbulence than the latter, and shows a decided peak in August. An interesting feature of the data is the absence of a high value of percentage of coupling echo observations with right-handed rotation in August, implying,

when combined with the main echo results, that although many irregularities were present during this month their amplitude must have been generally small. From the above considerations, then, it is felt that the minimum in N_c level height may be reasonably placed in July, at least until other data are available to lead to a different conclusion.

We may also obtain an estimate of the time of year at which the maximum height of the N_c level occurs. An inspection of Figs. 9 and 10 will show a maximum in the percentage of coupling echo observations with right-handed rotation in November, while the percentage of main echo observations having high tilt angles shows no maximum at all, unless possibly in December (night-time main echo data were too few in January to obtain a check on the latter). The reason for this discrepancy is not well understood at this time, since, although it may again imply a large number of low amplitude disturbances, a corresponding increase in ionospheric storminess index is not observed in Fig. 11. However, bearing in mind the coupling echo results we shall tentatively, at least, place the maximum in N_c level height in November, with the reservation that additional data from other sources may change this conclusion.

Having obtained a seasonal variation in the height of the N_c level, an attempt was made to break down the data on percentage of occurrence of the above phenomena by hours, in order to obtain additional data on the diurnal variation of this level. The results of this breakdown for percentage of main echo data with high tilt angles are shown in Fig. 12, and show a general tendency for a maximum percentage to occur in the hours shortly after midnight. This is what would be expected on the basis of a study of night-time recombination, with a vertical electron drift having a noticeable effect towards morning, both of which will be discussed in more detail in Section 3. A tendency for a secondary maximum before midnight may be observed in the curves for October to December, but since the variations for these months, in general, are much "flatter" throughout the night than for July to September, it is felt that the significance of this secondary maximum is questionable. An hourly breakdown of the percentage of coupling echo observations showing right-handed rotation was also carried out, but because of a general scarcity of data the results showed no significant diurnal tendencies, and it is felt that no useful purpose would be served by presenting them here.

VOL. 7 1955

D. *Summary of Conclusions from Experimental Results*

The conclusions reached above may be summarized as follows:

1. The excellent correlation between the appearance of the coupling echo and occurrence of high tilt angles for main echo indicates that both phenomena may be attributed to the same cause.

2. Both of the above phenomena may be satisfactorily explained by the coupling effects investigated theoretically in the preceding paper.

3. The irregular manner in which both high and low main echo tilt angles are observed on any given night may be explained by the presence of travelling disturbances at or near the coupling level.

4. There is a seasonal variation in the average height of the N_c level, with an increase of this height from summer to winter months. For the latter half of 1953, the minimum and maximum of this height variation are placed at about July and November, respectively.

5. There is a diurnal variation in the average height of the N_c level, with an

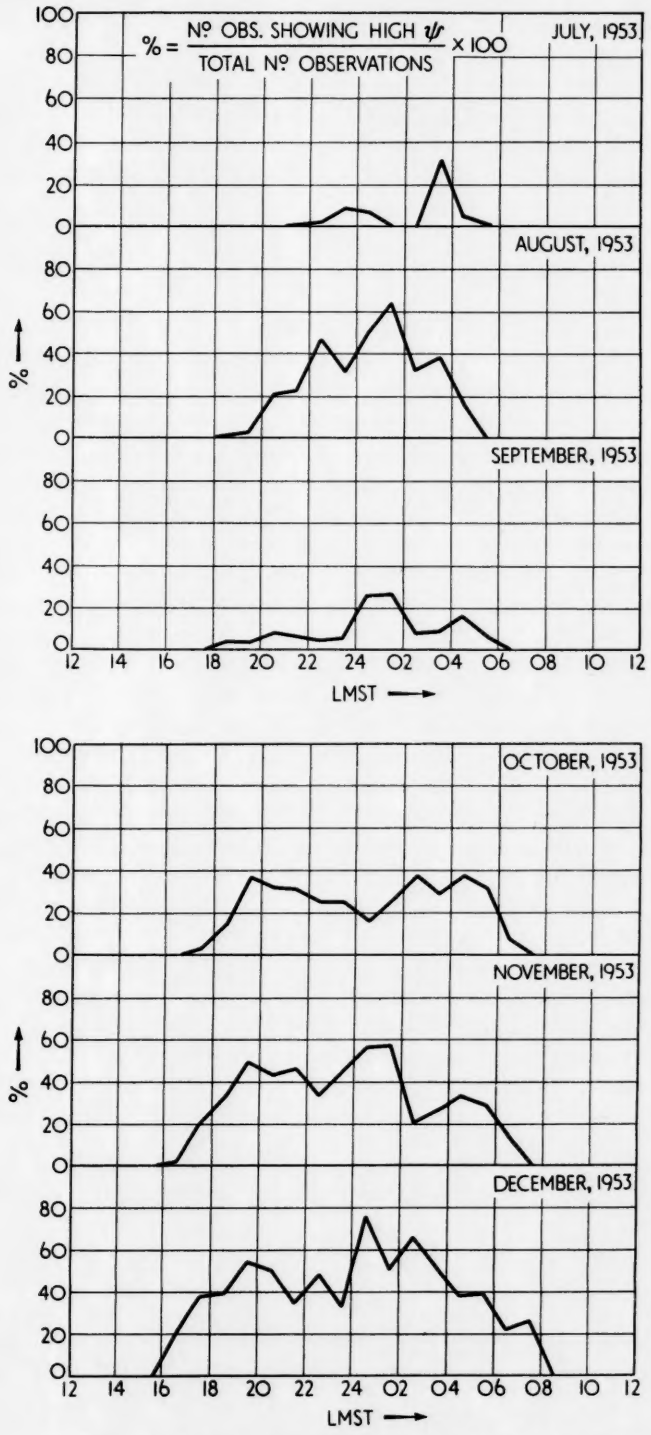

Fig. 12. Hourly percentages of night-time main echo observations with high tilt angles.

increase after sunset which levels off shortly after midnight, and then a decrease again towards morning.

6. The night-time *D*-region has a fairly high electron density gradient at the coupling level, with a value between that of the Jones-Mitra models and the Chapmanlike model, but somewhat closer to the latter. The shape of the night-time *D*-layer in the coupling region should be somewhat similar to that of the Chapmanlike model.

3. Determination of a Night-time *D*-Region Model

A. *Procedure*

The final phase of the study of coupling phenomena which has been under way at this Laboratory for the past several years is a correlated analysis of experimental and theoretical results in the hope of obtaining additional information concerning the physical characteristics of the lower night-time ionosphere. This has already been carried out, in part, in arriving at the conclusions regarding coupling phenomena stated in Section 2. The purpose of this section is to continue the analysis with the object of proposing a night-time model of the *D*-layer.

In proposing such a model, several factors must be considered in addition to the coupling results obtained above. These must include night-time recombination coefficient, the effect of vertical transport of electrons, any other low-frequency data which may be available, and the effect which the variation in electron density due to the solar cycle may have upon correlation of data. With all of these factors to consider, it is essential that the number of variables be reduced as much as possible. The procedure of obtaining the desired model will, therefore, be carried out along the following lines: A night-time recombination coefficient model will be chosen which is considered the best available at the present time. This will be assumed to be constant, although there is actually some dependence upon the sunset electron density model used, and this assumption will, therefore, be discussed further below. A sunset electron density model for the *D*-region will then be obtained by essentially a trial and error method which, upon application of the night-time recombination coefficient model, yields variations of electron densities with time which provide a good fit with the experimental data available. The resultant model, and its variation with time, will then be proposed as a provisional *D*-region model, subject to modifications which may be indicated by future work.

VOL. 7 1955

B. *Night-time Recombination Coefficient*

In general, it is possible to express the variation of electron density with time by the equation

$$\frac{dN}{dt} = q - \alpha N^2 \tag{3.1}$$

where N is the electron density, q the effective rate of electron production, and α the effective recombination coefficient. At night, the rate of electron production,

neglecting effects due to cosmic rays and meteors, is zero, so that equation (3.1) reduces to

$$\frac{dN}{dt} = -\alpha N^2 \tag{3.2}$$

The Mitra-Jones models (Figs. 4 and 6 of the preceding paper) were obtained by the use of this equation. However, although the recombination coefficients used in these calculations were considered to be functions of height, they were assumed to be constant in time, an assumption which is not true according to

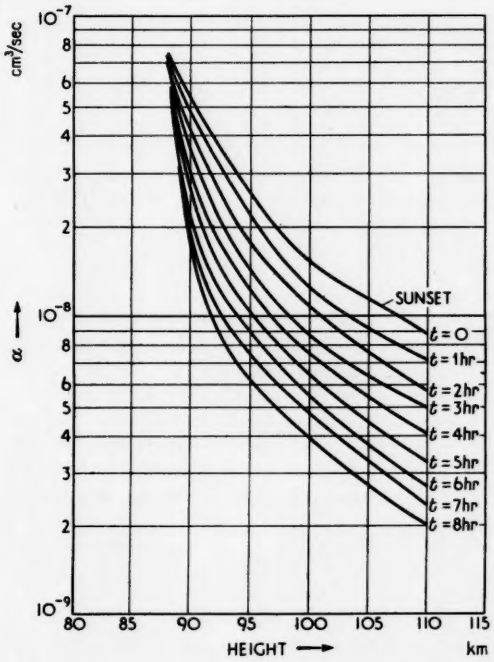

Fig. 13. Time-varying night-time recombination coefficient (after MITRA).

available experimental evidence. Recently, MITRA (1954a) has investigated this problem both from the experimental and theoretical point of view. Using the results of absorption measurements at 150 kc/sec and on 18·3 mc/sec cosmic radio noise, night-time *E*-region critical frequencies, phase height measurements at 16 and 150 kc/sec, and virtual height measurements at 50 and 150 kc/sec, he obtained a recombination model based on these experimental data which varied with time as well as height. Proceeding to an investigation of the general theory of night-time recombination in the lower ionosphere, including the effects of all positive and negative ions, he showed that time- and space-varying night-time recombination coefficients were obtained which agreed with these experimental results. The numerical values for the recombination coefficient, however, were dependent upon the sunset model of electron density initially assumed. Two

theoretical recombination coefficient models were thus calculated, one for the theoretical sunset electron density model from which models 1 to 4 used in the theoretical calculations of coupling phenomena were obtained, and the other for a sunset model based on 16, 50, and 150 kc/sec experimental observations. Since these same data will be utilized later in order to obtain our provisional *D*-region model, the second recombination coefficient model, shown in Fig. 13, will be accepted as more nearly representing actual conditions. The *D*-region model which will finally be proposed does not differ too much from that which MITRA assumed; in view of this, and of the uncertainties in the experimental data, the procedure of considering the accepted recombination coefficient model to be independent of the assumed sunset electron distribution, as outlined above, is considered justified.

One other factor must be considered before proceeding to a determination of a night-time *D*-region. Experimental observations at various frequencies have shown that the apparent height of reflection begins to decrease some time after midnight, but before the time of sunrise in the layer. This is an effect which cannot be explained by recombination alone, since it would require a negative value for the recombination coefficient. Now, horizontal electron motions called ionospheric "winds," similar to but distinct from the travelling irregularities previously discussed, have been observed in the upper atmosphere for some time (see, for instance, MILLMAN, 1951 and 1952). If the effect of the earth's magnetic field upon these horizontal winds is considered, it is found that the resultant electron velocity has an appreciable vertical component. A vertical drift of electrons is thus produced which may cause an overall distortion of the otherwise static layers. PEIFFER and MITRA (1955) have shown that the experimental observations may be explained by such a vertical electron drift, having a velocity of the order of 1–5 km/hr, which reverses in direction sometime after midnight. Also, in obtaining his theoretical models of recombination coefficient, MITRA (1954a) estimates that the effect of this vertical transport does not become appreciable in comparison with normal recombination effects until the recombination coefficient falls to a value of the order of 10^{-9} cm^3/sec. From Fig. 13, we see that this will again occur sometime shortly after midnight at heights of 90–100 km. In checking our night-time *D*-layer model for agreement with experiment, then, we shall concentrate upon the period from sunset to shortly after midnight, with the observation that the reversal of direction of movement of a given electron density level after this time may be satisfactorily explained by PEIFFER and MITRA's analysis.

VOL. 7 1955

C. *Experimental Data Available for Comparison*

In addition to satisfying the conditions deduced from coupling phenomena in Section 2, our proposed night-time *D*-region model must also agree with other low-frequency data which may be available for comparison. These may be divided into two groups, depending upon whether diurnal or seasonal variations are indicated. A further sub-division may then be made according to the type of data from which the diurnal and seasonal variations are obtained.

1. *Data indicating diurnal variations*

(a) *Phase height measurements*—Extensive measurements have been made in England of changes in the apparent height of reflection of low-frequency waves by observations of the changes in phase of the received signal. Most of this work has been done at a frequency of 16 kc/sec, although more recently experimental programmes at 30, 43, and 65 kc/sec have been reported. In a paper by BRACEWELL *et al.* (1951), the variations in the phase of the downcoming wave are given for

thirty-eight days between 28 June 1948 and 7 August 1948. By making measurements on a slightly different frequency from time to time, and comparing the difference in phase accompanying the known change in frequency, these workers have

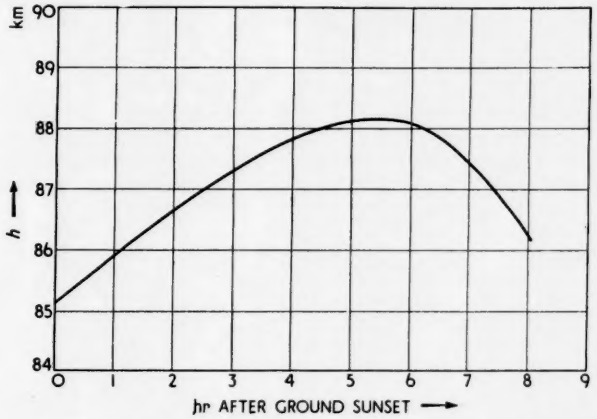

Fig. 14. Variation of apparent 16 kc/sec reflection height as a function of time after ground sunset (after BRACEWELL *et al.*).

also been able to measure the "actual" height of reflection. Fig. 14 shows a smooth curve obtained from the measurements during the above period. Further results at 16 kc/sec, giving only the change in apparent height with time, have been

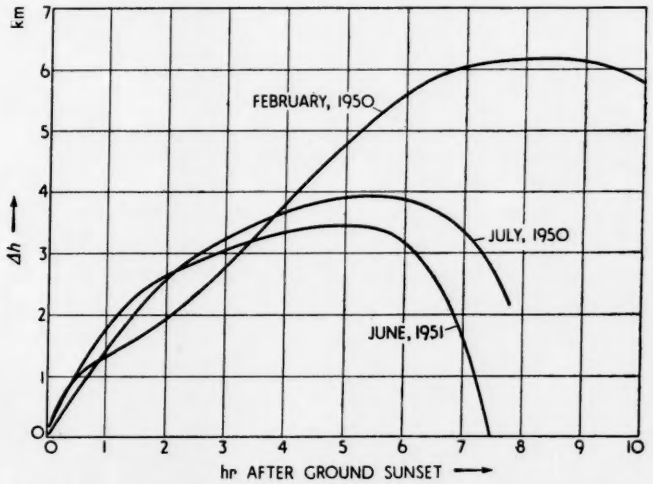

Fig. 15. Monthly average change in apparent 16 kc/sec reflection height as a function of time after ground sunset (after HOPKINS and REYNOLDS).

reported very recently by HOPKINS and REYNOLDS (1954). Curves taken from their results, giving the monthly average change in apparent reflection height with time for February and July 1950 and June 1951, are shown in Fig. 15.

Phase height results have also been reported by BAIN *et al.* (1952) at 16 kc/sec, BRACEWELL, HARWOOD, and STRAKER (1954) at 30, 43, and 65 kc/sec, and by WEEKES and STUART (1952) at 70 and 113 kc/sec. The curves given by all of these workers, unfortunately, are for isolated days; no monthly average results are shown and their data is, therefore, of little use for our purpose.

It will be noticed, on inspecting the curves obtained from HOPKINS and REYNOLDS' data (Fig. 15), that the curve for February 1950 shows a variation of reflection height with time which is definitely not similar to the curves for July 1950 and June 1951. The latter, however, are quite similar to the results obtained from BRACEWELL *et al.* (Fig. 14). It is believed that this second type of curve, rather than that for February 1950, represents typical behaviour, and the February 1950 data, therefore, will not be included in the comparisons to be made later in this section.

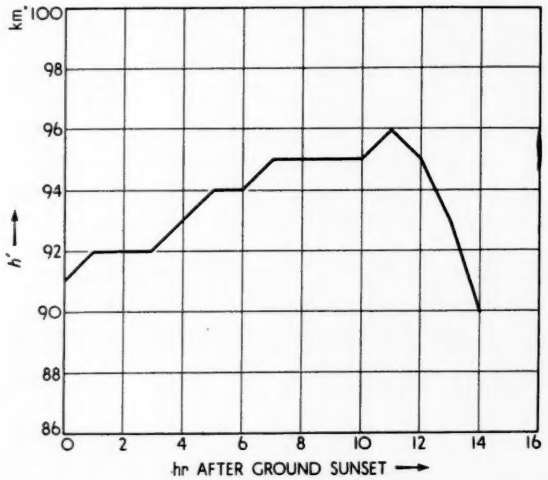

Fig. 16. Average 50 kc/sec group height, for January–April, 1950, as a function of time after ground sunset (after BROWN and WATTS).

(b) *Virtual height pulse measurements*—Although little work has been done at very low frequencies by the pulse method of radio sounding, BROWN and WATTS (1950, 1954) have obtained a few results from measurements of this type at a frequency of 50 kc/sec. The first reference gives preliminary results obtained over a one-day period; the second gives average group heights for the period January–April 1950, as shown in Fig. 16. Group height measurements have also been made by HELLIWELL *et al.* (1950) at 100 kc/sec, but since split night-time echoes are observed at this frequency, and their results do not differentiate between coupling and main echoes, the use of any average heights obtained from these data would be questionable. LINDQUIST (1953) has reported the results of group height measurements at 150 kc/sec; while these data pertain to the lower *E*-layer, which is somewhat outside of the region of interest in this paper, his results will be useful in determining the shape of the transition region between the *D*- and *E*-layers by giving the seasonal variation of the 150 kc/sec reflection point at sunset. This will be discussed further below.

VOL. 7 1955

2 *Data indicating seasonal variations*

(a) *Phase height measurements*—The English workers have also given results from which some idea of the seasonal variation of reflection height at sunset may be obtained. BRACEWELL *et al.* (1951) state that the phase heights at 16 kc/sec may be represented by the equation

$$h_\chi = h_{\chi=0} + A(t) \ln (\sec \chi)$$

where h_χ and $h_{\chi=0}$ represent the apparent heights for a sun's zenith angle of χ and 0, respectively. This equation is stated to hold up to $\chi = 85°$, with $A(t)$ varying throughout the year as shown in Fig. 17. BRACEWELL, HARWOOD, and STRAKER (1954) give a similar curve, obtained from measurements at 30 kc/sec, which is also shown in Fig. 17. As stated above, the equation from which these curves

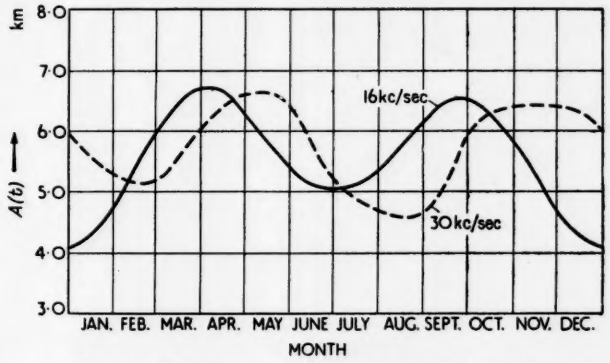

Fig. 17. Seasonal variation of the parameter $A(t)$ in the equation $h_\chi = h_{\chi=0} + A(t) \ln (\sec \chi)$ for 16 and 30 kc/sec.

are obtained holds up to $\chi = 85°$; since the time between $\chi = 85°$ and sunset ($\chi = 90°$) is virtually constant throughout the year, and it would be expected that the phase height curves would be of the same general shape during this interval, Fig. 17 should give us an indication of the seasonal variation of reflection height at sunset. Inspection of the curves shows that the variations are similar both in shape and magnitude, although there is a "phase difference" of about a month between the times of maxima and minima. This cannot be attributed to a variation from year to year, since the observations were made over approximately the same period. It is felt that the 16 kc/sec results are more representative of the actual conditions, since BRACEWELL, HARWOOD, and STRAKER state that their curve for 30 kc/sec has a relatively large probable error. If we average the two sets of results, then, weighing the 16 kc/sec data more heavily than the 30 kc/sec data, we obtain a seasonal variation with a minimum in July and a maximum at about the beginning of November. This is in good agreement with the variation deduced from coupling phenomena in the last section.

(b) *Absorption measurements*—Since most of the absorption at low frequencies is due to the *D*-layer, an investigation of the seasonal variation of absorption at sunset should give us a qualitative idea of the variation in electron density of the *D*-region at this time The results of such an analysis, using 150 kc/sec

data as given by NERTNEY (1953), are shown in Fig. 18. The curve indicates a minimum about November and a maximum near the end of April. Since a minimum absorption indicates a minimum overall electron density and thus a maximum in height of any given electron density, these results are in generally good agreement with those obtained from Fig. 17 and from the data on coupling phenomena.

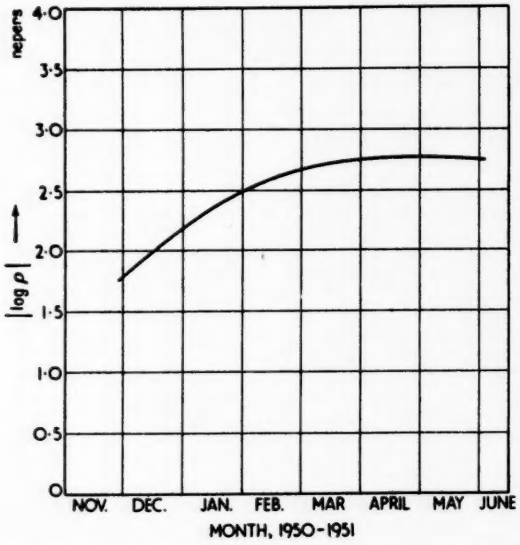

Fig. 18. Monthly variation of 150 kc/sec absorption at ground sunset.

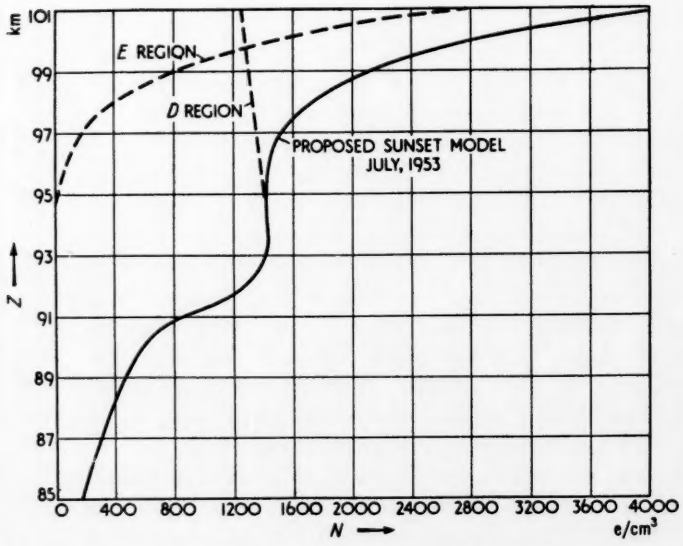

Fig. 19. Proposed sunset model—July 1953.

VOL. 7 1955

D. *The Proposed Model*

Two proposed night-time models, which are actually combined D- and lower E-region models, are shown in Figs. 19 and 20; the variation of these models during the night is shown with a larger scale in Figs. 21 and 22, where $t = 0$ refers to ground sunset. The times of the year for which these models are given correspond to the minimum and maximum of the seasonal variation of the layer as deduced above. Since the accepted models were obtained by a rather lengthy trial and error process, only the final results are given here.

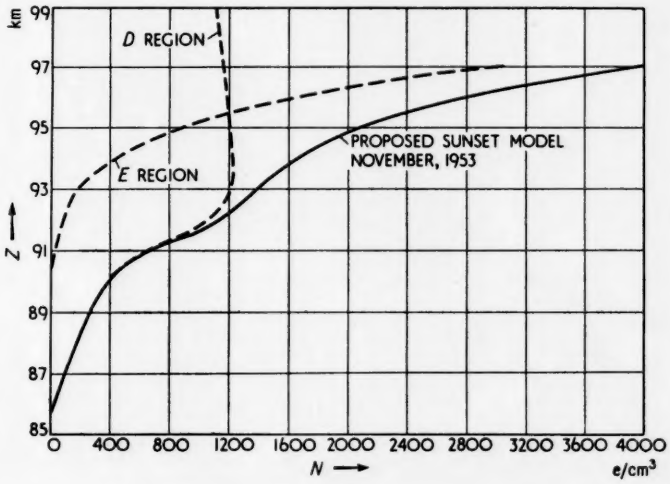

Fig. 20. Proposed sunset model—November 1953.

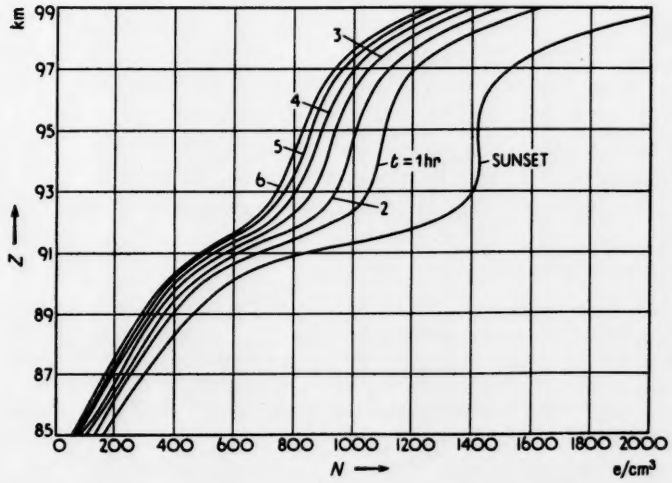

Fig. 21. Variation of July 1953 model with time after ground sunset.

In determining these models, certain approximations and experimental data were used other than those already stated. The diurnal height variation of the electron densities of interest were obtained by the use of the Mitra night-time recombination model of Fig. 13 in the equation

$$\frac{1}{N} = \frac{1}{N_{ss}} + \alpha t \tag{3.3}$$

where N is the electron density at a given height after a time t, and N_{ss} is the sunset value at this height. Equation (3.3) is the solution of (3.2), assuming α to

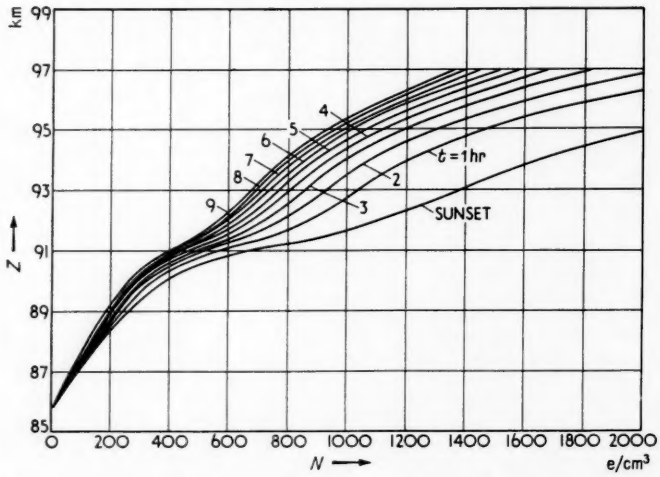

Fig. 22. Variation of November 1953 model with time after ground sunset.

be constant in time; since a time-varying recombination coefficient is to be used, equation (3.3) is obviously not correct. In order to avoid the necessity of using the integral expression which is the true solution of (3.2), however, the geometric average of the recombination coefficient between any two hours was obtained for a given height and the electron densities were calculated from hour to hour by means of (3.3). A check showed that the effective hourly recombination coefficient, which may be evaluated from the true integral solution of (3.2), agrees very closely with the geometric averages actually used in the calculations. In view of the uncertainties in the experimental data, this approximation is considered to be more than adequate.

It must also be remembered that the time $t = 0$ of Fig. 13 refers to sunset in the layer, whereas we are interested in variations starting with ground sunset. At State College, the time between ground and layer sunset is approximately one hour throughout the year. Therefore, calculations for the first hour after ground sunset were made using an effective recombination coefficient obtained by taking the average of the Mitra-Jones (1954) daytime values and the values for $t = 0$ of Fig. 13.

The extension of the models to the lower *E*-region was made utilizing 150 kc/sec group height data (LINDQUIST, 1953) to place the 3000 e/cc level. The

VOL. 7 1955

seasonal variation of the average group height at sunset as obtained from these data is shown in Fig. 23, and gives heights of about 101 km and 97 km for July and November, respectively. These values must be corrected for group delay, which, according to DAVIDS (1952), is of the order of 1 km at this time. His calculations, however, were carried out for a Chapmanlike E-region, and a somewhat smaller group delay would be expected for the Jones E-layer, which is sharper on the bottom. Considering this fact, and also the variation in electron density due to the solar sunspot cycle (to be discussed in more detail below), the 3000 e/cc point was finally placed at about 100·2 km and 96·2 km for the two months of interest.

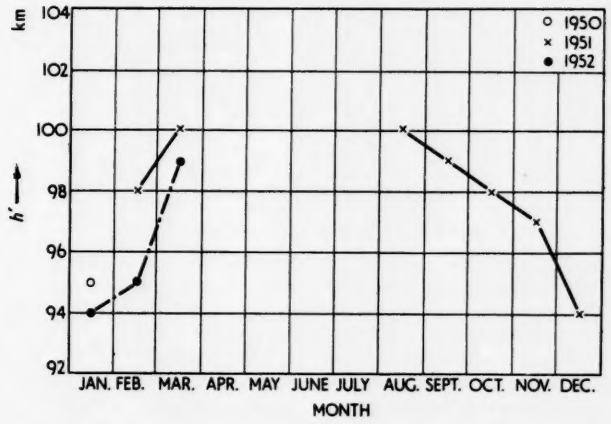

Fig. 23. Seasonal variation of average 150 kc/sec group height at ground sunset.

In order to compare the diurnal variations of reflection heights obtained from the proposed models with the above experimental data, it is necessary to consider the variation of electron density due to the solar sunspot cycle. Although few data are available on this variation for the D-region, MITRA (1952) gives an ionization change from sunspot maximum to minimum of 2·7 to 1 in summer and 1·4 to 1 in winter. According to BENNINGTON (1954), the last sunspot maximum occurred in May 1947, with a minimum predicted for about the middle of 1954. Lacking further information, we shall assume that the variation in D-region electron density with the solar cycle is approximately linear; then the level with 280 e/cc (16 kc/sec reflection point) at sunset in the summer of 1948 should have an electron density of about 230 e/cc in the summer of 1950, about 200 e/cc in the summer of 1951, and about 150 e/cc in the summer of 1953. Similarly, the level with 960 e/cc (50 kc/sec reflection point) at sunset in November 1950 should have an electron density of about 830 e/cc in November 1953. These values enable us to correct the 1953 models to the years in which the data used for comparison were obtained.

One other correction should be discussed before the final comparison with experiment is made. The results obtained at 50 kc/sec were pulse measurements, and consequently we must consider the problem of group delay, as was done for the 150 kc/sec group height data. From

Fig. 17, we see that if the 960 e/cc level has a seasonal variation similar to that for 280 e/cc, it should decrease in height from November to February (the middle of the period during which the 50 kc/sec data were obtained) by about the same amount as it increases in height from July to November. From Figs. 19 and 20, this would be about $\frac{1}{2}$ km. Now if we assume, again for lack of data, that the group delay is of the order of 1 km at sunset, the measured group heights at

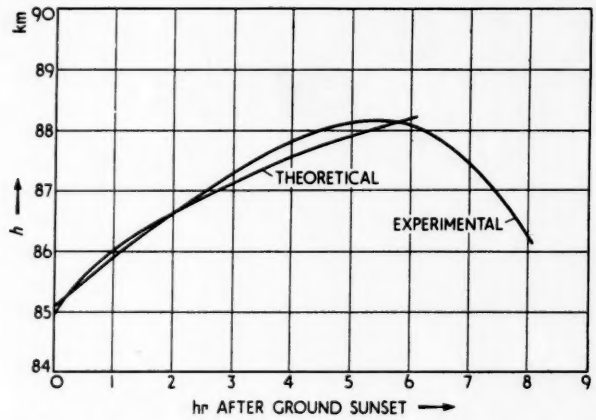

Fig. 24. Comparison of 16 kc/sec reflection level variation of proposed summer model, adjusted to 1948, with observed 16 kc/sec phase height variation.

VOL. 7 1955

50 kc/sec during the period when data were obtained should just about coincide with the heights of the true reflection level during the preceding November, at least to within the accuracy of the measurements themselves. In making our comparison with experiment, therefore, the height of the 960 e/cc level, after correction is made for the solar cycle, will be compared directly with the 50 kc/sec group heights of Fig. 16.

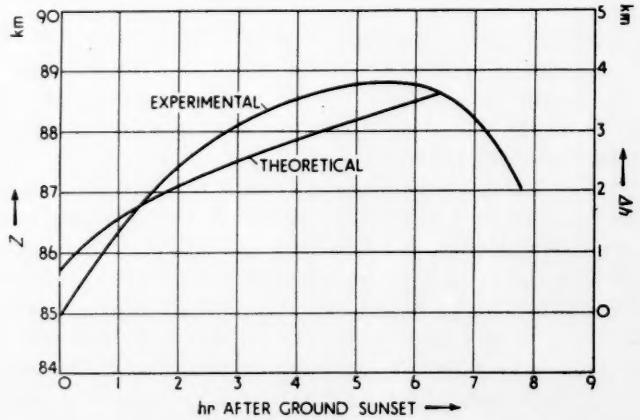

Fig. 25. Comparison of 16 kc/sec reflection level variation of proposed summer model, adjusted to 1950, with observed 16 kc/sec phase height variation.

Adjusting the proposed models to the years in which the experimental data are available, and applying the Mitra recombination coefficient in the manner described above, we obtain the diurnal variations of the 280 e/cc and 960 e/cc levels shown

in Figs. 24 to 27. The experimental results of Figs. 14, 15, and 16 are superimposed on the theoretical results to facilitate comparison. Inspection of the figures will show that agreement is quite good in all cases, especially when it is

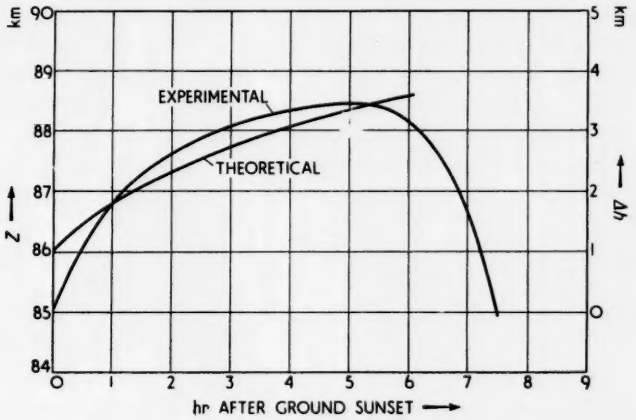

Fig. 26. Comparison of 16 kc/sec reflection level variation of proposed summer model, adjusted to 1951, with observed 16 kc/sec phase height variation.

remembered that the probable error of experimental measurements of these types is seldom less than 1 km.

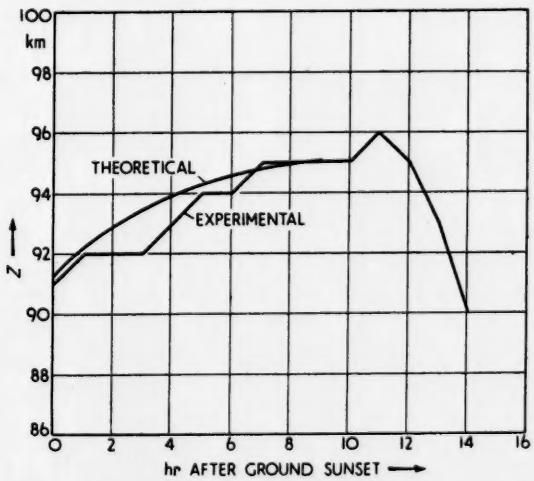

Fig. 27. Comparison of 50 kc/sec reflection level variation of proposed winter model, adjusted to 1950, with observed 50 kc/sec group height variation.

The proposed models thus satisfy the criterion of agreement with other experimental results, and with the conclusions obtained from coupling phenomena data in Section 2, at least as far as diurnal variations are concerned. Seasonally,

the models were chosen to correspond to the minimum and maximum N_c level as deduced above, and an inspection of Figs. 19 to 22 will show that the actual heights of the N_c level agree with the data on coupling phenomena in this respect. The models also show a change in height of the 16 kc/sec reflection point at sunset, from July to November, of 2·4 km; referring to Fig. 17, we note that this value agrees quite well with the observed 16 kc/sec phase height variation. Finally, we must compare the shape of the models near the critical levels with the conclusions in Section 2. Since the N_c levels for the November model are closer to the critical point than those of the July model, the former will be used for comparison. Fig. 28 shows the November model in the coupling region for ground sunset and, nine hours later, together with the Chapmanlike critical coupling

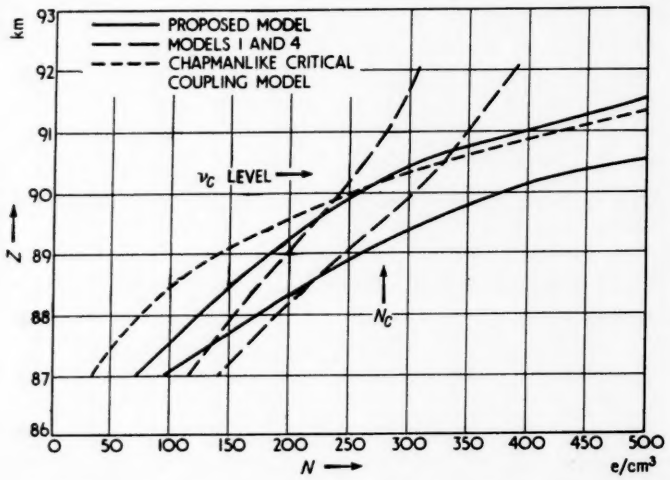

Fig. 28. Comparison of proposed model with models used for theoretical investigations.

model and the Jones-Mitra Models 1 and 4 which were used in the theoretical calculations. It will be noted that the proposed model has a slope whose value is between that for the Jones-Mitra models and that of the Chapmanlike model, but closer to the latter. Also, the proposed model has a shape near the critical levels which is much more similar to the Chapmanlike model than the Jones-Mitra models. If we refer to Section 2D, we find that these results are in excellent agreement with the conclusions obtained from the coupling phenomena data.

4. Summary and Conclusions

The experimental programme for the investigation of coupling phenomena at 150 kc/sec extended from 19 March 1953 to 26 January 1954. Sample data plots are presented to illustrate the type of data obtained. Average curves of tilt angle, ellipticity angle, and mode ratio, for both main and coupling echo, are shown. It is pointed out that "abnormal" high night-time tilt angles are observed for main echo, and data corresponding to these observations are averaged and presented separately.

VOL. 7 1955

An excellent correlation was obtained between the observation of high night-time main echo tilt angles and the appearance of the coupling echo. This correlation, together with a comparison of the theoretical and experimental results on coupling phenomena, allow the following conclusions to be made:

1. The occurrence of high night-time tilt angles for the main echo and the appearance of the coupling echo may be attributed to the same cause.

2. These phenomena may be satisfactorily explained by the results of the theoretical investigation of coupling effects.

3. The irregular manner in which both high and low main echo tilt angles occur on any given night may be explained by the presence of travelling disturbances at or near the coupling level.

4. There is a seasonal variation in the average height of the N_e level; for the last half of 1953, the minimum and maximum of this height variation are placed at about July and November, respectively.

5. There is a diurnal variation in the average height of the N_e level, with an increase after sunset which levels off shortly after midnight, and then a decrease again towards morning.

6. The night-time *D*-region has a fairly high electron density gradient near the coupling level. The shape of the *D*-layer in this region should be similar to that of the Chapmanlike model used in the theoretical calculations.

From these conclusions, and experimental data obtained elsewhere at other low frequencies, it has been possible to propose sunset *D-E* region models for July and November 1953. The variation of these models throughout the night has been determined by the use of a theoretical night-time recombination coefficient suggested by MITRA. Good agreement is obtained between the diurnal and seasonal variations of the proposed models and all available experimental data.

Acknowledgements—I wish to express my appreciation to Drs. A. H. WAYNICK, N. DAVIDS, and J. J. GIBBONS for their advice and guidance in the course of this work, and to other members of this Laboratory for their helpful advice and criticism.

Portions of this work are to be submitted in partial fulfilment of the requirements for the Ph.D. degree in the Department of Physics, the Pennsylvania State University.

REFERENCES

BAIN, BRACEWELL, STRAKER, and WESCOTT	1952	*Proc. Inst. Elect. Eng.* (*London*), Monograph No. 37
BENNINGTON, T. W.	1954	*Wireless World* **60,** 66
BRACEWELL, BUDDEN, RATCLIFFE, STRAKER, and WEEKES	1951	*Proc. Inst. Elect. Eng.* (*London*) **98,** 221
BRACEWELL, HARWOOD, and STRAKER	1954	*Proc. Inst. Elect. Eng.* (*London*) **101,** IV, 154
BROWN, J. N., and WATTS, J. M.	1950	*J. Geophys. Res.* **55,** No. 2, 179
BROWN, J. N., and WATTS, J. M.	1954	Private communication to A. P. Mitra (See Mitra, 1954a)
DAVIDS, N.	1952	*J. Atmosph. Terr. Phys.* **2,** 324
DAVIDS, N., and PARKINSON, R. W.	1955	*J. Atmosph. Terr. Phys.* **7,** 175

HELLIWELL, MALLINCKRODT, KRUSE, and WAMBSGANSS	1950	Pulse Studies of the Ionosphere at Low Frequencies, *Electronics Research Laboratory*, Stanford University, California
HOPKINS, H. G., and REYNOLDS, L. G.	1954	*Proc. Inst. Elect. Eng.* (*London*) **101,** III, 21
JONES, R. E.	1955	Accepted for publication in *J. Atmosph. Terr. Phys*
KELSO, NEARHOOF, NERTNEY, and WAYNICK	1951	*Ann. Geophys.* **7,** 215
LINDQUIST, R.	1953	*J. Atmosph. Terr. Phys.* **4,** 10
MILLMAN, G. H.	1951	*Ann. Geophys.* **7,** 272
MILLMAN, G. H.	1952	*Ann. Geophys.* **8,** 365
MITRA, A. P.	1954a	Nocturnal Recombination Processes in the Lower Ionosphere, Scientific Report No. 68, *Ionosphere Research Laboratory*, State College, Pennsylvania
MITRA, A. P.	1954b	*J. Atmosph. Terr. Phys.* **5,** 28
MITRA, A. P., and JONES, R. E.	1954	*J. Geophys. Res.* **59,** No. 3, 391
MITRA, S. K.	1952	*The Upper Atmosphere*, 2nd ed., The Asiatic Society, Calcutta
NERTNEY, R. J.	1953	*J. Atmosph. Terr. Phys.* **3,** 92
NICOLET, M.	1953	*J. Atmosph. Terr. Phys.* **3,** 200
PARKINSON, R. W.	1955	Accepted for publication in *Rev. Sci. Instrum.*
PEIFFER, H. R., and MITRA, A. P.	1955	The Effect of Vertical Ion Transport on the Night-time *E*-Region, accepted for publication in *J. Atmosph. Terr. Phys.*
PIERCE, J. A., and MIMNO, H. R.	1940	*Phys. Rev.* **57,** No. 2, 95
RYDBECK, O. E. H.	1944	*Trans. Chalmers Univ. Gothenberg*, No. 34
SCHRAG, R. L.	1955	A Method for Studying Large-Scale Irregularities in Region *E* of the Ionosphere, to be published in *Proceedings of the Physical Society Conference on the Physics of the Ionosphere*
WEEKES, K., and STUART, R. D.	1952	*Proc. Inst. Elect. Eng.* (*London*), Monograph No. 15, **99,** IV

VOL. 7 1955

Journal of Atmospheric and Terrestrial Physics, 1955, Vol. 7, pp. 235 to 243. Pergamon Press Ltd., London

Observations of the effects of ionospheric storms over a North Atlantic Circuit

T. W. Bennington
(The British Broadcasting Corporation, Kingswood Warren, Surrey)

(*Received* 18 *February* 1955)

ABSTRACT

From six months' observations of the signals of WWV Washington at Tatsfield, the median MUF for the Washington-Tatsfield circuit, for both the normal and disturbed propagation periods of each month, has been deduced, by a method based on the fact that the median MUF is the frequency below which signals are propagated for 50 per cent of the time in a given period.

Graphs are given which show, for each hour of day, the percentage reduction in the median MUF caused by ionospheric disturbances during the summer, equinox, and winter, this quantity representing the severity of the disruptive effects upon communications. These effects are shown to be far more severe during the period from about 0700 to 1100 LT than at other times of day. This result, obtained from data on the reception of obliquely incident waves, is in good correspondence with the findings of Appleton and Piggott, obtained from vertical incidence data, from which it appears to be due to a tendency for the disturbances to be most intense at these times.

At other times of day the severity of the disruptive effects is conditioned, not only by the intensity of the disturbances, but also by the value of the normal MUF at the time. Thus the effects are more severe during night than during day at all seasons, but more particularly during the winter night, when the normal MUF is particularly low.

Introduction

Ionospheric storms have been the subject of a great deal of investigation, most of which has been concerned with the physical causes of the disturbances, or with the nature of the effects in the ionosphere itself. The data used for this purpose have usually been the vertical incidence measurements of virtual heights and critical frequencies obtained at specific locations on the earth's surface.

It was thought that useful information about the effects of ionospheric storms upon practical radio communication might be obtained from regular observations of signals received at oblique incidence upon fixed frequencies over the North Atlantic transmission path. It has long been known that the most serious effect of an ionospheric storm is to cause the maximum usable frequency (MUF) for a circuit to become considerably lower than its normal value, another effect being that of an increase in ionospheric absorption, so that the lowest usable frequency (LUF) becomes higher than normal. It was the extent and nature of the first of these two variations which it was primarily desired to examine.

Data Used and Definition of Disturbed Periods

The basic data used in the investigation consisted of a series of observations made at the B.B.C. Receiving Station at Tatsfield, Surrey, during the last six months of 1953, upon the signals of WWV, the Standard Frequency Station at Washington, U.S.A. The transmission path WWV to Tatsfield traverses a region relatively near to the northern auroral zone, and thus it is particularly susceptible to the effects of ionospheric disturbances.

The Tatsfield observations were made at hourly intervals upon the fixed frequencies of 5, 10, 15, and 20 Mc/s used by WWV, and cover the period July–December, which thus includes a complete seasonal change in propagation conditions near the sunspot minimum period.

The data consisted of hourly field-strength measurements on the four frequencies, among these being many zero values obtained when the field was unmeasurably low, or else completely absent. At both transmitting and receiving locations vertical omni-directional aerials were used. For the purposes of this investigation the data were dealt with in the following way, the method being an adaptation of one used by J. W. C. SCOTT (HANSON, SERSON, and CAMPBELL, 1953).

If, for any period, the number of cases of zero field on the higher frequencies is counted for every hour of day and for each frequency, then, for any given frequency, the hour at which the number of zeros equals half the total count is the hour at which that frequency is the median MUF for the circuit. This is because the median MUF is defined as the frequency which is propagated (i.e., which does not penetrate the ionosphere) at any hour of day, for half the days of a given period. Thus the monthly median MUF is the frequency which conforms to these conditions at each hour of day, for half the days of a month. It should be noted that the actual strength of the signals does not affect this consideration, for, apart from the small effect of deviative absorption, signals just below the MUF should be efficiently propagated. The weaker signals should occur on frequencies so far below the MUF that the effects of non-deviative absorption become apparent.

It might have been possible, from a similar count of zeros for the observations on the lower frequencies, to determine the median LUF for the circuit, on the assumption that the median LUF is the frequency above which, at any hour, good signals are received for half the days of a given period. On frequencies below this, signals would be absent due to the effects of non-deviative absorption as mentioned above. But it is difficult to determine a realistic value for the LUF in this way, for the practical LUF is dependent on a number of factors, such as transmitter power, directivity of aerials, atmospheric noise, type of service, etc., as well as upon the absorption. Apart, therefore, from obtaining an *estimate* of the LUF in this way, nothing further was attempted.

It was desired, for this examination, to obtain the median MUF for the circuit for two separate periods during each month: firstly, for the periods when ionospheric conditions were undisturbed, and secondly, for the periods when ionospheric storms were in progress. It was necessary, therefore, to define these two periods, and the following procedure was adopted:

It has long been known that, when a magnetic disturbance is in progress, the ionosphere is also disturbed, but that the reverse is not necessarily true, because the ionospheric disturbance often persists after the magnetic field has returned to a "quiet" state. It was therefore decided to define the ionospheric disturbances by the use of Abinger magnetic data, in conjunction with the short-wave "disturbance ratings"—indicative of ionospheric disturbance—compiled at Tatsfield, in the following way.

The Abinger data is issued in the form of three-hourly 'K' figures—ranging from 0 (quiet) to 9 (highly disturbed)—and also as daily character numbers—ranging from 0·0 (quiet) to 2·5 (highly disturbed). Magnetic disturbances were considered to be in progress on all days when the daily character number was 1·0 or greater. The time of the start or end of the disturbance was taken to be the start

VOL. 7 1955

Table 1

Month	*Normal periods (GMT)*	*Disturbed periods (GMT)*	*Normal hours*	*Disturbed hours*	*Percentage of total time disturbed*
July		1st 0000 to 4th 2059		93	
	4th 2100 to 7th 1159	7th 1200 to 9th 2059	63	57	
	9th 2100 to 15th 1159	15th 1200 to 15th 1759	135	6	
	15th 1800 to 23rd 0259	23rd 0300 to 24th 2359	177	45	
	25th 0000 to 25th 2359	26th 0000 to 31st 2359	24	144	
			399	345	46·4
August		1st 0000 to 1st 2359		24	
	2nd 0000 to 9th 1159	9th 1200 to 13th 2359	180	108	
	14th 0000 to 22nd 2359	23rd 0000 to 31st 2359	216	216	
			396	348	46·7
September		1st 0000 to 6th 1759		138	
	6th 1800 to 15th 1159	15th 1200 to 17th 2059	210	57	
	17th 2100 to 19th 0559	19th 0600 to 25th 1159	33	150	
	25th 1200 to 26th 2359	27th 0000 to 27th 0559	36	6	
	27th 0600 to 30th 2359		90		
			369	351	48·7
October		1st 0000 to 1st 2059		21	
	1st 2100 to 15th 1159	15th 1200 to 25th 1159	327	240	
	25th 1200 to 26th 2359	27th 0000 to 28th 1159	36	36	
	28th 1200 to 29th 1159	29th 1200 to 30th 0259	24	15	
	30th 0300 to 30th 1759	30th 1800 to 31st 1159	15	18	
	31st 1200 to 31st 2359		12		
			414	330	44·4
November	1st 0000 to 5th 1159	5th 1200 to 6th 1759	108	30	
	6th 1800 to 12th 1759	12th 1800 to 24th 2359	144	294	
	25th 0000 to 26th 1759	26th 1800 to 26th 2359	42	6	
	27th 0000 to 30th 2359		96		
			390	330	45·8
December	1st 0000 to 9th 1759	9th 1800 to 16th 1159	210	162	
	16th 1200 to 24th 1759	24th 1800 to 24th 2359	198	6	
	25th 0000 to 31st 2359		168		
			576	168	22·6

or end of the three-hourly period for which the 'K' figure first or last had a value of 4 or more. Checking these periods against the Tatsfield figures showed that the periods were, in fact, periods of poor propagation conditions. At Tatsfield, from regular observations on the signals of North American stations, a check on propagation conditions over the North Atlantic path is maintained. The results are kept in the form of "disturbance ratings"; these take the form of figures ranging from 0·0 (propagation much better than normal) to 4·0 (blackout) which apply to various periods of the day.

The ionospherically disturbed periods were, therefore, defined as follows. The start and end of the period was first considered to coincide with those of the magnetically disturbed periods as defined above. If, however, there appeared a figure of 2·0 (moderately disturbed) or greater in the Disturbance Ratings after the end of a magnetically disturbed period, the ionospheric disturbance was considered to extend to the end of the period to which this figure applied. It is considered, after a check, that, by this means, the ionospherically disturbed periods were quite well defined.

Table 1 lists the periods of normal ionospheric conditions, and those when disturbed conditions prevailed, for the months July to December 1953, inclusive.

In the last column of this Table is given, for each month, the percentage of the total time during which ionospheric conditions were disturbed, and it will be noticed that, apart from the month of December, this amounted to almost half the total time each month. These months were, in fact, unduly disturbed in point of time, owing to the fact that there was a large number of recurring disturbances of the type attributed to the effects of '*M*'-regions on the sun.

VOL. 7 1955

Preparation of Normal and Disturbed MUF Curves

The number of zeros in the Tatsfield observations of WWV field strength was then counted for each frequency at each hour of day. This was done separately for the

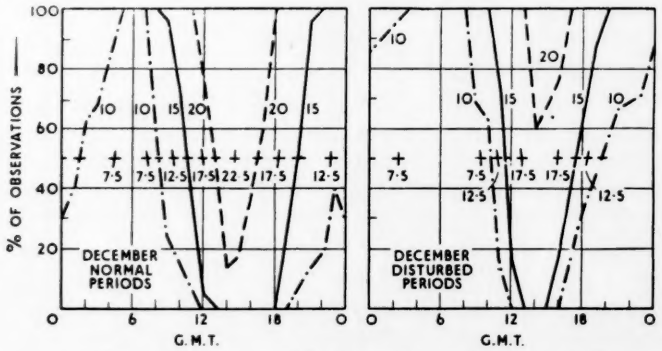

Fig. 1. Percentage of total time for zero field on WWV frequencies 10, 15, and 20 Mc/s.

normal and for the disturbed periods of each month. Graphs of the results were drawn for each period for the three higher frequencies, 10 Mc/s not being used during the midday period when zeros would only have indicated that it was below the LUF. Fig. 1 is an example of such a graph for the month of December

1953. The points where zero field was obtained for 50 per cent of the total observations, during either normal or disturbed periods, were marked by the short horizontal lines for each frequency, and these indicate the time at which that frequency was the median MUF for either the normal or the disturbed period. It was then possible to interpolate for the frequencies of 7·5, 12·5, 17·5, and 22·5 Mc/s. The times and frequencies thus indicated were then transferred to the graphs of Fig. 2, on which the co-ordinates are frequency and time of day. In this way it was possible to draw in the median MUF for both the normal and the disturbed periods for each month.

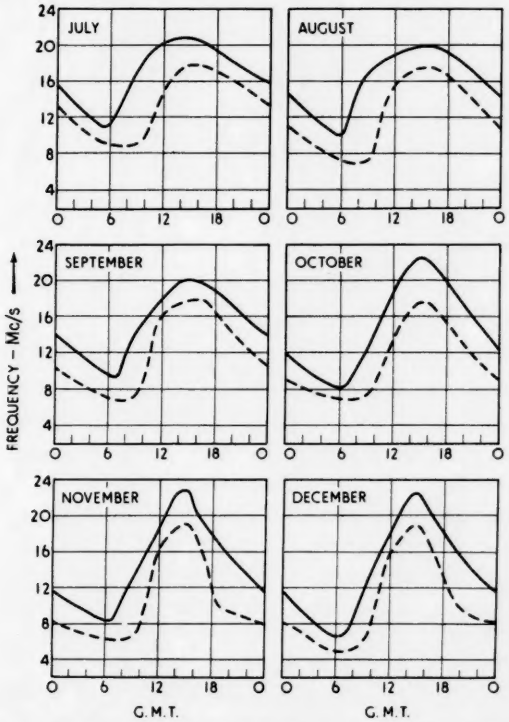

Fig. 2. Monthly median MUF for normal and disturbed periods, as deduced from observations at Tatsfield.

The graphs of Fig. 2 therefore give (as full lines) the median MUF for the normal periods of each month, and (as dashed lines) the median MUF for the disturbed periods, on the basis of the signals received over the Washington-Tatsfield circuit. From this information the practical effect of the ionospheric storms upon short-wave transmission and reception over the circuit can be assessed.

General Effects of the Storms

Fig. 2 shows that, as would be expected, the median MUF for the disturbed periods was, each month, considerably lower than that for the normal periods, at all hours of day. It may be remarked, also, that the estimates of median LUF,

obtained as previously mentioned, indicated that it was, during the disturbed periods, somewhat higher than during the normal periods, as would also be expected.

The most important effect of an ionospheric storm from the communication point of view is the reduction in the MUF, and this is attributed both to a decrease in the ionization of the F_2-layer (as evidenced by a decrease in the measured critical frequency) (APPLETON and PIGGOTT, 1952) and to an increase in the virtual height. It has been found, however, that the storm phenomena in the layer are not exactly the same, either in character or in the time of their occurrence, at all places, and in particular, that there are positive and negative phases to the storms

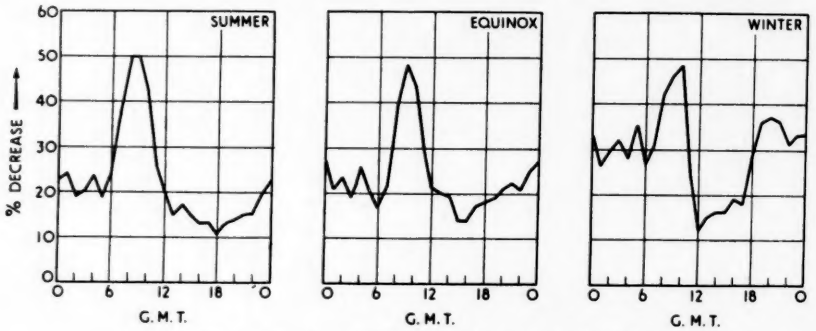

Fig. 3. Mean reduction in MUF, due to ionospheric disturbances, for each hour of day.

(APPLETON and PIGGOTT, 1950). However, in the region traversed by the Washington-Tatsfield transmission path, the negative phase is of principal importance, and it would not appear wrong to expect that, during the whole course of a storm, the ionization would be below normal, and that there would therefore be a marked decrease in MUF.

Fig. 2 indicates that the decrease in MUF on this circuit during disturbances is not the same at all times, but varies considerably both diurnally and seasonally. Since the effects of ionospheric storms are already known to be different during the summer, equinoctial, and winter seasons, the months for which the data were available were grouped accordingly, July and August being considered summer months, September and October equinoctial months, and November and December winter months. Fig. 3 gives the mean reduction in MUF, as a percentage of the normal MUF, for each hour of day during the three two-monthly periods, as obtained from the curves of Fig. 2.

STORM EFFECTS ON THE MUF

The results are presented in this way because the disruptive effects of ionospheric storms upon radio communication may be said to depend, at any time of day and season, not necessarily upon the intensity of the disturbances, but upon the percentage reduction in the MUF which they cause. Thus a given departure from the normal MUF (in Mc/s) will not disrupt communications so much during summer night, when the normal MUF is relatively high, as during the winter night, when it is low. Similarly, though storms may be more intense at the equinoxes,

VOL. 7 1955

their effects may not be so severe as during the winter night, when the normal MUF is so low. The graphs of Fig. 3 may therefore be taken as representing the severity of the effects of the disturbances upon communications.

The outstanding feature of the curves is the large increase in the MUF reduction during disturbances, which is seen to occur between 0700 and 1100 GMT (which is local time at Tatsfield). This occurs at all seasons, varying by a small amount of time from season to season. Thus the storm effects are always much worse during this period than at any other time of day. It may here be remarked that APPLETON and PIGGOTT (1952), in an examination of the statistical relationships for a large number of storms, found that there is a pronounced diurnal control of ionospheric storminess, such that the maximum degree of disturbance occurs between about 0600 LT and somewhat before noon. They show that this applies, not only to the reduced F_2 critical frequencies, but also to the increased virtual heights. Furthermore, they note that storms (negative phases) start most frequently when the local time is 0600 to 0700, with a subsidiary maximum for the starting time between 1800 and 2300 LT. Fig. 3 shows no evening peak in summer or equinoctial periods, but in winter it shows that, between 1900 and 2100 GMT, there is an increase in the MUF reduction due to the disturbances. Altogether, therefore, the times for maximum MUF reduction on the North Atlantic circuit, here found on the basis of actual radio reception over the circuit, appear to be in good correspondence with those for maximum storm effects found from the detailed examination of ionospheric measurements quoted above.

Apart from these periods of maximum MUF reduction, the relative severity of the storm effects on this circuit at different times of day and seasons are rather interesting. Fig. 3 shows that they are least severe during the period 1200 to 2300 LT in summer, 1200 to 2000 LT at the equinox, and 1200 to 1700 LT in winter, hours during which, during each season, the normal MUF is relatively high; so that the period during which the disturbing effects are relatively slight is most prolonged in summer, less so at the equinox, and shortest during winter. During the remainder of the twenty-four hours (mainly hours of darkness), a greater degree of disturbing effect results from the storms, this being of about the same degree in summer and at the equinox, but considerably higher in winter. Thus, apart from the period 0700 to 1100 GMT, the effects of the disturbances are greatest and most prolonged (diurnally) during winter, in spite of the fact that the storms themselves are usually most frequent and intense at the equinoxes. On the North Atlantic circuit, therefore, it would appear that, taken over the whole twenty-four hours, the effects of ionospheric storms upon communications are more pronounced during the winter months than at any other time of year, a fact which would seem to confirm the general experience of engineers on this circuit.

POSSIBLE STORM EFFECTS ON THE LUF

It is not intended here to go far into the measures which might be taken in order to maintain communication during the storms, but it may be suggested that, if the normal working frequency is reduced, at any season or time of day, by the percentages indicated in Fig. 3, then it should be below the MUF on the stormy

days. Good communication would, however, only result if the working frequency were then, at the same time, above the LUF, which itself is increased during the disturbances.

As was mentioned earlier, it was not thought possible, by the process used for finding the MUF, to obtain a precise value for the LUF for the Washington-Tatsfield circuit. But by using the results of the observations on the lower frequencies of 5 Mc/s and 10 Mc/s (the latter only during the midday period) in a similar manner to that described, and illustrated in Fig. 1, it was possible to obtain an estimate of times at which these frequencies became the lowest on which signals could be obtained, owing to the effects of ionospheric absorption, for each month, during both the normal and the disturbed periods. As an example, in order to illustrate the nature of the disturbance effect upon communication, Fig. 4 is given, and it may be remarked that, even if the LUF is only an estimate, the nature of the variation as between the normal and the disturbed periods is correctly indicated. Fig. 4, therefore, shows, as a dashed line, the MUF for the disturbed periods, as a full line the indications of LUF for the normal periods, and, as a dot-dashed line those for the disturbed periods of August 1953. It will

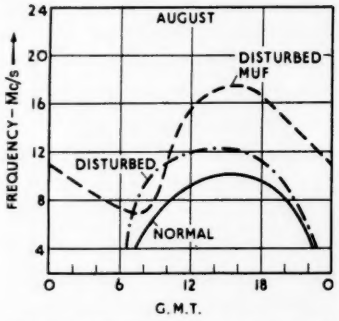

Fig. 4. Nature of LUF variation due to disturbances.

be seen that the increase in the LUF estimates for disturbed periods above those for the normal periods also varied diurnally, ranging from about 0·5 to 3·0 Mc/s over the period when indications were obtainable. Furthermore, that the greatest increase occurred during the period 0700 to 1100 GMT, at the same time that the storm effects in reducing the MUF were greatest, and that for the greater part of this time the disturbed LUF appeared to be greater than the disturbed MUF for the circuit. Summarizing these results, it might be inferred that during disturbed periods it ought to be possible to maintain communication, if the working frequencies were reduced by the percentages shown in Fig. 3, except during the period 0700 to 1100 GMT, when it would be more economical to suspend operations altogether.

Conclusions

(1) The disruptive effects of ionospheric disturbances upon communication over the North Atlantic circuit would appear to be far more severe between 0700 to 1100 LT than at other times of day, because of a tendency for the disturbances to be most intense during those hours.

VOL. 7 1955

(2) Their effects are least severe during the periods 1200 to 2300 LT in summer, 1200 to 2000 LT at the equinoxes, and 1200 to 1700 LT in winter, because, during those times, the normal median MUF is relatively high.

(3) During the remaining hours of day (mainly the dark hours) the effects are more severe than the last-mentioned periods, but particularly so during the winter season, because, at that time, the normal median MUF is particularly low.

Acknowledgements—The author is indebted to Mr. H. V. GRIFFITHS, E.i.C. Tatsfield, for the supply of the data used.

REFERENCES

APPLETON, E. V., and PIGGOTT, W. R.	1950	World Morphology of Ionospheric Storms, *Nature* (*London*) **165,** 130.
APPLETON, E. V., and PIGGOTT, W. R.	1952	The Morphology of Storms in the F_2-layer of the Ionosphere, *J. Atmosph. Terr. Phys.* **2,** 236
HANSON, G. H., SERSON, H. V., and CAMPBELL, W.	1953	Maximum Usable Frequencies and Lowest Usable Frequencies for the Path Washington to Resolute Bay, *J. Geophys. Res.* **58,** 487

Journal of Atmospheric and Terrestrial Physics, 1955, Vol. 7, pp. 244 to 246. Pergamon Press Ltd., London

On the variation of ionospheric absorption at different stations

W. R. PIGGOTT

(Official Communication from D.S.I.R. Radio Research Station, Slough)

(Received 17 February 1955)

ABSTRACT

The possibility that the day-to-day changes in absorption at Slough, Swansea, and Freiburg are identical is examined statistically. After allowing for known sources of error, it is considered that the residual differences in summer months are too small to be significant, but that it is probable that real differences occur in winter. In both cases the minimum probable correlation for the Swansea-Slough comparison is very high—about 0·92.

IN recent papers, RAWER (1951) and BEYNON and DAVIES (1954) have compared measurements of ionospheric absorption made at Slough, Freiburg, and Swansea. The results obtained suggest a rather rapid decrease in the correlation of absorption as measured on 2 Mc/s with distance both in summer and winter This is surprising in view of the generally high correlation with time of day and from day to day (APPLETON and PIGGOTT, 1954) and the presence of well marked 27-day recurrence tendencies at temperate and low latitudes (LANGE-HESSE, 1953). Local variations might well be expected on days of anomalous absorption in winter, since the winter anomaly occurs in local winter in both hemispheres, is not found at low latitudes, and is thus clearly an atmospheric and not a solar phenomenon (DIEMINGER, 1952).

It is therefore worth while enquiring whether the observations can be reconciled with the hypothesis that the actual absorption at the stations was the same, the lack of correlation being ascribed to sampling and other errors.

Let the mean square deviations of the measured absorption at two stations during a given month be σ_x^2 and σ_y^2, and the mean square errors of observation be σ_a^2, σ_b^2 respectively The most probable relation between the measured correlation coefficient, r, and the correlation coefficient with no errors, r_0, is

$$r = r_0[(1 - \sigma_a^2/\sigma_x^2)(1 - \sigma_b^2/\sigma_y^2)]^{1/2}$$

This relation becomes more accurate as the number of observations per month increases. It is difficult to estimate σ_a^2 and σ_b^2 accurately, though the contributions from rapid and focus fading can be easily computed. We shall, therefore, first estimate r_0 after correcting for known errors, and then ask whether the difference between r_0 and 1 can be reasonably ascribed to other sources of error.

BEYNON and DAVIES have given curves from which the standard errors due to fading can be estimated for observations occupying periods up to about half an hour. In addition, an error can be incurred due to the average field of an echo over half an hour being different from that appropriate to the absorption present. Thus observations at night, for which the absolute absorption can be deduced with considerable accuracy (PIGGOTT, 1953), show that the mean echo amplitude averaged over half-hour periods can vary over a range of 2 : 1 while the absorption

VOL. 7 1955

remains constant. A reasonable value of σ^2 for this phenomenon, measured in nepers^2 (n^2), is about 0·06. The sampling errors at Swansea and Slough estimated from BEYNON and DAVIES are $0{\cdot}01n^2$ and $0{\cdot}05n^2$. The mean apparent absorption changes σ_x^2, σ_y^2 at Swansea and Slough are $0{\cdot}40n^2$ and $0{\cdot}45n^2$ in summer, $1{\cdot}00n^2$ and $1{\cdot}71n^2$ in winter, giving $r/r_0 = 0{\cdot}79$ in summer and $r/r_0 = 0{\cdot}93$ in winter, the observed mean values of r being 0·68 and 0·86 respectively.

Examining the data in more detail, we note that, as mentioned by BEYNON and DAVIES, the absolute absorptions for the first two months are not consistent, probably owing to calibration difficulties when starting the sequence. Also the low correlation for April is due to one large discrepancy caused by an error in the published data. Omitting the first two months and correcting the error in April 1951, we get r in summer equal to 0·73. Using this value of r, we find that the minimum probable values of r_0 are 0·92 and 0·93 in summer and winter respectively. Thus, if there are no further sources of error, the incoherent fluctuations at each station are approximately proportional to the day-to-day fluctuations at all seasons. This type of variability is most probable if the day-to-day fluctuations are mainly due to changes in deviative absorption.

The other extreme interpretation is to ascribe the difference between the observed values of r_0 and unity to uncorrected errors. This implies the existence of additional errors at both stations with standard deviations of $0{\cdot}15n$ in summer and $0{\cdot}30n$ in winter. The uncertainty due to changes in the roughness of the ionosphere (PIGGOTT, 1953) is about $0{\cdot}15n$, and unaccountable irregularities of this order are often found when examining diurnal variations at a single station. Thus the summer data may well be consistent with $r_0 = 1$.

There does not seem to be any reason why errors should be greater in winter than summer. Assuming that they are equal in both seasons, we must attribute the difference to real changes in the ionosphere. We then find that the winter results imply $r_0 = 0{\cdot}94$, the standard deviation (S.D) of the uncorrelated absorption changes, assumed equal at both stations, being about $0{\cdot}26n$. Thus both extreme interpretations suggest that the winter correlation was about 0·93, the uncorrelated fluctuations having S.D's between $0{\cdot}25n$ and $0{\cdot}30n$, whereas the summer correlation may lie between 0·92 and 1·00. In both seasons the probable correlation is very high, and the residual discrepancies small compared with the total absorption observed, $3n$ to $8n$.

Turning to the Freiburg-Slough comparison, we note that the correlation for 2 Mc/s is expressed in "correlation numbers" which cannot be directly corrected by our methods. However, in view of the enormous range of correlation number found, from $-0{\cdot}34$ to 0·68 in summer and from $-0{\cdot}22$ to $+0{\cdot}99$ in winter, the differences between correlation coefficients and correlation numbers is insignificant. The large range suggests the presence of discrepancies in deducing the absorption comparable with the day-to-day changes in absorption in summer, i.e., about $0{\cdot}35n$ (0·7 : 1 in amplitude of signal.) The mean and median correlation numbers are 0·20 and 0·22 in summer, 0·71 and 0·81 in winter. The high average correlation in winter, when the day-to-day absorption changes are large enough to swamp such errors, supports this deduction. If the discrepancies are as large as suggested above in both winter and summer, the correlation coefficient r_0 in winter will be

considerably increased. We may conclude that we cannot draw firm conclusions from this comparison until it is clear that the discrepancies are not due to the fundamentally different techniques in use at the two stations.

Thus the statistical evidence in favour of a low correlation between the absorption at stations separated by up to 800 km is not convincing, though, of course, some examples of widely differing conditions must occur.

Acknowledgement—The work described above was carried out as part of the programme of the Radio Research Board, and this note is published by permission of the Director of Radio Research of the Department of Scientific and Industrial Research.

REFERENCES

APPLETON, E. V., and PIGGOTT, W. R.	1954	Ionospheric Absorption Measurements during a Sunspot Cycle, *J. Atmosph. Terr. Phys.* **5**, 141
BEYNON, W. J. G., and DAVIES, K.	1954	Simultaneous Ionospheric Absorption Measurements at Widely Separated Stations, *J. Atmosph. Terr. Phys.* **5**, 273
DIEMINGER, W.	1952	On the Causes of Excessive Absorption in the Ionosphere on Winter Days. *J. Atmosph. Terr. Phys.* **2**, 340
LANGE-HESSE, G.	1953	27-Day Variations in the Absorption of the *D*-Region of the Ionosphere over Singapore and Slough, *J. Atmosph. Terr. Phys.* **3**, 153
PIGGOTT, W. R.	1953	The Reflection and Absorption of Radio Waves in the Ionosphere, *Proc. Instn. Elect. Engrs.* III. **100**, 61
RAWER, K.	1951	Comparison des Resultats de Mesures de l'absorption Ionospherique Effectuees, *J. Atmosph. Terr. Phys.* **2**, 38

VOL. 7 1955

Journal of Atmospheric and Terrestrial Physics, 1955, Vol. 7, pp. 247 to 253. Pergamon Press Ltd., London

Measurements of the mean lifetime of the metastable ^1S-state of the oxygen atom in the upper atmosphere during auroral displays

A. Omholt and L. Harang
The Auroral Observatory, Tromsö, and Astrophysical Institute, Blindern, Oslo

(*Received* 28 *February* 1955)

ABSTRACT

The intensity variations of the green oxygen line 5577 Å ($^1D-^1S$) and the first negative nitrogen band 4278 Å (N_2^+, $B^2\Sigma_u^+ - X^2\Sigma_g^+$) are measured in rapidly changing aurorae. The mean lifetime of the upper state of the nitrogen band is of the order 10^{-8} sec, the intensity variations of this band will probably therefore at the same time represent the instantaneous relative excitation rate of the metastable OI ^1S-level. The mean lifetime of the metastable OI ^1S-level is theoretically calculated to be of the order $\tau = 0{\cdot}75$ sec (Garstang, 1951). One should therefore expect a time-lag in the intensity curve of the 5577-line relative to the 4278-band. This effect is demonstrated on the records, and the mean lifetime of the OI ^1S-level is found to vary between 0·45 and 0·75 sec. The upper value (0·75 sec) confirms the theoretical value found by Garstang (1951), the lower value found indicates that a probability of collisional deactivation of the metastable OI ^1S-level of the order 1 sec^{-1} may appear in the auroral region of the upper atmosphere.

1. Introduction.

Four of the most intense lines and bands in the auroral spectrum are the atomic oxygen lines, the red doublet 6364,6300 Å ($^3P_{1,2} - {}^1D_2$) and the green line 5577 Å ($^1D_2 - {}^1S_0$), and the nitrogen bands 4278 and 3914 Å (N_2^+, $B^2\,\Sigma_u^+ - X^2\,\Sigma_g^+$, 0-1 and 0-0). The lifetime of the upper state of the nitrogen bands is assumed to be of the order 10^{-8} sec, whereas the lifetime of the metastable states $^1S_0$ and $^1D_2$, from which the red and green lines originate, is theoretically assumed to be of the order 0·7 and 110 sec (Garstang, 1951).

If therefore the luminosity in an aurora is rapidly changing, one should expect a time-lag in the intensity curves of the oxygen lines compared with the nitrogen bands. From the relative displacements of the intensity curves it should be possible to calculate the mean lifetime τ of the ^1S- and ^1D-states. In the following, the records of the intensity variation of the 5577-line and the 4278-band will be discussed, and the values of the mean lifetime τ of the ^1S-state of the oxygen atom in an auroral display will be given.

In the upper atmosphere, the lifetime τ of the ^1S-state will be modified by collisional deactivation through neighbouring atoms, molecules, and electrons (Vegard and Tönsberg, 1937; Seaton, 1954). The population n of the ^1S-level is given by the equation

$$dn/dt = Q - (\sum_m A_{nm} + d_n)n = Q - \frac{1}{\tau}n \qquad (1)$$

where

$$\frac{1}{\tau} = \sum_m A_{nm} + d_n \qquad (2)$$

Here A_{nm} are the spontaneous transition probabilities from the ^1S-level to respectively the ^1D- and ^3P-levels, d_n is the probability of an OI atom in the ^1S-state suffering collisional deactivation, τ is the mean lifetime of an OI atom

in the ^1S-state, and Q the excitation rate of the ^1S-level. If we assume that the excitation of the ^1S-level and the nitrogen band are proportional, we have

$$Q = kI_N \tag{3}$$

where I_N is the intensity of the band. This is due to the very short lifetime of the upper state of this band (N_2^+, $B^2\Sigma_u^+$), of the order 10^{-8} sec.

The intensity of the green oxygen line is given by

$$I_0 = h\nu A_{32} n \tag{4}$$

The levels ^3P, ^1D, and ^1S are denoted by 1, 2, and 3. This gives, by equations (1) and (3)

$$dI_0/dt = k h\nu A_{32} I_N - (A_{32} + A_{31} + d_3)\, I_0 \tag{5}$$

or

$$KI_N = I_0 + \tau\, dI_0/dt \tag{6}$$

where

$$K = k h\nu A_{32}/(A_{32} + A_{31} + d_3) = k h\nu A_{32}\tau \tag{7}$$

Measurements of I_N, I_0, and dI_0/dt may thus give us informations about K and τ. Since τ is of the order of 1 sec, it appears from equation (6) that I_0 and dI_0/dt must be of the same magnitude if a reliable estimate of τ is to be obtained. This means, however, that only the most rapid intensity variations in the aurora can be used. K is more easily derived with sufficient accuracy.

VOL. 7 1955

2. THE PHOTOMETER

The supposition for equation (6) is that the green line and the nitrogen band are emitted from an infinitesimal volume in the auroral form. Equation (6) is, however, valid even if we integrate over any volume and time-interval, assuming that K and τ can be regarded as constant within this volume and time-interval. Two types of photometric arrangements were used, as shown in Fig. 1a and 1b.

The optical system consisted of an objective of $F = 60$ cm or $F = 25$ cm, both with an effective diameter of 10 cm, which focused the sky on the 6 × 12-mm opening of the photomultiplier. The area of the sky covered was thus $0{\cdot}6° \times 1{\cdot}2°$ or $1{\cdot}4° \times 2{\cdot}8°$, which during an auroral display cuts out only a small fraction of the total auroral form appearing.

The interference filters used had a half-width of about 70 Å. This width is somewhat extended towards shorter wavelengths, due to the convergence of the beam, but within the total width of the filters there are no strong auroral emissions likely to cause serious errors in the intensities measured. The photometer could be easily moved in height and azimuth directions.

The photocurrent was amplified through a cathode follower and through a shielded cable connected to the amplifier and Y-plate of a CRT (or the two Y-plates in a double beam CRT). The deflections were recorded on a continuous moving film.

The split-beam photometer in Fig. 1a was tried first on a number of aurorae. It turned out, however, that for the rapidly moving auroral forms a serious error was introduced in the intensity curves due to the different sensitivity distributions on the photocathode of the two photomultipliers. This gave for the two

intensities a different effective integration over the area of the sky covered by the photometer. Equation (6) is thus not valid for these integrated intensities. On the other hand, it was in this case necessary to use a fairly wide area of the photocathodes to obtain the sufficient signal-to-noise ratio. By mapping the photocathodes and choosing suitable, restricted areas of these, this difficulty may be overcome in cases where a lower signal-to-noise ratio is sufficient.

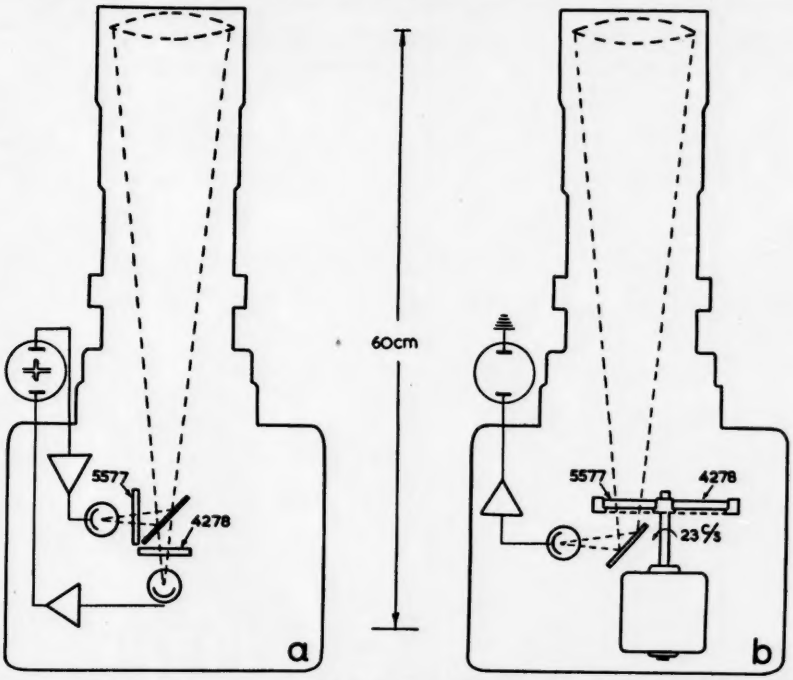

FIG. 1. Photometric arrangements for simultaneous recording of the intensities of the green line 5577 Å and the nitrogen band 4278 Å.
(a) The light beam is *split* up into two identical ways by means of a 50 per cent reflecting and transmitting mirror.
(b) The light beam is *chopped* by a rotating filter desk and the two intensity curves consisting of light pulses from alternatively 5577 Å and 4278 Å are recorded through one common amplifier on the same film strip.

The chopping photometer in Fig. 1b worked satisfactorily even on rapidly moving auroral forms. The speed of rotation of the filter plate was 23 c/sec, which determines the upper limit of the band-width of variations to be recorded. The time constant of the current pulses from the photomultiplier was of the order 10^{-2} sec. All measurements given in this paper were carried out with this photometer.

The photomultiplier was not cooled, and this limited the application of the instrument to record only the stronger components of the auroral spectrum.

3. Observations

The observations were made at the Auroral Observatory in Tromsö during the autumn of 1954. In Fig. 2 is shown an original record from a rapidly moving

auroral form. In Figs. 3(a–m) are given twelve typical curves from various auroral forms. These have been redrawn from the photographic records.

On all the curves there is a delay of the green line 5577 Å relative to the nitrogen band 4278 Å.

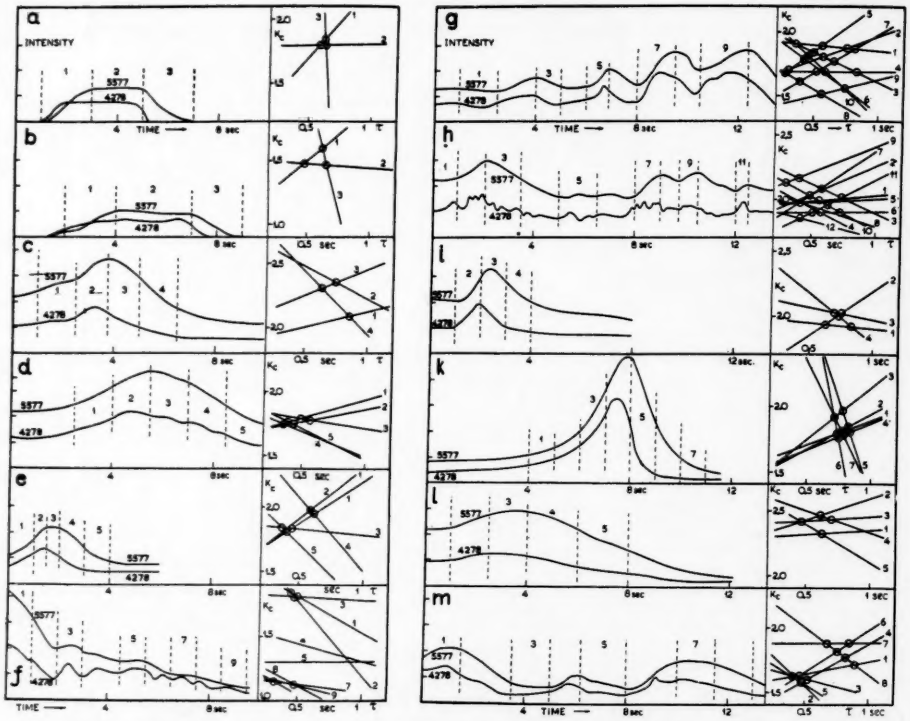

FIG. 3(a) to (m): Intensity curves of 5577 Å and 4278 Å from various auroral forms.

4. DISCUSSION OF THE OBSERVATIONS

The main problem is to investigate if the intensity curves recorded are consistent with equation (6)* and to derive numerical values of K and τ which give the best consistency. As the intensities I_N and I_0 are in arbitrary scales, we cannot derive K given by equation (7), but a constant K_c, dependent on K as well as instrumental constants.

From the intensity curves a number of sets of values $c_N I_N$, $c_0 I_0$, and $c_0 dI_0/dt$, c_N and c_0 being instrumental constants, may be determined for different values

* We may point out that equation (6) or (1) is identical with the equation well known in the physics of the ionosphere which describes the temporal variations of ionization in a layer in which we have ion production due to solar control and the electrons are disappearing by way of attachment. The coefficient of attachment, β, corresponds to $1/\tau$. APPLETON (1953) has in a note on the "sluggishness" of the ionosphere pointed out that β (or $1/\tau$) can easily be determined from the displacement in time, $\Delta t \approx 1/\beta$, between local noon and the maximum in the electron density curve. This method of determination presupposes, however, that in the present case the mean lifetime τ is small compared with the time of intensity fluctuations. This is not the case in the auroral experiments, and we have therefore to use the more elaborate graphical method described in this chapter.

VOL. 7 1955

L.
55

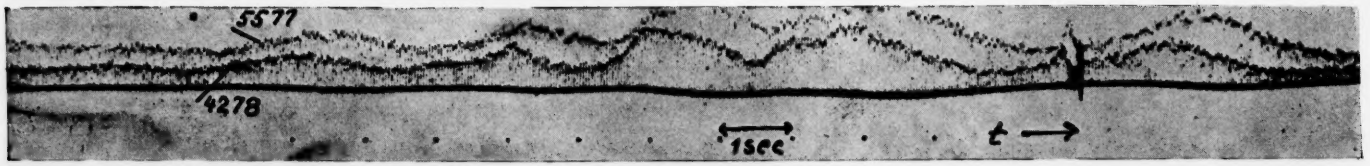

FIG. 2. Record of the intensity variations of an auroral drapery in 5577 Å and 4278 Å taken with the chopping photometer. The time lag of the 5577 Å curve is visible.

VOL.
7
1955

of time t, each set of values assumed to satisfy equation (6). Because of the errors introduced by the noise in the photomultiplier, it seemed more convenient to integrate the values of I_N, I_0, and dI_0/dt over suitable time-intervals $t_p \rightarrow t_{p+1}$, and from equation (6) one then gets:

$$c_0 \int_{t_p}^{t_{p+1}} K c_N I_N \, dt = c_N \int_{t_p}^{t_{p+1}} c_0 I_0 \, dt + c_N \int_{t_p}^{t_{p+1}} c_0 \tau \, (dI_0/dt) \, dt \tag{8}$$

If it is justified to regard τ and K as constant during the time-interval, we have for each of the time-intervals chosen:

$$K_c J_{Np} = J_{0p} + J'_{0p} \tau \tag{9}$$

where

$$J_{Np} = \int_{t_p}^{t_{p+1}} c_N I_N \, dt, \; J_{0p} = \int_{t_p}^{t_{p+1}} c_0 I_0 \, dt,$$

$$J_0{}'_p = \Big[c_0 I_0 \Big]_{t=t_p}^{t=t_{p+1}}, \; K_c = K c_0 / c_N$$

The noise give random errors in the intensities I. These errors are reduced by the integration (8); the greatest experimental error is thus undoubtedly introduced by $J_0' \, . \, (\Delta J_0' \approx \Delta I_0)$. To minimize this error we have to select time-intervals over which the integration gives the highest possible relative numerical value of J_0'. This means that dI_0/dt should be either positive or negative over the whole time-interval considered. The time-intervals chosen were from 0·5 to 2·0 sec duration.

On a record the number of time-intervals considered was of the order 3 to 12. This means that from one record one might get a set of equations (9) from which τ could be computed by means of the method of least-squares. We found it, however, more reliable to use a graphical method of solution, by means of which one more easily could estimate the reliability of the evaluation of τ. In an orthogonal K_c, τ co-ordinate system the set of equations (9) are represented by a number of straight lines. If K_c and τ were constant during the whole record, these lines should cross at one single point, giving the true values of K_c and τ. Graphical solutions according to this method are shown in Fig. 3(a–m) to the right. The intervals of integration chosen are indicated on the intensity curves through numbers. In estimating the mean position of the point (K_c, τ) we have only used intersection points of lines crossing at fairly large angles.

Now, the intensities recorded have been integrated over a column in radial direction from the photometer, and K_c and τ may vary within this column. The values deduced will therefore represent a mean value over this volume during the time recorded. The most probable values of τ and the error estimated are given in Table 1, column 4, for each of the twelve cases analyzed. K_c given in Table 1, column 5, is derived through integration of the intensities over all time-intervals during one record. From the record shown on Fig. 3(m) were deduced two values of τ and K_c, one from the first five and one from the last three time-intervals.

5. DISCUSSION OF THE NUMERICAL VALUES OBTAINED

Attempts have been made theoretically (PASTERNACK, 1940; GARSTANG, 1951) as well as experimentally (SAWYER and EMELEUS, 1952) to determine the spontaneous transition probabilities A_{nm} for the metastable OI ^1S-level. The value obtained theoretically by GARSTANG (1951) of $A_{32} + A_{31} = 1{\cdot}36$ sec^{-1} is in good agreement with the greatest values of τ derived from the auroral measurements (Table 1, $\tau = 1/(A_{32} + A_{31})$). HERMAN (private communication to SAWYER and EMELEUS, 1952) has during laboratory experiments obtained the value $\tau = 0{\cdot}67$ sec, which is probably the effective lifetime when the effect of deactivation by the surrounding gas and tube walls is taken into account. The value of $\tau = 0{\cdot}75$ sec is

Table 1. *The mean lifetime τ and the collisional deactivation probability d for the OI atoms in the $^1S_0$-state in the upper atmosphere.*

Record fig.	*Auroral form*	*Height* (°)	τ (sec)	K_c	d (sec^{-1})	d_{min} (sec^{-1})
3a	Puls. surface	65	0·60 ± 0·1	1·82	0·3	0·1
b	Puls. surface	65	0·55 ± 0·1	1·50	0·5	0·2
c	Band w. ray st.	27	0·80 ± 0·2	2·23	0	0
d	Drapery	32	0·50 ± 0·2	1·75	0·6	0·1
e	Drapery	35	0·55 ± 0·15	1·85	0·5	0·1
f	Drapery	23	0·45 ± 0·1	var.	0·7	0·5
g	Drapery	35	0·55 ± 0·1	1·69	0·5	0·2
h	Drapery	23	0·45 ± 0·1	2·00	0·9	0·5
i	Drapery	23	0·70 ± 0·1	2·00	0·1	0
k	Moving band	80	0·75 ± 0·05	1·85	0	0
l	Drapery	35	0·60 ± 0·2	2·41	0·3	0
m	Drapery	30	0·45 ± 0·05	1·60	0·9	0·7
			0·75 ± 0·1	1·83	0	0

probably a fairly correct value of the lifetime for an undisturbed OI atom in the metastable ^1S-state. This gives $A_{32} + A_{31} = 1{\cdot}3$ sec^{-1}.

From Table 1 it is seen that τ in most cases has a value which is below 0·75 sec. This means that a collisional deactivation is present in the auroral region. Using the value 1·3 sec^{-1} for $A_{32} + A_{31}$ it is possible from equation (2) to deduce the probability of collisional deactivation d. The derived values of d are given in Table 1, columns 6 and 7, together with the lowest possible value d_{min}, the possible error in τ taken into account. From Table 1 we conclude that in the auroral region there is a deactivation probability of the ^1S-state of the order 0-1 sec^{-1}. This is in fair agreement with the results of SEATON (1954). He finds, from intensity ratios between the red OI-doublet ($^3P - {}^1D$) and the green OI line in spectra from upper and lower limit of auroral arcs a deactivation probability of the same order of magnitude for the metastable ^1D-state of the OI-atom in the lower part of the aurora.

VOL. 7 1955

Acknowledgements—The authors wish to express their thanks to Mr. R. LARSEN and Mr. S. BERGER at the Auroral Observatory for valuable assistance during the observations, and to the Director, Mr. E. TÖNSBERG, for putting the facilities of the observatory at our disposal. We are also indebted to Professor S. ROSSELAND for placing a camera at our disposal, and to the Norwegian Defence Establishment, Kjeller, through chief scientists T. HVINDEN and F. LIED, for placing at our disposal the theodolite and photomultipliers. One of us (A. O.) is indebted to the Research Council for Science and the Humanities and to Kr. Birkelands and Norsk Hydros Funds for financial support.

REFERENCES

APPLETON, E. V.	1953	*J. Atmosph. Terr. Phys.* **3**, 282
GARSTANG, R. H.	1951	*Mon. Not. R.A.S.* **111**, 115
PASTERNACK, S.	1940	*Astrophys. J.* **92**, 129
SAWYER, N. D., and EMELEUS, K. G.	1952	*Proc. Roy. Soc.* **A65**, 219
SEATON, M. J.	1954	*J. Atmosph. Terr. Phys.* **4**, 285
VEGARD, L., and TÖNSBERG, E.	1937	*Geofys. Publ.* **11**, No. 16

Journal of Atmospheric and Terrestrial Physics, 1955, Vol. 7, pp. 254 to 277. Pergamon Press Ltd., London

Atmospheric noise interference to broadcasting in the 3-Mc/s band at Poona

S. V. Chandrashekhar Aiya and K. R. Phadke
College of Engineering, Poona
(*Received* 15 *April*, 1955)

Contents

PAGE

1. Introduction 255
2. Experimental Work 255
   (a) Design of the experiments 255
   (b) Equipment and its installation 256
   (c) Experimental results 257
   (d) Noise data for broadcast services 259
   (e) Accuracy of the results 260
   (f) Conversion data 260
   (g) Some stray phenomena 261
3. Comparison Between the New and the Existing Noise Data . . . 261
   (a) Available data 261
   (b) Comparison with the estimates of CRPL, Washington 262
   (c) Comparison with the measurements of RRB, London 264
4. Estimations of Noise from Lightning Discharge Data 266
   (a) Approach to the problem 267
   (b) Propagation calculations 268
   (c) Probable sources of noise 270
   (d) Estimation of power radiated by noise sources 271
   (e) Estimation of noise levels 274
   (f) Comparison of estimated and measured values 275
5. Conclusion 276

ABSTRACT

Systematic measurements of atmospheric radio noise at 2·9 Mc/s were taken at Poona (18.31 N, 73.55 E), during the hours, 18 to 23 I.S.T., for the whole year 1953 by a method previously described by one of the authors. The details of the experimental work and the analysis of the results are given in the paper. Noise data as required for broadcast services have been calculated. These new data have been compared with the estimates of noise as deduced from Circular No. 462 of the U.S. National Bureau of Standards and with the experimental results as reported in the Radio Research Special Report No. 26, London. Noise levels have been estimated from lightning discharge data on the basis of the known distribution of thunderstorm activity over the globe and compared with measured values.

VOL. 7 1955

1. Introduction

A possible way of assessing atmospheric noise interference to broadcasting has already been reported (Aiya, 1954a). The object of the present paper is to describe the first experiments carried out, and discuss the results obtained. Measurements at 2·9 Mc/s were taken at Poona for the whole year 1953 during the hours 18 to 23 I.S.T. In the first section, the experimental work is described in detail and utilized to deduce the noise data as required for broadcast services. The second section is devoted to a comparison between the new and the existing noise data. In the last section, an attempt is made to estimate noise levels from lightning discharge data and compare them with the results obtained by experiments described in the paper.

2. Experimental Work

(a) *Design of the experiments*

In order to interpret the results theoretically, it is necessary to know as many factors as possible with reasonable accuracy. Ground constants not being known sufficiently well, it was decided to avoid ground-ray reception as far as possible. For ionospheric propagation, calculations become less indeterminate during night, when absorption is negligible and reflection is only possible through the F_2-layer.

On examining the charts giving the distribution of thunderstorm activity over the globe (Brooks), it is found that there are sources of thunderstorms both to the east and the west of Poona. The western sources could be eliminated and night conditions could be realized for all eastern sources as far as Java and Sumatra by choosing for the hours of observation the period, 18 to 23 hr I.S.T. (Indian Standard Time is 5 hr 30 min ahead of G.M.T.). Even during this period, the first hour of observation would be under daylight conditions for months near the summer solstice. The period, 18 to 23 hr I.S.T., is of importance to Indian broadcasting and is a period of high noise level.

Except for extremely local thunderstorms, ground-ray has to be completely eliminated. The frequency must be such that reliable propagation should be possible all the year round during the hours stated for regions to the east of Poona up to distances of 4500 km. Further, it should be possible to see without ambiguity for the sources involved whether the transmission is by a single or double hop path via the F_2-layer. Noise is reported to be higher, the lower the frequency. Taking all these factors into account, it was found that the 3-Mc/s band was suitable. The 90-m band broadcast transmissions in India add interest to investigations in the 3 Mc/s band. In this band, interference could be avoided and observations taken continuously by working at 2·9 Mc/s.

Atmospheric noise, therefore, was measured at 2·9 Mc/s during the hours 18 to 23 I.S.T., continuously, at Poona. Periodically, investigations have been carried out for twenty-four hours to study the diurnal variation of noise. An examination of these results indicates that the assessments made for the period 18 to 23 hr can be taken as valid for the period of day 18 to 24 hr I.S.T.

(b) *Equipment and its installation*

Measurements were carried out, using the equipment designed for investigations in the 2·5–20-Mc/s band, and its details are as follows:—

A vertical aerial, 8 ft 3 in. high, is mounted at a height of 8 ft from the terrace of a laboratory which is 50 ft from ground. All the constants of the aerial are determined at site. Its effective height is 1·22 m. The aerial terminates into a cathode follower mounted at the bottom of the aerial. The output of the cathode follower is taken through a feeder to a receiver mounted in the room below. Necessary precautions are taken for balancing, shielding, etc., so that the stray pick-up is 40 db below that of the aerial. The receiver used is a Hammerlund SP-400-SX. The R.F. stages are carefully aligned and the I.F. stages are aligned using the alignment oscilloscope. The band-width characteristics of the receiver are shown in Fig. 1. The second channel selectivity of the receiver is 80 db down. The receiver is used with AVC off and its R.F. volume control is replaced by fixed resistances and a switch to provide ranges for the noise meter. Power is supplied

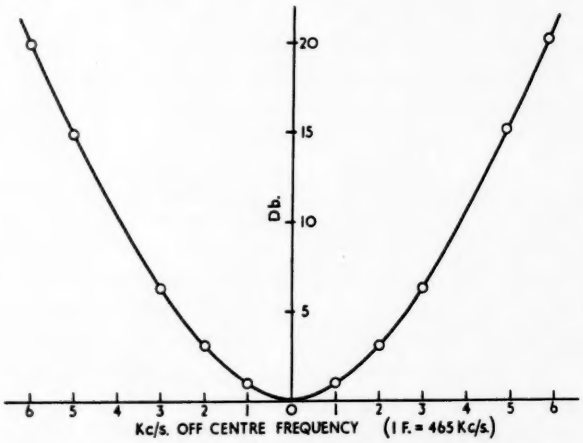

Fig. 1. Receiver frequency response characteristic.

to the receiver through a constant-voltage transformer. The receiver gain is checked twice a week. The A.F. output of the receiver is fed to the output unit built specially for these experiments, and shown in Fig. 2.

The value of the choke in the output unit is 25 henrys. Since it has to record impulses, some overload protection is necessary and, for this purpose, it must have some form of logarithmic response. Further, the value of the choke must be such that it has no effect on the time constants of the circuit. The procedure adopted for the design of the output unit is as given by Hunt (1933). An additional feature introduced into the design of the output unit was to provide a linear response from 100 to 5000 c/s. This represents the range of frequencies of interest in the reproduction of broadcast programmes, and the A.F. output resulting from noise within this range had, therefore, to be provided with a high-fidelity reproduction. The charging and discharging time constants of the meter are 10 and 500 milliseconds respectively.

VOL. 7 1955

The noise meter thus set up is calibrated by using signals from a standard signal generator modulated 30 per cent by a 400-c/s note. The signals from the signal generator previously tested and checked are fed through the equivalent impedance of the aerial to the cathode follower at the point at which the aerial is connected. At any frequency at which the calibration is carried out, the strength of the signal from the signal generator is gradually varied and the noise meter read. The results obtained are reduced to correspond to an aerial of 1 m effective

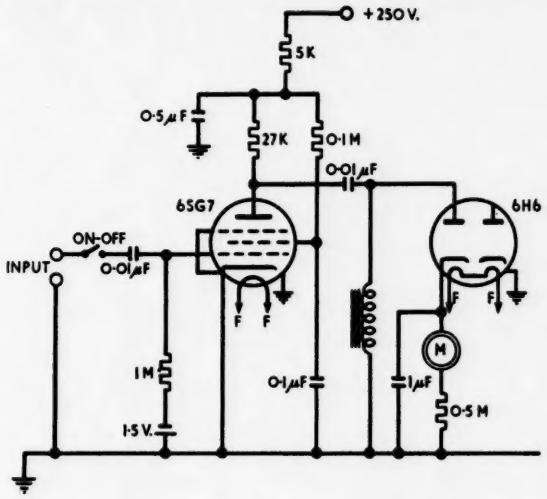

Fig. 2. Circuit diagram of output unit.

height. This calibration is checked at one point in each range twice a month. The equipment thus set up can be used in the range, 0·5 to 500 μV/m. A higher range has also been provided.

The procedure for the recording and analysis of observations is as previously reported (AIYA, 1954a).

(c) *Experimental results*

In a previous communication (AIYA, 1954a), atmospheric noise has been classified into three types:—(a) Type A noise giving the impression of continuous noise, (b) type B noise coming as distinct impulses, and (c) type C noise, a special form of type B noise arising from local thunderstorms. This classification is followed in reporting the results. When only type A noise is present, or when the number of impulses due to type B or type C noise is less than five per minute, only type A noise values are computed. When the number of impulses due to type B or type C noise is between five and ten per minute, values of both type A and type B or type C noise are computed and stated. When the number of impulses due to type B or type C noise exceeds ten per minute, only type B or type C noise values are calculated and type A noise observations are ignored.

Systematic observations were taken during the period, 18 to 23 hr I.S.T. for the whole year 1953, at 2·9 Mc/s. As stated in section 2(a), these results can be

Table 1. *Measured values of atmospheric noise*

Place: Poona (18.31 N, 73.55 E) Year: 1953
Frequency: 2·9 Mc/s. Time: 18–23 hr I.S.T.

Month	*Type of noise*	*Med. value in* μV/m	*H.D. value in* μV/m	*% days*	*Remarks*
January	A	0·7	1·2	90	
February	A	0·8	1·2	100	
	B	3·6	4·6	100	5 impulses/min
March	B	5·4	8·0	66	
	B	10·8	14·2	33	
	B	7·2	10·1	100	weighted value
	C	—	—	—	one day only
April	B	10·0	14·0	75	
	C	66·0	100·0	25	
May	B	10·0	15·0	67	18–23 hr
	B	11·0	15·4	67	19–23 hr
	C	24·0	64·0	33	
June	B	10·3	15·5	60	18–23 hr
	B	10·6	15·7	60	19–23 hr
	C	17·8	28·0	40	
July	B	10·4	15·4	72	18–23 hr
	B	11·0	15·6	72	19–23 hr
	C	17·8	25·8	28	
August	B	5·0	7·3	40	
	B	10·4	14·8	45	
	B	7·8	11·2	85	weighted value
	C	16·3	20·0	15	
September	B	5·6	8·1	38	
	B	11·0	15·0	50	
	B	8·7	12·0	88	weighted value
	C	14·8	19·8	12	
October	B	6·2	9·6	50	
	B	9·9	13·6	25	
	B	7·4	10·9	75	
	C	14·3	20·4	25	
November	A	1·0	1·2	90	
December	A	1·1	1·4	90	

Note: During November–January, there can be type B or type C noise for about 10 per cent of the days, and values can go up to 30 μV/m. Data are not adequate for analysis.

VOL. 7 1955

taken as valid for the period, 18 to 24 hr I.S.T. To assist theoretical understanding, if two forms of type B noise are received, their values are computed separately as also the weighted value for the month. Similarly, during the period May to July, values are also computed for the hours 19 to 23, as 18 to 19 hr falls under daylight conditions. Table 1 summarizes the results.

(d) *Noise data for broadcast services*

The experimental results given in Table 1 are of direct scientific interest and can be useful for a theoretical understanding of the problem. Further, it is known that the approach and recession of thunderstorm activity varies from year to year. Therefore, the percentage days given in Table 1 can only be considered useful for giving an idea of the number of days in a month when a particular type of noise is predominant. However, if a longer period than a month, viz., a quarter, is considered, it is very probable that the percentage days when a particular noise predominates will remain the same from year to year. Therefore, for service purposes, the data of Table 1 can be utilized to calculate noise values for satisfactory service during 50, 75, and 90 per cent of the time in the four quarters of the year and the complete year. The results are given in Table 2. Calculated values have been rounded off to the nearest higher whole numbers. The letter in brackets below the value indicates the type of noise.

Table 2. Noise values in $\mu V/m$ for 50, 75, and 90 per cent of the time-satisfactory broadcast service
Place: Poona (18.31 N, 73.55 E) Time: 18–24 hr I.S.T.
3-Mc/s band

I *Season*	II 50%	III 75%	IV 90%
Dec.–Feb.	1 (A)	2 (A)	6 (B)
Mar.–May	13 (B)	42 (C)	85 (C)
June–Aug.	14 (B)	18 (C)	25 (C)
Sept.–Nov.	8 (B)	12 (B)	15 (C)
Whole year	11 (B)	15 (B)	20 (C)

Note 1—The letter in brackets below value indicates the type of noise.
Note 2—The value in column IV for December–February is an estimate based on scanty data and actual values for March and October.

An examination of Tables 1 and 2 shows clearly that the median and higher-decile values of any one type of noise do not necessarily represent the noise values

for satisfactory service for 50 and 90 per cent of the time. Such a coincidence can, however, occur at high latitutes where only type A noise may be observed for a whole season.

(e) *Accuracy of the results*

In discussing this question, the first problem is instrumental accuracy. This is as good as one can expect it to be and is estimated to be correct to within 5 per cent for measurements exceeding 2 μV/m. For values of the order of 1 μV/m and lower, the accuracy may be as poor as 20 per cent. Measurements of such low values are beset with several difficulties. Other noises, including man-made noise and interference, enter into the picture. Occasions arise when it becomes extremely difficult to say that only atmospheric noise is being measured. Over the whole spectrum, there is always a small background due to radiations from stations at their authorized frequencies or their harmonics. This is generally so bad that no useful purpose may be served by measuring atmospheric noise of values of the order of 1 μV/m. Fortunately, in the 3-Mc/s band, this interference has not been so bad as to prevent measurement.

The statistically computed values are expected to hold from year to year, but for possible variations of ionospheric absorption, etc., and the year-to-year variations of thunderstorm activity. The latter become important for type C noise, and this assumes significance during March–May. Observations have been taken for some months during 1952 and 1954. A comparison of the results for the corresponding months shows agreement within 3 db or better. Most satisfactory agreement is obtained for type B noise. All these facts appear to support the conclusion that the averaged seasonal values for service purposes should be considered satisfactory from year to year and do not need a factor of safety beyond 3 db.

VOL. 7 1955

(f) *Conversion data*

In the results presented, the ten highest impulses recorded during a minute are averaged to give the noise value. It is not outside the limits of probability that some may consider five, fifteen, or twenty impulses per minute to have an annoyance value. To make the results useful in such cases, thirty-six hourly sets of observations selected at random from type B noise data were analyzed. In each case, the average value of the ten highest impulses per minute, the five highest impulses per minute, the fifteeen highest impulses per minute, and the twenty highest impulses per minute were calculated. These values were converted into ratios in terms of the value calculated for the ten highest impulses per minute. The results are shown in Table 3. They represent the arithmetically averaged ratios for all the hours.

From the limits of error, it is seen that the ratio is about the same for all the hours selected for averaging. Such tables are not necessary for type A noise. The type C noise data is not large enough to attempt any such generalization.

The bandwidth characteristics of the receiver have already been described. This can be used to convert the results to other bandwidths approximately.

Table 3. Data for converting ten impulses/min type B noise value to five, fifteen, or twenty impulses/min value

	Average of 5 highest peaks/min	*Average of 15 highest peaks/min*	*Average of 20 highest peaks/min*
Ratio to value of 10 per min	1·14 ± 0·03	0·912 ± 0·013	0·843 ± 0·020
db above value of 10 per min	1·15	−0·85	−1·45

The results in this paper are given in terms of signals modulated 30 per cent by a 400 c/s note. The equipment was also calibrated, using signals modulated 15 per cent and 50 per cent with the same note. By multiplying the results in this paper by 2·5 and 0·58 respectively, values corresponding to 15 and 50 per cent modulation calibrations can be obtained, but they will be approximate to 5 per cent.

(g) *Some stray phenomena*

It is now necessary to mention some stray phenomena noticed during the measurements. During the period, March–October, there can be a day or two when thunderstorm activity occurs over the point of observation. In such cases, continuous noise exceeding 100 μV/m and lasting for periods ranging from half to one minute may be observed for an hour. This may be followed by impulsive noise having values of the order of 800 μV/m and lasting about an hour. The number of such high-value impulses is of the order of ten per minute. In addition, there can be three or four days when the average value for the hour exceeds 100 μV/m for several hours and can have values of the order of 250 μV/m for an hour or so. Before the break of the monsoon (April, May), precipitation static of value 100 μV/m can be observed for a minute or so, occasionally, when it starts raining or the intensity of rainfall increases.

3. Comparison Between the New and Existing Noise Data

In a previous communication (Aiya, 1954a) it has been pointed out that the following information is necessary for making a fair comparison of the results of different workers:—(a) details of the aerial, (b) bandwidth characteristics of the receiver, (c) detailed particulars of the receiver and the measuring system, (d) method of calibration, (e) criteria of the number of impulses per minute and, if possible, suitable data for converting the results to other criteria, (f) the details of the way the observations have been recorded and assessed, and (g) standards of satisfactory signals in relation to the noise level as measured. When details on the several points mentioned above are not available, comparisons become difficult and will not be made in this paper.

(a) *Available data*

Estimates of noise level can be deduced from the data provided by the Central Radio Propagation Laboratory (CRPL) in Circular No. 462 of the United States

National Bureau of Standards on Ionospheric Radio Propagation (National Bureau of Standards, 1949). These estimates will be compared with the data given in Table 2.

Atmospheric noise has been measured at the places given below, which are in or around India:—

(1) Calcutta (Chakravarti, Ghosh, and Ghosh);
(2) Dacca (Khastgir and Ali; Khastgir and Rao);
(3) Lahore (All India Radio);
(4) Calcutta, Delhi, and Colombo (Radio Research Board, 1953).

For (1), (2), and (3), the details necessary for making a fair comparison are not available. Therefore, the data of Table 2 will be compared with the results of the Radio Research Board, London, only.

(b) *Comparison with the estimates of CRPL, Washington*

In the circular No. 462 referred to above, the world is divided into atmospheric radio-noise zones. Areas of the world in which thunderstorms are most frequent are indicated as zones 4 and 5. The areas most remote from the principal thunderstorm areas and in which little atmospheric radio noise may be expected are indicated as zone 1. The other zones are intermediate in radio-noise expectations. Thus the world is divided into five noise zones. Four noise maps are drawn to correspond to four different seasons of the year, and each map indicates the noise zone to which any place in the world belongs during the season. The five noise zones correspond to five noise grades. Corresponding to each noise grade, the required field intensity for telephony with 100 per cent modulation for satisfactory service in the presence of atmospheric radio noise is given in the form of graphs for six different times of the day. The required field intensity is given in r.m.s. values and is believed to represent a signal to "average noise" ratio of 15 db. The graphs give the field intensity, and the average noise can be deduced from the field intensity by assuming the former to be 15 db lower than the latter. "Satisfactory Service" in these calculations is expected to assure radio telephone communication for 90 per cent of the time and is expected to provide 90 per cent intelligibility of 100 per cent modulated radio telephone service.

Average noise values can be deduced from the circular for 16, 20, and 24 hr L.M.T. Having regard to the measurements reported in this paper, it is adequate to abstract the necessary information for 20 hr L.M.T. This has been done for Poona, Delhi, Calcutta, and Colombo, and is reproduced in Table 4. Noise values have been rounded off to the nearest whole numbers. The noise grades have been estimated from the maps in intervals of half a unit. The values of noise given are average noise values as described in the circular quoted, and are for a receiving-set bandwidth of "3 kc each side of the carrier frequency."

In examining the extent to which noise-grade maps can be satisfactory, the following questions arise:—

(a) Whether one noise grade can satisfactorily represent noise levels at a place at all frequencies, having regard to the varying propagation characteristics at different frequencies and the known thunderstorm distribution over the globe.

VOL. 7 1955

Table 4. Estimated noise grade and noise value in $\mu V/m$ at 20 hr L.M.T. for 3 Mc/s
(From Circular No. 462 of the National Bureau of Standards, Washington)

Place	Dec.–Feb.		Mar.–May		June–Aug.		Sept.–Nov.	
	Grade	Value	Grade	Value	Grade	Value	Grade	Value
Poona	2·5	8	3·5	16	3·5	16	3·0	11
Delhi	2·5	8	3·0	11	3·5	16	3·0	11
Calcutta	2·5	8	3·5	16	3·5	16	3·0	11
Colombo	3·0	11	3·5	16	3·0	11	3·0	11

(b) Whether it is at all possible to give noise levels for 90 per cent of the time-satisfactory service by such noise-grade maps.

These questions will not be discussed here, as it is proposed to examine them along with the significance of the noise grade, and a possible way of revision of the noise grade, as assigned at present to different places in a future paper.

A careful examination of the description and graphs given in Circular No. 462 of the National Bureau of Standards leads to the following inferences:—

(a) The calculations, on which the CRPL estimates of noise at 3 Mc/s as given in Table 4 are based, appear to be restricted to considering the noise received by sky-wave propagation only at the places listed in the table. Type C noise which arises from local thunderstorms appears to have been ignored.

(b) The calculations appear to have been carried out without any criterion for the minimum number of impulses per minute. In this paper, if the number of impulses received is less than five per minute, type B noise observations are ignored. Type B noise values only are computed when the number of impulses per minute exceeds ten. There appears to be no such criteria for the CRPL estimates.

The net effect of (a) is to make the estimate lower than the actual value during periods of significant local thunderstorm activity. This is actually the case for Poona during March–May, June–August, and September–November. The net effect of (b) is to make the estimate higher than the actual value when a few stray impulses are being received. This is the case for Poona during the season, December–February. The above conclusions follow by a comparison of the values in Table 4 with those in Table 2.

The values given in Table 4 can be deduced from the experimental results as given in Table 1 by adopting the assumptions (a) and (b) as stated above. Adoption of such assumptions is certainly not a justifiable step, but it is useful for a rational understanding of the estimates in Table 4. If Table 1 is examined carefully after ignoring type C noise, it will be noticed that there is one type B noise having a median value between 10 and 11 μV/m and a higher decile value between 14 and 16 μV/m. This noise can be assigned to one set of sources. It will be shown later in Section 4(e) that this arises from sources spread over an area lying between 400 and 1000 km from Poona and having a mean distance of 700 km. In round

figures, the median value of noise due to this source can be taken as 11 μV/m, and the higher decile value as 16 μV/m. This follows by an examination of the results in Table 1. This noise is predominant during March–May and June–August. Therefore, for 90 per cent of the time-satisfactory service, the higher decile value has to be adopted, and this value, 16 μV/m, agrees with the value given in Table 4 for March–May and June–August. During September–November, this noise is very much less frequent. Therefore, for this season, the median value of this noise, viz., 11 μV/m, has to be adopted for 90 per cent of the time-satisfactory service, and this is the value given in Table 4.

An examination of Table 1 shows that there is a second-type B noise which is observed quite prominently during March, August, and September. It has a median value between 5 and 6 μV/m and a higher decile value between 7 and 8 μV/m. This noise can be assigned to a second set of sources. It will be shown later in Section 4(e) that this noise arises from sources for which a mean distance of 2000 km from Poona can be assigned. Noise from this source has been noticed in the measurements during the period December–February, but the number of impulses per minute was very small for most of the time. The scanty data indicated that the number of impulses per minute for this noise did not exceed ten per minute for more than 10 per cent of the time. Therefore, its median value rounded off is given in Table 2 for 90 per cent of the time-satisfactory service as 6 μV/m. But, if the number of impulses per minute criterion is ignored, the higher decile value of this noise, viz., 8 μV/m, will have to be taken as the value for 90 per cent of the time-satisfactory service. This corresponds to the value given in Table 4 for the period December–February.

VOL. 7 1955

The above discussion appears to indicate that only two possible sources have been taken into account for arriving at an estimate of noise level as given by the CRPL data. It is obvious that these estimates cannot be considered entirely satisfactory.

(c) *Comparison with measurements of RRB, London*

On behalf of the Radio Research Board, London, measurements of atmospheric noise at high frequencies (2 to 20 Mc/s) have been in progress at a number of stations spread all over the world. The results of such measurements during the years 1945–1951 have been published as Special Report No. 26 (Radio Research Board, 1953). The method used has been described by THOMAS (1950). It measures the minimum required field intensity for 95 per cent intelligibility of C.W. signals sent at ten words per minute in the presence of atmospheric noise. It is a subjective method, and the values recorded by observers are their estimates of the signal strength required. Subjective tests have revealed that the maximum range of error of this method is from +4 to −7 db above the correct value. The method is not likely to give rise to an error beyond ±5 db. The likely error can be regarded to be within ±3 db. The signal generator used with the equipment has a coarse calibration in steps of about 3 db. The measurements are carried out with a receiver bandwidth of 10 kc/s.

Each station at which measurements are taken produces one measurement of noise level each hour on each of the five frequencies 2·5, 5·0, 10, 15, and 20 Mc/s.

These results are utilized for determining the monthly median, higher, and lower decile values for each hour. The number of observations from which the results are computed is not very large. This is partly compensated for by observations being available for a number of years. Mean diurnal curves for the whole period of observation for each season of the year have been given in an appendix to the special report No. 26, and they can be used for the abstraction of data.

The Radio Research Board results give the minimum required field intensities for satisfactory reception in the presence of noise. To compare these results with the results reported in this paper, it becomes necessary to make a statement about standards, but this should be considered *tentative*. For steady signals, it appears that a signal of r.m.s. value equal to one-half type A noise, one-fourth type B noise, and one-fifth type C noise can give 90 per cent intelligibility of C.W. signals. The values of noise to be used are those as given actually in the paper. The bandwidth of the receiver is as stated in Section 2(b).

The special report No. 26 of the Radio Research Board gives the results of measurements at 2·5 Mc/s for Delhi, Calcutta, and Colombo. For purposes of comparison, it is adequate to abstract the data for 20 hr L.M.T. On the basis of Table 4, Poona is in the same noise grade as the other places in the table; viz., Delhi, Calcutta, and Colombo during September–November. During the other seasons, two out of the other three places have the same noise grade as Poona. Therefore, *assuming* that places having the same noise grade have the same noise level, a comparison can be made.

Table 5 gives the data abstracted from the special report No. 26 of the Radio Research Board. The median and higher decile values as used in the table are the terms used in the report, and they really correspond to "50 and 90 per cent of the time-satisfactory service" values in Table 2. Using the tentative standard, as stated earlier, and the data from Table 2, the minimum r.m.s. signal values for satisfactory reception of C.W. signals in the presence of atmospheric noise on the basis of the results reported in this paper for Poona have been calculated, and are shown in Table 6. While comparing the results in Table 6 with those in Table 5 for the same noise grade, it is useful to take account of the differences in the two sets of measurement, and they are listed in Table 7. It may further be added that, if noise due to local thunderstorms is taken into account, the assignment of

Table 5. Minimum signal r.m.s. values in μV/m at 2·5 Mc/s for satisfactory reception of C.W. signals in the presence of atmospheric noise at 20 hr L.M.T.
(Radio Research Board—Special Report No. 26)

Place	*Dec.–Feb.*		*Mar.–May*		*June–Aug.*		*Sept.–Nov.*	
	Med.	*H.D.*	*Med.*	*H.D.*	*Med.*	*H.D.*	*Med.*	*H.D.*
Delhi	—	—	2·0	7·1	2·5	7·9	0·8	1·6
Calcutta	—	2·0	2·5	10·0	1·8	5·6	1·3	3·2
Colombo	1·6	3·2	2·8	6·3	2·0	3·2	2·2	5·0

Table 6. Minimum signal r.m.s. values in $\mu V/m$ at 2·9 Mc/s for satisfactory reception of C.W. signals in the presence of atmospheric noise during 18–24 hr I.S.T.
(Calculated from Table 2 of this paper)

Place	Dec.–Feb.		Mar.–May		June–Aug.		Sept.–Nov.	
	50%	90%	50%	90%	50%	90%	50%	90%
Poona	0·5	1·5	3·3	17·0	3·5	5·0	2·0	3·0

Table 7. Differences of experimental details for measurements reported in Table 5 and in Table 6

Table No.	Frequency in Mc/s	Receiver bandwidth in kc/s	Time of day	Percentage intelligibility
5	2·5	10	20 L.M.T.	95
6	2·9	6 at 6 db down	18–24 I.S.T.	90

the noise grades as in Table 4 is not satisfactory on the basis of the distribution of thunderstorm days on the land mass of India (AIYA, 1954b).

A comparison of the results as given in Tables 5 and 6 appears to indicate generally that the Radio Research Board measurements give lower values of noise than what is to be expected on the basis of the Poona experiments. The two sets of results can, however, be reconciled by making an allowance of 6 db for errors. Since the statement about standards is tentative, no useful purpose can be served by a detailed discussion at this stage.

4. ESTIMATIONS OF NOISE FROM LIGHTNING DISCHARGE DATA

The source of all atmospheric radio noise appears to be the natural electrical discharges associated with thunderstorms. Extensive investigations have revealed "no evidence that is incompatible with the provisional hypothesis that every atmospheric received on a set of high sensitivity within the commercial range is radiated by a lightning flash" (Radio Research Board, 1947). Therefore, estimation of noise from lightning discharge data and its comparison with measured values is of importance to our understanding of the problem of atmospheric radio noise.

Useful data on the distribution of thunderstorm activity over the globe have been published. Valuable information on lightning discharges and their associated fields, and on the nature of atmospherics which are responsible for the noise, is available in the classical papers of APPLETON, CHAPMAN, WATSON WATT, SCHONLAND, and their collaborators, and of BERGER, LUTKIN, MCEACHRON, NORINDER, and others. The data can be utilized to determine the position, form, and power of a radiator that can be considered as equivalent to the natural phenomenon at any given frequency during a specified period of day in a month or a season. The

VOL. 7 1955

field strength at any point due to such an equivalent radiator can then be calculated on the basis of the known laws of propagation. It is thus possible to estimate atmospheric radio noise levels from lightning discharge data.

Attempts have been made to estimate the frequency distribution of energy radiated by a lightning flash, and to calculate the noise levels, by OLLENDORF, JAEGAR, and THOMAS and BURGESS (OLLENDORF, JAEGAR, Radio Research Board, 1947). The most recent of such attempts is that of THOMAS and BURGESS. Their calculations are based on the data for the return stroke, and the lightning discharge thus becomes equivalent to a long linear aerial. They assume a value for the rate of occurrence of the impulses. In carrying out field-strength calculations from the working equations, they assume that radiation at all angles to the assumed vertical discharge channel is the same as that computed for the normal. The return stroke is of no real importance in the case of tropical thunderstorms which are responsible for the noise as measured and reported in this paper. A critical summary of the present position of noise estimations from lightning discharge data is given elsewhere by one of us (AIYA, 1955), and it has been shown therein that a fresh approach to the problem is necessary.

(a) *Approach to the problem*

When the intensity of the electric field at some point in the cloud exceeds the disruptive strength of the dielectric, a discharge occurs, and this leads to the initiation of a lightning flash. Theoretically, such a flash can occur (a) within the cloud, (b) from a cloud to the upper atmosphere, and (c) from a cloud to the earth. At higher latitudes, especially in temperate regions, the third type is common and, hence, the return stroke from the earth to the cloud becomes important. Owing to the greater height of the tropopause, thunderstorms occur at a higher altitude in the tropics. Consequently, the most common type of a flash is the one that occurs within the cloud. Therefore an analysis of the lightning discharge data as they apply to typical tropical thunderstorms becomes necessary.

A lightning discharge radiates an impulse. The field strength measured depends, therefore, on the several processes involved in the technique of measurement. Further, the results reported in this paper are based on the collection and assessment of data on a certain statistical basis. These facts have to be taken into account in evolving the equivalent radiator from lightning discharge data.

The whole problem has been examined in detail by one of us and reported elsewhere (AIYA, 1955). It has been shown that a step in a stepped leader stroke is responsible for the radiation that appears as radio noise. Lightning discharge data have been utilized to deduce an idealized, statistically valid representation of a typical lightning flash as it occurs in a tropical thunderstorm. An expression is deduced for the average electric field due to a stroke in a flash. This is used to evaluate the power at the source that should correspond to the noise-field strength as measured by the noise meter used for the experiments reported in this paper. It has also been shown that the radiator is equivalent to a short vertical dipole in free space. All the deductions are expected to be valid in the frequency range, 1–20 Mc/s. The power radiated by this equivalent dipole is given by the formula:

$$\text{Power in watts} = W = 45/f^2 \qquad (1)$$

where f is the frequency in Mc/s.

Equation (1) is based on an idealized, statistically valid representation of a lightning flash. It is, therefore, strictly not applicable to an individual thunderstorm. In a paper by AIYA, PHADKE, KHOT, and SANE (1955) the growth and decay of the activity of tropical thunderstorms is discussed, and the peak activity defined. It is shown therein that this peak activity lasts four to six hours and that, in the majority of cases, the maximum is reached after local sunset. Equation (1) gives the mean power during the period of peak activity. Since the hours of observation for the measurements reported in the paper are 18–23 I.S.T., it is found that the power given by equation (1) can be used for the calculation of statistically assessed results.

Having fixed the form and power of the equivalent radiator, it is now necessary to fix its position. Suppose that, during a certain period, say a month, the thunderstorm activity is spread over a certain area, then the mean centre of this area is located and it is supposed that the equivalent radiator is at this mean centre.

(b) *Propagation calculations*

Impulses radiated by lightning flashes travel via the ground, via the ionosphere, via the troposphere, or as an optical ray in exactly the same manner as other radio waves. A Fourier analysis of an impulse shows that it consists of a large number of components of different amplitudes and frequencies. Any receiver turned to a frequency f picks up all frequencies lying within the receiver bandwidth at the frequency f. This is exactly what happens with the noise meter and, when it is tuned to a frequency f, it picks up all the Fourier components of the impulse radiated by a lightning flash which are within 3 kc each side of the carrier frequency f to which the receiver of the noise meter is tuned. For these Fourier components lying within a bandwidth of 6 kc at a frequency f, it will be assumed that the propagation characteristics are the same as for the frequency f. This type of assumption is usual in considering the propagation of modulated waves as in radio telephony or broadcasting.

Change of propagation characteristics with frequency, however, become perceptible for changes of frequency much larger than are implied by the "bandwidth of a receiver." This can be expressed in general terms by saying that, as the carrier frequency f varies, the propagation characteristics vary. This paper is concerned with only one value of frequency f, viz., 2·9 Mc/s.

Detailed numerical calculations in this paper are restricted to only one type of propagation, viz., ionospheric propagation. During the period of observation, 18–23 hr I.S.T., reliable and continuous propagation from the sources involved to Poona is via the F_2-layer. In the results reported in the paper, the average of the ten highest impulses out of the large number received every minute is taken as a measure of the noise. Hence, in almost all cases, values measured correspond to maximum values. Fading can, therefore, be neglected. For these pulses of short duration, focusing can also be neglected. There may be absorption, but this will be small during the period of observation.

It has been shown in Section 4(a) that the noise source is equivalent to a short vertical dipole in free space. Since the height of the clouds above ground-level is not very high, it can be assumed that this dipole is practically at ground-level

VOL. 7 1955

for long-distance calculations. The unabsorbed field intensity, E_T, in μV/m due to this dipole is given by

$$E_T = \frac{212\sqrt{P}\sin^2\theta}{d} \tag{2}$$

where θ = angle the direction of radiation makes with the vertical dipole,

d = distance of the source from the point of reception in 10^6 metres,

P = power of the source at the frequency in kilowatts.

The power, P, can be obtained from equation (1) for any particular frequency. Equation (2) gives the field intensity for a single-hop transmission. Assuming a suitable loss factor for ground reflections, the field intensity for a double-hop transmission can be calculated.

If there is absorption, following the CRPL method (National Bureau of Standards, 1949), the following relations can be written:

$$\text{Absorption index} = \alpha = JQKS = \log (E_T/E_E) \tag{3}$$

$$\log (E_T/E_E) = AS \tag{4}$$

The significance of the different symbols in the equations and the source from which numerical values have been obtained for the calculations in this paper are given below.

(i) J is called the seasonal variation factor. Values for different months are given in Circular No. 462 of the National Bureau of Standards quoted earlier.

(ii) Q is the solar cycle variation factor. It can be calculated for each month on the procedure described in Circular 462 quoted, and using the CRPL predictions.

(iii) K is the absorption factor. This is a quantity to be deduced from experimental results if necessary.

(iv) E_T is the unabsorbed field intensity. It is the field intensity for $K = 0$, i.e., $A = 0$.

(v) E_E is the observed field intensity for different values of K, i.e., for different values of A.

(vi) $A = JQK$. This can be calculated from the values of J, Q, and K.

(vii) S is a function of the frequency and the distance travelled in the absorbing medium.

The only other quantity required for calculations is the loss factor for ground reflection, and this is required for double-hop calculations. From Circular 462 quoted above, this will be taken as 0·63. The height of the F_2-layer will be assumed to be 320 km, the value given in the circular mentioned.

S values are not directly given in the circular mentioned. They can, however, be calculated from the data in the circular mentioned as follows. Figs. 7.11 to 7.30 in Circular 462 give the field intensity for different values of A, including the value, $A = 0$. Each figure gives the field intensity for a particular distance at

different frequencies for different values of A for 1 kW effective radiated power. Therefore, from each figure, the value of S can be calculated by using equation (4). Thus S values can be obtained for single hop transmissions for different distances like 400, 800 etc., in km. Then, a graph is plotted "S value–distance." From this graph, the required values of S can be read off for the distances for which they are necessary.

It will thus be seen that the numerical data required for the different constants in propagation calculations are chosen entirely from Circular No. 462 of the U.S. National Bureau of Standards.

The CRPL method of calculations for the F_2-layer ionospheric propagation has been chosen for the calculations in this paper because of its simplicity. The method has been used for propagation calculations in connection with some field-strength and absorption measurements in the laboratory, and is found to give consistent and satisfactory results.

(c) *Probable sources of noise*

For defining the position of the equivalent radiator, the probable sources of atmospheric radio noise have to be indicated and their position defined by a mean distance from Poona. The distribution of thunderstorm days over the globe is available in the form of charts (Brooks). The latest available information on the distribution of thunderstorm days on land masses has been published in the form of tables (World Meteorological Organization). The latest available information on the distribution of thunderstorm days on the land mass of India has been analyzed (Aiya, 1954b). It is, therefore, possible to indicate the regions from which noise arises during different months and estimate the mean distance of such sources from Poona. The details of the possible sources of atmospheric noise at 2·9 Mc/s at Poona during the period of day 18–23 hr I.S.T., are as follows.

(i) Regions lying in or about Malaya, Java, etc.: These are equatorial regions lying within about 5 degrees of the equator. There is intense thunderstorm activity all the year round. At any given time, several thunderstorms may be in progress. Noise from these sources is made up of a very large number of impulses and will give the impression of type A noise. The mean distance of these sources from Poona is 4000 km. The noise radiation probably reaches Poona by a double-hop transmission. The received noise-field strength will be low and will become important in the absence of other nearer sources. They thus appear to be responsible for type A noise received during November, December, January, and February.

(ii) Bay of Bengal: There is, throughout the year, some activity in the Bay of Bengal. Very reliable and detailed data are not yet available. The World Meteorological Organization is at present busy converting the available data on lightning seen to thunder heard by a statistical process. The available data indicate that the activity extends over a wide area. At a mean distance of about 2000 km from Poona, there is always some activity, but it is not such as to give rise to more than ten impulses per minute all the year round. However, the activity becomes pronounced from February onwards, and continues in this

VOL. 7 1955

manner till about November. This is particularly so in regions nearer the land mass of India. These sources lie between 5 and 20 degrees north. They give rise to impulsive noise, i.e., type B noise, and the magnitude of the noise will be greater than that due to sources listed in (i). Between February and November, noise due to these sources will predominate during periods of a month when the activity on the land mass of India is weak, i.e., during February, early November, and some days of March, August, and September. During October, noise due to activity on the land mass of India round Bengal being more probable, the effect of these sources may not be felt in Poona.

(iii) Land mass of India: From March to October, there is enough activity on the land mass of India to give rise to noise at Poona. There can be local thunderstorms giving rise to type C noise. During March–May, the clouds are very high, and noise due to extremely local thunderstorms may be received as an optical ray. If the E-layer persists for some time after sunset, some reflection from the E-layer may be possible. Similarly, there is the possibility of reflection from the sporadic E-layer. In all such cases, type C noise has been noticed, but these are all exceptions. Ordinarily, type C noise which is due to ground-ray propagation and arises from local thunderstorms occurring within about 40 km from Poona, is what is to be expected at 2·9 Mc/s, and is what is actually observed. In this common case, there is no abrupt or very sudden change of noise value from hour to hour. Changes of noise value from before sunset to after sunset are also gradual, and show the general trend that corresponds only to the growth and decay of the activity of a thunderstorm.

The equivalent of a tropical thunderstorm as a noise radiator is a short vertical dipole in free space. Therefore, for F_2-layer propagation, the sky-wave intensity due to sources between 400 and 1000 km from Poona will be greater than the sky-wave intensity due to sources within 400 km. Hence, the major sources of atmospheric noise in Poona during March–October are sources lying between 400 and 1000 km from Poona. All of them are between 8 and 28 degrees north. They give rise to type B noise, and can be assumed to be at a mean distance of 700 km from Poona.

During October, sources in and around Bengal at a mean distance of 1500 km from Poona may predominate when nearer sources are weak or inactive. The South Indian sources continue in activity during November and even December, and are probably responsible for impulsive noise received occasionally during these months. The mean distance of these sources is about 1300 km.

(d) *Estimation of power radiated by noise sources*

As explained in Section 4(a), the noise source is equivalent to a short vertical dipole. The median value of the power radiated by this equivalent radiator, which corresponds to the noise-field strength as measured by the noise meter used for measurements reported in this paper during the period of peak activity of the source, is given by equation (1). This gives a power of 5·35 watts at 2·9 Mc/s. This value of power will be used to estimate noise levels.

It is seen from Section 4(c) that there are various sources responsible for noise in Poona. All of them are in the tropics, but some are on land masses and some

over the sea. Equation (1) is based on the idealized statistically valid representation of a lightning flash. Before using the power given by the equation, it is necessary to examine how far this statistically idealized representation is a true picture of lightning flashes associated with thunderstorms occurring over land and sea during the period of observation, 18–23 hr I.S.T. There is no simple and direct way of doing this. It is, however, possible to draw some inference on this point indirectly. It is possible to estimate the power radiated from the statistically assessed noise-field strengths for the same type of noise arising in the same month from two different sources, by assuming that the power radiated by both the sources is the same. If this estimate is of the same order as that given by equation (1), it would be reasonable to assume that the power given by equation (1) is valid for the different sources. An attempt will, therefore, be made to estimate the power on the lines indicated from the results given in Table 1.

Suppose there are two sources of noise in the same month. One may be called source 1, and the other source 2. Assume, for argument purposes, that there is a small absorption in the ionosphere for the F_2-layer propagation under night conditions and that it is the same for both the sources during the month. Then, using equations (2) and (3), the following can be written:—

$$\frac{\log \dfrac{212\sqrt{P}\sin^2\theta_1}{d_1E_1}}{\log \dfrac{212\sqrt{P}\sin^2\theta_2}{d_2E_2}} = \frac{\alpha_1}{\alpha_2} = \frac{JQKS_1}{JQKS_2} = \frac{S_1}{S_2} = \delta \qquad (5)$$

and, therefore,

$$\log \sqrt{P} = \frac{1}{1-\delta}\left\{\log \frac{d_1E_1}{212\sin^2\theta_1} - \delta \log \frac{d_2E_2}{212\sin^2\theta_2}\right\} \qquad (6)$$

In equations (5) and (6), the letters have the same significance as in equations (2) and (3). The subscripts 1 and 2 stand respectively for the corresponding values of the two sources. E_1 and E_2 stand for the respective median values of noise field strength of the two sources as given in Table 1. P can be calculated from equation (6).

Table 8. Estimates of source power from two sets of type B noise data

Month	δ	E_1	d_1	θ_1	E_2	d_2	θ_2	*Power in watts*
March	$\frac{2\cdot1}{3\cdot1}$	10·8	0·7	50	5·4	2	77	6·1
August	$\frac{2\cdot1}{3\cdot1}$	10·4	0·7	50	5·0	2	77	7·5
September	$\frac{2\cdot1}{3\cdot1}$	11·0	0·7	50	5·6	2	77	5·7

Mean value of source power = 6·4 watts.

VOL. 7 1955

An examination of Table 1 shows that, during March, August, and September, type B noise is received from two sources. From the discussion in Section 4(c), it is clear that one is probably due to a source on the land mass at a mean distance of 700 km, and that the other is probably due to a source at a mean distance of 2000 km from Poona. The latter source is over the sea. The relevant data and the calculated value of power from equation (6) are given in Table 8.

The accuracy of the estimated power in the last column of Table 8 depends on the accuracy of all the seven quantities listed in the table and particularly on the value of δ. Since all the quantities except the values of E_1 and E_2 are the same for all the three months, the differences in the calculated values of P power are due to the differences in the values of E_1 and E_2. It is possible that the actual mean distance of the sources may be differing slightly, from month to month, from the mean distance assumed. Further, the values of θ depend on the assumed height of the F_2-layer. It is not impossible that this height may differ slightly from month to month from the assumed mean height of 320 km. The mean value of the estimated power is 6·4 watts, and this is within one db of the power estimated from lightning discharge data, viz., 5·35 watts. In the light of the discussion, this agreement should be considered satisfactory. It will, therefore, be reasonable to assume the power as deduced from lightning discharge data viz., 5·35 watts, as the power of the equivalent radiator for all noise estimations.

Table 9. Estimated noise levels from lightning discharge data at Poona at 2·9 Mc/s during 18–23 hr I.S.T. for sources other than local

No.	*Source*	*Mean distance in km*	*Type of noise*	*Value in $\mu V/m$*	*Mode of trans.*	*Months when expected*
1.	Land mass of India	700	B	13·0	one hop.	Very frequently between March and October.
2.	Do.	1300	B	10·2	do.	Sometimes during Nov.–Dec.
3.	Do.	1500	B	9·2	do.	Occasionally during October.
4.	Bay of Bengal	2000	B	7·3	do.	Throughout the year whenever stronger sources are not active. Ten impulses per min not always probable during Nov.–Feb.
5.	Malaya, Java, etc.	4000	A	2·3	two hop.	All the year round, but presence felt when all other sources are absent, i.e., Nov.–Feb.

(e) *Estimation of noise levels*

The noise level at Poona at 2·9 Mc/s can be estimated from lightning discharge data on the basis of the discussion in this section. A lightning flash is equivalent to a short vertical dipole carrying a power of 5·35 watts. This equivalent radiator is considered to be located at a distance from Poona equal to the mean distance of the particular set of sources involved. The noise received by the sky-wave has been calculated in the manner explained in Sub-section 4(b), and the results are shown in Table 9. The values of noise-field strength given in the table are median values.

Noise received by sky-wave propagation at Poona at 2·9 Mc/s appears to arise from three principal sources, viz., 1, 4, and 5. Sources 1 and 4 are responsible for type B noise, and source 5 for type A noise.

Type C noise arises from local thunderstorms and is received mainly as a ground-ray. Assuming that $\sigma = 10^{-13}$ e.m.u. and $\varepsilon = 4$ for regions round Poona, if ground-ray calculations are carried out by following the procedure given by BREMMER (1949), it is found that the field strength varies from 13 to 290 μV/m as the distance of the source decreases from 40 to 10 km from Poona. Values of special interest are those which can be compared with the 90 per cent of the time-satisfactory service data in Table 2. A possible way of estimating these is given below.

A thunderstorm day is defined as a local calendar day on which thunder is heard. This requirement limits the area covered to a circle of radius 20 km. Suppose, during a season, a place is in an area having n local thunderstorm days. Then, the radius, R, of the circle in which ten local thunderstorms occur is given by

$$\frac{10}{n} = \frac{\pi \,.\, R^2}{\pi \,.\, (20)^2} \tag{7}$$

Hence, R can be calculated, if n is known. This R, therefore, is the maximum distance from the place at which any one of the ten local thunderstorms can occur. Hence, the minimum noise-field strength due to local thunderstorms during a season when the number of local thunderstorms is taken as ten, is the field strength due to a local thunderstorm occurring at a distance R from the place. Let this field strength be called E_C.

In a season, there are ninety to ninety-two days. Therefore, if there are ten

Table 10. *Minimum values of local storm noise at Poona at 2·9 Mc/s for* 10 *per cent of the time in a season for the hours* 18–23 *I.S.T.*

Season	n *Number of thunderstorm days*	*Corrected number of thunderstorm days for* 18–23 *I.S.T.*	R *Radius of circle in which ten thunderstorms occur in km*	E_c *Noise value in* $\mu V/m$
March–May	8	8	22·5	51
June–Aug.	4	4	31·6	25
Sept.–Nov.	9	3	36·5	16
Dec.–Feb.	1	—	—	—

VOL. 7 1955

local thunderstorm days in a season, the noise value for 90 per cent of the time-satisfactory service is that due to local thunderstorms. Hence, E_C gives the noise value for 90 per cent of the time-satisfactory service, when E_C is greater than noise received by sky-wave. The values of n for Poona have been published (AIYA, 1954b). These values have to be corrected if the local thunderstorms do not show their peak activity after sunset. Experimental observations for the last three years have shown that this correction is necessary for the season September–November, when only 30 per cent of the local thunderstorms show peak activity after sunset. Table 10 gives the results.

Type C noise estimations cannot be carried out for a month, as the number of local thunderstorms are too few and calculations will have no significance. Even for a season, calculations of Table 10 are for ten local thunderstorms only. If these occur in a circle of radius R, it is assumed that the field strength due to the source being at this extreme distance of the area is the noise value. The value of power used for the calculations is the statistical median value of 5·35 watts. Taking into consideration all these facts, it appears that the calculated values may be lower than actual values by factors up to 6 db. These questions will be discussed in detail in a future communication referred to already in Section 3(b), in discussing noise grade, etc.

(e) *Comparison of estimated and measured values*

For noise received by sky-wave propagation, there are three principal sources. The estimates of noise for these sources and the corresponding measured values during different months from Table 1 are given in Table 11. It will be observed from the table that the measured values of type B noise are within 3 db of the estimated values. Having regard to the wide range of data required, this agreement appears to be very satisfactory. For type A noise, the measured values are

Table 11. *Measured and estimated sky-wave noise at Poona at 2·9 Mc/s during 18–23 hr I.S.T.*

Probable source	*Type of noise*	*Mean distance of source in km*	*Estimated noise from lightning discharge data in μV/m*	*Measured values of noise in μV/m*											
				January	*February*	*March*	*April*	*May*	*June*	*July*	*August*	*September*	*October*	*November*	*December*
Land Mass of India	B	700	13·0	—	—	10·8	10·0	11·0	10·6	11·0	10·4	11·0	9·9	—	—
Bay of Bengal	B	2000	7·3	×	×	5·4	—	—	—	—	5·0	5·6	×	×	×
Regions near Malaya, Java, etc.	A	4000	2·3	0·7	0·8	—	—	—	—	—	—	—	—	1·0	1·1

— indicates "not observed." × indicates "observed occasionally."

lower than the estimated values by 6 db. Even after allowing for possible inaccuracies of calculation or data and experimental inaccuracies, this difference between measured and estimated values appears to be rather large. This fact and the general trend of all type B noise measured values being consistently lower than the estimates indicate that (a) either there is some quantity in the data for estimates which is perhaps high or (b) that there is probably a very small absorption in the ionosphere even for F_2-layer propagation under night conditions. The increase of the difference between measured and estimated values with increase of distance of the source appears to indicate that some small absorption may possibly be one of the factors contributing to the difference between measured and estimated values. Calculations carried out on the procedure described in Section 4(b) show that the difference between measured and estimated values of noise can be explained by assuming an absorption factor of value between 0·03 and 0·05 for the period 18–23 hr I.S.T. for a month. No conclusions about the possibility of absorption in the ionosphere of this order can possibly be drawn from noise measurements. However, the discussion indicates that measurements of ionospheric absorption under night conditions would be of interest to workers in the field of noise interference.

A comparison of the results in Table 10 with those in the last column of Table 2 shows satisfactory agreement for type C noise.

Actual noise estimations, as required for a detailed comparison with the results as given in Table 2, have to be based on a generalized analysis of the distribution of thunderstorm activity over the globe for noise estimation purposes, the definition of noise grade, etc.; these questions will be discussed, as mentioned earlier, in a future communication.

VOL. 7 1955

5. CONCLUSION

There appears to be reasonable agreement between measured and estimated values of noise at 2·9 Mc/s at Poona for the period of day, 18–23 hr I.S.T. It seems that an objective method of measuring noise evolved out of subjective considerations, when used for the collection and assessment of noise data on a statistical basis, can prove useful for noise measurements. The results reported in this paper are for one service, viz., broadcasting. From the comparison of the results reported in this paper with the measurements of the Radio Research Board, London, it appears that the data as collected for this paper may prove useful for another service, viz., low-speed C.W. telegraphy.

The probability of some ionospheric absorption at night, i.e., after sunset, has recently been reported (APPLETON and PIGGOTT). It has been indicated in the section on comparison of measured and estimated values of noise that some data on night absorption in the ionosphere can prove helpful in understanding the differences between estimated and measured values.

Acknowledgement—A grant from the University of Poona and a scholarship to one of us (K. R. P.) by the Government of India in the Ministry of Education are gratefully acknowledged. The authors' thanks are also due to L. A. RAMDAS and K. N. RAO for permission to use the library of the India Meteorological Department.

References

Aiya, S. V. C.	1954a	*J. Atmosph. Terr. Phys.* **5,** 230
	1954b	*J. Sci. Industr. Res.* **13A,** 314
	1955	*Proc. Inst. Radio. Engrs.* (in print)
Aiya, S. V. C., Khot, C. G., Phadke, K. R., and Sane, C. K.	1955	*J. Sci. Industr. Res.* (in print)
All India Radio	1939	*Report on Progress of Broadcasting in India,* New Delhi
Appleton, E. V., and Piggott, W. R.	1954	*J. Atmosph. Terr. Phys.* **5,** 141
Bremmer, H.	1949	*Terrestrial Radio Waves,* Elsevier Publishing Co., London
Brooks, C. E. P.	1925	Meteorolog. Office, Geophys. Mem. and Prof. Notes, No. 24
Chakravarti, S. P., Ghosh, P. B., and Ghosh, H.	1939	*Proc. Inst. Radio. Engrs.* **27,** 780
Hunt, F. V.	1933	*Rev. Sci. Instr.* **4,** 672
Jaegar, J. C.	1943	*Coun. Sci. Ind. Res.* (*Aust.*), Report No. 184
Khastgir, S. R., and Ali, M. I.	1942	*Ind. J. Phys.* **15,** 399
Khastgir, S. R., and Rao, M. K.	1940	*Proc. Inst. Radio. Engrs.* **28,** 511
National Bureau of Standards	1949	*Ionospheric Radio Propagation,* Circular No. 462, Washington
Ollendorf, F.	1930	*Elekt. Nachr. Tech.* **1,** 108
Radio Research Board	1947	*Radio Research Special Report No.* 15, London
	1953	*Radio Research Special Report No.* 26, London
Thomas, H. A.	1950	*J. Inst. Elect. Engrs.* **97(3),** 329
World Meteorological Organization	1953	*World Distribution of Thunderstorm Days, Part I—Tables,* Geneva

Journal of Atmospheric and Terrestrial Physics, 1955, Vol. 7, pp. 278 to 284. Pergamon Press Ltd., London

A theoretical model for high-frequency backscatter from the sea surface via the ionosphere

WILLIAM C. HOFFMAN*

(*Received* 4 *March* 1955)

ABSTRACT

The sizable backscatter from the ocean for high-frequency radio waves propagated via the ionosphere is accounted for, using an essentially realistic model of the sea surface. The sea surface is in fact random; however, a good working approximation (at least in the case of high-frequency radio waves) is a perfectly-conducting doubly-trochoidal or doubly-sinusoidal surface. The average far-zone backscattered power is computed for each type of surface on the basis of the "current distribution" method and Breit-Tuve theorem. The assignment of realistic values to the ocean parameters then yields values of the back-scattered power which are of the same order of magnitude as those observed.

1. INTRODUCTION

THE sizable backscatter from the sea surface for ionospheric propagation of high-frequency radio waves has been noted by many investigators (VILLARD and PETERSON, 1952a, b), and at first sight appears somewhat surprising in view of the radio wavelengths involved (10–300 m). The observed backscatter from the sea is often of the same order as that from such irregular terrain as the Rocky Mountains or the Alps. However, in the analogous situation of a polished mirror, it seems to be well known (KELVIN, 1904) that the mirror can be considered as polished, and therefore as specularly reflecting, only if the surface roughness does not exceed 1/200 of the wavelength of the incident radiation. In the present application a reasonable average for the height of ocean waves is, say, two metres. On the basis of the above criterion one is therefore led to expect some nonspecular reflection at high radio frequencies. That the roughness of the sea surface is sufficient to explain the order of magnitude of the observed backscatter is the burden of this paper.

It seems to be well established on the basis of the observed travel times that the normal backscatter echo originates at the earth's surface, and not at some ionospheric layer (PETERSON, 1951; DIEMINGER, 1951; ABEL and EDWARDS, 1951). Some observers (PETERSON, 1951) have noted no appreciable difference between backscatter from land and sea, while others† (TAYLOR and YOUNG, 1929) have detected noticeable differences. If there does in fact exist a difference between land and sea backscatter for comparable degrees of roughness of the illuminated area, it may perhaps be attributed to the fact that the conductivity of sea-water exceeds that of ground by a factor of at least 100.

VOL. 7 1955

---

* Work done at U.S. Navy Electronics Laboratory. Author's present address is Rand Corp., Santa Monica, California, U.S.A.

† K. MIYA, T. KOBAYASHI, and N. WAKAI. "Field Intensity of Scattered Wave in Radio Wave Propagation," *Rep. Ionosph. Res.* (*Japan*) **5**, 55–73 (1951). While this investigation dealt primarily with forward-scatter, the forward-scatter was observed to be appreciably lower in propagation over sea. It is plausible that at least some of the non-specularly reflected energy went into backscatter.

2. Possible Models for the Sea Surface

According to Stoke's results of 1847, the free surface of waves in a fluid which is not wind-driven very nearly takes the shape of a trochoid (Sverdrup *et al.*, 1946). This is a wave profile (that is, the wave crests are assumed to be infinitely long), rather than a wave surface, and an actual sea profile is described only very approximately by this model (Sverdrup *et al.*, 1946; Bigelow and Edmundson, 1947).

The existence of "cross-sea," i.e., waves travelling in various directions, the so-called short-crested waves, should also be taken into account in the model. Jeffreys (Sverdrup *et al.*, 1946) has shown theoretically the existence of doubly-sinusoidal ocean waves of the form $z = a \cos(\sigma t - \kappa x) \cos \kappa' y$. This surface (with $t = 0$), and the doubly-trochoidal surface, will be assumed as models of the sea surface in the analysis to follow.

It is well known that the sea surface is in fact random, so that the models assumed above can only be regarded as rough approximations (Sverdrup *et al.*, 1946). However, some justification may perhaps be gleaned from the fact that the radio wavelengths under consideration (of the order of 10–300 metres) are presumably sensitive only to the larger variations in the sea surface, and the latter are almost trochoidal. However, it is definitely not the case that sea waves repeat with the same height and period, and the surfaces assumed here are admittedly unrealistic in this regard. It follows that the approach of the present paper can give order-of-magnitude relations, but no more.

In a similar approach to the problem of scattering from a random surface, the author has expressed the mean and covariance of the scattered field in terms of the mean and covariance of the perfectly-conducting random surface. However, statistical estimation of the correlation function of the sea surface appears to be an oceanographic problem of considerable magnitude, and numerical results can be obtained at present only for the rough models described in this paper.

In regard to the electrical properties of the sea surface, perfect conductivity will be assumed. While this is not exactly true, the fact that at the radio frequencies under consideration the skin depth is only a few centimetres (Stratton, 1941) indicates the closeness of the approximation.

3. The Backscattered Energy

Since we are interested in order-of-magnitude relations only, no essential loss of accuracy results from assuming a plane-earth plane-ionosphere geometry. Then, by the Breit-Tuve theorem, one may regard the ionosphere as a perfect mirror at the virtual height h, and the geometry is as appears in Fig. 1A and 1B. It is clear from Fig. 1B that the range to the centre of the illuminated area on the earth's surface is given by

$$R = \frac{2h}{\cos \iota} \tag{1}$$

where ι is the angle of incidence. Then, for an antenna of beamwidth B, and a pulse of duration τ, the width of the illuminated area is

$$w = \frac{2h}{\cos \iota} \tan (B/2). \tag{2}$$

and the length of the illuminated area is*

$$l = \frac{\frac{1}{2}c\tau}{\sin \iota} \tag{3}$$

Expressions for the far-zone field backscattered from a large doubly-trochoidal or doubly-sinusoidal surface have been derived elsewhere.† The derivation is based on the "current distribution" method of antenna theory (SILVER, 1949), and

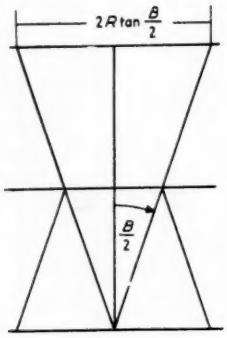

Fig. 1A. End view of earth-ionosphere geometry

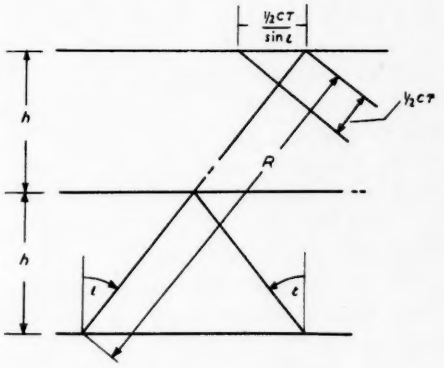

Fig. 1B. Side view of earth-ionosphere geometry

so the expressions given below are subject to the condition that there exists no shielding of parts of the surface by other parts, and to the approximations inherent in the Kirchhoff approximation (BOUWKAMP, 1954).

It can then be shown‡ that the average backscattered power received by an antenna in the far-zone is given by

$$P_r = \frac{P_0 G^2}{24\pi^2 R^4} \tag{4}$$

where P_0 is the average transmitted power, G is the gain over a dipole, R is given by formula (1), and $\mathcal{J}$ is a parameter characteristic of the surface with values given by the formulas below. In terms of voltage delivered to the terminals of an antenna of resistance Ω, the received energy is

$$E_r^2 = \frac{P_0 G^2}{24\pi^2 R^4} |\mathcal{J}|^2 \Omega. \tag{5}$$

---

* The factor ½ arises from the fact that we are considering two-way transmission. See L. N. RIDENOUR, "Radar System Engineering," McGraw-Hill Book Co., 1947, p. 85.

† *Trans. Inst. Radio Engrs. Prof. Group on Antennas and Propagation*, Vol. AP-3, no. 3, July, 1955.

‡ All derivations are given in the article referred to in the preceding footnote.

VOL. 7 1955

Consider first a doubly-trochoidal surface with waves of height δ and wavelengths Λ and Λ' in the x and y directions, respectively, and let

ι be the angle of incidence (Fig. 2);

λ be the wavelength of the incident radiation;

$$N = \Lambda/\delta; \quad M = \Lambda'/\delta; \tag{6}$$

w and l be given by (2) and (3) respectively;

W and L be the *nearest* integers to w/Λ' and l/Λ respectively;

$$\beta = 2\,\frac{\Lambda}{\lambda}\sin\iota; \tag{7}$$

$$\gamma = k\delta\cos\iota = 2\,\frac{\Lambda}{\lambda}\,\frac{\pi}{N}\cos\iota; \tag{8}$$

$$\Theta = \beta\left(\pi\,\frac{l}{\Lambda} - \frac{\pi}{N}\sin\pi\,\frac{l}{\Lambda}\right); \tag{9}$$

$$\Phi = \gamma\cos\pi\,\frac{l}{\Lambda} \tag{10}$$

Then for a doubly-trochoidal surface the parameter $\mathscr{J}$ is given by the expression

$$\mathscr{J} = \frac{1}{2\pi}\,W\Lambda'\lambda\cot\iota\left[\sin\Theta J_0(\Phi) + \frac{\pi}{M}\cos\Theta J_1(\Phi)\right] + \frac{\delta}{2\sin\iota}\,W\Lambda'\,\frac{\sin L\beta\pi}{\sin\beta\pi}\,e^{-i\beta\pi}$$
$$\times\int_0^{2\pi}\exp\left\{i\beta\left(\xi \mp \frac{\pi}{N}\sin\xi\right)\right\}\left\{\pm\frac{\pi}{2M}\left[J_0(\gamma\cos\xi) - J_2(\gamma\cos\xi)\right]\right.$$
$$\left. + iJ_1(\gamma\cos\xi)\right\}\sin\xi\,d\xi, \tag{11}$$

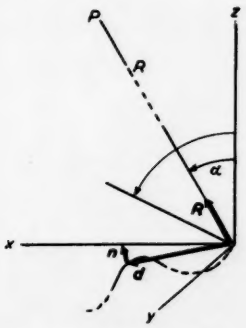

Fig. 2. Co-ordinate system for far-zone backscattered field.

with the upper sign being chosen for L even and the lower sign for L odd. It appears that the integral in equation (11) can only be evaluated numerically. Due to the rapid oscillation of the complex exponential in the integrand, a large number of subintervals must be employed in the numerical integration.

In the case of a doubly-sinusoidal surface, the expression for the parameter $\mathscr{J}$ takes the form

$$\mathscr{J} = \frac{1}{2\pi} W\Lambda\Lambda' \left\{ -\frac{\lambda}{\Lambda} \tan \iota J_0(\Phi) \sin\left(\beta\pi \frac{l}{\Lambda}\right) + \frac{2}{\cos \iota} \sum_{n=0}^{\infty} \varepsilon_n (-1)^n \frac{J_n{}^2\left(\frac{\gamma}{2}\right)}{(2n)^2 - \beta^2} \left[2n \sin\left(2n\pi \frac{l}{\Lambda}\right) \cos\left(\beta\pi \frac{l}{\Lambda}\right) - \beta \cos\left(2n\pi \frac{l}{\Lambda}\right) \sin\left(\beta\pi \frac{l}{\Lambda}\right) \right] \right\}, \tag{12}$$

where the various parameters in the expression are defined in the same way as for the doubly-trochoidal case (equations (6)–(10), etc.). The series in expression (12) converges quite rapidly for the range of values of γ encountered in connection with high-frequency backscatter from the sea surface—in fact, two or three terms are ordinarily enough. The doubly-sinusoidal surface thus leads to considerably more convenient computations than the doubly-trochoidal surface.

4. Comparison with Experiment

Values of backscatter observed with the equipment at the U.S. Navy Electronics Laboratory fall in the range 4–100 microvolts. It will be shown below that values of the backscattered energy computed from formula (5) for the doubly trochoidal and doubly-sinusoidal models of the sea surface fall within this range.

The equipment at the U.S. Navy Electronics Laboratory consists of a rhombic antenna with a switching device capable of aiming it in two directions; over land from San Diego to Washington, D.C., and over sea toward Australia. The antenna and transmitter parameters required for use in expressions (2), (3), and (5) have the following values:

P_0 = effective (average) radiated power = 1·25 kW.

$G = 10$

$\Omega = 600$ ohms

$B = 12°$

$\iota = 78°$

Assuming a virtual ionospheric height of 300 kilometres, expression (1) gives for the range

$$R = 2886 \text{ km} \tag{13}$$

Thus

$$\frac{P_0 G^2}{24\pi^2 R^4} \Omega = 0{\cdot}4564 \times 10^{-20} \tag{14}$$

The remaining factor $|\mathscr{J}|^2$ in equation (5) has to be evaluated by numerical integration in case of a doubly-trochoidal surface, and by summing the first few

VOL. 7 1955

terms of a series for a doubly-sinusoidal surface. The results of such a programme for a few common ocean wavelength to waveheight ratios (BIGELOW and EDMUNDSON, 1947): $N = \Lambda/\delta$ and $M = N$, a waveheight δ of 2 metres, radio frequencies of 6 and 15 mc, and pulses of 0·1 and 1 millisecond duration, are given in the following tables:

f = 6 mc

Λ (*metres*)	*Doubly-trochoidal surface*		*Doubly-sinusoidal surface*	
	E_τ		E_τ	
	$\tau = 100\ \mu s$	$\tau = 1$ ms	$\tau = 100\ \mu s$	$\tau = 1$ ms
14	12·1 μV	36·6 μV	2·9 μV	33·1 μV
20	9·4	19·2	1·8	14·1
30	6·7	18·5	1·7	13·0
36	1·0	9·1	3·3	13·9
40	5·9	9·2	2·4	13·8

f = 15 mc

Λ (*metres*)	*Doubly-trochoidal surface*		*Doubly-sinusoidal surface*	
	E_τ		E_τ	
	$\tau = 100\ \mu s$	$\tau = 1$ ms	$\tau = 100\ \mu s$	$\tau = 1$ ms
14	14·1 μV	4·9 μV	1·8 μV	2·2 μV
20	25·5	10·6	11·3	5·5
30	6·5	4·2	2·9	9·2
36	0·2	0·3	2·5	5·7
40	7·4	6·6	0·08	1·5

From the above tabulations it is clear that the backscattered energy falls within the range mentioned at the beginning of this section, and so can be regarded as in agreement with respect to order of magnitude. The fact that for the same surfaces the computed backscatter is in general less for a 15-mc radio wave than for a 6-mc radio wave may perhaps be attributed to the very special choice of an ocean waveheight of two metres. In view of the fact that an ordinary sea consists of waves of heights from zero to four metres, and all wavelength-to-waveheight ratios from 7 : 1 to 100 : 1, it is apparent that predictions cannot be based on expression (5) unless the evaluation of $\mathcal{J}$ is radically modified. The present results apply only to average backscattered power, and then only with respect to order of magnitude. It can, however, be argued on the basis of the order of magnitude agreement between theory and observation as well as the travel-time evidence previously referred to, that backscatter originates from the sea surface for high-frequency ionospheric propagation.

REFERENCES

ABEL, W. G., and EDWARDS, L. C.	1951	The source of long distance backscatter. *Proc. Inst. Radio Engrs.* **39,** 1538–1541
BIGELOW, H. B., and EDMUNDSON, W. T.	1947	*Wind Waves at Sea, Breakers and Surf.* U.S. Navy Hydrographic Office, Public. No. 602, pp. 47–49
BOUWKAMP, C. F.	1954	Diffraction theory. *Rep. Progr. Phys.* **17,** cf. p. 49
DIEMINGER, W.	1951	The scattering of radio waves. *Proc. Phys. Soc. London* **B64,** No. 2, 142–158
KELVIN, Lord	1904	*Baltimore Lectures on Molecular Dynamics and the Wave Theory of Light* (Clay & Sons, London), pp. 327–8, 374
PETERSON, ALLEN M.	1951	The mechanism of *F*-layer propagated back-scatter echoes. *J. Geophys. Res.* **56,** No. 2, 221–237
SILVER, S.	1949	*Microwave Antenna Theory and Design,* (McGraw-Hill Book Co.) Sections 5.7–5.8
STRATTON, J. A.	1941	*Electromagnetic Theory* (McGraw-Hill Book Co.) p. 505
TAYLOR, A. HOYT, and YOUNG, L. C.	1929	Studies of echo signals. *Proc. Inst. Radio Engrs.* **17,** 1491–1507, esp. p. 1495
SVERDRUP, H. U., JOHNSON, M. W., FLEMING, R. H.	1946	*The Oceans* (Prentice-Hall), Chap. XIV
VILLARD, O. G., Jr., and PETERSON, A. M.	1952a	Scatter-sounding: a new technique in ionospheric research. *Science* **116,** 221–224
VILLARD, O. G., Jr., and PETERSON, A. M.	1952*b*	Scatter-sounding: a technique for study of the ionosphere at a distance. *Trans. Inst. Radio Engrs.*, Professional Group on Antennas and Propagation PGAP–3 (Aug)

VOL. 7 1955

Journal of Atmospheric and Terrestrial Physics, 1955, Vol. 7, pp. 285 to 291. Pergamon Press Ltd., London

Infrared spectrum of the night sky from 1·0 μ to 2·0 μ

H. P. GUSH* and A. VALLANCE JONES†
University of Saskatchewan, Saskatoon

(*Received* 4 *January* 1955)

ABSTRACT

The spectrum of the night sky from 1·0 to 2·0 μ has been obtained, using a scanning spectrometer equipped with a PbS cell detector. The spectral slit width employed varies from 100 Å to 200 Å. It has been concluded, from a comparison with synthetic spectra, that the observed spectrum must arise predominantly from the rotation-vibration bands of the OH molecule.

INTRODUCTION

PHOTOGRAPHIC investigations of the infrared spectrum of the night-glow are at present limited to wavelengths shorter than 0·9 μ. KRON (1950) and MEINEL (1950) have obtained spectra extending to 1·2 μ by using a CsO-Ag photocell as detector, while KRASOVSKI (1949, 1950) and LUKASHENIA and KRASOVSKI (1951) have examined this same region in detail, using a CsO-Ag image converter. This paper reports an extension of the observed spectrum to nearly 2 μ; this advance has been possible by the use of a PbS photoconductive cell detector.

Preliminary experiments carried out in 1952–53 (VALLANCE JONES and GUSH, 1953) showed that a PbS cell could detect radiation from the night sky in the 1–2 μ region. Low resolution spectra were obtained at that time by placing a Kodak Ektron PbS cell in the plateholder of an f/0·8 auroral spectrograph. Recently, improved spectra have been obtained with a new spectrometer which was specially designed to use a PbS cell detector. This instrument can record a spectrum of the night-glow from 1·5 μ to 1·9 μ with a spectral slit width of 200 Å in four minutes.

THE SPECTROMETER

A scale drawing of the spectrometer is shown in Fig. 1. To reduce energy losses, no lens is used in front of the slit of the spectrometer; consequently the field of view (3° × 4°) is determined by the focal length of the collimator mirror, *a* (120 in.), and the dimensions of the diffraction grating, *e*, which is the field stop. The entrance slit, which is 6 in. long, is mounted at the end of the light tunnel, *g*. Radiation from the spherical collimator mirror is dispersed by a 4-in. × 5-in. 600-line per mm plane diffraction grating (Bausch & Lomb Optical Co.). This grating is blazed at 1·08 μ. The dispersed radiation is focused on the exit slit by an off-axis paraboloid of 34-in. focal length.

The spectrum is scanned across the exit slit by rotating the grating with a cam and lever system. The scanning period may be either 4 min, 1 min, or 15 sec;

* This work was carried out during the tenure of a National Research Council of Canada Bursary by H. P. G.

† The research reported in this paper has been sponsored by the Geophysics Research Directorate of the Air Force Cambridge Research Center, Air Research Development Command, under Contract AF19(122)–152.

8 – 12 pp.

the wavelength range of the scan may be adjusted continuously from 0·7 μ to zero. In the work described here the scanning speed varied from 1200 to 600 Å/min.

The radiation passing through the exit slit is condensed on to the PbS cell by means of a "cone" channel condenser (Williamson, 1952), which provides an effective relative aperture at the detector of f/0·8. The cone channel, which is of

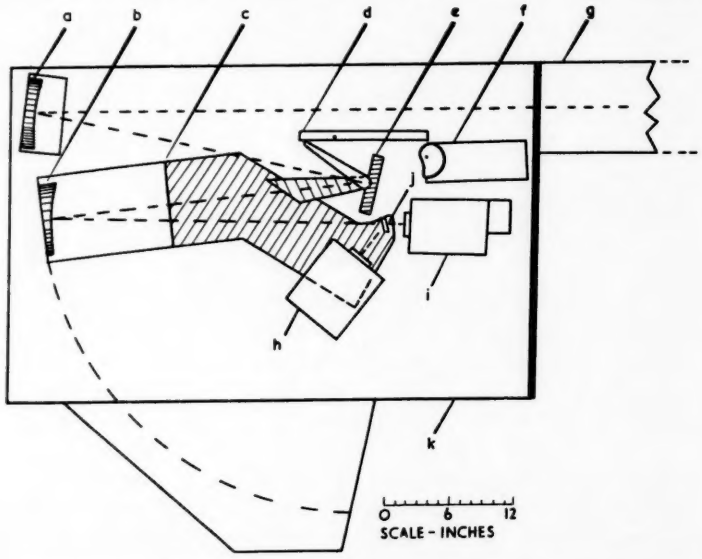

Fig. 1. Scale drawing of spectrometer. (*a*) collimator mirror; (*b*) camera mirror; (*d*) cam and lever system for rotating grating; (*e*) grating; (*i*) PbS-detecting unit with cone channel; (*g*) light tunnel at the far end of which is mounted the slit (not shown).

rectangular cross-section, is constructed from perspex; its interior surfaces are silvered. A field lens of focal length 8·5 cm is fitted just behind the slit at the entrance to the cone channel. The field lens, channel, and PbS cell, which are all enclosed in an evacuated envelope, are refrigerated with dry ice. A heated double window prevents the outer window of the detecting unit from fogging. Trial calculations showed that, for this type of spectrometer, the cone channel should be at least as good as condensing systems employing ellipsoidal mirrors. The principal advantage of the cone channel is its simplicity and its ability to work well with long slits. The radiation entering the spectrometer is modulated at 90 c.p.s. by a chopper at the entrance slit. The signal from the PbS cell is amplified by a tuned 90-c.p.s. amplifier of 1-c.p.s. band width; the amplified signal is then demodulated by a phase-sensitive detector, of which the output is displayed on an Esterline Angus recording milliammeter. The time constant of the amplifier was adjusted to a value appropriate to the scanning speed and spectral slit width.

Results

A spectrum of the 1·0–2·0-μ region, obtained with a spectral slit width of 200 Å, is shown in Fig. 2. This spectrum was obtained by averaging the results of ten runs obtained on the night of May 7, 1954. The traces obtained in the individual

VOL. 7 1955

runs are similar in all important details to the average spectrum shown in Fig. 2. These spectra were obtained with the spectrograph directed toward the north at a zenith angle of 75°. This direction of observation was chosen since the open prairie to the north of the University is free from nearby artificial lights. Since spectra similar to Fig. 2 have been obtained on many occasions during the summer of 1954 and previously (VALLANCE JONES and GUSH, 1953), it may be concluded that this emission is a permanent property of the night sky as observed from Saskatoon.

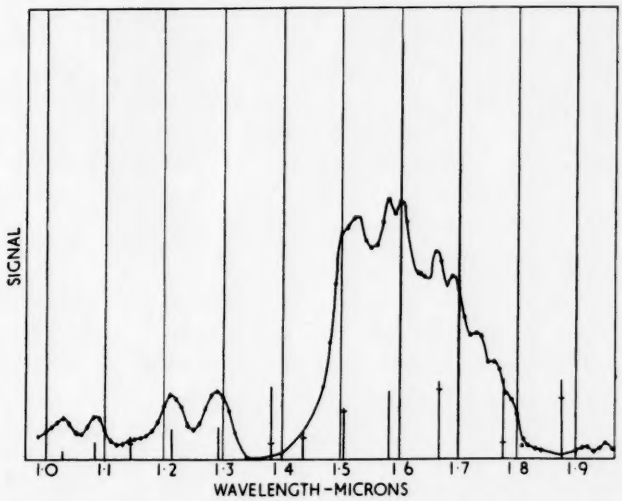

Fig. 2. Spectrum of night sky 1·0 to 2·0 μ. Spectral slit width 200 Å. Average of ten traces obtained May 7, 1951. The theoretical origins and intensities of the OH bands are shown by vertical lines across which strokes have been drawn to indicate approximately the reduction in intensity caused by atmospheric water-vapour.

It is necessary, however, to consider the possibility that the observed infrared radiation arises from scattered artificial lights, in view of the high infrared intensity of such sources. The spectrum of Fig. 2 bears a general resemblance to that of an incandescent source, as it would be modified by the atmospheric absorption bands at 1·4 and 1·9 μ. A strong argument against this interpretation is provided by the fact that the intensity maximum for radiation from an ordinary tungsten lamp (colour temperature 2800°K) falls close to 1·0 μ, whereas the maximum intensity of the night-sky spectrum lies near 1·6 μ, corresponding to a colour temperature of 1800°K. A direct experimental test was made by observing the spectrum of an automobile headlamp source set up 14·5 km from the spectrometer. This spectrum, obtained with a spectral slit width of 200 Å, is shown in Fig. 3. It is clear that there is no similarity between this spectrum and that of the night-glow, except that both show strong absorption caused by the 1·4-μ and 1·9-μ water-vapour bands. As a further check, a spectrum of the sun was obtained; this spectrum also was completely different from the night-sky spectrum.

It was possible to obtain spectra in the 1·6-μ region with a spectral slit width of 100 Å, because the emission is very intense. Fig. 4 shows the results of averaging

six runs from 1·5 μ to 1·7 μ. The standard deviation of the measured intensities is represented by the lengths of the vertical lines through the points representing the mean intensity at each wavelength.

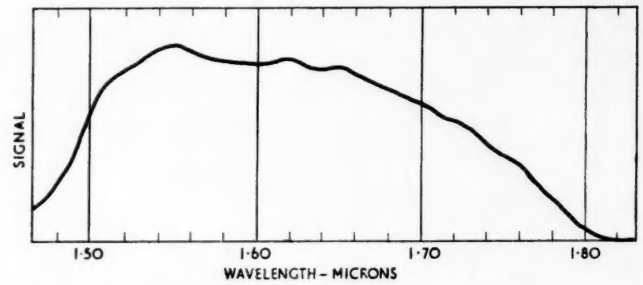

Fig. 3. Spectrum of automobile headlamp, 14·5 km from spectrometer. Spectral slit width 200 Å.

Discussion of Results

(a) *Identification of the emitted radiation*

In view of the great intensity of the OH rotation-vibration bands discovered by Meinel (1950) in the photographic infrared region of the night-glow spectrum, it is natural to suppose that this band system would contribute materially to

VOL. 7 1955

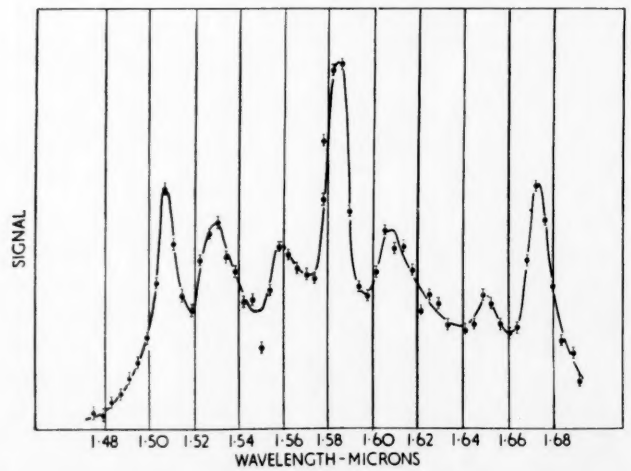

Fig. 4. Spectrum of night sky from 1·50 to 1·70 μ. Spectral slit width 100 Å. Average of six runs obtained June 13, 1954.

emission in the 1·0-μ to 2·0-μ region. Heaps and Herzberg (1952) have carried out quantitative calculations of the intensity of the bands of the system. Kron has shown experimentally that the night-glow emission from 0·9 to 1·2 μ can be accounted for in terms of OH bands. Our preliminary results showed that there was good agreement between the intensity maxima of the observed low resolution spectrum from 1·4 to 1·9 μ and the origins of the $\Delta v = 2$ sequence of OH bands.

The higher resolution spectra reported in this paper have made it possible to test more decisively the identification of the spectrum with the OH bands. Synthetic spectra of the 3,1 and 4,2 OH bands, for spectral slit widths of 200 Å and 100 Å, were constructed. The wavelengths of the rotational lines were calculated from the energy levels of the OH radical listed by DIEKE and CROSSWHITE (1948). The line intensities were calculated, using the line-strength factors given

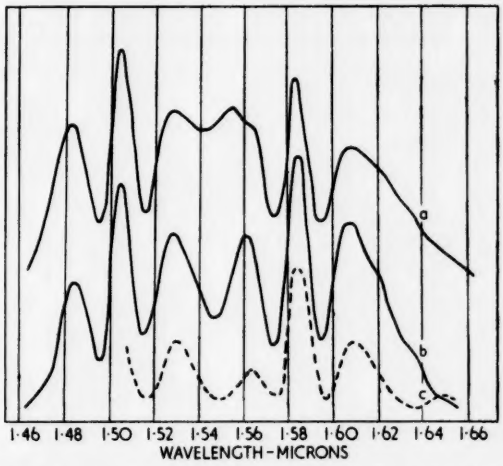

Fig. 5. (*a*) Synthetic spectrum of OH bands, spectral slit width 100 Å, temperature 260°K.
(*b*) Synthetic spectrum of OH bands, spectral slit width 100 Å, temperature 200°K.
(*c*) Observed spectrum (mean of eleven runs June 16, 1954).

by PLYLER, BENEDICT, and HUMPHREYS (1953). A triangular transmission function was assumed for the spectrometer. The synthetic spectra were calculated for 200°K and for 260°K. The latter temperature is that found by MEINEL (1950) from measurements of the rotational intensity distribution of the OH bands in the photographic infrared region.

The synthetic spectra obtained are shown in Fig. 5. Comparison between the observed spectra (Fig. 4) and the synthetic spectra for the same spectral slit width indicates that good qualitative agreement is obtained for a temperature of 200°K. This provides strong evidence that the observed spectrum is mainly that of the OH radical.

In the calculation of the synthetic spectra it is difficult to take quantitative account of the effect of the telluric water-vapour absorption lines, because the absorption profiles of these lines are not known with sufficient accuracy. This absorption probably accounts for our failure to observe the *R* branch of the 3,1 band, since the lines of this branch will be strongly attenuated by almost coincident water-vapour lines. The 2,0 band appears to be entirely extinguished for the same reason.

Between 1·0 and 1·4 μ, the peaks observed in the night-glow spectrum correspond closely with the origins of the $\Delta v = 3$ sequence of OH bands. The 6,3 and 9,6 bands appear to be extinguished by water-vapour absorption.

There can be little doubt that a major part of the radiation from the night sky from 1·0 to 2·0 μ is due to the OH molecule.

(b) *The temperature of the emitter*

It should be possible to estimate the temperature of the emitting OH radicals from the intensity distribution of the rotational lines. The form of the synthetic spectrum changes rapidly with temperature; this change is shown in Fig. 5, which shows the synthetic spectra calculated for 200°K and 260°K, and a spectral slit width of 100 Å. The observed spectrum (of which the standard deviation is

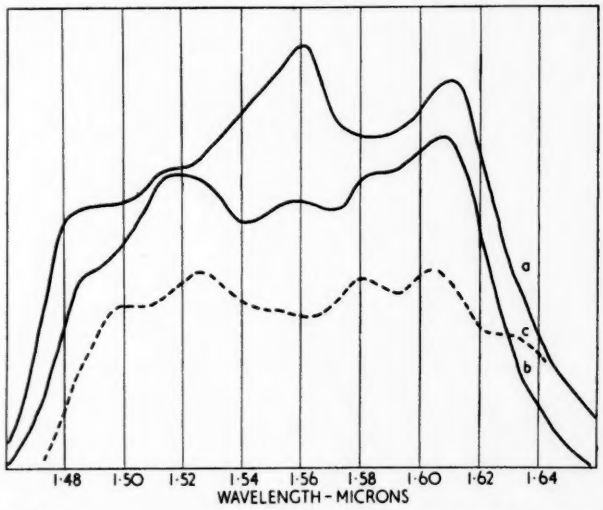

Fig. 6. (*a*) Synthetic spectrum of OH bands; spectral slit width 200 Å, temperature 260°K.
(*b*) Synthetic spectrum of OH bands; spectral slit width 200 Å, temperature 200°K.
(*c*) Observed spectrum.

indicated), is also plotted in Fig. 5. The observed spectrum appears to correspond to a temperature of 200° $\pm$ 20°. Fig. 6 shows plots of synthetic spectra of the 3,1 and 4,2 bands at 200 Å resolution, together with the observed spectrum. Since the 200°K synthetic spectrum agrees fairly well with the observed spectrum, while the 260°K synthetic spectrum is completely different, a temperature about 200°K is again indicated.

As was pointed out above, measurements of the higher sequences of OH bands in the visible region by Meinel (1950) and Oliver (1954) indicate a temperature in the neighbourhood of 260°K for the latitude of Saskatoon. A difference between the rotational temperatures of the sequences of the OH bands would be of considerable theoretical importance. While the evidence presented above for the temperature of 200°K for the $\Delta v = 2$ sequence seems strong, it would be desirable to carry out further observations with higher resolution.

A knowledge of the relative and absolute intensities of the OH bands would be of great theoretical interest. The problem is complicated by the difficulty of correcting the results for water-vapour absorption. Further work, now in progress, will enable a table of intensities to be drawn up.

VOL. 7 1955

References

Dieke, G. H., and Crosswhite, H. M.	1948	Bumblebee Report No. 87, Johns Hopkins University
Heaps, H. S., and Herzberg, G.	1952	*Z. Phys.* **133,** 48
Krasovski, V. I.	1949	*Dokladi. Akad. Nauk.* **66,** 53
	1950	*Dokladi. Akad. Nauk.* **70,** 999
Kron, G. E.	1950	*Pub. Astron. Soc. Pac.* **62,** 264
Lukashenia, V. I., and Krasovski, V. I.	1951	*Dokladi. Akad. Nauk.* **79,** 241
Meinel, A. B.	1950	*Astrophys. J.* **111,** 555; **112,** 120
Oliver, N. J.	1954	Private Communication.
Plyler, E. K., Benedict, W. S., and Humphreys, C. J.	1953	*J. Chem. Phys.* **21,** 398
Vallance Jones, A., and Gush, H.	1953	*Nature* **172,** 496
Williamson, D. E.	1952	*J. Opt. Soc. Amer.* **42,** 712

OL.
955

RESEARCH NOTE

The detection of the S_q current system in ionospheric radio sounding

(*Received* 4 *September* 1955)

USING the results now available from the world's ionospheric stations, a critical examination of the behaviour of the *E*-layer of the ionosphere has been conducted with the object of discovering how far such behaviour is explicable in terms of CHAPMAN's classical theory of ionized layer formation. It has been found that, although this theory certainly gives a broad general explanation of *E*-layer phenomena, a number of anomalies have been identified which indicate the operation of certain perturbing factors not envisaged in its formulation. Some of these anomalies have already been reported (APPLETON, 1955). The present note deals with the results of a further examination of one of them, namely the effect of electron transport phenomena on diurnal variations of maximum electron density.

We may first note that the theory of CHAPMAN is based on the simple continuity equation

$$\frac{\partial}{\partial t} N(h) = q(h, \chi) - \alpha[N(h)]^2 \tag{1}$$

where $N(h)$ is the electron density at height h and time t; $q(h, \chi)$ expresses the rate of electron production per unit volume, and so is a function of both height and solar zenith distance χ, while α is the recombination coefficient, assumed independent of both h and t. In a recent paper (APPLETON and LYON, 1955), two of us have shown how, under quasi-stationary conditions such as are believed to obtain in the *E*-layer, the layer maximum electron density N_m itself obeys an equation, similar to (1), as follows:—

$$\frac{dN_m}{dt} = q_0 \cos \chi(1 - a^2) - \alpha N_m{}^2 \tag{2}$$

where a^2 is a quantity which can be estimated, but which is usually negligible compared with unity except when χ is large.

An approximate solution of (2), with "a" neglected, suffices to express the theoretical variation of N_m over the central part of the day. This solution shows, as we should expect, that N_m should generally be greater in the afternoon than in the forenoon. Also, the maximum of N_m should occur shortly after noon. Methods of determining α' the *effective* value of the recombination coefficient, can be based on each of these two effects (APPLETON, 1937 and 1953). In the first method we compare the values of N_m for similar values of χ, before and after noon. The value of α' is then given by

$$\alpha' = \frac{\left|\frac{dN_m}{dt}\right|}{\Delta N_m \cdot N_m} \tag{3}$$

where $\left|\frac{dN_m}{dt}\right|$ and N_m are the numerical averages of the a.m. and p.m. values, and ΔN_m is the amount by which the p.m. value of N_m exceeds the corresponding a.m. value. In the second method we use the theoretical relation expressing the delay (Δt) of the N_m maximum relative to noon. This is

$$\Delta t = \frac{1}{2\alpha' N_m} \tag{4}$$

VOL. 7 1955

We may note, then, that, if simple Chapman theory were applicable to the E-layer, we should find α', as determined by way of (3) or (4), to be constant under all conditions.

As a result of the examination of a great wealth of diurnal data in relation to equations (3) and (4), we can report the most flagrant disagreements between experiment and theory, if α' is assumed constant. Indeed, estimates of the values of α', using (3) and (4), reveal relatively enormous variations of that quantity. Since it seems clear (APPLETON, 1955) that the value of the natural recombination coefficient α could not possibly vary by the amounts exhibited by α', we believe that the non-constancy of the latter is an expression of the existence of some form of perturbation. An obvious type of perturbation to be considered is the effect of electron transport.

Let us suppose, for example, that electron transport of some kind is present. Our basic continuity equation must then be written

$$\frac{dN}{dt} = q(t) - \alpha N^2 - \text{div}\,(Nv) \tag{5}$$

where v is the velocity of electron transport. If electron transport occurs in the form of vertical drift, as suggested by MARTYN (1947, 1948), it is possible to calculate theoretically (APPLETON and LYON, 1955) how the height of maximum ionization, and the value of maximum ionization itself, are altered under E-layer conditions. It is also possible to estimate the effect of vertical drift on the value of the effective recombination coefficient, α', as determined by either (3) or (4).

For example, when α' is obtained from the noon delay Δt via the simple relation (4), it may be shown that

$$\alpha' = \alpha + \frac{1}{2N}\frac{\partial(v'N)}{\partial N} \tag{6}$$

where v' is $\dfrac{\partial v}{\partial h}$, and the second term is to be evaluated at noon. If, then, the vertical drift gradient is appreciable we should expect the value of α' (and the corresponding value of Δt) to vary with latitude and any other conditions which may affect electron transport.

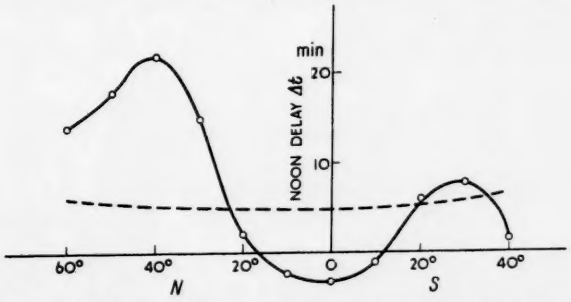

Fig. 1. The full line shows the relation between Δt (noon delay of maximum N_m) and geographical latitude for June (mean of values for the years 1953 and 1949). The broken line shows the theoretical variation for $\alpha = 10^{-8}$ cm^3/sec.

We now turn to a sample of our experimental results. In Fig. 1 the full line shows the variation of Δt (noon delay of N_m) over a wide range of latitudes for the same period of observation, and the broken line indicates the theoretical values of Δt for $\alpha' = 10^{-8}$ cm^3/sec. It will be seen that although Δt does not vary in the manner to be expected if α' were constant, it nevertheless has a definite pattern. We suggest that the pattern is related to

the S_q overhead current system which, by way of the earth's magnetic field, would be expected to cause a vertical drift pattern having a configuration related to it.

Thus MARTYN (1953) has shown that "in a given region of the ionosphere the vertical drift of ionization depends entirely on the *east-west current in that region.*" Now, near the S_q current focus the east-west component of current is always small, but at higher and lower latitudes it becomes large near noon, and the directions of flow are opposite in the two cases. Hence "it seems certain that, at the ionospheric levels where flow the currents mainly responsible for the solar and lunar magnetic variations, the daily oscillations of these regions at low latitudes must be *in phase opposition* to those at high latitudes" (MARTYN, *ibid*).

Now, if we examine the perturbation of Δt shown in Fig. 1 (relative to its theoretical value for a simple Chapman layer) we see at once that it shows precisely such a phase opposition between low and high latitudes. Increasing or decreasing α will, of course, lower or raise the broken curve in Fig. 1, but this statement will remain true for all values of α greater than about $0{\cdot}5 \times 10^{-8}$ cm^3/sec. It might be objected that the transition latitudes indicated by Fig. 1 do not agree very precisely with those obtained for the S_q current system from geomagnetic data. Thus CHAPMAN and BARTELS (1940, Fig. 16, p. 229) show the main current focus in summer at 30° N, whereas the cross-over point in Fig. 1 lies between 20° N and 25° N (depending on the value of α chosen). There are, however, several reasons why a very close agreement in this respect is not to be expected.

First, as noted by CHAPMAN and BARTELS (*ibid.*), there is very considerable variability (of the order of 10° to 15°) in the latitude of the current focus as shown by geomagnetic data, and the average appropriate to our data may differ appreciably from the value quoted.

Secondly, the geomagnetic data refer to the integrated value of the currents throughout the whole ionosphere, whereas our results refer to the maximum of the E-layer only.

Thirdly, the perturbation we have measured will depend not so much on v as on $\partial v/\partial h$, and it is not to be expected that these will necessarily be zero at the same latitude.

Fourthly, the angle between the plane of the earth's field and that of the geographical meridian is not in general negligible and may well affect the latitude of zero drift effect.

So far as the southern (winter) hemisphere is concerned, it is clear that there is agreement at any rate to the extent that both the currents flowing and the perturbations observed are much smaller. On the other hand, since the focus in this hemisphere is near 50° S, it is doubtful if the apparent change of phase at 20° S is significant. (As there are fewer stations in operation in the southern hemisphere, our values of Δt are less reliable in this region.)

Further confirmation of the above interpretation has been obtained, using some equinox results. As has already been reported, Slough equinox diurnal measurements of fE indicate that α', as determined by (3), increases rapidly as χ increases. Now, Slough is situated north of the S_q northern-current focus, and so the ionosphere there is subject to an east-west overhead current. We have, however, found that, near the latitude of the current focus itself (say between latitudes 25° and 40°), at which location the S_q currents do not run athwart the horizontal component of the earth's magnetic field in the daytime period, the application of (3) leads to sensibly constant values of α' over a considerable range of χ. In other words, the diurnal variation of E-layer ionization appears to be most nearly Chapman-like near the S_q current focus, just where we should expect vertical drift to be at a minimum. On the other hand, corresponding results of the application of (3), at both higher and lower latitudes, are subject to marked perturbations, but of opposite sense in the two cases, expressed in the inconstancy of α'. The average value of α', which

VOL. 7 1955

we have obtained, as indicated above, from stations near the current focus, is $1{\cdot}0 \times 10^{-8}$ cm^3/sec; but it should be mentioned that a relatively small residual perturbation in this region (from whatever cause) might well render this value considerably in error.

The above remarks refer to the *latitude* of the S_q current focus. We have, however, been able, by further studies of the diurnal asymmetry in E-layer ionization, to identify the *longitude* of the current focus, (15° to 30° W), relative to that of the noon meridian.

In conclusion, however we may choose to interpret points of detail, it seems clear that the S_q current system exerts a small but readily detectable influence on the diurnal variation of E-layer ionization, and most probably does so by way of some form of vertical drift mechanism.

The above results relate, as stated, to the E-layer. We find that the F_1-layer exhibits somewhat similar phenomena.

Acknowledgement—This work has been supported by way of a grant from the Department of Scientific and Industrial Research and has been carried out as part of the programme of the Radio Research Board of that Department.

E. V. Appleton
A. J. Lyon
(Mrs.) A. G. Pritchard

The University,
Edinburgh

References

Appleton, E. V. 1955 Proceedings of 4th Meeting of the Mixed Commission on the Ionosphere, pp. 14 to 22, Brussels.

Appleton, E. V., and Lyon, A. J. 1955 The Physical Society, Report of 1954 Cambridge Conference on the Physics of the Ionosphere, pp. 20 to 39.

Appleton, E. V. 1937 *Proc. Roy. Soc.* **A162,** 451.

Appleton, E. V. 1953 *Journ. Atmos. Terr. Phys.* **3,** 282

Chapman, S., and Bartels, J. 1940 Geomagnetism (Oxford: at the Clarendon Press)

Martyn, D. F. 1947–8 *Proc. Roy. Soc.* **A189,** 241, and **190,** 273; and **194,** 429 and 445

1953 *Phil. Trans.* **A246,** 281

Book review

DAUVILLIER, A.; **Les Rayons Cosmiques dans leurs rapports avec l'Electricité atmosphérique, la Métrologie, la Géomagnétisme et l'Astronomie.** Tome 1.—xii + 248 pages 16 × 25, 116 fig. 1954. Broché. 1.750 F. Tome ii.—xii + 318 pages 16 × 25, 137 fig. 1954. Broché. 2.600 F. Les deux tomes en un seul volume relié toile. 4.700 F. Dunod, Paris.

The full title of this book is Cosmic Rays and Their Relationship to Atmospheric Electricity, Meteorology, Geomagnetism, and Astronomy. In addition to the main topic, a short account is given of the more important properties of the cosmic radiation together with some details of the experimental techniques used in cosmic-ray physics. There are sections on ionization chambers, counters, and cloud chambers, and a brief description of nuclear emulsion techniques. It is to be regretted, however, that a rather disproportionate amount of space is devoted to detailed descriptions of apparatus and techniques which are now of historical interest only.

As implied by the title, the greater part of the book is concerned with the effect of the earth's magnetic field on the distribution and intensity of the primary cosmic rays, and with the variations of the cosmic-ray intensity with time. These variations in time are partly due to changing pressure and temperature distribution in the atmosphere, and partly to variations in the primary intensity which are closely linked with solar and geomagnetic activity. The process of disentangling and interpreting these primary intensity variations is far from complete, and the author has been content to give a comprehensive and up-to-date survey of the established experimental results which will be of considerable value to all the workers in this field.

H. ELLIOT

VOL.
7
1955

Journal of Atmospheric and Terrestrial Physics, 1955, Vol. 7 ,pp. 297 to 309. Pergamon Press Ltd., London

Nitrogen oxides and the airglow

MARCEL NICOLET*
Ionosphere Research Laboratory, The Pennsylvania State University,
University Park, Pennsylvania

(*Received* 18 *May* 1955)

ABSTRACT

The chemospheric processes lead to various possibilities for description of the contribution of nitrogen oxides in the airglow. An excitation of the Vegard-Kaplan system is indicated when nitric oxide is formed by a three-body collision process involving molecular nitrogen. A bimolecular association leading to nitrogen peroxide must show a continuous airglow during dark hours as well as in a sunlit atmosphere. Electronic systems emission of NO_2 is also possible because of a reaction between ozone and nitric oxide.

A reaction leading to an excitation of the O_2 red atmospheric band system with its peculiar emissions is also discussed.

Since these various processes causing day, twilight, and night airglow occur in the mesosphere and at the mesopause level, dynamic effects may lead to strong variations in the airglow.

1. INTRODUCTION

THE study of the identification of the airglow radiations suggests that additional processes are required to explain ultraviolet and visible features. Using results obtained in a preceding paper (NICOLET, 1955), we discuss various possibilities here that may be of importance in the airglow. Before accepting a high-altitude origin for all of the emissions of the airglow, it is necessary to assess the likelihood of occurrence of some chemical reactions; and, in particular, the contributions of the nitrogen oxides have to be studied. An initial study, made by BATES (1952, 1954) and BATES and WITHERSPOON (1952), has led to our brief analysis of the aeronomic problem of nitrogen oxides (NICOLET, 1955) in which several reactions involving atomic oxygen and ozone were discussed. It appears that the main processes thus far discussed can provide possible mechanisms of excitation for the airglow.

2. NITRIC OXIDE FORMATION AND THE VEGARD-KAPLAN SYSTEM

It does not appear possible to accept the previous identifications of night-airglow radiations with the Vegard-Kaplan intercombination system of N_2. However, bands which seem to show a degradation toward the red lead, as may be expected from synthetic spectra, to the possibility that some night-airglow emissions would be due to a relatively small number of these N_2 bands.

In the thermosphere, the presence of nitrogen and oxygen atoms results in the formation of nitric oxide. It is interesting to consider the following mechanism:

$$(O + N)(Y) + N_2\,(X^1\Sigma_g^+) \rightarrow NO(X^2\Pi) + N_2(A^3\Sigma_u^+) \qquad (1)$$

* Present address: Royal Meteorological Institute of Belgium, Department of Radiation, UCCLE.

The research reported in this paper has been sponsored by the Geophysics Research Directorate of the Air Force Cambridge Research Center, Air Research and Development Command, under Contracts AF19(122)-44 and AF19(604)-1304.

instead of the reaction usually invoked:

$$(N + N)(Y) + N_2 \rightarrow N_2(^1\Sigma_g^+) + N_2(A^3\Sigma_u^+) \qquad (2)$$

for the excitation of the Vegard-Kaplan bands.

BATES (1952) has discussed the process of type (2) and shown that it is not able to give an observable intensity of Vegard-Kaplan band-system emission unless the nitrogen-atom concentration is considerable.

With (1), the presence of oxygen atoms is of interest, since it increases the the rate of the process. Nevertheless, other objections can be made, such as those BATES (1952) has indicated. It seems, however, that the conditions are less severe with (1) than with (2); and a limited excitation is to be expected.

If an effort is made toward finding a possible mechanism for the excitation of Vegard-Kaplan bands in the night airglow, attention may be drawn to the fact that (1) is energetically possible. The dissociation energy of nitric oxide is about 150 kcal (GAYDON, 1947; BRIX and HERZBERG, 1954), while the excitation energies of $N_2(A^3\Sigma)$ are as follows:

$$v' = 0 \quad 142{\cdot}2 \text{ kcal}$$
$$v' = 1 \quad 146{\cdot}3 \text{ kcal}$$
$$v' = 2 \quad 150{\cdot}3 \text{ kcal}$$

Adopting the conditions BATES (1952) has chosen for (2), $n(N)$ would have smaller values using (1). Instead of 10^{11} cm^{-3}, for example, about 6×10^8 nitrogen atoms would be needed.

For the formation of NO we may write

$$\frac{dn(NO)}{dt} = 5 \times 10^{-34} T^{1/2} n(M) n(O) n(N) \qquad (3)$$

in which the rate coefficient has chosen to be the same as for the formation of O_2 by three-body collisions (BATES and NICOLET, 1950).

The excitation from $^1\Sigma$ to $A^3\Sigma(v' \leq 2)$ of N_2 will be

$$\frac{dn(N_2, A^3\Sigma)}{dt} = 4 \times 10^{-34} T^{1/2} n(N_2) n(O) n(N) p_{12} \qquad (4)$$

in which p_{12} denotes the probability factor for the excitation, and $n(N_2) = \frac{4}{5} n(M)$.

The emission from $A^3\Sigma$ to $A^1\Sigma$ will be

$$\frac{dn(VK)}{dt} = p_{12} p_{21} 4 \times 10^{-34} T^{1/2} n(N_2) n(O) n(N) \qquad (5)$$

in which p_{21} denotes the probability factor for the deactivation.

At 120 km, a yield for the total emission in the Vegard-Kaplan bands of the order of 10 cm^{-3} sec^{-1} requires a concentration of nitrogen atoms of about 2×10^8 cm^{-3} if $p_{12} p_{21} = 1$.

With the same conditions ($p_{12} p_{21} = 1$), and keeping the day concentration of oxygen atoms, it is possible to reach the same yield with 2×10^6 nitrogen atoms cm^{-3} at 50 km and 2×10^7 cm^{-3} at 80 km.

VOL. 7 1955

In other words, the presence of Vegard-Kaplan bands would be detected in airglow spectra if $p_{12}p_{21} = 1$ and, therefore, the emission would be more important at mesospheric levels than in the thermosphere. However, as deactivation must occur,

$$p_{21} \ll 1 \tag{6}$$

and p_{21} increases towards low altitudes. From 120 km to 50 km, the variation of the factor p_{21} should be more than 10^4; for example,

$$p_{21}^{(120\,\mathrm{km})} : p_{21}^{(90\,\mathrm{km})} : p_{21}^{(55\,\mathrm{km})} = 1 : 10^{-2} : 10^{-4} \tag{7}$$

The detection of Vegard-Kaplan bands in airglow spectra requires:

(i) an atomic nitrogen concentration not less than 10^8 cm^{-3};

(ii) a complete excitation in the association process (1); and

(iii) no deactivation effect.

Therefore, there is maximum probability of the emission in the thermosphere where $n(\mathrm{O})n(\mathrm{N})$ is maximum. However, the exact rate of such an emission cannot be determined without knowledge of the deactivation factor. In any case, the emission rate should be less than 10 cm^{-3} sec^{-1}, and the observation of Vegard-Kaplan bands, even if possible, should be difficult. Because of a deactivation effect, the final possibility is the emission of bands from $A^3\Sigma\,(v' = 0)$.

3. Nitrogen Peroxide and the Atmospheric Oxygen System

If the concentration of NO_2 is sufficiently large, the following process may be considered for an excitation of O_2,

$$NO_2 + O \rightarrow NO + O_2, \tag{8}$$

for which the rate coefficient b_3 is not well known at mesospheric temperatures (Nicolet, 1955).

According to data deduced from the chemical equilibrium, $NO_2 = NO + \frac{1}{2}O_2$, the dissociation energy of NO_2 is about 72 kcal. The data of Bodenstein and Lindner (1922), considered by Zeise (1936), lead to

$$E_0^0 = -25{\cdot}55 \text{ kcal} = 2D_0^0(\mathrm{NO}) + D_0^0(\mathrm{O_2}) - 2D_0^0(\mathrm{NO_2}) \tag{9}$$

in which E_0^0 is the heat of reaction at 0°K and D_0^0 the atomic heats of formation (or the heat of dissociation for diatomic molecules).

Since the heat of dissociation of O_2 is 117·96 kcal (Brix and Herzberg, 1954), the following equation can be written,

$$NO_2 = NO + O + 71{\cdot}75 \text{ kcal}. \tag{10}$$

The photochemical decomposition is complete at λ3650 Å (Hg line), while at λ4050 Å (Hg line) the efficiency is not complete (predissociation?), and at λ4360 Å no detectable effect was found (Norrish, 1929; Holmes and Daniels, 1934). According to Noyes and Leighton (1941), excited molecules are produced by $\lambda > 3700$ Å, and a few of these may be expected to dissociate by acquisition of thermal energy. The predissociation has been considered (Herzberg, 1931;

NOYES and HENRIQUES, 1939); however, it is difficult to determine a precise value of the dissociation energy of NO_2, since that for thermal decomposition is only an average value. It may be pointed out that HALL and BLACETT (1952), having separated the absorption spectra of NO_2 and N_2O_4, indicate an effect of the NO_2 spectrum at 3900 Å which could alter the photochemistry of the system.

In any case, it appears that the energy of dissociation of NO_2 into NO + O cannot be greater than 77 kcal, and is probably near 72 kcal. Considering (8), the excitation of O_2 may correspond to

$$NO_2 + O \rightarrow NO + O_2(^1\Sigma, v' \leq 2) \qquad (11)$$

i.e., to an excitation at $v' \leq 2$ for the lowest value of the NO_2 dissociation energy and $v' = 0$ for the largest value.

In order to explain an emission from $O_2(^1\Sigma, v' = 0)$ alone, as is observed in the airglow, when $D(NO_2) = 72$ kcal, it is necessary to suppose that resonance is not effective or to introduce BATES'S process (1954), in which the vibrational energy is transformed by collision to the zeroth vibrational level of the excited electronic state.

Because of the uncertainty of the coefficient values, it is not possible to determine the exact rate of (11). However, by using extreme values for (11) (NICOLET, 1955), we may obtain estimates as follows:

At 200°K, with $n(NO_2) = 10^7$ cm^{-3}, a yield of 50 photons cm^{-3} sec^{-1} in the atmospheric bands of O_2 requires an atomic oxygen concentration between 10^{11} and 4×10^{10} cm^{-3}. At mesospheric levels, the reaction rates of (11) would be of the order of 10^{-5} cm^{-3} sec^{-1} to 5×10^{-5} cm^{-3} sec^{-1} between 80 km and 90 km. Therefore a total rate of $2{\cdot}5 \times 10^8$ photons cm^{-2} sec^{-1} needs only an average concentration $n(NO_2) = 10^7$ cm^{-3}. Since such a value can be reached after twilight (NICOLET, 1955), process (11) does exist, and leads to an emission which must be variable according to the mesospheric conditions.

Finally, it is interesting to notice that KAPLAN (1952) was the first to observe the atmospheric bands in oxygen afterglows containing small amounts of nitrogen. These afterglows are much more intense than those observed in pure oxygen. There is strong emission in the visible and in the photographic infrared due to NO_2.

VOL. 7 1955

4. NITROGEN PEROXIDE AND AFTERGLOW

The radiative process

$$O + NO \rightarrow NO_2 + h\nu \qquad (12)$$

has been studied in the laboratory by a number of investigators (RAYLEIGH, 1910; STODDARD, 1934; NEWMAN, 1935; SPEALMAN and RODEBUSH, 1935; GAYDON, 1944; TANAKA and SHIMAZU, 1948). Other investigations are those of NORRISH (1929) and BAXTER (1930) pertaining to fluorescence, and of KONDRATJEW (1937) concerning the thermal radiation of nitrogen peroxide. They also show that the general spectrum may be considered as a continuous spectrum with a possible banded structure.

Let us first discuss the bimolecular association (12), which corresponds to the continuous afterglow found by RAYLEIGH (1910) from about 4200 Å to 6700 Å,

and observed in more detail by STODDARD (1934) and NEWMAN (1935) in a discharge through air or through oxygen with traces of nitrogen. The similarity of the colours of this afterglow and the emission of flames containing oxides of nitrogen (GAYDON, 1944) indicate that process (12) is an important one.

TANAKA and SHIMAZU (1948) have observed the chemiluminescence in the reactions between nitric oxide and oxygen and ozone, using discharges through air, NO, NO_2, and mixed gas. They have found various afterglows indicating that NO is necessary, and O_3 is perhaps not essential.

Adopting the value of 10^{-17} cm^{-3} sec^{-1} for the rate coefficient of (12) (BATES, 1954), a yield of 10^3 photons cm^{-3} sec^{-1} at $\lambda \geq 3900$ Å would result from only 2×10^{11} oxygen atoms if we adopt 5×10^8 NO molecules per cm^3.

Considering the possible values of $n(\mathrm{NO}) \geq 10^8$ cm^{-3} (NICOLET, 1955), there is no doubt that (12) may produce a continuous airglow spectrum, for the rate of (12) between 80–90 km is of the order of $2 \times 10^{-6}\, n(\mathrm{NO})$ cm^{-3} sec^{-1}. A total continuous emission of more than 10^9 photons ($\lambda \geq 3900$ Å) per cm^2 and sec can be obtained in the night airglow.

As has been shown (NICOLET, 1955), the bimolecular reaction involving ozone molecules leads to the excitation of NO_2,

$$\mathrm{O_3 + NO \rightarrow O_2 + NO_2^{*}}, \tag{13}$$

which corresponds to an energy of not less than 48 kcal. In other words, the energy released by this reaction is used for an excitation of NO_2 in an electronic level leading most certainly to an emission of bands at $\lambda > 5950$ Å. Since we know that the visible oxygen afterglow also consists of bands, for example at $\lambda\lambda$5980–6320–6400 Å, it is possible to consider an airglow spectrum having such a behaviour. This conclusion can be used to explain the experimental results of TANAKA and SHIMAZU (1948). Furthermore, it is interesting to note that the observed airglow seems to show a diffuse spectrum in the region of the sodium and red oxygen lines.

The activation energy of (13) being very low, the rate coefficient is large. In the mesosphere, at 65 km for example, where a value of more than 10^9 O_3 molecules cm^{-3} and a temperature of the order of 250°K may be adopted, the rate of formation of NO_2 by (13) would be of the order of

$$\frac{dn(\mathrm{NO_2})}{dt} \geq 10^{-5} n(\mathrm{NO})\ \mathrm{cm^{-3}\text{-}sec^{-1}}. \tag{14}$$

Considering a possible concentration for $n(\mathrm{NO})$ of 10^9 cm^{-3} sec^{-1}, the rate of excitation in (14) would be of the order of 10^4 cm^{-3} sec^{-1}.

This process will be efficient during twilight, and it must therefore be considered as playing a disturbing role in the twilight emissions as observed in the red lines of atomic oxygen and even, perhaps, for the sodium line.

As was shown in a preceding paper (NICOLET, 1955), all the reactions discussed here are very sensitive to the concentrations adopted, and depend on the activation energy chosen for (11). If chemical data were more precise, it would be possible to discuss in a more quantitative manner the diurnal variation of nitrogen oxide concentrations.

These various results on the possible effects of nitrogen oxides in the night airglow may be related with observational data. For example, the continuum of the airglow spectrum, starting at about 3900 Å, should be affected by these reactions even if the major part is due to a stellar continuum (CHAMBERLAIN and OLIVER, 1953; MEINEL, 1953).

5. DAY AIRGLOW

Observational data obtained by rocketborne photoelectric photometers (MILEY, CULLINGTON, and BEDINGER, 1952) have been discussed recently by BATES and DALGARNO (1954). After this analysis, it is interesting to make an attempt to describe the behaviour of nitrogen oxides in the day airglow.

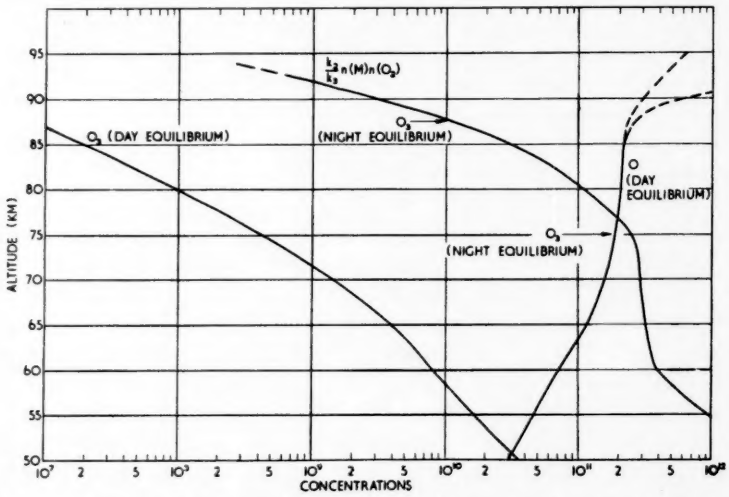

Fig. 1. Concentrations of ozone and atomic oxygen in an atmosphere in which the effect of minor constituents is neglected.

To make the position clear, the vertical distributions of ozone and atomic oxygen between 50 km and 90 km are given in Fig. 1. The atomic oxygen concentration is greater than the ozone concentration under daytime photoequilibrium conditions. At any time during the day, the photoequilibrium does exist for ozone. During dark hours, the problem is entirely different, and is not studied here. It must be pointed out that the night-time distribution shown in Fig. 1 deals with night-time equilibrium values in an oxygen atmosphere. Insofar as atomic oxygen is concerned, the problem of photoequilibrium is different. In Fig. 2 various states of recombination are shown. The upper curve corresponds to the loss-rate coefficient of oxygen atoms by association with O_2. The lower curve corresponds to a recombination effect by reaction between O and O_3 in a sunlit atmosphere. The right heavy curve represents the same process with the maximum possibility during hours of darkness. The heavy curve in the left part of that figure shows the effect of the recombination of two oxygen atoms. This effect becomes preponderant above 85 km. Furthermore, the surface limited

VOL. 7 1955

by the heavy curves shows the possible limits for the recombination of oxygen atoms in an oxygen atmosphere. It indicates that below 60 km the time of recombination is less than one day. At 75 km the minimum time is obtained during dark hours and is of the order of twenty-four hours. At 80 km, this minimum time is of the order of three days.

In view of the above, we cannot increase the oxygen concentration below 65 km by vertical transport, for the recombination by collision between O_3 and O is effective in less than one hour for $n_0(O) = 3 \times 10^{11}$ cm^{-3} But from 65 to 75 km the concentration of 2×10^{11} cm^{-3} may have a lifetime of not less than three hours. Thus, it may be concluded that the vertical transport of oxygen atoms to lower heights is possible. Above 80 km, we may have a concentration of oxygen

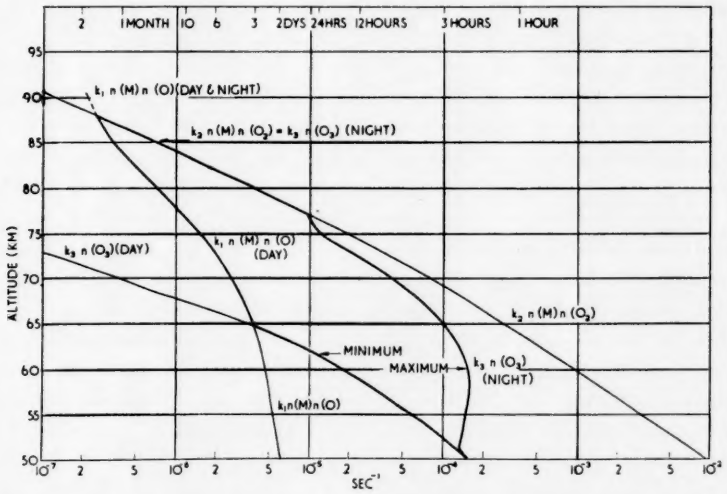

Fig. 2. Recombination rate coefficients of oxygen atoms versus height or lifetimes of oxygen atoms.

atoms larger than the photochemical value, because the time of dissociation is longer than two days.

At 90 km, the process which plays an effective role in the recombination of oxygen is the normal association of oxygen by a three-body collision.

The aeronomic problem is more complicated than the problem in an oxygen atmosphere. It was shown by BATES and NICOLET (1950) that the presence of hydrogen may affect the general behaviour. However, the aeronomic study of nitrogen oxides (NICOLET, 1955) shows difficulties such that preliminary conclusions are hardly changed by use of an oxygen atmosphere.

In any case, the assignment of a night-airglow spectrum to reactions between nitric oxide and atomic oxygen or ozone, and between nitrogen peroxide and oxygen, suggests possible effects resulting in an important day airglow.

In a sunlit atmosphere, process (12) attains its maximum rate, since n(NO) and n(O) certainly have their maximum values under these conditions. When

NO_2 is produced by (12), this molecule emits its continuous spectrum and, afterwards, is dissociated after a mean lifetime of 200 seconds (BATES, 1954). But before dissociating, NO_2 can be excited to an excited electronic level from which fluorescence occurs. This last process was observed in the laboratory (NORRISH, 1929; BAXTER, 1930) when there were recognized two characteristic bands lying in the red-orange and yellow-green regions, namely broad bands between 6200–6500 Å and 5600–6050 Å. BAXTER (1930) has assumed a mean lifetime of the electronic state of the order of 10^{-7} sec, and HEIL (1932) has obtained a time of about 10^{-5} sec by a diffusion method. Since the absorption coefficient of NO_2 has a peak near 4000 Å (HALL and BLACETT, 1952) of the order of 10^{-18} cm^2, and is still about 7×10^{-19} cm^2 at 5000 Å, in a spectral region where the solar emission is most important, it seems, therefore, that an absorption process leading to an excitation giving fluorescence is not less effective than a photodissociation process due to the ultraviolet radiation. In other words, during its lifetime of 200 seconds, nitrogen peroxide can be excited to an electronic level to emit a fluorescence spectrum. Unfortunately, the experimental data are not suitable for theoretical determinations. The recent analysis of NEUBERGER and DUNCAN (1954) shows that the fluorescence spectrum of NO_2 excited by λ4358 Å is apparently continuous at low dispersion, and extends from the exciting line to the limit of observation at about 8000 Å. The fluorescence spectrum excited by a radiation of longer wavelength, namely λ5461 Å, shows relatively sharp emission bands superimposed on an apparently continuous emission. Since the interpretation of such experimental data is difficult (the knowledge of the electronic levels of NO_2 being very poor), no simple suggestion can be offered; the fluorescence spectrum due to relatively short wavelengths must be ascribed to a series of different levels which partly overlap. However, the narrow bands obtained by the excitation of λ5461 Å may be of importance in the day airglow. These bands have the following approximate wavelengths: $\lambda\lambda$5890, 6160, 6385, 6460, 6540, and 6700 Å. They come from electronic levels having a very short lifetime ($\sim 10^{-7}$ sec), and cannot be excluded from twilight phenomena. A certain number of features observed in twilight spectra which are not due to OH emissions may belong to NO_2. As far as the apparently continuous spectrum is concerned, its lifetime is relatively long and is of the order of $4{\cdot}4 \times 10^{-5}$ sec, according to NEUBERGER and DUNCAN (1954). Without any additional contribution toward the interpretation of this spectrum it is not possible to reach a more precise conclusion concerning the fluorescence of the day or twilight airglow.

The whole problem is complicated, for it is a problem of radiation transfer involving absorption of solar radiation by NO_2, eventual fluorescence after collisions at low height, photodissociation, and, perhaps, subsequent absorption. Nevertheless, the way in which nitrogen oxides and their various reactions may behave in the day airglow must be shown.

Let us consider the photoequilibrium which does exist between NO_2 and NO. The equation of photoequilibrium is (see NICOLET 1955, equation(18)),

$$\frac{n(NO_2)}{n(NO)} = \frac{b_2 n(O) + b_4 n(O_3)}{J_{NO_2} + b_3 n(O) + b_5 n(N)} \qquad (15)$$

VOL. 7 1955

in which the rate coefficients correspond to the following reactions

$$O + NO \rightarrow NO_2 + h\nu \qquad (b_2)$$
$$O_3 + NO \rightarrow NO_2 + O_2 \qquad (b_4)$$
$$NO_2 + h\nu \rightarrow NO + O \qquad (J_{NO_2})$$
$$O + NO_2 \rightarrow NO + O_2 \qquad (b_3)$$
$$N + NO_2 \rightarrow NO + NO \qquad (b_5)$$

Inserting numerical values in (15), the ratio $n(NO_2)/n(NO)$ for day equilibrium has been found and is shown in Fig. 3. It is less than unity in the atmospheric region which was analyzed, and decreases with increasing heights.

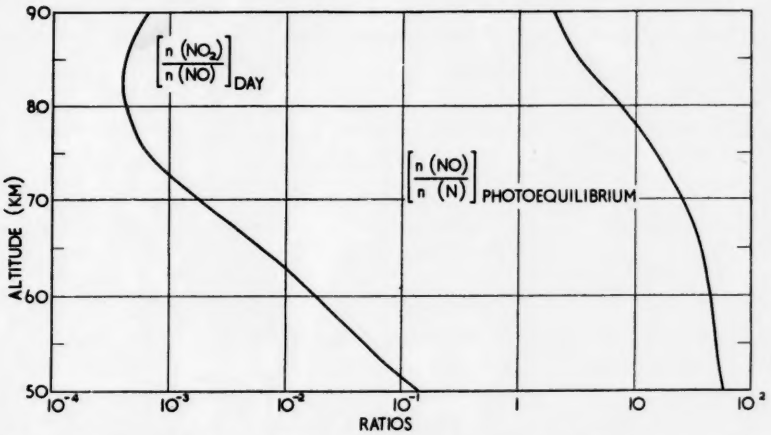

Fig. 3. Photoequilibrium conditions. $n(NO_2)/n(NO)$ corresponding to real conditions. $n(NO)/n(N)$ for a limiting case, since departure from photoequilibrium conditions does exist.

Using the complete set of reactions, the equation governing the rate of change of $n(NO)$ is (see NICOLET, 1952, equation (32)).

$$\frac{dn(NO)}{dt} = b_1 n(M) n(O) n(N) - \left[J_{NO} + b_6 n(N) \right] n(NO) \qquad (16)$$

in which the rate coefficients correspond to the following reactions:

$$O + N + M \rightarrow NO + M \qquad (b_1)$$
$$NO + h\nu \rightarrow N + O \qquad (J_{NO})$$
$$NO + N \rightarrow N_2 + O \qquad (b_6)$$

It is not possible to find the variation of $n(NO)$ from equation (16), because of its dependence on the atomic nitrogen concentration. Furthermore, photoequilibrium cannot be accepted because of the long lifetime of NO and, since in any case, the lifetime of atomic nitrogen is more than one day. Nevertheless, by considering the ratio $n(NO)/n(N)$, which under equilibrium conditions depends on the association between oxygen and nitrogen atoms, it is possible to reach

preliminary conclusions using (16) in which $\frac{dn(\mathrm{NO})}{dt} = 0$. Such a hypothesis means that the variation of NO due to photodissociation is less rapid than the loss of nitrogen atoms entering into the formation of nitric oxide. We can assume such a process, for the mean lifetime of a nitrogen atom is of the order of $1{\cdot}5 \times 10^5$ sec at 50 km and $1{\cdot}3 \times 10^6$ sec at 75 km.

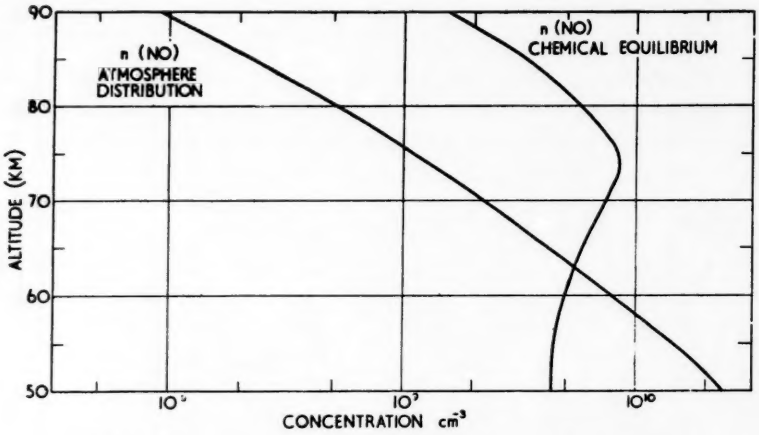

Fig. 4. Extreme cases of the vertical distribution of nitric oxide.

Since this behaviour implicitly assumes that $n(\mathrm{NO}) > n(\mathrm{N})$, which is correct below 90 km, we can write the following condition

$$J_{\mathrm{NO}} > b_6 n(\mathrm{N}), \tag{17}$$

and therefore

$$\frac{n(\mathrm{NO})}{n(\mathrm{N})} = \frac{b_1 n(\mathrm{M}) n(\mathrm{O})}{J_{\mathrm{NO}}} \tag{18}$$

corresponding to photochemical conditions. Using numerical values in (18), we find approximate results which show (Fig. 3) a decrease of the ratio $n(\mathrm{NO})/n(\mathrm{N})$ from about 50 near 50 km to unity above 90 km.

It is not possible to deduce the vertical distribution of $n(\mathrm{NO})$ from (16) or (18). However, utilizing a chemical equilibrium by employing the condition,

$$J_{\mathrm{NO}} < b_6 n(\mathrm{N}), \tag{19}$$

instead of (17), the following equation can be written,

$$n(\mathrm{NO}) = \frac{b_1}{b_6} n(\mathrm{M}) n(\mathrm{O}) \tag{20}$$

which leads to the vertical distribution of nitric oxide concentration shown in Fig. 4. Such a distribution corresponding to the limiting case of chemical equilibrium, does not correspond to aeronomic conditions, as has been shown (NICOLET, 1955); we must consider the problem of the departure from equilibrium conditions so far as nitric oxide is concerned. Taking an average value of 5×10^8 cm^{-3}

VOL. 7 1955

for the nitric oxide concentration at 80 km, a value which may be used to interpret the ionospheric behaviour of region *D* (NICOLET, 1955), it is possible to invoke mixing (complete departure from photochemical conditions) in order to adopt the atmospheric distribution for nitric oxide (Fig. 4).

In considering the content of a column of about 30 km between 50–90 km, one is permitted to use the same total number of molecules accurate to within one

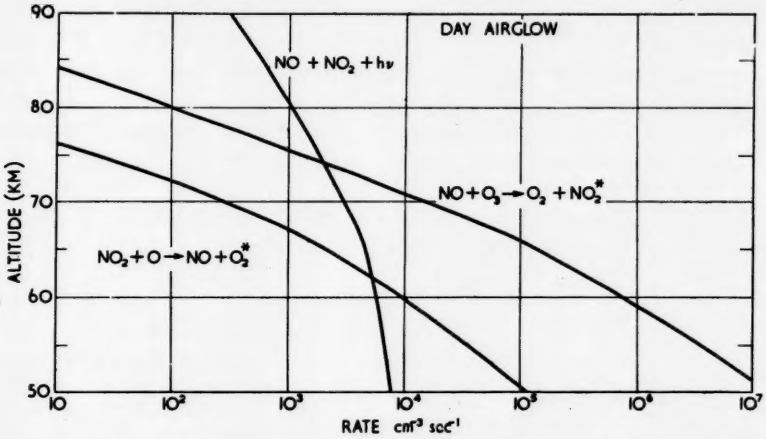

Fig. 5. Rates of the principal reactions affecting nitrogen oxides and occurring in the day airglow when nitric oxide follows the atmospheric distribution.

order of magnitude for any vertical distribution which is adopted. Owing to lack of other basic data, we adopt nitric oxide concentrations following the atmospheric distribution in order to compute the yields corresponding to processes (11), (12), and (13). The results are plotted in Fig. 5.

The continuous spectrum at $\lambda > 3900$ Å due to the reaction

$$NO + O \rightarrow NO_2 + h\nu \qquad (12)$$

leads to photon emission rates per cm^3 sec not less than 10^3 photons in a layer of 30 km. Therefore, the total yield due to the continuous day-airglow spectrum is not less than 2×10^{10} photons cm^{-2} sec^{-1}.

The reaction between nitric oxide and ozone leading to an electronic excitation of NO_2 according to

$$NO + O_3 \rightarrow O_2 + NO_2 \qquad (13)$$

has a very strong rate at low altitudes. If the ozone and nitric oxide concentrations are of the same order, as adopted here, 10^7 photons cm^{-3} sec^{-1} could be emitted when there is no quenching of fluorescence by atmospheric gases.

Finally, the reaction between nitrogen peroxide and atomic oxygen which leads to an excitation of the first atmospheric system according to

$$NO_2 + O \rightarrow NO + O_2^* \qquad (11)$$

is very effective at low heights and should play a role which may be detected in twilight spectra.

6. CONCLUSIONS

The theoretical considerations regarding the possible effects of nitrogen oxides in the airglow have revealed that these minor constituents cannot be neglected.

Since the presence of nitric oxide in the lower ionospheric region seems to be justified in explaining its behaviour, it is conceivable that nitrogen oxides play a role in the airglow. However, in order to make such an exploration it has been necessary to assume values of the rate coefficients for various reactions in the thermosphere.

In spite of the fact that tentative values have been used because of the lack of basic laboratory data, it has been possible to draw attention to promising sources of emission, and to show how the presence of nitrogen oxides appears to offer attractive possibilities for the explanation of the airglow.

Acknowledgements—The author is indebted to Professor D. R. BATES for his comments on the draft manuscript written at the Pennsylvania State University.

REFERENCES

BATES, D. R. 1952 *Ann. Géophys.* **8,** 194

BATES, D. R. 1954 The Physics of the Upper Atmosphere, Chap. 12 of *The Solar System*, Ed. G. P. Kuiper, Vol. 2, University of Chicago Press.

BATES, D. R., and DALGARNO, A. 1954 *J. Atmosph. Terr. Phys.* **5,** 329

BATES, D. R., and NICOLET, M. 1950 *J. Geophys. Res.* **55,** 301

BATES, D. R., and WITHERSPOON, A. E. 1952 *Mon. Not. Roy. Astron. Soc.* **112,** 101

BAXTER, W. P. 1930 *J. Amer. Chem. Soc.* **52,** 3920

BODENSTEIN, M., and LINDNER, K. 1922 *Z. Phys. Chem.* **100,** 82

BRIX, P., and HERZBERG, G. 1954 *Canadian J. Phys.* **32,** 110

CHAMBERLAIN, J. W., and OLIVER, N. J. 1953 *Astrophys. J.* **118,** 197

GAYDON, A. G. 1944 *Proc. Roy. Soc.* **A183,** 111

GAYDON, A. G. 1947 *Dissociation Energies and Spectra of Diatomic Molecules*, Chapman Hall, London

HALL, T. C., and BLACETT, F. E. 1952 *J. Chem. Phys.* **20,** 1745

HEIL, O. 1932 *Z. Phys.* **77,** 563

HARTECK, P., and DONDES, J. 1954 *J. Chem. Phys.* **22,** 758

HERZBERG, G. 1931 *Ergb. der Naturwiss.* **10,** 207

HOLMES, H. H., and DANIELS, F. 1934 *J. Amer. Chem. Soc.* **56,** 630

JOHNSTON, H. S. 1951 *J. Chem. Phys.* **19,** 663

KAPLAN, J. 1952 "The Optical Study of the Earth's Atmosphere," Mém. Soc. Roy. Sc. Liège, **12,** 295

KONDRATJEW, V. 1937 *Physik. Zeit. Sowjetunion*, **11,** 320

MEINEL, A. B. 1950 *Astrophys. J.* **112,** 464

MILEY, H. A., CULLINGTON, E. H., and BEDINGER, J. F. 1952 *Trans. Amer. Geophys. Union* **33,** 321

NEUBERGER, D., and DUNCAN, A. B. F. 1954 *J. Chem. Phys.* **22,** 1693

NEWMAN, F. H. 1935 *Phil. Mag.* **20,** 777

NICOLET, M. 1954 Dynamic Effects in the High Atmosphere, Chap. 13 of *The Solar System*, Ed. G. P. Kuiper, Vol. 2, University of Chicago Press

VOL. 7 1955

NICOLET, M.	1955	*J. Atmosph. Terr. Phys.*
NOYES, W. A., and HENRIQUES, F. C.	1939	*J. Chem. Phys.* **7,** 767
NOYES, W. A., and LEIGHTON, P. A.	1941	*The Photochemistry of Gases,* Reinhold Publ. Corp., New York
NORRISH, R. W.	1929	*J. Chem. Soc.* p. 1611
RAYLEIGH, LORD (R. J. STRUTT)	1910	*Proc. Phys. Soc.* **23,** 66
SPEALMAN, M. L., and RODEBUSH, W. H.	1953	*J. Amer. Chem. Soc.* **57,** 1474
STODDART, E. M.	1934	*Proc. Roy. Soc.* **A147,** 454
TANAKA, Y., and SHIMAZU, N.	1948	*J. Sci. Res. Inst.* **43,** 241
ZEISE, H.	1936	*Z. Elektrochem.* **42,** 785

L.
55

Journal of Atmospheric and Terrestrial Physics, 1955, Vol. 7, pp. 310 to 321. Pergamon Press Ltd., London

A new index of solar activity based on ionospheric measurements

C. M. MINNIS

Official communication from D.S.I.R. Radio Research Station, Slough

(*Received* 29 *April* 1955)

ABSTRACT

The monthly mean relative sunspot number (R_M) is assumed to contain a component (R_v) which has a one-to-one correlation with the critical frequency of the F_2-layer in an undisturbed ionosphere and which is, therefore, an idealized index of solar activity. The residual component (R_z) may be regarded as an error which has a Standard Deviation of about 20 per cent. A new index (I_{F_2}) has been constructed for the period 1938–1954; like R_M, it can also be regarded as giving an approximate value of R_v, but its residual error component (R_z) has an S.D. which is only about one tenth that of R_z. The magnitude of I_{F_2} for a given month is computed from the mean noon critical frequencies in the F_2-layer at Slough, Huancayo, and Watheroo, which are normally available within a few weeks of the end of each month. The index is based, in effect, on a calibration of the F_2-layer critical frequencies at these observatories in terms of R_v, using data extending back as far as possible. Precautions have been taken to reduce to negligible proportions the effects of ionospheric disturbances on the magnitude of the new index.

1. INTRODUCTION

IT has been known for many years that the long-term changes in electron density in the ionosphere follow closely those in solar activity, as indicated by measurements made at optical frequencies. The reflecting properties of the ionospheric layers have been responsible for the development of the highly organized world-wide network of high-frequency communications which now exists. However, the ionosphere is not static, and the continually changing characteristics of the reflecting layers have made it essential for communication engineers to ensure that the operating frequency in use on each circuit always falls within the narrow frequency limits, determined by the ionosphere, which allow satisfactory communication to be maintained. This requirement has led to the establishment of ionospheric forecasting services in several countries, and such services are now regarded as necessary to the most efficient operation of high-frequency communications.

The basis for ionospheric forecasts reduces ultimately to a knowledge of how solar activity is changing; although sunspot numbers are the most frequently used index of this activity, they suffer from certain defects, and in recent years there has been a demand for a more satisfactory index. Quite apart from this purely practical requirement, it would also be of considerable scientific interest to have an index which was more closely related to ionospheric parameters than the sunspot number. Such an index would assist, for example, in the investigation of the relation between electron production and the intensity of the ionizing radiation, and in the study of the relation between solar particle radiation and ionospheric and magnetic storms.

2. GENERAL CONSIDERATIONS

As seen from the earth, the sun appears to rotate about its axis once in twenty-seven days. Consequently, when the sources of ionizing radiation on the sun are

VOL. 7 1955

not uniformly distributed, the electron density in the principal ionospheric layers tends to vary with a twenty-seven day period. These short-term changes are not of great importance in the present connection, and they will be eliminated by the use of monthly mean values of both solar and ionospheric parameters. The aim of the investigation is to produce an index of solar activity which is capable of representing the mean activity during each month. Since the intention is to use the index for the study of the relation between solar radiation and the ionosphere, it must be available for at least a complete solar cycle. This minimum period would also provide a suitable background of experience to allow the index to be used as a means of extrapolating solar activity up to about twelve months into the future.

It is not proposed to deal with extrapolation beyond this limit, because this would involve the consideration of the nature of the long-term changes in solar activity; for this it is essential to have data covering many solar cycles, and only the sunspot number satisfies this requirement. The need for data extending over at least a cycle rules out the possibility of using direct measures of solar-noise flux as an index, but it seems possible that such methods may prove to be useful eventually when sufficient data have accumulated.

Since the ionosphere itself is so closely controlled by solar radiation, it seems logical to attempt to use the various critical frequencies in the construction of a solar activity index. The remainder of this paper describes how the changes in critical frequency which are due to seasonal and other effects can be eliminated, so as to leave an index number which is very insensitive to terrestrial influences and which reflects only the month-by-month changes in solar activity which are responsible for ionospheric ionization.

3. Choice of Layer

For the E-layer, the day-to-day fluctuations, and therefore the sampling error in the monthly mean critical frequency, are less than for the F_2-layer. On the other hand the sensitivity of the F_2-layer to changes in solar activity is three or four times as great as that of the E-layer; also the fact that the critical frequencies of both layers are measured to the nearest 0·1 Mc/s means that the percentage accuracy of the measurements is greater for the F_2-layer. Since ionospheric forecasting is concerned primarily with the F_2-layer, and bearing in mind the points just mentioned, it was decided to use the F_2-layer rather than the E-layer in constructing an index. The F_1-layer was not seriously considered, because in winter it tends to coalesce with the F_2-layer at many observatories, and its critical frequency cannot be measured accurately when this happens.

4. Theoretical Basis

If an exact functional relation existed connecting the mean intensity of the ionizing radiation and the mean sunspot number, and if, in addition, the ionosphere was not subject to any irregular disturbances, it is reasonable to suppose that the monthly mean value of the F_2-layer critical frequency (f) could be expressed exactly as a single-valued function of the monthly mean sunspot number (R). It is well known, however, that the measured values of these quantities (f_M, R_M) cannot be related exactly in this way, although the correlation between them may

be quite high. The assumption will be made, however, that both R_M and f_M contain components (R_v, f_{vc}) which do have a functional relationship, and which include constants such that, over a long period, the mean value of the residual components (R_x, f_x) is zero. The F_2-layer changes in a fairly consistent manner with changes in magnetic activity, and it is necessary, for this reason, to include in the expression for f_{vc} a term which allows for this; the monthly mean value (C) of the international magnetic character figure is a convenient index to use.

The assumptions which have been made above may be summarized concisely in the expressions:

$$R_M = R_v + R_x \tag{1}$$

$$f_M = f_{vc} + f_x \tag{2}$$

$$f_{vc} = a + bR_v + kC \tag{3}$$

$$\Sigma R_x = \Sigma f_x = 0 \tag{4}$$

where a, b, k are constants for a given month and time of day at a given observatory Although a linear relation has been used to connect f_{vc} and R_v, this assumption is not quite true in practice, but has been retained merely to simplify the analysis which follows. In constructing the index described in Sections 5 and 6, this restriction was not applied and non-linear relations were used where this was necessary.

The character figure C is itself a function of solar activity, and if a linear relation were assumed to connect C and R_v, viz.

$$C = C_{\min} + C_s + \beta R_v \tag{5}$$

then (3) could be re-written as:

$$f_{vc} = (a + kC_{\min}) + R_v(b + k\beta) + kC_s \tag{6}$$

where $C_{\min}$ is the minimum value of C, and C_s is an irregularly occurring component of C which is zero except during magnetic disturbances, and is independent of R_v.

Using (1), (2), and (3), the expression relating the measured values of sunspot number and critical frequency can be shown to be:

$$f_M = (a + k\bar{C}) + bR_M - bR_x + k(C - \bar{C}) + f_x \tag{7}$$

where $\bar{C}$ is the mean value of C during the whole period under consideration. If f_M is plotted against R_M, the scatter of the points on either side of the best-fit line can be attributed to fluctuations in the magnitudes of the last three terms in (7). If the equation of the best-fit line drawn through the points (f_M, R_M) is represented by:

$$f_M = (a' + k\bar{C}) + b'R_M \tag{8}$$

this relation may be used to define the parameter (R'_M) given by

$$R'_M = \frac{f_M - (a' + k\bar{C})}{b'} \tag{9}$$

VOL. 7 1955

The magnitudes of $(a' + k\bar{C})$ and b' can be obtained from the fitted line and, having evaluated these constants, they can be used in conjunction with a measured value of f_M for a given month to give the corresponding value of R'_M for that month. Monthly values of R'_M obtained in the manner just described form the basis of the index (I_{F_2}), which is defined in Section 5 and which is shown to be closely related to R_v.

5. Characteristics of R'_M

From (3),

$$R_v = \frac{f_{vc} - (a + kC)}{b} \tag{10}$$

and the resemblance of this expression to that already given for R'_M (9) suggests that R'_M may be regarded as an approximate value of R_v. In fact it can be shown, using the relations already given, that

$$R'_M = R_v + \left[\frac{f_M - a'}{b'} - \frac{f_M - a}{b}\right] + \frac{f_x}{b} - k\left(\frac{\bar{C}}{b'} - \frac{C}{b}\right) \tag{11}$$

$$= R_v + R_y + R_c \tag{12}$$

where $$R_y = \left[\frac{f_M - a'}{b'} - \frac{f_M - a}{b}\right] + \frac{f_x}{b}$$

and $$R_c = -k\left(\frac{\bar{C}}{b'} - \frac{C}{b}\right)$$

Table 1. I_{F_2} *(sunspot number units)*

Year	*Jan.*	*Feb.*	*Mar.*	*Apr.*	*May*	*June*	*July*	*Aug.*	*Sept.*	*Oct.*	*Nov.*	*Dec.*
1938	99	105	120	110	108	119	138	135	115	99	113	107
39	121	85	86	91	114	118	111	101	125	111	101	74
40	66	66	78	79	70	76	85	89	89	81	76	53
41	60	49	46	31	36	42	50	60	58	50	48	48
42	42	41	50	53	47	24	19	22	24	11	27	29
43	24	28	26	23	14	15	22	13	1	2	1	12
44	6	2	16	0	2	−1	2	17	17	21	21	19
45	23	28	23	19	31	39	39	39	37	55	63	43
46	44	68	90	88	90	103	116	114	100	103	109	122
47	113	131	135	142	160	168	169	169	138	128	133	126
48	103	98	115	128	140	157	148	140	125	116	109	108
49	117	130	144	141	127	120	119	110	127	116	126	109
50	105	98	99	105	106	101	83	72	48	53	51	37
51	44	43	46	68	68	75	78	67	55	54	44	44
52	35	31	26	28	21	34	34	39	29	21	20	16
53	16	11	2	5	12	9	11	8	11	11	9	6
54	4	4	−2	−1	2	−7	−4	5	−1	8	12	4
55	10	12	8	3	19	28						

If a reasonably large number of f_M, R_M values are available, it follows from (4) and (7) that $a \simeq a'$, $b \simeq b'$ and, if f_x is small, that R_y should also be small. In any particular month, however, R_c is capable of introducing an appreciable error which may be either positive or negative, depending on the location of the observatory for which R'_M has been computed. It is possible to reduce this dependence of R'_M on magnetic activity by combining the values of R'_M derived from a number of selected observatories for which k differs in sign. It has been found that the values of f_M measured at noon at Slough, Huancayo, and Watheroo provide such a combination, and that the mean value of R'_M for these three observatories (I_{F_2}) is comparatively insensitive to change in C.

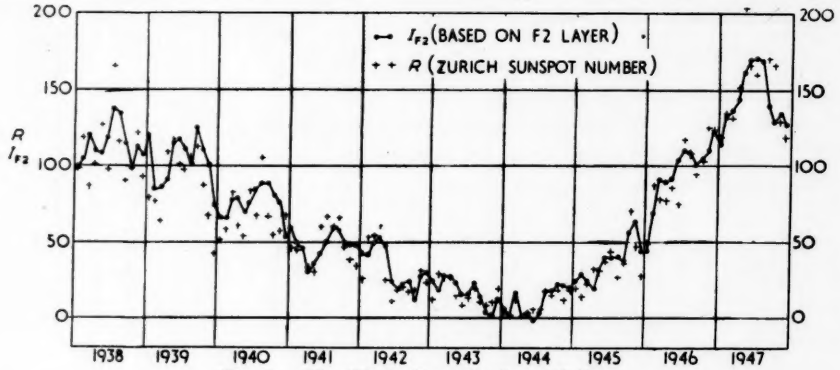

Fig. 1a. Monthly indices of solar activity.

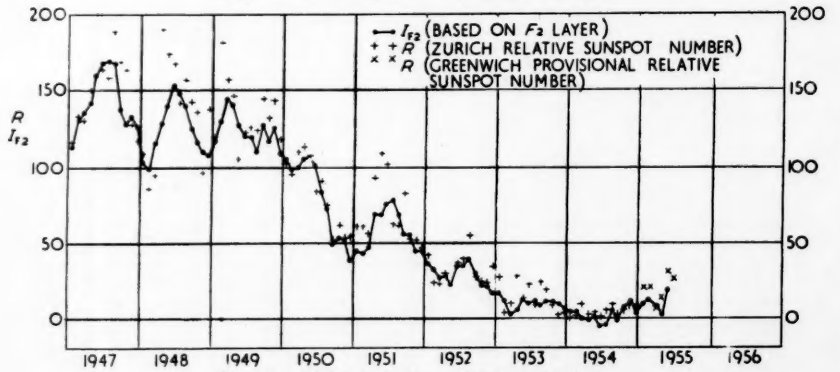

Fig. 1b. Monthly indices of solar activity.

Thus, by definition,

$$I_{F_2} = \overline{R'_M} = R_v + \bar{R}_y + \bar{R}_c = R_v + R_z \qquad (13)$$

The values of I_{F_2} are given in Table 1; in Figs. 1a and 1b they have been plotted together with the values of R_M, the observed monthly mean sunspot number, for comparison.

6. Characteristics of I_{F_2}

It is evident from an examination of the changes in I_{F_2} since 1938 that this index has a strong tendency to pass through a maximum during northern summer.

VOL. 7 1955

Such an effect might, at first sight, be attributed to a residual seasonal influence, but it is possible to show that this inference is not correct by comparing the mean values of I_{F_2} and R_M (Fig. 2a), and also the differences $(R_M - I_{F_2})$ (Fig. 2b) for each month of the year. Both indices exhibit the same summer maximum, and the monthly differences give no evidence for the existence of any significant seasonal component in I_{F_2}.

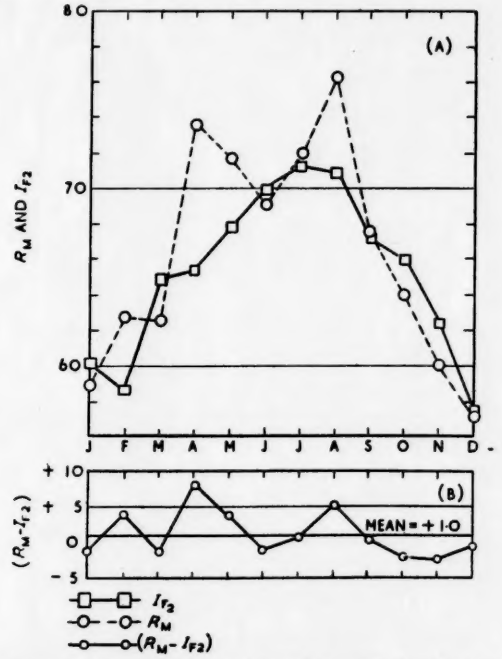

Fig. 2. Mean monthly values of R_M and I_{F_2}, 1938–1954.

The discussion in Section 5 has led to the conclusion that both I_{F_2} and R_M may be regarded as approximations to an idealized index (R_v) defined in Section 4, while the residual terms R_x and R_z may be regarded as random errors of measurement, i.e.

$$R_M = R_v + R_x \tag{1}$$

$$I_{F_2} = R_v + R_z \tag{13}$$

It is evident from Fig. 1 that, whereas R_M often fluctuates violently from one month to another, I_{F_2} is much more conservative, and this suggests that the variance of R_x exceeds that of R_z.

It is possible to obtain some information on the relative magnitudes of these variances by using the well-known superposed epoch method. During the period 1938–1953 there were 36 peak values in I_{F_2}, and its mean value has been computed for these months and also for several months before and after the peak months. For these same months the mean values of R_M were also computed; the resulting "pulse" was compared with that already obtained for I_{F_2}, and was found to have a

closely similar peak value (Fig. 3a). This procedure was then repeated, commencing with 46 peak values of R_M, and deriving the I_{F_2} and R_M pulses as before. In this case both the amplitude and the peak value of the R_M pulse were found to be

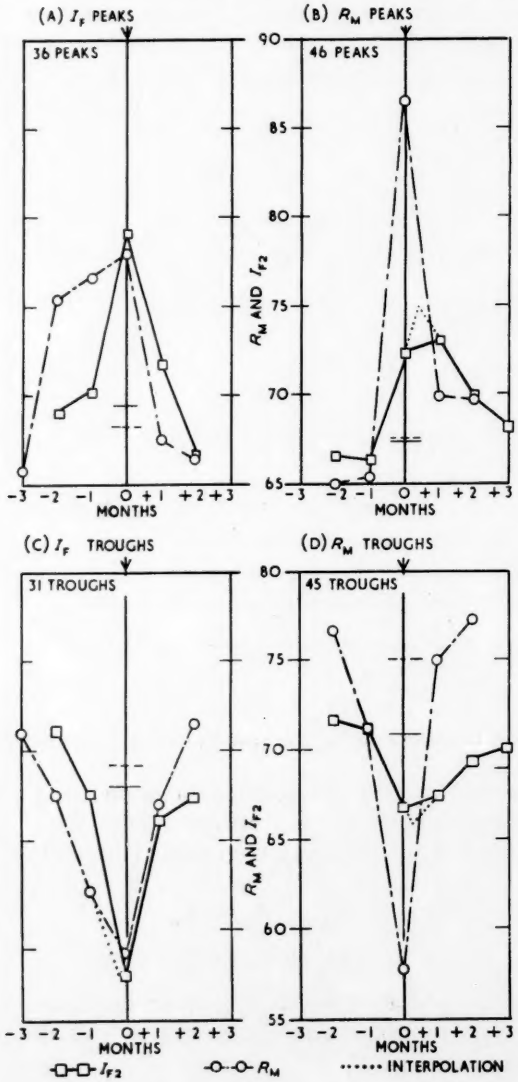

Fig. 3. Superposition of peaks and troughs in R_M and I_{F_2} (1938–1953). The reference levels of R and I_{F_2} are indicated by short lines on the zero month line.

much greater than those of the I_{F_2} pulse (Fig. 3b). Both these results were confirmed by comparing the negative pulses obtained by superposing the values of I_{F_2} and R_M in troughs (Figs. 3c, 3d).

VOL. 7 1955

It follows from (1) and (13) that the points on the superposed epoch diagrams can be represented by:

$$\bar{R}_M = \bar{R}_v + \bar{R}_x \tag{14}$$

$$\bar{I}_{F_2} = \bar{R}_v + \bar{R}_z \tag{15}$$

When peaks or troughs in I_{F_2} form the starting point (Figs. 3a, 3c), the agreement between $\bar{R}_M$ and I_{F_2} suggests that both $\bar{R}_x$ and $\bar{R}_z$ are small. On the other hand, the large difference between $\bar{R}_M$ and $\bar{I}_{F_2}$, which is found when high or low values of R_M are selected, shows that these extreme values are at least partly due to the inclusion in them of consistently positive or negative values of R_x. Since R_x and R_z are uncorrelated, it can be assumed that $\bar{R}_z \simeq 0$ and that the difference $(\bar{R}_M - \bar{I}_{F_2})$ can be used as an estimate of $\bar{R}_x$. In the same way, when peaks or troughs in I_{F_2} are selected, $(\bar{I}_{F_2} - \bar{R}_M)$ allows the value of R_z to be estimated. The magnitudes of these differences, after making certain small adjustments, are given in absolute values in Table 2. Alternatively, instead of comparing the absolute values at the peaks and troughs, it is possible to compare the amplitudes of the pulses, and this method also leads to estimated values of $\bar{R}_x$ and $\bar{R}_z$ which are quoted in Table 2.

Table 2. Estimated values of R_x and R_z (sunspot number units)

Method		R_x	R_z
Peaks	Absolute values	+ 9·6	+0·5
	Pulse amplitudes	+11·7	−1·0
Troughs	Absolute values	− 8·7	+0·9
	Pulse amplitudes	−12·4	+1·2
	Mean modulus	10·6	0·9

The reference level from which the amplitude is measured on each diagram is the mean value of the parameter for the four months symmetrically placed in relation to the pulse. There appears to be a time lag of a week or two in the occurrence of the I_{F_2} pulse relative to that of R_M, and it is very likely that the diagrams do not reproduce the true maximum and minimum values of the pulses in the parameter which did not control the selection process. To allow for this a rough interpolated value of the peak or trough has been added in Figs. 3b, c, d; but in Fig. 3a, since the simple construction used was not applicable, the peak value of the R_M pulse has been augmented by one unit. When computing the absolute peak values of R_M and I_{F_2}, an allowance was made for the fact that for the whole period 1938–1954 there is a small difference between the mean monthly values of R_M and I_{F_2}, which varies from month to month (Fig. 2b). An appropriately weighted correction was applied to take account of this when computing the absolute values in Table 2.

If the selection process used in constructing, for example, Fig. 3b, retained only positive values of R_x, then $(\bar{R}_M - \bar{I}_{F_2})$ would be the Mean Deviation of R_x. It

seems likely, however, that $\bar{R}_x$ may include some negative values, and will probably be somewhat less than the M.D. In order to obtain a rough figure for the

Table 3. *Mean and standard deviations of errors in* R_M *and* I_{F_2} (R_x *and* R_z)
(*sunspot number units*)

	R_x	R_z
M.D. (approx.) (Table 2)	10·6	0·9
S.D. (approx.)	13·3	1·1
Mean of index	$R_M = 70{\cdot}0$	$I_{F_2} = 68{\cdot}9$
S.D. (approx.)	19·0%	1·6%

S.D's of R_x and R_z, it will be assumed that the mean values of the moduli of $\bar{R}_x$ and $\bar{R}_z$ given in Table 2 represent approximate values of the M.D's, and that both parameters have normal distributions. These assumptions lead to the conclusion that the S.D. of $R_x \simeq 20$ per cent and of $R_z \simeq 2$ per cent (Table 3).

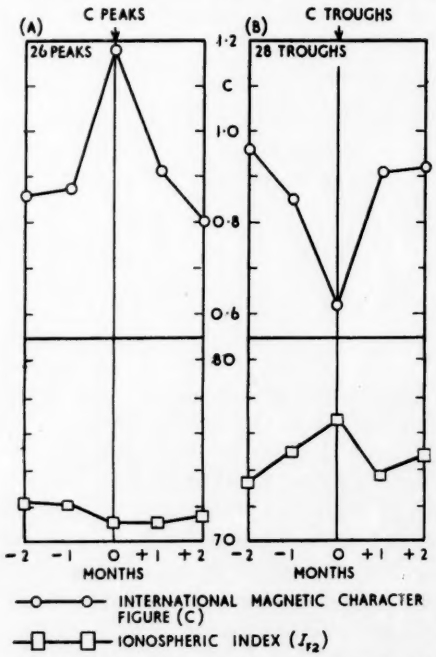

Fig. 4. Superposition of peaks and troughs in C and corresponding change in I_{F_2} (1938–1953).

The comparatively low S.D. of the fluctuations of I_{F_2} on either side of R_v accounts for the much greater conservatism shown in the trend of I_{F_2} as compared with that of R_M. This implies that the changes in the flux of the ionizing radiation which is responsible for the existence of the F_2-layer are much less erratic than might be inferred from the changes in relative sunspot number.

VOL. 7 1955

As explained in Section 5, I_{F_2} ought to be much less sensitive to changes in magnetic activity than R'_M. To test this supposition, superposed epoch diagrams were made by selecting peaks and troughs in the monthly mean value of the international magnetic character figure (C), and comparing the amplitudes of the pulses with those which occurred simultaneously in I_{F_2} (Figs. 4a, b). It is doubtful whether the resulting I_{F_2} pulses can be regarded as significant, but assuming that they do indicate associated changes in I_{F_2} and C, the evidence indicates that I_{F_2} changes by about five units per unit change in C. From data quoted by APPLETON and PIGGOTT (1955) it can be shown that the sensitivity of R'_M, deduced from measurements made at Slough alone, is four or five times as great as the figure just quoted for I_{F_2}. Since the total range in the monthly mean value of C during the solar cycle is only about 0·6, the maximum error in I_{F_2} due to disturbed ionospheric conditions is unlikely to exceed three units. It should be remembered that errors due to magnetic disturbances are already included in the estimated S.D. of R_z (equation 13).

7. Other Indices of Solar Activity

(a) *Twelve-month running-mean sunspot number*

A simple method of eliminating the seasonal component from a series of monthly values of the critical frequency of the F_2-layer is to compute the twelve-month running mean (f_{12}), and several authors have discussed the relation between f_{12} and the twelve-month running mean (R_{12}) of the sunspot number.

There are some obvious disadvantages in using R_{12} and its relation with f_{12} to forecast the mean critical frequency for a particular month:

(i) since the most recent available value of R_{12} always refers to a date at least six months earlier, it is necessary to make a larger extrapolation than if a monthly index were used;

(ii) short-term changes in solar activity having quasi-periods of under a year tend to be suppressed in various degrees and cannot be taken into account in the extrapolation.

(iii) A further consequence of (ii) is that the correlation of R_{12} with the mean critical for a single month is not high.

An additional and hitherto unsuspected objection to the use of R_{12} and f_{12} has emerged from this investigation. Equation (8) relates f with R only for a particular month, but both the solar cycle and seasonal changes can be represented by an expression of the form:

$$f = \alpha + \beta R + \gamma R^2 + m(\lambda + \mu R + \nu R^2) \qquad (16)$$

in which, for a given observatory, α, β, γ, λ, μ, and ν are constants, and m represents a function which oscillates between limits ± 1 and has a period of one year. Although m is roughly sinusoidal, it contains harmonics which are characteristic of the observatory but which have not been fully investigated Since both m and

R are functions of time ($m(\theta)$, $R(\theta)$, where $\theta = 2\pi t$), the twelve-month running mean of f centred on the month for which $\theta = \phi$ is given by:

$$f_{12} = \frac{1}{2\pi}\int_{\phi-\pi}^{\phi+\pi} f(\theta)\, d\theta$$

$$= \alpha + \beta\,\overline{R(\theta)} + \gamma\,\overline{R^2(\theta)} + \int_{\phi-\pi}^{\phi+\pi} [\mu m(\theta)R(\theta) + \nu m(\theta)R^2(\theta)]\, d\theta \qquad (17)$$

Equation (17) has two implications:

(i) f_{12} is a function not only of the mean value of R but also of its mean square, and consequently it depends on how R changes during the twelve-month period

(ii) If, for simplicity, it is assumed that $m(\theta) = \cos\theta$, and that $R(\theta)$ contains terms up to θ^2, the integral terms in (17) will have the form:

$$\int_{\phi-\pi}^{\phi+\pi} \theta^r \cos\theta\, d\theta \qquad (18)$$

where $r = 1$, 2, 3, or 4. Integrals of this type do not vanish when the integration covers 2π, but depend on ϕ and the coefficients of θ in the expression for $R(\theta)$.

On account of both (i) and (ii), it is concluded that the twelve-month running mean of the critical frequency of the F_2-layer is not uniquely determined by the twelve-month running mean of R, which, in consequence, cannot be regarded as a suitable index for use in forecasting ionospheric behaviour.

VOL. 7 1955

(b) *Relative critical frequency*

ALLEN (1946, 1948) has made use of an alternative method of eliminating the seasonal changes from the monthly mean values of the critical frequency of the F_2-layers. The "relative critical frequency" is defined as the ratio (A) of the mean critical frequency for a given month, when the mean sunspot is R, to that for the same month at zero sunspot number Using the linear terms in the relation between f and R (equation 16), A can be expressed approximately by:

$$A = \frac{\alpha + m\lambda + R(\beta + m\mu)}{\alpha + m\lambda} = 1 + \frac{\beta}{\alpha} R\left(\frac{1 + m\dfrac{\mu}{\beta}}{1 + m\dfrac{\lambda}{\alpha}}\right) \qquad (19)$$

Since A is a function of m, it must contain a seasonal component except when $\mu\alpha = \lambda\beta$. However, by averaging the values of A derived from a number of observatories, ALLEN has reduced any seasonal changes in his final index to negligible proportions.

The principal objection to the use of A as an index of solar activity is that its magnitude depends on the value of β/α at an observatory, or on the mean value of β/α when values of A from several observatories are combined. Thus A is not a pure solar index, since its magnitude is a function of certain ionospheric parameters and depends consequently on which observatories are selected to provide the ionospheric measurements.

During the analysis of F_2-layer data for the construction of the index I_{F_2}, approximate values of β/α were obtained for several observatories, viz., Slough, 66×10^{-4}; Huancayo, 81×10^{-4}; Watheroo, 88×10^{-4}. A comparison of the mean values of A for 1938–1947, tabulated by ALLEN, with I_{F_2} for the same period, shows that the mean value of β/α in ALLEN's index is 65×10^{-4}. Both ALLEN's index ($\bar{A}$) and I_{F_2} are, as might be expected, closely correlated ($r = 0{\cdot}977$) and are related by the expression:

$$\bar{A} = 1{\cdot}04 + 65 \times 10^{-4} I_{F_2} \tag{20}$$

8. CONCLUSIONS

The monthly mean value of the relative sunspot number (R) can be regarded as an approximation to the magnitude of an idealized index of the intensity of the solar ionizing radiation, but it includes an error having a Standard Deviation of about 20 per cent, which accounts for the erratic fluctuations in R. A method has been devised which allows the behaviour of the F_2-layer to be used to give the magnitude of the idealized index mentioned above. The new index (I_{F_2}) includes an error the S.D. of which is only about one-tenth that of R.

Acknowledgements—The author wishes to acknowledge useful criticisms made by Dr. H. G. HOPKINS.

The work described above was carried out as part of the programme of the Radio Research Board. This paper is published by permission of the Director of Radio Research of the Department of Scientific and Industrial Research.

REFERENCES

ALLEN, C. W. 1946 *Terr. Magn. Atmos. Elect.* **51**, 1
1948 *Terr. Magn. Atmos. Elect.* **53**, 43

APPLETON, E. V., and PIGGOTT, W. R. 1955 Rpt. Phys. Soc. Conference on The Physics of the Ionosphere, Sept. 1954, p. 219.

Journal of Atmospheric and Terrestrial Physics, 1955, Vol. 7, pp. 322 to 332. Pergamon Press Ltd., London

The interaction of pulsed radio waves in the ionosphere

J. A. FEJER
Telecommunications Research Laboratory of the South African Council
for Scientific and Industrial Research, Johannesburg

(*Received* 6 *April* 1955)

ABSTRACT

Preliminary daytime measurements of radio-wave interaction in the lower ionosphere with pulse transmitters are described. Interpretation of the results with the aid of the theory of BAILEY and MARTYN (1934a, 1934b, 1935) yields the collision frequency, the electron density, and the energy-loss coefficient G.

The resulting collision frequencies are in substantial agreement with results based on laboratory measurements by CROMPTON, HUXLEY, and SUTTON (1953), and with a value obtained from the observation of partial reflections by GARDNER and PAWSEY (1953). The electron densities are near the values of GARDNER and PAWSEY. The value obtained for G is very much higher than those resulting from laboratory measurements (CROMPTON, HUXLEY, and SUTTON, 1953). The latter apply, however, to high excess electron energies, while the excess electron energy during the present measurements was low.

The results of the observations described in this paper appear to lend support to the original form of the theory of BAILEY and MARTYN and not to its alternative development recently suggested by HUXLEY (1953).

1. INTRODUCTION

THE study of radio-wave interaction has been used previously (RATCLIFFE and SHAW, 1948; HUXLEY, 1950; SHAW, 1951) as a tool for the investigation of the lowest layers of the ionosphere. In these investigations the disturbing transmitter was sinusoidally modulated, and the wanted transmitter radiated a continuous wave. Pulse modulation of the disturbing transmitter only was used by CUTOLO (1947), and by BAILEY, SMITH, LANDECKER, HIGGS, and HIBBERD (1952). Pulse modulation of both the wanted and the disturbing transmitter was proposed in the Report of the Canadian National Committee to the 1952 meeting of the General Assembly of U.R.S.I.

This paper describes a method, which uses the observation of radio-wave interaction with two pulse transmitters, as a means of determining the collision frequency and the electron density, as functions of height, in the lowest parts of the ionosphere. Information about the rate of loss of the excess electron energy acquired by absorption is also obtained.

The present observations, which were exploratory in nature, were handicapped by the lack of sufficient radiated power (the mean power radiated by the disturbing transmitter was only 10 W). The experimental data nevertheless reveal some information about the lowest regions of the ionosphere, which is not easily obtained by other means.

2. EXPERIMENTAL PROCEDURE

2.1. *Basic principles*

Two pulse transmitters and a receiver for the ionospheric echo from the wanted transmitter are used on a common site with separate aerials. The disturbing transmitter pulse precedes the arrival on the ground of the wanted echo pulse by an adjustable time-interval t_0. The two aforementioned pulses are made to meet in the ionosphere at the height h_0. If the velocity of propagation is not greatly

VOL. 7 1955

modified by the presence of free electrons below the height h_0, the relationship $h_0 = ct_0/2$ exists, where c is the velocity of light.

The passing of the disturbing pulse through any height h raises the mean electron temperature above that of the neutral particles. The consequent increase of the collision frequency of electrons with neutral particles modifies the absorption of the wanted echo pulse, provided that the latter passes during its downward journey through the height h after the disturbing pulse. The condition for this is $h < h_0$. The amplitude of the echo received on the ground is therefore modified, if there are absorbing regions below the height h_0.

The aim of the present method is the measurement of this change in echo amplitude as a function of h_0. For this purpose the disturbing pulses are transmitted at half the recurrence frequency of the wanted pulses. The recurrence period of the wanted pulses is made much longer than the decay time of excess electron temperature. In this way the amplitude of only every second echo pulse is modified. The change of amplitude is measured by applying the amplified, detected, and strobed echoes at a controlled level to a selective amplifier tuned to half the recurrence frequency of the wanted pulses.

The output of this amplifier is applied to a phase-sensitive detector, which measures both the absolute value and the sign of the fractional change of echo amplitude.

2.2. *Equipment*

The block diagram of Fig. 1 shows the essential details of the equipment. Some of its more important parameters are:

Disturbing transmitter

Peak radiated power	5 kW
Equivalent omnidirectionally radiated peak power	80 kW
Frequency	1·82 Mc/s
Pulse length	50 microsec
Recurrence frequency	40 c/s

Aerial: Four horizontal half-wave dipoles 55 ft above the ground forming the sides of a square and producing circular polarization. The circuit employed for the production of circular polarization is similar to that described by GARDNER and PAWSEY (1953).

Wanted transmitter

Peak radiated power	2 kW
Frequency	2·4–2·6 Mc/s
Pulse length	50 microsec
Recurrence frequency	80 c/s

Aerial: Horizontal half-wave dipole 30 ft from the ground.

Receiver

Effective bandwidth	30 kc/s
Time constant of phase-sensitive detector	10 sec
Width of output strobe	50 microsec

Aerial: Horizontal half-wave dipole 30 ft from the ground.

Calibration is carried out by applying the disturbing instead of the wanted pulses at the same controlled level from the receiver output, after 2000 : 1 attenuation, to the selective amplifier, simulating a fractional change of $5 \cdot 10^{-4}$ in echo amplitude.

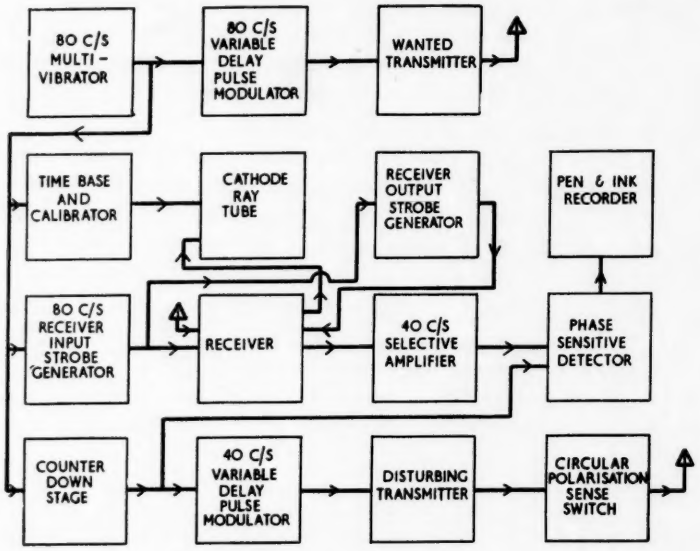

Fig. 1. Block diagram of equipment.

3. OBSERVATIONS

Observations were carried out during the months of October and November 1954 at Frankenwald, about fourteen miles from Johannesburg. Man-made noise was higher at Frankenwald than at the Burragorang Valley site described by GARDNER and PAWSEY (1953), corresponding to an equivalent aerial temperature of about 3000°K under favourable conditions. The 70-km partial reflections described by GARDNER and PAWSEY (1953) were regularly observed at Frankenwald, but no study of these echoes was made. During the present observations, which were restricted by atmospheric noise to the period of about 9 a.m. to 1 p.m., the wanted echo was reflected by the E-layer. During the winter it should be possible to use the F_2 echo.

Circularly polarized disturbing pulses were used throughout the measurements. The wanted echo had right-handed polarization on account of the large absorption suffered by the extraordinary wave.

Fig. 2 shows sections from some typical records taken with an extraordinary disturbing wave. The records show the fractional difference, T, in subsequent parts of the paper referred to as transferred modulation, between alternate echo amplitudes as a function of time. The value of h_0 was changed at about five-minute intervals, and is indicated on the records. The vertical scale for T is indicated on the left of each record. Levels below zero (T positive) show that the amplitude of the disturbed echo is smaller than that of the undisturbed echo.

VOL. 7 1955

All three records of Fig. 2 show the largest interaction effect for $h_0 = 80$ km, and some of the records show an effect for $h_0 = 70$ *km* and $h_0 = 90$ km. No definite effect is shown at the other levels. The interaction effect seen on these records is little above the level of spurious fluctuations. These fluctuations appear to be partly due to man-made noise, partly to atmospheric noise, and partly to fading.

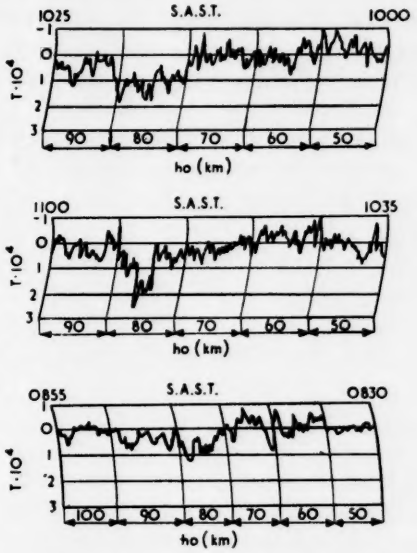

Fig. 2. Three respective sections from records of the transferred modulation T taken on three different days, the dates being (from top to bottom): 14.10.54, 13.10.54, and 8.10.54. The time is shown on the top, the value of h_0 at the bottom of each record.

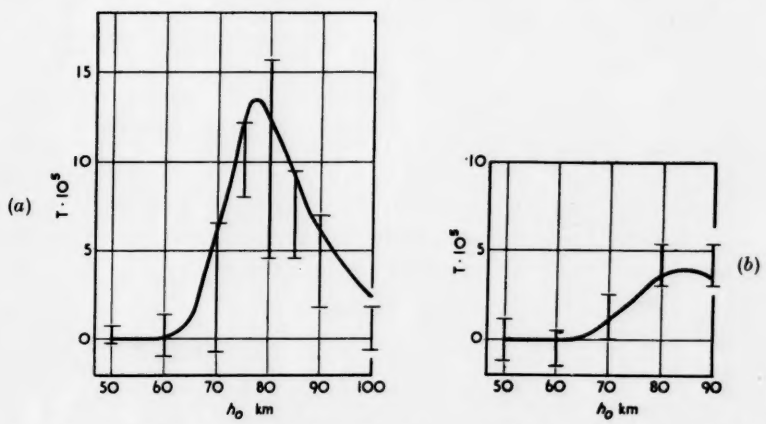

Fig. 3. Mean values and standard deviations of records for different values of h_0. Fig. 3a represents records taken with extraordinary polarization, Fig. 3b records taken with ordinary polarization of the disturbing wave. The lengths of the vertical lines are equal to twice the standard deviation, their midpoints indicate mean values. The solid theoretical curve corresponds to the conditions of Fig. 4.

Fig. 3 indicates the results obtained from all the records of the type shown by Fig. 2. For each value of h_0 except 100 km there were about fifteen records of five-minute duration available with the disturbing transmitter radiating an extraordinary wave, and about five records with the disturbing transmitter radiating an ordinary wave. For 100 km only five records were available with the disturbing transmitter radiating an extraordinary wave. The average value of each five-minute section was estimated. The centres of the vertical lines in Fig. 3 represent the means of these average values, while the lengths of the vertical lines indicate twice their standard deviation. The meaning of the curves of Fig. 3 will be discussed in a later part of the paper.

While the standard deviations of Fig. 3 are rather large, there is little doubt of the existence of the effect or of the sharp maximum at 75–80 km for the extraordinary wave. It was difficult to obtain records for much higher values of h_0 than 90 km because in the present method the disturbing transmitter pulse must not coincide with, or precede, the wanted transmitter pulse. Records for much higher values of h_0 could be obtained by using the F_2 echo.

4. INTERPRETATION

4.1. *Theory*

Let a pulsed radio wave of infinitely short duration be perpendicularly incident on a thin homogeneous layer of thickness dh containing N free electrons per cm^3. Let the energy absorbed from the wave per unit area of the layer be dI. The mean thermal energy of the electrons is $3k\theta/2$, where k is BOLTZMANN'S constant and θ the temperature of the layer. The mean fractional increase of electron temperature caused by the energy absorbed from the wave is then $2dI/(3Nk\theta dh)$, and this is equal to the fractional increase in collision frequency ν, the latter being proportional to temperature (CROMPTON, HUXLEY, and SUTTON, 1953). The fractional decrease in the amplitude of a wanted wave passing through the layer immediately after the disturbing pulse is then

$$\frac{\partial \kappa_2}{\partial \nu} d\bar{h} \frac{2dI\nu}{3Nk\theta dh} \tag{1}$$

where κ_2 is the absorption coefficient for the wanted wave.

If the above-mentioned pulsed radio wave is radiated from the ground by a disturbing transmitter, and if the equivalent energy radiated upward in one pulse, assuming a transmitter radiating equally in all directions, is E, then the disturbing energy per unit area of the wave front at the height h is

$$EF(h)/(4\pi h^2) \tag{2}$$

where

$$F(h) = \exp\left(-\int_0^h 2\kappa_1 \, dh\right) \tag{3}$$

and where κ_1 is the absorption coefficient for the disturbing wave. The disturbing energy absorbed in the thin layer between h and $h + dh$ is

$$dI = EdF/(4\pi h^2) \tag{4}$$

VOL. 7 1955

If equations (1) and (4) are used to calculate the fractional decrease in the amplitude of the wanted wave caused by all absorbing layers below the height h_0, it must be remembered that at the height h there is a time interval $2(h_0 - h)/c$ between the passing of the disturbing pulse and the wanted echo pulse. The excess electron temperature is thus less at the time of the passing through of the wanted echo pulse than it is immediately after the passing through of the disturbing pulse. The excess electron temperature existing immediately after the passing of the disturbing pulse is assumed here to be a small fraction of the temperature of the neutral particles. It is also assumed, after BAILEY and MARTYN (1934a, 1934b, 1935) that this small excess electron temperature decreases exponentially with a time constant $(G\nu)^{-1}$, where G is a constant. These assumptions are justified in a subsequent part of the paper. One obtains then with the aid of equations (1) and (4) for the fractional decrease dT in the amplitude of the wanted echo caused by interaction in the layer between h and $h + dh$,

$$dT = \frac{2\nu}{3Nk\theta} \frac{\partial \kappa_2}{\partial \nu} \frac{E dF}{4\pi h^2} \exp\left[-2(h_0 - h)G\nu/c\right] \tag{5}$$

and thus the total transferred modulation is

$$T = \int_0^{h_0} \frac{E\nu}{6\pi Nk\theta h^2} \frac{\partial \kappa_2}{\partial \nu} \exp\left[-2(h_0 - h)G\nu/c\right] \tag{6}$$

Substituting

$$T_h = \frac{E\nu}{6\pi Nk\theta h^2} \frac{\partial \kappa_2}{\partial \nu} \tag{7}$$

equation (6) may be rewritten in the form

$$T = \int_0^{h_0} T_h \exp\left[-2(h_0 - h)G\nu/c\right] dF \tag{8}$$

Equations (7) and (8) are of a very general nature. No assumptions are made in them about the dependence of the absorption coefficients on the various parameters involved. Equation (8), together with equation (3), indicates the calculating procedure, based on equation (7), which must be used when the interaction effect takes place over a range of heights.

The physical significance of T_h is best seen by assuming that the disturbing pulse is completely absorbed at a single height h, and that the wanted pulse passes through this height immediately after the disturbing pulse. In this case the transferred modulation T is equal to T_h, as $\int dF = 1$. It should be noted that T_h is independent of the electron density, because κ_2 is proportional to N.

Apart from the zone near the magnetic equator, the absorption coefficients κ_1 and κ_2 for non-deviative absorption at frequencies far enough above the gyro frequency are given with sufficient accuracy by the quasilongitudinal approximation to the magneto-ionic theory (APPLETON, 1937)

$$\kappa_1 = \frac{2\pi e^2}{mc} \frac{N\nu}{\nu^2 + (\omega_1 \pm \omega_L)^2} \tag{9}$$

$$\kappa_2 = \frac{2\pi e^2}{mc} \frac{N\nu}{\nu^2 + (\omega_2 \pm \omega_L)^2} \tag{10}$$

where e is the electronic charge, m the electronic mass, ω_1 and ω_2 the angular frequencies of the disturbing and the wanted waves respectively, and ω_L the angular frequency corresponding to the longitudinal component of the earth's magnetic field. The positive sign refers to the ordinary, the negative to the extraordinary wave. Differentiation of equation (10) gives

$$\frac{\partial \kappa_2}{\partial \nu} = \frac{2\pi e^2 N}{mc} \frac{(\omega_2 \pm \omega_L)^2 - \nu^2}{[(\omega_2 \pm \omega_L)^2 + \nu^2]^2} \tag{11}$$

Substituting $\partial\kappa_2/\partial\nu$ from equation (11) into equation (7)

$$T_h = \frac{e^2 E \nu}{3mck\theta h^2} \frac{(\omega_2 \pm \omega_L)^2 - \nu^2}{[(\omega_2 \pm \omega_L)^2 + \nu^2]^2} \tag{12}$$

Equation (12) shows that T_h only depends, apart from physical constants, on ν, ω_2, ω_L, θ, and h. Of these, ω_2 is independent of the height and ω_L, θ, h are slowly varying functions of the height when compared with ν. Thus the extreme values of T_h may be found approximately by differentiation with respect to ν.

According to equation (12), T_h is positive for $\nu < \omega_2 \pm \omega_L$ and negative for $\nu > \omega_2 \pm \omega_L$. The largest positive value of T_h occurs for $\nu = (\sqrt{2}-1)(\omega_2 \pm \omega_L)$ and is equal to $e^2E/[12mck\theta h^2(\omega_2 \pm \omega_L)^2]$, while the (absolutely) largest negative value occurs for $\nu = (\sqrt{2}+1)(\omega_2 \pm \omega_L)$ and is equal to $-e^2E/[12mck\theta h^2(\omega_2 \pm \omega_L)^2]$. Thus the largest transferred modulation of both signs occurs near the height, for which $\nu = \omega_2 \pm \omega_L$, although at this height itself there is no interaction.

VOL. 7 1955

4.2. *Methods of interpretation*

The result of the experimental procedure described in Section 2 usually has the form of two curves, one for the ordinary and one for the extraordinary disturbing wave respectively, representing T as a function of h_0. Some methods of interpretation based on these two curves are suggested here. The choice of a method depends on the error in the measured points defining the curve.

The methods of interpretation to be discussed make use of equation (8) re-written with the summation instead of the integral sign:

$$T_i \cong \sum_{j=1}^{j=i} T_{hj} \Delta_j F \exp[-2(h_i - h_j)G\nu_j/c] \tag{13}$$

Here $h_{j+1} > h_j$, so that h_1 is the lowest height at which an interaction effect T_1 is measured. T_{hj} is the value of T_h for $h = h_j$, while $\Delta_j F = F(h_j) - F(h_{j-1})$ for $j > 1$ and $\Delta_1 F = F(h_1)$ for $j = 1$. Then in principle, if a tentative value of G is assumed, and T_1, T_2, ... have all been measured for both an ordinary and an extraordinary disturbing wave, the values of ν_1, ν_2, ... and N_1, N_2, ... can be obtained from the two sets of equations for $i = 1, 2, \ldots$ provided by equation (13). The temperature is assumed known for this purpose; its exact value influences the results only slightly. The solution of these equations is simple enough, if one starts with the pair of equations for $i = 1$ to obtain ν_1 and N_1, and then proceeds step by step to higher values of i. A rather sensitive check on the value of

G chosen is provided by the fact that the value of N near the centre of the E-region is known from routine measurements.

While this method appears at first sight a very comprehensive one, it requires more accurate experimental results than one is likely to obtain, even in future measurements of this nature.

In a more practical method of interpretation, which is used to interpret the present observations, the assumption is made that the collision frequency ν, and therefore also $G\nu$, is proportional to rocket pressure data (HAVENS, KOLL, and LAGOW, 1952). This is probably true at the heights of interest, for which the chemical composition of the air is the same as on the ground (CROMPTON, HUXLEY, and SUTTON, 1953). A value of $G\nu_1$ for the height h_1 is tentatively assumed. The numerical values $\theta = 200°\text{K}$ and $p_L = 5{\cdot}2 \cdot 10^6$ are used. Equation (13) then makes the calculations of the quantities $T_{hj}\Delta_j F$ possible. In practice it is usually known that $\Delta_j F$ vanishes above a certain height where the disturbing wave is almost completely absorbed, particularly if an extraordinary disturbing wave is used. This provides a check on the value of $G\nu_1$ chosen for h_1. The continued vanishing of $T_{hj}\Delta_j F$ above a certain height should also provide proof of the correctness of the theory as well as of the rocket data.

The next step is to assume a tentative value for G. Then, ν_j being tentatively known, the values of T_{hj} can be calculated from equations (7) and (11), and thus the $\Delta_j F$ can be obtained from the previous results for $T_{hj}\Delta_j F$. It is usually known for at least the extraordinary disturbing wave that $\Sigma\Delta_j F = 1$ above a certain height, and this provides a simple check on the chosen value of G. When the correct value of G has been ascertained, and thus the collision frequencies ν_j are known, the values of the N_j can be determined from the $\Delta_j F$ with the aid of equations (3) and (9). This can be done for both the ordinary and the extraordinary disturbing wave, and the values of N_j obtained in these two ways should agree; this provides a further check.

Two other methods could be used (they were not used in the present investigation) to find an absolute value of ν for a single height. Firstly, the reversal of the sign of T_h for $\nu = \omega_2 \pm \omega_L$ may be used to determine the collision frequency at the height concerned. If this reversal could be observed, it would occur at a rather low height, for which the time $(G\nu)^{-1}$ is very short, and it would therefore be sufficiently accurate to observe the reversal in the sign of T instead of T_h.

In the second method the ratio of the values of T for the ordinary and for the extraordinary disturbing waves is obtained at the smallest values of h_0 for which reliable values of both have been measured, and for which the absorption suffered by both is small. From equation (9) the value of this ratio is

$$\frac{\nu^2 + (\omega_1 - \omega_L)^2}{\nu^2 + (\omega_1 + \omega_L)^2} \tag{14}$$

and thus the value of ν may be determined.

4.3. *Discussion of the experimental results*

The data shown by Fig. 3 do not define the two curves required for interpretation very accurately. A tentative curve for the extraordinary disturbing

wave based on these data was first used and the second method described in Section 4.2 was applied to it. In this way $T_{hj}\Delta_j F$ was determined for 2-km intervals with the aid of rocket pressure data (HAVENS, KOLL, and LAGOW, 1952), and with tentatively assumed values of $G\nu_1$ at 70-km height. The condition that $T_{hj}\Delta_j F$ vanishes at the height of 90 km was used to determine the correct value of $G\nu_1$. The condition $\Sigma\Delta_j F = 1$ was then used to determine the value of G. The value obtained for G was very near to 10^{-2}, while the value of the collision frequency obtained for 70 km was $5 \cdot 10^6$. The methods of Section 4.2 were then used to obtain the values of N_j. These values should in theory also fit the, so far disregarded, curve for the ordinary disturbing wave. In practice, however, the curve

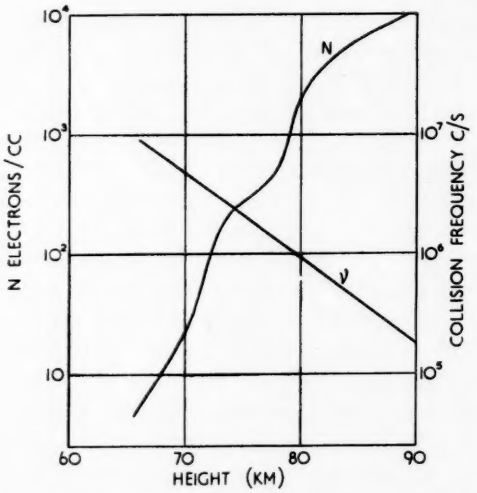

Fig. 4. Collision frequencies and electron densities derived from the experimental data of Fig. 3.

for the extraordinary wave does not define the values of N_j over about 80 km very accurately, and therefore the values of N_j obtained by the method described above were afterwards modified to fit the curve for an ordinary disturbing wave better, especially in the 80 to 90 km region.

The values of collision frequency and electron density obtained in this way are shown by Fig. 4, while the T, h_0 curves resulting from the curves of Fig. 4 (with $G = 10^{-2}$) are shown by Fig. 3, which, as previously mentioned, also shows the experimental data. A correction for the finite width of the disturbing pulse was made in the calculation of the curves of Fig. 3.

The values of G, ν, and N are not determined very accurately by the experimental data. The uncertainty in the values of G and ν is estimated as about ± 40 per cent, while the values of N especially above 80 km are very much less certain.

The collision frequencies shown by Fig. 4 are identical with those suggested by CROMPTON, HUXLEY, and SUTTON, and the collision frequency shown by Fig. 4 for 65 km agrees within the limits of experimental error with the figure obtained by GARDNER and PAWSEY (1953) from measurements on D-layer partial reflections.

VOL. 7 1955

The values of N shown by Fig. 4 are not very different from those of GARDNER and PAWSEY (1953), and would be still nearer if the results of GARDNER and PAWSEY were re-interpreted by using the collision frequencies of Fig. 4 of this paper. Their results show a stronger stratification at 70 km and somewhat larger electron densities below 70 km.

4.4. *Alternate developments of the theory of radio-wave interaction*

The high value of G obtained here is rather significant in view of the two possible alternative developments of the theory of radio-wave interaction pointed out by HUXLEY (1953). In the first of these developments the mean excess energy lost by an electron in a collision is in HUXLEY's notation

$$\Delta Q = G(Q - Q_0) \tag{15}$$

while in the second development (HUXLEY's equation (16))

$$\Delta Q = 4{\cdot}13 \,.\, 10^{-38} \frac{n}{\nu} (Q - Q_0)^2 / Q\, Q_0{}^2 \cong 3{\cdot}73 \,.\, 10^{-3} \frac{k_T - 1}{k_T{}^2} (Q - Q_0) \tag{16}$$

According to the second development, the decay of the excess energy in the absence of a disturbing wave is not exponential. One could, however, re-write (16) in the form

$$\Delta Q = G_{\text{eff}} (Q - Q_0) \tag{17}$$

where

$$G_{\text{eff}} = 3{\cdot}73 \,.\, 10^{-3} \frac{k_T - 1}{k_T{}^2} \tag{18}$$

and the value of G_{eff} immediately after the passing of the disturbing pulse would determine the rate of decay accurately at that moment, although further decay would show the slow tail mentioned by HUXLEY.

The value of k_T can be estimated from the following expression derived from equation (4) for the energy absorbed by an electron, neglecting absorption below the height h

$$\frac{2\pi e^2}{mc} \frac{\nu}{\nu^2 + (\omega_1 \pm \omega_L)^2} \frac{E}{4\pi h^2} \tag{19}$$

This expression, taking the extreme case of $\nu = \omega_1 - \omega_L \cong 6 \,.\, 10^6$, can at the most be equal to $3{\cdot}1 \,.\, 10^{-16}$ ergs. With this value one obtains $k_T = 1{\cdot}005$, corresponding (according to equation (18)) to $G_{\text{eff}} = 1{\cdot}87 \,.\, 10^{-5}$, a value too small by a factor of 500. Thus the present observations strongly favour the first and original development of the theory of radio-wave interaction.

This finding contradicts the view, expressed by HUXLEY (1953), that the results of measurements of radio-wave interaction using large powers support the second alternative development rather than the first one. HUXLEY bases his view on a consideration of the rise in electron temperature (his Section 5), which fails to take the magnetic field of the earth into account. If the magnetic field is not neglected, the calculation of the rise in electron temperature for HUXLEY's experimental conditions results in very much smaller figures than those of HUXLEY. This would

mean values of k_T near unity rather than of the order of 2 or 3. With such values of k_T the measurements of HUXLEY (1950), and RATCLIFFE and SHAW (1948), lend support to the original theory rather than to the modification suggested by HUXLEY, and lead to about the same high value of G as was obtained from the present experiments, if the collision frequencies suggested by HUXLEY (1953), and apparently confirmed by the present experiments, are adopted.

5. CONCLUSIONS

It has been established that radio-wave interaction between pulsed radio waves with frequencies of the order of 2 Mc/s takes place above the Transvaal during the day at heights of about 70–90 km. The use of this effect appears to be a promising method of exploring the lowest regions of the ionosphere.

The results of the present observations support, for the case of small excess electron energies, the original form of the BAILEY-MARTYN (1934, 1935) theory of radio-wave interaction rather than the modification suggested by HUXLEY (1953). The results for the collision frequency appear to be in agreement with results derived from laboratory measurements by CROMPTON, HUXLEY, and SUTTON (1953), and also with the collision frequency at the height of 65 km obtained from observations of partial reflections by GARDNER and PAWSEY (1953).

The present results for the electron density do not differ greatly from the results of GARDNER and PAWSEY (1953).

If further observations are undertaken, it would be desirable to increase the pulse power substantially and to improve the range resolution.

Acknowledgements—This paper is published with the permission of the South African Council for Scientific and Industrial Research.

REFERENCES

APPLETON, E. V.	1937	*Proc. Roy. Soc.* **A162,** 451
BAILEY, V. A., SMITH, R. A., LANDECKER, K., HIGGS, A. J., and HIBBERD, F. H.	1952	*Nature* **169,** 911
BAILEY, V. A., and MARTYN, D. F.	1934a	*Nature* **133,** 218
BAILEY, V. A., and MARTYN, D. F.	1934b	*Phil. Mag.* **18,** 369
BAILEY, V. A., and MARTYN, D. F.	1935	*Nature* **135,** 585
CROMPTON, R. W., HUXLEY, L. G. H., and SUTTON, D. J.	1953	*Proc. Roy. Soc.* **A218,** 507
CUTOLO, M.	1947	*Nature,* **160,** 834
GARDNER, F. F., and PAWSEY, J. L.	1953	*J. Atmosph. Terr. Phys.* **3,** 321
HAVENS, R. J., KOLL, R. T., and LAGOW, H. E.	1952	*J. Geophys. Res.* **57,** 59
HUXLEY, L. G. H.	1950	*Proc. Roy. Soc.* **A200,** 486
HUXLEY, L. G. H.	1953	*Proc. Roy. Soc.* **A218,** 520
RATCLIFFE, J. A., and SHAW, I. J.	1948	*Proc. Roy. Soc.* **A193,** 311
SHAW, I. J.	1951	*Proc. Phys. Soc.* **B64,** 1

VOL. 7 1955

Journal of Atmospheric and Terrestrial Physics, 1955, Vol. 7, pp. 333 to 340. Pergamon Press Ltd., London

Ionospheric wind determination from spaced radio receiver fading records

G. W. G. COURT
Dominion Physical Laboratory, Department of Scientific and Industrial Research, New Zealand*

(*Received* 28 *April* 1955)

ABSTRACT

A simple physical model provides an interpretation of the fading records obtained when using the system described by MITRA (1949) for the observation of drift in the ionosphere. This seems to be confirmed by a new practical method of analysis of the records, and the results support a proposal for an alternative method of determining the winds.

This paper is intended to present a brief survey of the proposals and initial experimental results.

INTRODUCTION

THE method proposed by MITRA (1949) to determine winds in the ionosphere by the examination of the fading records of reflected radio signals on three spaced receivers has been discussed in the literature. In particular, RATCLIFFE (1954) and NEWSTEAD (1954) have discussed the analysis of the records obtained, and have suggested various means of interpreting these analyses. It is proposed in this paper that no particular distribution of the orientations of field strength patterns with respect to the wind be assumed, and it is shown that direct analysis of the records can indicate the true wind and also indicate the changes in orientations of the patterns. As discussed by RATCLIFFE, "lines of maximum amplitude" are considered, and are approximated by straight lines for the basis of this analysis. Effects of curvature of the "line of maximum curvature" are discussed in a paper by N. J. RUMSEY (1955).

The results obtained in specific cases support the proposal for a method of determining the winds, in which a single fixed aerial, and an aerial moving on a circular path around it, are used. This method overcomes the difficulty of reducing the field strength patterns to lines of maximum amplitude, and indicates the true wind in direction and amplitude directly.

GENERAL

It will be assumed that, insofar as the records from the Mitra assembly of aerials is concerned, the field-strength patterns can be reduced to lines of maximum amplitude as defined by RATCLIFFE. Further, it is assumed that these lines may be considered to be straight as a first approximation.

Let the true wind velocity be V (Fig. 1) and the aerials N, C, and E. If M_1M_1' is a line of maximum amplitude moving over this aerial system, then by the Mitra analysis the component of velocity v_1 normal to the line M_1M_1' is derived. For any other line M_2M_2', the component v_2, normal to M_2M_2', is derived. In fact, generally, this component velocity v is measured.

* Now at Civil Aviation Administration, Air Department, Wellington, New Zealand.

Now $v = V \cos \theta$ where θ is the angle between V and the normal to the line of maximum amplitude, and if we assume that, for the duration of a record, V is constant, then the construction shown in Fig. 2 is to be realized.

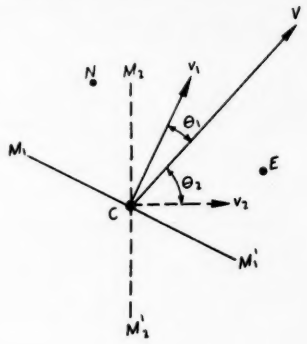

Fig. 1.

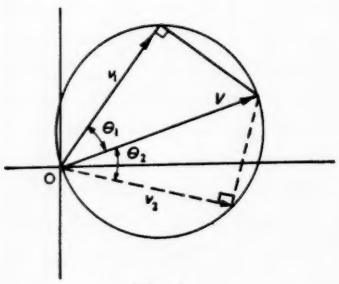

Fig. 2.

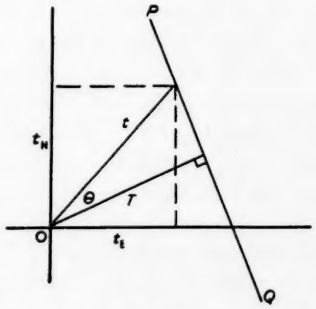

Fig. 3.

The vectors $v_1, v_2, \ldots, v_n$ are drawn from an origin O, and since in each case the individual vector is equal to $V \cos \theta_n$, where θ_n is the appropriate angle as defined, then the ends of the vectors must lie on a circle of which V is the diameter through the origin O.

Equally well $$1/v_n = 1/V \cos \theta_n$$

or $$t = T \sec \theta_n$$

where $t \propto 1/v$ and $T \propto 1/V$

and it will be seen that

$$t = \sqrt{t_N{}^2 + t_E{}^2}$$

where t_N and t_E are the time-intervals between similarities occurring in the central and north, and central and east aerials, respectively (MITRA, 1949).

Using t_N and t_E the construction of Fig. 3 is realized, since $t = T \sec \theta$ defines the straight line PQ, where T is the normal to PQ through the origin O.

Plotting appropriate values for t_N and t_E should produce a straight line, and the normal to it from the origin will indicate the velocity of the true wind V.

VOL. 7 1955

It will be noted that no assumption as to the distribution of the orientation of the patterns is assumed, and, provided the construction is realized, the actual variation of θ may be determined.

Proposed Method of Analysis

Carrying out the analysis for t_N and t_E from the north, central, and eastern records, by the method described by Mitra, involves the identification of points of correspondence in these records. This has been attempted, and the results generally fail to define a unique circle or straight line. It is desirable therefore to determine if a more satisfactory method of analysis is possible, and it is of interest to consider

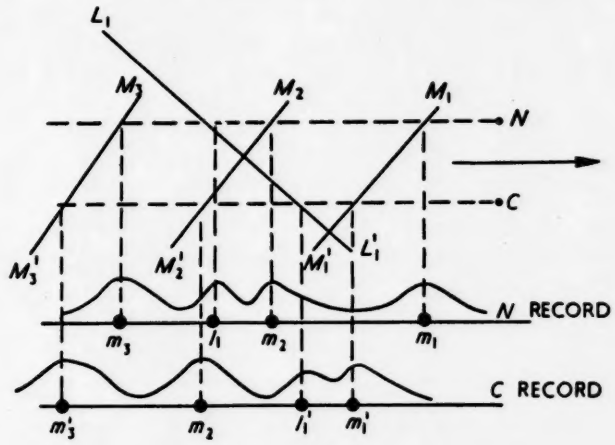

Fig. 4.

how the records arise in a simple case. As an example, we can examine a set of field-strength patterns due to a simple diffraction pattern, over which is superimposed a second set at a different orientation. The possibilities are innumerable, but we may make some deductions from an oversimplified case.

Consider a set of patterns reduced to straight lines of maximum intensity M_1M_1', M_2M_2', etc., and a second set of which LL' is an individual example (Fig. 4). If the patterns are moving with a velocity V, then the occurrence of maxima in the N and C aerial records may be as indicated m_1m_1', l_1l_1', etc. An analysis of these records by attempting to associate similarities directly may be confusing, and the values of t_N derived possibly misconstrued. Nevertheless, there is a definite pattern due to m_1m_1', m_2m_2', and m_3m_3', and the values of t_N for these would be appropriate for lines of maximum intensity at the appropriate orientation. It can be seen that, if the record for C is superimposed on that for N. and moved to obtain the optimum correspondence, then the m maxima will match, and the l maxima will appear as secondary effects, provided that the amplitudes of l and m are comparable. As a result, the appropriate value of t_N may be measured for the appropriate relative shift of the C and N records, and by similar considerations t_E may be measured.

Although this is clearly an oversimplified case, the method has been tried practically with some success. The fading records, similar to those illustrated in MITRA's paper, are familiar to workers in the field, and will not be discussed in detail. The analysis has been carried out in the following manner.

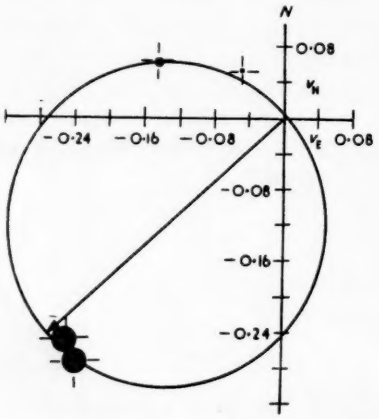

Fig. 5. V_N and V_E scales in arbitrary units.
07·00, 20.6.53. 110 km.
V = 102 m/s, 132° W of North.

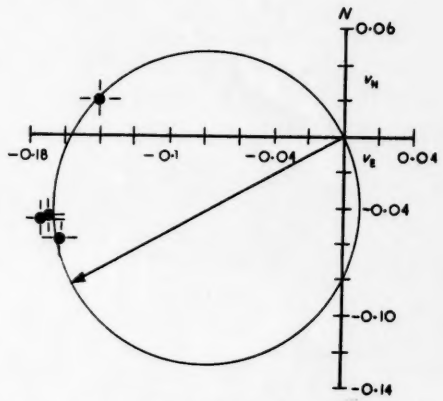

Fig. 6. V_N and V_E scales in arbitrary units.
08·00, 21.6.53. 110 km.
V = 48 m/s 118° W of North.

VOL. 7 1955

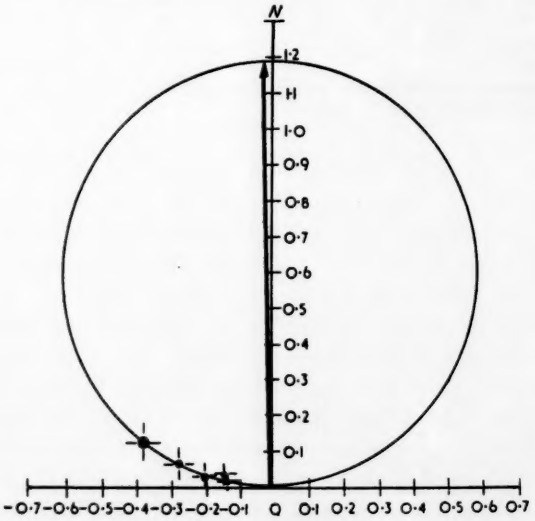

Fig. 7. V_N and V_E scales in arbitrary units.
01·20 , 17.9.54. 110 km.
V = 325 m/s 1·25° W of North (circle construction).
V = 350 m/s North (approx) (moving aerial deduction).

The record of the central aerial is traced, and the tracing compared in turn with corresponding portions of the north and east records. It is found that short portions of the pairs of records, i.e., central and north, and central and east, when

compared in this way, show immediately a suitable relative shift to give optimum correspondence. As indicated above, it is often found that a group of similarities will match well, with perhaps one or two odd points which are obviously incorrect. In records of two or three minutes duration it has been found that three or four short portions of the records can be taken, and corresponding values of t_N and t_E measured by this method.

From these results both the circle and straight-line constructions have been carried out, and the results are shown in Figs. 5, 6, 7, 8 for the circle, and Figs. 9,

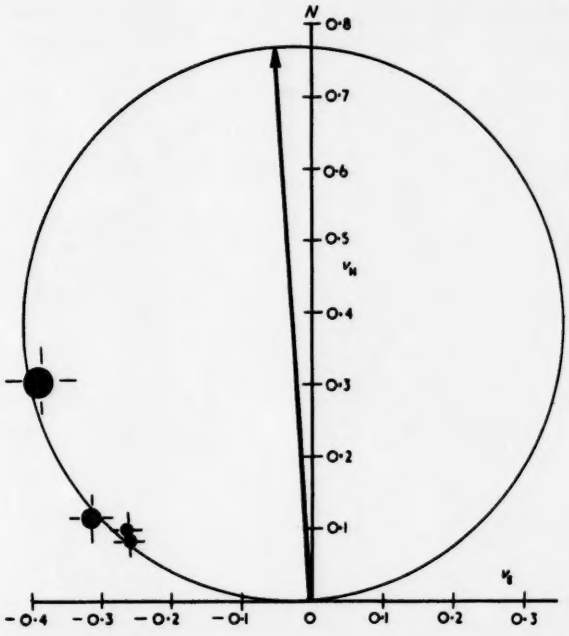

Fig. 8. V_N and V_E scales in arbitrary units.
00·00, 16.9.54. 110 km.
V = 212 m/s 4° W of North (circle construction).
V = 234 m/s North (approx.) (moving aerial deduction).

10 for the straight-line construction. It is apparent that the straight line is preferable for a general application of an analysis, but the use of the vector construction gives a better physical picture for discussion purposes. The size of the plotted points is an indication of the uncertainty of their precise position.

Generally, so far as it has been applied, the method is satisfactory, although on a few records no successful construction could be carried out from the results. This is taken to indicate that the basic assumption of a constant wind V, or effectively straight lines of maximum amplitude, has not been met, and the result must be ignored. Insufficient numbers of records have so far been analyzed by this method to completely determine its usefulness, but it is considered that the results that have been obtained justify a full-scale application of it.

However, another method of determining the wind V is proposed, and it will be seen that the results of this analysis on specific records provide evidence in favour of its usefulness.

New Method of Observation

It is immediately apparent that if, and only if, two aerials are in line with the direction of movement of the field-strength patterns over the ground, then, provided the patterns do not change in the time-interval required to move from one aerial to the other, the records obtained at the aerials will be identical.

Consider a single fixed aerial F, Fig. 11, and a moving aerial M, arranged to move on a semi-circular path centred on F. Now, if the records of these aerials are

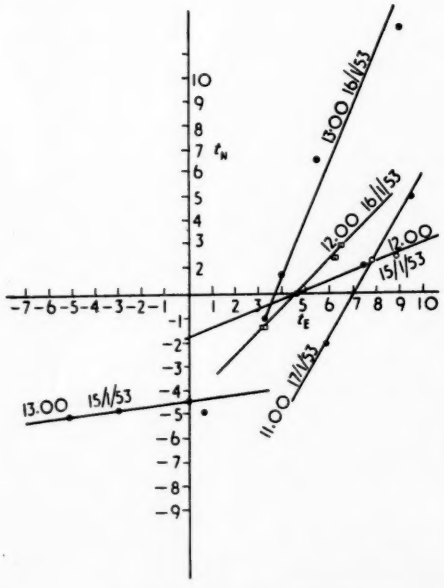

Fig. 9. t_N and t_E scales in arbitrary units.

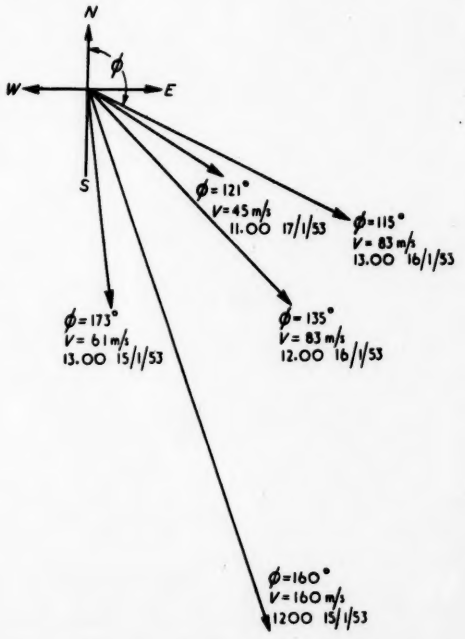

Fig. 10. Wind velocity V deduced from Fig. 9.

displayed suitably, a direct comparison between them can be made by an observer, particularly if arrangements are made to shift one relative to the other. Comparisons of records by the tracing system described earlier give reason for believing that when two identical records are observed, the fact will be immediately apparent. The wind determination would be carried out therefore by having the aerial moved around its path, while an observer compared the records from the two aerials. The wind direction will be determined by the direction indicated by the line of the aerials, when optimum correspondence of records resulted, and the time delay required for this correspondence would indicate the velocity, the distance between aerials being constant. Various electronic and mechanical aids

VOL. 7 1955

have been suggested to produce a complete practical method, but it is proposed in this paper to merely indicate the basic proposal and draw attention to the results in Figs. 8 and 9. In these records it was found that the north and central records were practically identical, and this suggested a wind in the N–S direction. From the time-interval required to give optimum correspondence, the magnitude of the

Fig. 11.

velocity was calculated, and as will be seen the result compares favourably with the result of the new analysis of the Mitra aerial system.

It is to be noted that the time-intervals for the central-east correspondence of records, differed for various portions of it, indicating a change in orientation of the lines of maximum amplitude which is essential for the circle construction. The use of a third aerial in this way may well provide useful information on the field-strength patterns.

It will be seen that the method is unaffected by curved lines of maximum amplitude, but will fail if the field-strength contours are in effect a series of parallel lines. Inspection of many records from the Mitra method indicates that this is not a usual occurrence. The practical success of the method as outlined will depend to a major extent on the stability of the field-strength patterns during the time-intervals involved. However, it is considered that an extension of the scheme to a process of automatic correlation rather than subjective observation could overcome this difficulty, but a complete discussion is not appropriate to this paper. It may be mentioned that the moving aerial could then be replaced by a set of fixed aerials suitably distributed around the semi-circular path, if this arrangement is more suitable from a mechanical point of view.

Conclusion

An interpretation of the fading records of the Mitra system has been given and a new method of analysis described. Initial results have shown promise, and have provided some evidence in favour of an alternative method of determining ionospheric winds. It is intended to publish a more detailed discussion and summary of results at a later date.

Acknowledgements—The author would like to acknowledge, with thanks, discussions with Mr. N. F. Barber and other members of the Department.

This paper is published with the permission of the Secretary of the Department of Scientific and Industrial Research, New Zealand.

REFERENCES

MITRA, S. N.	1949	*Proc. Inst. Elect. Engrs.* **96,** (Pt. IV), 441
NEWSTEAD, G.	1954	*J. Atmosph. Terr. Phys.* **5,** 182
RATCLIFFE, J. A.	1954	*J. Atmosph. Terr. Phys.* **5,** 173
RUMSEY, N. J.	1955	To be published

VOL.
7
1955

Journal of Atmospheric and Terrestrial Physics, 1955, Vol. 7, pp. 341 and 342. Pergamon Press Ltd., London

The measurement of normal *E*-layer critical frequencies at night

W. R. PIGGOTT

Official communication from D.S.I.R. Radio Research Station, Slough

(*Received* 11 *February* 1955)

ALTHOUGH the characteristics of the normal *E*-layer during the day have been studied intensively, practically no reliable measurements of its critical frequency at night have been obtained. Such measurements are needed both for theoretical purposes and to provide a sound basis for studies of the propagation of medium waves at night.

Identifying the normal *E*-layer critical frequency at night is, however, very difficult, because the typical group retardation observed during the day becomes small when the critical frequency is comparable with the gyro-frequency and vanishes at lower frequencies. Thus at night the $h'f$ patterns for normal and sporadic E reflections are indistinguishable.

The difficulty can be overcome by measuring the variation of absorption with frequency and time during the night, the absorption band associated with the critical frequency remaining very obvious even when no group retardation can be detected (e.g., for $\Delta P' < 2$ km).

The shapes of the absorption-frequency patterns, when plotted in the form $(-\log/\rho)$ against log (frequency), are very similar during any month, changing slightly with sunspot cycle and perhaps also with season. Using these shapes, one can deduce the critical frequency with good accuracy, even when echoes on frequencies below the absorption band cannot be measured or are not observed. It is, however, essential that the measurements should be made at closely spaced frequencies in order to define the shape of the absorption band.

The alternative procedure of observing the changes of absorption with time on a fixed frequency is not so satisfactory. The observed absorption contains two terms: the non-deviative loss which decreases steadily with time, and a deviative loss which first increases and then decreases with time. In addition, there are the disturbing effects of slow period fading to be eliminated. Thus the interpretation is difficult, especially when the critical frequency falls below about 0·8 Mc/s, since it then varies very slowly with time.

The results of some typical measurements are shown in Fig. 1. Near sunset, measurements could be made on frequencies above about 1 Mc/s, thus enabling the shape of the absorption band and the critical frequency of the *E*-layer to be determined with considerable accuracy. The deduced critical frequency could also be confirmed by observing the group retardation on a normal $h'f$ record. Later, echoes could be detected occasionally below the absorption band with amplitudes roughly consistent with those to be expected, but the signal-to-noise ratio was inadequate for accurate measurement. The curves shown were obtained at Slough, using a sender with a peak output power of about 0·5 kW and a standard D.S.I.R. absorption measuring receiver having a large linear dynamic range (PIGGOTT, 1955). Aerials originally designed to work between 1·5 Mc/s and 3·0 Mc/s were employed. Intense medium-wave interference from broadcasting stations limited the accuracy. It was, however, clear that the experiment would be very easy, given about ten times as much power from the sender. It is perhaps worth pointing out that while it is very advantageous to increase the size of the sending aerials, signal-to-noise ratio is most

important when designing the receiving aerials. Thus the latter need only be fairly short, but should be carefully balanced to reject vertically polarized medium-wave interference.

When the main trend of the critical frequency variation had been obtained, it was found possible to identify the absorption band on a few of the routine $h'f$ patterns obtained at night at Slough. Usually this was difficult owing to the presence of E_s reflections and occasional fades due to layer irregularities. An interesting feature of the results was that the critical frequency was remarkably consistent on different occasions at corresponding times after sunset, differences greater than the experimental error of measurement being

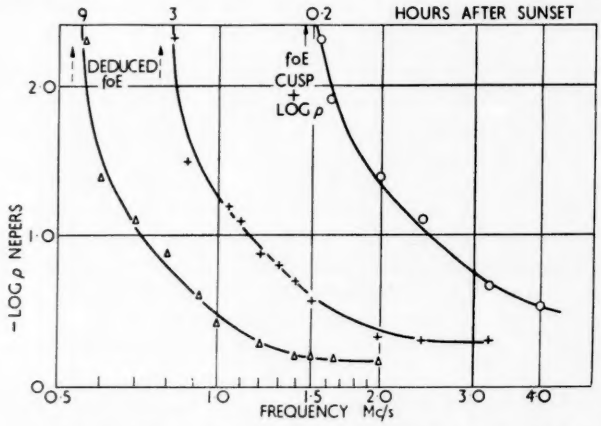

Fig. 1. $-\log \rho$: Frequency measurements, January 1947

very unusual. The variation with time fitted a recombination law in which the recombination coefficient was about $1 \cdot 10^{-8}$ for values of critical frequency above about 0·7 Mc/s, the lowest on which measurements could usually be obtained with the inefficient system available. It was also found that the weaker forms of sporadic E reflections often varied remarkably smoothly with time after sunset, the average difference between the critical frequencies of the E_s- and normal E-layers decreasing very slowly with time. The resultant variation of E_s critical frequency imitates a recombination law with a very small recombination coefficient.

Thus, useful information about the characteristics of normal E-layer at night can be obtained using comparatively cheap and simple equipment, and it is probable that absorption changes with frequency observed with high-power equipment would be very enlightening.

Acknowledgements—The main portion of this work was carried out in 1942–3, and formed part of a joint investigation on the propagation of medium waves at night sponsored by the British Broadcasting Corporation and the Department of Scientific and Industrial Research. This paper is published by permission of the Director of Radio Research of the Department of Scientific and Industrial Research.

REFERENCES

PIGGOTT, W. R. 1955 The D.S.I.R. Ionospheric Absorption Measuring Equipment. *Wireless Engineer* **32**, 164

VOL. 7 1955

RESEARCH NOTES

On the level at which fading is imposed on waves reflected vertically from the ionosphere

(*Received* 13 *June* 1955)

IT has been shown by BOOKER, RATCLIFFE, and SHINN (1950) that the autocorrelation function over the ground of the field of a downcoming radio wave from the ionosphere is the same as the autocorrelation function existing at emergence from the ionosphere, provided that structure across the wave front finer than the wavelength is not present. In the H.F. band this result has been used to deduce the correlation distance of irregularities in the E-region (and in some cases also the F-region), values of the order of 200 metres being obtained. At lower frequencies, however, the wavelength is too long for the fine structure in the ionosphere to be recorded at the ground. Nevertheless, some interesting information about scattering in the ionosphere can be deduced from observations of the correlation function over the ground at the lower frequencies.

Consider a plane wave incident normally upon a diffracting screen in which the structure is small compared with the wavelength λ in the surrounding medium. Let us calculate the autocorrelation function of the field over a plane parallel to the screen, following the methods of BOOKER, RATCLIFFE and SHINN (1950). The result is

$$\frac{\sin(2\pi x/\lambda)}{(2\pi x/\lambda)}$$

if the irregularities in the screen involve a function of one cartesian co-ordinate x only, or

$$\frac{J_1(2\pi r/\lambda)}{(\pi r/\lambda)}$$

if the irregularities involve a function of two orthogonal cartesian co-ordinates x and y and $r = (x^2 + y^2)^{\frac{1}{2}}$. From these expressions we see that the width of the autocorrelation function over the ground at the lower frequencies should be proportional to wavelength, and this is what is observed.*

When comparing the above expressions with experimental autocorrelation functions, however, an interesting numerical discrepancy arises. To make the above expressions fit the experimental results approximately, it is necessary to make λ about six or seven times the free space wavelength λ_0*. This shows that the irregularities causing the fading are occurring at a level in the ionosphere where the local wavelength λ is six or seven times λ_0. It follows that the irregularities concerned are located where the ionization-density is within a few per cent of the critical value required for classical reflection. In other words, the fading of a radio wave reflected normally from the ionosphere is imposed upon the wave within, or close to, the reflecting stratum.

This result, although important, is perhaps not surprising. For a scattering formula such as that used by BAILEY *et al.*[3] (1952), the scattered power increases as the square of the mean ionization-density, if the r.m.s. fractional deviation of ionization-density remains

*Unpublished results of the Cambridge Radio Group.

constant. Fading is therefore most likely to be imposed where the greatest ionization-density is encountered, and this is in the reflecting stratum. In addition, there is the possibility of plasma resonance of irregularities in and near the reflecting stratum, as suggested by HERLOFSEN (1951).

It should perhaps be mentioned that the scattering which we have shown to be taking place in or near the reflecting stratum is by no means a trivial phenomenon. Even in a quiet ionosphere the resulting amplitude of fading is nearly always comparable to the mean amplitude of the signal (MCNICOL, 1949). Thus, scattering by irregularities in and near the classical reflecting stratum is nearly as important a mechanism for returning energy as classical internal reflection itself.

H. G. BOOKER

Cavendish Laboratory,
Cambridge, England.
June, 1955.

REFERENCES

BOOKER, RATCLIFFE, and SHINN	1950	*Phil. Trans.* **A242,** p. 579
BAILEY *et al.*	1952	*Phys. Rev.* **86,** 141
HERLOFSEN	1951	*Ark. fys*, **3,** 247
MCNICOL	1949	*Proc. Instn. Elect. Engrs.* **96,** 3, p. 517

VOL.
7
1955

Accuracy of solar-flare observations

(*Received* 4 *July* 1955)

THE connection between solar flares and solar radio emission has given further importance to the solar-flare observations published in the I.A.U. *Quarterly Bulletin on Solar Activity*, which have already proved useful in correlating a wide range of geophysical data with solar activity. In the approaching years of increased activity, and especially during the International Geophysical Year, there will be considerable need to know the importance of a flare, which at present is only coarsely estimated on a scale of 1 to 3.

The practicability of a more precise scale has obvious interest; in addition, the accuracy of present solar-flare reports is brought into question by such items as a flare reported by seven different observers as importances 1, 1–2, 2, 2, 2, 2, 3.

For that reason an elementary statistical investigation was made of consistency among observations by two or more observers of the same flare. To determine whether solar-flare observations have improved in the last few years, the periods covered were 1947 and 1952–4. No significant differences appeared.

The mean value of the standard deviation was about 0·45 over most of the importance range, falling off to zero at the extreme ends of the scale where observational error would be difficult. For flares reported by three or more observers, the standard deviation did not decrease with more observations, suggesting the scatter is real and not the result of one or two observers being out of line.

Using the statistical distribution of flare importances, and making allowance for the

fact that very large or very small flares can hardly be misclassified, the percentages of flares of given importance likely to be reported as importance 1, 2, or 3 were computed:

Flare observation scatter

Reported as	True Importance 1	True Importance 2	True Importance 3
3	0	11%	81%
2	9%	63%	19%
1	91%	26%	0

Evidently classes 1 and 3 are fairly reliable, mainly because the observer can err in only one direction. As for class 2, it can at least be said that the observers are right more often than they are wrong.

It appears that the division of solar flares into more than three classes is not at present feasible; division into three classes is barely justifiable. The classifications 1+, 1–2, 2–, etc., which occasionally appear in the literature, seem of doubtful significance. Solar-flare observations would be increased in value if more uniform as well as more detailed reporting could be achieved.

L. W. Ross

Leuschner Observatory,
University of California,
Berkeley, California.

The recombination coefficient in the *E*-layer during aurorae

(*Received* 14 *April* 1955)

Recent investigations (Omholt, 1955) show that the connection between the primary ionization q and the electron density n_e in the E-layer during aurorae, at least for $n_e \leqslant 3 \cdot 10^5$ electrons/cm^3, the upper limit of n_e during the observations, when $\frac{d}{dt} n_e = 0$, can be described by

$$q = \alpha n_e^2 \qquad (1)$$

where α is found to be about 10^{-7} cm^3 sec^{-1}, independent of n_e. For the E-layer by daylight the effective recombination coefficient is about $2 \cdot 10^{-8}$ cm^3 sec^{-1}, and must be explained by dissociative recombination (Bates and Massey, 1946, 1948; Mitra and Jones, 1954). The greater value of α during aurorae may be explained by dissociative recombination if the relative concentrations of positive ions differ appreciably from the concentrations at daytime (Omholt, 1955).

An alternative explanation may be given by assuming a high value of the negative-ion-to-electron ratio, λ, during aurorae. This gives, as shown by Appleton and Sayers (1938),

at equilibrium, equation (1) with

$$\alpha = (1 + \lambda)(\alpha_e + \lambda\alpha_i) \tag{2}$$

when $\alpha_i n^+ n^-$ is the rate of ionic recombination and $\alpha_e n_e n^+$ the rate of electronic recombination, including dissociative recombination. n, n^-, and n^+ are the numbers/cm^3 of neutral particles, negative ions, and positive ions. When ρn^- is the rate of detachment due to the incoming particles causing the aurorae, $\kappa n^- n$ the rate of collisional detachment and $\eta n_e n$ the rate of attachment, one may show (from equation (35), BATES and MASSEY, 1946) that for $\frac{d}{dt} n^- = 0$,

$$\lambda = n^-/n_e = \eta n/\rho + \kappa n + \alpha_i(1 + \lambda)n_e \tag{3}$$

To make α independent of n_e requires λ to be constant:

$$\kappa n = k(\rho + \alpha_i(1 + \lambda)n_{e\,\max}) \tag{4}$$

where $k \gg 1$ and $n_{e\,\max} = 3 \cdot 10^5$ cm^{-3}, the maximum value of n_e obtained during the observations for which equation (1) was proved to hold. ρ can probably be ignored. Taking ρn to be of the same order of magnitude as q, it may be shown from the observations that for $n_e \leqslant 3 \cdot 10^5$ cm^{-3}, $\rho \leqslant 10^{-8}$ sec^{-1}. Taking n to be 10^{13} cm^{-3}, equations (4), (3), and (2) give

$$\kappa = k\alpha_i(1 + \lambda) \cdot 3 \cdot 10^{-8} \tag{5}$$

$$\eta = \lambda\kappa = k\alpha_i\lambda(1 + \lambda) \cdot 3 \cdot 10^{-8} \tag{6}$$

$$\alpha = \alpha_e + \lambda(\alpha_e + \alpha_i) + \lambda^2\alpha_i \tag{7}$$

Putting $\alpha = 10^{-7}$ and $\alpha_e = 2 \cdot 10^{-8}$ cm^3 sec^{-1}, equation (7) has been solved for different values of α_i, and κ and η are derived from equations (5) and (6). The results are given in the table.

α_i cm^3 sec^{-1}	λ	κ cm^3 sec^{-1}	η cm^3 sec^{-1}	
10^{-7}	0·5	$k \cdot 45 \cdot 10^{-16}$	$k \cdot 22 \cdot 10^{-15}$	
10^{-8}	1·7	$k \cdot 8 \cdot 10^{-16}$	$k \cdot 1{\cdot}4 \cdot 10^{-15}$	$k \gg 1$
10^{-9}	3·3	$k \cdot 1{\cdot}3 \cdot 10^{-16}$	$k \cdot 0{\cdot}4 \cdot 10^{-15}$	

According to BATES and MASSEY (1946), α_i is probably of the order 10^{-7} — 10^{-8} cm^3 sec^{-1}, but it may be smaller. Further, they do not find values of κ and η of the order given in the table impossible, though they are probably lower. We must, with the present knowledge of the values of α_i, κ, and η, assume that the value of λ may be large enough to explain the high value of α during aurorae.

A. OMHOLT

*The Auroral Observatory, Tromsö, Norway.**

REFERENCES

APPLETON, E. V., and SAYERS, J.	1938	*Rec. Un. radio-sci. int.* 272
BATES, D. R., and MASSEY, H. S. W.	1946	*Proc. Roy. Soc.* **A187,** 261.
	1948	*Proc. Roy. Soc.* **A192,** 1.
MITRA, A. P. and JONES, R. E.	1954	*J. Geophys. Res.* **59,** 391.
OMHOLT, A.	1955	*J. Atmosph. Terr. Phys.* **7,** 73

* Present address: Department of Applied Mathematics, Queen's University, Belfast, Northern Ireland.

VOL. 7 1955

Changes in the absorption of cosmic noise observed during two ionospheric disturbances

(*Received* 9 *April* 1955)

It has been shown by Mitra and Shain (1953), that although the D-region generally makes the greater contribution to the absorption of 18·3 Mc/s cosmic noise during daylight hours, the F-region may produce considerable attenuation when f_0F_2 is high. During ionospheric storms f_0F_2 often departs considerably from its usual value for short periods, and it would be expected that, for at least the largest increases, there would be corresponding increases in the attenuation of cosmic noise.

Such an effect is illustrated in the record taken at Hornsby (latitude 34° S, longitude 151° E) for November 25, 1950. Fig. 1(a) shows the measured total absorption (in both the D- and F-regions) for the periods from 1100 to 1500 on each of the three days November 23, 24, and 25; also shown are the values of f_0F_2, recorded at 10-min intervals, at Canberra (latitude 35° S, longitude 149° E) and Brisbane (latitude 28° S, longitude 153° E) during the same periods. It is apparent that, corresponding to the increase in absorption commencing at about 1220 on November 25, there are large increases in f_0F_2 at both stations. Mitra and Shain found that the F-region contribution to the total absorption of 18·3 Mc/s cosmic noise was less than 0·2 db for f_0F_2 equal to 7 Mc/s, but increased rapidly for higher values of f_0F_2, the rate of increase being roughly 0·25 db per Mc/s at 8·5 Mc/s. The increase in absorption is therefore consistent with the hypothesis that it is due to F-region attenuation.

Marked variations in absorption occurred during the severe ionospheric disturbance on August 20, 1950. Fig. 1(b) shows the observations on this occasion. As before, abnormally high absorption is associated with high f_0F_2. However, although f_0F_2 at Canberra was very low on August 20 between 1400 and 1500, the absorption was actually higher than on the other two days (differences in the zeros on successive days should be less than 0·1 db). This unusual effect is most probably associated with the marked and rapid changes which took place in the shape of the F-region; during this hour $h'F_2$ fell from about 600 km to 320 km. Examination of the Canberra ionospheric records showed that the sudden rise in f_0F_2 at 1600 was probably due to the movement over the station of a region in which there was a very marked gradient of ionization density. Between 1500 and 1600, besides the spread traces of the ordinary and extraordinary rays with critical frequencies near 7 Mc/s and 8 Mc/s respectively, there was a separate group of echoes between 10 and 12 Mc/s. The virtual height of this group decreased gradually from about 1000 km, until at 1600 they suddenly became part of a normal h'-f record with very little spread on the first F reflection. At 1520, besides the 12-Mc/s echo at 650 km, there was a further very faint echo at 980 km. The difference, 330 km, would correspond well with a ground reflection after oblique reflection at the F-region level.

It will be noticed in Fig. 1(a) that there is a difference in the times of maxima of the three curves for November 25. The Hornsby absorption maximum occurs about 20 min after the Canberra f_0F_2 maximum, and the Brisbane f_0F_2 maximum is delayed a further 30 min. Taking account of the relative locations of the stations, it is found that the delay in the maxima of the curves could be explained if there were a disturbance travelling roughly towards the north-east at a speed of about 700 km per hour. Similarly, Fig. 1(b) shows that the Hornsby absorption maximum is probably delayed about 10 min after the maximum at Canberra; comparatively short-term variations at Brisbane mask any time delays between Brisbane and either Canberra or Hornsby. Similar travelling disturbances, although generally of a less intense nature, have been studied in detail by Munro (1950).

It has been shown already (SHAIN and MITRA, 1954) that observations of cosmic noise give a sensitive means of detecting the numerous short-term increases in *D*-region absorption due to solar flares. The two observations noted here show that the continuous records

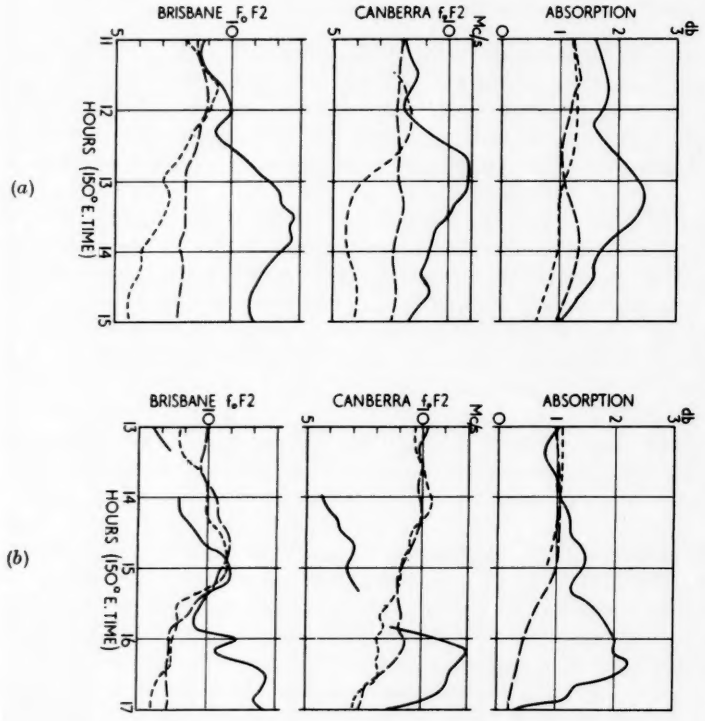

Fig. 1. Observed total absorption at Hornsby, and f_0F_2 at Canberra and Brisbane.
(a) Between 1100 and 1500 on November 23 (— — —), 24 (- - - - -) and 25 (————).
(b) Between 1300 and 1700 on August 19 (— — —), 20 (————) and 21 (- - - - -).

of absorption provided by the cosmic-noise technique, although sometimes difficult to interpret by themselves, should be of value in bringing to notice other rapid changes in ionospheric conditions which would repay further study.

C. A. SHAIN

Division of Radiophysics, C.S.I.R.O.,
Sydney, Australia.

REFERENCES

MITRA, A. P., and SHAIN, C. A. 1953 *J. Atmosph. Terr. Phys.* **4**, 204-217
MUNRO, G. H. 1950 *Proc. Roy. Soc.* **A202**, 208-223
SHAIN, C. A., and MITRA, A. P. 1954 *J. Atmosph. Terr. Phys.* **5**, 316-328

VOL. 7 1955

Solar H_α filaments and geomagnetic disturbances

(*Received* 13 *June* 1955)

ROBERTS and TROTTER (1955) recently investigated the relation of prominences visible in H_α at the solar limb to geomagnetic disturbances for the periods May–November 1951, February–October 1953, and February–June 1954. These periods fall in the declining phases of the last solar-activity cycle. The purpose of the study was to test a previously announced hypothesis of KIEPENHEUR (1947), which identified the recurrent *M*-region geomagnetic disturbances with dark filaments on the solar disc. Limb prominences and disc filaments are generally regarded as manifestations of the same phenomenon

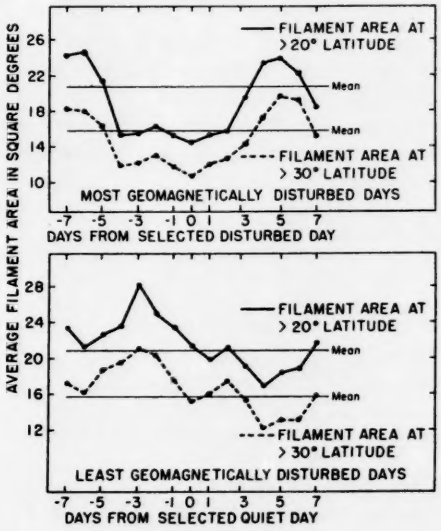
AVERAGE FILAMENT AREA IN SQUARE DEGREES
FILAMENT AREA AT > 20° LATITUDE
Mean
Mean
FILAMENT AREA AT > 30° LATITUDE
MOST GEOMAGNETICALLY DISTURBED DAYS
DAYS FROM SELECTED DISTURBED DAY
FILAMENT AREA AT > 20° LATITUDE
Mean
Mean
FILAMENT AREA AT > 30° LATITUDE
LEAST GEOMAGNETICALLY DISTURBED DAYS
DAYS FROM SELECTED QUIET DAY

Fig. 1.
Above: Average H_α dark-filament area at the solar central meridian on days preceding and following zero days representing the five most geomagnetically disturbed days each month.
Below: Same for zero days representing the five least geomagnetically disturbed days.

(D'AZAMBUJA, 1948), so that the use of limb-prominence measures was considered a reasonable test of the hypothesis. The results were negative; that is, they did not confirm the statistical results of KIEPENHEUR derived from earlier years of low solar activity.

To make certain that the negative results did not derive from the use of limb prominences rather than disc filaments, the present authors repeated the analysis, using dark-filament areas measured from the solar activity maps of M. D'AZAMBUJA, published monthly in *l'Astronomie*. We also examined photographs of filament from the McMath-Hulbert Observatory, and concluded that the use of data from these would not differ significantly from the use of the D'AZAMBUJA maps.

The results of our analysis are shown in Fig. 1, where we have treated the filament areas just as ROBERTS and TROTTER (1955) treated the prominence areas. Included are average filament areas for latitudes greater than 20° and 30°, represented in superposed epoch graphs, where the zero dates were: (a) the five most magnetically disturbed days of the

month, and (b) the five most geomagnetically quiet days, giving us 105 days of each kind (CRPL 1951–1954). The mean filament areas shown are the means for all days in the period studied, and thus are not equal to the means of the curves shown which are based on selected days. In the analysis by ROBERTS and TROTTER the means were computed for the same days entering the superposed epoch analysis and are therefore equal to the means of their curves. Otherwise the results are exactly comparable.

Our results confirm the limb-prominence analysis, and thus are not in agreement with the hypothesis of KIEPENHEUER. They show a tendency for filament areas to be at a minimum for the two or three days preceding the disturbed days. The tendency for filament areas to reach a maximum on the third day preceding the most magnetically quiet days is much more definite than of ROBERTS and TROTTER for the limb prominences. This peak arises, however, from a relatively small number of cases in which there were unusually large filament areas.

One should not expect the curves of Fig. 1 to agree in detail with those of ROBERTS and TROTTER, since the latter are based on the areas of prominences seen in vertical projection, whereas our study utilizes the filament area observed by very different techniques, and in horizontal projection. Nevertheless, our study leads to the same conclusion; namely, that M-regions are not to be identified, at least in the period studied, with intermediate and high latitude solar filaments seen in H_α.

HOPE I. LEIGHTON
DONALD E. BILLINGS

National Bureau of Standards
and High-Altitude Observatory,
Boulder, Colorado

VOL.
7
1955

REFERENCES

D'AZAMBUJA, L. and M. (1948) *Prominences and their Evolution.* Annals of Observatory of Paris, Astrophysics Section at Meudon, Vol. 6. Gauthier-Villars, Paris

CRPL F-Series, *Monthly Ionospheric Data* (1951–54) issued by United States Department of Commerce, National Bureau of Standards, Central Radio Propagation Laboratory, Boulder, Colorado

KIEPENHEUER, K. O. (1947) *Astrophys. J.* **105,** 408

ROBERTS, W. O., and TROTTER, D. E. (1955) *J. Atmosph. Terr. Phys.* **6,** 282

Indices of geomagnetic activity

of the Observatories ABINGER (*Ab*), ESKDALEMUIR (*Es*) and LERWICK (*Le*)

May to June 1955

The figures given on pages 351 and 352 represent the *K*-indices for three-hour intervals, beginning with 00–03 hrs for the first and ending with 21–24 hrs for the eighth figure.

May 1955

Day	*Ab* Range for $K = 9 : 500\gamma$			*Es* Range for $K = 9 : 750\gamma$			*Le* Range for $K = 9 : 1000\gamma$			*Day*
	K-Indices		*Sum*	*K-Indices*		*Sum*	*K-Indices*		*Sum*	
1	2211	1123	13	2211	1223	14	3211	1112	12	1
2	1012	3322	14	0012	2222	11	0111	2212	10	2
3	2122	2322	16	2111	2321	13	2111	1311	11	3
4	1123	3333	19	1012	3223	14	1112	2223	14	4
5	1222	3422	18	1122	3422	17	2211	3311	14	5
6	3223	5445	28	3223	5335	26	3223	4326	25	6
7	5434	3334	29	5334	3334	28	5443	2234	27	7
8	4434	4454	32	4433	3454	30	4343	3444	29	8
9	3222	2332	19	2222	2332	18	4112	2332	18	9
10	3223	1333	20	3223	1233	19	3322	1223	18	10
11	1221	2321	14	1111	1221	10	1111	1112	9	11
12	1222	1234	17	0112	1233	13	0212	1224	14	12
13	3223	3332	21	2112	3332	17	3112	2232	16	13
14	2334	3321	21	2323	3322	20	2322	2322	18	14
15	2222	2223	17	2221	1223	15	2221	1212	13	15
16	4423	2211	19	4423	1111	17	4532	1111	18	16
17	2121	2212	13	1110	1102	7	1111	1102	8	17
18	3121	2321	15	2110	2321	12	1110	2211	9	18
19	1122	2111	11	1121	1111	9	0111	2111	8	19
20	1212	2322	15	1112	1222	12	1112	1121	10	20
21	1122	3212	14	1011	2212	10	0001	2211	7	21
22	1212	1232	14	2201	1231	12	1111	1221	10	22
23	0112	3311	12	1011	2210	8	0011	2200	6	23
24	0112	2321	12	0110	2321	10	0111	1211	8	24
25	1122	4465	25	1111	4456	23	0111	3358	22	25
26	5434	3432	28	5435	3431	28	8644	3322	32	26
27	2222	4544	25	2111	4544	22	2111	4545	23	27
28	3343	3333	25	3343	3333	25	4344	3323	26	28
29	2223	2322	18	2122	2312	15	2222	2312	16	29
30	1112	2321	13	1121	2221	12	1121	1221	11	30
31	2222	2222	16	2221	2112	13	2111	1112	10	31

June 1955

Day	*Ab* *Range for* $K = 9 : 500\gamma$			*Es* *Range for* $K = 9 : 750\gamma$			*Le* *Range for* $K = 9 : 1000\gamma$			*Day*
	K-Indices		*Sum*	*K-Indices*		*Sum*	*K-Indices*		*Sum*	
1	2222	3321	17	2222	3311	16	2211	3321	15	1
2	2122	3322	17	2112	2322	15	2111	2221	12	2
3	2322	2331	18	1211	2331	14	1211	1321	12	3
4	1232	3322	18	2221	3322	17	1122	2221	13	4
5	1111	2321	12	1112	2321	13	1112	2221	12	5
6	0122	3334	18	0001	2333	12	0111	2333	14	6
7	3333	4323	24	3323	3323	22	3322	2213	18	7
8	2433	4534	28	2523	3533	26	2532	3434	26	8
9	1222	3333	19	1122	3233	17	1212	2223	15	9
10	2222	2221	15	1112	2211	11	1111	1211	9	10
11	0122	3323	16	0122	3232	15	1112	3323	16	11
12	2333	3222	20	3222	3122	17	2322	3112	16	12
13	2122	3333	19	1021	3322	14	2111	3321	14	13
14	2234	3431	22	2234	3431	22	2123	3321	17	14
15	3343	3333	25	3333	3333	24	4333	3323	24	15
16	4333	4322	24	4223	3321	20	4323	3311	20	16
17	2223	3423	21	2223	3323	20	2223	3323	20	17
18	1323	3222	18	1223	2211	14	1222	1211	12	18
19	3322	3321	19	3322	3221	18	3321	3220	16	19
20	1122	3422	17	0001	2431	11	1111	2321	12	20
21	2122	2221	14	2111	2211	11	2111	2211	11	21
22	2214	3433	22	2103	3333	18	1003	3333	16	22
23	4333	3354	28	3332	2344	24	2331	2234	20	23
24	4333	4332	25	4333	3332	24	4433	3322	24	24
25	3233	3331	21	2132	3231	17	3133	2231	18	25
26	1212	2213	14	1111	1212	10	1111	1112	9	26
27	1222	2331	16	1122	2321	14	1121	2320	12	27
28	2212	2323	17	2212	2223	16	2212	3113	15	28
29	2222	3332	19	2022	3232	16	2021	3221	13	29
30	2222	1221	14	2211	1211	11	2211	1211	11	30

VOL. 7 1955

L.
55